SEDIMENTOLOGY, ICHNOLOGY, AND SEQUENCE STRATIGRAPHY OF BLACK SHALES FROM THE UPPER JURASSIC - LOWER CRETACEOUS VACA MUERTA FORMATION, NEUQUÉN BASIN, ARGENTINA

A Thesis Submitted to the
College of Graduate and Postdoctoral Studies
In Partial Fulfillment of the Requirements
For the Degree of Doctor of Philosophy (Ph.D)
In the Department of Geological Sciences,
University of Saskatchewan
Saskatoon, Saskatchewan, Canada

By

Maximiliano Paz

PERMISSION TO USE

In presenting this thesis/dissertation in partial fulfillment of the requirements for a Postgraduate degree from the University of Saskatchewan, I agree that the Libraries of this University may make it freely available for inspection. I further agree that permission for copying of this thesis/dissertation in any manner, in whole or in part, for scholarly purposes may be granted by Drs. María Gabriela Mángano and Luis Alberto Buatois who supervised my thesis/dissertation work or, in their absence, by the Head of the Department of Geological Sciences or the Dean of the Colleges of Graduate Studies and Research (CGSR). It is understood that any copying or publication or use of this thesis/dissertation or parts thereof for financial gain shall not be allowed without my written permission. It is also understood that due recognition shall be given to me and to the University of Saskatchewan in any scholarly use which may be made of any material in my thesis/dissertation.

DISCLAIMER

Reference in this thesis/dissertation to any specific commercial products, process, or service by trade name, trademark, manufacturer, or otherwise, does not constitute or imply its endorsement, recommendation, or favoring by the University of Saskatchewan. The views and opinions of the author expressed herein do not state or reflect those of the University of Saskatchewan, and shall not be used for advertising or product endorsement purposes.

Requests for permission to copy or to make other uses of materials in this thesis/dissertation in whole or part should be addressed to:

Head
Department of Geological Sciences
University of Saskatchewan
114 Science Place
Saskatoon, Saskatchewan, S7N 5E2, Canada

OR

Dean
College of Graduate and Postdoctoral Studies
University of Saskatchewan
116 Thorvaldson Building, 110 Science Place
Saskatoon, Saskatchewan, S7N 5C9, Canada

ABSTRACT

During the past decades, the study of fine-grained successions has received considerable attention, mainly due to the groundbreaking work of various mudstone sedimentologists who suggested bottom transport processes as plausible mechanisms for mud sedimentation. Moreover, an increased interest has been growing due to the extensive development of unconventional shale reservoirs in USA. In this context, the Upper Jurassic-Lower Cretaceous Vaca Muerta Formation from the Neuquén Basin, Argentina, stands as a valuable shale reservoir for both industry and academic research that can be used to expand our knowledge on ancient fine-grained, organic-rich depositional environments. This Formation is the most important unconventional shale reservoir in South America, with exceptional characteristics for oil and gas extraction. It is well exposed in central western Argentina and contains a fair amount of core data that can be used to evaluate sedimentary processes and trace fossils. The present study analyzed sedimentologic, ichnologic and sequence stratigraphic datasets of the Vaca Muerta Formation to construct a robust depositional model and compare the results with other studies in order to test previous models and propose new ideas. For this purpose, outcrops from a basin margin location (Picún Leufú area), as well as outcrops (Yesera del Tromen) and cores (wells 1 to 9) from the basin centre (where most of the unconventional development is currently active), were analyzed in detail.

In the basin margin location (Picún Leufú area), ten sections were logged in the Kimmeridgian to Tithonian succession. The interval encompasses two third-order sequences formed in continental environments and a mixed carbonate-siliciclastic, shelf-margin clinoform system. At the base, the Quebrada del Sapo Formation represents sandstone, conglomerate and mudstone of eolian and fluvial origin. On top, marine carbonaceous, mixed to calcareous mudstone and sandstone of the Vaca Muerta (bottomset and foreset of the clinoform) and Picún Leufú (topset) formations occur. At the base, the clinoform system consists of a thin, retrograding, open bay facies association comprising beach, bay margin, proximal bay and distal bay facies. Above, a siliciclastic basin facies association is constituted by basin, hyperpycnal lobe, lobe fringe, channel-fill complex and overbank facies, developed at the bottomset of the clinoform system. In the foreset and topset, slope mud belt, mixed slope, slope sand bodies, sandy shoal, sand bar complex and lagoonal facies are part of the foreset facies association. This analysis challenged the previous paradigm of a catastrophic transgression at the onset of deposition of the Vaca Muerta

Formation. Catastrophic rates of sea-level rise (metres per day) are incompatible with the existence of a basal, retrograding, marginal marine succession suggesting a transition between continental and marine facies. A comparison to modern analogues of marine flooding over dunes indicates that rates of sea-level rise similar to Holocene ones (mm to cm per year) are plausible and may have generated a rapid, yet not catastrophic transgression. Hence, rapid transgressions represent an alternative to "catastrophic" and "normal" scenarios of marine flooding over eolian deposits. The Late Jurassic represents a non-glacial time, and the global sea-level maximum highstand pre-dated the Vaca Muerta transgressive event, indicating that part of the sea-level rise has to be attributed to tectonic/thermal subsidence and compaction. In addition, the combined analysis provides insights into sedimentary processes affecting bottomset and foreset of a fine-grained clinoform system, highlighting the role of wave-influenced hyperpycnal flows associated with higher fluvial input in Picún Leufú and their effect on diluting organic matter content.

In the basin centre (Yesera del Tromen and cores from wells 1 to 9), the succession was represented by the Tithonian to Valanginian, mixed carbonate-siliciclastic, shelf-margin clinoform system of the Vaca Muerta (bottomset and foreset) and Quintuco (topset) formations. The succession mostly comprises mixed to calcareous mudstone and bioclastic to intraclastic wackestone developed in four third-order sequences (Sequence 1 to 4). Sequence 1 and 2 start with a transgressive, marginal marine facies association comprising beach and open bay facies. Above, the bottomset and lower foreset of the clinoform shows starved, anoxic, dysoxic and oxic basin facies grouped into the basin facies association, and crinoid-rich, bioclastic- and silt-rich drift, and mixed drift and fluid mud facies, included in the drift facies associations. In the foreset, distal, mid, proximal, and fluid mud-rich slope facies occur as part of the slope facies associations. The slope association evolves from dominantly hemipelagic facies in the older, low-angle clinoforms, to mostly fluid mud-rich slope facies due to higher foreset angles in younger clinoforms. Sequence 3 and 4 are poorly cored, yet low- and high-energy outer ramp facies of the outer ramp facies association with subordinate basin and slope facies associations can be observed. This analysis provides several insights into the understanding of the Vaca Muerta Formation and other ancient fine-grained depositional environments. First, climate and consequent basin circulation were found to control sediment partitioning along the clinoform. Warmer climates triggered equatorward migration of the arid belt, humid conditions and estuarine circulation, producing high TOC and siliciclastic content due to anoxia and enhanced riverine input, respectively. In contrast, cooler

climates associated with a poleward migration of the arid belt generated arid conditions and anti-estuarine or weakened estuarine circulation, triggering intense contour currents at deep waters. Low TOC and high carbonate content is recorded, due to high burndown of organic matter under upper dysoxic to oxic conditions, and enhanced shelf export of carbonate sediments by cascading. Organic matter content was sourced from the water column (pelagic), indicating that bottom currents and sediment-gravity flows dilute the TOC content of these deposits. Second, the trace-fossil analysis shows an ichnofauna differing from the classic *Chondrites* and *Zoophycos* ichnoguild recorded in organic-rich mudstone successions. In contrast, cryptobioturbation, pellet-rich ichnocoenoses, and biodeformational structures are abundant in this formation. This characteristic can be explained by bioturbation in a food-rich benthic environment, which precluded specialized feeding and the development of tiered communities. Limited oxygenation is deemed responsible for reduced bioturbation index, penetration depth, burrow size, and ichnodiversity. Moreover, biodeformational structures in mudstone are associated with soupy to very soft substrates, whereas a change to soft and stiffgrounds during ash deposition enhanced preservation of discrete trace fossils. This last relationship indicates that tuff deposits and rock fabric can be used to evaluate bioturbation in homogeneous, fine-grained successions in order to claim biogenicity of structures or delineate bottom water oxygenation.

Finally, the characteristics of this Formation (low bioturbation intensity due to oxygen deficiency and low foreset angles hampering gravity flow transport) allowed the delineation of contourite deposits. Contourite deposits (drifts) can be differentiated from sediment-gravity flow deposits by their evidence of long-term transport, low sediment concentration, and long-term oxygen introduction at the sea-floor. Furthermore, contourites are host to a particular trace-fossil assemblage that was controlled by food (deposited at the surface or in suspension), oxygenation (increasing oxygen levels), hydrodynamic energy (precluding biogenic reworking during higher energy events) and water turbidity (allowing suspension feeding). The basin-wide increase in oxygenation generated by contourites indicates that these were produced by a wind- and thermohaline-driven circulation system of deep waters that was intensified during arid and cooler climates, which were times of enhanced cascading of dense, shelf waters. The trace fossil data supports the existence of high bioturbation intensity in contourite deposits, yet indicate that sedimentary structures can be preserved in muddy contourites when different stress factors are combined.

ACKNOWLEDGEMENTS

A short paragraph such as the following is not enough to really appreciate how much I am grateful of the people I have met while working on my thesis. Celeste and my family, Carlos, Vivi, Manu and Jere, were well-trained, first responders to the minor problems and difficulties I have found at my home (both Canadian and Argentinian), while being instrumental in my well-being. Gabriela Mángano and Luis Buatois were foster parents in the remote field of the -30 °C, bringing warm and actively listening every time you meet and talk to them. They have been a profound source of inspiration for me, both from their academic but also, very importantly, from their political and social justice background. Juan Ponce and Patricio Desjardins were the masterminds that proposed and encouraged many of the projects that manufactured this thesis. I will keep grateful to them for all the time, support, critics, calls and e-mails they have spent with me. Martín Parada, Maximiliano Rodríguez, Claudio and Camila García, Débora Campetella, and the Painemilla family, are friends and were field work partners in the beautiful outcrops of Picún Leufú and Yesera del Tromen. Romain Gougeon, Neal Handkamer, Andrei Ichaso, Mayra Zuñiga, Mario González, Diego and Sol Muñoz, Gabriel Mendoza, Fernando and Gustavo Valencia, Fadhia Arocha, Carla Almendariz, Kai Zhou, Brittany Laing, Charlie Zheng, Gerry and Shirley Falk, Cristian España, Mayra Samaniego, Eliza Mae, and Gurpreet Singh are the friends to which I relied on any time I needed. These people made me fully enjoy every minute I spent in Canada and it was a great satisfaction to meet them. Silvio Casadío, Josefina Pons, Adolfo Giusiano, Noelia Carmona, Cecilia Cábana, Pablo González, Victor García, Maisa Tunik, Alberto Caselli and specially, Dr. Ponce, were the people who taught me field geology during my undergrad, and watched me growing from a would-be, to a fully grown baker. Juan, Silvio, and Noe introduced me to Luis and Gaby after organizing the field school on Vaca Muerta in 2015. I specially thank the enlightening feedback and discussions received from Andreas Wetzel, Federico González Tomassini, Daniel Minisini, Germán Otharán and Martín Cevallos, people from which I borrowed many ideas. Maximiliano Rodríguez, Egberto Pereira, Raúl Notta, Manuel Fantín, Hernán Reijenstein, María Dolores Vallejo, Carlos Zavala, Gonzalo Veiga, Juan Pedro Rodríguez-López, Agustín Arguello-Scotti, Lauren Birgenheier, Massimo Moretti, Diego Kietzmann, Ernesto Schwarz, João Trabucho Alexandre and Patrick Orr reviewed and remarkably improved different versions of the chapters. Elisabeth Steel, Camille Partin, Bruce Eglington, and Christopher Hawkes

reviewed the complete thesis and provided multidisciplinary feedback during the committee meetings. Chantal Strachan-Crossman, Michelle Howe, Blaine Novakovski, and Tom Bonli supported our study through administrative and lab work. This thesis was possible thanks to funding from the University of Saskatchewan (Dr. Rui Feng Graduate Studies Award and Dean's Scholarship), Natural Sciences and Engineering Research Council of Canada (NSERC), Universidad Nacional de Río Negro (UNRN), and the Consejo Nacional de Investigaciones Científicas y Técnicas (CONICET). I have received Student Research Grants from the Society for Sedimentary Geology (SEPM), the American Association of Petroleum Geologists (AAPG), the International Association of Sedimentologists (IAS), and two Grants from the Geological Society of America (GSA), which were fundamental for our field work. We are in debt with Germán Canto, Adrián Dolso, Sebastián Estrada, Sebastián Galeazzi, and Fabián Lamarque who allowed access to the cores of Total Austral, Shell, YPF, and Chevron, companies that also shared with us their core information. To conclude, I want to thank all the friends and pieces of inspiration that I found while wandering in the amazing land of the living skies.

TABLE OF CONTENTS

LIST OF TABLES

LIST OF FIGURES

CHAPTER 1: INTRODUCTION AND LITERATURE REVIEW

Fine-grained sediments constitute about 70-75% of the modern and ancient depositional record and much of the cover of shelves, slopes and abyssal plains (McCave, 1972; Gorsline, 1984; Stow and Piper 1984), yet sedimentology has been historically skewed towards coarser grained deposits due to a focus on conventional hydrocarbon reservoir characterization (Schieber and Zimmerle, 1998; Scott and Bouma, 2004), difficulties on imaging clay-size particles (Potter *et al.*, 1980), and the high weathering observed in outcrops that precludes the study of ancient successions (Li and Schieber, 2018). Therefore, understanding of transport and deposition of fine-grained sediments historically relied on physical models (McCave, 1972) or experimental studies by engineers aimed at evaluating mud effects on coastal management (Schieber, 2011). Nevertheless, many books concerning mud and mudstone have covered fields such as for instance, sedimentology, clay microstructure and geochemistry (e.g. Potter *et al.*, 1980; Stow and Piper, 1984; Weaver, 1989; O'Brien and Slatt, 1990; Bennett *et al.*, 1991; Tyson, 1995; Schieber *et al.*, 1998). Mudstone successions are important as petroleum source rocks, unconventional shale reservoirs and base metal mineral deposits, and hence their study is critical from an academic but also from an economic standpoint (Aplin and Macquaker, 2011).

In the last decades, a growing number of research papers have increased our knowledge on muddy systems. Field and modeling studies have demonstrated gravity-driven, bottom transport of mud across shelves (Sternberg *et al.*, 1996; Ogston *et al.*, 2000; Traykovsky *et al.*, 2000; Wright and Friedrichs, 2006; Hill *et al.*, 2007; Nittrouer *et al.*, 2007), indicating an alternative process to the paradigm of mudstones as products of low-energy, suspension fallout (Schieber *et al.*, 2007). Seminal experimental studies on mud transport revealed that mud can produce ripples composed of floccules, generating structures such as parallel, low-angle or current and wave ripple cross-lamination (Schieber *et al.*, 2007, 2013; Schieber and Southard, 2009; Schieber, 2011; Yawar and Schieber, 2017). Moreover, flume experiments on mixed mud and sand transport provided a framework to understand transitional flows and the role of turbulence modulation by muds (Baas and Best, 2002; Baas *et al.*, 2011, 2016). Since these achievements, the interest in fine-grained depositional systems has been increasing, paralleling the growing importance of unconventional hydrocarbon reservoirs in USA and the need for their characterization by means of sedimentology. Several ancient fine-grained successions have been described in detail, and bottom transport has

been recognized (e.g. Pratt, 1984; Schieber, 1994, 1999a, 2016; O´Brien, 1996; Loucks and Ruppel, 2007; Macquaker *et al.*, 2007; Singh *et al.*, 2008; Varban and Plint, 2008; Bhattacharya and MacEachern, 2009; Ghadeer and Macquaker, 2011; Trabucho-Alexandre *et al.*, 2012; Egenhoff and Fishman, 2013; Frébourg *et al.*, 2013; Leonowicz, 2013; Nyhuis *et al.*, 2014; Wilson and Schieber, 2015; Poyatos-Moré *et al.*, 2016; Birgenheier *et al.*, 2017; Knapp *et al.*, 2017; Newport *et al.*, 2017; Ayranci *et al.*, 2018; Li and Schieber, 2018; Minisini *et al.*, 2018; Boulesteix *et al.*, 2019; Otharán *et al.*, 2020). However, many questions regarding mud sedimentology remain. For instance, the mechanism and origin of bottom current transport are varied, and a facies model is still being developed (Lazar *et al.*, 2015a; Schieber, 2016). For epicontinental seas, Schieber (2016) disregarded storm and sediment-gravity flow processes as likely transport agents redistributing mud on distal locations and hypothesized that mud can be carried away by wind- or tide-driven circulation. Bottom current deposits show extensive traction structures and high bioturbation intensities (Shanmugam *et al.*, 1993a, 1993b; Martín-Chivelet *et al.*, 2003; Stow and Faugères, 2008; Wetzel *et al.*, 2008), and might represent an alternative to interpret low-density flows otherwise described as fine-grained turbidites or tempestites (e.g. Stow and Shanmugam, 1980). Another issue comprises the understanding of organic matter distribution in muddy successions, as some authors have suggested preservation and enrichment by bottom transport mechanisms (Lash, 2016; Otharán *et al.*, 2020). All these innovative ideas contribute to delineate sediment partitioning in fine-grained successions, which have extensive applications in the research area of unconventional shale reservoirs.

Moreover, the ichnological characterization of fine-grained successions needs further development, specially to understand the role of oxygen and substrate on trace fossils. The benthic paleo-oxygenation stress generates burrow size reduction and low bioturbation intensities and depth, resulting in cryptobioturbation by meiofauna to small macrofauna (Savrda and Bottjer, 1989a; Wignall, 1991; Schieber, 2003; Mángano, 2011). Meiofaunal activity in ancient deposits was recorded from faecal pellet production (Löhr and Kennedy, 2015), yet claims of meiofauna burrows in ancient carbonaceous mudstone (black shale) deposits remains dubious (cf. Egenhoff and Fishman, 2013; Schieber, 2014; Schieber *et al.*, in press). The description of "cryptobioturbation" further complicates the delineation of paleo-oxygen levels, because the ability to recognize a cryptic feature depends on the observer (Schieber and Wilson, 2021). In addition to oxygenation, substrate control is substantial, as muds are typically soupy with high

water contents, precluding preservation of discrete trace fossils (Wetzel and Uchman, 1998; Schieber, 2003). Hence, biodeformational structures or indistinct trace fossils occur, preventing proper ichnotaxonomic treatment and creating a growing number of informally named structures and ethologies in the literature (e.g. pyrite burrows, mantle and swirl structures, Navichnia; Schieber, 2003; Li and Schieber, 2018).

In this context, the Vaca Muerta Formation represents an example that provides an opportunity to understand fine-grained depositional environments and paleoecological controls on trace-fossil distribution. This formation occurs in the Neuquén Basin, a triangular-shaped basin located in western central Argentina, showing an Upper Triassic-lower Cenozoic infill. The basin was developed during three different stages: (1) a Late Triassic-Early Jurassic syn-rift stage, generated by an extensional regime associated with NW-SE-elongated half-grabens, (2) an Early Jurassic-Early Cretaceous post-rift stage, characterized by subsidence in the back-arc location and a volcanic arc towards the west, and (3) a Late Cretaceous-early Cenozoic foreland phase, showing a compressional tectonic regime (Howell *et al.*, 2005; Arregui *et al.*, 2011; Casadío and Montagna, 2015). The Vaca Muerta Formation was developed during the post-rift (back-arc) stage, and is considered together with the overlying Picún Leufú and Quintuco formations as a shallow-marine, mixed carbonate-siliciclastic, shelf-margin, subaqueous clinoform system that migrated due to the accumulation of sediments derived from along and across shore sources (Spalletti *et al.*, 1999, 2000; Kietzmann *et al.*, 2008, 2014a, 2016; Leanza *et al.*, 2011; Zeller *et al.*, 2015a; Desjardins *et al.*, 2018; Paz *et al.*, 2019; Minisini *et al.*, 2020a; Otharán *et al.*, 2020). In the eighties, the Vaca Muerta Formation clinoforms were detected from seismic data (Mitchum and Uliana, 1985), and since then, several authors have refined their characterization, with extensive sequence-stratigraphic interpretations (e.g. Massaferro *et al.*, 2014; Reijenstein *et al.*, 2014; Desjardins *et al.*, 2018; Domínguez *et al.*, 2020a), integration of outcrop-based data (Zeller 2013, Zeller *et al.*, 2014; 2015b), and delineation of their organic-rich intervals (Domínguez *et al.*, 2020a). Clinoform-shaped units are encountered in deltas, shelf- or continental-margin locations, and their morphology can be differentiated into topset (upper horizontal strata), foreset (clinoform strata) and bottomset (lower horizontal strata) areas (Gilbert, 1885; Steel and Olsen, 2002; Porębski and Steel, 2003; Helland-Hansen and Hampson, 2009; Patruno *et al.*, 2015). The clinoform framework is useful to assess the nested nature of marine successions, define the locus of sediment deposition, and predict a substantial number of quantitative measures (e.g. Patruno *et al.*, 2015). In the present

study, sedimentary processes and depositional environments have been delineated across the clinoform system. Further research is needed to integrate quantitative measures of the Vaca Muerta clinoforms with sedimentary facies and understand its control in sequence stratigraphy and reservoir characterization.

The Vaca Muerta, Picún Leufú and Quintuco system can be considered as relatively well-studied, as illustrated by the several sedimentological and sequence stratigraphic studies that have been done in the locations analyzed in the present work, both from cores (Fantín and González, 2014; González Tomassini *et al.*, 2014; Pose *et al.*, 2014; Repol *et al.*, 2014; Notta *et al.*, 2017, 2020; Barredo *et al.*, 2018; Desjardins and Aguirre, 2018; Desjardins *et al.*, 2018; Gómez Rivarola and Borgnia 2018; Vallejo *et al.*, 2018; Estrada *et al.*, 2020; Minisini *et al.*, 2020a; Reijenstein *et al.*, 2020) and outcrops (Leanza, 1973; Spalletti *et al.*, 1999, 2000; Freije *et al.*, 2002; Zavala and Freije, 2002; Leanza *et al.*, 2011; Zeller, 2013; Massaferro *et al.*, 2014; Zeller *et al.*, 2014, 2015a; Kietzmann *et al.*, 2016; Ponce *et al.*, 2015, 2016; Krim, 2015; Krim *et al.*, 2017; Capelli *et al.*, 2018; Otharán, 2020; Rodríguez Blanco *et al.*, 2020). These studies are coupled with other geochemical, diagenetic, biostratigraphic and paleontological studies (Leanza and Hugo, 1977; Leanza *et al.*, 1977; Leanza, 1993; Aguirre-Urreta *et al.*, 2014; Catalano *et al.*, 2018; del Rosario Lanz *et al.*, 2021). Regional sequence stratigraphic analyses by Legarreta and Gulisano (1989), Mitchum and Uliana (1985), Leanza *et al.* (2011, 2020a), Kietzmann *et al.* (2014), Desjardins *et al.* (2018), and Domínguez *et al.* (2020a) helped to summarize the information at a basinal scale. In contrast, ichnologic evidence has received less attention. Trace fossils have been mentioned from the study area (Ponce *et al.*, 2015; Kietzmann *et al.*, 2016; Desjardins and Aguirre, 2018), but detailed analysis is only available for the northern Neuquén Basin (Doyle *et al.*, 2005, see also Leanza *et al.*, 2020b). In addition, the topset (shelf) deposits of the Picún Leufú and Quintuco formations are host to abundant trace fossils (Mángano and Buatois, 1991; Olivo *et al.*, 2016; Parada, 2019). Many of the following chapters helped to refine or propose new depositional models and define the ichnological dataset, yet still several areas of study remain poorly studied, such as the correlation of bottomset and topset stratigraphy (e.g. Zeller, 2013) or the quantification of the different sedimentary processes occurring along and across clinoforms.

From an economic standpoint, the Vaca Muerta Formation shows exceptional characteristics for unconventional shale development, with high average TOC levels (5.0% to a maximum of 31%), high thickness of organic-rich units (up to 380 m), moderate depth (2.440 m),

over-pressured conditions, and multiple landing zones compared with other unconventional plays (Fig. 1.1; Boyer *et al.*, 2011; Brisson *et al.*, 2020; Minisini *et al.*, 2020b), constituting an extremely valuable asset for the country. The Vaca Muerta rocks have been mentioned by Charles Darwin in 1835 while in his stop-over from the HMS Beagle voyage in the Paso Piuquenes, Andean Cordillera of Argentina (Aguirre-Urreta and Venari, 2009), and in 1931 the Vaca Muerta Formation was formally added to the literature (Weaver, 1931; Leanza, 2012). Unconventional reservoir exploration started in 2009 by Repsol-YPF, drilling a well in the Loma la Lata-Sierra Barrosa block (Minisini *et al.*, 2020b). However, it was not until 2012 that renewed interest on this unit resulted from the strategic re-acquisition of the ex-public company YPF by the Argentinian government administration of 2007-2015. The new public-private authority utilized the know-how from foreign companies and increased its investments in exploration, expanding production and drilling, and creating jobs in the provinces where they operate (CEPAL, 2015; Bilmes, 2018). It was also under the same government administration when many national universities and the Y-TEC technological centre for hydrocarbon research were opened, generating increasing funding and human resources for research. One of these universities was the Universidad Nacional de Río Negro, where I obtained my undergraduate Geology degree and where a field school on unconventional reservoirs was held on 2015 (Ponce *et al.*, 2015). Another great achievement happened in 2014, when a >300 km-long seismic section displayed in the Argentinian Hydrocarbon Exploration and Development Congress encouraged researchers from industry and academy to publish the "dark book" in 2016 (and its 2018 English edition, González *et al.*, 2018), making available a growing amount of data and cultivating a co-opetition work environment that continues until today. Later, consortiums between industry and academia (e.g. Universidad de Buenos Aires, University of Miami, Colorado School of Mines, University of Texas at Austin) resulted in the recent American Association of Petroleum Geologists Memoir, another astounding contribution that summarizes a multidisciplinary body of data on the Vaca Muerta Formation (Minisini *et al.*, 2020c). Within this context, all the sedimentologic knowledge on this unit can supplement petrophysical, geochemical and geomechanical datasets to drive exploration, determine landing zones, and lower extraction costs (Minisini *et al.*, 2020a).

The previous paragraphs are short summaries of the extremely valuable potential of the Vaca Muerta Formation for academic and industry research, and delineate the importance of this work. The objectives of this study are to:

(1) collect sedimentologic, ichnologic, and sequence stratigraphic data from the Vaca Muerta Formation

(2) analyze these datasets in order to understand sedimentary processes and paleoenvironmental controls on trace-fossil distribution and construct a depositional model.

The hypotheses to be tested are the following:

(1) The Tithonian transgression at the beginning of the deposition of the Vaca Muerta Formation shows similarities to transgressions displaying Holocene-like rates of sea-level rise.

(2) Hyperpycnal flows were instrumental in transporting sediment in basin margin locations.

(3) Weakened estuarine or anti-estuarine basin circulation dominated during specific intervals of time, generating extensive contour current activity at the sea-floor.

(4) Oxygen and substrate consistency represent the main stress factors influencing the benthos as recorded by their trace fossils.

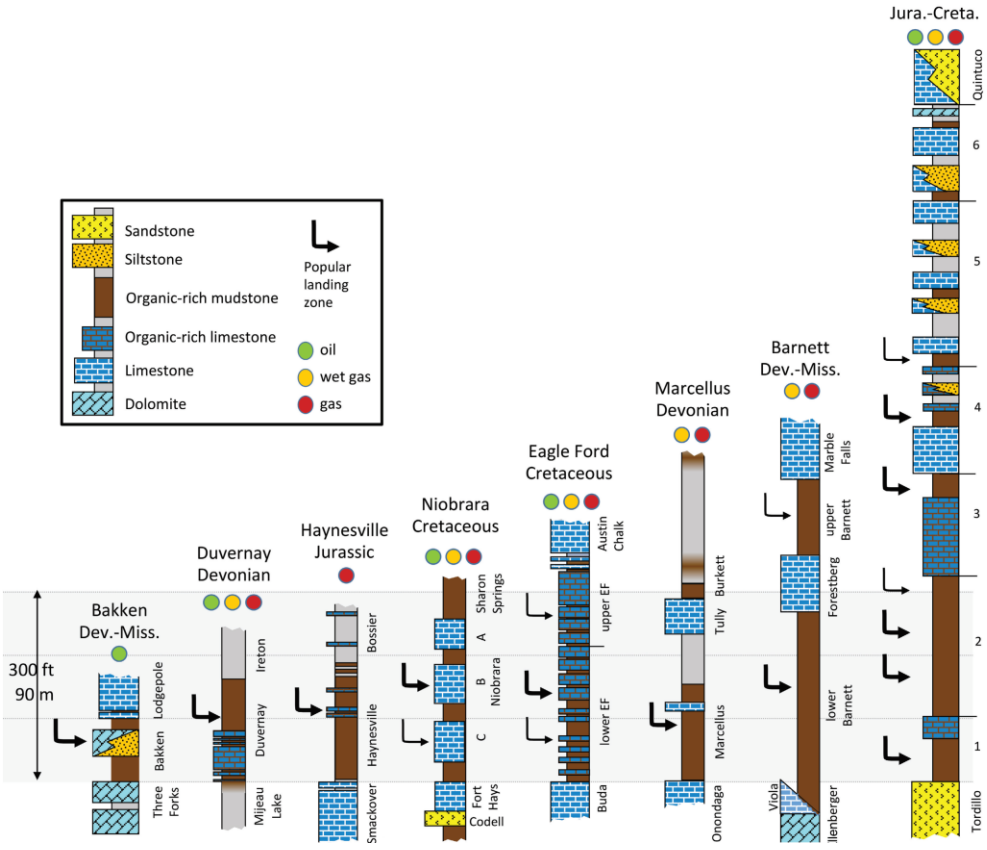

Fig. 1.1. Stratigraphy, thickness, and landing zones of the Vaca Muerta Formation compared with other unconventional plays from North America. From Minisini *et al.* (2020b).

1.1 Thesis structure

In addition to Introduction (Chapter 1) and Conclusions (Chapter 8), the present thesis consists of six chapters. The study area can be subdivided into basin margin (ten sections in the Picún Leufú area outcrops) and basin centre (cores from nine wells from the Embayment area, and one section in Yesera del Tromen outcrop) locations.

The basin margin data was laid down in chapters 2 and 3. Chapter 2 deals in detail with the transgressive event at the beginning of deposition of the Vaca Muerta Formation. For this purpose, the underlying Quebrada del Sapo Formation was studied in addition to the basal Vaca Muerta Formation in order to evaluate the paleoenvironmental changes in the transition from eolian to marine deposits. The finding of marginal marine deposits in the basal, Tithonian transgressive interval of the Vaca Muerta Formation rejected the current paradigm of a catastrophic flooding during that time. Thus, we propose that Holocene-like rates of sea-level changes could have produced the recorded transition. Chapter 3 outlines the sedimentologic, ichnologic, and sequence stratigraphic information of the Vaca Muerta Formation and part of the Picún Leufú Formation, with a special focus on the description of wave-influenced hyperpycnal flows.

The basin centre data was compiled in chapters 4, 5, 6 and 7. Chapter 4 characterizes the sedimentologic and sequence stratigraphic interpretation of the study area, discussing the implications for facies model and sediment partitioning in clinoform systems. Chapter 5 is focused on the ichnologic content of the formation, with a specific analysis on the oxygenation and substrate consistency stresses. Both sedimentologic and ichnologic datasets indicate the presence of contourite deposits in the Vaca Muerta Formation, which were previously described as tempestites, sediment-gravity flows, or tidal deposits. Therefore, chapter 6 describes and discusses the evidence to suggest contour current transport, and propose an origin from a wind- and thermohaline-driven circulation system fed by cascading of dense waters. Chapter 7 defines the trace-fossil content of these contourites and delineates paleoecologic controls on the ichnofauna.

The results revealed the impact of our research for timing of ancient marine transgressions over eolian dunes (Chapter 2), clinoform sedimentary characterization (Chapter 3), clinoform sequence stratigraphy and sediment partitioning (Chapter 4), trace-fossil models in organic-rich,

muddy systems (Chapter 5), differentiation of sediment-gravity flows and bottom current deposits (Chapter 6), and contour current paleoecological controls on trace fossils (Chapter 7).

TRANSITION

Chapter 1 presents an introduction to the importance of the Vaca Muerta Formation, the literature of the study area, and an explanation of the thesis structure. Chapter 2 deals with the transition between the eolian Quebrada del Sapo Formation and the marine Vaca Muerta Formation observed in the basin margin location of the study area. Our sedimentological and ichnological analysis suggests the existence of a marginal marine succession at this transition, rejecting the previous hypothesis of a catastrophic flooding at the onset of deposition of the Vaca Muerta Formation.

CHAPTER 2: THE VACA MUERTA TRANSGRESSION (UPPER JURASSIC), NEUQUÉN BASIN, ARGENTINA: INSIGHTS INTO THE EVOLUTION AND TIMING OF EOLIAN-MARINE TRANSITIONS

Paz, M., Ponce, J.J., Mángano, M.G., Buatois, L.A., Beatriz Carmona, N., Wetzel, A., Pereira, E. and Rodríguez, M.N. (2021). The Vaca Muerta transgression (Upper Jurassic), Neuquén Basin, Argentina: Insights into the evolution and timing of aeolian–marine transitions. *Sedimentology*, doi: 10.1111/sed.12872.

Keywords: Bioturbation, catastrophic flooding, embayment, rapid transgression, transgressive systems tract, Picún Leufú area.

Abstract

Considering the evolution of aeolian to marine transitions for the geological record, either catastrophic or gradual transgressive scenarios showing high or low rates of coastal migration have been proposed. A critical evaluation of modern analogues suggests that a catastrophic transgression shares many characteristics with Holocene transgressions, yet they are caused by different rates of sea-level rise. The present study provides insights into the evolution of eolian to marine transitions in order to discuss different scenarios of sea-level rise. For this purpose, a sedimentological and ichnological analysis was carried out on ten stratigraphic sections of the Picún Leufú area, Argentina. There, marine deposits of the Vaca Muerta Formation accumulated over the eolian deposits of the Quebrada del Sapo Formation during the early Tithonian. The sedimentary evolution of the transition can be summarized in: (i) a shutdown of eolian dune field deposition, generating a planation surface in somewhat elevated areas and reworked megadunes in lowlands; (ii) beach sedimentation caused by episodic marine flooding that contributed to megadune reworking; and (iii) deposition in an embayed marginal-marine setting at the coast, recorded by bay margin bindstone, proximal bay and distal bay sedimentation. This transition indicates very rapid coastline migration and a condensed Transgressive Systems Tract succession throughout the study area. Rates of sea-level rise similar to Holocene ones (millimetres to centimetres per year) may have produced the transition between the Quebrada del Sapo and Vaca

Muerta formations. The Late Jurassic represents a non-glacial time, and the global sea-level maximum highstand pre-dated the Vaca Muerta transgressive event. Thus, part of the sea-level rise has to be attributed to tectonic/thermal subsidence and compaction of underlying strata, which may have generated these atypical rapid rates of sea-level rise.

2.1 Introduction

During transgressions, a relative sea-level rise fosters landward migration of facies and sediment reworking through ravinement erosion, as well as sediment storage within marginal-marine environments and a decrease in sediment transfer towards the basin centre (Swift, 1968; Nummedal & Swift, 1987; Cattaneo & Steel, 2003). Shoreline trajectories can record sediment thickness variations depending on the coastal gradient (Cattaneo & Steel, 2003). While thick successions occur in incised valleys (Belknap & Kraft, 1981), transgressive deposits are thinner, have a lower preservation potential, and represent a telescoped record of sea-level rise in interfluve areas (e.g. Joeckel & Korus, 2012). When a transgression takes place over a dune field, eolian bedforms can be reworked in different ways and stratigraphic hydrocarbon traps form in many cases (e.g. van West, 1972; Vincelette & Chittum, 1981; Moore, 1983; Desmond *et al.*, 1984; Fryberger, 1984). Flooding of dune fields results in an 'inherited', 'reworked' or 'erosional' relief or a planation surface, depending on the amount of reworking (Fryberger, 1986; Eschner & Kocurek, 1988). This is controlled by several factors, such as eolian-dune sand-budget, dune orientation with respect to the coast, prevailing wind direction, marine processes, precipitation and rate of relative sea-level rise (Eschner & Kocurek, 1988).

At present, ancient examples of eolian to marine transitions are explained using either gradual transgressions occurring in the range of Myr and represented by several parasequences showing a retrogradational stacking pattern (Jordan & Mountney, 2012), or invoking catastrophic rates of sea-level rise (metres per day; Garcia-Castellanos *et al.*, 2009) that generates limited transgressive successions (Ahmed Benan & Kocurek, 2000), such as the abrupt flooding of the Mediterranean Sea (Blanc, 2002; Abril & Periáñez, 2016). This study presents an alternative model where a transgression can be constituted by a thin retrogradational succession over an eolian dune field that may have been deposited following Holocene rates of sea-level rise (millimetres to centimetres per year; Hanebuth *et al.* 2000).

The Picún Leufú area in Argentina (Fig. 4.1), offers exceptional outcrops exposing the transgression of the Upper Jurassic–Lower Cretaceous Vaca Muerta Formation over the Kimmeridgian Quebrada del Sapo Formation (lateral equivalent of the Tordillo Formation). The aims of this study are to: (i) describe and interpret the sedimentary facies of the transgressive succession of the Vaca Muerta Formation; (ii) decipher the processes and factors that affected its development; (iii) critically evaluate previous hypotheses about flooding of modern and ancient eolian dune fields; and (iv) discuss a classification scheme comprising gradual, rapid and catastrophic transgressions over eolian successions. A further facies characterization of the Vaca Muerta Formation in the Picún Leúfu area is provided in Chapter 3.

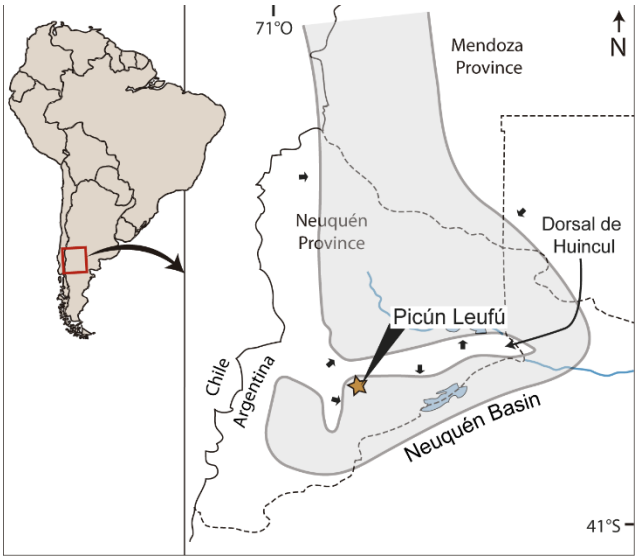

Fig. 2.1: Location of the study area. Left – South America, red frame represents detailed map shown tothe right. Right – Study area marked by orange asterisk in the Kimmeridgian palaeogeographic reconstruction of the Neuquén Basin (grey shaded). Black arrows show sediment source areas. Modified from Vergani *et al.* (1995).

2.2 Geological setting

The Neuquén Basin is located in western-central Argentina, bounded by cratonic areas at its north-east and south-east margins, and by the Andean magmatic arc to the west (Fig. 2.1). The basin contains about 7000 m thick sediments deposited from Late Triassic–Early Jurassic to Cretaceous times (Fig. 2.2; Arregui *et al.*, 2011). The development of the basin is commonly subdivided into

three major stages according to the tectonic setting, namely syn-rift, back-arc (post-rift) and foreland stage (Howell *et al.*, 2005). Upper Triassic–Lower Jurassic volcaniclastic and siliciclastic continental deposits constitute the syn-rift stage, grouped into the Precuyano Cycle (Gulisano, 1981; Carbone *et al.*, 2011). During the Early Jurassic, a magmatic arc formed along the western margin of Gondwana and a back-arc basin developed within the continent due to the onset of subduction (Mpodozis & Ramos, 2008). Since this time and until the Early Cretaceous, marine and continental sedimentation alternated in response to sea-level fluctuations, subsidence and deposition, as recorded by the Cuyo, Lotena and Mendoza groups. During the Late Cretaceous, a compressional tectonic regime led to the closure of the connection with the Pacific Ocean, and the Neuquén Basin entered a foreland basin stage (Ramos & Folguera, 2005; Tunik *et al.*, 2010).

The Vaca Muerta Formation comprises upper lower Tithonian to lower Valanginian marine deposits of the Mendoza Group (Stipanicic *et al.*, 1968). The Vaca Muerta Formation belongs to the Lower Mendoza Mesosequence (Fig. 2.2; Legarreta & Gulisano, 1989), a sequence-stratigraphic entity bound at the base and top by the intra-Upper-Jurassic and the intra-Valanginian unconformity, respectively. This mesosequence starts with the continental deposits of the Tordillo Formation and their lateral equivalents (for example, Quebrada del Sapo Formation), which are covered by marine deposits of the Vaca Muerta Formation. The transgression approached from the Pacific Ocean due to a relative sea-level rise (Leanza *et al.*, 2011). At the top, the Vaca Muerta Formation shows a transitional and diachronous contact with the overlaying nearshore deposits of the Quintuco Formation and its lateral equivalents (Legarreta & Gulisano, 1989). The Vaca Muerta Formation is composed of mudstone, marl and limestone that are commonly referred to as black shales due to their high organic matter content [on average 3–8% total organic carbon (TOC) and peak values of 10–12%; Uliana *et al.*, 1999].

The transgression of the Upper Jurassic–Lower Cretaceous marine Vaca Muerta Formation over the Upper Jurassic continental Tordillo Formation constitutes an excellent example of an eolian–marine transition that has been recurrently studied (Mutti *et al*., 1994; Boll & Valencio, 1996; Cevallos, 2005; Borbolla *et al*., 2014; Ponce *et al.*, 2015; 2016). Contrasting hypotheses concerning the transgression were proposed. Originally, the shift from the Tordillo to the Vaca Muerta formations was seen as transitional, resulting in a conformable contact (e.g. Leanza *et al*., 1977; Zanettini, 1979). Later, Mutti *et al.* (1994) and Legarreta (2001, 2002) emphasized the abrupt shift from continental Lowstand Systems Tract (LST) dune facies to marine conditions

during the Transgressive Systems Tract (TST). Consequently, the transition from the Tordillo to the Vaca Muerta formations was suggested to represent a Jurassic equivalent to the catastrophic flooding of the Mediterranean Sea during Zanclean times at the end of the Messinian Salinity Crisis (Mutti *et al.*, 1994). In contrast, based on seismic, well log and outcrop information, Boll & Valencio (1996) proposed a transgression characterized by a basal transgressive deposit above an erosive unconformity that truncates the Tordillo Formation. Later, Cevallos (2005) recognized a partly inherited to partly reworked eolian megadune's relief in plan-view seismic records on top of the Catriel Formation (lateral equivalent of the Tordillo Formation), and argued in favour of a catastrophic transgression. In this case, the transgression was seen in terms of its timing to represent an equivalent to the Holocene flooding of the Black Sea (Ryan & Pitman, 1998). Since then, a catastrophic flooding has been the widely accepted hypothesis for the transgression of the Vaca Muerta Formation (Leanza *et al.*, 2011).

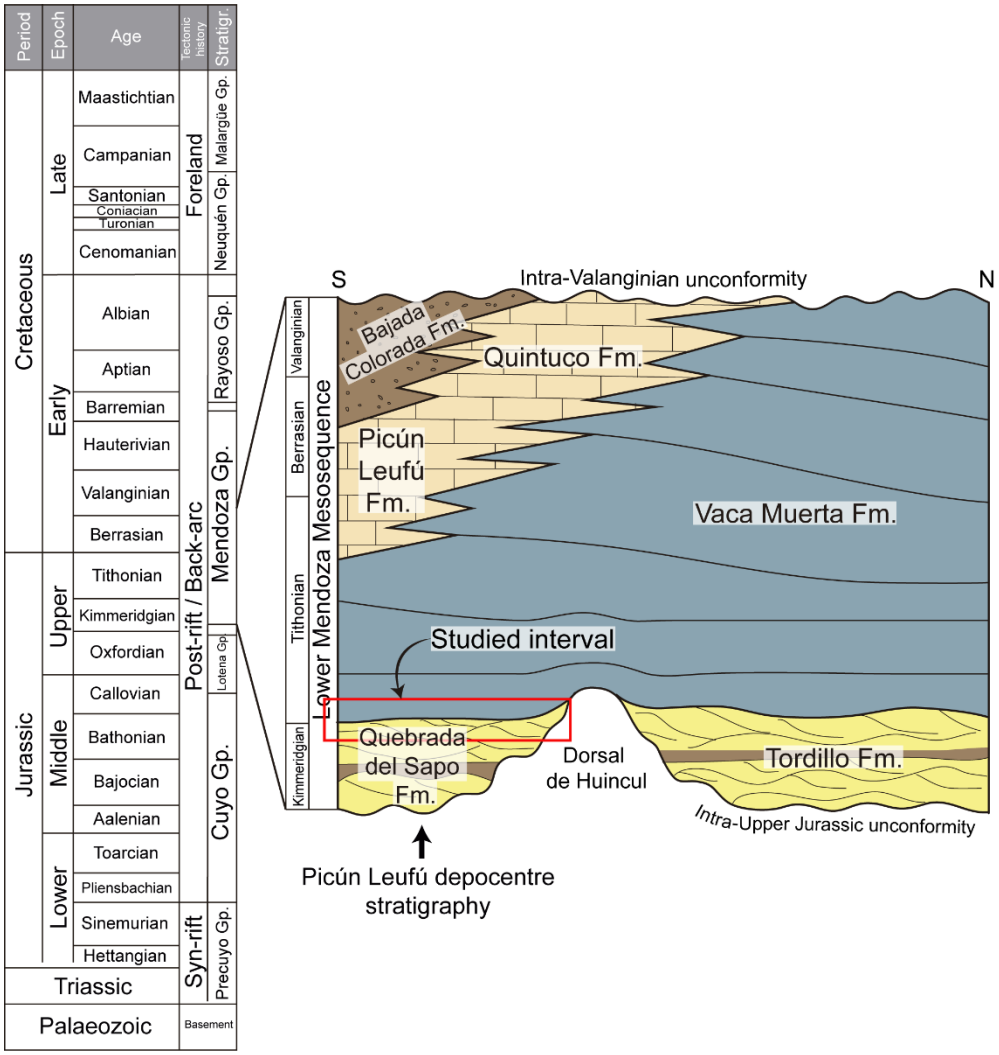

Fig. 2.2: Stratigraphy of the Neuquén Basin, fourth column from the left indicates tectonic stages of the Neuquén Basin. To the right a south–north section of the Lower Mendoza Mesosequence in the Picún Leufú area, traversing the Dorsal de Huincul (modified from Howell *et al.*, 2005); the studied interval is marked by a red frame.

2.2.1 Picún Leufú anticline and Quebrada del Sapo domain

The study area is located near the intersection between the Picún Leufú creek and National Route 40. It comprises the north-western part of the Picún Leufú depocentre and the westernmost edge of the Dorsal de Huincul ridge system (Fig. 2.1), in particular, the south-verging, east–west trending Picún Leufú anticline. The study area can be differentiated in the Picún Leufú domain

(PL, sections 1 to 4) and an area associated with a NNE-oriented ravine, known as Quebrada del Sapo (QdS, sections 5 to 10, Fig. 2.3, Appendix A).

In the study area, the Lower Mendoza Mesosequence is represented by the Quebrada del Sapo, Vaca Muerta and Picún Leufú formations (Fig. 2.2). The Quebrada del Sapo Formation (Parker, 1965; Digregorio, 1972) is Kimmeridgian in age as evidenced by lithostratigraphic correlation with the Tordillo Formation (Veiga & Spalletti, 2007). However, a supposed unconformity between both units may indicate a slightly younger age for the Quebrada del Sapo Formation (Zavala *et al.*, 2008). The latter is composed of conglomerate, sandstone and mudstone deposited in fluvio-lacustrine, fluvial and eolian settings (Zavala *et al.*, 2005; Spalletti & Veiga, 2007; Veiga & Spalletti, 2007). The eolian facies covers an extensive area and, hence, it was interpreted as recording a dune field (Zavala *et al.*, 2005). A sharp to erosive surface separates the Vaca Muerta Formation above from the Quebrada del Sapo Formation below (see Ponce *et al.*, 2015, 2016, for details).

The Vaca Muerta Formation comprises up to *ca* 350 m of marine siliciclastic and carbonate deposits in the study area. At the top, the Picún Leufú Formation overlays the Vaca Muerta Formation by a gradational contact. The latter formation consists of shallow-marine sandstone, mudstone and limestone, reflecting an overall upward increase in carbonate content. Correlation based on ammonite biostratigraphy shows an early Tithonian to early Berrasian age for both formations (Leanza & Hugo, 1977). Several sedimentological and sequence stratigraphic studies agree that the Vaca Muerta and Picún Leufú formations record a mixed carbonate–siliciclastic system (Leanza, 1973; Spalletti *et al.*, 2000; Freije *et al.*, 2002; Zavala & Freije, 2002; Zeller, 2013; Zeller *et al.* 2015a; Krim *et al.*, 2017, 2019; Paz *et al.*, 2019). In this area, most of these sedimentological studies have dealt with the basal TST and envisaged a catastrophic transgression, yet they did not address the transgressive deposits from an integrated sedimentological and ichnological perspective.

Early Jurassic to Early Cretaceous syn-sedimentary tectonics in the Dorsal de Huincul area played a major role for the development and configuration of facies and sediment source areas. Stratal geometry and associated unconformities of the Picún Leufú anticline record successive pulses of growth (Freije *et al.*, 2002; Zavala & Freije, 2002; Naipauer *et al.*, 2012). During the Kimmeridgian to middle Tithonian (lower *A. proximus* ammonite zone of Parent *et al.*, 2011), syn-sedimentary deformation affected the Lower Mendoza Mesosequence in the anticline, whereas in

the QdS domain the strata are almost undeformed. Tectonic movements caused progressive development of unconformities and normal faults within the Mendoza Mesosequence. An upward gradually decreasing dip of the Quebrada del Sapo Formation and the lowermost *ca* 100 m of the Vaca Muerta Formation record waning deformation that ends with subhorizontal strata of the middle and upper Vaca Muerta and Picún Leufú formations. The progressive unconformities are represented by a change in dip between the Lotena and Quebrada del Sapo formations (30°), the fluvial and eolian unit of the Quebrada del Sapo Formation (9°), the Quebrada del Sapo and Vaca Muerta formations (2–17°), and above the first 80 to 120 m of the Vaca Muerta Formation (10–23°). Syn-sedimentary normal faults cross-cut the uppermost part of the Quebrada del Sapo Formation dune deposits and up to *ca* 50 m of the lowermost Vaca Muerta Formation. A post-depositional deformational episode generated an additional *ca* 30° tilt of the whole succession, showing its maximum to the east of the anticline and a decrease towards the west (QdS).

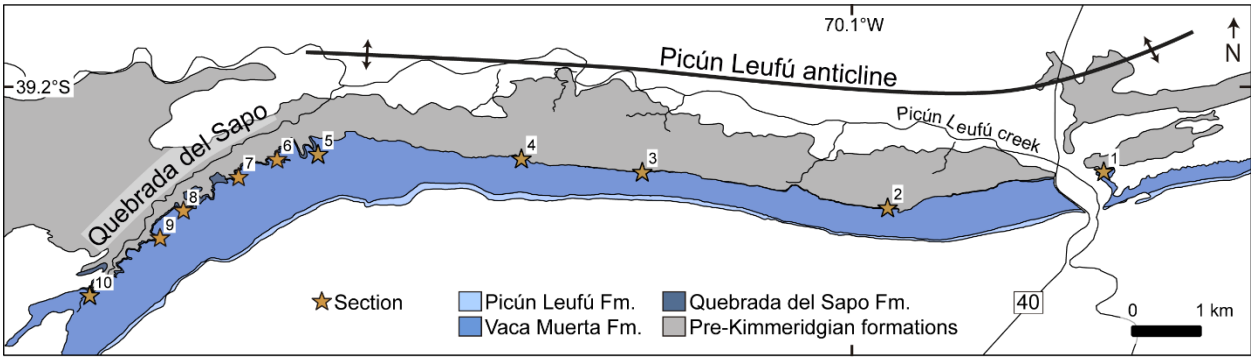

Fig. 2.3: Map of the study area showing the location of sections.

2.3 Methods

The Picún Leufú area shows exceptional outcrops of the Quebrada del Sapo and Vaca Muerta formations, 12 km long in the east–west direction at PL and 5.5 km long in the north-east/south-west direction at QdS, that were suitable for logging sedimentary sections. The main analysis is focused on the eolian-marine transition represented by the uppermost 0.5 to 2.0 m of the Quebrada del Sapo Formation and the lowermost 3 to 25 m of the Vaca Muerta Formation. Dip angle and azimuth were measured with a clinometer and compass to assess the tectonic deformation of the succession. A short description of the Quebrada del Sapo Formation continental deposits is provided, in order to unravel the pre-flooding topography and determine its associated sedimentary

environments based on previous studies in the area (Zavala *et al.*, 2005; Spalletti & Veiga, 2007; Veiga & Spalletti, 2007). In contrast, the Vaca Muerta Formation facies are numbered because of a higher detail of analysis.

Sedimentological and ichnological analyses of the top of the Quebrada del Sapo Formation and the Vaca Muerta Formation transgressive succession were carried out while logging ten sections on a bed by bed scale (Fig. 2.3, Appendix A), four sections in PL and six sections in QdS. The lithology, sedimentary structures, trace fossil and body fossil content of each facies have been recorded. Lithofacies classification was used as a descriptive term to subdivide rocks showing different sedimentological aspects within a facies. Facies comprises sedimentary features and related processes in a specific subenvironment of deposition. Facies association was used to describe a group of facies occurring in a depositional environment. Petrological observations were made on thin sections of seven samples from the Vaca Muerta Formation. The ichnological analyses comprise the description of ichnotaxa and estimation of the degree of bioturbation that is expressed as bioturbation index (BI) as proposed by Taylor & Goldring (1993), ranging from unbioturbated (BI = 0) to completely bioturbated (BI = 6). Mudstones are classified following Lazar *et al.* (2015b). The sequence stratigraphic interpretation was based on facies stacking pattern and interpretation of stratigraphic surfaces, following the nomenclature of Catuneanu (2006).

2.4 Sedimentary facies

2.4.1 Quebrada del Sapo Formation: Fluvial facies association

2.4.1.1 Sandy conglomerate and pebbly sandstone facies

Description. This facies consists of thin to thick-bedded, clast or matrix-supported sandy conglomerate, pebbly sandstone, and medium to coarse-grained sandstone (Fig. 2.4). The conglomerate and sandstone display normal grading, trough cross-bedding, low-angle cross-bedding, horizontal bedding and subordinate current ripples in the sandstone. The conglomerate is polymictic and consists of rounded cobbles to granules of predominantly volcanic and plutonic origin. The gravelly sandstone is medium to coarse-grained with a minor content of cobbles and pebbles. The conglomerate occurs in lenticular-shaped, amalgamated, 10 to 50 cm thick, stacked packages that commonly have a slightly convex, erosive base. Sandstone beds are 20 to 100 cm

thick and commonly encase conglomerate. The complete facies forms 3 to 21 m thick intervals, and rests on red mudstone facies or trough cross-stratified sandstone facies (see below).

Interpretation. The trough cross-bedded deposits were formed by migration of three-dimensional dunes, whereas the low-angle cross-bedded and horizontal-bedded deposits represent migration of low-relief sediment waves (Paola *et al.*, 1989). The stacking of conglomerate within lenticular-shaped bodies suggests bedform migration in fluvial channels, constituting channel-bar deposits. Zavala *et al.* (2005) interpreted these facies as dense flows of fluvial origin. Veiga & Spalletti (2007) differentiated between lenticular bodies representing the accumulation of in-channel and marginal bars and minor channel fills, and sheet-like geometries comprising short-lived, high-energy sheetfloods.

Fig. 2.4: Facies of the Quebrada del Sapo Formation. (A) Panoramic view close to section 7 showing the fluvial and eolian facies association (Fluvial FA and Eolian FA) and the overlying Vaca Muerta Formation. (B) Fluvial facies association in outcrop showing trough cross-bedded conglomerates overlain by red and green lacustrine mudstone. (C) Large-scale trough cross-bedded sandstone of the eolian facies association (people for scale are *ca* 1.7 m tall).

2.4.1.2 Red to green mudstone facies

Description. This facies is represented by 1 to 15 m thick successions of red to green massive mudstone. The facies is interbedded with sandy conglomerate and pebbly sandstone facies.

Interpretation. In the study area, these fine-grained deposits associated with sandstone and conglomerate facies were interpreted as lacustrine because of lacking evidence for subaerial exposure (Zavala *et al.*, 2005), or as deposited on an ephemerally flooded mudplain due to their association with fluvial facies (Veiga & Spalletti, 2007). The latter authors suggested that the massive appearance of the mudstone can be related to bioturbation and incipient pedogenesis (Veiga & Spalletti, 2007).

2.4.1.3 Matrix-supported pebble to cobble conglomerate facies

Description. This facies comprises 5 to 10 cm thick, matrix-supported, structureless pebble to cobble conglomerate. It occurs locally at the top of sandy conglomerate facies, towards the transition to the Vaca Muerta Formation.

Interpretation. This facies represents fluvial deposits modified by erosive processes. The formation of thin beds of massive conglomerate in close proximity to eolian deposits is likely related to deflation processes. Deflation surfaces were also described in the study area at the transition from fluvial to eolian units (Zavala *et al.*, 2005; Veiga & Spalletti, 2007).

2.4.2 Quebrada del Sapo Formation: Eolian facies association

2.4.2.1 Trough to planar cross-stratified sandstone facies

Description. This facies consists of trough or planar cross-stratified, well-sorted, fine to coarse-grained sandstone (Fig. 2.4C). Inversely graded intervals occur within the foresets, having a thickness of 0.5 to 5.0 cm. Foresets can dip as steep as 32°. The cross-stratified sandstone occurs in medium (10–30 cm) to very thick (1–2 m) beds, showing internal reactivation surfaces. Palaeocurrent indicators are directed mostly towards the north-east and subordinately towards the north and east (N = 10). Locally, parallel-crested, low-amplitude ripples having a high ripple index (length/height of 20–25) are present. Towards the top, near the contact with the Vaca Muerta Formation, a 1 to 2 m thick sandstone interval shows convolute bedding and water-escape structures. Abundant, 1 mm wide pyrite cubes replaced by iron oxides and 5 to 10 cm wide carbonate concretions are present. This facies shows a thickness of 3 to 28 m.

Interpretation. Steep foresets, very good sorting, and low-amplitude ripples characterize an eolian setting. Although palaeocurrent data is limited, its low dispersion suggests that the sandstone

succession possibly resulted from migration of barchanoid or transverse eolian dunes (see also Zavala *et al.*, 2005; Veiga & Spalletti, 2007). Previous studies in the area have recognized third-order (reactivation), second-order (superimposition) and first-order (interdune) surfaces, indicating the development of composite draas formed by dunes (Zavala *et al.*, 2005; Veiga & Spalletti, 2007). Liquefaction towards the top of the succession resulted from the collapse of water-saturated sands experiencing mechanical loading during a water-table rise associated with marine flooding (*e.g.* Collinson, 1994).

2.4.3 Vaca Muerta Formation: Marginal-marine and shallow-marine facies association

2.4.3.1 Facies 1 (F1): Low-angle cross-bedded to horizontal-bedded sandstone

Description. This facies can be subdivided into two lithofacies. Lithofacies 1a (F1a) consists of sharp to erosive-based, thin to medium-bedded (3–20 cm-thick), low-angle cross-bedded to horizontal-bedded, medium-grained with minor fine-grained sandstone (Figs 2.5A and 2.6). Asymmetrical and symmetrical ripples displaying a low index (length/height of 10–15) are common on bedding planes (Fig. 2.5B). The low-angle cross-bedding shows variable dips, but predominant slopes are towards ESE and WSW, and subordinately towards the north and north-east (N = 6), whereas current-ripple foresets dip towards the south and WNW (N = 4, palaeocurrent data in Fig. 2.7B). Lithofacies 1b (F1b) comprises 10 to 30 cm-thick, erosive to sharp-based, trough cross-stratified, medium-grained to minor coarse-grained sandstone (Fig. 2.5D). This lithofacies is locally observed at the base of or interbedded within F1a. In places, the sandstone exhibits organic matter drapes. Both lithofacies locally display water-escape structures and syn-sedimentary faults. The water-escape structures constitute 1 to 3 m of deformed strata that occur isolated or laterally associated with the low-angle cross-bedded sandstone (Fig. 2.5C). The synsedimentary normal faults exhibit displacements of centimetres to a few metres and associated drag folds, and they commonly cross-cut this facies and the underlying eolian deposits of the Quebrada del Sapo Formation (Fig. 2.5D). F1a shows a tabular to subtle lenticular geometry that laterally grades into F1b (Fig. 2.6). At a large-scale, F1 displays a tabular geometry and thickness variations of 0.5 to 2.0 m.

Interpretation. Facies 1 documents episodic marine flooding and reworking of the Quebrada del Sapo Formation eolian dune deposits in a beach area (for example, ‘Laminated and Cross-bedded

Sandstone facies' of Blakey *et al.*, 1983; or 'Planar-Bedded Sandstone lithofacies' of Desmond *et al.*, 1984). The subaqueous reworking is similar to wet interdune facies (Ahlbrandt & Fryberger, 1981; Kocurek, 1981), yet adjacent dunes are not preserved. F1a suggests low-relief bedforms that were later reworked into ripple surfaces by repeated flooding (*e.g.* Fryberger *et al.*, 1990). The lithofacies does not show bimodal sorting or inverse grading, precluding the hypothesis of eolian climbing translatent strata. The low-index current ripples are typically produced in rather shallow centimetre-deep water (Tanner, 1967), whereas the symmetrical ripples indicate wave reworking. The water-escape structures suggest soft-sediment deformation of water-saturated sands. Lagoons adjacent to dune fields can expand over interdune areas during high water level and generate shallow-water, wind-induced wave reworking (Inman *et al.*, 1966; Shinn, 1973). These parts of the eolian dune field show an enhanced preservation potential due to their position below the water table (Hummel & Kocurek, 1984). F1b may record the formation of small subaqueous dunes generated during marine flooding and scouring of beach deposits (Kocurek, 1981). Subaqueous tractive processes reworking the previous eolian deposits generated segregation of the coarser grains into these bedforms. The organic matter drapes probably represent material reworked from the adjacent coastal areas (for example, F2). In modern settings, thin, cross-bedded and ripple cross-laminated sandstone beds having an erosional base and showing water-escape structures are typical of subaqueous marine reworking (Fryberger *et al.*, 1988). The erosive, irregular stratal contacts imply sand stabilization by damp conditions and later erosion during marine flooding. Synsedimentary normal faults cross-cutting F1 and the underlying Quebrada del Sapo Formation dune deposits suggest tectonic extension at the time of deposition.

2.4.3.2 Facies 2 (F2): Bindstone

Description. This facies comprises 5 to 30 cm thick bindstone beds (Figs 2.5D and 2.8A). Macroscopically, the bindstone displays dark, millimetre-thick, parallel to irregular, planar to wrinkle lamination. In thin section, the bindstone shows alternating wavy to lenticular, sand-rich and organic-rich laminae (Fig. 2.8B). The organic-rich laminae contain sand grains displaying a preferential orientation of their long axes parallel to lamination (Fig. 2.8B). Pyrite crystals occur abundantly aligned sub-parallel to stratification. The organic carbon content of the bindstone can reach 20% C_{org} (N = 2). Indistinct ammonite moulds and bivalve shells occur scattered in the bindstone.

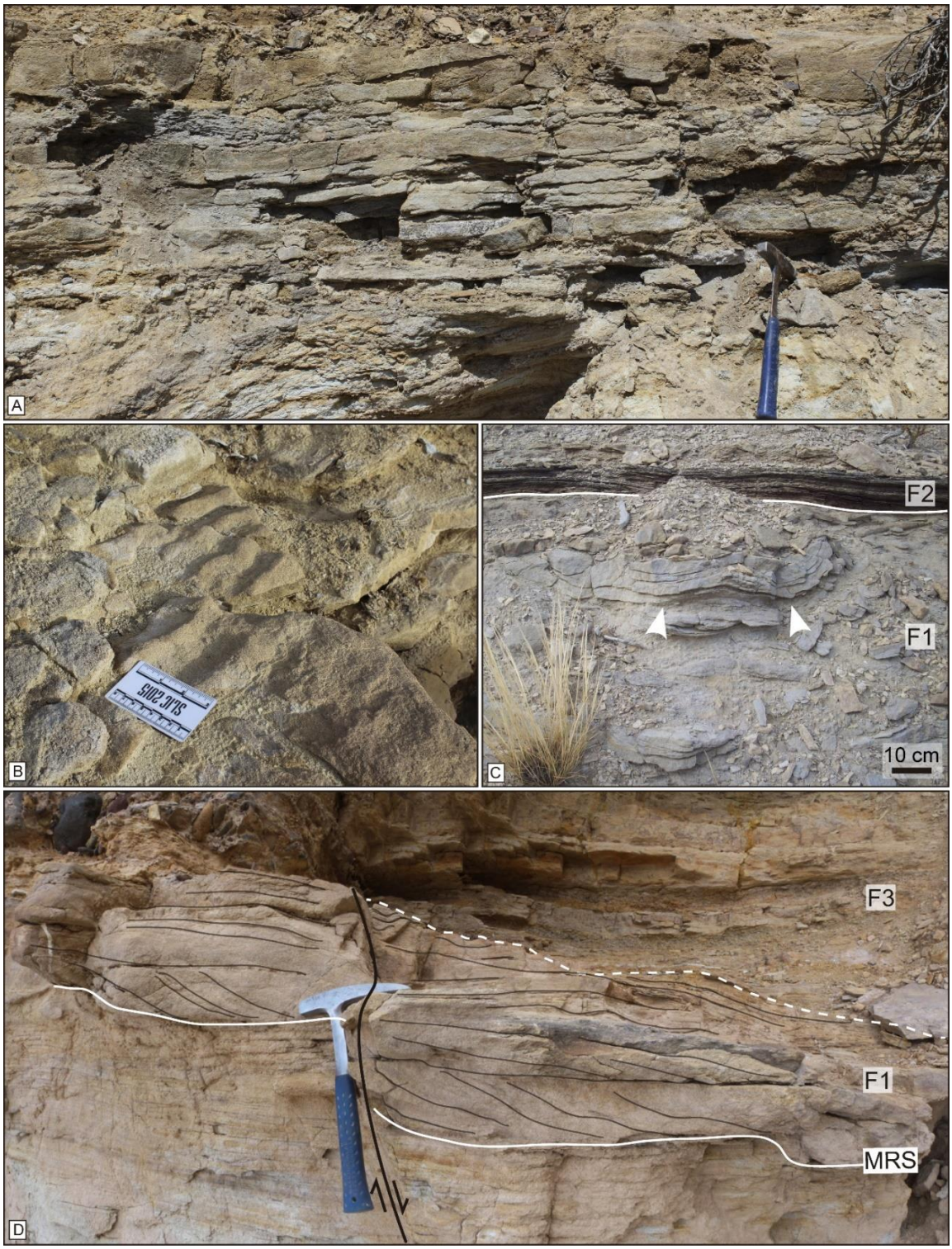

Fig. 2.5: Facies F1 of the Vaca Muerta Formation. (A) and (B) Low-angle cross-bedded sandstone overprinted by current ripples on bedding planes. (C) Water-escape structures in F1 (arrow), overlain by bindstone of F2. (D) Trough cross-bedded sandstone of F1 erosively overlying the eolian facies association

of the Quebrada del Sapo Formation. The contact represents a maximum regressive surface (MRS) cross-cut by a syn-sedimentary normal fault and overlain by facies F3 (hammer for scale is *ca* 30 cm long).

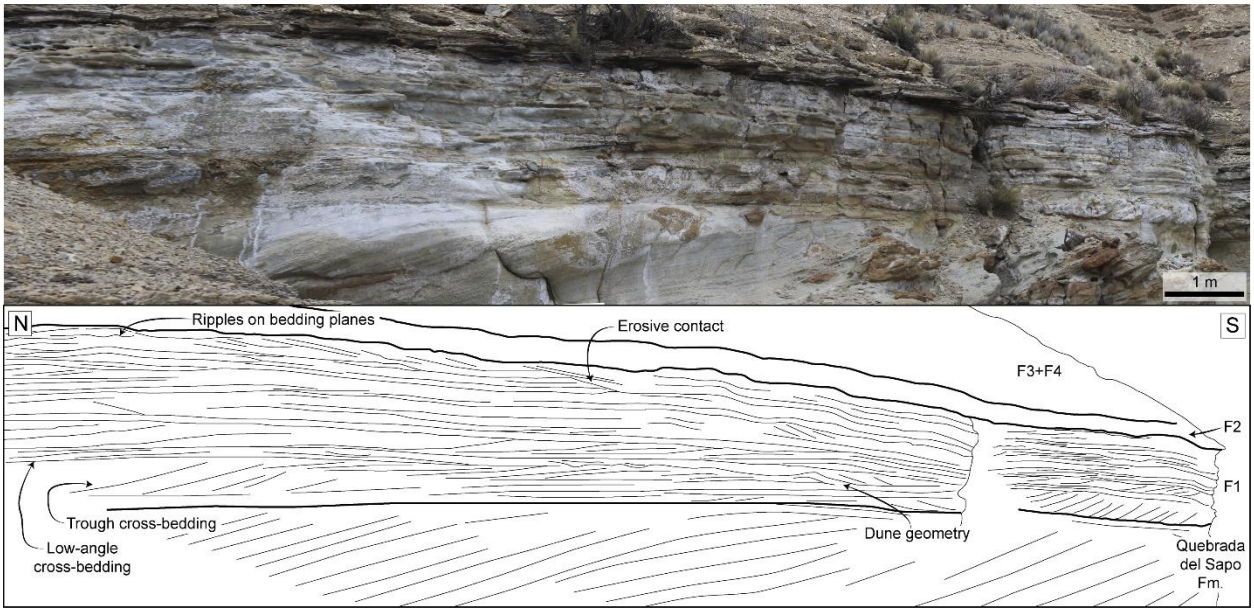

Fig. 2.6: Bedding planes and characteristics of F1. This facies sharply rests on the eolian sandstone succession of the Quebrada del Sapo Formation, and it is covered by F2, F3 and F4.

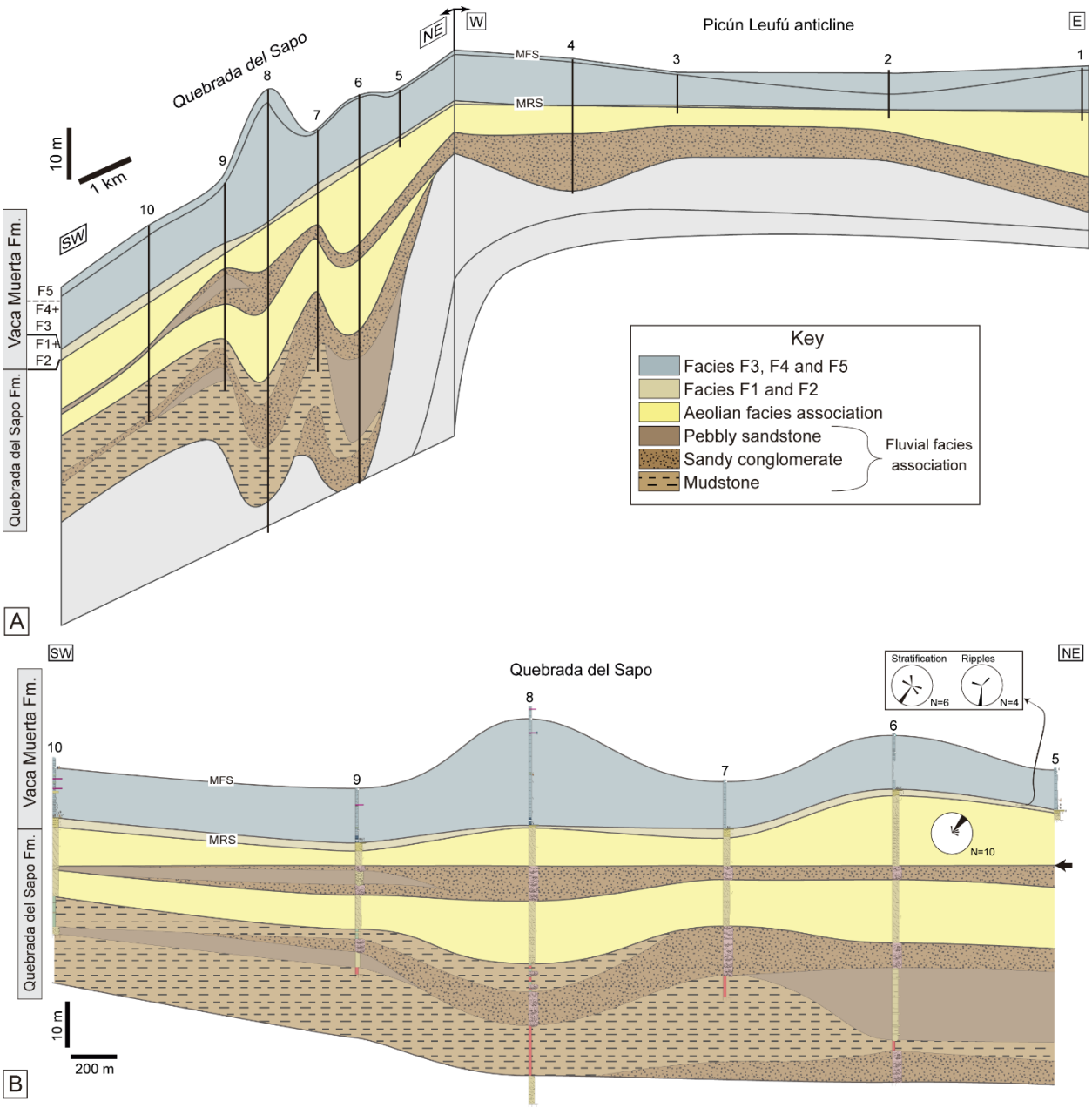

Fig. 2.7: Stratigraphic correlation of sections in the Picún Leufú domain (PL) and Quebrada del Sapo (QdS). (A) General correlation of the study area. (B) Stratigraphic correlation in the QdS, with the base of the last eolian succession of the Quebrada del Sapo Formation drawn as horizontal reference level (arrow). Note thickness changes in the eolian interval and the overlying TST succession.

Interpretation. Facies 2 resulted from vertical accretion of microbial mats in a bay-margin area associated with an open-bay depositional environment (see below). The wavy to lenticular laminae are very similar to the wavy-crinkly laminated structure typical of microbial mats (Schieber, 1986,

2007). In addition, oriented grains and layered pyrite indicate microbial activity (Noffke, 2010). Similar microbial mats thrive in protected, transitional areas at the coast of the Guerrero Negro area, Mexico, yet they are related with hypersaline environments (Fryberger *et al.*, 1990).

Fig. 2.8: Bindstone of F2 (dark interval). (A) Outcrop, F2 overlying F1 (sandy interval at the base). Hammer for scale is *ca* 30 cm long. (B) Thin section of the bindstone showing alternating sand-rich and organic matter-rich laminae and oriented sand grains. Scale is 1 mm.

2.4.3.3 Facies 3 (F3): Mudstone with interbedded sandstone layers, bioclastic wackestone and packstone

Description. This facies consists of cycles of thin-bedded (1–10 cm), carbonaceous–calcareous medium mudstone, bioclastic wackestone and packstone (Fig. 2.9A and B). Thin, gradational-based, medium to coarse-grained, calcareous sandstone occurs in PL (Fig. 2.9C), while 1 to 5 cm thick, muddy heterolithic beds are present in section 1. Symmetrical ripples occur locally in the bioclastic wackestone and medium to coarse-grained sandstone (Fig. 2.9B). The TOC content shows values of 2% and 17% (N = 2). In the medium mudstone, carbonate locally occurs as fine-grained mineral clusters in between millimetre-thick laminae of kerogen seams, whereas in the calcareous sandstone it is observed as matrix and cement. In the wackestone and packstone, debris and shells of bivalves, ammonites and gastropods are present. Well-preserved to fragmented bivalve (2–4 cm wide) and ammonite (5–20 cm wide) shells occur loosely packed (5–25%; Fig. 2.9D). Locally, ammonite shells have bivalves attached. These ammonite-rich and bivalve-rich beds are observed in all sections. In contrast, a monospecific gastropod fauna was only encountered in the QdS (sections 5 to 10). It comprises well-preserved, 2 to 5 mm long and 1 to 2

mm wide shells (Fig. 2.9E), and highly fragmented shell debris, 0.1 to 0.5 mm in size. The gastropods occur in 1 to 5 cm thick beds randomly or concordant to stratification, sparsely dispersed (2–5%) or loosely packed (10–15%). Bioturbation is recorded by poorly defined biodeformational structures, *Teichichnus rectus* (Fig. 2.9A) and *Thalassinoides* isp. A. Deposits containing biodeformational structures are moderately to intensely bioturbated (BI = 4–5), whereas those with discrete burrows tend to be slightly less bioturbated (BI = 3–4). A second generation of low density (BI = 1) *Thalassinoides*, referred to as *Thalassinoides* isp. B, cross-cuts all other trace fossils, has sharp, unlined walls, and is passively filled by medium to coarse-grained sand (Fig. 2.9E and F). Laterally, F3 varies from 1 m to *ca* 2 m in thickness.

Interpretation. Facies 3 formed at a proximal bay location. The symmetrical ripples suggest oscillatory flow reworking associated with fair-weather or storm wave action. The shell accumulations may indicate low sedimentation rates because low-energy winnowing of fines occurred during the transgression (Kidwell & Aigner, 1985). The sand grains of the calcareous sandstone were probably delivered by wind from the adjacent eolian dunes or beach deposits (F1). The muddy heterolithic deposits are interpreted to have accumulated in a protected low-energy environment, where suspended particles settled down to the seafloor during tranquil periods. The millimetre-thick kerogen laminae and the high TOC content are typical of microbial mats that stabilized the substrate (Carmona *et al.*, 2011, 2012). Gastropods are similar to the cerithioid gastropods analyzed by Gründel & Parent (2001, 2006). The good preservation of some cerithioid gastropods and the absence of erosive surfaces below the shell beds imply their autochthony, whereas randomly disposed shells suggest minor reworking and parautochthony. The shell debris was probably delivered from higher-energy areas. Cerithioid gastropods have been reported from nearshore, mud-rich environments offshore southern Vietnam (Szczuciński *et al.*, 2013), from tidal flats in South Thailand (Waite & Strasser, 2011), and in the Bay of Bengal where they occur in high abundance and produce grazing trails (De, 2000). In addition, such gastropods are also associated with microbial mats thriving in the moist supratidal depressions (De, 2019). However, cerithioid gastropods, such as those belonging to the Turritellidae family, show a wide bathymetric range and can tolerate a broad range of salinity and temperature (Allmon, 1988). During microbial mat growth, the substrate below dewatered and became firm and, thus, suitable for exploitation by *Thalassinoides* producers that cross-cut the biodeformational structures. The sharp, unlined walls and the passive, allochthonous infill of *Thalassinoides* are diagnostic of the *Glossifungites*

Ichnofacies, and indicate firmground conditions (Pemberton & Frey, 1985; MacEachern *et al.*, 1992). The coarse-grained sandstone infilling burrows probably originated from sand-rich flows that bypassed the area. These flows deposited their load in the distal-bay areas where sandstone beds are preserved (F4, see below). The absence of proximal, storm-generated shoreface or foreshore deposits, such as cross-bedded, parallel-laminated, or hummocky cross-stratified sandstone, supports the above interpretation. Therefore, a low-energy, protected coast is suggested, and pronounced lateral thickness changes imply sedimentation rates varying along an irregular-shaped shoreline. An open-bay setting is more plausible than an estuarine environment because incised valley fill or flooded fluvial channel deposits are absent (MacEachern & Gingras, 2007).

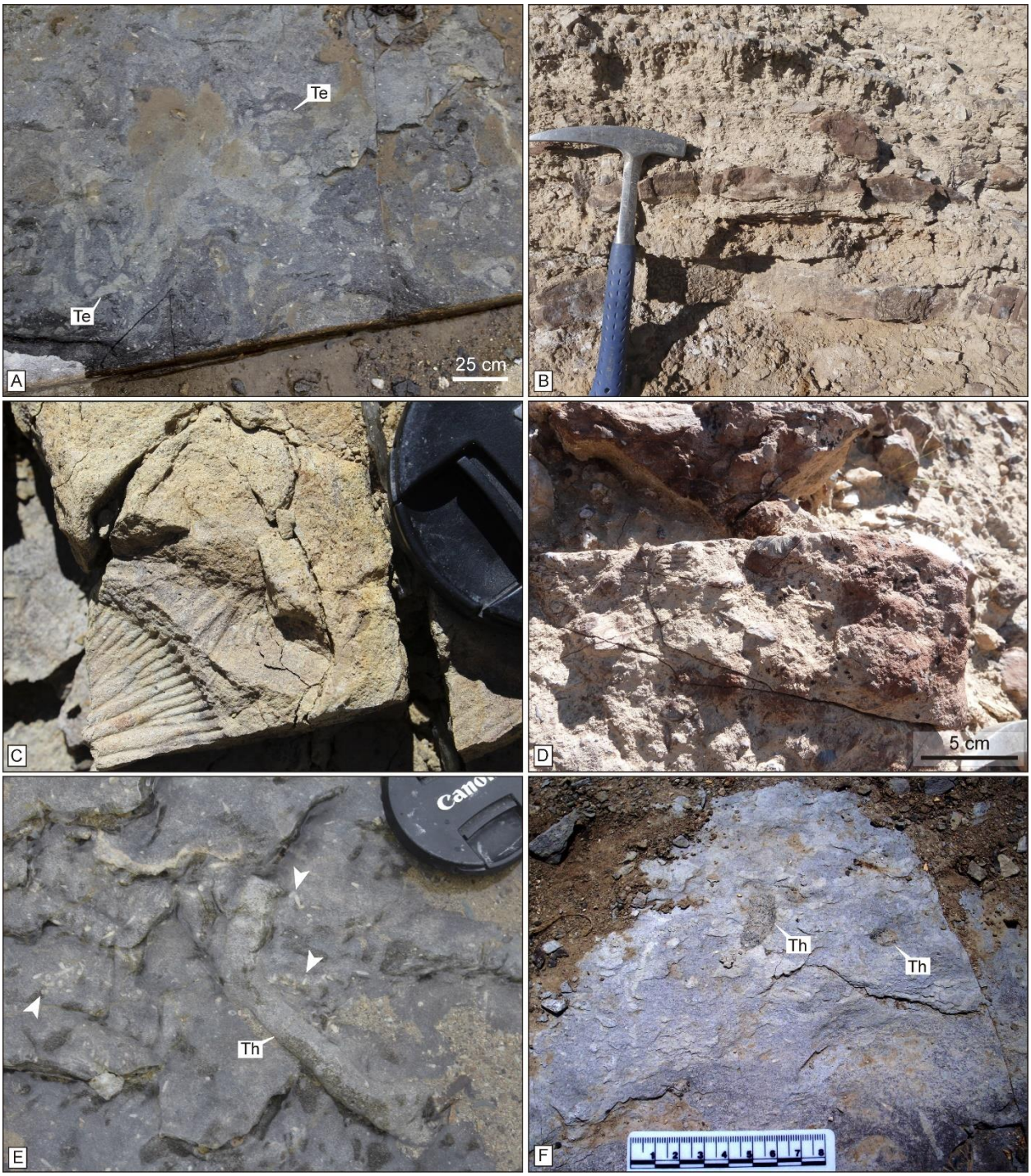

Fig. 2.9: Proximal bay facies. (A) Bioclastic wackestone exhibiting monospecific occurrence of *Teichichnus rectus* (Te). (B) Bioclastic wackestone to packstone showing symmetrical ripples (hammer for scale is *ca* 30 cm long). (C) Medium to coarse-grained calcareous sandstone (lens cap is 5.5 cm diameter), alternating with bioclastic wackestone showing ammonite moulds. (D) Close-up picture of the bioclastic wackestone showing fragmented to partially preserved bivalves, ammonites and gastropods. (E) and (F)

Bioclastic wackestone showing gastropods (white arrows), cross-cut by *Thalassinoides* isp. (Th) passively infilled by medium to coarse-grained sandstone.

2.4.3.4 Facies 4 (F4): Medium mudstone with interbedded greyish-green fine mudstone beds, sandstone beds and tuff layers

Description. This facies consists of grey, carbonaceous, medium mudstone showing subordinate 5 to 20 cm thick, sharp to erosive-based, greyish-green, fine mudstone beds, medium-grained sandstone and tuff beds (Fig. 2.10A, B and C). The TOC content is moderate (*ca* 2.5%; N = 2). The background carbonaceous mudstone displays abundant, 0.2 to 1.0 mm long, ellipsoidal to round-shaped pellets in the matrix, whereas the greyish-green mudstone contains pellets at the base. The sandstone is composed by organic-rich intraclasts of coarse-sand size located 1 to 2 cm above the base, giving an inverse to normal-graded appearance (Fig. 2.10B). Ammonite and bivalve shells are minor components of the mudstone. This facies is highly bioturbated, displaying biodeformational structures and discrete trace fossils, such as *Thalassinoides* isp., *Palaeophycus tubularis, Teichichnus rectus* and *cf. Teichichnus patens* (Fig. 2.10D, E and F). The discrete trace fossils are seen in the basal part of a bed, where a distinct colour contrast between mudstone, sandstone and tuff intervals occurs (Fig. 2.10B). Locally, *Teichichnus rectus* constitutes monospecific occurrences (Fig. 2.10C and F). The burrows are 3 to 10 mm wide. The burrow boundaries of *Teichichnus* are sharp to irregular, and commonly show ellipsoidal pellets (Fig. 2.10F). The bioturbation index is 2 to 3 for intervals containing only discrete trace fossils and 5 to 6 if biodeformational structures occur. This facies is 2 to 10 m thick.

Interpretation. This facies is ascribed to a distal-bay environment where mudstone is indicative of low-energy, hemipelagic sedimentation. The greyish-green mudstone and medium-grained sandstone beds are interpreted as muddy tempestites and concentrated sand-rich density flows originating at the coast. The concentrated density flows eroded the underlying organic-rich mudstone and transported the mudstone mainly as intraclasts. Massive sandstone beds deposited by sandy mass flows occur in marine environments above eolian successions, where storms erode adjacent eolian systems and transport material seaward by subaqueous flows (Eschner & Kocurek, 1986). The muddy distal-bay deposits are similar to the sediments described from the central Eckernförde Bay in the south-west Baltic Sea, where laminated muddy tempestites and pelletized strata are interbedded (Bentley & Nittrouer, 1999).

The sharp burrow margins of *Teichichnus rectus* characterize a stiff to firm substrate. Furthermore, a stiffground scenario is indicated by the insignificant compaction of burrows in the fine-grained sediment (Wetzel & Uchman, 1998; Lobza & Schieber, 1999). The low ichnodiversity and moderate to high degree of bioturbation reflect an opportunistic population strategy that is characteristic of brackish-water environments (Pemberton & Wightman, 1992). Particularly, the monospecific, high-density occurrence of *Teichichnus rectus* is typical of marginal marine environments experiencing salinity fluctuations (Buatois *et al.*, 2005; MacEachern *et al.*, 2007a; Díez-Canseco *et al.*, 2015). A similar lagoonal bay, nearshore setting was inferred from the abundant *Teichichnus* occurring in Middle Jurassic deposits of the North Sea (Petersen *et al.*, 1998), and in Lower and Middle Jurassic deposits of Denmark (Bromley & Uchman, 2003). In addition, the common occurrence of *Teichichnus* in bay and lagoonal facies associated with brackish waters has been extensively documented (Pemberton *et al.*, 2001; Buatois *et al.*, 2005). The absence of bay-mouth facies and the lack of other salinity fluctuation indicators as, for example, trace fossil size reduction and syneresis cracks, suggest to assign these embayment deposits to an open rather than to a restricted bay (MacEachern & Gingras, 2007).

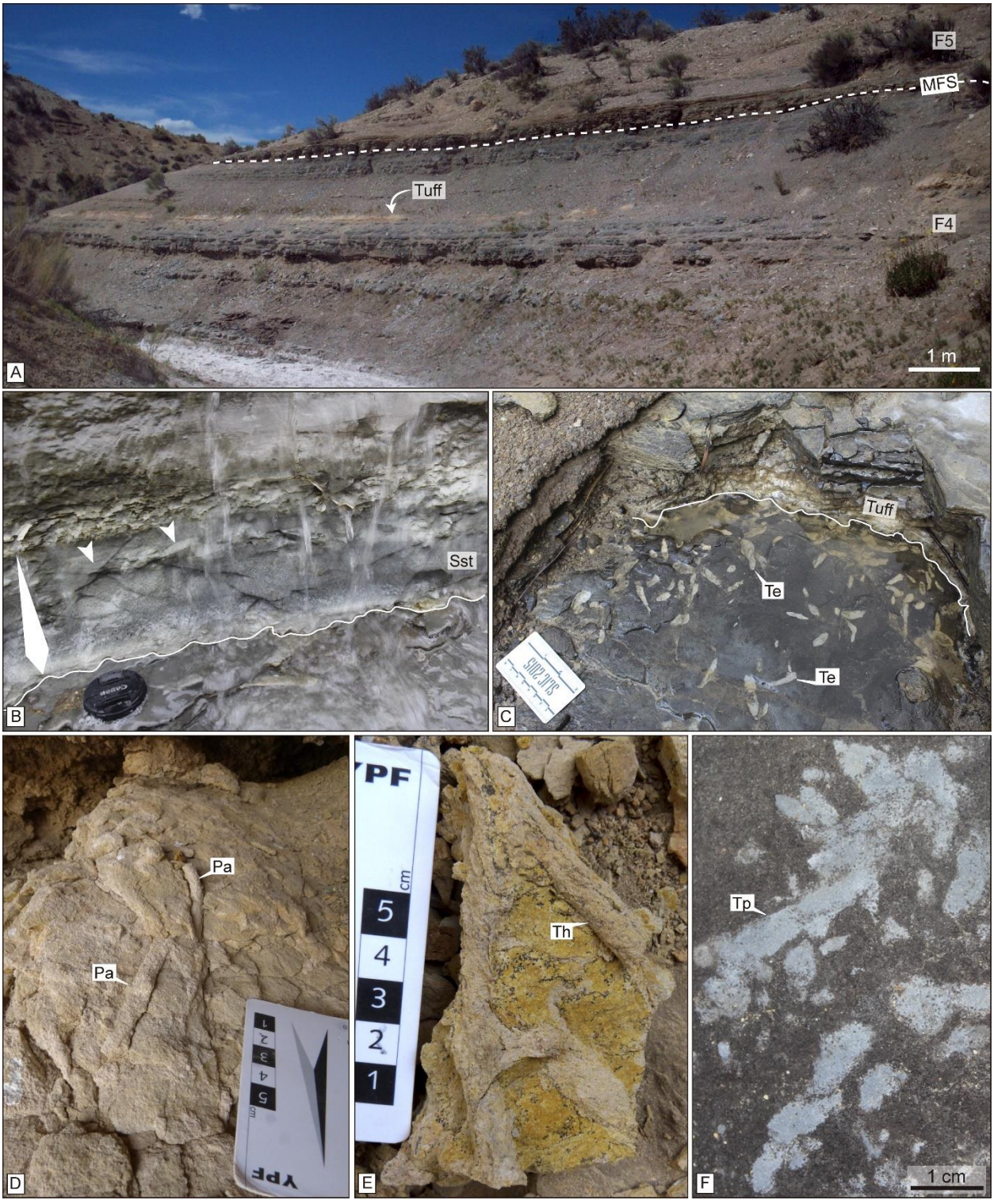

Fig. 2.10: Distal-bay facies (F4). (A) Outcrop showing the transition of F4 to the siliciclastic basin facies F5 while the supposed probable maximum flooding surface (MFS) is located in between. (B) Medium-grained sandstone (Sst) showing inverse to normal grading, with trace fossils originating from the overlying intervals (white arrows). Lens cap is 5.5 cm diameter. (C) Tuff intervals passively infilling *Teichichnus*

rectus (Te). (D), (E) and (F) *Palaeophycus tubularis* (Pa) and *Thalassinoides* isp. (Th) in intensely bioturbated intervals, and monospecific occurrences of *cf. Teichichnus patens* (Tp) with pellets along the wall.

2.4.4.5 Facies 5 (F5): Parallel-laminated medium to fine mudstone

Description: This facies is the thickest facies of the Vaca Muerta Formation, yet the basal transgressive succession is only considered. It is composed of very thin-bedded, parallel-laminated medium to fine mudstone (Fig. 2.11A). Discontinuous, anastomosing, wrinkle laminae of kerogen seams are denser in the fine than in the medium mudstone. In the studied interval, the TOC content ranges between 1 to 12% (mean *ca* 5%; N = 5). Locally, sharp-based, 2 to 3 cm thick massive tuff layers occur (Fig. 2.11B). In both medium and fine mudstone, soft-sediment deformation structures include slumps, sand dykes and syn-sedimentary faults. Ellipsoidal, 20 to 70 cm long carbonate concretions occur, and become more abundant upsection. Moderate to high concentrations of well preserved, flattened, 2 to 20 mm wide pectinid bivalve shells (*Huncalotis,* Damborenea & Leanza, 2016) are present on bedding planes. Some of the larger bivalves are spatially associated with ammonite shells. Ammonites, plant debris and fish scales are minor constituents. Ammonites are well-preserved to partially fragmented. Some specimens are up to 20 cm in diameter.

Interpretation: This facies formed in a basinal environment. High amounts of organic matter and kerogen seams, as well as the absence of macrofauna burrows, point to an at least temporary oxygen deficiency. The relative absence of event beds (sharp or erosive, discrete beds) indicates that the predominant processes were hemipelagic. In this sense, organic matter was provided by marine snow, whereas the silt grains of the medium mudstone were airborne (e.g. Gabbott *et al.*, 2001). Sand dykes and syn-sedimentary faults are related to gravity-driven mass movements that likely were triggered by the tectonic activity in the study area. The colour contrast provided by tuffs documents the absence of macrofaunal burrows (Fig. 2.11B; compare with F4, Fig. 2.10C). The lack of bioturbation structures implies oxygen deficiency of bottom and pore water. *Huncalotis* is found in upper Tithonian deposits of the Vaca Muerta Formation in western-central Neuquén Basin, and is considered a pseudoplanktonic epibyssate living on swimming ammonites (Damborenea & Leanza, 2016). Bivalve shell pavements may reflect short-term benthic settlement representing an opportunistic strategy (Damborenea & Leanza, 2016) due to fluctuating

oxygenation, similar to some black shales in the Posidonia Shale of Germany (Röhl *et al.*, 2001). Because concretions need time to grow (e.g. Raiswell & Fisher, 2004), their strata-bound arrangement suggests intermittent sediment accumulation (Wetzel & Allia, 2000).

Fig. 2.11: Siliciclastic basin facies (F5). (A) Discontinuous, anastomosing, parallel lamination in the medium to fine mudstone produced by kerogen seams. (B) Unbioturbated tuff intervals (white arrows), which contrast with the tuff intervals occurring in F4 bioturbated by producers of *Teichichnus rectus* (scale in inches).

2.5 Facies distribution and sequence stratigraphy

Facies distribution can be differentiated into two areas: PL (sections 2, 3 and 4), and QdS and section 1 (sections 1, 5, 6, 7, 8, 9 and 10). In PL, the Quebrada del Sapo Formation continental deposits show a reduced development of fluvial and eolian units (Fig. 2.7). Locally, a conglomeratic fluvial deposit with a deflation surface above occurs towards the top. The contact between the Quebrada del Sapo and Vaca Muerta formations is represented by a flat surface, overlying eolian dune deposits (Fig. 2.12A) or locally the conglomeratic fluvial deposits. The entire sequence of the Vaca Muerta Formation shifts from bay-margin bindstone (F2) to shallow-marine (F3 and F4) sediments, comprising a retrogradational stacking pattern (F1 is not observed). Therefore, the contact between the Quebrada del Sapo and Vaca Muerta formations represents a maximum regressive surface (MRS) overlain by a Transgressive Systems Tract (TST). In places, the bindstone (F2) is not observed and proximal bay deposits (F3) rest on top of the contact. This TST is within the *V. mendozanus* ammonite zone (Parent *et al.*, 2011), which has been assigned to the late early Tithonian–early middle Tithonian (Riccardi, 2008). However, there is still

considerable debate about the age of the Andean ammonite biozones (Vennari *et al.*, 2014; Riccardi, 2015; Kietzmann *et al.*, 2018a).

In QdS, the Quebrada del Sapo Formation continental facies comprises two fluvial to lacustrine and two eolian successions (Fig. 2.7; see also Zavala *et al.*, 2005). Here, the contact between the Quebrada del Sapo and Vaca Muerta formations is variable depending on the scale of observation. In outcrops, the contact represents a planation to erosional surface and the previous dune relief is not preserved (Figs. 2.6 and 2.12B). However, at a larger scale, the topography of partially preserved megadunes constitutes a reworked relief. This topography is evidenced by minor thickness changes in the Quebrada del Sapo Formation, that can be observed when the strata correlation is normalized to the deflation surface at the base of the last eolian interval (Fig. 2.7B) (top of unit T3 of Zavala *et al.*, 2005). The eolian interval is thicker in sections 6, 8, and 10 (15.2 m, 8.3 m and 8.4 m respectively) and thinner in sections 7 and 9 (6.3 m). F1 and F2 are thicker (1.7 m, 1.8 m and 1.9 m) in sections 7, 9 and 10 and thinner (0.4 m and 1.1 m) in sections 6 and 8. Thus, the thickness of the eolian deposits is slightly inverse to the thickness of F1 and F2. F3 and F4 vary between 8.2 m and 22.8 m in thickness, and exhibit no relation to the thickness of the eolian deposits.

Beach (F1), bay-margin (F2), proximal bay (F3) and distal bay (F4) deposits of the Vaca Muerta Formation occur on top of the planation to reworked contact in QdS and section 1. Similarly, as in PL, the retrogradational pattern suggests a TST overlying a MRS occurring at the base of F1. Basin facies (F5) mantles all the underlying facies in both PL and QdS. In the first 1 to 3 m of F5, a level with carbonate concretions occurs, indicating condensation due to the development of a maximum flooding surface (MFS) and marking the top of the TST.

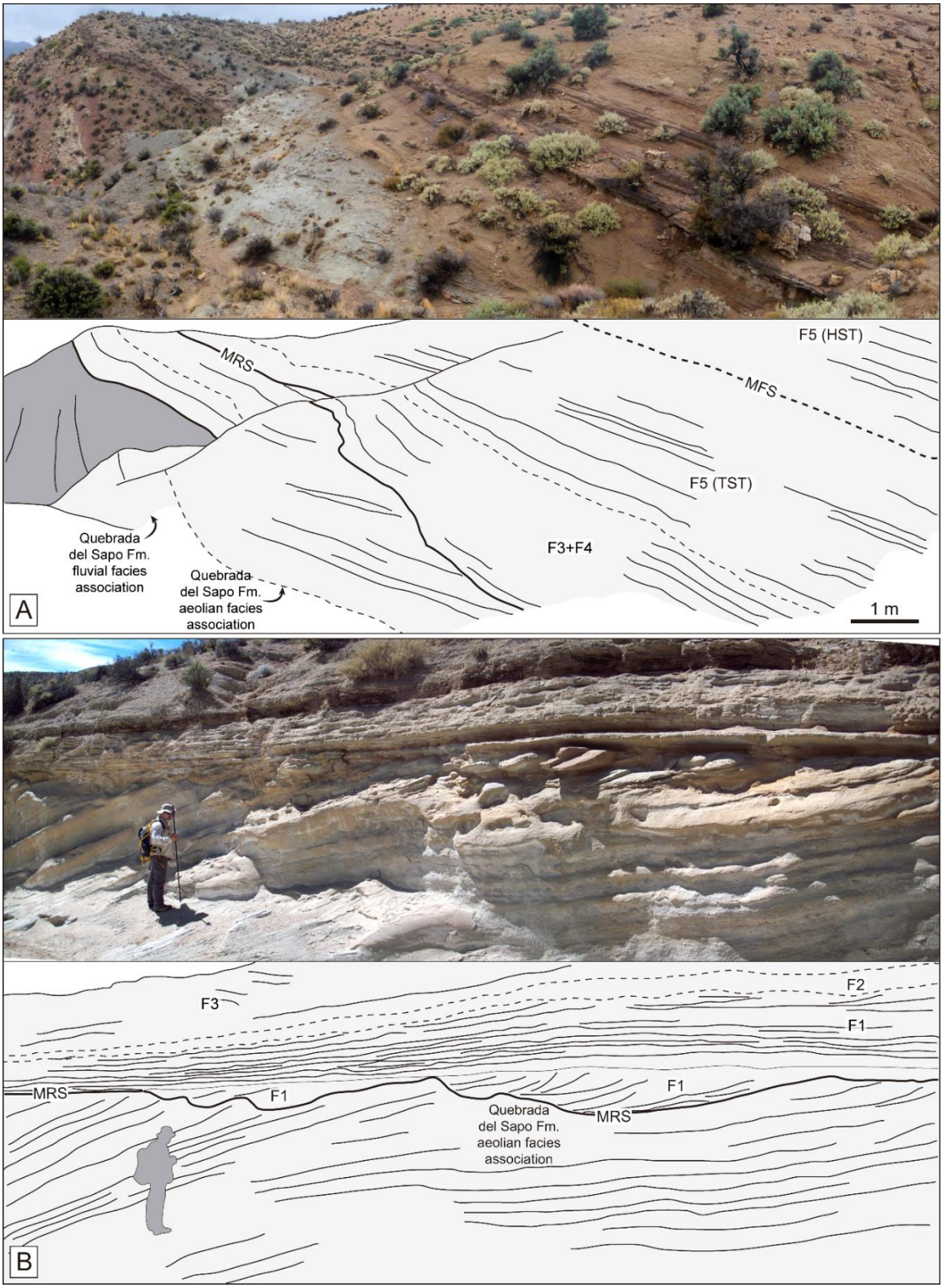

Fig. 2.12: Contrasting development of the Quebrada del Sapo Formation and the TST of the Vaca Muerta Formation in (A) topographic high areas located close to the Picún Leufú anticline (picture from section 4), and (B) low areas (Quebrada del Sapo, picture from section 10). Person for scale is *ca* 1.7 m tall.

2.6 Depositional model

The sedimentological and ichnological observations form the base to develop a depositional model for the eolian to marine transition of the Quebrada del Sapo and Vaca Muerta formations in the study area (Figs. 2.13 and 2.14). A decrease in thickness towards PL in both the Quebrada del Sapo Formation (23–62 m in QdS to 10 m in PL) and Vaca Muerta Formation (9–25 m in QdS to 5–9 m in PL; Fig. 2.7; Zavala & Freije, 2002) suggests the existence of topographically higher domains with lower accommodation rate in this area. One hypothesis considers that this topographic difference originated from the extensive tectonic activity of the anticline. Palaeocurrent indicators in fluvio-lacustrine deposits and detrital zircon ages suggest that the anticline constituted a source area prior to the deposition of the eolian unit (Zavala & Freije, 2002; Zavala *et al.*, 2005, 2008; Naipauer *et al.*, 2012). The progressively developed unconformities of the Picún Leufú anticline indicate continuous deformation throughout deposition of the Quebrada del Sapo and Vaca Muerta formations (Fig. 2.12A; Freije *et al.*, 2002; Naipauer *et al.*, 2012). Particularly, deformation is expressed as a change of dip (2–17°) between the Quebrada del Sapo and Vaca Muerta formations, and as normal faults affecting the uppermost Quebrada del Sapo Formation (Fig. 2.5D; Freije *et al.*, 2002, fig. 11A), indicating tectonic influence during the transgression. A second hypothesis implies that the topographic difference is related to a different position within an erg, with the higher domains (PL) occurring in the centre of the erg (Veiga & Spalletti, 2007). The relative constant thickness of the uppermost fluvial and eolian units of the Quebrada del Sapo Formation supports this idea, with less influence of tectonics towards the end of continental deposition (Fig. 2.7A).

The pre-transgression topography of the eolian dune field affected facies distribution and sediment accumulation of the Quebrada del Sapo and Vaca Muerta formations (Fig. 2.7A). Both the fluvio-lacustrine and eolian successions suggest alternating wet and dry conditions during deposition of the Quebrada del Sapo Formation in the study area. Many studies of this formation arrived at a similar environmental interpretation (Parker, 1965; Digregorio, 1972; Leanza & Hugo, 1997; Freije *et al.*, 2002; Zavala & Freije, 2002; Zavala *et al.*, 2005, 2008; Spalletti & Veiga, 2007; Veiga & Spalletti, 2007). Increasing accommodation space towards the low domains of QdS, enhanced by tectonic loading effects, generated thicker continental successions and development

of lacustrine deposits. Predominance of eolian facies towards the top implies increasingly arid and dry conditions that might have resulted from the growth of the Andean magmatic arc or lowering of water table due to basin compartmentalization (Veiga & Spalletti, 2007). Veiga & Spalletti (2007) suggested a shallower water table because the thickness of the eolian dune field decreased towards the Chacaico–Charahuilla area (7 km south of QdS), located in an upwind erg-margin position.

The pre-transgression continental environment was characterized by transverse dunes oriented north-west/south-east that migrated towards the north-east (Fig. 2.14A; Zavala *et al.*, 2005; Veiga & Spalletti, 2007). The existence of a topographic high in the Picún Leufú anticline suggests that the coast advanced from the south. Flooding of the sand source areas located to the south might have decreased the continental sand budget of the study area, leading to the partial destruction of the eolian dune field (Eschner & Kocurek, 1988). However, the oblique orientation of the dunes with respect to the coast counteracted the destructive processes by restricting the area of dune erosion, therefore promoting preservation of the eolian palaeotopographic relief (Eschner & Kocurek, 1988).

The reworked to planated MRS indicates that the record of the last stage of eolian accumulation in the Quebrada del Sapo Formation was partially eroded. The monotonous eolian dune facies with soft-sediment deformation is the typical deposit below the MRS, yet locally, other facies were documented. In section 2, the top of the Quebrada del Sapo Formation shows deflation processes overlying the eolian dune deposits. Sand sheet deposits occur above the last eolian dune units in a location close to section 1 (Veiga & Spalletti, 2007). Deflation surfaces and sand sheets overlying the uppermost eolian dune deposits and below the MRS were also recorded 30 km to the north-east of the study area (fig. 16 of Cevallos, 2005). All of this evidence suggests a switch towards a negative sediment budget at the end of the eolian dune field phase, associated with the regional rise of the water table caused by the transgression. However, Veiga & Spalletti (2007) described an overall drying upward succession of the Quebrada del Sapo Formation for the study area, indicating that deflation observed at the top might be unrelated to the transgressive event, and represents a local process.

The transgression began with a base-level rise affecting the continental water table inland (Kocurek *et al.*, 2001). The occurrence of soft-sediment deformation structures in the eolian dunes located below the Vaca Muerta Formation indicates that water table rise caused by the marine

flooding affected unconsolidated eolian sand (F1). The continuous flooding by seawater and probably the negative sediment budget of the eolian dune field associated with a flooded source area generated a large-scale reworked surface (*sensu* Eschner & Kocurek, 1988; Fig. 2.7B). The distance between the sections suggests a low-relief palaeotopography characterized by ridges with widths of *ca* 1500 m and heights of 2 to 9 m (Fig. 2.7D), interpreted to be megadunes (e.g. Cevallos, 2005). Minor scouring by channelized subaqueous dunes (F1b) caused by episodic flooding locally generated an erosive surface at an outcrop scale. In the elevated domains (PL), similar processes might have formed a planation surface (*sensu* Eschner & Kocurek, 1988).

As the coast retreated, beach processes reworked the preexisting Quebrada del Sapo eolian dunes (F1; Figs. 2.7B and 2.12B). The marine flooding also fostered soft-sediment deformation structures within this facies. During F1 deposition, the Quebrada del Sapo Formation dunes were stable as syn-sedimentary normal faults cross-cut both. Low-relief beach bedforms developed while eolian dune construction was hindered by wave erosion and damp sediment being stabilized by capillary forces. Recurrent marine flooding may have characterized this transition, generating demanding conditions for the benthos and, thus, preventing burrowing by macro-organisms. Microbial mats (F2) established in the transitional zone between the beach and the coastline (Fig. 2.14B). The microbial mats also facilitated preservation of eolian and beach deposits by binding and covering them.

On top of F1 and F2, proximal bay deposits (F3) accumulated above fair-weather wave base. The proximal bay was a low-energy, sheltered embayment protected against strong waves and storms and does not show proximal shoreface facies, such as cross-bedded or HCS sandstone. Abundant fragmented or complete ammonite and bivalve shells became enriched due to winnowing of fines by waves. The producers of *Thalassinoides*, *Palaeophycus* and *Teichichnus* record a suspension-feeding/passive-predation or deposit-feeding mode that indicate the presence of nutritious particles in suspension and on the seafloor, respectively (Buatois & Mángano, 2011). Microbial mats probably stabilized the sediment and favoured the development of a stiffground later exploited by burrowing organisms. Sandy flows bypassed the area as recorded by the passive infill of the *Thalassinoides*. F3 marks the onset of marine processes above fair-weather wave base and therefore, its base constitutes a wave ravinement surface. The low-energy nature of the ravinement surface is supported by the absence of the *Glossifungites* Ichnofacies at F3 base, which

is a distinguishing feature of high-energy wave ravinement erosive surfaces (MacEachern *et al.*, 1992, 2012).

Continuous sea-level rise triggered deposition of the distal-bay facies (F4), composed of predominant hemipelagic sediments and intercalated event beds. In the distal bay, large amounts of mud accumulated in the turbidity maximum. The existence of sandy mass-flows in the distal bay suggest that unconsolidated eolian dunes occurred adjacent to the coast (Eschner & Kocurek, 1986). Low ichnodiversity and a high degree of bioturbation indicate an opportunistic population strategy typical of brackish-water environments. Further up, increasing distance to coast led to decreasing sediment accumulation. Siliciclastic basinal deposits (F5) contain high amounts of organic matter and document oxygen-deficient conditions, evidenced by the absence of burrowing organisms. The interval ends with strata-bound carbonate concretions and associated indicators of lowered, intermittent sedimentation, marking the end of the transgression at the maximum flooding surface (MFS).

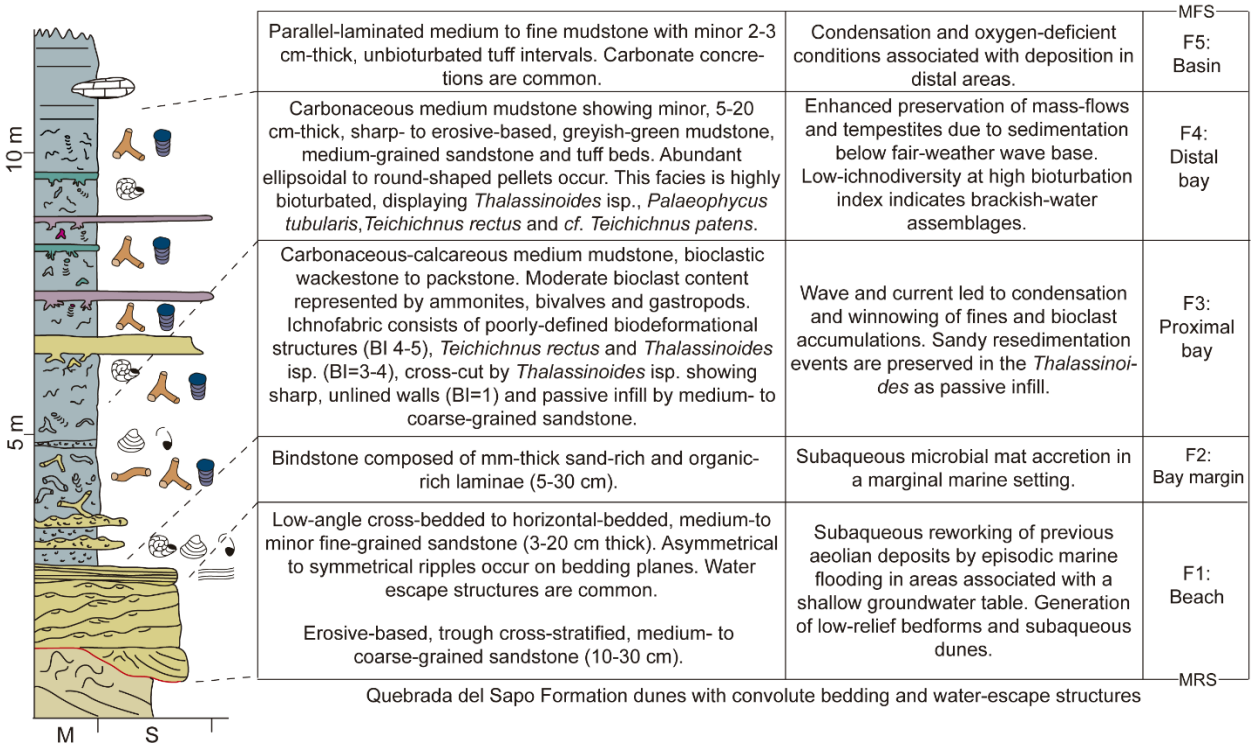

Fig. 2.13: Idealized depositional evolution of the Vaca Muerta Formation transgressive succession.

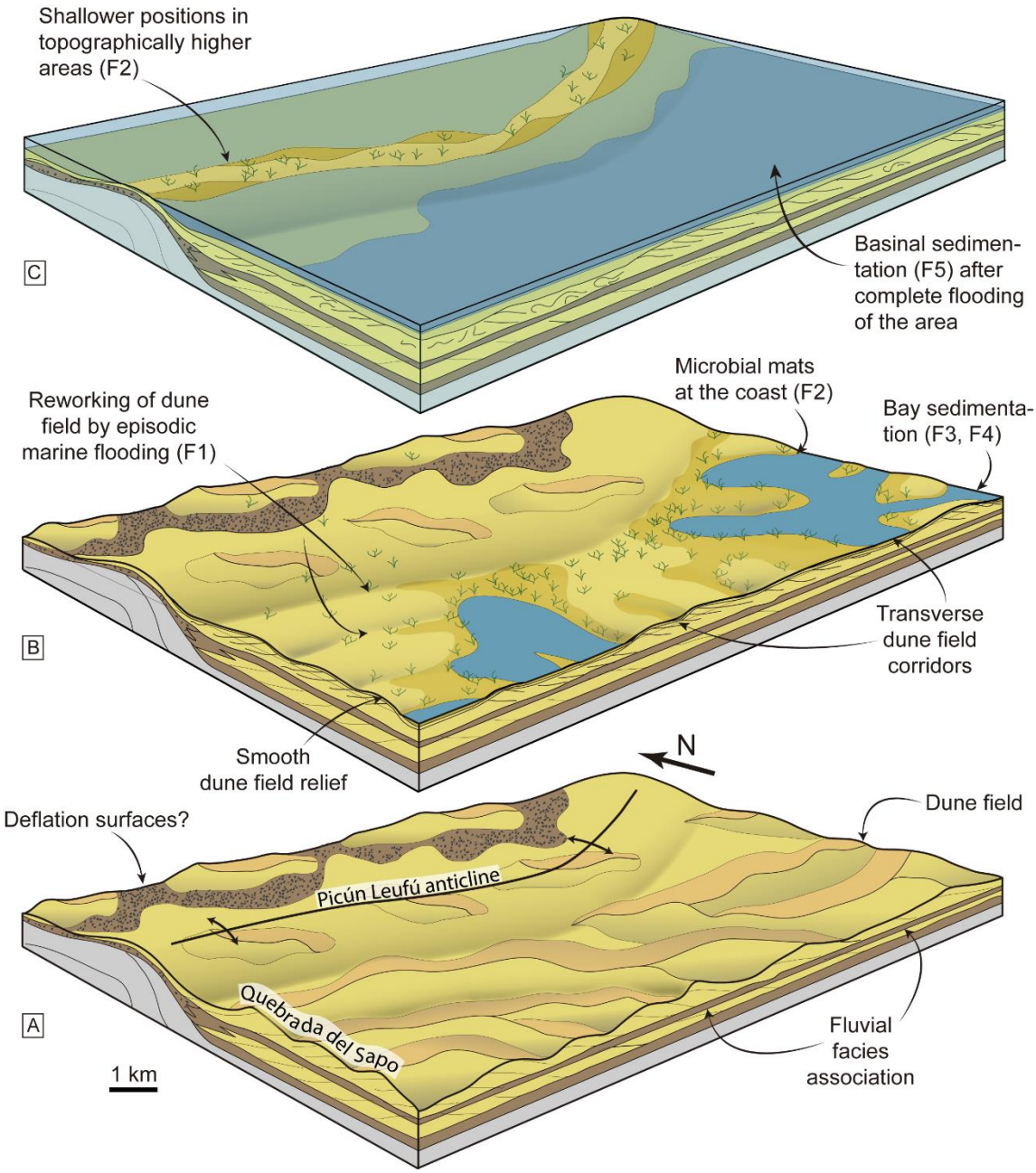

Fig. 2.14: Depositional model of the Vaca Muerta Formation transgression showing: (A) the pre-flooding topography; (B) the transgressive coast; and (C) the complete flooding of the study area.

2.7 Discussion

2.7.1 Current hypotheses about the transgression of the Vaca Muerta Formation

The current hypothesis for the Vaca Muerta Formation transgression envisages an instantaneous catastrophic Tithonian flooding preserving the eolian fields (Mutti *et al.*, 1994; Cevallos, 2005). This hypothesis relies on four main lines of evidence: (i) relative absence of onlap relationships to the underlying continental LST deposits (Cevallos, 2005); (ii) lack of transitional facies between the eolian and marine deposits (Mutti *et al.*, 1994); (iii) preservation of the underlying dune-field topography indicating subordinate marine reworking (Cevallos, 2005, Reijenstein *et al.*, 2014; Acevedo & Bande, 2018); and (iv) presence of soft-sediment deformation structures in the upper part of the eolian deposits (Cevallos, 2005; Veiga & Spalletti, 2007).

In the Neuquén Basin, catastrophic transgressions were interpreted at different basin-filling episodes. The catastrophic transgression of the Vaca Muerta Formation was described at the Dorsal de Huincul, 30 km north-east of the study area (Cevallos, 2005). There, the upper beds of the eolian Kimmeridgian deposits (Catriel Formation) show liquefaction structures generated by flooding over unconsolidated deposits (Cevallos, 2005). The megadune topographic relief is preserved below the transgressive surface (Cevallos, 2005; see also Reijenstein *et al.*, 2014; Acevedo & Bande, 2018). Overlying the transgressive surface, the TST consists of a few centimetres to >10 m thick succession of marl, black mudstone and limestone with bivalve bioclasts and siltstone and fine-grained sandstone intraclasts, named as the Rapid Transgression Remnant. This succession is covered by a 20 to 40 m interval of dark, laminated mudstone, referred as VM-A (Cevallos, 2005). The TST was interpreted to have been formed by sedimentation of the coarser-grained material because of subordinate reworking in its lower part, and by suspension fallout in its upper part (Cevallos, 2005). A catastrophic transgression was also suggested for the Lower Cretaceous Lower Troncoso Member of the Huitrín Formation based on the preservation of an eolian palaeorelief and existence of subaqueous mass flows produced by reworking of unconsolidated sediment (Strömbäck *et al.*, 2005; Argüello Scotti & Veiga, 2015).

The sections studied in this work provide clear evidence of a TST composed of retrograding beach, open-bay and siliciclastic-basin facies (Fig. 2.13), followed by prograding siliciclastic-basin facies. Facies transitions are indicated by: (i) beach deposits revealing a shallow groundwater table at the beginning of the flooding; (ii) microbial mats at the coast; (iii) symmetrical ripples recording wave reworking of proximal bay deposits; and (iv) aggradation of distal-bay deposits with alternating infaunal communities, as recorded by trace fossils. Therefore, the transgression occurred during a time span lasting long enough to allow the establishment of

transitional environments and biotas. This time span is not consistent with a catastrophic transgressive scenario, where the coast migrates at a rate of kilometres per day (see below).

Another issue with the current hypothesis of the transgression is that preservation of an eolian landscape is not restricted to catastrophic flooding, but it is also facilitated by a low-energy transgression in embayments (e.g. Jennings, 1985) or submergence of early-stabilized dunes (e.g. Al-Hinai *et al.*, 1987; Carmona *et al.*, 2012; Hanebuth *et al.*, 2013; see review by Eschner & Kocurek, 1988). For instance, in the Fitzroy Delta in King Sound, Australia, low-energy, tidal-flat environments migrate over Quaternary eolian dunes during the rapid Holocene marine transgression (Jennings, 1975). Stabilization by vegetation and a cover of tidal-flat mud favour the preservation of the dune topography (Jennings, 1975). In addition, early cementation of coastal dunes is promoted by groundwater seepage (Kocurek & Nielson, 1986; Chan & Kocurek, 1988; Pye, 1983). Microbial mats also stabilize the sediment and promote preservation of the transgressive deposits (Carmona *et al.*, 2011, 2012).

Dune-field relief preservation has to be differentiated between megadune and dune relief, because the former constitutes a large-scale bedform commonly preserved in the rock record (for example, Fig. 2.7B), whereas the latter is hardly preserved in modern and ancient settings. A well-documented example of dune preservation is the Jurassic Entrada Formation, USA (Ahmed Benan & Kocurek, 2000). In the study area, dunes are not completely preserved because a sharp surface truncates their top at outcrop scale (Figs. 2.6 and 2.12B), yet a megadune relief can be observed at a larger scale (Fig. 2.7B). Similar preservation of eolian relief has been observed during different basin-fill stages of the Neuquén Basin (Cevallos, 2005; Strömback *et al.*, 2005; Reijenstein *et al.*, 2014; Argüello-Scotti & Veiga, 2015; Acevedo & Bande, 2018).

Moreover, soft-sediment deformation structures not only result from a catastrophic transgression; they just indicate unconsolidated sediment, and they do not document the rate of coastline migration. A rise of the groundwater table facilitates soft-sediment deformation in the wet, highly porous, eolian dune sand (see review by Doe & Dott, 1980; Kocurek *et al.*, 2001).

To summarize, the findings of the present study do not support the previous hypothesis of an instantaneous catastrophic flooding for the Vaca Muerta Formation. The transgressive deposits clearly differ from ancient examples of catastrophically flooded dune fields as substantiated by three examples: (i) lower Permian Weissliegend Sandstone of Europe (Smith, 1979; Blaszczyk, 1981; Glennie & Buller, 1983; Strömbäck & Howell, 2002); (ii) Jurassic Entrada Formation, USA

(Tanner, 1970; Vincelette & Chittum, 1981; Ahmed Benan & Kocurek, 2000; Kocurek *et al.*, 2019); and (iii) Cretaceous Lower Troncoso Member of the Huitrín Formation, Argentina (Strömbäck *et al.*, 2005, Argüello Scotti & Veiga, 2015). These examples contrast with the Vaca Muerta Formation in three aspects: (1) reduced or absent coastal or marginal-marine facies transitions; (2) mass-flow deposits originating from sediment shedding from dunes; and (3) a relatively higher degree of eolian relief preservation. In contrast, the studied case shows an eolian to marine transition consisting of coastal and marginal-marine environments (beach and bay deposits) similar to ancient examples of gradual transgressions (e.g. Blakey *et al.*, 1983; Desmond *et al.*, 1984). Considering the degree of eolian palaeotopography preservation, the transition to the Vaca Muerta Formation is an intermediate case between gradual and catastrophic, with a planation to erosive relief observed at an outcrop scale (i.e. no dune-relief preservation, Fig. 2.12B), but megadune preservation at a large scale (Fig. 2.7).

2.7.2 Revised scenario for the transgression of the Vaca Muerta Formation

In the study area, during the transgression of the Vaca Muerta Formation a low-energy, embayed facies migrated rapidly over the continental deposits of the Quebrada del Sapo Formation. A rapid marine transgression is implied by the thin coastal deposits (F1, 0.5–2.0 m thick) prior to open-bay sedimentation and the absence of punctuated shoreline movements that would record a gradual transgression associated with a retrogradational parasequence set (Cattaneo & Steel, 2003). Erosion by wave reworking and deflation on the one hand, and stabilization provided by microbial mats and early cementation on the other hand, controlled the preservation of the eolian relief. In seismic sections, the lack of onlap relationships and the absence of retrogradation represent additional evidence for a rapid transgression draping the basin topography (Cevallos, 2005).

The sharp basal MRS overlying the eolian deposits of the Quebrada del Sapo Formation represents the first expression of the transgression. Deflation and marine flooding might have generated the planated to reworked relief. A good analogue to illustrate marine reworking of eolian sediments is the western coast of Baja California near Guerrero Negro, Mexico (Fryberger *et al.*, 1990). In this area, marine deposits truncate underlying eolian cross-bedded deposits, commonly modified by water-escape structures or slumping during short-term flooding (Fryberger *et al.*, 1990). Marine transgressive scouring of cemented eolian strata formed an irregular erosional

surface similar to that at the base of the trough cross-bedded sandstone (F1). In addition, subaqueous wave reworking comparable to F1 occur within the interdune areas during episodic marine flooding (Inman *et al.* 1966).

The beach deposits are replaced by bay-margin facies characterized by microbial mats similar to the Holocene transgression of the carbonate coast of Abu Dhabi, UAE, where reworked eolian deposits are covered by microbial mats (Strohmenger *et al.*, 2010). The open-bay scenario for the Vaca Muerta Formation matches the observation of low-energy, non-incised, transgressive lithosomes that lack barrier facies and proximal shoreface facies. The reduced thickness of the open-bay sediments and the absence of progradational stacking patterns indicate a continuous transgression (Cattaneo & Steel, 2003). Within the embayment, the environmental conditions showed high lateral variability that is also typical of transgressive successions.

The low-energy, rapid transgression of the Vaca Muerta Formation could have evolved in an open bay similar to the Fitzroy delta of King Sound, Australia (Jennings, 1975; see above). Marginal-marine conditions established in corridors traversing the megadunes and fostered later inundation of the megadune crests (Fig. 2.14B; e.g. Jennings, 1975; Carmona *et al.*, 2012). According to this scenario, it was possible to preserve the smoothed, reworked long-wavelength megadunes observed in the Dorsal de Huincul (Cevallos, 2005). The thin strata of the TST indicate a low-gradient transgressive surface (e.g. Ghinassi, 2007) that facilitated high rates of coastline migration. A modern example of a transgression over a gently sloped area is the Gulf of Tonkin, South China Sea; there, the coastline prograded over 700 km in 12 kyr while the transitional deposits are gradational and bioturbated (Wetzel *et al.*, 2017), similar to those deposits documented in connection with the wave ravinement surface at F3.

2.7.3 Timing of marine transgressions over dunefield deposits

Considering the rate of landward migration of the coastline, eolian to marine transitions can be subdivided into three main categories: catastrophic, rapid and gradual. The rate of coastline migration is controlled by the rate of sea-level rise and the slope of the transgressive surface. This rate affects the preservation of the dune topography by the time available for marine reworking (Chan & Kocurek, 1988; Eschner & Kocurek, 1988), whereas the slope of the transgressive surface controls the accommodation space for transgressive deposits.

The sediment record of eolian to marine transitions during *catastrophic* transgressions shows a limited representation of coastal or marginal-marine transitional settings (for example, shallow marine reworking associated with sudden flooding), high preservation of the eolian landscape, and eventually sandy mass-flows shed from dunes (Fig. 2.15A). A catastrophic transgression occurs if the rise of water level is in the range of several metres during one to 10 years caused, for instance, by sill or dam-breaks. This type of flooding requires that the water level within the basin is considerably below current eustatic sea level. A representative example is the catastrophic Zanclean flood filling the Mediterranean Sea at the end of the Messinian dry period (5.32 Ma; Blanc, 2002). Peak rates of sea-level rise could have exceeded 10 m day^{-1} (Garcia-Castellanos *et al.*, 2009). High rates of sea-level rise are also suggested for the Holocene catastrophic flooding of the Black Sea (tens of centimetres per day; Ryan *et al.*, 1997), although this is still a matter of discussion (Yanko-Hombach *et al.*, 2007, and references therein). Assuming the rates of sea-level rise suggested by Garcia-Castellanos *et al.* (2009), a coastal plain sloping at 0.5 m km^{-1} (a value typical of low-gradient continental shelves; Harris & Macmillan-Lawler, 2016) would generate shoreline migration rates of kilometres per day.

Rapid transgressions in the range of the Holocene rates of sea-level rise lead to a thin TST composed of coastal or marginal-marine deposits that records the complete transition from eolian to marine facies and may preserve the eolian landscape relief (Fig. 2.15B; e.g. Jennings, 1975; Steele, 1983). Holocene rates of sea-level rise are of several to several tens of metres on timescales of 10^2 to 10^3 years, as for example after the Last Glacial Maximum when sea-level rise was on average 4.1 to 13.3 mm yr^{-1} and peak rates reached 1.25 to 5.33 cm yr^{-1} (Hanebuth *et al.*, 2000, 2009; Yokoyama *et al.*, 2001). On gentle slopes, these rates result in fast landward migration of the coastline. For example, the Holocene transgression (20 to 8 kyr) in the Gulf of Tonkin, South China Sea, caused an average coastline migration of 60 m yr^{-1} for a low-gradient shelf (*ca* 0.2 m km^{-1}) and up to 150 m yr^{-1} for the Red River incised valley area (Wetzel *et al.*, 2017). In this case, the rapid transgression resulted in low sediment supply to coastal and offshore areas. Therefore, commonly less than metre-thick deposits accumulated outside incised valleys, while inside the valleys tidal bars or coastal barriers did not form due to shortage of sand (Wetzel *et al.*, 2017). Dune field topography (in the scale of megadunes) can be preserved if the coastal processes are of low-energy as encountered at estuarine or embayed coasts (e.g. Jennings, 1975; Wetzel *et al.*,

2017). Because a lower rate of landward migration leads to increased dune-field reworking, preservation of the dune field relief might be lower than in catastrophic transgressions.

Gradual transgressions over eolian systems show low rates of coastline migration, and are only known from the sediment record. Most gradual transgressions lead to formation of retrogradational parasequence sets (punctuated transgressions of Cattaneo & Steel, 2003). They comprise several inland marine incursions and, thus, interbedded eolian and marine deposits occur recurrently (e.g. Havholm & Kocurek, 1994; Blakey *et al.*, 1996; Jordan & Mountney, 2010, 2012; Rodríguez-López *et al.*, 2012). In addition, these transgressions record a rising groundwater table and upward increasing humid conditions on the continent, as evidenced by the switch to fluvial deposits (e.g. Jordan & Mountney, 2010, 2012). During that time, dunes below supersurfaces became stabilized and eolian sedimentation resumed. An erosional relief may indicate a prolonged time span that allowed reworking of the eolian topography by continental and marine processes (e.g. Moore, 1983; Huntoon & Chan, 1987). Therefore, gradual transgressions are recorded by transitions towards marine environments characterized by several short seawater incursions (parasequences of 400 kyr; Jordan & Mountney, 2012) and preservation of planation surfaces or reworked relief towards the top of the eolian succession. Marine and eolian facies are interbedded (Fig. 2.15C).

The transition from the Quebrada del Sapo to the Vaca Muerta Formation resembles the sediment record of a Holocene rapid transgression at high rates of sea-level rise. Using sedimentation rates of modern estuarine systems as a measure (Nichols, 1989, and references therein), the basal TST of the Vaca Muerta Formation could have formed during a period lasting about 10^4 to 10^5 years. The calculation considers a compaction of 70% for the Vaca Muerta Formation estimated from the laminae bent around early diagenetic concretions, formed within the deposits of the *ca* 23 m embayment succession accumulated during TST. Thus, Holocene rates of sea-level rise can result in such a flooding scenario.

The proposed rates of sea-level rise in the range of the Holocene ones for the Late Jurassic face the problem of reconciling this data with the Jurassic sea-level curve (Haq, 2018). The global maximum sea-level highstand of the Jurassic occurs in the late Kimmeridgian–early Tithonian (Haq, 2018), slightly pre-dating the Vaca Muerta Formation. In the Neuquén Basin, therefore, compaction-induced, tectonic and/or thermal subsidence has to be taken into account to explain the discrepancy in the global sea-level chart with respect to the timing of the transgression. The

Vaca Muerta Formation formed during the initial Aluk deformation stage, which represented the time of maximum areal extent of the deformation in the Dorsal de Huincul (Mosquera *et al.*, 2011). The Vaca Muerta transgression was nearly simultaneous with an extensional phase of the Picún Leufú anticline (Freije *et al.*, 2002), as documented by syn-sedimentary normal faults cross-cutting the contact between Quebrada del Sapo and Vaca Muerta formations. In addition, based on biostratigraphy and palaeobathymetric calculations, the Mesozoic rates of sea-level change were estimated to have had a magnitude of several metres to tens of metres per Myr (Immenhauser, 2005), supporting the idea that subsidence must have contributed to the high rates of relative sea-level rise in the study area. However, glacio-eustasy was also suggested to have occurred during the Mesozoic while modulated by high-altitude perennial ice shields (Immenhauser, 2005), which can result in similar rates of sea-level variations as in the Holocene. The origin of the transgression is still contentious and needs further investigations to understand which variable accounted for such rates of sea-level change.

The hypothesis of a rapid, Holocene-like transgression questions the current idea of a catastrophic transgression. A normal evolution of the Tithonian transgression in the Neuquén Basin has been proposed previously by Boll & Valencio (1996) and recently by Ponce *et al.* (2015, 2016). This is consistent with the overall increase in accommodation space of the continental Tordillo Formation recorded in the northern Neuquén Basin (Spalletti & Colombo-Piñol, 2005; Spalletti & Veiga, 2007). Furthermore, transgressive lag deposits and/or *Glossifungites* Ichnofacies were recorded at the base of the Vaca Muerta Formation in other areas (Boll & Valencio, 1996; Borbolla *et al*., 2014). The rate of coastline migration for the whole Neuquén Basin is far from being resolved because time resolution provided by biostratigraphy based on ammonites is too low to establish the specific timing of the transgression. Therefore, there is a need for these analyses conducted in basinal positions, which might provide a framework to understand how the transgression started and evolved.

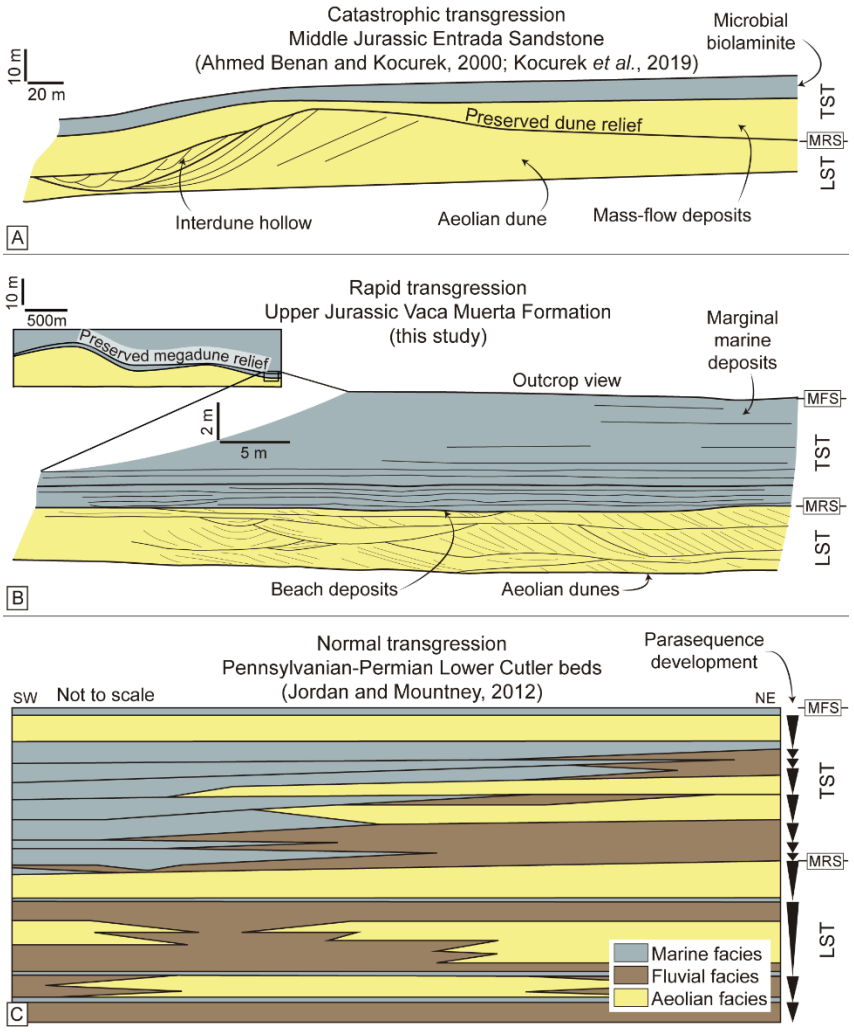

Fig. 2.15: Stratigraphic representation of three different transgressive scenarios over eolian dune fields: (A) catastrophic; (B) rapid; and (C) gradual.

2.8 Conclusions

The Kimmeridgian continental deposits of the Quebrada del Sapo Formation represent fluvial, lacustrine and eolian facies. Jurassic deformation generated an irregular topography prior to flooding. The growth of the Picún Leufú anticline controlled the development of the continental facies of the Quebrada del Sapo Formation and the sedimentary environments of the basal transgressive systems tract (TST) of the Vaca Muerta Formation (both of them thinning towards the anticline). Within the Picún Leufú domain (PL; sections 2, 3 and 4), a planated eolian–marine contact is present, whereas in the Quebrada del Sapo (QdS; sections 5 to 10) and PL section 1, a

reworked dune-field relief characterized by megadunes is preserved, as indicated by a planation or erosive surface at outcrop-scale and slight thickness changes of strata at large scale. The Vaca Muerta transgression smoothed the pre-flooding relief and a succession accumulated, which is thinner in the topographically high PL domain than in the topographically low QdS domain.

The transgression constituted a rapid, low-energy period representing the transition between the eolian deposits of the Quebrada del Sapo Formation and the marine basinal facies of the Vaca Muerta Formation. The evolution of the transgression can be subdivided into: (1) onset of the TST, where rising sea level induced a rising groundwater table that generated a negative sediment budget and facilitated liquefaction and early stabilization of the Quebrada del Sapo eolian deposits; (2) beach sediments (F1) accumulated above a sharp to erosive maximum regressive surface due to damp conditions and episodic marine flooding; (3) early Tithonian extension induced faulting of the beach and eolian deposits underneath; (4) an embayed coastline developed and microbial mats established (F2); (5) a low-energy, proximal bay with evidence of condensation and winnowing formed above fair-weather wave base (F3); (6) a distal-bay setting characterized by sandy concentrated density flows and storms developed under brackish-water conditions (F4); and (7) distal siliciclastic basin hemipelagic sedimentation established, recording deposition under oxygen-deficient conditions (F5) and showing the maximum flooding surface at the top.

Because a transitional marginal-marine facies association is fairly well-developed, a rapid transgression of the Vaca Muerta Formation is postulated in contrast to previous hypotheses favouring a catastrophic flooding of the eolian succession. Modern and ancient studies of eolian to marine transitions suggest three types of transgressions that can be distinguished with respect to timing: (i) *catastrophic* – abrupt filling of basins after sill or dam break; (ii) *rapid* – fast sea-level rise events as the Holocene flooding after the Last Glacial Maximum; and (iii) *gradual* – expressed by stacked parasequences documenting punctuated shoreline migration and producing interbedded eolian and marine deposits. Modern estuarine sedimentation rates suggest that the embayment succession may have accumulated in a time span of 10^4 to 10^5 yr, supporting the rapid transgression hypothesis. At such high rates of sea-level rise, eolian deposits flooded during low-energy transgressions may record a thin marginal-marine succession with the eolian landscape preserved below. For the Vaca Muerta Formation, however, the eustatic contribution to relative sea-level rise was relatively small as indicated by the global eustatic sea-level chart and, therefore, thermal and tectonic subsidence played a major role.

Acknowledgements

We thank to Martin Parada, Claudio García, Camila García, Debora Campetella, and the Painemilla family, who offered exceptional support in the Picún Leufú village during field work. We also thank M. Cevallos (CGC), who shared his ideas and provided enormous feedback to the manuscript, and H. Leanza (Universidad Nacional de La Plata), who helped in the determination of bivalves. Valuable comments by Sedimentology reviewers A. Argüello Scotti and J.P. Rodriguez-López, and Associate Editor G.D. Veiga significantly improved the manuscript. This work was financially supported by the Natural Sciences and Engineering Research Council of Canada (NSERC) Discovery Grants 311727–20, PI-UNRN 2016 40-A-468 and PUE 0031CO to JJP, PI-UNRN 2017 40-A-616 and PIP CONICET 2017 11220170100129CO to NBC, 2016 Student Research Grant from Society for Sedimentary Geology (SEPM), 2016 and 2018 Research Grants from the Geological Society of America (GSA), and 2016 Grants-in-Aid Program of the American Association of Petroleum Geologists (AAPG), and 2017 International Association of Sedimentologists (IAS) post-graduate grant. Field work of AW was financially supported by the Swiss National Fund (grant 200021-169042/1). EP thanks to FINEP, CNPq and FAPERJ to support the Laboratório de Estratigrafia Química e Geoquímica Orgânica (LGQM).

TRANSITION

Chapter 2 is focused on the transition between the Quebrada del Sapo Formation and the Vaca Muerta Formation at the basin margin location in order to construct a depositional model of this transgressive event. Chapter 3 consists of a sedimentological, ichnological, and sequence stratigraphic analysis of the complete succession of the Vaca Muerta Formation at the same basin margin area. This study characterizes sedimentary processes in a mixed clinoform system, highlighting the role of wave-influenced hyperpycnal flows in transporting sand towards distal, basinal locations.

CHAPTER 3: BOTTOMSET AND FORESET SEDIMENTARY PROCESSES IN THE MIXED CARBONATE-SILICICLASTIC UPPER JURASSIC-LOWER CRETACEOUS VACA MUERTA FORMATION, PICÚN LEUFÚ AREA, ARGENTINA

Paz, M., Ponce, J.J., Buatois, L.A., Mángano, M.G., Carmona, N.B., Pereira, E., and Desjardins, P.R. (2019). Bottomset and foreset sedimentary processes in the mixed carbonate-siliciclastic Upper Jurassic-Lower Cretaceous Vaca Muerta Formation, Picún Leufú Area, Argentina. *Sedimentary Geology*, 389, 161-185. doi: 10.1016/j.sedgeo.2019.06.007

Keywords: Wave-influenced hyperpycnal flows, bioturbation, Neuquén Basin, fine-grained systems, unconventional reservoirs

Abstract

The Upper Jurassic-Lower Cretaceous Vaca Muerta Formation at the Picún Leufú area constitutes bottomset and foreset marine deposits comprising open bay, siliciclastic basin and mixed carbonate-siliciclastic shelf facies. Detailed sedimentological, ichnological and sequence stratigraphic analysis of six stratigraphic sections allows establishing two depositional sequences. Depositional Sequence 1 (DS1) begins with lowstand eolian deposits included in the Quebrada del Sapo Formation, and continues with thin, retrograding, transgressive open bay facies of the Vaca Muerta Formation encompassing beach, bay margin, proximal bay and distal bay facies. Above the transgressive deposits, the regressive hemicycle of DS1 consists of bottomset deposits representing a siliciclastic basin facies association. Lobe and lobe fringe hyperpycnal flow sedimentation alternated with hemipelagic basinal deposition in an oxygen-deficient environment. A relative sea-level fall generated a sequence boundary, which coincides with an angular unconformity that marks the base of Depositional Sequence 2 (DS2). This sea-level fall triggered the formation of an extensive lowstand channel-fill and lobe complex at the base of the slope, followed by retrogradational lobe facies during the subsequent transgression. The regressive hemicycle of DS2 represents foreset mixed carbonate-siliciclastic shelf facies, forming a slope mud belt and slope sand bodies. Near the top, sedimentation in a foreset-topset transition resulted in the accumulation of bioturbated mixed slope and sandy shoal deposits. Sand bars and lagoonal

facies occur on top of all sections and are truncated by a sequence boundary. The combined analysis provides insights into the sedimentary processes affecting bottomset and foreset deposition, underscoring the role of wave-influenced hyperpycnal flows, and the effect on organic matter dilution in one of the most important unconventional reservoirs from Argentina.

3.1 Introduction

Clinoform-shaped deposits are found in deltas, shelves and carbonate environments, and their analysis aids to identify sea-level variations which in turn are key for sequence stratigraphic interpretations (Steel and Olsen, 2002; Helland-Hansen and Hampson, 2009). Systems showing clinothems (i.e. clinoform-shaped rocks) typically encompass three distinctive depositional areas: topset, foreset and bottomset (Gilbert, 1885; Bates, 1953; Pirmez *et al.*, 1998; Steel and Olsen, 2002; Swenson *et al.*, 2005; Patruno *et al.*, 2015). The Upper Jurassic-Lower Cretaceous Vaca Muerta Formation of the Neuquén Basin, Argentina, consists of mudstone, marl and limestone representing a mixed carbonate-siliciclastic shelf showing well-developed bottomset to foreset strata, overlain by topset carbonate deposits of the Picún Leufú Formation. This unit shows an intermediate paleogeomorphology varying between sloping foreset, rimmed shelves and slope-absent ramps (see Williams *et al.*, 2011). Mitchum and Uliana (1985) highlighted the importance of basin, slope and shelf positions as distinctive depositional areas of the Vaca Muerta Formation comparable to bottomset, foreset and topset areas. Later, several workers continued differentiating these segments for sequence stratigraphic interpretations (e.g. Reijenstein *et al.*, 2014; Domínguez *et al.*, 2014; Desjardins *et al*., 2018), incorporating new techniques (Zeller, 2013; Zeller *et al.*, 2014, 2015a) and recognizing their plain-view geometry (Domínguez *et al.*, 2017). All of these efforts are useful for understanding depositional environments and sedimentary processes in each segment of the depositional system.

Several studies focused on the most prolific Central Neuquén Basin area (González *et al.*, 2018 and references therein), where carbonate-rich facies were deposited. In contrast, siliciclastic-dominated facies occur in the Picún Leufú area, where well-exposed outcrops of the Vaca Muerta-Picún Leufú mixed system occur. The Picún Leufú area is located in the NW area of the Picún Leufú depocenter (Fig. 3.1), comprising a distinctive sub-basin located at the south of the east-west trending Huincul Ridge structural system that divides the Neuquén Basin at its 39°S latitude.

An east-west anticline exposes the clinoform geometries of the formation and represents an exceptional opportunity to study the relationship between foreset and bottomset sedimentary facies in mixed depositional environments. The objective of this study is to integrate the sedimentological, ichnological, and sequence stratigraphic datasets of the Vaca Muerta Formation in the Picún Leufú area, to construct a depositional model. The proposed model has implications for understanding bottomset and foreset sedimentary processes, with a particular emphasis on the importance of wave-influenced hyperpycnal flows for bottomset sedimentation and organic matter dilution.

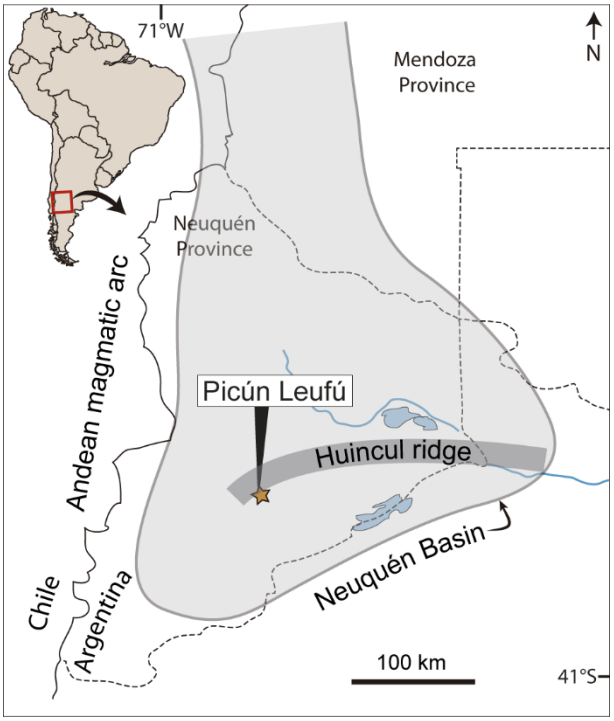

Fig. 3.1: General map showing location of the study area.

3.2. Geological setting

The Neuquén Basin constitutes a triangular-shaped basin located in western-central Argentina, bounded by cratonic areas at the northeast and southeast margins and by the Andean magmatic arc at the west. The stratigraphic record of this basin consists of approximately 7000 m of Jurassic and Cretaceous strata deposited since Late Triassic-Early Jurassic times (Arregui *et al.*, 2011). Tectonics controlled basin development, and its evolution can be subdivided in three different

stages, namely syn-rift, back-arc (post-rift) and foreland stage (Howell *et al.*, 2005). The syn-rift phase occurs during the Late Triassic to Early Jurassic (Gulisano, 1981; Carbone *et al.*, 2011). During the Early Jurassic, subduction in the active western margin of Gondwana generated a magmatic arc (Mpodozis and Ramos, 2008) and a subsequent shift to a back-arc basin stage. Since this time and up to the Early Cretaceous, alternating marine and continental sedimentation as a response to relative sea-level fluctuations was recorded by the Cuyo, Lotena and Mendoza groups. A Late Cretaceous compressional tectonic regime led to the closure of the connection with the Pacific Ocean and the establishment of the foreland stage (Ramos and Folguera, 2005; Tunik *et al.*, 2010).

The Vaca Muerta Formation comprises upper lower Tithonian to lower Valanginian marine deposits of the Mendoza Group (Stipanicic *et al.*, 1968) and records one of the back-arc stage transgression pulses of the Pacific Ocean over continental deposits (Leanza *et al.*, 2011). It is mainly composed by mudstone, marl and limestone that are commonly referred to as black shales due to their high organic matter content (3-8 % TOC with upper values of 10-12%, Uliana *et al.*, 1999). The Vaca Muerta Formation is grouped into the Lower Mendoza Mesosequence (Fig. 3.2, Legarreta and Gulisano, 1989), a sequence stratigraphic subdivision bounded at the base and top by the intra-Malmic and intra-Valanginian unconformities, respectively. This mesosequence starts with the establishment of the Tordillo Formation continental deposits and their lateral equivalents, which are covered by the Vaca Muerta Formation offshore deposits (Legarreta and Gulisano, 1989). At the top, the Vaca Muerta Formation has a transitional and diachronic contact with the overlying nearshore deposits of the Quintuco Formation and their lateral equivalents, such as the Picún Leufú Formation (Legarreta and Gulisano, 1989). The intra-Valanginian unconformity marks the end of the Lower Mendoza Mesosequence by a relative sea-level fall (Gulisano *et al.*, 1984).

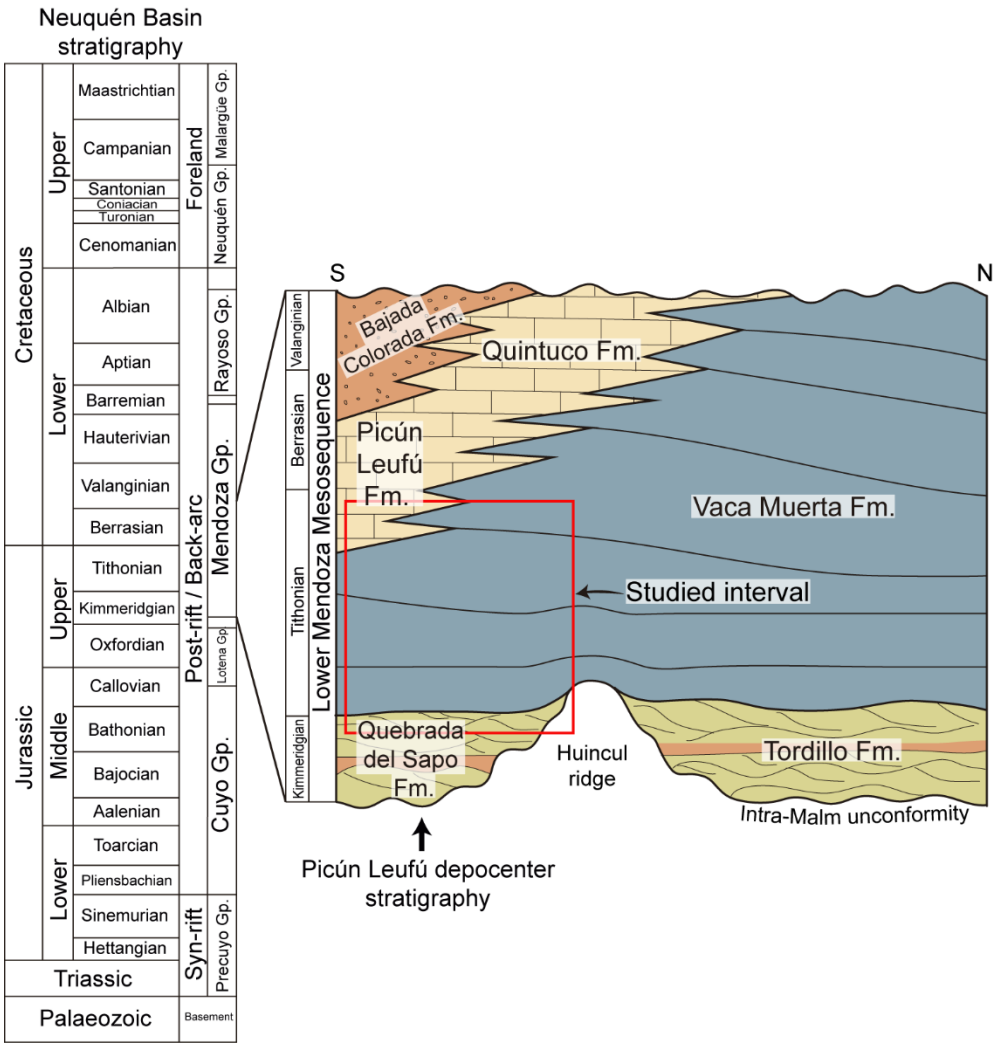

Fig. 3.2: Neuquén Basin and Picún Leufú depocenter stratigraphy, with an S-N section of the Lower Mendoza Mesosequence locating the studied interval. Modified from Howell *et al.* (2005).

3.2.1. The Picún Leufú anticline and Quebrada del Sapo areas

The Picún Leufú study area comprises the northwestern part of the Picún Leufú depocenter and the westernmost edge of the Huincul ridge system (Fig. 3.1). The area shows the convergence of two Huincul ridge structures: a south-verging, east-west anticline affecting the Cuyo, Lotena and Mendoza groups, namely the Picún Leufú anticline, and a NNE-oriented ravine associated with the Sierra de Chacaico anticline, known as Quebrada del Sapo (Fig. 3.3).

The stratigraphy of the Lower Mendoza Mesosequence in the study area is represented by the Quebrada del Sapo, Vaca Muerta and Picún Leufú formations (Fig. 3.2). The Quebrada del Sapo Formation (Digregorio, 1972) is regarded as Kimmeridgian in age based on its

lithostratigraphic correlation with the Tordillo Formation (Veiga and Spalletti, 2007), although evidence of an unconformity between these two units has been suggested, indicating that the Quebrada del Sapo Formation may be younger (Zavala *et al.*, 2008). Sedimentological and stratigraphic studies indicate that this formation consists of conglomerate, sandstone and mudstone deposited in fluvial, eolian (Veiga and Spalletti, 2007) and lacustrine systems (Zavala *et al.*, 2005).

The Vaca Muerta Formation overlays the Quebrada del Sapo Formation by a sharp to erosive transgressive surface. The contact between the Vaca Muerta and the overlying Picún Leufú formations is gradational. An early Tithonian-early Berrasian age based in ammonite zones has been assigned for this system in the Picún Leufú area (Leanza and Hugo, 1977).

Several sedimentological and sequence stratigraphic studies focusing on different intervals of these two lithostratigraphic units have been conducted in this area (Leanza, 1973; Spalletti *et al.*, 2000; Freije *et al.*, 2002; Zavala and Freije, 2002; Armella *et al.*, 2007; Zeller, 2013; Massaferro *et al.*, 2014; Zeller *et al.*, 2014, 2015b; Ponce *et al.*, 2015, 2016; Krim *et al.*, 2017; Otharán, 2020). Summarizing all the previous studies, the Vaca Muerta and Picún Leufú formations constitute a mixed carbonate-siliciclastic system, the first one being the seaward siliciclastic equivalent of the latter. Initially Spalletti *et al.* (2000) suggested the development of two shallowing-upwards sequences of a tidally-influenced siliciclastic-carbonate system. Zeller (2013) interpreted this interval as a mixed carbonate-siliciclastic succession with the Vaca Muerta Formation comprising one third-order transgressive-regressive succession (Massaferro *et al.*, 2014; Zeller *et al.*, 2015b). Otharán (2020) emphasized siliciclastic sedimentation by turbidity currents and hyperpycnal flows at slope and offshore positions, with the development of two third-order sequences. The last interpretation implies a siliciclastic shelf and a mixed ramp arranged in two low-frequency transgressive-regressive sequences (Krim *et al.*, 2017). These papers added plenty of sedimentological information to the study area, yet the hyperpycnal deposits are still poorly documented.

The Picún Leufú anticline records successive pulses of growth since the Early Jurassic and up to the Early Cretaceous, represented in outcrop by growth unconformities and thickness changes (Freije *et al.*, 2002; Zavala and Freije, 2002; Naipauer *et al.*, 2012). Kimmeridgian to middle Tithonian (lower *A. proximus* ammonite zone of Parent *et al.*, 2011) syn-sedimentary deformation affected from east to west the Lower Mendoza Mesosequence in the Picún Leufú anticline, whereas in Quebrada del Sapo the strata is almost undeformed. Deformational events

caused normal faults and progressive unconformities within this mesosequence. The syn-sedimentary normal faults crosscut the uppermost part of the Quebrada del Sapo Formation dune deposits and up to ~50 m of the lowermost Vaca Muerta Formation. The progressive unconformity represents a deformational event showing a gradual decrease in dip in the Quebrada del Sapo Formation and the lowermost ~80-120 m of the Vaca Muerta Formation. On top of the progressive unconformity, an angular unconformity occurs within the Vaca Muerta Formation, represented by change of dips of 15°-40° in the strata below, to 7°-30° in the strata on top, and suggesting a dip difference of 10° in sections 4, 3 and 2, to 23° near section 5 (Fig. 3.4). Dips on top of the unconformity remain constant, indicating the end of the progressive unconformity affecting the anticline. A post-sedimentation deformational event is responsible for an additional ~7-30° tilting in the whole succession, showing its maximum expression to the east of the anticline and decreasing towards the west (Quebrada del Sapo).

3.3. Methodology

Sedimentological and ichnological analysis was carried on in six stratigraphic sections of the Vaca Muerta Formation (230-330 m) and part of the Picún Leufú Formation (~30 m). Two of the six bed-by-bed stratigraphic sections were measured in Quebrada del Sapo and four in the Picún Leufú anticline (Fig. 3). Twenty five samples were taken to analyze lithofacies in thin section under petrographic microscope. Total organic carbon (TOC) analysis (52 samples) were performed using LECO SC 632 at the Laboratório de Estratigrafia Química e Geoquímica Orgânica of the Universidade do Estado do Rio de Janeiro, Brazil. The fine-grained siliciclastic and carbonate rocks were classified according to Lazar *et al.* (2015b) and Wright (1992), respectively. The ichnological analysis consists of the description of ichnotaxa and assessment of ethologies, ichnodiversity and degree of bioturbation (from 0 to 6, after Taylor and Goldring, 1993). For the sequence stratigraphic analysis, Google Earth imagery was analyzed together with a published seismic line parallel to our section and distant ~10 km SE (Zeller, 2013; Massaferro *et al.*, 2014) to understand stratal geometry and to visualize large-scale stratal terminations.

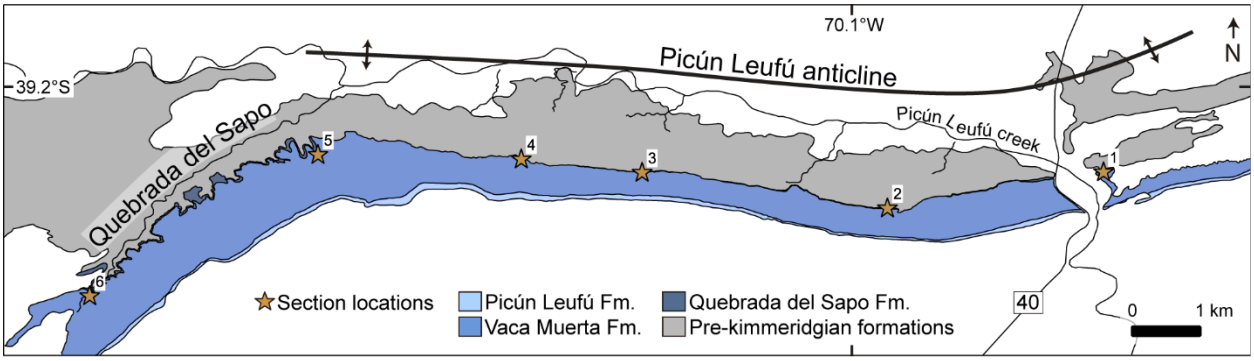

Fig. 3.3: Map of the study area showing location of the measured sections.

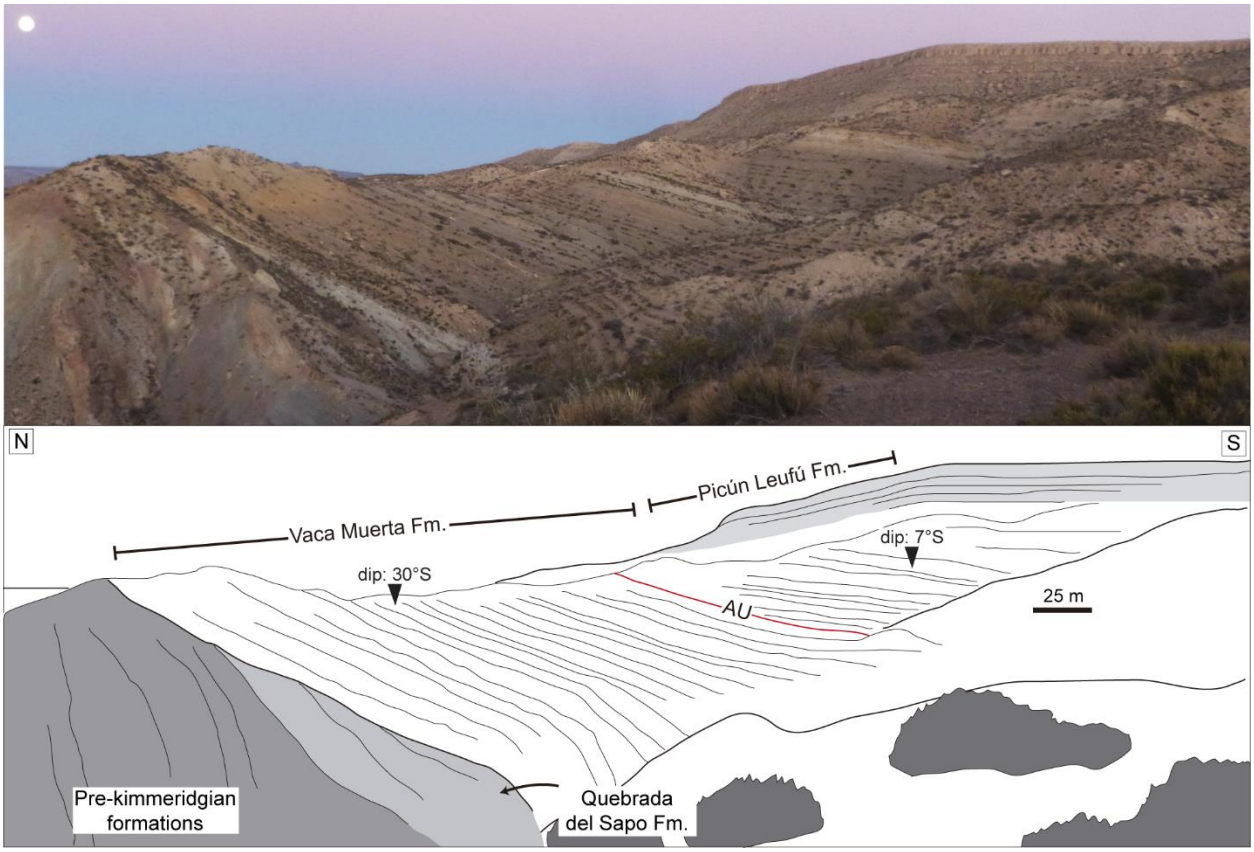

Fig. 3.4: Angular unconformity (AU) observed in areas close to section 5 (see fig. 3.3 for location). Dip data shows angle and dip direction.

3.4. Sedimentary facies

Integration of sedimentological and ichnological information allowed recognition of twelve facies grouped into three facies assemblages (Table 3.1, Fig. 3.5). Facies assemblage A was extensively analyzed in Chapter 2; thus, a brief description is provided here.

3.4.1. Facies assemblage A (FAA)

3.4.1.1. Facies 1 (F1)

This facies consists of sharp-based, thin- to medium-bedded (3-20 cm-thick), low-angle cross-bedded to horizontal-bedded, medium-grained with minor fine-grained sandstone (Fig. 3.6A, B). Asymmetrical and symmetrical ripples are commonly seen on bedding planes. The low-angle cross-bedding shows dips towards ESE and WSW, and minor towards N and NE, whereas current ripples have paleocurrents towards S and WNW. A 10-30 cm-thick, interval of erosive-based, trough cross-stratified, medium- to minor coarse-grained sandstone is observed below the low-angle lithofacies, displaying a patchy distribution, and locally showing organic matter drapes. F1 locally shows water escape structures. F1 is 0.5-2 m thick, and has a large-scale tabular geometry. This facies occurs in the easternmost and in the Quebrada del Sapo sections, where the Quebrada del Sapo Formation eolian deposits shows the thicker succession.

F1 records sedimentation in a beach area associated with a shallow groundwater table. Low-angle cross bedding suggests low-relief bedforms that were later reworked into rippled surfaces by frequent tidal flooding (e.g. Fryberger *et al.*, 1990). The current ripples are produced by water-lain sedimentation, whereas the symmetrical ripples indicate wave reworking in a high water-table environment. The patchy trough cross-bedded sandstone reflects small subaqueous dunes generated during marine flooding (Kocurek, 1981). The water escape structures suggest soft-sediment deformation in water-saturated sands.

Table 3.1: Open bay, siliciclastic basin and mixed carbonate-siliciclastic shelf sedimentary facies of the Vaca Muerta Formation in the Picún Leufú area.

Facies	Bedding thickness	Geometry	Lithology	Sedimentary structures	Ichnology	Fossil content	Interpretation	Distribution in the section
F1: Beach	3-20 cm	Tabular	Medium-grained to minor fine- and coarse-grained sandstone	Low-angle cross-bedding to horizontal-bedding. Symmetrical and asymmetrical ripples on bedding surfaces. Local trough cross-bedding	Unbioturbated	-	Low-relief bedforms associated with tidal flooding in a high water table environment	At the base of the Formation, in areas with eolian deposits
F2: Bay margin	5-30 cm	Tabular	Bindstone	Wavy-crinkly lamination	Unbioturbated	Ammonites and bivalves	Bindstone accretion in stressed environments	At the Formation base, after the transgressive surface.
F3: Proximal bay	1-10 cm	Large-scale thickness variation	Medium mudstone, bioclastic wackestone and packstone	Wave ripples	Poorly-defined biodeformational structures (BI=4-6), crosscut by *Thalassinoides* isp.	Fragmented ammonite molds and bivalve shells	Wave reworking in a low-energy environment showing stressed conditions	At the Formation base or on top of facies F2, in a retrogradational succession
F4: Distal bay	5-20 cm	Large-scale	Medium mudstone, with minor medium-	Normal gradation in the sandstone	Highly bioturbated, displaying	Bivalve, ammonite and	Deposition below fair-weather wave base.	On top of facies F3, in a

		thickness variation	grained sandstone and tuff		*Thalassinoides* isp., *Palaeophycus tubularis* and *Teichichnus rectus* and biodeformational structures Ichnodiversity is low and bioturbation index is 2-3	gastropod shells	Intercalation of muddy tempestites and sandy concentrated density flow deposits	retrogradational succession
F5: Sediment-starved basin	1 m	Tabular	Carbonaceous-argillaceous fine mudstone to argillaceous medium mudstone, minor thin, massive fine mudstone	Parallel-lamination, slumps, sand dykes and syn-sedimentary faults	Unbioturbated	Pectinid bivalves, ammonites, plant debris and fish scales	Organic carbon enrichment due to low sedimentary input from hemipelagic and eolian deposition, minor buoyant plume deposition	Above facies F4, in bottomset areas
F6a: Hyperpycnal lobe fringe (sand-rich)	10-50 cm	Tabular to lenticular beds	Fine to very fine-grained sandstone	Structureless, some wave ripples, combined-flow ripples, parallel lamination, and minor current ripples	Unbioturbated	Plant debris	Hyperpycnal flows reworked by combined-flows	Encased in F6b, located in bottomset areas
F6b: Hyperpycnal lobe	1-10 cm	Tabular	Heterolithic successions of argillaceous	Structureless, minor ripple	Unbioturbated	Plant debris	Muddy hyperpycnal flow	Vertically and laterally associated

fringe (mud-rich)			coarse to fine mudstone, minor very fine-grained sandstone	cross-lamination			and lofting processes	with F6a and F7
F7: Hyperpycnal lobe	5-50 cm	Tabular beds	Medium to fine-grained sandstone	Structureless, parallel lamination, combined-flow ripples, and HCS. Water escape structures occur	Unbioturbated	Plant debris	Hyperpycnal flows reworked by combined flows	Occur in bottomset areas, intercalated with minor facies F6a or F6b
F8a: Channel-fill complex	0.1-3 m	Tabular to lenticular bodies with lateral accretion	Medium-grained sandstone	Structureless, parallel-bedding, trough cross-bedding, HCS, combined-flow ripples, and minor current and climbing ripples and sigmoidal cross-stratification	Unbioturbated	Bivalve bioclasts	High-energy bedload sedimentation in a meandering, subaqueous sandy channel	Occurs in bottomset to foreset areas, in a landward position
F8b: Overbank	5-30 cm in the sandstone and 0.5-1 cm in the heterolithics	Tabular	Fine-grained sandstone and mud-rich heterolithic successions of very fine-	Massive and ripple cross-lamination	Unbioturbated	-	Crevasse splay deposition and suspension fallout sedimentation	Occurs in bottomset to foreset areas, in a landward position

			grained sandstone and argillaceous fine mudstone				from lofting clouds	
F9a: Slope mud belt	5-10 cm	Tabular	Argillaceous fine mudstone, minor very fine-grained sandstone	Silt laminae, slumps, sand dykes and syn-sedimentary faults	Unbioturbated	Bivalve and ammonite shells	Higher siliciclastic input by mud redistribution processes and mass movements	Lower and middle foreset areas
F9b: Mixed slope	1-10 cm	Tabular	Intraclastic wackestone, minor calcareous fine-grained sandstone	Structureless	Biodeformational structures	Bivalve and ammonite shells	Mixed sedimentation in an oxic environment	Upper foreset areas
F10: Slope sand bodies	0.1-3 m	Lenticular to tabular	Calcareous fine-grained sandstone and minor intraclastic wackestone	Structureless, locally parallel lamination and low-angle cross stratification	Unbioturbated	Bivalve shells	Spillover lobes	Foreset areas
F11a: Sandy shoal	1-3 m in the sandstone and 0.1-1 m in the wackestone and packstone	Tabular	Calcareous sandstone, wackestone and packstone	Structureless, minor low-angle cross-bedding and wave ripples	Biodeformational structure, some *Thalassinoides* isp. and *Palaeophycus tubularis*	Bivalve and ammonite shells	Wave reworking and sand shoal progradation in an oxic environment	Foreset to topset transition

F11b: Sand bar complex	1-5 m	Tabular to large-scale lenticular	Rudstone, floatstone and calcareous coarse- to medium-grained sandstone	Planar to trough cross-stratification, minor ripple cross-lamination	Escape traces	Bivalve, gastropod and ammonite shells	Subaqueous dune migration in a high energy environment	Top of the sections
F12: Lagoon	mm-thick	Tabular	Medium-grained sandstone	Structureless to parallel-lamination	Unbioturbated	Bivalve bioclasts	Protected, stressed environment	Topset to foreset transition

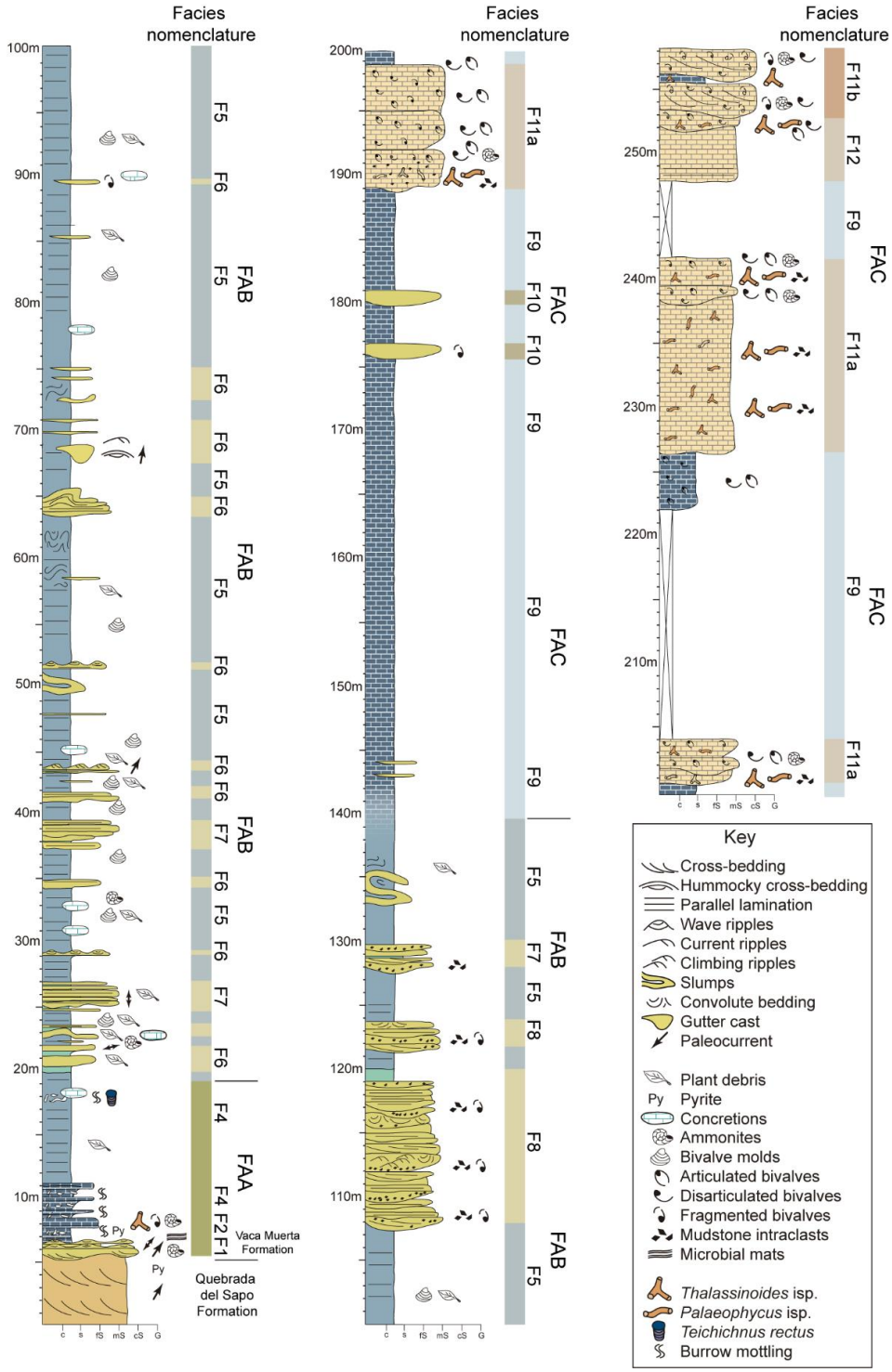

Fig. 3.5: Westernmost stratigraphic section (number 6 in Fig. 3.3) of the Vaca Muerta Formation, showing the sedimentary facies (see text) grouped into open bay (FAA), siliciclastic basin (FAB) and mixed carbonate siliciclastic shelf (FAC) facies assemblages.

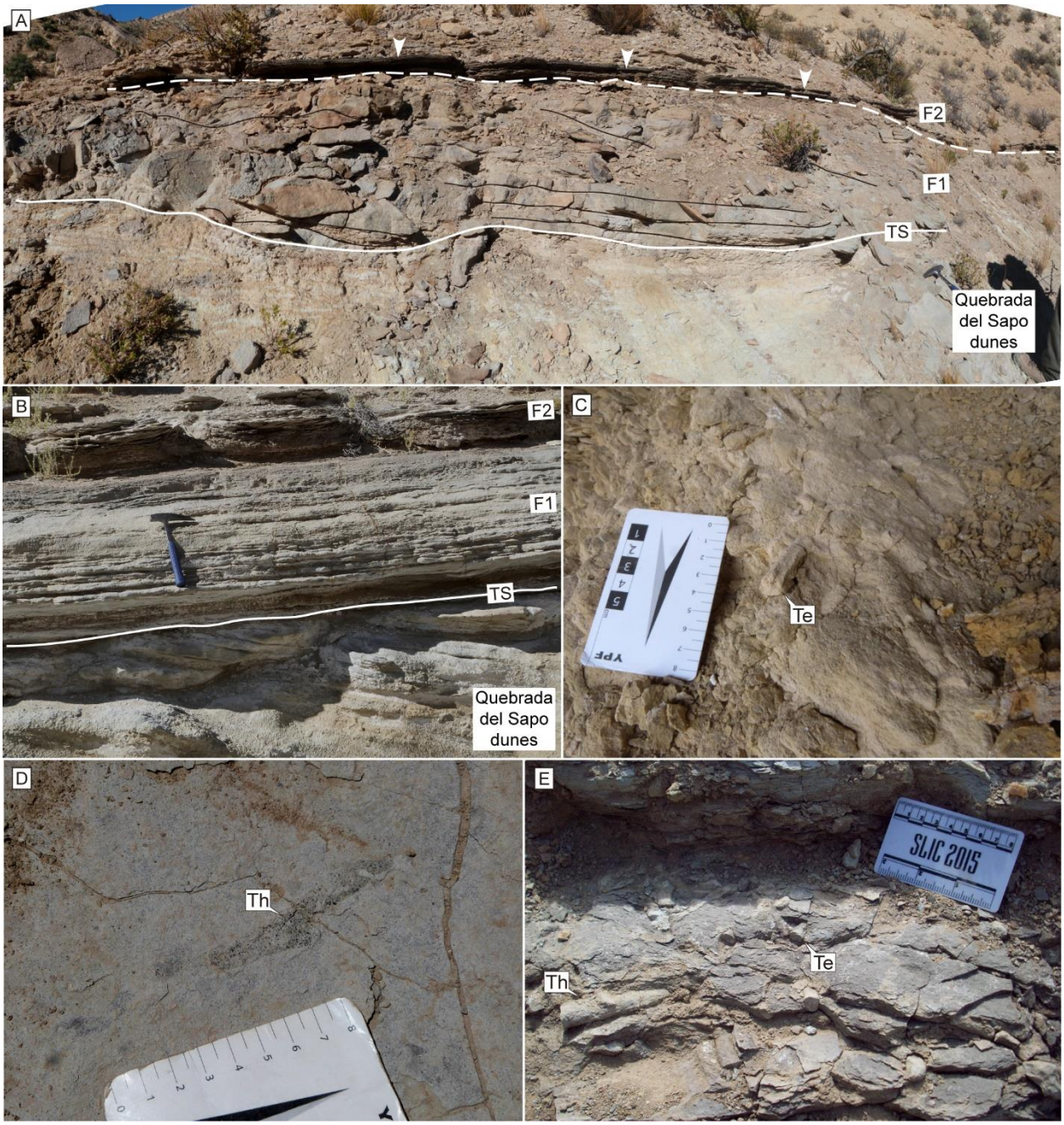

Fig. 3.6: Open bay facies (FAA) of the transgressive basal sequence. A) Microbial bindstone (white arrows) of the bay margin facies (F2) overlying the Quebrada del Sapo Formation dune deposits by a Transgressive Surface (TS T1). Note the deformation in the eolian deposits. B) Wave-rippled sandstone of the proximal bay facies (F3), overlying the Quebrada del Sapo Formation dunes. C) *Teichichnus rectus* (Te) in highly bioturbated F3. D) *Thalassinoides* isp. (Th) passively infilled by coarse-grained sandstone and e) *Thalassinoides* isp. and *Teichichnus rectus* of the second trace fossil association, in distal bay facies (F4).

3.4.1.2. Facies 2 (F2)

This facies consists of a bindstone interval of 5-30 cm thick (Fig. 3.6A, B). TOC is high (mean=20.15%, N=2). In thin section, the bindstone shows an alternation of sandstone-rich and organic matter laminae with a wavy to lenticular pattern. The organic matter laminae contains grains displaying a preferential orientation of their major axes, which are arranged parallel to the pseudo-lamination. Ammonite molds and bivalve shells occur intercalated in the bindstone. This facies overlies the Quebrada del Sapo eolian dune deposits or F1 by a sharp surface.

Facies 2 resulted from microbial mat vertical accretion in a low-energy, bay margin area subject to stress conditions. The laminae showing wavy to lenticular pattern representing a wavy-crinkly laminated structure (Schieber, 1986, 2007) and the oriented grain texture and pyrite in the lamination indicate a microbial mat origin (Noffke, 2010).

3.4.1.3. Facies 3 (F3)

This facies is composed by cycles of thin-bedded (1-10 cm), carbonaceous-calcareous medium mudstone, bioclastic wackestone and packstone. Symmetrical ripples are locally preserved on top of the cycles. TOC content is moderate (mean=2.01%, N=2), with one high value of 17%. Locally, thin-bedded (1-5 cm), muddy heterolithic successions occur. Wackestone and packstone are composed of well-preserved to partially fragmented, bivalve, ammonite, and gastropod shells. Poorly defined biodeformational structures are crosscut by *Thalassinoides* isp. showing sharp, unlined walls (Fig. 3.6D). *Thalassinoides* is passively infilled by medium- to coarse-grained sandstone. Bioturbation instensity is extremely variable (BI-1-6). F3 shows a high lateral variation of thickness (1-2 m), and overlies the Quebrada del Sapo Formation where F2 and F1 are absent.

F3 represents sedimentation in a proximal bay environment, above fair-weather wave base. Symmetrical ripples and bioclastic wackestone and packstone suggest wave reworking and sediment bypass associated with transgressive condensation. The *Thalassinoides* isp. suite crosscutting the biodeformational structures was emplaced under firmground conditions evidenced by the sharp, unlined walls and passive infill. The coarse-grained sandstone infilling burrows was probably bypassed from this area of high-energy to the distal bay area (F4), where sandstone beds are preserved.

3.4.1.4. Facies 4 (F4)

This facies consists in carbonaceous medium mudstone showing minor, 5-20 cm-thick, sharp- to erosive-based, grayish-green mudstone, medium-grained sandstone and tuff beds. TOC content is moderate (mean=2.37%, N=2). The background carbonaceous mudstone displays abundant 0.2-1 mm-long, oval to round-shaped pellets in the matrix, whereas the grayish-green mudstone shows pellets at the base. The sandstone shows normal gradation with organic-rich intraclasts located at the base. Ammonite, bivalve and gastropods shells are minor components of the mudstone. This facies is moderately bioturbated (BI 2-3), displaying biodeformational structures. Discrete trace fossils, such as *Thalassinoides* isp., *Palaeophycus tubularis* and *Teichichnus rectus,* can be observed when sediment contrast provided by a change in mudstone color, sandstone or tuff intervals occur (Fig. 3.6C, E). This facies also has variable thickness (2-10 m).

This facies records deposition in a distal bay environment with medium mudstone deposits indicative of low-energy, hemipelagic sedimentation. Deposition below the fair-weather wave base promoted preservation of sandstone and grayish mudstone beds probably representing sandy concentrated density flows (e.g. Eschner and Kocurek, 1986) and muddy tempestites bypassed from the higher energy coast, respectively. The trace fossil content shows the establishment of suspension feeders and passive predators with minor deposit feeders (Buatois and Mángano, 2011).

3.4.1.5. FAA Interpretation

The absence of proximal, storm-generated shoreface deposits indicates a low-energy, retrograding coast developing an open bay succession (MacEachern and Gingras (2007). An absence of bay mouth facies suggests the deposits can be assigned to an open bay rather than to a restricted bay (MacEachern and Gingras, 2007).

3.4.2. Facies assemblage B (FAB)

3.4.2.1. Facies 5 (F5)

F5 is composed by thick-bedded (1 m) cycles grading from parallel-laminated carbonaceous-argillaceous fine mudstone (Fmud) to argillaceous medium mudstone (Mmud, Fig. 3.7A). Rare isolated, very thin (0.5-2 cm) massive fine mudstone beds also occur (Fig. 3.7B). The parallel-laminated mudstone shows a discontinuous, anastomosing, wrinkle lamination produced by kerogen seams (Fig. 3.7C). TOC content in the parallel-laminated mudstone is high (0.03-12.20%, mean=3.24%, N=31), compared with the massive fine mudstone (1.18% of TOC). Soft-sediment deformation structures include slumps, sand dykes and syn-sedimentary faults. Oblate-shaped, 20 to 70 cm long carbonate concretions are observed in the lower and middle part of the sections. The fossil content mainly consists of high- to moderate-density accumulations of flattened bivalve shells occurring on bedding planes. Pectinid bivalves (*Huncalotis*; H. Leanza, written communication) are found as shell pavements and include both a widespread small-sized (2-5 mm long) population and a more localized one of larger (1-2 cm long) bivalves. Ammonites, plant debris and fish scales are minor constituents. Ammonites are well-preserved to fragmented, with specimens up to 20 cm wide. Trace fossils are absent.

High amounts of organic matter and a relative absence of event, discrete beds suggest deposition in a sediment-starved basinal environment. Hemipelagic deposition dominated this area, with the organic matter provided by marine snow and silt derived by eolian input (Gabbott *et al.*, 2010). Occasionally, massive fine mudstone could represent buoyant plumes advected from the slope area, diluting organic matter content (e.g. Wright and Nittrouer, 1995). As the study area is located at a tectonically active zone at the time of deposition, soft-sediment deformation structures were probably triggered by seismicity, at the base of the slope. In thin section, the wrinkled lamination and bed contacts observed are not crosscut or disrupted by bioturbation structures, suggesting oxygen deficiency at bottom and interstitial waters. Bivalve shell pavements are abundant in some black shale successions, such as the Posidonia Shale of Germany, and may reflect short-term benthic colonization due to fluctuating oxygen conditions (Röhl *et al.*, 2001).

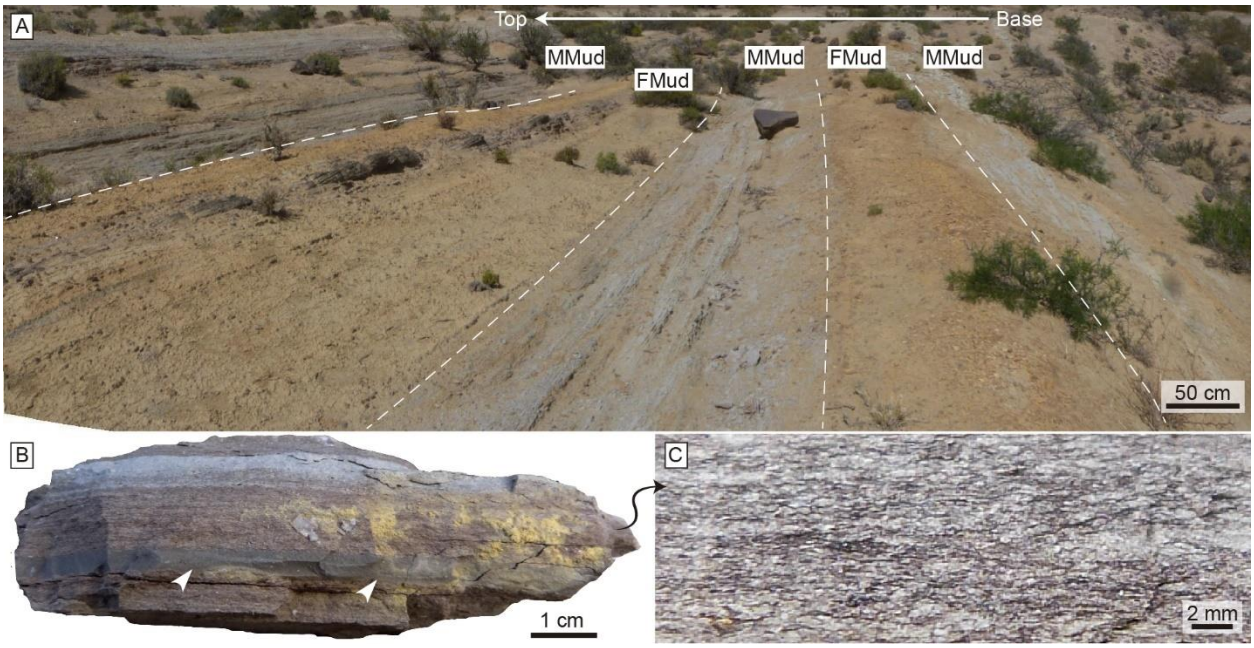

Fig. 3.7: Sediment-starved basin facies (F5), showing A) the fine (FMud) to medium mudstone (MMud) cycles. B) Rare massive fine mudstone intervals within the parallel-laminated mudstone. C) Close-up photograph of parallel-laminated mudstone displaying the kerogen seams (darker wrinkled laminae).

3.4.2.2. Facies 6 (F6)

This facies is composed by sharp- to erosive-based, medium-bedded (10-50 cm), fine- to very fine-grained sandstone (F6a, Fig. 3.8), and mud-rich heterolithic successions of thin-bedded (1-10 cm), massive, argillaceous coarse to fine mudstone (F6b, Fig. 3.9A). TOC content in the mudstone is low (0.18-0.99%, mean=0.48%, N=5). Although the sandstone is mostly massive, some sedimentary structures, including wave ripples (Fig. 3.8B, C), combined-flow ripples, parallel lamination, and minor current ripples, occur. Grooves are common at the base of the sandstone and within amalgamated sandstone delineating erosive surfaces. Paleocurrents from current ripples and grooves have two mean vectors, NNE-SSW and E-W (n=8). The sandstone contains chaotically distributed, 1-3 mm long plant debris (1-2 %, Fig. 3.8D) or concentrated together with minor rip-up mudstone clasts in discrete beds at the base (20-30 %). The coarse mudstone shows abundant, up to 2 cm long plant debris (30-50%), micas (5%), and deformed rip-up fine mudstone intraclasts (0-10%, Fig. 3.9B), whereas the fine mudstone contains smaller (1 to 0.5 mm long) plant remains (5-10%, Fig. 3.9C), which can show a plant-debris normal grading

from base to top. This facies occurs as alternations of tabular or lenticular beds showing F6a encased in F6b (Fig. 3.8A).

This facies is associated with sandy and muddy hyperpycnal flow sedimentation in a lobe fringe, basinal setting. Wave ripples and combined-flow ripples indicate oscillatory and combined wave oscillatory and unidirectional geostrophic flow reworking due to storm influence (Plint, 2010). Paleocurrent trends of current ripples (NNE) and groove casts (ENE-WSW) show a vector of transport parallel to the direction of clinothem progradation (NE). Plant debris in the sandstone and mudstone indicates an extrabasinal origin for these flows (Mulder and Chapron, 2011; Ponce and Carmona, 2011a, b; Zavala *et al.*, 2012), supporting a hyperpycnal flow origin. The sedimentary structures can be compared with the genetic facies model of hyperpycnal flows put forward by Zavala *et al.* (2011). Therefore, the massive fine-grained sandstone was formed by progressive aggradation from high-suspended load long-lived currents, whereas the minor parallel-laminated and ripple cross-laminated sandstone indicates traction processes. The coarse mudstone was produced by turbidity currents that reworked plant debris and unconsolidated fine mud from an early phase of deposition (Zavala and Arcuri, 2016). In addition, lofting occurs by negative buoyancy reversal of a hyperpycnal flow as a result of flow deceleration (Sparks *et al.*, 1993), generating the fine mud and sorting process of the smaller plant debris. Encasement of F6a within mud-rich F6b indicates a waxing to waning current showing its higher energy peak in the sandy F6a deposits.

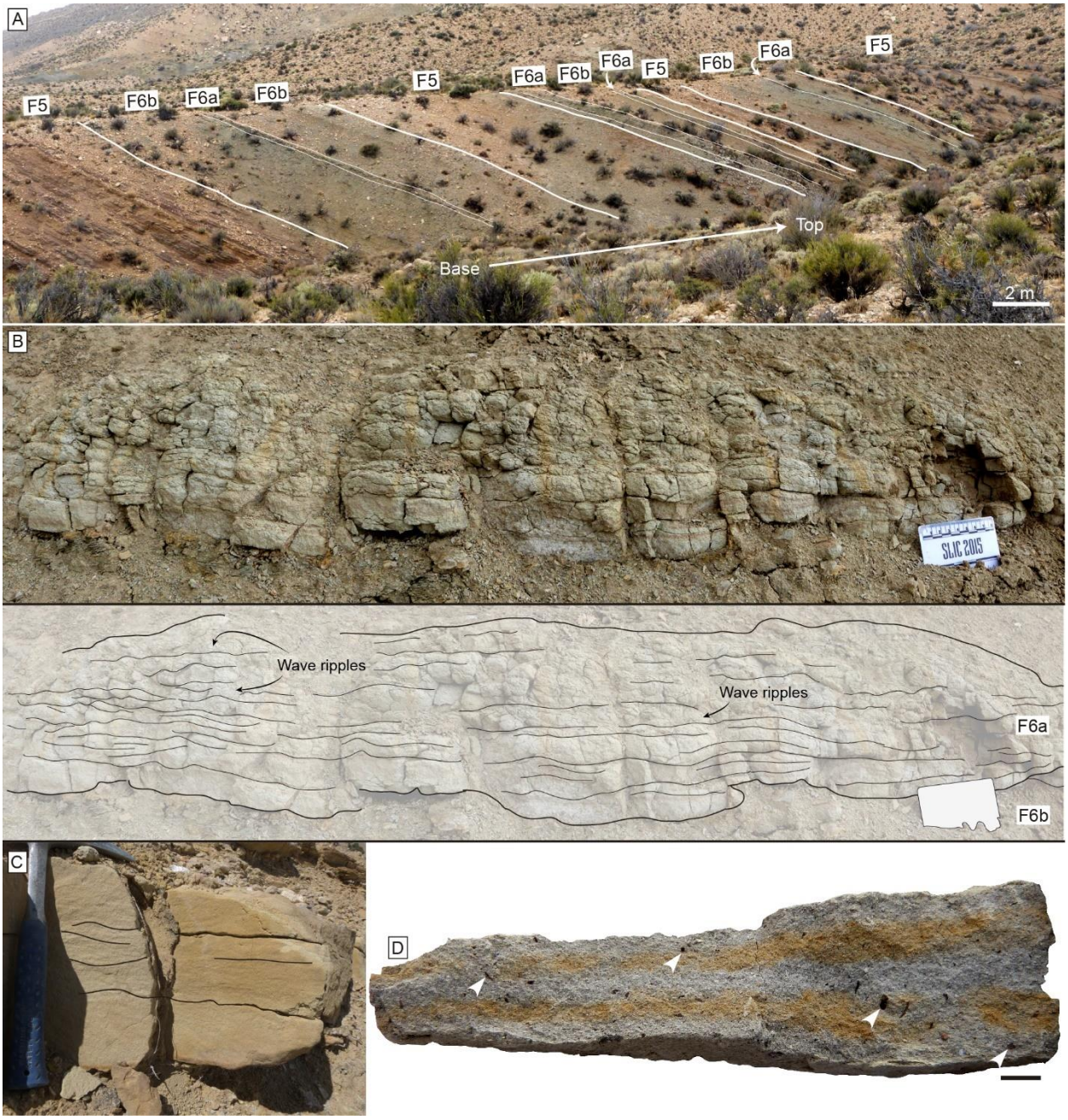

Fig. 3.8: Hyperpycnal lobe fringe facies (F6) of the basin facies assemblage (FAB). A) Outcrop appearance of lobe fringe facies, commonly intercalated with basin facies (F5). Sandy lobe fringe facies (F6a) occurs encased in thick packages of muddy lobe fringe facies (F6b). B, C) Wave-rippled sandstone of F6a, showing D) randomly distributed plant debris in the matrix (white arrows, scale bar is 1 cm.

Fig. 3.9: Mud-rich lithofacies of the hyperpycnal lobe fringe facies (F6b). A) Coarse and fine mudstone intercalations of F6b overlying sandy lobe fringe facies (F6a). Plant debris and rip-up mudstone clasts occur in the coarse mudstone (B, scale bar is 1 cm), whereas fine mudstone contains smaller plant material (C, white arrows).

3.4.2.3. Facies 7 (F7)

This facies comprises sharp- to erosive-based, medium- to thin-bedded (5-50 cm), medium- to fine-grained sandstone (Fig. 3.10A). The sandstone contains, in order of abundance, massive beds, parallel lamination, combined-flow ripples, and hummocky cross-stratification (HCS). Water escape structures also occur. Load casts and grooves are preserved at the base of the sandstone. Grooves exhibit paleocurrents trending N-S and ENE-WSW (n=2). The sandstone contains isolated and randomly distributed, 1-5 mm long plant debris, up to 10 cm wide rip-up mudstone clasts, and minor bivalve shell fragments. Discrete, high-concentrated layers of plant debris (30-40%) and mudstone clasts (30-40%) are also common (Fig. 3.10B, C), with plant debris delineating sandstone parallel lamination in some cases. This facies commonly occur grouped in bedsets, developing coarsening- and thickening-upward patterns at the base, and fining- and thinning-upward patterns at the top. Beds are tabular, with some swale and hummock geometries on the top. Intra-bed erosive surfaces delineated by mudstone clast breccias are also common. This facies is locally intercalated with thin intervals of facies 6.

This facies represents hyperpycnal flow sedimentation affected by combined-flow action (as indicated by combined-flow ripples and HCS) in a lobe setting. Deposition of massive and

parallel-laminated, plant debris-rich sandstone reflects the transition from relatively high to lower fallout rates that promoted plant debris trapping in the sandstone (Zavala *et al*., 2012). The mudstone-clast breccia indicates erosion and bedload deposition. Evidence of alternation between massive and parallel-laminated facies in the same interval and intra-bed erosive surfaces indicate fluctuations in the flow regime. Deposition from more concentrated density currents in comparison with the lobe fringe facies (F6) is indicated by the coarser grains, common occurrence of rip-up mudstone clasts, thicker sandstone lithofacies, and relative lack of lobe fringe muddy deposits (F6b). The thickening at the base and thinning at the top patterns of the bedsets can be explained by the shifting of the lobe depocentre at different scales (Prélat and Hodgson, 2013), generating intercalation of lobe and lobe fringe deposits.

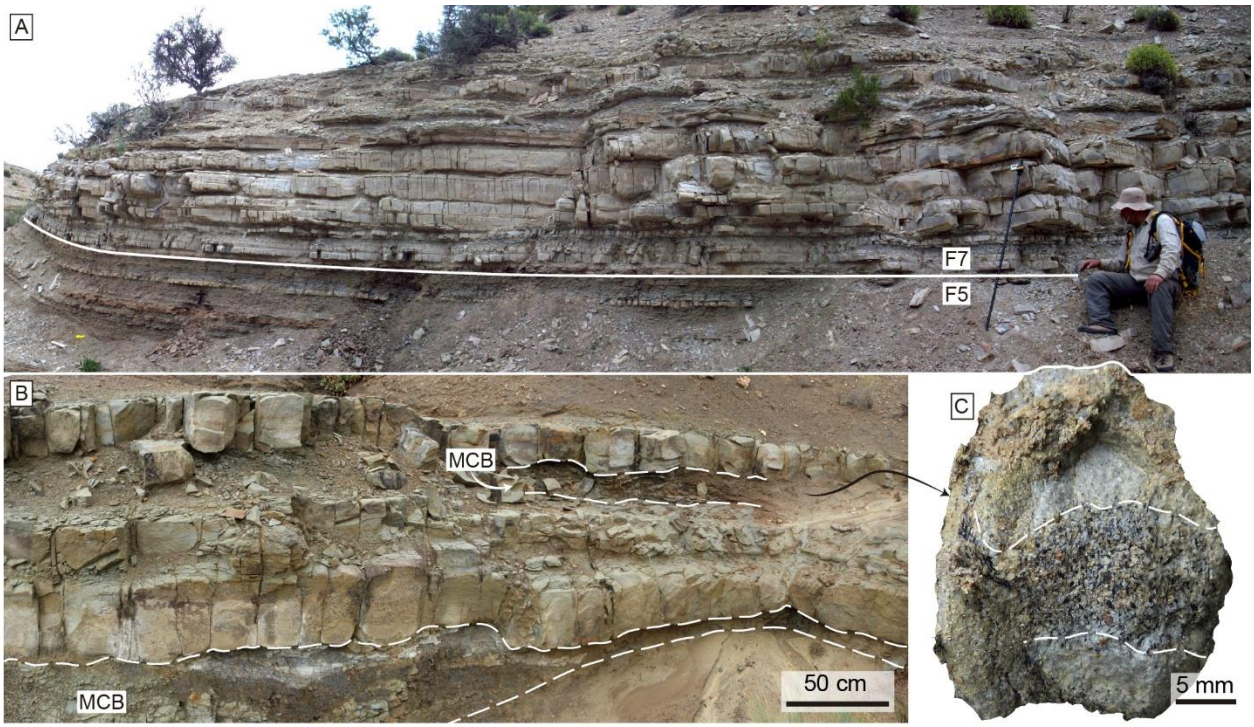

Fig. 3.10: A) Hyperpycnal lobe facies (F7) comprising massive to parallel-laminated fine-grained sandstones, overlying basin facies (F5). B) Lobe facies displaying mudstone-clast breccias (MCB) at the sandstone bases. C) Close-up view of high-concentrated plant debris layers that delineates lamination.

3.4.2.4. Facies 8 (F8)

This facies is composed by erosive-based, medium- to thick-bedded (0.1-3 m), medium-grained sandstone (F8a, Fig. 3.11A) and by thin- to medium-bedded (5-30 cm), fine-grained

sandstone and mud-rich heterolithic successions of very thin-bedded (0.5-1 cm), very fine-grained sandstone and argillaceous fine mudstone (F8b, Fig. 3.12B). Although massive beds are distinctive, sedimentary structures in the sandstone include parallel-bedding, trough cross-bedding (Fig. 3.11B) and HCS, combined-flow ripples, and minor current and climbing ripples and sigmoidal cross-stratification. The sandstone in the heterolithic succession shows ripple cross-lamination, with organic matter in the lamination (Fig. 3.12C). Large-scale water escape structures (Fig. 3.11A, C) and slumps are common in the otherwise massive beds. Bioclast and rip-up mudstone clasts occur at the base of the sandstone, forming mudstone-clast breccia that delineates bed contacts or isolated in the sandstone. The mudstone shows mm-thick medium- to fine-grained sand and organic matter lags. At an outcrop scale, F8a constitute tabular or lenticular bodies, the latter exhibiting lateral accretion (Fig. 3.12A). Minor gutter cast geometries also occur. These bodies are stacked forming 50 to 100 m wide and up to 12 m thick units. F8b is laterally and vertically associated with facies 8a.

This facies is interpreted as a meandering channel-fill complex (F8a) and overbank (F8b) subject to hyperpycnal flow sedimentation. Multiple erosive reactivation surfaces and rip-up mudstone clasts indicate high-energy bedload sedimentation and erosion in or at the channel base (Zavala *et al*., 2011). Deposition from dense cohesion-less suspension can generate liquefied flows with water escape structures (Mulder and Alexander, 2001). High amounts of massive beds and large-scale water escape structures indicate rapid deposition due to loss of flow capacity by a change in slope (slope break location) or by translation of the river plunge point (Lamb and Mohrig, 2009). HCS, combined-flow ripple, and gutter cast occurrence point towards a storm-influenced setting. Bypassing of the low-density turbidity cloud and/or erosion by the successive hyperpycnal flows prevented fine-grained sediment and plant debris accumulation. The fine-grained sandstone of F8b represents crevasse splays, whereas the heterolithic succession shows the combination of unidirectional traction structures in very fine-grained sandstone produced by turbidity currents that overtop the channel margins, and mudstone lithofacies interpreted as suspension fallout from lofting clouds developed adjacent to the channel. The sand and organic matter lags probably indicate the resuming of hemipelagic conditions characteristic of the basin facies (F5).

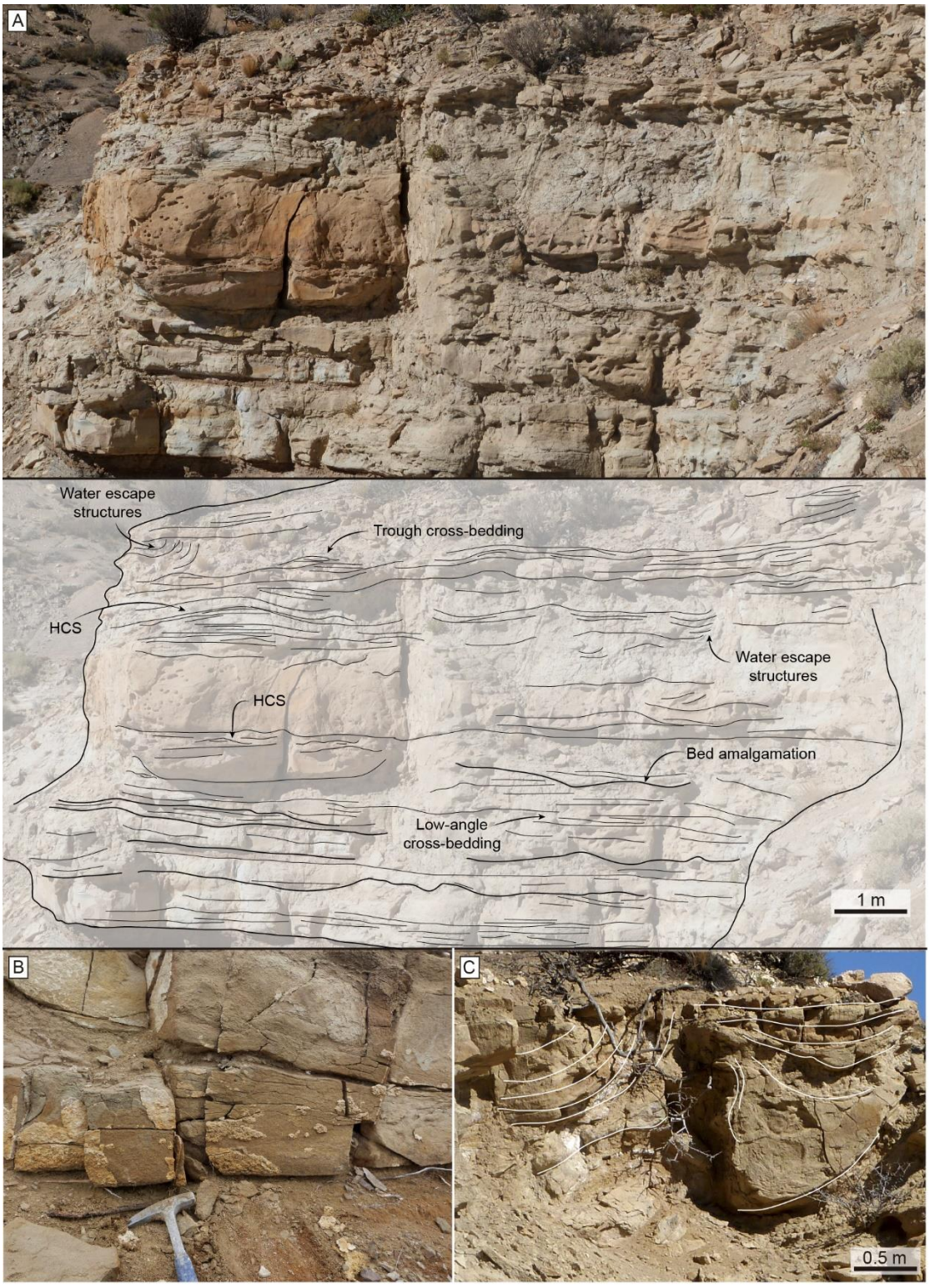

Fig. 3.11: Photographs of hyperpycnal channel-fill complex (F8a). A) Thick-bedded, medium- to fine-grained sandstone of facies F8a showing multiple sedimentary structures. B) Cross-stratification and C) high-scale water escape structures in facies F8a.

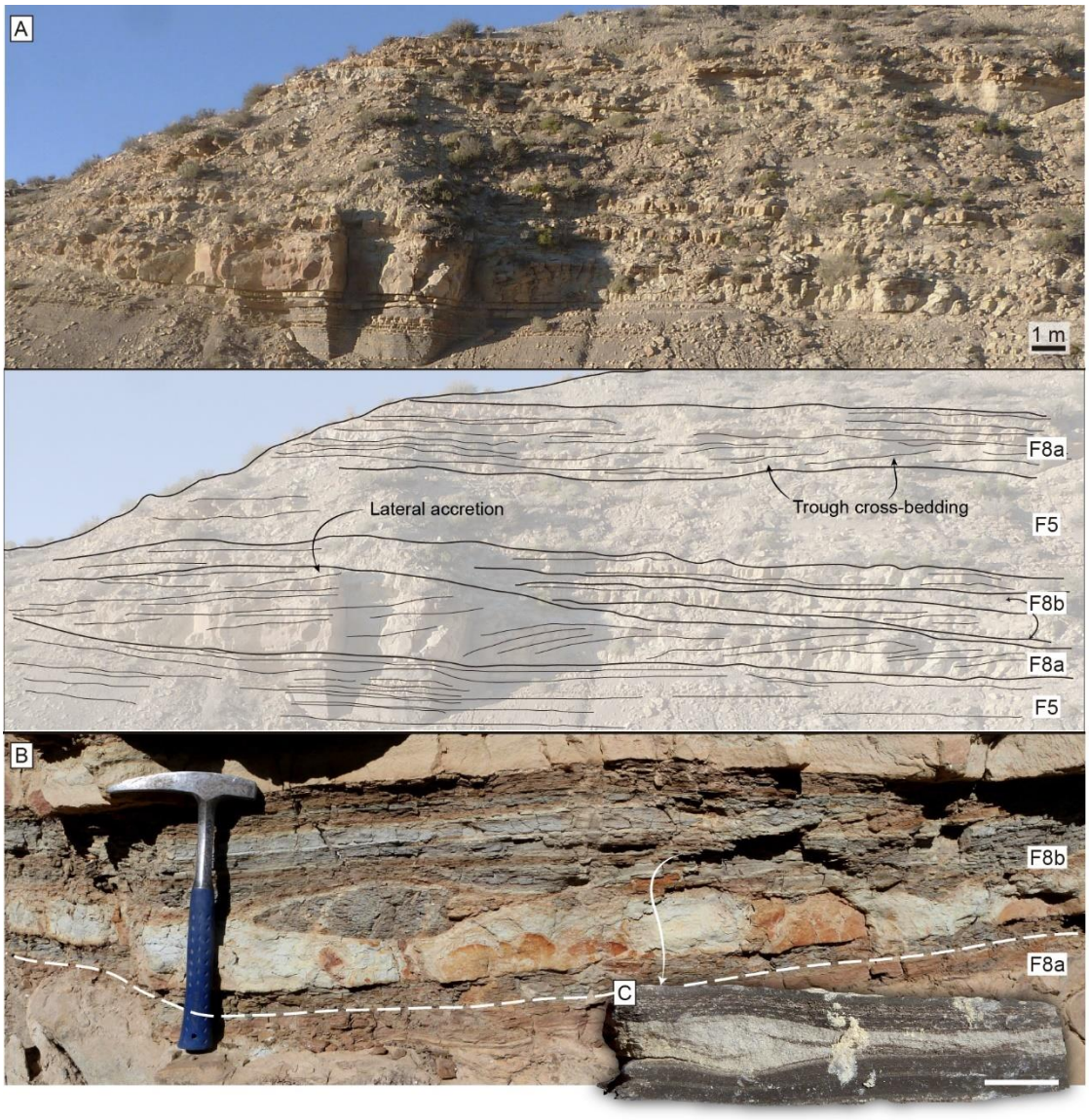

Fig. 3.12: Photographs of hyperpycnal channel-fill complex (F8a) and overbank facies (F8b). A) Lateral accretion in facies F8a, associated with facies F8b and basin (F5) deposits, with drawing of structures below. B) Facies F8b intercalated within channel-fill complex facies (F8a), showing crevasse-splay sandstone and heterolithic successions containing C) ripple cross-laminated sandstone (scale is 1 cm).

3.4.2.5. FAB interpretation

This facies assemblage is characterized by bottomset geometries (Fig. 3.13) and alternation of hyperpycnal deposits and sediment-starved, hemipelagic conditions, suggesting a siliciclastic basin environment associated with a mixed shelf (see below). The hyperpycnal system is described with the turbidity element nomenclature utilized by Mutti and Normark (1991).

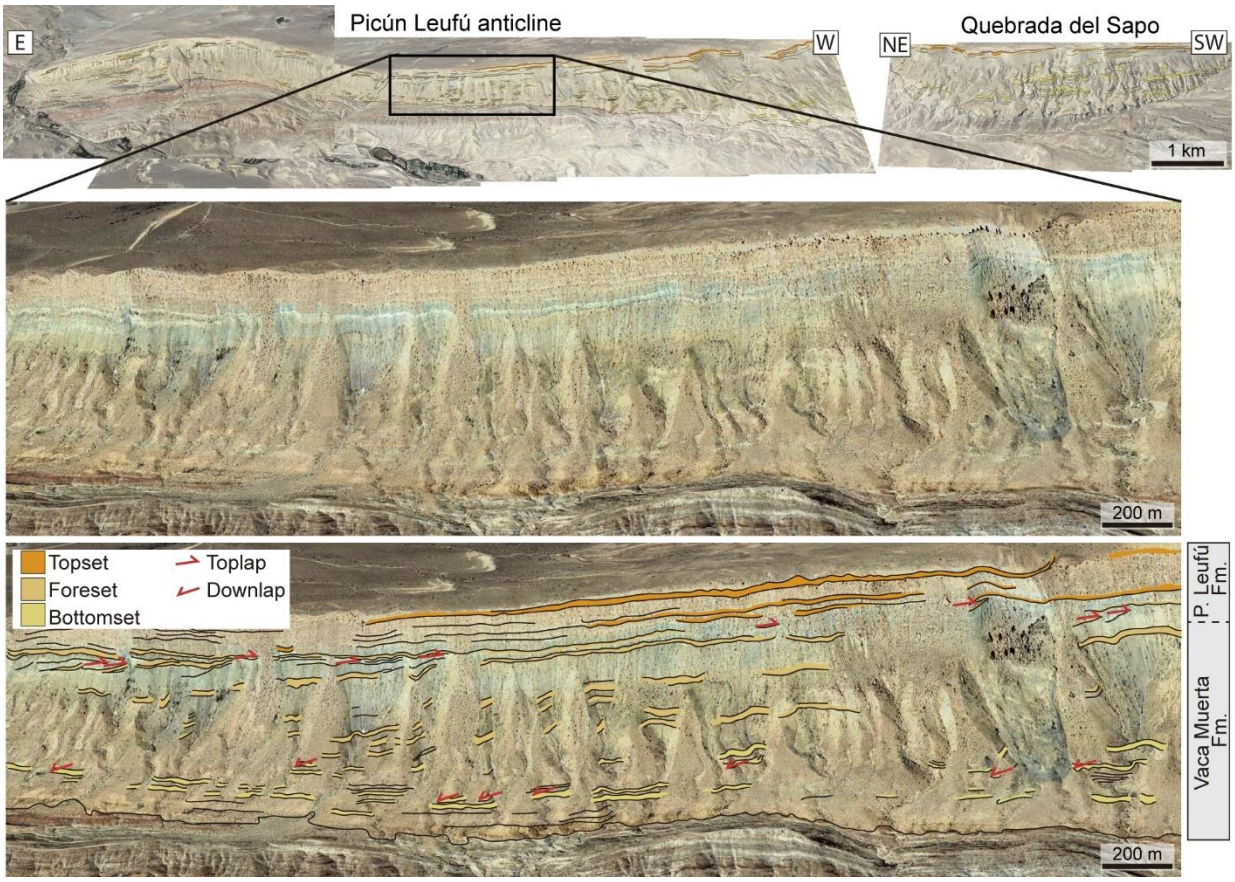

Fig. 3.13: Topset, foreset and bottomset geometries with their stratal terminations observed in satellite imagery of the Picún Leufú anticline and Quebrada del Sapo areas.

3.4.3. Facies assemblage C (FAC)

3.4.3.1. Facies 9 (F9)

This facies consists of parallel-laminated, grey, argillaceous fine mudstone, with minor thin-bedded (5-10 cm) very fine-grained sandstone (F9a, Fig. 3.14A, B) and coarsening upwards successions of thin-bedded (1-10 cm), massive to mottled, green, dolomitic intraclastic wackestone capped by medium-bedded (10-50 cm), calcareous fine-grained sandstone beds (F9b, Fig. 3.14A, C). Laminae in F9a is mm-thick and composed of silt showing very angular clast. TOC content is low (0.23-2.50%, mean=0.97%, N=12). The mudstone contains 50 cm wide, carbonate concretions, and minor bivalves and ammonite shells. Slumps, sand dykes and large scale syn-sedimentary faults occur. In addition, 5-10 m wide, shallow-marine olistoliths are observed within

the mudstone. The olistoliths comprise massive fine-grained sandstone, wackestone or mudstone. Bioturbation structures are absent in F9a, whereas mottlings are common in F9b (BI=3-6) and no discrete trace is recognized (Fig. 3.14C, D).

This facies is interpreted as a slope mud belt (F9a) and a mixed slope (F9b). High-energy near-bed shear stress in the topset produced by wave, tidal and oceanographic currents generated mud bypass towards the deeper foreset area (Pirmez *et al.*, 1998). Mixed sedimentation in coarsening upwards succession suggests minor scale sea-level changes, with the calcareous fine-grained sandstone representing increased siliciclastic export from the topset during sea-level lowstands (Kendall and Schlager, 1981; Yose and Heller, 1989). Angular shapes in clasts indicate eolian dust delivery caused the observed silt laminae, as eolian abrasion in silt-sized grains is relatively low (Kuenen, 1960). Other possible interpretations for the silt laminae as produced by current ripples flattened by compaction (cf. Yawar and Schieber, 2017) are less likely because of the absence of downlapping relationships in the laminae or erosive surfaces. Soft-sediment deformation structures and olistoliths originated from mass movements due to tectonic influence and slope construction. Along-shore redistribution by geostrophic currents (Swift *et al.*, 1986), and across-shore sediment delivery by storm-ebb surge currents (Aigner, 1985; Snedden and Nummedal, 1990), hyperpycnal flows (Bhattacharya and MacEachern, 2009) and wave-enhanced sediment gravity flows (Wright and Friedrichs, 2006) transport mud to this area, yet structures associated with these processes were not observed. Compaction constitutes the main problem when analyzing fine-grained depositional environments because of their high water content at the time of deposition, and therefore, samples from carbonate-cemented concretions could be helpful to elucidate the relative importance of these processes (e.g. Otharán *et al.*, 2020). Existence of bioturbation structures in F9b indicates a change to oxic environments in the mixed slope.

3.4.3.2. Facies 10 (F10)

This facies consists of thick- to medium-bedded (0.1-3 m), massive, calcareous fine-grained sandstone to intraclastic wackestone, intercalated with minor thin-bedded (1-5 cm), heterolithic intervals (Fig. 3.15A). Locally, subtle parallel lamination to low-angle cross stratification is observed. Some of the beds are amalgamated showing lenticular geometries with erosive bases. The sandstone contains minor isolated, small bivalve shells and mudstone rip-up

clasts. This facies comprises 3-10 m thick intervals encased in facies F9 and located in a foreset position.

This facies is interpreted as slope sand bodies produced by resedimented material from the shelf topset. The sand bodies are similar to the spillover lobes generated during times of strong tidal-ebb currents on the slope and consequent resedimentation (Tucker and Wright, 1992; Playton *et al.*, 2010), with sufficient energy to rework the muddy clinothem and transported it as rip-up clasts. The existence of faint sedimentary structures suggests development of concentrated density flows (Mulder and Alexander, 2001). Absence of well-defined structures precluded paleocurrent measurements and interpretation of likely triggering factors (wave, tidal or storm).

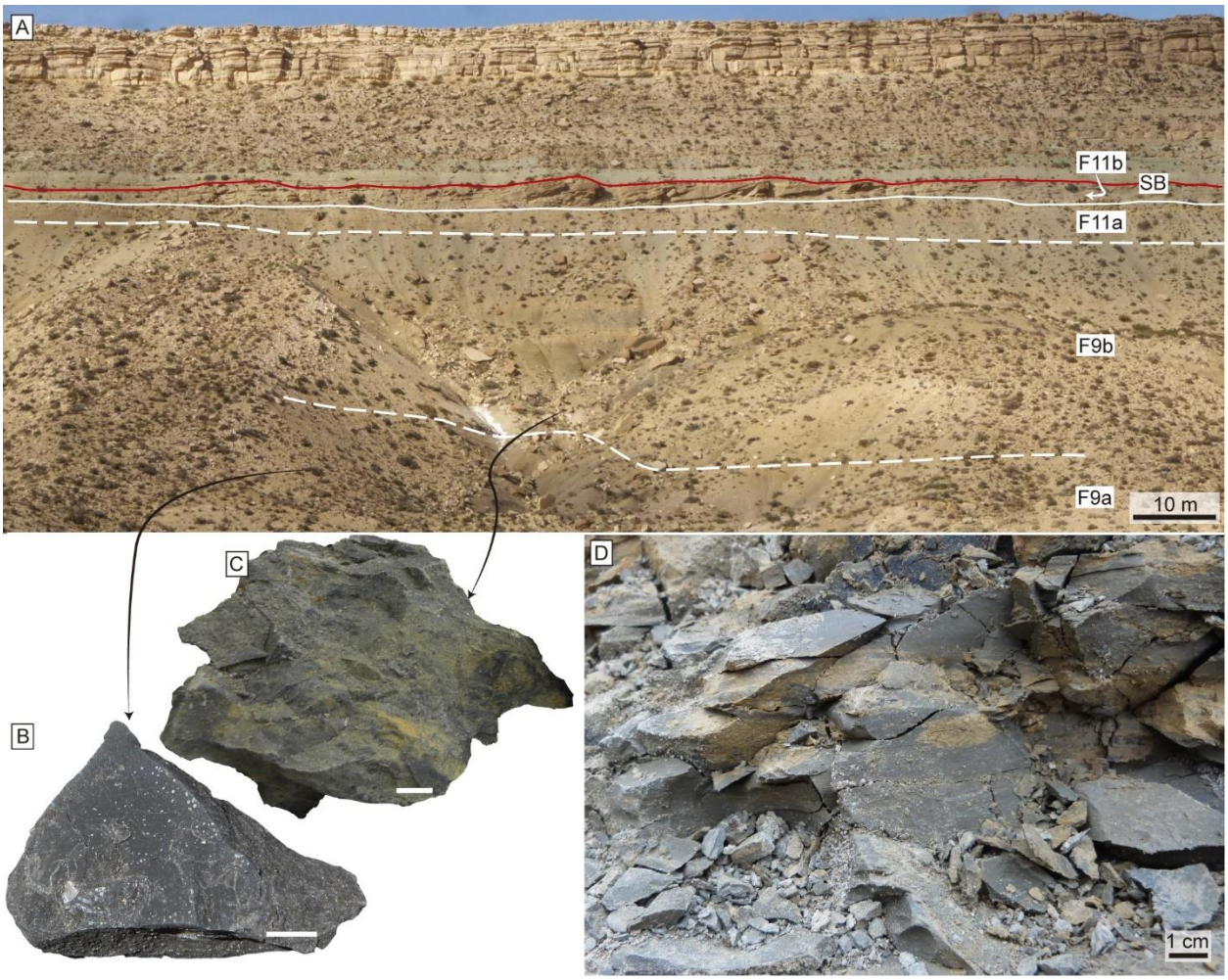

Fig. 3.14: Mixed carbonate-siliciclastic shelf facies association (FAC). A) Outcrop panorama of the foreset and topset area, showing slope mud belt (F9a) and mixed slope facies (F9b), grading towards bioturbated sandy shoal (F11a) and sand bars (F11b), with delineation of the uppermost sequence boundary (SB T3).

B, C) Samples of F9a and F9b, respectively. Note the change of color and mottling of F9b. Scale bars are 1 cm. D) Outcrop photograph of a calcareous fine-grained sandstone encased in intraclastic wackestone showing burrow mottlings in facies F9b.

Fig. 3.15: Photographs of slope sand bodies (F10), sandy shoal (F11a) and sand bar complex (F11b). A) Facies F10 (white beds) encased in fine-grained mixed slope facies. B, C) Undetermined trace fossil from facies F11a, and wave-rippled to parallel-laminated calcareous sandstone to wackestone from the same facies. D) Ripple cross-laminated medium-grained sandstone from facies F11b showing E) escape structures.

3.4.3.3. Facies 11 (F11)

This facies is composed of very thick successions (1-3 m) of medium- to coarse-grained, calcareous sandstone intercalated with medium- to thick-bedded (0.1-1 m), bioclastic wackestone and packstone (F11a, Fig. 3.15C) and erosive-based, thick-bedded (1-5 m), planar to trough cross-stratified, rudstone, floatstone and calcareous coarse- to medium-grained sandstone (F11b, Fig. 3.14A). F11a is mostly massive, although minor low-angle cross-bedding and wave ripples occur. F11b shows minor ripple cross-lamination showing escape trace fossils (Fugichnia) (Fig. 3.15D, E). Cross-stratification and lamination display paleocurrents towards SW and NE to E. The wackestone and packstone intervals are intercalated in the sandstones with gradational contacts. The matrix is composed by clay to fine-grained sand-size sediments, and the fossil content comprises articulated to disarticulated ammonites and bivalves (bioclastic fraction is 20-50%). The bioclastic material is abundant in the rudstone and floatstone (80-70%), and is composed of fragmented to partially preserved, disarticulated, large (up to 7 cm long) bivalve, gastropod and ammonite shells. Bioturbation completely reworked this facies (BI 4-6), giving a massive appearance, although *Thalassinoides* isp., *Palaeophycus tubularis* and horizontal to vertical undetermined trace fossils can be recognized (Fig. 3.14B). Burrow infill is commonly similar to the host rock, except for some grey mud infill.

This facies represents deposition in an oxygenated sandy shoal (F11a) with associated sand bars (F11b). The presence of trace fossils of a suspension feeding and active predator infauna in the calcareous sandstone (F11a) suggests suspended particles in a relatively moderate energy environment. Low-angle cross-bedding can be produced by bedform migration of the shoal edges (Ball, 1967), whereas wave ripples indicate oscillatory reworking in a relatively shallow environment. The packstone was produced during storm events due to the winnowing of the underlying sediment (Schlager, 2005), whereas the wackestone with clay matrix was generated during fair-weather times. High-energy currents scoured the underlying bioturbated sandy shoal deposits and generated migration of 2D and 3D subaqueous dunes (Hine, 1977; Tucker and Wright, 1992; Schlager, 2005). SW paleocurrents opposite to the direction of general coastal and clinothem progradation (NE) suggest a tidal influence in the origin of the bars (Spalletti *et al.*, 2000). High energy levels and high sedimentation rate limited bioturbation, and therefore, trace fossils are excluded or represented only by escape structures in the sand bars (F11b).

3.4.3.4. Facies 12 (F12)

This facies is only recorded in the upper part of the Quebrada del Sapo section comprising a ~4.5 m-thick interval. It is composed by green, structureless to parallel-laminated, medium-grained sandstone. Isolated, up to 4 cm long, bivalve bioclasts are common. Bioturbation is represented by biodeformational structures (BI 0-2).

This facies is interpreted as a lagoonal deposit in a protected setting. The paucity of body fossils and bioturbation points towards an environmental stress caused by restricted water circulation.

3.4.3.5. FAC interpretation

The FAC represents the foreset and topset deposits of the mixed carbonate-siliciclastic shelf facies (Fig. 3.13). The FAC slope refers to a low-angle, shelf-prism slope (0.91-1.15° angles observed in seismic reflections; Zeller, 2013) prograding into a relatively shallow basin floor comparable to an epicontinental shelf, instead of exemplifying the conventional usage of continental margin slope (see Patruno *et al.*, 2015).

3.5. Depositional model

Analysis of sedimentological and ichnological datasets allows the proposal of a depositional model for the Vaca Muerta Formation and part of the Picún Leufú Formation in the study area (Fig. 3.16). Jurassic deformation generated a heterogeneous pre-Vaca Muerta relief, represented by an E-W topographic high located in the Picún Leufú anticline area (Zavala and Freije, 2002; Zavala *et al.*, 2005, 2008; Naipauer *et al.*, 2012). This high constituted an important controlling factor for open bay facies assemblage (FAA), which generated paleorelief smoothing through sediment shedding from topographically elevated areas towards depocenters. Consequently, the initial transgression generated thicker FAA deposits in low areas and thinner in high areas.

The relative sea-level rise started with a rapid upward migration of the water table in the Quebrada del Sapo eolian deposits (Fig. 3.16a), generating liquefaction of active coastal dunes. Beach deposits (F1) were developed laterally from the soft-sediment deformation structures, where a high-water table generated eolian reworking, and constituted the first expression of the Vaca Muerta Formation.

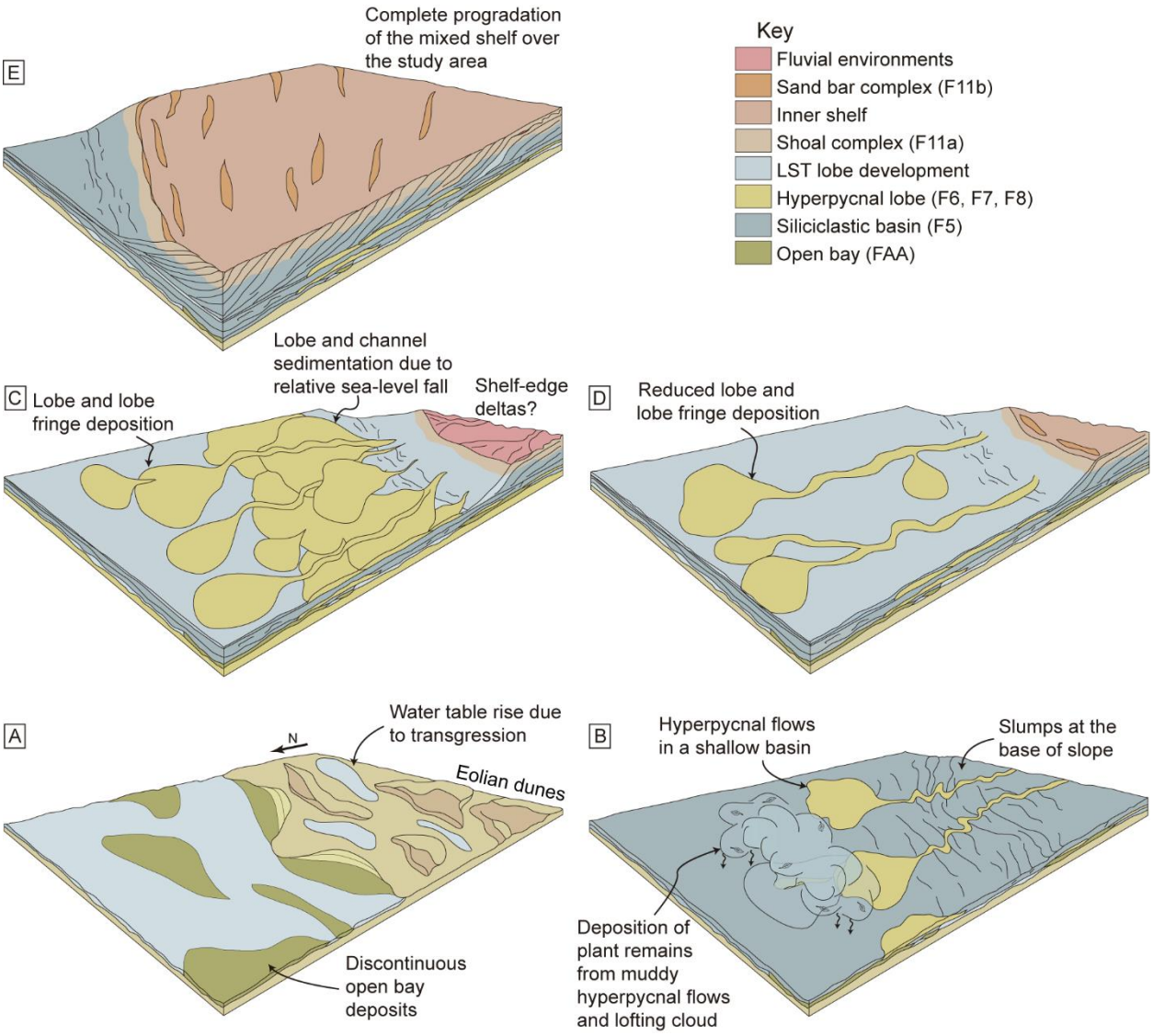

Fig. 3.16: Depositional model for the Vaca Muerta Formation (see text for explanation).

Bay margin (F2), proximal bay (F3) and distal bay (F4) environments were developed in a low-energy, sheltered embayment area (Fig. 3.16A) weakly affected by waves. The distal bay deposits are only present in the Quebrada del Sapo area and section 1, probably due to its position as a topographic low with respect to the anticline. The area was subject to suspension fallout sedimentation, punctuated by minor sandy concentrated density flows and muddy tempestite sedimentation. Opportunistic, low-diversity communities were sparsely developed in the distal bay, generating highly bioturbated intervals. On top of the FAA, a basinwide flooding led to deposition of the basinal facies (F5). The entire transgressive event ended with condensation and sediment starvation in the basin, leading to the formation of carbonate concretions.

After development of retrogradational FAA, alternating hemipelagic basinal (F5) and hyperpycnal flow sedimentation (F6 and F7) dominated in the bottomset area (Fig. 3.16B). Development of a low-angle coastal profile generated a basin of relatively shallow depth, allowing wave and combined-flow reworking of the hyperpycnal flow deposits. Oxygen-deficient conditions in the basin prevented bioturbation and produced short-term benthic colonization by bivalves during fluctuations of oxygen levels. In addition, the combined effect of oxygen deficiency and sediment starvation contributed to organic matter enrichment. Slumps were generated in a base of slope area by active tectonic deformation affecting the Picún Leufú anticline, which is recorded by the progressive unconformity lasting until the angular unconformity within the formation. Extensive slump and olistolith generation were produced nearby section 5, where the Picún Leufú anticline showed its maximum deformation.

Wave-influenced hyperpycnal flows moving across-shelf (NE paleocurrents) punctuated hemipelagic deposition at the basin and contributed to siliciclastic dilution of organic matter content. Moreover, slump deformation indicates that turbidite flows probably affected the bottomset area. The hyperpycnal flows generated lobe fringe (F6) and lobe (F7) deposits that can be traced 5 to 10 km laterally, losing energy in a seaward direction. Therefore, lobe sedimentation was restricted to the landward sections (SW), and lobe fringe facies occur in the seaward sections (to the E). Amalgamation of hyperpycnal flow deposits occurred in the lobe area, whereas lobe fringe settings were subject to occasional flows alternating with basinal hemipelagic sedimentation (Fig. 3.9A). The continuous shifting of lobes generated thickening and coarsening upward patterns and controlled abandonment of lobe fringes seaward. The energy gradation of combined-flow structures from lobe fringe containing wave and combined-flow ripples, to the lobe area with HCS sandstone suggests reduced oscillatory energy in deeper lobe fringe positions. Sandy lobe fringe facies (F6a) encased in thick muddy lobe fringe deposits (F6b) shows the waxing and waning behavior represented by sandy and muddy hyperpycnal sedimentation. Evidence of flow regime fluctuations also occurs in the lobe facies (F7) with alternated S1 and S2 facies (sensu Zavala *et al.*, 2011) and intra-bed erosive surfaces. Absence of these wax and wane energy changes in some lobe and lobe fringe facies can be attributed to the pervasive reworking by wave and combined-flows.

The extensive lateral distribution of hyperpycnal sedimentation and common lack of vertical gradation or connection between lobe fringe and lobe facies is noteworthy. These

observations can be related with (1) the low-frequency, intermittent nature of hyperpycnal deposition, which is restricted to specific bottomset intervals associated with extraordinary river discharges, and (2) an angle-independent behavior of these flows, showing occurrences distally in the bottomset area in contrast with surge-like flows deposited near the base of slope (Zavala and Arcuri, 2016). The two probably source areas for these flows were the Somuncurá Massif to the SE, and the active Andean volcanic arc to the SW.

Rejuvenation of hyperpycnal sedimentation occurs after progressive anticline deformation ceased, and the angular unconformity was developed (Fig. 3.16C). Tectonic uplift related with the last phase of deformation at the end of progressive unconformity may have triggered base-level changes. In this scenario, deltas approached to the foreset break and delivered high amounts of sediment to the bottomset, reactivating hyperpycnal sedimentation. Hydrodynamic energy decreased seaward, and therefore channel-fill (F8a), overbank (F8b) and lobe (F7) facies were produced at a base of slope position in the landward sections (SW), whereas lobe fringe facies (F6) occurs seaward in the basin (to the E). Facies F8a rests erosively on the underlying basin facies (F5) in the highly active tectonic area (section 5), where the higher energy facies occur. On top of facies F8a, hyperpycnal sandy deposits initiated a retrogradational pattern, displaying an increased amount of hemipelagic basin sedimentation (Fig. 3.16D).

The foreset area comprises clinoforms of the mixed carbonate-siliciclastic shelf (FAC) showing progradation towards the NE and downlapping relationships with the underlying bottomset strata (Fig. 3.13). These shelf-prism clinoforms developed a distinctive zonation of a topset, high carbonate productivity area, and a foreset showing mud belt accretion (Fig. 3.16E). The seaward area of the sections (section 1 and 2) also developed minor bottomset basinal sedimentation during the beginning of clinoform progradation. Hyperpycnal sedimentation in the bottomset was restricted due to the evolution of the lower angle siliciclastic basinal system into a mixed carbonate-siliciclastic shelf prone to more sediment redistribution by coastal diffusion processes in a wider topset area. The addition of higher foreset angles to the mixed shelf system also prevented storm action in foreset and bottomset areas.

The lower foreset area comprises mud belt deposits (F9a) representing the shelf siliciclastic counterpart, whereas upper foreset and foreset to topset transition showed mixed siliciclastic-carbonate sedimentation (F9b). Mass movements in the foreset generated slump and olistoliths, which are also more pervasive in the tectonically active area (section 5). Higher sedimentation

rates of the foreset mud belt compared with those of the sediment-starved bottomset basin contributed to organic matter dilution. Rivers supplied siliciclastics towards the topset, which were later bypassed by across- and along-shore currents reaching the foreset. Sand bodies (F10) were an additional source of sediment, supplied from the shoal and sand bar complex (F11) located at the shelf break. The chemocline was located in the F9a-F9b transition and restricted bioturbation and organic matter preservation. The foreset-topset transition constituted an area of carbonate production with oxygenated waters, where organisms thrived and intensely reworked mixed slope facies (F9b) and sandy substrates of the sandy shoal (F11a). The sand bars (F11b) protected the lagoon in the topset and represented a sediment source as well. Bioturbation was precluded in the lagoon (F12) or restricted to escape structures in the sand bars due to salinity and sedimentation rate stresses, respectively. The whole FAC sedimentation ended with an erosional surface recording erosion of the foreset and truncation towards topset structures (Fig. 3.14A).

3.6. Sequence stratigraphy

The sequence stratigraphy analysis of the correlation panel is presented in Fig. 3.17. The analysis follows Depositional Sequence Model II of Posamentier *et al.* (1988), to avoid confusion with delineation of a Falling Stage Systems Tract (FSST). The ammonite biostratigraphic zonation of Riccardi (2008), following Parent *et al.* (2011) analysis in the easternmost of our sections was utilized to calibrate chronostratigraphically the correlation, although the proposed new zone (Picunleufuense) is not used due to a lack of consensus (cf. Riccardi, 2008, 2015). Progradation or aggradation of lobe deposits were considered as product of autocyclic changes, as they are likely generated either by lobe migration or aggradation and progressive smoothing of the depositional surface (Mutti and Sonnino, 1981), or by changes in the fluvial input related with climatic factors (Zavala and Arcuri, 2016). Two depositional sequences (DS1 and DS2) were recognized in the study area.

3.6.1. Depositional Sequence 1 (DS1)

The base of DS1 is placed at the base of the Quebrada del Sapo Formation LST deposits. The first expression of marine facies of the Vaca Muerta Formation indicates the development of a

Transgressive Surface (TS) located on top of eolian dune facies and deflation surfaces of the Quebrada del Sapo Formation (Fig. 3.6A, B). On top, FAA shows a retrogradational stacking pattern and constitute the TST. Proximal bay facies (F3) represent wave reworking and therefore, a wave ravinement surface is developed at the base. The TST is within the *V. mendozanus* ammonite zone, which has been assigned to the late early Tithonian-early middle Tithonian. The maximum flooding zone (MFZ) is suggested by the extensive occurrence of carbonate concretions indicating condensation and high TOC values within basin facies (F5) and marks the top of the TST.

Above the MFZ, facies F5 shows coarsening upwards cycles, and the first hyperpycnal facies occur, indicating the beginning of HST. At a larger scale, a progradational 55-110 m-thick siliciclastic basin facies assemblage (FAB) is observed. The HST was deposited during the middle Tithonian, constituting the upper *V. mendozanus*, the *P. zittelli* and the lower *A. proximus* ammonite zones.

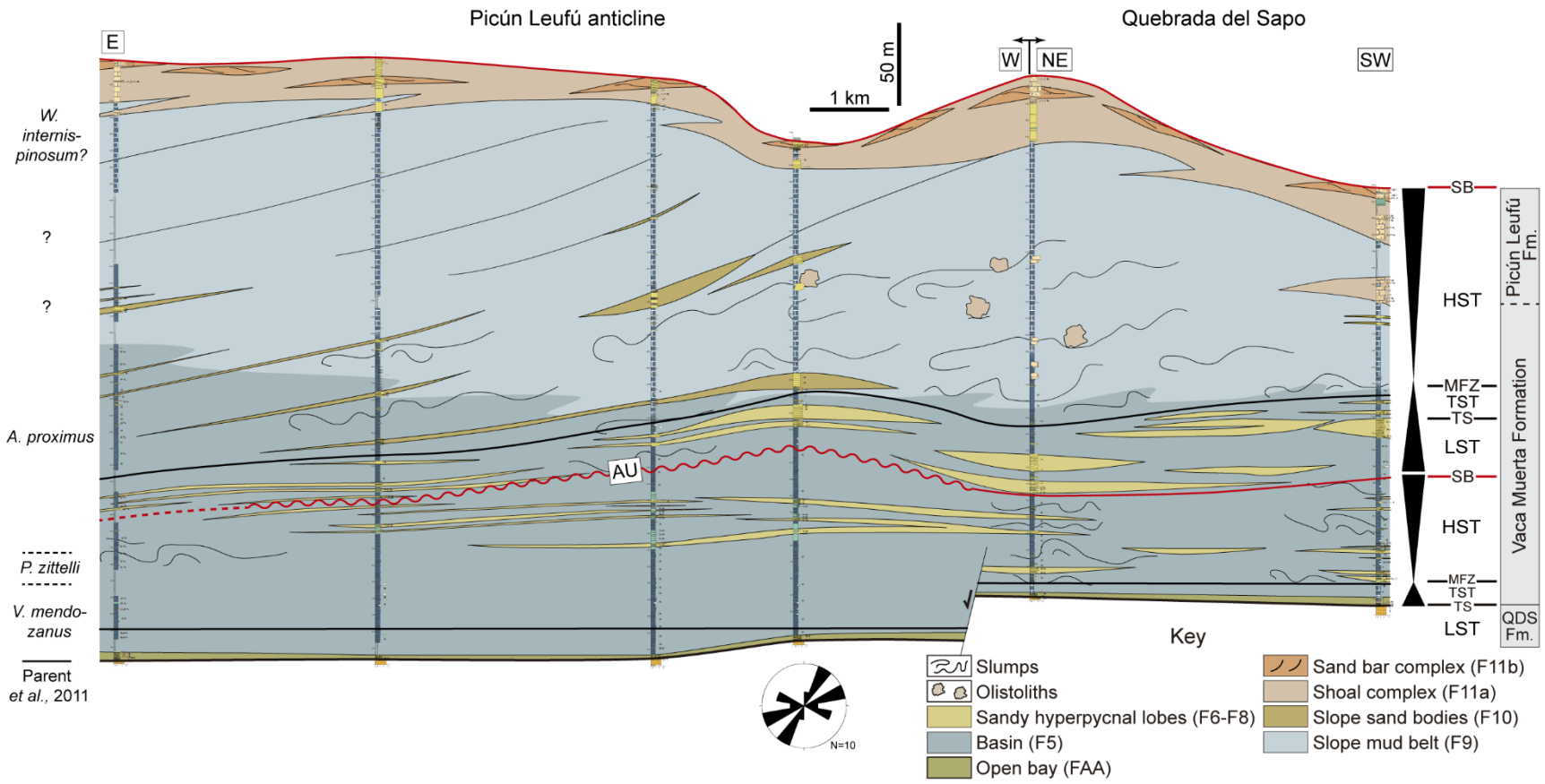

Fig. 3.17: Sequence stratigraphy analysis of the correlation, showing the angular unconformity location (AU). The correlation datum is the lower MFZ. Paleocurrents measurements are restricted to F6a and F7.

3.6.2. Depositional Sequence 2 (DS2)

The angular unconformity within the Vaca Muerta Formation occurs at the 80-120 m of the section (Figs. 3.4 and 3.18, "AU"), representing the end of the progressive unconformity affecting the anticline. Above the angular unconformity, the abrupt reactivation of sandy hyperpycnal flow facies and existence of shallow-water wave and storm reworking suggest a relative sea-level fall associated with a Sequence Boundary (SB) and LST sedimentation, marking the beginning of DS2. The coincidence of the angular unconformity with the SB indicates tectonic movements along the anticline could be associated with base-level and accomodation space changes. Hyperpycnal facies (F6, F7 and F8) overlaying the LST display retrogradational stacking patterns with increased deposition of F5, indicating a TST developed upon a transgressive surface (TS). The LST and TST are 25-50 m thick and are middle Tithonian in age based on the *A. proximus* ammonite zone location. The MFZ occurs at the top of the TST and is suggested by carbonate concretions and higher TOC values within F5 interval.

The overlying mixed carbonate-siliciclastic shelf (FAC) facies display foreset geometries prograding towards the NE with downlap relationships with the MFZ, as revealed in outcrop and seismic images (Fig. 3.13), indicating development of HST (DS2). The HST comprises the *A. proximus* to *W. internispinosum* ammonite zones, suggesting a middle to late middle Tithonian age. The foreset shows a significant lateral thickness variation from NE to SW of ~254 to ~119 m caused by an irregular truncation surface at the top, which deepens towards the SW and represents a SB (Fig. 3.14A, 3.16).

3.6.3. Correlation of outcrop-based sequence stratigraphy with seismic section

The sequence stratigraphy analysis from outcrops was correlated with the seismic section from Zeller (2013) and Massaferro *et al.* (2014), which is parallel to our outcrop section (Fig. 3.19). The seismic section clearly differentiates bottomset, foreset and topset reflectors. The bottomset displays continuous reflectors in its lower and upper part, and a low-amplitude middle part, which has subtle downlapping relationships with the lower bottomset. The bottomset thins basinward, towards the NE. The foreset reflectors are above the bottomset, showing mostly downlap

terminations towards the upper bottomset top, with minor internal downlap and onlap surfaces. At the top, the foreset-topset contact constitutes an irregular truncation surface that is dipping towards SW, underlying a topset composed by continuous horizontal reflectors.

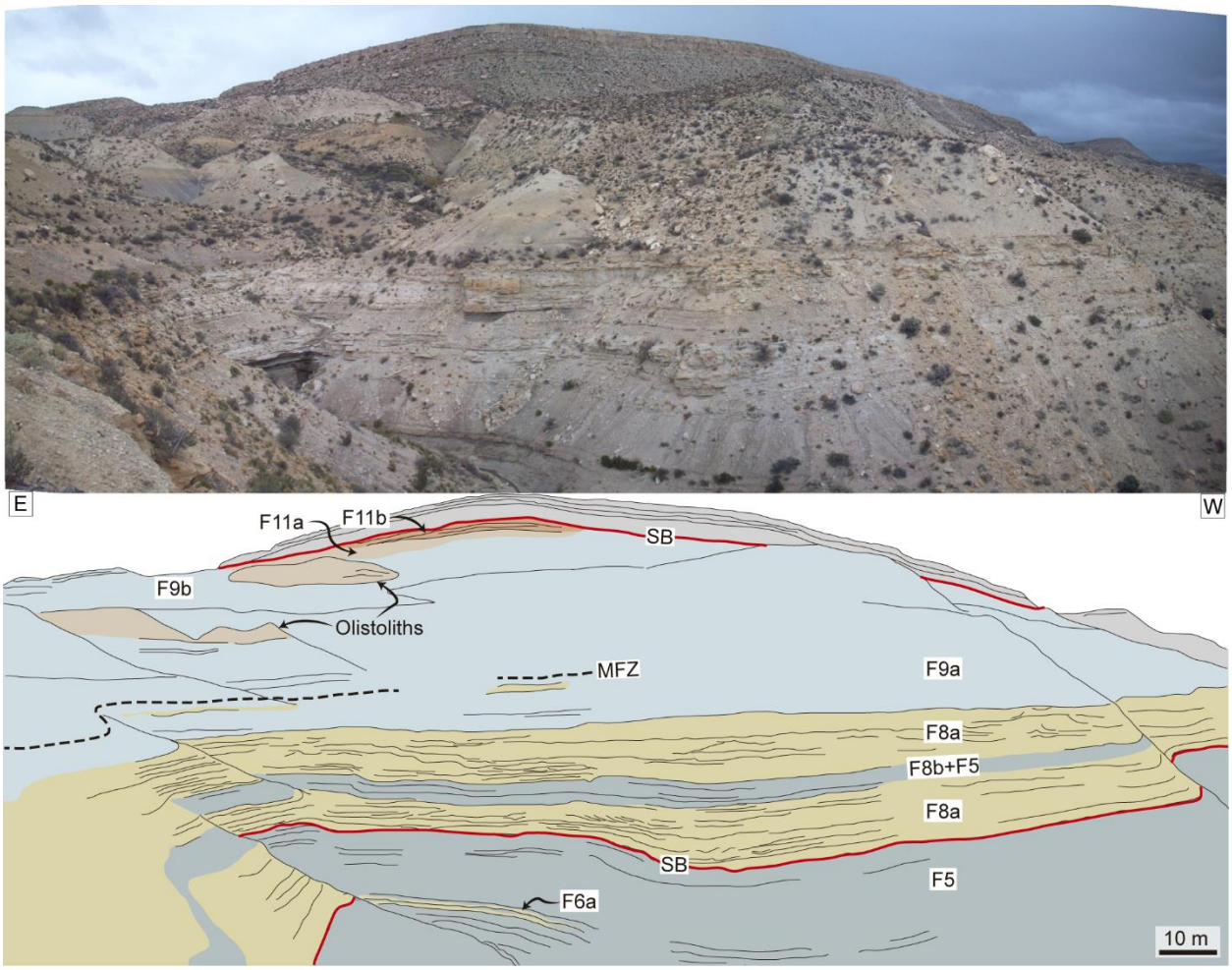

Fig. 3.18: Interpreted panorama photograph displaying the facies succession and sequence-stratigraphic surfaces. F5: basin, F6a: sandy lobe fringe, F8a: channel-fill complex, F8b: overbank, F9a: slope mud belt, F9b: mixed slope, F11a: bioturbated sandy shoal, F11b: sand bar complex.

The correlation from outcrop to seismic was created adjusting the thickness of the easternmost Picún Leufú section to the NE edge of the seismic line, tying the TS to the Vaca Muerta Formation base, and the uppermost SB to the foreset truncation surface. The Picún Leufú section was chosen for being a more homogeneous depositional environment with less hyperpycnal flow sedimentation, and its proximity with the seismic section. After adjustment,

bottomset and foreset outcrop geometries match with the seismic image. The lower bottomset correlates with TST (DS1), and the middle low-amplitude bottomset corresponds to the HST (DS1) siliciclastic basin (FAB) sedimentation. The upper bottomset coincides with LST and TST (DS2) position: the base matches with SB (DS2), whereas the top, which is a downlap surface, correlates with MFZ (DS2). The continuity of the upper bottomset reflectors with an absence of terminations (Fig. 3.19B) supports its correlation with an aggradational-retrogradational LST and TST. HST (DS2) shows foreset reflectors in a landward position and bottomset reflectors seaward, both of them downlapping over the MFZ (DS2). On top, the truncation surface is highly irregular, similarly as it is observed in outcrops.

3.7. Discussion

3.7.1. The hyperpycnal sedimentation model for basinal sand deposits

Analysis of sedimentological evidence of the basinal sandstone intervals hereby described (F6, F7 and F8) indicates a wave-influenced hyperpycnal flow origin for most of the turbidity and concentrated density currents responsible for sedimentation. Three models are meaningful in the discussion of the origin of these deposits: waning flow model (Kneller, 1995; Mulder and Alexander, 2001), tempestite model (Aigner, 1985; Myrow and Southard, 1996), and hyperpycnal flow model (Mulder *et al.*, 2003; Zavala *et al.*, 2011), and these are revised in detail in the following paragraphs.

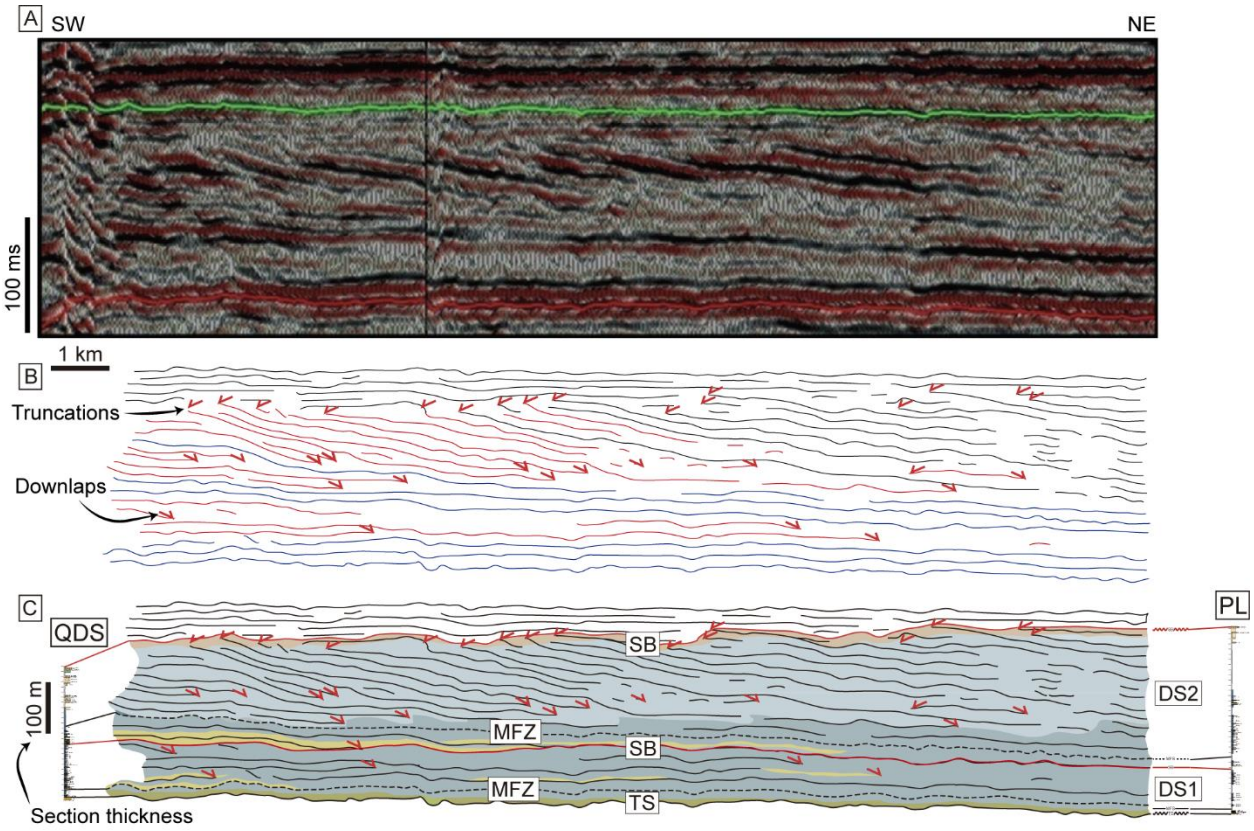

Fig. 3.19: Correlation of seismic sequence stratigraphy with the correlation panel of Fig. 3.17. A) Seismic 2D section from Massaferro *et al.* (2014). Red and green line represents Vaca Muerta Formation base and their MFS II, respectively. Vertical scale is in time. B) Seismic interpretation showing truncation, downlap and minor onlap and toplap stratal termination. Blue reflectors comprise continuous, aggradational strata, whereas red reflectors are prograding, downlapping deposits. C) Interpretation of seismic image based on the position of stratigraphic surfaces and correlation with the westernmost Quebrada del Sapo (QDS) and easternmost Picún Leufú (PL) sections of Fig. 3.17 (sedimentary environments key in Fig. 3.17, and sequence stratigraphy terminology referred in the text). Vertical scale on the left corresponds to stratigraphic section thickness (relationship between time and depth in seismic line is unknown).

The waning flow model follows the classic turbidite model proposed by Bouma (1962), which was intended to explain the processes and products of waning, unidirectional turbidity flows. These flows are differentiated from hyperpycnal flows mainly by the steadiness of sedimentation: while hyperpycnal flows are considered quasy-steady currents, waning flows are unsteady flows (Mulder and Alexander, 2001). Many factors can trigger waning flows, although commonly they are related to slumping produced by gravity-collapse or seismogenic activity. The model is useful to explain the occurrence of erosive bases and unidirectional structures in the

sandstone, yet fails to account for the riverine signal provided by the plant debris occurrence and the wave and combined-flow reworking.

Second, the tempestite model explains deposition of storm-generated beds across the shelf, in offshore areas (Aigner, 1985; Myrow and Southard, 1996). The possibility for a density flow to be offshore-transported is controlled by the interplay between offshore pressure gradient, Coriolis forces, bottom friction and excess-weight forces (Myrow and Southard, 1996). Offshore pressure gradient is produced by coastal set-up and set-down generated by storm wind energy, which consequently trigger currents that are deflected along-shore by Coriolis forces (geostrophic flows, Swift *et al.*, 1986). Excess-weight forces refer to the downslope force produced by a sediment suspension, and its magnitude is related with sediment concentration and the available slope. High offshore pressure gradient, high excess-weight forces and weak Coriolis forces facilitate across-shelf sediment transport; however, high excess-weight forces achieved by catastrophic introduction of sediment are particularly emphasized by Myrow and Southard (1996) as a likely triggering factor. These authors suggested that many tempestites represent across-shelf transport during storms with high bottom sediment concentration, with the sediment-rich suspensions being provided by river floods or earthquakes. Consequently, this model can successfully interpret the storm (wave and combined-flow structures and gutter casts) and riverine input (plant debris), evidence of our basinal sandstone facies.

Lastly, hyperpycnal flows are negatively buoyant, freshwater density underflows generated during times of river flood (see Mulder and Syvitski, 1995; Mutti *et al.*, 1996; Mulder *et al.*, 2003; Ponce, *et al.*, 2008; Zavala *et al.*, 2011; Wilson and Schieber, 2014; Canale *et al.*, 2015; Zavala and Arcuri, 2016). Negative buoyancy is easily achieved in freshwater bodies, yet in marine settings, the concentration of suspended sediment in the flows needs to be large enough in order to overcome seawater density (Mulder and Syvitski, 1995). These flows differ from waning flows by the duration and steadiness of the event: hyperpycnal flows are originated by a continuous fluvial discharge that may last for days or weeks, which generates a quasy-steady current, whereas waning, surge-like flows are very short duration, unsteady and strongly non-uniform events (Mulder and Alexander, 2001). Hyperpycnal flow deposits display a typical coarsening-up to fining-up trend as a result of the waxing-waning behavior of the fluvial discharge (Mulder *et al.*, 2003), which contrasts with the waning, surge-like turbidite sequence. In addition, hyperpycnal flows are able to transport extrabasinal material as plant debris in their suspended load (Ponce and

Carmona, 2011a, b; Zavala *et al.*, 2012; Canale *et al.*, 2015). Hence, the hyperpycnal model can account for the abundance of plant debris in our basinal sandstone deposits.

Following these definitions, a combination of the tempestite and hyperpycnal flow models can explain the evidence detected by our analysis. As pointed out before, evidence of flow regime fluctuations occurs in the lobe facies (F7), and lobe fringe facies (F6). Typical waxing and waning flow sedimentary structures are not observed in the lobe fringe sandy facies, probably due to the pervasive reworking by waves and combined-flows and the abundance of massive beds. Nevertheless, massive bed deposition do not exclude interpretation of river-derived flows, as structureless beds produced by hyperpycnal flows occur in Holocene subaqueous fans in southern California (Steel *et al.*, 2016).

The high amount of plant debris constitutes a direct evidence suggesting a connection with riverine systems (Plink-Björlrklund and Steel, 2004; Ponce *et al.*, 2008; Mulder and Chapron, 2011; Paim *et al.*, 2011; Ponce and Carmona, 2011a, b; Zavala *et al.*, 2011; Zavala and Arcuri, 2016). Not only plant debris have been extensively found in the fine-grained deposits, but also randomly disposed in the sandstone and draping sandstone parallel lamination. In addition, it is difficult to explain the abundant plant remains in the mudstone facies as being reworked from prodelta or delta front deposits, as biological and physical reworking contributes to oxidize the organic material deposited in these areas (Zavala and Arcuri, 2016). However, abundant slump structures indicate turbidite flows probably contributed to bottomset sedimentation.

These hyperpycnal flow deposits were reworked by wave and combined flows during storms in a shallow basin. Storm imprint in hyperpycnal facies was only possible during siliciclastic basin development (HST of DS1, and LST and TST of DS2) due to its gentler angle of slope compared with mixed shelf systems and consequent lower water depth. Other possible origins to consider for combined-flows include internal waves associated with density contrast in the upper interface of the flows (Mutti *et al.*, 1996), or reflection and ponding processes by flowing against obstacles (Edwards *et al.*, 1994, Kneller *et al.*, 1997). The storm-generated combined-flow hypothesis is the most plausible explanation due to (1) the genetic association with oscillatory flow reworking, which may reflect a decelerating later phase of the unidirectional component and consequent shift to pure oscillatory movement, and (2) the existence of combined and/or oscillatory flow reworking in mostly every bottomset sandstone bed, suggesting deposition above storm wave base.

Therefore, the basinal sandstone facies are interpreted as wave-influenced hyperpycnites produced by sediment-rich riverine discharges during a superimposed storm event. Shore-perpendicular paleocurrents suggest offshore-directed sedimentation and exclude the hypothesis of along-shore geostrophic currents. Studies on modern continental shelves showed that sediment gravity flows are of prime importance in distributing sediment across-shelf (Hill *et al.*, 2007), with some examples associated with fluvial discharges (Wright and Friedrichs, 2006; Ma *et al.*, 2008). Boundary shear stress produced by storm-generated waves or currents aid to sustain suspended sediment and maintain negative buoyancy (Wright *et al.*, 2001; Wright, 2012). Sediment suspensions generated during storms without associated riverine discharge were probably deflected by along-shore currents and contributed to foreset construction landward from the study area. The superimposed storm-generated, wave and combined-flow action over a sandy sediment-gravity flow associated with fluvial discharges has been described in the fossil rock record as a wave-modified (or wave-influenced) turbidite (Myrow *et al.*, 2002, 2008; Higgs, 2004; Pattison, 2005; Pattison *et al.*, 2007; Lamb *et al.*, 2008; Pattison and Hoffman, 2008; Buatois *et al.*, 2019) or shelfal hyperpycnite (Zavala *et al.*, 2011).

3.7.2. Sedimentary and sequence stratigraphic models: Regional and global importance

Bottomset and foreset represent two contrasting areas of deposition, impacting on siliciclastic, organic matter and carbonate accumulation (Fig. 3.20). The bottomset area was characterized by extensive sediment-starvation and oxygen deficiency, allowing higher organic matter concentration produced by hemipelagic sedimentation. The absence of bioturbation and an abundance of pectinid bivalves indicate this environment could represent the exaerobic zone of Savrda and Bottjer (1987), where low oxygen bottom waters coexist with reducing substrates, contrasting with trace element geochemistry that suggests oxic bottom waters and reducing pore waters (Krim *et al.*, 2017). The mudbelt accretion and eolian input contributed to dilution of organic matter in the foreset. These models are similar to the mudbelt and sediment-starved shelf descriptions of Birgenheier *et al.* (2017) for the Mancos Shale, USA, with their limit representing the most seaward extension of mud delivery by coastal redistribution processes.

In addition, slumping and olistolith formation related with tectonic activity represented an important sediment contributor to both bottomset and foreset areas. Tectonic movements along the

Picún Leufú anticline affected early development of the siliciclastic basin (Krim *et al.*, 2017) up to the end of HST (DS1), and also during SB and LST (DS1) formation. Krim *et al.* (2017) located slumps as a facies association on top of their high-frequency cycle S2 and related them with a gently prograding slope. However, random slump distribution in both bottomset and foreset positions and association of the siliciclastic basin with a progressive unconformity suggest a mixed sedimentary and tectonic origin for the slope triggering slump deformation. Slumps and other deformational structures were also documented at the bottomset-foreset transition in seismic sections from the central Neuquén Basin (Pose *et al.*, 2014; Arregui, 2014; Notta *et al.*, 2017; Reijenstein *et al.*, 2017a). In addition, hyperpycnal and minor surge-like flows also contributed to bottomset sediment accumulation. Otharán (2020) recognized the sandstone deposits as produced by shelfal hyperpycnal flows, a similar interpretation to the one favored here.

Delineation of the base of DS2 described in the present contribution agrees with the "SB2" proposed by Spalletti *et al.* (2000), and the "discontinuity 8" described by Freije *et al.* (2002). In addition, this SB coincides in age with the T2 surface recognized in seismic analysis (Desjardins *et al*., 2018), yet regional seismic correlation of stratigraphic surfaces is needed to confirm this hypothesis. Seismic information provided by Massaferro *et al.* (2014) and outcrop delineation of facies geometry also support SB interpretation. The correlation with the seismic section was helpful to confirm the location of the conformable, non-erosive SB seaward, in an area where absence of abrupt facies changes makes its recognition difficult. This sequence stratigraphic interpretation adds more detail to bottomset reflectors analysis in seismic, which were described as a transgressive succession (Massaferro *et al.*, 2014).

LST (DS2) shows extensive hyperpycnal flow sedimentation in both bottomset to foreset positions. These LST sandstone intervals from the Quebrada del Sapo section were correlated with the LHo.x-1 well log, located 35 km southeast from the area (Santiago *et al.*, 2014), and also interpreted as turbiditic resedimentation processes in a slope setting (Otharán *et al.*, 2017). Slumps and water escape structures support the existence of a slope, yet the seaward association of high-energy LST facies with lobe fringe, plant debris-rich deposits, probably indicates an extrabasinal origin.

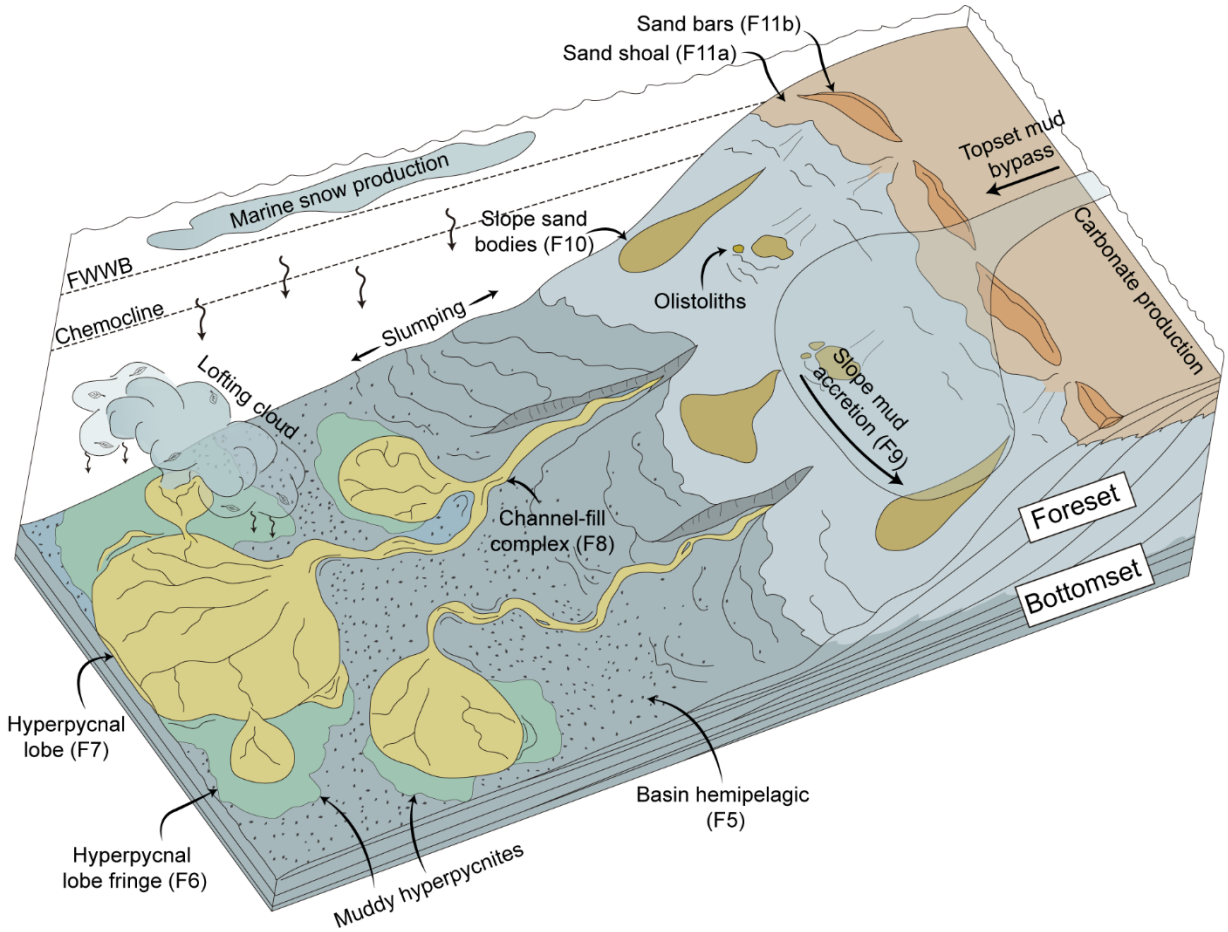

Fig. 3.20: Summary of sedimentary facies and processes occurring during siliciclastic basin and mixed carbonate-siliciclastic shelf progradation in bottomset and foreset segments. FWWB: Fair-weather wave base location.

Carbonate productivity increased during HST (DS2) and was exported towards the foreset. Siliclastic elements were probably fed by riverine buoyant plumes bypassing the high-energy topset and contributing to clinothem progradation in deeper areas. Alternation of HST carbonate and TST siliciclastic deposition were explained by an along-shelf current system redistributing sediment during TST and being terminated during HST by a lack of accommodation space in the shelf topset (Zeller, 2013; Zeller *et al.*, 2015b). In addition, several authors described the tidal influence of the system (Spalletti *et al.*, 2000; Armella *et al.*, 2007; Zeller *et al.*, 2015b; Krim *et al.*, 2017) and associated this process to tidal amplification caused by the embayed geometry of the Neuquén Basin and existence of the Huincul Ridge (Spalletti *et al.*, 2000). Evidence presented in this contribution underscores the action of fluvial input in the bottomset showing across-shore

paleocurrents, expanding and modifying the knowledge of sedimentary processes affecting the system.

Presence of a slope with olistoliths and pervasive slumping, and absence of a clear and graded outer-mid-inner ramp partitioning lead us to utilize the shelf terminology instead of ramp. The system has been also considered as a gently inclined shelf (Zeller, 2013; Zeller *et al.*, 2015b), which might be a reasonable alternative terminology. The foreset and foreset-topset transition ended with a SB truncating HST (DS2) on top correlated with surface T3 of Desjardins *et al.* (2018), that has been also observed in seismic section and correlation with outcrops from Sierra de la Vaca Muerta (Zeller, 2013; Massaferro *et al.*, 2014).

The analysis of bottomset and foreset sedimentary processes in the Vaca Muerta Formation has implications for understanding shelfal sand sedimentation in sequence stratigraphic models and organic matter enrichment in one of the most important unconventional reservoirs in the world (cf. Wang *et al.*, 2016). Warrick *et al.* (2013) and Steel *et al.* (2016) described sandy hyperpycnites in the modern Santa Barbara channel, USA, indicating sandy shelfal sedimentation disconnected from offshore tempestite processes was not restricted to LST deposition or TST shelf sand ridges (Berne *et al.*, 1998; Snedden and Dalrymple, 1999), as conventional sequence stratigraphic models suggest (Posamentier and Vail, 1988; Catuneanu, 2006). Similarly, the Vaca Muerta sandy shelfal sedimentation shows *en masse* deposition of wave-enhanced currents with massive beds and dewatering structures during HST and additionally, LST development. Therefore, the Vaca Muerta Formation represents a direct fossil example of the Santa Barbara channel deposits that occur in bottomsets associated with short topset distances able to bypass the littoral energy fence.

In addition, organic matter distribution in this unconventional reservoir shows a clear pattern affected by dilution of siliciclastic material. Organic matter enrichment constitutes a process balanced by the effects of dilution by inorganic components, production and preservation of organic matter (Tyson, 2005), and the question of which of these processes represents the main driving factor constitutes an extensive debate (Hedges and Keil, 1995; Sageman *et al.*, 2003; Katz, 2005; Macquaker *et al.*, 2010a). Recently, many studies underscored the contribution of sediment-density flows in trapping organic matter towards deep, fine-grained depositional environments (Könitzer *et al.*, 2014; Lash, 2016, DeReuil and Birgenheier, 2019), in addition to studies from the Vaca Muerta Formation (Otharán *et al.*, 2020). The present analysis shows low TOC content associated with buoyant plume (minor massive fine mudstone in facies F5) and fine-grained

hyperpycnal flows (facies F6b) deposits in the bottomset, and with mudbelt (facies F9a) deposits in the foreset, suggesting that, dilution of sediment-starved, hemipelagic basinal areas constitutes the main controlling factor for organic matter enrichment in the study area. However, more analysis focused on the organic matter quality and type should be conducted to fully understand the processes of organic carbon burial in the Vaca Muerta Formation.

3.8. Conclusions

Two third-order sequences (DS1 and DS2) representing bottomset, foreset and foreset-topset transition sedimentation accumulated in the Vaca Muerta Formation. TST (DS1) started with deposition in an open bay setting, represented by beach, bay margin, proximal bay and distal bay environments showing retrogradational patterns, and ended during a MFZ developed within a sediment-starved basin. Bioturbation suggests firmground conditions in the bay margin and opportunistic behaviors in the distal bay. HST (DS1) records hemipelagic deposition in a shallow, sediment-starved basin, punctuated by wave-influenced, hyperpycnal lobe and lobe fringe sedimentation and minor turbidite flows. A progressive unconformity affected the anticline area until the end of DS1. An angular unconformity separates DS1 and DS2, constituting a SB. DS2 started with LST deposition of wave-influenced, hyperpycnal channel-fill complex, lobe, and lobe fringe facies, and ended with retrogradational hyperpycnal facies encased in basin deposits during TST. LST and TST deposits correlate in seismic sections with two continuous bottomset reflectors, indicating large-scale aggradational stacking patterns during their development. HST (DS2) developed the foreset mixed-carbonate siliciclastic shelf, associated with slope mud belt and slope sand body facies. The foreset-topset transition constituted a low-energy, bioturbated sandy shoal crosscut by high-energy, sand bar complexes, with minor laterally associated, lagoonal deposits. The chemocline marks the transition between unbioturbated muddy slope facies and bioturbated mixed slope facies. Bioturbation occurs as a burrow mottling in the mixed slope, massive structures in the sandy shoal or as escape structures in high-energy bar facies. The foreset deposits ended by a truncation on top, representing an erosive SB. Based on the Vaca Muerta Formation time frame, the stratigraphic surfaces within the two third-order sequences could be correlated with T1 and T3 surfaces of the regional sequence stratigraphic framework.

3.9. Acknowledgments

We thank to Martin Parada, Debora Campetella, Maximiliano Rodríguez and the Painemilla family, who were of exceptional support in the Picún Leufú village field work, Fernando Valencia for his help with thin section descriptions, the feedback provided by C. Zavala to an early draft, and the valuable comments of reviewers Lauren Birgenheier and Massimo Moretti. This work was financially supported by the Natural Sciences and Engineering Research Council of Canada (NSERC), PI 40-A-468 IA 1 from the Universidad Nacional de Río Negro (UNRN), 2016 Student Research Grant from Society for Sedimentary Geology (SEPM), 2016 Research Grant from the Geological Society of America (GSA), and 2016 Grants-in-Aid Program of the American Association of Petroleum Geologists (AAPG). E.P thanks the CNPq and FAPERJ by financial support.

TRANSITION

Chapter 3 analyzes and discusses the sedimentological, ichnological, and sequence stratigraphic datasets of the basin margin location. In contrast, Chapter 4 consists of a sedimentological and sequence stratigraphic analysis but from the basin centre location. This study provides insights into understanding sedimentary processes and sediment partitioning in mixed clinoform systems, and evaluating the impact of basin circulation on sediment reworking and bottom water oxygenation.

CHAPTER 4: INTERPLAY OF SEDIMENTARY PROCESSES IN A FINE-GRAINED CARBONATE-SILICICLASTIC, SUBAQUEOUS CLINOFORM: THE UPPER JURASSIC-LOWER CRETACEOUS VACA MUERTA FORMATION, NEUQUÉN BASIN, ARGENTINA

Paz, M., Buatois, L.A., Mángano, M.G., Desjardins, P.R., Rodríguez, M.N., Ponce, J.J., Minisini, D., González Tomassini, F., Pereira, E., Carmona, N.B., Fantín, M. and Vallejo, M.D., (in review), Interplay of sedimentary processes in a fine-grained carbonate-siliciclastic, subaqueous clinoform: The Upper Jurassic-Lower Cretaceous Vaca Muerta Formation, Neuquén Basin, Argentina. *GSA Bulletin*.

Abstract

Over the last years, extensive research on fine-grained depositional systems triggered new ideas on sedimentary processes occurring in distal environments. In particular, fine-grained sediments deposited under oxygen-deficient conditions are enriched in organic matter and hold considerable economic interest as unconventional shale reservoirs. The present analysis integrates stratigraphic, sedimentologic, ichnologic, and sequence stratigraphic datasets to understand depositional processes in the Upper Jurassic-Lower Cretaceous Vaca Muerta Formation (Argentina), the most important economical unconventional play outside North America. For this purpose, cores from nine wells and one outcrop were examined. The stratigraphic succession comprises four third-order depositional sequences that can be subdivided into fifteen facies and five facies associations, deposited in a mixed carbonate-siliciclastic, shelf-margin, subaqueous clinoform system. Sedimentary processes include suspension fallout under anoxia dominating in the bottomset, and hypopycnal/mesopycnal plumes and fluid muds in the foreset in anoxic to oxic conditions. Estuarine circulation produced a stable oxycline and dominated the delivery of sediments to the basin. However, the typical estuarine circulation changed to weakened estuarine or anti-estuarine during arid and cooler climates, and wind- and thermohaline-driven contour currents reworked and oxygenated the complete clinoform system. This study provides insights into differentiating bottom current from sediment-gravity flow deposits, delineating paleoecological conditions using trace fossils, understanding forcing mechanisms of surface and

bottom water circulation, and evaluating sediment partitioning (carbonate, siliciclastics and organic matter) in fine-grained clinoform systems.

4.1 Introduction

Fine-grained depositional systems represent an important component of modern sedimentary successions, comprising about 70% of basin-fill history (Aplin and Macquaker, 2011), yet their analysis has been hampered by the technical difficulties of observing depositional processes in distal, relatively deep marine environments, with most of the first interpretations relying on models (Hill *et al.*, 2007). However, over the last years, flume experiments and analyses of the stratigraphic record sparked considerable progress on the understanding of depositional processes and sedimentary facies of fine-grained units (Baas and Best, 2002; Schieber *et al.*, 2007; Schieber, 2011). These findings suggested that mud transport at the seafloor represents an important contributor to sediment accumulation, contrasting with the traditional idea of dominantly hemipelagic deposition of mud in distal environments (Macquaker and Bohacs 2007; Schieber *et al.*, 2007). Since then, several fine-grained successions have been interpreted as deposited after bottom transport (e.g. Varban and Plint, 2008; Ghadeer and Macquaker, 2011; Nyhuis *et al.*, 2014; Birgenheier *et al.*, 2017; Newport *et al.*, 2017; Li and Schieber, 2018).

The increasead interest in fine-grained depositional systems follows the extensive exploration of unconventional shale reservoirs. These organic-rich shales typically comprise successions recording variable bottom transport activity and intermittent oxygen-deficient conditions (Hammes and Frébourg, 2012; Egenhoff and Fishman, 2013; Frébourg *et al.*, 2013; Wilson and Schieber, 2015; Birgenheier *et al.*, 2017; Borcovsky *et al.*, 2017; Minisini *et al.*, 2018). The Upper Jurassic-Lower Cretaceous Vaca Muerta Formation (Neuquen Basin, Argentina), object of this contribution, represents the first economical unconventional play outside North America, characterized by a prograding clinoform system with exceptional thickness (100-700 m) and extent (30,000 km^2). Hydrocarbons are mainly produced from horizontal wells drilled in the proximal bottomsets, showing the best unconventional reservoir characteristics (averages: TOC 5%; porosity 12%; clay 10-20%, water saturation 20%), yet distal bottomset and foreset reservoirs are also developed (Minisini *et al.*, 2020a). As a consequence, the Vaca Muerta Formation has been extensively studied in the last years by industry and academia in order to pursue further

exploration and optimize production (González *et al.*, 2018; Minisini *et al.*, 2020c). In this context, the new sedimentologic knowledge on fine-grained depositional environments can be integrated with petrophysical, geochemical and geomechanical datasets, creating an important tool to refine petroleum play concepts and determine well landing zones.

In fact, the availability of new datasets and increased resolution of the studies triggered new ideas on the origin of bottom transport processes, which is important to improve the prediction of reservoir quality, and reservoir distribution and extent of the reservoir quality. In a broad discussion on the different mud transport processes, Schieber (2016) highlighted the importance of wind- and tide-driven circulation to account for the deposition of considerable amounts of mud in distal environments. In more proximal environments, other ideas emerged, such as mud-rich hyperpycnal flow deposition or flows triggered and enhanced by wave and current activity (Bhattacharya and MacEachern, 2009; Macquaker *et al.*, 2010b; Wilson and Schieber, 2015; Lin and Bhattacharya, 2021; Zavala *et al.*, in press). However, a comprehensive model for these different processes is still under elaboration, and progress in this area may be stimulated by a proper understanding of processes in modern systems (e.g. Ogston *et al.*, 2000; Traykovski *et al.*, 2000; Cattaneo *et al.*, 2003; Hill *et al.*, 2007). Moreover, the role of each of these processes on the deposition of organic matter seems to be variable (Lash, 2016; Otharán *et al.*, 2020), underscoring the potential influence of sedimentologic studies on reservoir characterization.

This paper analyzes the sedimentology, ichnology, and sequence stratigraphy of cores from nine wells and an outcrop along the muddy, shelf-margin clinoform system of the Vaca Muerta Formation. The objetctives of this study are to characterize facies and facies associations, and determine sedimentary processes, paleoecological controls on trace fossils and organic matter distribution in order to generate an integrated depositional model. In particular, this study focuses on the complex interplay of depositional processes along the clinoform, namely 1) hemipelagic suspension fallout sedimentation, 2) wind- and thermohaline-driven contour currents, 3) hypopycnal/mesopycnal plumes, and 4) wave- or current-enhanced fluid mud flows. The description of both bottom current and sediment-gravity flow deposits provides insights into their differentiation using sedimentologic and ichnologic data. On the other hand, trace fossils were helpful to delineate paleoenvironmental conditions and characterize ichnofacies in fine-grained deposits. In addition, this multidisciplinary and integrated characterization of the Vaca Muerta

Formation may shed light on other organic-rich fine-grained depositional systems potentially hosting unconventional reservoirs.

4.2 Geologic setting

The Neuquén Basin is in central western Argentina and encompasses approximately 7000 m of mostly Jurassic and Cretaceous strata (Figs. 4.1, 4.2; Arregui *et al.*, 2011; Casadío and Montagna, 2015). Sedimentation began with an extensional event and subsequent syn-rift deposition during the Late Triassic to Early Jurassic, represented by the Precuyano Cycle (Carbone *et al.*, 2011). From Early Jurassic to Late Cretaceous, thermal subsidence with local tectonic inversions gradually generated a single broad basin, showing alternating continental and marine deposition in response to sea-level fluctuations (Cuyo, Lotena, Mendoza and Bajada del Agrio Groups; Arregui *et al.*, 2011). A compressional regime started during the Late Cretaceous (Andean uplift) closing the connection between the Neuquén Basin and the Pacific Ocean with subsequent deposition of the continental Neuquén Group in a foreland stage (Tunik *et al.*, 2010). The last transgression entered from the Atlantic Ocean during Late Cretaceous to early Paleogene, generating marine sedimentation recorded in the Malargüe Group (Arregüi *et al.*, 2011).

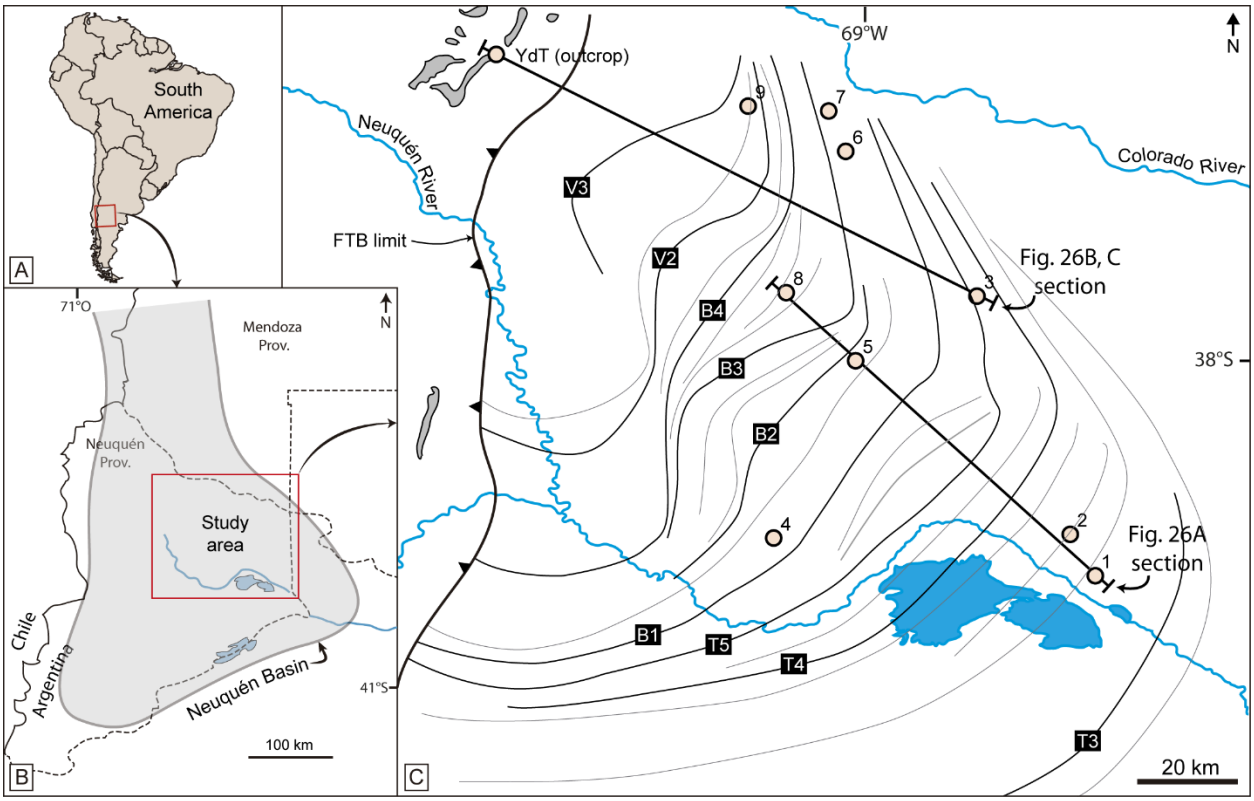

Fig. 4.1. Location maps. A) Location of the Neuquén Basin in Argentina. B) Neuquén Basin shape and extent (gray). C) Study area with location of well with cores (1-9), outcrop (YdT: Yesera del Tromen), and transects displayed in fig. 4.20. Clinoforms of the Vaca Muerta-Quintuco system prograde NW-ward and their evolving shelf breaks are shown, from older to younger: T3, T4, T5, B1, B2, B3, B4, V2, V3, see Fig. 4.3 (after Domínguez *et al.*, 2020a). Grey polygons are outcrops of the Vaca Muerta Formation, bounded to the east by the fold and thrust belt limit (FTB).

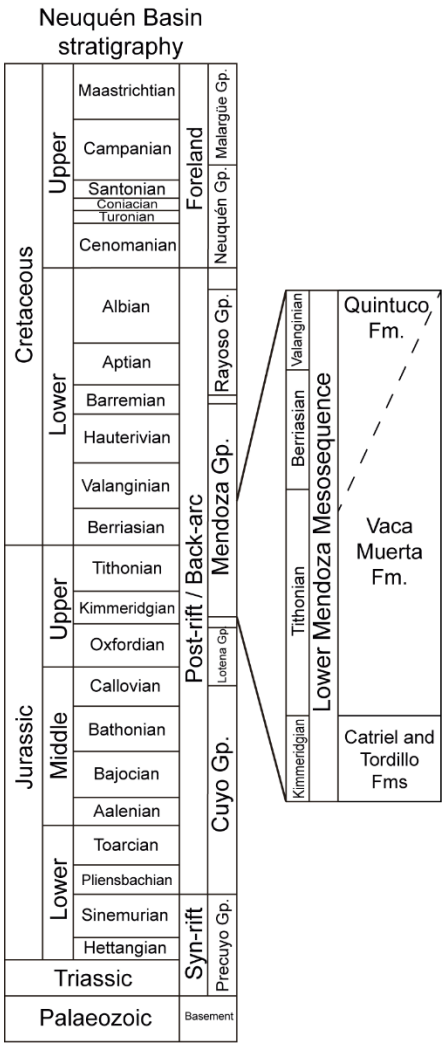

Fig. 4.2. Regional stratigraphy of the Neuquén Basin, displaying a detail of the stratigraphy in the study area.

The Vaca Muerta-Quintuco system (part of the Mendoza Group) consists of subaqueous clinoforms, deposited from early Tithonian to early Valanginian, and represents a shallowing-upward sedimentary cycle of second order (Fig. 4.3) (Mitchum and Uliana, 1985; Legarreta and Gulisano, 1989; Leanza *et al.*, 2020a), subdivided into six chrono-stratigraphic units (*sensu* Desjardins *et al.*, 2018; Minisini *et al.*, 2020b). The Vaca Muerta Formation corresponds to the bottomsets and foresets of the clinoforms, consisting of carbonaceous (organic-rich) mixed and calcareous mudstone interbedded with limestone and extremely thin volcaniclastic layers (i.e. bentonite, tuff, tephra; Kietzmann and Rodríguez Schelotto, 2018), whereas the Quintuco Formation represents the coeval topsets (Fig. 4.3). Acoustic impedance from seismic inversions

shows that high values relate to carbonate-rich units, whereas low values relate to organic-rich, porous units (Reijenstein *et al.*, 2020, Fig. 4.3). The Vaca Muerta–Quintuco system is uncomformably underlain by the continental Tordillo Formation, and topped by the regional intra-Valanginian uncomformity (Fig. 4.2; Gulisano *et al.*, 1984; Mitchum and Uliana, 1985; Leanza *et al.*, 2011). The stratigraphic architecture, sequence stratigraphy, and structural elements of this system have been extensively studied after multiple seismic data acquisitions (Mitchum and Uliana, 1985; Maretto and Pángaro, 2005; Reijenstein *et al.*, 2017b; Desjardins *et al.*, 2018; Domínguez *et al.*, 2020a).

The subsurface study area represents the sweet spot of the unconventional exploration (Fig. 4.1C), hence it has been subject to numerous sedimentologic and sequence stratigraphic studies (e.g., Fantín and González, 2014; González Tomassini *et al.*, 2014; Pose *et al.*, 2014; Repol *et al.*, 2014; Notta *et al.*, 2017; Barredo *et al.*, 2018; Desjardins and Aguirre, 2018; Desjardins *et al.*, 2018; Gómez Rivarola and Borgnia, 2018; Vallejo *et al.*, 2018; Estrada *et al.*, 2020; Minisini *et al.*, 2020a; Reijenstein *et al.*, 2020). The surface study area (outcrop) was also previously studied from sedimentologic, geochemical and sequence stratigraphic perspectives (Mitchum and Uliana, 1985; Spalletti *et al.*, 1999, 2014, Krim, 2015; Ponce *et al.*, 2015; Kietzmann *et al.*, 2016; Capelli *et al.*, 2018; Catalano *et al.*, 2018; Rodríguez Blanco *et al.*, 2020; del Rosario Lanz *et al.*, 2021), coupled with biostratigraphic and paleontologic analyses (Leanza and Hugo, 1977; Leanza *et al.*, 1977; Leanza, 1993; Aguirre-Urreta *et al.*, 2014). Trace fossils were mentioned in both cores and outcrops from the study area (Ponce *et al.*, 2015; Kietzmann *et al.*, 2016; Desjardins and Aguirre, 2018; see also Doyle *et al.*, 2005).

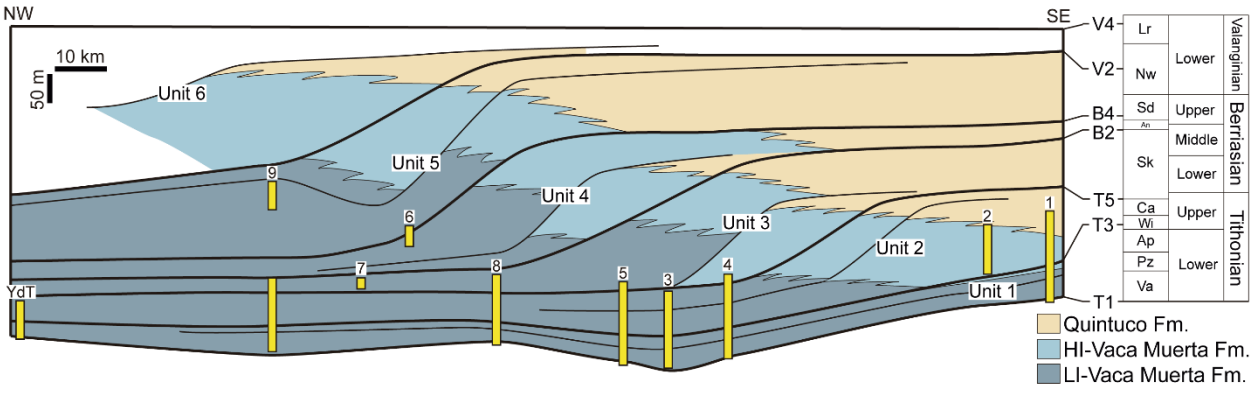

Fig. 4.3. NW-SE simplified cross-section of the Quintuco-Vaca Muerta system, showing the projected locations of the cores and outcrop analyzed (modified from Sattler *et al.*, 2018 and Reijenstein *et al.*, 2017b).

The Vaca Muerta Formation is divided in a high acoustic impedance succession (HI, correlated with carbonate-rich rocks) and a low acoustic impedance succession (LI, correlated with organic-rich rocks). Units, stratigraphic surfaces and ages are after Minisini *et al.* (2020b -see their Fig. 5). Note ammonite zones: Va: *Virgatosphinctes andesensis*, Pz: *Pseudolissoceras zittelli*, Ap: *Aulacosphinctes proximus*, Wi: *Windhauseniceras internispinosum*, Ca: *Corongoceras alternans*, Sk: *Substeueroceras koeneni*, An: *Argentiniceras noduliferum*, Sd: *Spiticeras damesi*, Nw: *Neocomites wichmanni*, Lr: *Lissonia riveroi*).

4.3 Methodology

This study analyzed and correlated cores from nine wells and an outcrop (Figs. 4.1C, 4.3, Appendix B). The outcrop (Yesera del Tromen, 148 m thick) shows a fault at 115 m that repeats the *W. internispinosum* ammonite zone (Aguirre-Urreta *et al.*, 2014). The analysis is based on sedimentologic, ichnologic, and geochemical data. Descriptions of rocks were improved by spraying samples with ethanol and consequently applying image enhancement techniques to photographs, such as brightness, contrast, and level adjustment. The mudstones were characterized following terminology proposed by Lazar *et al.* (2015b), whereas the lithofacies rich in carbonate constituents followed the carbonate terminology of Wright (1992).

Bioturbation index (BI) was asessed in intervals of 5 cm, following Taylor and Goldring (1993). However, a higher resolution was adopted in intervals showing changes in bioturbation intensity at a smaller scale. Tuffs were used as marker beds to measure penetration depth for discrete trace fossils. In heterolithic or highly bioturbated successions, penetration depth was estimated measuring the distance between discrete trace fossils and the inferred colonization surface. Thin sections were described on a petrographic microscope (59 sections from cores, 18 from outcrop). Rock composition derives from XRD analysis on cores. Total organic carbon (TOC) was obtained in cutting samples from cores (n=156) and outcrop samples (n=18) using LECO SC 632 at the Laboratório de Estratigrafia Química e Geoquímica Orgânica of the Universidade do Estado do Rio de Janeiro, Brazil. Three samples coated in 200Å of carbon were subject to backscattered electron (BSE) analysis. BSE images were obtained on a JEOL 8600 Superprobe electron microprobe analyzer using a Gellar Microanalytical dPict image adquisition system at the University of Saskatchewan Electron Microprobe Laboratory. Qualitative spot analyses were performed using energy dispersive spectrometry (EDS). The BSE and EDS data helped characterize mudstone and pellets composition.

A scheme of three hierarchies was adopted to analyze the Vaca Muerta deposits, namely lithofacies, facies, and facies associations. Lithofacies were named following the code of Kietzmann and Rodríguez Schelotto (2018) based on lithology, composition, and sedimentary structures. Lithofacies were combined with ichnologic and geochemical data to define facies characterizing depositional environments. In turn, genetically related facies were grouped into facies associations depending on the general environmental location. The whole succession was analyzed along two transects to define a sequence stratigraphic framework (Fig. 4.1C). Definition of time lines, stratigraphic surfaces and units is based on the most updated and integrated sequence stratigraphic analysis of the Vaca Muerta-Quintuco system, compiled by Minisini *et al.* (2020b - see their Fig. 5), modified after Desjardins *et al.* (2018) and González Tomassini *et al.* (2016). These stratigraphic surfaces were preferred over surfaces defined in previous stratigraphic analyses (e.g. Mitchum and Uliana, 1985; Reijenstein *et al.*, 2017b; Domínguez *et al.*, 2020a) because they were defined evaluating all the nomenclature utilized in different companies operating in the study area (Desjardins *et al.*, 2018), and therefore, they were helpful for correlation across wells. Sequence stratigraphic surfaces and system tracts nomenclature are taken from the Depositional Sequence IV model (Hunt and Tucker, 1992), but following the recommendation of Catuneanu (2006) of using the Regressive Systems Tract of Embry and Johannessen (1992) when the different regressive deposits cannot be differentiated.

4.4 Facies analysis

Lithofacies and trace-fossil data are summarized in Tables 4.1 and 4.2, respectively. For a further analysis and discussion of trace-fossils, see Chapter 5. The clinoform system of the Vaca Muerta and Quintuco formations started with a low-angle slope (0.2-0.3°) during deposition of Unit 1, and changed to higher angles for the following Units (1-3°; Figs. 4.4, 4.5; Minisini *et al.*, 2020a). The clinoform system has been previously described as part of a mixed ramp or shelf, mainly depending on the angle of slope (e.g. Spalleti *et al.*, 1999; Zeller *et al.*, 2015a; Kietzmann *et al.*, 2016). In this study, the shelf nomenclature was preferred (e.g. Pose *et al.*, 2014; Zeller *et al.*, 2015a; Paz *et al.*, 2019) because of the existence of slump structures indicating slopes, and the low amount of storm deposits to define ramp subenvironments. However, it must be noted that slopes (clinoforms) are absent in transects located in the northern sector of the study area (close to

wells 6, 7 and 9, Fig. 4.1C), where less cores are available, in which case the ramp nomenclature was utilized (e.g. Spalletti *et al.*, 1999; Kietzmann and Palma, 2011; Kietzmann *et al.*, 2015).

In the cores and the Yesera outcrop, the Vaca Muerta Formation (up to 300 m thick) overlays the eolian Catriel Formation and the coeval fluvial-to-lacustrine Tordillo Formation, respectively. The basal transgressive interval is constituted by 3-4 m-thick, marginal-marine facies association. Upward, the prograding clinoform displays deposits differentiated into basin, drift, and slope facies associations, whereas cores from the northern part of the study area (well 6, 7 and 9) shows an outer ramp facies association. The uppermost slope facies association indicates the most proximal environment, representing the transition to the Quintuco Formation.

Table 4.1. Lithofacies of the Vaca Muerta Formation defined in the study area. Codes refer to lithology, composition, and sedimentary structures following the proposal of Kietzmann and Rodríguez Schelotto (2018). Lithofacies with similar composition and interpretation were grouped in the same row to simplify the chart.

Code	Lithofacies description	Composition	Interpretation
Sm, Sh, Sl, Sr	1-30 cm-thick, massive, parallel-, low-angle and ripple-cross-laminated, medium- to coarse-grained sandstone (Fig. 4.6A). Sharp to erosive bases. Local 0.5-2 mm-thick mudstone drapes.	Granule- to pebble-sized organic matter intraclasts and sand-size heavy minerals.	Tidal flood and storm surge reworking of the Catriel Formation eolian deposits during the marine Vaca Muerta transgression. Mudstone drapes indicating mud deposition during slack water conditions in a diurnal tidal cycle, generating flaser bedding (Reineck and Wunderlich, 1968). Erosive bases in cross-bedded sandstone suggestive of local development of channels.
B_{m1}	5-10 cm-thick bindstone with crinkly lamination. Local sand-rich cracks (Fig. 4.6A, B)	Lamination with alternated microsparite dolomite, organic matter, and cubic pyrite. Silt and sand grains displaying a preferential orientation of their long axes parallel to lamination.	Microbial mat development suggesting a stressed environment associated with marginal marine conditions. Cracks probably subaqueous, formed by salinity changes or sediment loading over decaying, void-rich mats (Harazim *et al.*, 2013).
M_{cm}b-w	Massive (bioturbated) to wavy, calcareous to mixed, coarse to fine mudstone. Minor parallel lamination and current ripple cross-lamination (Fig. 4.6C, D, E). Mm-thick drapes of tuffaceous material. Local sand-rich cracks.	Carbonate and pyrite intraclasts and fragmented bivalves and ammonites.	Wavy surfaces indicative of reworking by oscillatory flows above fair-weather wave base and rare combined flows.

M_mh, F_b, R_b	Parallel-laminated to bedded (up to 1 cm thick), carbonaceous, mixed to minor siliceous, argillaceous or calcareous, fine mudstone. 3-30 cm-thick, bioclastic floatstone to rudstone (Fig. 4.7A, B, C).	Fine sand to silt-sized quartz, plagioclase, carbonate-replaced clasts, volcanic glass, organic matter aggregates, phosphatic fragments, and pellets. Fossils: calcite-replaced radiolarians, bivalves and ammonite shells and molds, and minor fish scales, echinoderms, agglutinated foraminifera and benthic foraminifera tests. F_b/R_b displaying dense to loose packing of ammonites and bivalves, and rarely fragmented bioclasts. Matrix with microcrystalline quartz, clays, coccoliths, and framboidal pyrite (Fig. 4.8J, K).	Pelagic and occasional hemipelagic deposition in organic-rich, dysoxic to anoxic environments. F_b/R_b representing shell condensation during reduced pelagic sedimentation. R_b with bioclasts suggesting minor bottom current events. Bivalve fauna pointing toward local development of exaerobic conditions (Savrda and Bottjer, 1987) or short-term benthic colonization due to fluctuating oxygen conditions (Röhl *et al.*, 2001).
P_ph	Discontinuous, parallel-laminated, peloidal packstone. Internally, laminaset boundaries comprising gradational to minor sharp to erosive contacts (Fig. 4.7D, E). Transitional gradation from M_mh (Fig. 4.7F). Commonly associated vertically with volcaniclastic intervals.	Sand- to granule-sized, lens- to oval-shaped peloids elongated parallel to locally non-parallel to bedding, very fine-grained sand- to silt-sized plagioclase, muscovite, pellets, quartz, and undifferentiated skeletal fragments. Fossils: radiolarians, bivalves and ammonites.	The transitional gradation from M_mh and the fact that this lithofacies is similar to the texture of uncompacted strata of carbonate concretions (Fig. 4.7F) suggestive of a variant of M_mh affected by early carbonate cementation.
M_{bm}h, M_{cm}b	M_{bm}h is planar, parallel to non-parallel-bedded (1-10 cm-thick), bioclastic, mixed to rarely calcareous, fine to medium mudstone. M_{cm}b is massive	Silt-sized carbonate intraclasts, quartz, plagioclase, mica, and organic-rich and clay-rich pellets (Fig. 4.8A, B). Fossils: foraminifera tests, agglutinated foraminifera, calcite-replaced radiolarians, bivalves, gastropods, *Saccocoma*	Transitional bed and laminae contacts indicative of pelagic and hemipelagic deposition or probably low energy bottom currents under different degrees of oxygenation.

	(bioturbated) to irregularly parallel-bedded (1-30 cm-thick) calcareous to mixed, fine to medium mudstone (Fig. 4.9A, B, C)	microcrinoids, ammonites, and undetermined tube-like fossils, Bioclastic mudstone with a predominance of radiolarians. Matrix with microsparite dolomite, clays, and organic matter.	
Mh, Ml, M_sh, M_sl, M_sr, M_sw	Mh/Ml are 0.2-5 cm-thick, calcareous fine mudstone showing continuous, planar, parallel to low-angle downlapping, coarse mudstone laminae. M_sh,/M_sl/M_sr/M_sw comprise 0.5-5 cm-thick, parallel to low-angle, current- and wave-ripple cross-laminated, calcareous coarse mudstone (Fig. 4.9D, E, F, G). Sharp to erosive bases, tabular to lenticular geometries and sharp to bioturbated tops.	Silt-sized plagioclase, carbonate intraclasts, undifferentiated skeletal fragments, mudstone intraclasts, quartz, pellets, and echinoderm fragments. Fossils: calcite-replaced radiolarians, forams and bivalves. Laminae composed of silt- to very fine-grained sand-sized fragments of *Rhaxella*, forams, calcite-replaced radiolarians and mudstone intraclasts. Illitic and coccolith-rich matrix.	Bottom current activity (see Paz *et al.*, in review a). Mh and Ml representing bedload sediment segregation from mixed clay-silt suspensions and consequent floccule and silt ripple formation (Yawar and Schieber, 2017). M_sh, M_sl and M_sr originated during bedload traction transport of higher velocity and sedimentation rate (Yawar and Schieber, 2017). Sharp tops and absence of the typical normal graded interval precluding a turbidite interpretation (Shanmugam *et al.*, 1993a). M_sw caused by oscillatory flow reworking associated with long wavelength waves during storm conditions, or irregular bed development in a unidirectional, clay-rich flow (Baas *et al.*, 2016).
M_{cr}b, M_{cr}t, M_{cr}h, M_{cr}l,	5-50 cm-thick, massive (bioturbated) crinoidal mudstone. 5-15 cm-thick, cross-bedded crinoidal mudstone. 2-10 cm-thick crinoidal mudstone with discontinuous to continuous, planar,	Silt-sized plagioclase, quartz, and volcanic rock fragments. Fossils: dominant *Saccocoma* microcrinoids and minor radiolarians, ammonites and bivalves.	Bottom current activity affecting a pelagic crinoid community. M_{cr}b produced during low-velocity currents and oxic environments. M_{cr}t represents bioclastic dunes. M_{cr}h and M_{cr}l interpreted as bioclastic lags indicating bedload traction transport

$M_{cr}w$, $M_{cr}r$,	parallel-, low-angle to rare wavy (1-2 mm-thick) crinoid-rich laminae. 5-15 cm-thick crinoidal mudstone showing (0.5-3 mm thick and 2-20 mm long) crinoid-rich lenses (Fig. 4.10). Transitional ($M_{cr}b$), erosive ($M_{cr}t$), and sharp ($M_{cr}h$, $M_{cr}l$, $M_{cr}w$, $M_{cr}r$) bases.		and winnowing of muds during higher energy bottom currents. Crinoid-rich lenses interpreted as starved ripples due to their common gradation from lenticular structures to the laminae (Fig. 4.10B).
M_pl	20-70 cm-thick, low-angle cross-bedded peloidal mudstone to packstone, displaying 1-5 cm-thick ripple cross-laminated and trough cross-bedded intervals in bedding planes (Fig. 4.11). Minor undulatory lamination, symmetrical ripples, and climbing ripples. Sharp bases. One bidirectional paleocurrent (NE and SW) in outcrop.	Silt-sized, lens-shaped peloids, quartz, plagioclase and micas, and pebble-sized carbonate intraclasts (Fig. 4.8C). Fossils: calcite-replaced radiolarians, gastropods, microcrinoids, ammonites and bivalves. Gastropod and bivalve shell cavities typically filled with sparite.	Compound dunes generated by bottom currents. Low-angle cross-bedding representing second-order surfaces in which ripples and 3D dunes accrete (master bedding surfaces; Dalrymple, 2010). Bidirectional paleocurrent direction suggestive of a tidal origin (e.g. Neumeier, 1998), yet slack-water mudstone intervals are absent.
M_ch, M_cm, M_ccomp	Parallel-laminated to thin-bedded (0.25-10 mm-thick), calcareous medium mudstone with gradational to sharp bases. 1-50 mm-thick, massive, calcareous medium to coarse mudstone and composite beds	Pebble-sized, elongated, deformed, mudstone intraclasts and coarse sand-sized, rounded, carbonate intraclasts. Silt-sized, terrigenous (quartz and plagioclase) grains, dolomite microspar, clay and organic aggregates, bivalve bioclasts and peloids. Fossils: calcite-replaced	Gradational bases and absence of sedimentary structures in M_ch supporting hypopycnal or mesopycnal plumes or low-density flow deposition. M_cm and M_ccomp representing fluid mud flows. Lack of normal grading pointing towards a flow suffering *en masse* deposition, such as a high-density

	of calcareous mudstone, with erosive to sharp bases (Fig. 4.12). $M_c$comp showing local current-ripple cross-lamination, parallel-lamination, normal and inverse grading, micro-hummocky cross-lamination, wave ripples and/or intra-bed erosive surfaces. Minor small scour marks, load casts, mudstone pseudonodules, and flame structures. Sharp to rare irregular or wavy tops.	radiolarians. Lamination delineated by organic matter aggregates. Clay to micrite matrix.	mud flow showing low Reynold numbers. Deformed mudstone intraclasts within the bed suggesting low turbidity and probably incipient matrix strength supporting mechanisms. Minor current ripples indicative of the existence of turbulence within the flow and the occurrence of upper transitional plug flows with more varied mud concentrations (Baas and Best, 2002; Baas *et al.*, 2016). Local occurrence of wavy tops and micro hummocky cross-stratification indicative of rare oscillatory flows during and after deposition.
M_cw, M_cb	M_cw is 2-10 mm-thick, massive to normal graded, calcareous, fine to medium mudstone locally with wavy tops. Lenticular to minor tabular geometries. M_cb is 2-10 cm-thick, massive (bioturbated) to minor irregular- to wavy-laminated, calcareous to mixed mudstone (Fig. 4.13A, B).	Coarse- to medium-grained sand-sized, ovoid-shaped peloids, carbonate and quartz clasts, black grains and bioclasts. Silt-sized, quartz, plagioclase, mica, calcite and dolomite microspar, and clay-rich pellets in a micrite matrix. Fossils: ostreids, microcrinoids, calcite-replaced radiolarians and gastropods.	Low-energy, muddy environment affected by hemipelagic deposition (M_cb) and oscillatory flow reworking during storm events (M_cw).
M_sg, M_sm, Mcomp Scomp	0.2-20 cm-thick, normal graded or massive, fine to coarse mudstone to rare coarse-grained sandstone. 1-10 cm-thick, composite beds of	Silt- to granule-sized, pellets, organic matter aggregates, plagioclase, quartz, volcanic glass and carbonate and bindstone intraclasts (Fig. 4.8E). Fossils: bivalve, microcrinoid, and carbonate-	Normal graded beds suggesting differential settling of particles in a low-density turbidity flow (Mulder and Alexander, 2001). Composite beds indicative of velocity and/or sediment concentration variations

	bioclastic or intraclastic fine to coarse mudstone, and fine- to coarse-grained sandstone. Composite beds represented by alternation of normal to inverse gradation, massive, parallel- or ripple cross-lamination. Sharp to rarely erosive bases and sharp to gradational tops (Fig. 4.13D, E).	replaced radiolaria. Grains replaced by cubic and rarely framboidal pyrite or carbonate. Abundant granular microsparite dolomite as cement.	within a flow, generating current ripples at the turbulent base of lower density flows. Scomp are sand-rich concentrated density flows derived from erosion of the adjacent eolian environments (Chan and Kocurek, 1988).
W_{ib}hcs	15-30 cm-thick, hummocky cross-stratified and normal-graded, intraclastic to bioclastic wackestone, packstone to floatstone. Sharp- to erosive-bases and wavy tops (Fig. 4.13C).	Pebble- to sand-sized, tabular mudstone intraclasts, pellets, carbonate intraclasts and bioclasts. Fossils: ammonites, microcrinoids, carbonate-replaced radiolarians and bivalves.	Hummocky cross-stratification suggestive of combined oscillatory and unidirectional flows caused by storm waves and geostrophic currents (e.g. Kietzmann and Palma, 2011). Wavy tops reflecting lower energy conditions during a waning phase (Duke *et al.*, 1991).
B_{m2}, B_mb, M_{bind}	B_{m2} is 0.5-30 cm-thick bindstone, B_mb is 1-10 cm-thick, irregularly distributed, discontinuous bindstone laminae, and M_{bind} is 2-10 mm-thick, sharp-based mudstone with pebble- to granule-sized, bindstone intraclasts. Local bindstone showing thinner, black-colored laminae. Laminae with a crinkly texture and	Laminae composed by microsparite dolomite and minor organic matter and cubic pyrite (Fig. 4.8F).	Wavy-crinkled texture considered as an ancient analog of the lamination created by modern microbial mats (Schieber, 1999b). Tabular clasts and folding indicating that sediment cohesion was provided by trapping and binding generated by the extracellular polymeric substances from the mat-forming community. Activity of small bioturbators that disrupted the lamination and fed from the mat generated B_mb (e.g. Fenchel, 1998). M_{bind} produced

	rare superimposed wavy texture, showing downlapping relationships with underlying contacts and folding (Fig. 4.13F, G, H).		by bottom currents reworking the microbially stabilized sea floor and generating "mat chips" (Noffke, 2010).
Tm, Tg, Tr	1-10 cm-thick and minor 10-70 cm-thick, massive, graded and ripple cross-laminated tuff and lapilli-ash tuff. Alternation of normal or inverse grading, ripple cross-lamination and parallel-lamination. Double grading occurs (i.e. a fining-upward succession of several cm-thick beds showing normal grading). Local 5-10 cm-thick volcanic breccias. Sharp to erosive or transitional bases. Parallel-laminated or wavy tops. Soft-sediment deformation structures, such as convolute bedding and dish structures.	Very fine-grained sand- to silt-sized euhedral plagioclase, quartz (crystaloclasts) and arcuate to tabular glass shards, minor mudstone intraclasts, radiolaria, forams, benthic pellets and pumice fragments (Fig. 4.8G, 4.13I). Radiolarians within the benthic pellets. Plagioclase and quartz grains showing an upward decrease in abundance and glass shards showing an upward increase in some beds. Matrix completely replaced by calcite and minor pyrite (5%) cementation. Graded tops showing interlaminated tuff and organic-rich fine mudstone consisting of silt- and sand-sized, lens- and tabular-shaped, pelagic aggregates and ovoid, coccolith-rich planktonic pellets (Fig. 4.8G, H, I). Pelagic aggregates composed of coccoliths, radiolaria, microsparite, illite floccules, and minor silica replacements, plagioclase and volcanic glass shards (Fig. 4.8L).	Submarine volcanic fallout deposition and resedimented volcaniclastic deposits. Upward decrease in plagioclase and quartz crystals and increase in lower density material (glass shards) indicative of submarine fallout processes (Dimroth and Yamagishi, 1987). Soft-sediment deformation due to rapid sedimentation of the fallout deposits (Pedersen and Surlyk, 1977). Tuffs with ripples and erosive surfaces representing resedimentation processes. Double grading is typical of turbidity currents reworking sediment of different grain size as it settles in the seafloor (Fiske and Matsuda, 1964). Pelagic aggregates representing marine snow flocs associated with resuming of pelagic deposition at the end of the fallout events (Alldredge and Silver, 1988).
W_ib, W_ih, F_bb	10-30 cm-thick, massive (bioturbated), to parallel-bedded,	W_ib/W_ih show, very fine-grained to coarse-grained sand- to minor pebble-size carbonate	Oxic environment subject to moderate to high-energy currents. Bioclastic lags above erosive surfaces

	intraclastic wackestone. 5-20 cm-thick, massive (bioturbated), bioclastic floatstone to minor rudstone (Fig. 4.14). Fossil-rich intervals or lags mantling erosive to sharp surfaces.	intraclasts and grapestones, and minor phosphate intraclasts. Silt-sized quartz, carbonate clasts, plagioclase, micas, and clay-rich pellets (Fig. 4.8D). Fossils: calcite-replaced radiolarians and microcrinoids. F_bb dominated by ostreids, ammonites, and gastropods. Fossils concordant to bedding with minor randomly disposed bivalves.	indicative of storm events or currents capable of winnowing mud (Kidwell and Aigner, 1985).

Table 4.2. Trace-fossil content in the Vaca Muerta Formation described in the study area. BI: Bioturbation index.

Ichnotaxa	Characteristics	Interpretation and ethology
Alcyonidiopsis longobardiae	Actively pellet-infilled, horizontal to vertical, straight to minor curved, seldom branching unlined burrows. 0.5-2.3 mm wide and 3-20 mm long. Preserved as full relief in tuffs.	Polychaete detritus feeding trace. Fodinichnia.
Coprulus oblongus	125-500 μm wide and 250-800 μm long, ellipsoidal pellets. Length to width ratio is 2.01-2.6. Matrix composed of microcrystalline quartz and minor framboidal pyrite. Containing radiolarians, carbonate clasts and clay floccules. Preserved in tuffs.	Benthic polychaete faecal pellets.
Crininicaminus isp.	Horizontal, passively infilled burrows with bioclastic lining made up of crinoids. Burrows are 5-6 mm wide. Preserved as full relief in crinoidal mudstone.	Polychaete tube building associated with predation or suspension feeding. Domichnia.
Diplocraterion isp.	Vertical, U-shaped, passively infilled burrow displaying protrusive and retrusive spreite. Tube is 1-1.6 mm diameter, and 25-26 mm long. Preserved as full relief in tuffs.	Worm-like, suspension-feeding organism. Domichnia.
Lockeia siliquaria	Passively infilled, oval- shaped structures with rounded bases. Locally, one end with a straight tapering and another rounded end. Burrows are 2-5 mm wide and 5-7 mm long. Associated with equilibrium structures. Preserved as negative epirelief or positive hyporelief in calcareous mudstone.	Bivalve resting traces with suspension feeding strategies. Domichnia-Cubichnia.
?Lockeia isp.	Passively infilled, bowl-shaped structures with rounded bases. Burrows are 1.3-9.5 mm wide. Only observed in cross-sections, but vertically associated with *Lockeia siliquaria*.	Bivalve resting traces with suspension feeding strategies. Domichnia-Cubichnia.
Nereites isp.	Horizontal burrows with an actively filled, muddy dark core and a white to gray mantle. Burrows are 2.5-11 mm wide. Preserved as full relief in tuffs or coarse mudstone.	Deposit or detritus feeding worm like organism. Fodinichnia.

Palaeophycus heberti	Horizontal to oblique, passively infilled burrows with a 1 mm-thick white muddy wall. Burrows are 4-8 mm wide. Preserved as full relief in fine to coarse mudstone.	Dwelling burrow of a predaceous or suspension-feeding nereid or terebellid polychaete. Domichnia.
Palaeophycus isp.	Horizontal, curved to straight, passively infilled, typically lighter core and thin dark lined burrows. Burrows are 1-2.5 mm diameter. Preserved as full relief in tuffs or coarse mudstone.	Dwelling structure of a predator or suspension feeding vermiform organism. Domichnia.
Phycosiphon incertum	Oblique to horizontal, actively infilled burrows with a dark muddy core and white mantle. Burrows are 0.5 mm wide. Preserved as full relief in tuffs and fine to coarse mudstone.	Deposit-feeding structure of vermiform organism. Fodinichnia.
Planolites isp.	Simple, dominantly horizontal, unlined, straight to curved burrows with a dark or white infill. Burrows are 1-4 mm wide. Preserved as full relief in tuffs or coarse mudstone.	Deposit-feeding structure of vermiform organism. Fodinichnia.
?Skolithos isp.	Vertical, tube-shaped, passively infilled structures. Burrows are 3-7 mm long and 0.5-3 mm wide. Preserved as full relief in calcareous mudstone.	Dwelling structure of a vermiform organism. Domichnia.
Teichichnus patens	Straight to minor curved or sinuous, passively infilled horizontal burrows with vertical spreite, locally showing secondary successive branching. Causative burrow is 5-10 mm diameter. Preserved as full relief in tuffs.	The restriction of *Teichichnus* to organic-poor sediment (tuffs) suggest a dwelling or equilibrium structure of a surface-deposit, deposit, or suspension-feeding organism. Domichnia, Equilibrichnia.
Teichichnus rectus	Straight, passively infilled, arcuate-shaped burrow showing vertical to minor oblique spreite. Causative burrow is 0.5-2 mm diameter. Preserved as full relief in tuffs, mudstone or wackestone.	
Teichichnus zigzag	Horizontal to oblique, passively infilled burrows displaying a vertical spreite that switch directions horizontally in a zigzag pattern. Causative burrow is 0.5-1 mm diameter. Preserved as full relief in tuffs.	
Thalassinoides isp.	Horizontal to oblique, unlined, passively infilled burrows. Uncompacted specimens are common. Burrow diameter is 3-40 mm. Preserved as full relief in mudstone or tuffs.	Dwelling structure of a suspension or deposit

		feeding shrimp. Domichnia.
Zoophycos isp.	Horizontal to oblique burrows with horizontal spreite. 5-10 mm diameter. Preserved as full relief in tuffs.	Feeding structure of a vermiform organism. Fodinichnia.
Benthic pellet trails	Horizontal, curved to straight trails of pellets. 0.3-0.7 mm wide and 2-4 mm long. Preserved as full relief at the base of tuffs.	Grazing structures of polychaetes. Pascichnia.
Escape and equilibrium trace fossils	Oblique to vertical, U- and V-shaped, nested structures. Locally sharp-lined ?*Lockeia* isp is associated. 0.5-3 mm diameter and 1-15 mm long. Preserved as full relief in calcareous mudstone.	Differentiated between the two structures was difficult, yet sharp-lined burrows indicate re-establishment of organism in a colonization surface (typical of equilibrium traces). Fugichnia, Equilibrichnia.
Mantle and swirl structures	Highly compacted, horizontal, oblique or vertical burrows with irregular walls and locally an irregular concentric fill. 6-9 mm diameter. Preserved as full relief in tuffs and fine to coarse mudstone.	Movement of vermiform organisms in soupy substrates. Repichnia.

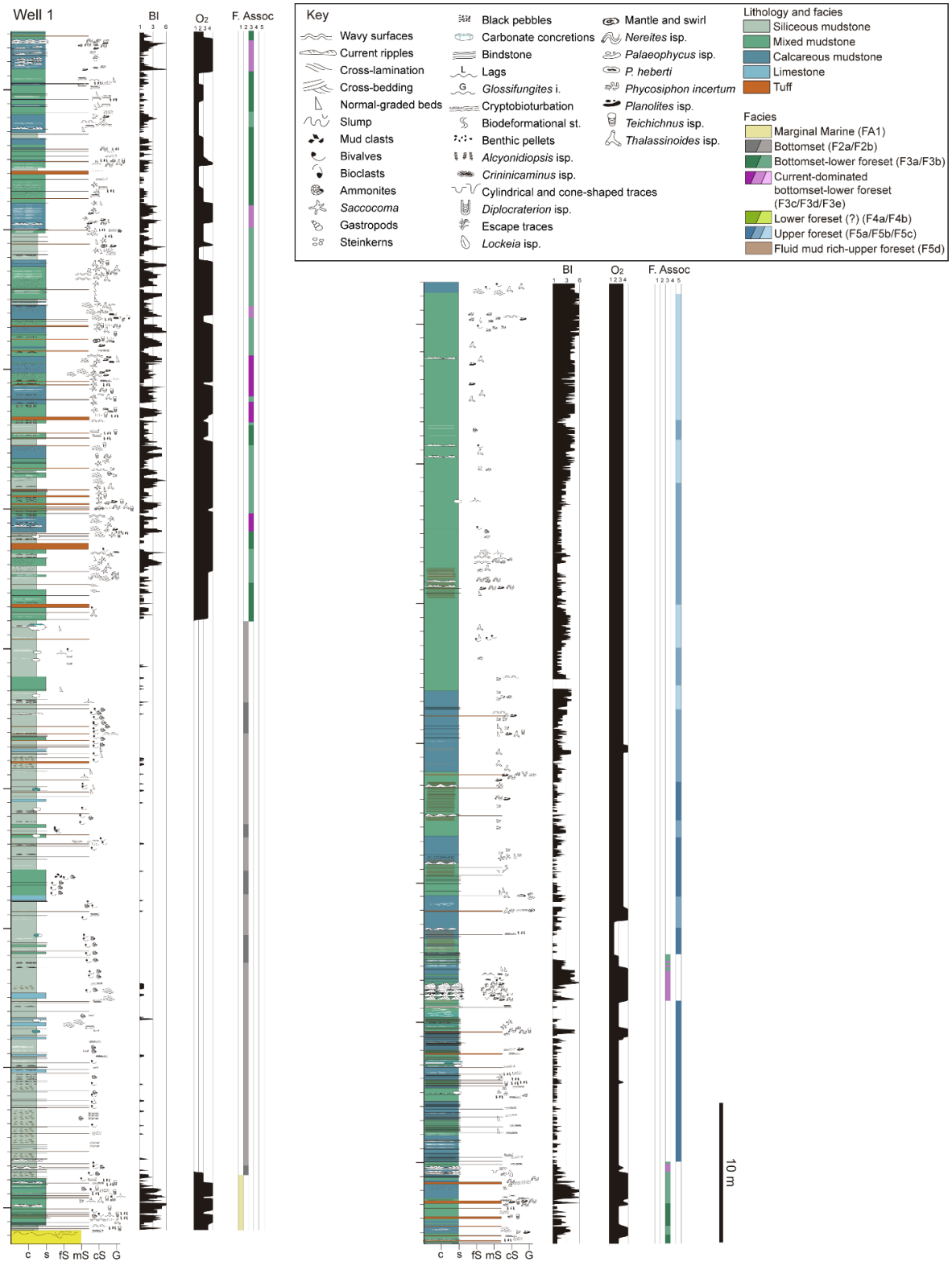

Fig. 4.4. Facies distribution in well 1. Ichnologic data, such as bioturbation index (BI), was documented along the section. Bottom water oxygen interpretation (O_2) based on mudstone fabric and trace fossil occurrence. Detail of the complete logs can be found in Appendix B.

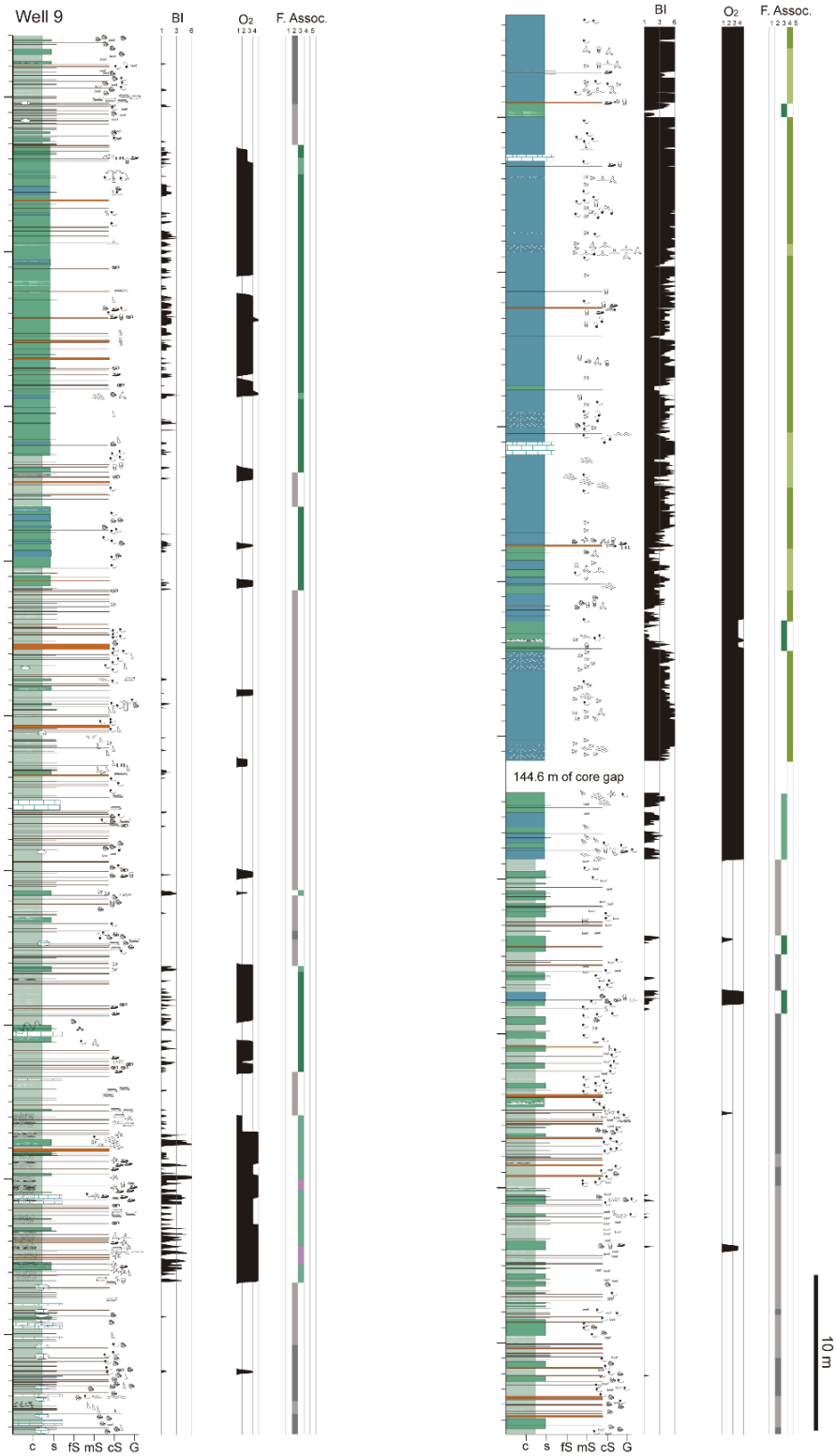

Fig. 4.5. Facies distribution in the cores located further offshore (well 9). Key in Fig. 4.4. Detail of the complete logs can be found in Appendix B.

4.4.1 Facies association 1 (FA1): Marginal-marine areas

FA1 comprises marginal-marine environments associated with the transition between the Kimmeridgian eolian deposits of the Catriel Formation and the marine Vaca Muerta Formation (e.g. Cevallos, 2005). Similar and roughly coeval transgressive deposits over an eolian complex have been documented in the Picún Leufú area (Paz *et al.*, 2021). FA1 is subdivided into two facies reflecting different positions within the coast. FA1 does not occur in the clinoform because the prograding marine system was yet not formed; however, at a larger scale (e.g. seismic data), this FA is delineated as part of the bottomset.

4.4.1.1 Facies 1a (F1a): Medium- to coarse-grained sandstone

Description. This facies consists of massive, parallel-laminated, low angle to current-ripple cross-laminated medium- to coarse-grained sandstone with mudstone drapes lithofacies (Sm, Sh, Sl, Sr; Figs. 4.6A, 4.15A; Table 4.1). Drapes are locally developed in pairs. A 5-cm-thick, micro-hummocky cross-stratified, tuffaceous medium- to coarse-grained sandstone is also observed. Pyrite cementation occurs as bed-parallel horizons (0.5-1.0 cm thick), or as laminae draping cross-laminated ripple (0.5-1 mm thick).

Ichnology. F1a is unbioturbated.

Interpretation. This facies represents marine reworking of the Catriel Formation continental deposits in a beach. The coast was affected by tidal flooding (Sr, Sl) that contributed to the reworking of the sandy coast (e.g. Inman *et al.*, 1966; Fryberger *et al.*, 1990). Pyrite cementated the areas with fine-grained accumulation on the ripples (mud drapes) or the eolian sandstone lamination. The hummocky-cross stratified sandstone suggests rare storm events.

4.4.1.2 Facies 1b (F1b): Bindstone and calcareous to mixed mudstone

Description. This facies consists mostly of bindstone (B_{m1}) and calcareous to mixed mudstone (M_{cm}b-w) lithofacies (Figs. 4.6B, C, D, E, F, 4.15A; Table 4.1). Thin- to thick-bedded, composited sandstone (Scomp), low-angle cross-bedded peloidal mudstone (M_pl), tuff to lapilli-ash tuff lithofacies (Tm) are interbedded locally. 1-30 cm-thick bioclastic and intraclastic lags and 0.5-1 mm-thick beefs are common.

Ichnology. B_{m1} is unbioturbated, but M_{cm}b-w shows variable intensity of bioturbation, with typical alternation of highly bioturbated (BI = 4-6) and unbioturbated (BI = 0) intervals. Mean BI is 3.04 (n=268), mean burrow diameter is 7.31 mm (n=16), and mean maximum bioturbation depth is 44.3 mm (n=12). Biodeformational structures are abundant in the mudstone lithofacies (M_{cm}b-w, Fig. 4.6D). Trace fossils include *Teichichnus rectus, T. zigzag, Thalassinoides* isp., *Phycosiphon incertum, Alcyonidiopsis longobardiae, Coprulus oblongus, Planolites* isp., and mantle and swirl structures (Fig. 4.6C, D, E). *Teichichnus patens* is observed in a 30 cm-thick tuff interval in the Yesera del Tromen outcrop (basal tuff of Aguirre-Urreta *et al.*, 2014). These discrete trace fossils occur within mudstone or tuff lithofacies (M_{cm}b-w, Tm). Uncompacted *Thalassinoides* isp. with sharp burrow boundaries can also be observed.

Interpretation. This facies was deposited in a bay environment subject to salinity changes above fair-weather wave base (MacEachern and Gingras, 2007; Paz *et al.*, 2021). The microbial mats (B_{m1}) and the high mudstone content suggest stressed and low-energy conditions. The bay alternated with high energy conditions generating the lags, and intercalation of sand-rich concentrated density flows (Scomp; Paz *et al.*, 2021). Biodeformational structures indicate the development of soupy to soft substrates. However, the sharp burrow margins, lack of compaction and passive infill in *Thalassinoides* isp. (Table 4.2) suggests the local development of the *Glossifungites* Ichnofacies, which illustrates firmground colonization after erosive events during transgressive scouring (Paz *et al.*, 2021). Erosional scouring is consistent with the presence of carbonate intraclast lags. High bioturbation intensity suggests oxic conditions, indicating an area above fair-weather wave base, with pulses of dysoxia and anoxia, as supported by the unbioturbated intervals.

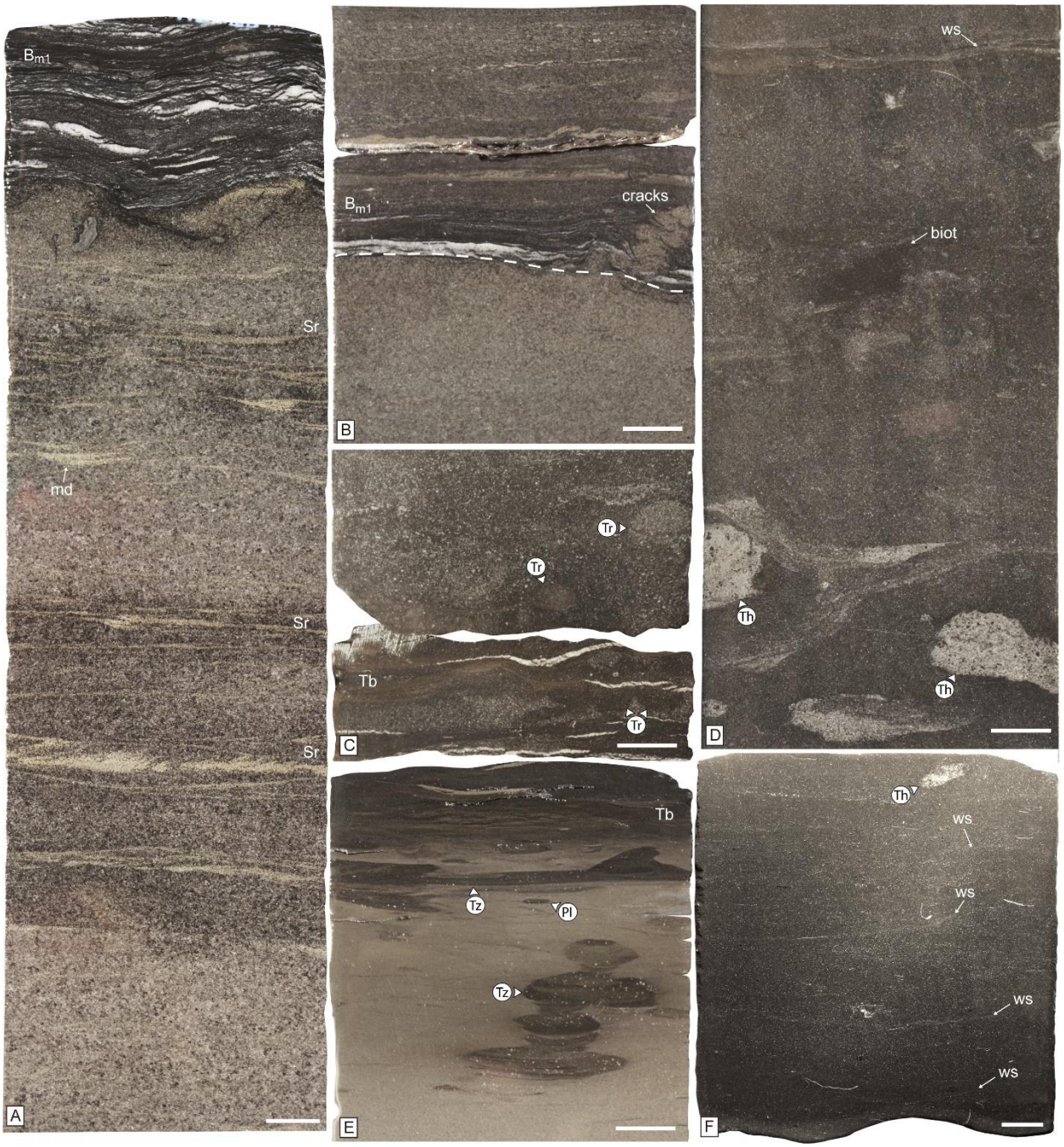

Fig. 4.6. Medium- to coarse-grained sandstone, bindstone and calcareous to mixed mudstone of marginal-marine facies association (FA1). A) Current-ripple cross-laminated sandstone (Sr) with mudstone drapes cemented by pyrite (md), with overlying bindstone (B_{m1}). B) Bindstone (B_{m1}) at the base of the Vaca Muerta Formation showing probably subaqueous cracks. C) Intraclastic, calcareous to mixed mudstone (M_{cm}b-w) highly bioturbated by *Teichichnus rectus* (Tr), with intercalated bioturbated tuff (Tb). D) Highly bioturbated calcareous mudstone, with biodeformational structures (biot) and *Thalassinoides* isp. (Th). Note faint wavy surfaces (ws) at the top of the core delineated by volcaniclastic material. E) *Teichichnus zigzag* (Tz) and

Planolites isp. (Pl) in bioturbated tuff. F) Laminated calcareous mudstone displaying faint wavy surfaces. Scale bars are 1 cm.

4.4.2 Facies association 2 (FA2): Basin

FA2 is represented by basin facies showing dominantly pelagic and hemipelagic deposition and located in bottomset and lower foreset positions of the clinoform system. It consists of a starved basin displaying evidence of sediment condensation, and three basin facies differentiated by their degree of oxygenation (anoxic, dysoxic and oxic).

4.4.2.1 Facies 2a (F2a): Carbonaceous, mixed mudstone and bioclastic floatstone to rudstone

Description. This facies mainly comprises carbonaceous, mixed mudstone (M_mh), bioclastic floatstone to rudstone (F_b, R_b), and bindstone (B_{m2}) lithofacies (Figs. 4.7A, B, C, 4.13F, 4.15B). Rare discontinuous parallel-laminated, peloidal packstone (P_ph, Fig. 4.7D, E, F), and tuff to lapilli-ash tuff (Tm, Tg, Tr) lithofacies occur as well. Pyrite replaced intraclasts and fossils. Carbonate cementation is observed as granular microsparite dolomite, generating 5-50 cm-thick carbonate concretions or concretionary levels (P_ph). Bitumen veins and calcite beef (0.1-2 cm thick) are observed in the highest TOC-rich intervals of this facies (Av. TOC of 5.43%, N=13).

Ichnology. This facies is commonly unbioturbated with very rare sparsely bioturbated intervals (BI 1-2, Fig. 4.7A). BI is typically 0, with rare intervals of 1 (mean BI of 0.05, n=1530), burrow diameter is *ca.* 0.89 mm, and maximum bioturbation depth is *ca.* 4.04 mm. The very rare bioturbated intervals are tuffs showing *Alcyonidiopsis longobardiae, Coprulus oblongus, Planolites* isp., pyrite-rich burrows, and mantle and swirl structures (Table 4.2). In addition, irregular, disturbed lamination on top of tuffs is preserved.

Interpretation. This facies association suggests condensation (F_b, R_b) and low sedimentation rate in a sediment-starved basin. Dominance of pelagic deposition is suggested by the abundance of pelagic microfauna (radiolarians and forams) and low amounts of bedload transport. Because P_ph preserves uncompacted strata of basinal deposition, the gradational boundaries between the laminasets indicate compositional changes from pelagic to occasional hemipelagic input. In contrast, rare sharp bed boundaries indicate minor event beds or hypopycnal plume deposition. Bottom current events are recorded by the small bioclasts of F_b/ R_b. The paucity of trace fossils suggests a highly reducing environment with anoxic conditions in bottom and

interstitial waters, punctuated by very rare dysoxic events. Microbial mats of sulfur-oxidizing bacteria can thrive in areas subject to stress conditions associated with oxygen deficiency (Oschmann, 2000), such as the oxygen minimum zones in the Santa Barbara Basin (Soutar and Crill, 1977) or areas associated with the coastal upwelling zone off central Chile (Fossing *et al.*, 1995). Low sedimentation rates and probably the establishment of a sulfate reduction zone enabled early carbonate cementation (Wetzel and Allia, 2000; Raiswell and Fisher, 2004). Heavy ^{13}C whole rock isotope values from concretions in the analyzed outcrop suggest methanogenesis was active during deposition (Catalano *et al.*, 2018), and supports the idea of a sulfate reduction zone close to the seafloor, generating early cementation.

4.4.2.2 Facies 2b (F2b): Carbonaceous, mixed mudstone

Description. This facies mainly comprises carbonaceous, mixed mudstone (M_mh) lithofacies. Bioclastic floatstone to rudstone (F_b, R_b), discontinuous parallel-laminated peloidal packstone (P_ph) and bioclastic mixed mudstone (M_{bm}h) are also regularly intercalated (Figs. 4.7, 15C). Very thin- to thin-bedded and rare thick-bedded intervals showing fine mudstone with coarse mudstone laminae (Mh), sharp- to erosive-based, graded to massive, fine to coarse mudstone (M_sg, M_sm), bindstone (B_{m2}), sharp-based mudstone with pebble- to granule-sized, bindstone intraclasts (M_{bind}), and tuff to lapilli-ash tuff (Tm, Tg, Tr) lithofacies are less common (Fig. 4.13G, H). Locally, peloidal mudstone with asymmetrical ripples (M_pl) was observed. Tuff intervals are more abundant than in other facies. Carbonate concretions or concretionary levels (30-50 cm-thick) are interbedded. Carbonate cementation locally occurs associated with bioclast-rich intervals, M_sg, M_sm, or volcaniclastic intervals (Tm, Tg, Tr, Fig. 4.9C).

Ichnology. This facies is commonly unbioturbated with very rare thin intervals with BI 1-2 (mean BI of 0.09, n=7580), burrow diameter is *ca.* 1.96 mm, and maximum bioturbation depth is *ca.* 6.84 mm. Some tuffs contain *Alcyonidiopsis longobardiae*, *Planolites* isp., *Coprulus oblongus*, pyrite-rich burrows, mantle and swirl structures, and biodeformational structures (Table 4.2).

Interpretation. This facies was deposited in an anoxic basin environment dominated by pelagic deposition with rare sediment-gravity flows (M_sg, M_sm) and bottom current activity (Mh, M_pl, M_{bind}). Pelagic sedimentation is suggested by the pelagic aggregates on top of the tuff intervals (Tm, Tg, Tr) and the abundance of pelagic fauna. The association of carbonate intervals with

porous media (M_sg, M_sm, Tm, Tg, Tr) indicates that carbonate-rich beds do not constitute event beds but areas of intensive carbonate cementation during early diagenesis (e.g. Westphal *et al.*, 2008). The fact that carbonate cementation enhances visibility of sediment-gravity flow deposits supports the idea of low bedload transport, as cementation might have prevented sediment compaction of these event beds. The less common sediment-gravity flows (M_sg, M_sm) may have been originated by destabilization of the slope or constitute hyperpycnal flows (e.g. Paz *et al.*, 2019; Otharán *et al.*, 2020). Basin environments are typically below the oxycline, which reflects a strong gradient from the relatively better mixed waters of shallower areas. Bottom and interstitial waters were anoxic for the most part, evidenced by the lack of bioturbation, and carbonate cementation might suggest sulfate reduction zones within the sediment (P_ph). The bottom currents that reworked this area probably did not modify the anoxic conditions of the sea-floor (Paz *et al.*, in review a), although the local presence of bioturbated beds suggests very rare short-term bottom-water dysoxic events.

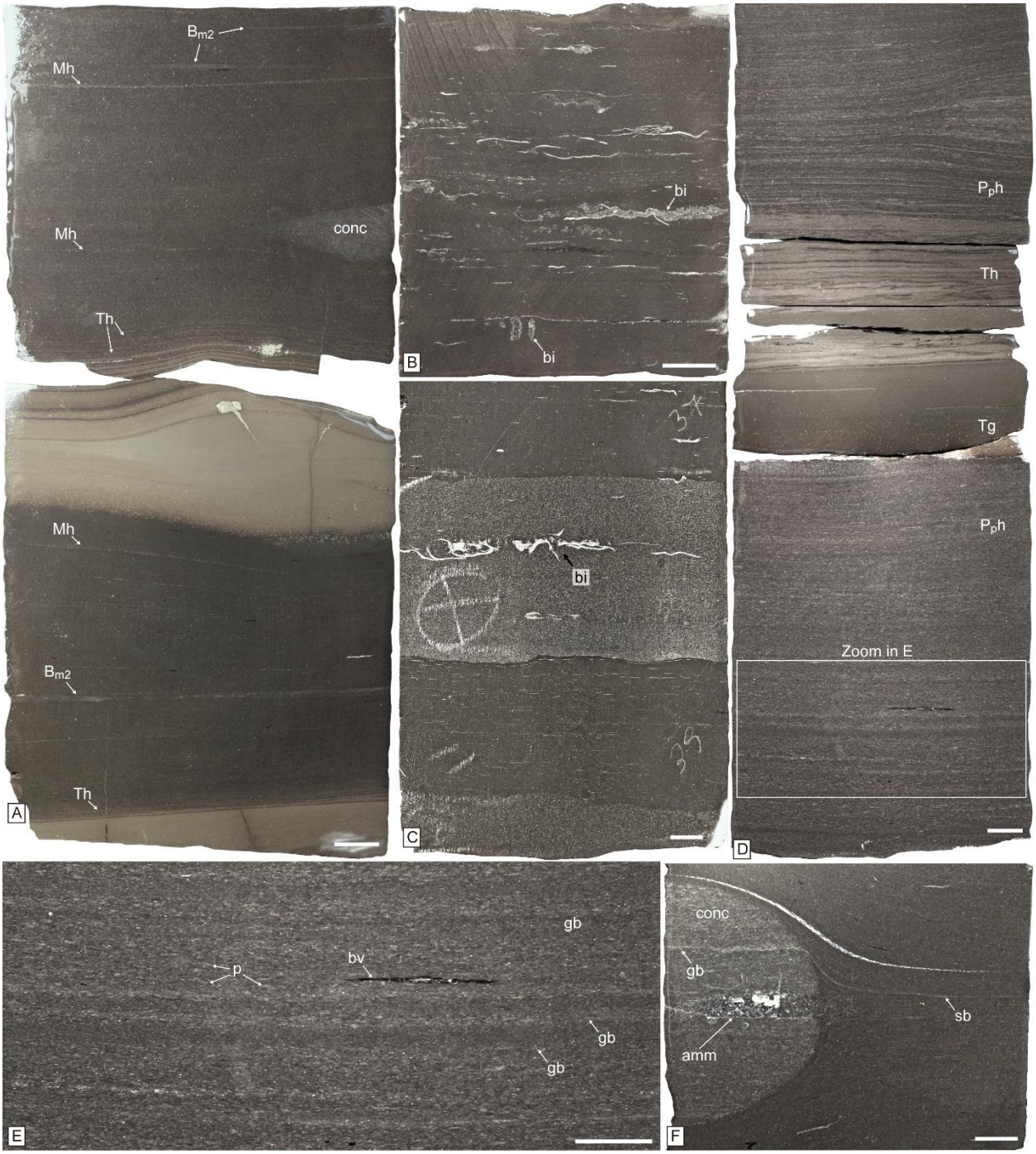

Fig. 4.7. Carbonaceous mixed mudstone and bioclastic floatstone to rudstone of basin facies association (FA2). A) General view of parallel-laminated mixed mudstone (M_mh) with intercalated laminated tuff intervals (Th), bindstone (B_{m2}), and carbonate concretions (conc). Note coarse mudstone laminae (Mh) on the fine mudstone and parallel-laminated top of the tuffs, suggesting absence of bioturbation. B) Bioclastic floatstone (F_b) with bivalves and ammonites bioclasts (bi). C) Parallel-bedded, bioclastic mixed mudstone (M_{bm}h) showing intercalation of carbonate-rich intervals with bioclasts (bi). D) General view of the parallel-

laminated peloidal packstone (P_ph), with intercalated, normal graded tuff (Tg), laminated (unbioturbated) towards the top (Th). E) Close-up image of the mudstone, with a detail of the peloids (p), bitumen veins (bv) and the gradational boundaries of the lamination (gb). F) Core showing the relationship between the discontinuous lamination observed within concretions (conc) and the encasing mudstone. The gradational boundaries (gb) may change to sharp boundaries (sb) due to compaction. An ammonite shell is observed (amm). Scales are 1 cm.

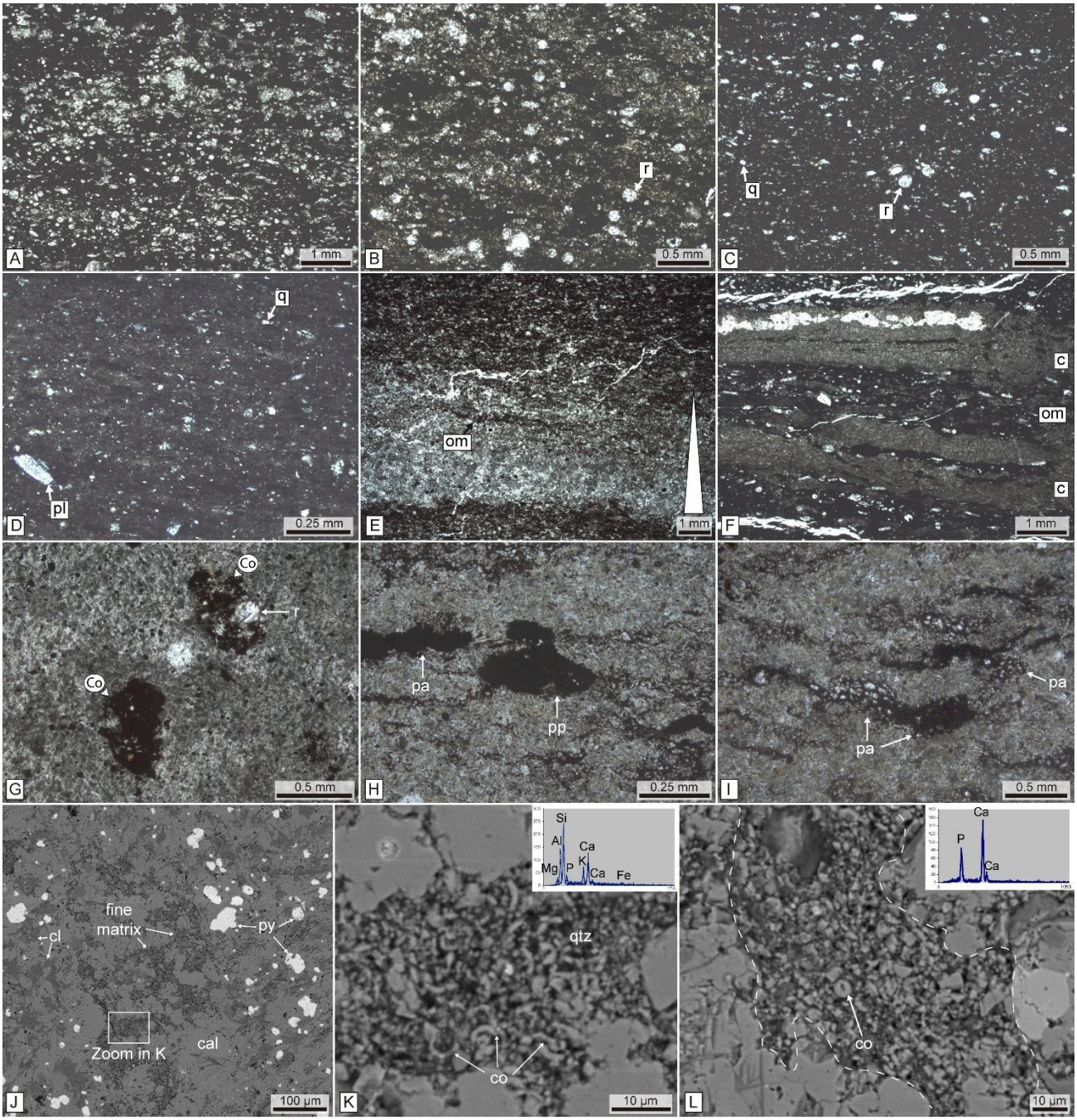

Fig. 4.8. Thin sections backscattered electron images of selected lithofacies. A) Bioclastic, mixed mudstone with carbonate-replaced radiolarians ($M_{bm}h$). B) Calcareous to mixed mudstone ($M_{cm}b$) cemented by microsparite, containing carbonate-replaced radiolarians (r). C) Peloidal mudstone ($M_p l$) showing abundant radiolarians (r) and silt-sized quartz (q). D) Intraclastic wackestone ($W_i b$), with silt-sized quartz (q) and plagioclase (pl). E) Sharp-based, normal graded calcareous mudstone ($M_s g$) displaying organic matter-rich aggregates (om). F) Bindstone (B_{m2}) comprising an alternation of carbonate (c) and organic matter-rich (om) laminae. G, H, I) Pelagic constituents observed at the top of tuff intervals (Tm), such as *Coprulus*

oblongus (Co) composed of radiolaria (ra), coccolith-rich, planktonic pellets (pp) and pelagic aggregates (pa). J) Backscattered electron image of the parallel-laminated, mixed mudstone (M_mh). Note calcite (cal), pyrite (py), and clay minerals (cl), associated with a fine-grained matrix. K) Close up photo of the fine-grained matrix displaying coccoliths (co) and microcrystalline quartz (qtz). The EDS analysis from this matrix suggests a mixed composition from the coccoliths, quartz and clays. L) Coccolith-rich, pelagic aggregates observed at the pelagic tops of tuff intervals. EDS analysis is predominantly calcareous due to predominance of coccoliths.

4.4.2.3 Facies 2c (F2c): Carbonaceous and bioclastic, mixed mudstone

Description. This facies comprises for the most part carbonaceous (M_mh) and bioclastic (M_{bm}h), mixed mudstone lithofacies (Figs. 4.9A, B, C, 4.16A). Massive, calcareous to mixed mudstone (M_{cm}b), massive crinoidal mudstone (M_{cr}b), very thin-bedded intervals of fine mudstone with coarse mudstone laminae (Mh, Ml), current-ripple cross-laminated, fine to coarse mudstone (M_sr), crinoid-rich parallel laminae (M_{cr}h), sharp- to erosive-based, graded to massive, fine to coarse mudstone (M_sg, M_sm), bindstone (B_{m2}), and tuff to lapilli-ash tuff (Tm, Tg, Tr) lithofacies are less common (Fig. 4.13D, E). Locally, carbonate cementation occurs associated with M_sg, M_sm, Tm, Tg or Tr (Fig. 4.9C).

Ichnology. This facies shows either unbioturbated intervals or successions with variable bioturbation levels (BI 2-4, mean BI of 0.75, n=2994). Mean burrow diameter is 4.59 mm (n=17), and mean maximum bioturbation depth is 14.41 mm (n=37). Biodeformational structures are abundant in the massive mudstone lithofacies (M_{cm}b). Trace fossils mainly occur in the tuffs, and include *Teichichnus rectus, Alcyonidiopsis longobardiae, Coprulus oblongus, Thalassinoides* isp., *Planolites* isp., and mantle and swirl structures (Table 4.2). *Teichichnus zigzag, Nereites* isp., and *Phycosiphon incertum* are less common.

Interpretation. The facies represents alternation of pelagic, hemipelagic, and bottom current processes in a dysoxic basin. A higher carbonate content occurs due to mixed mud transport exported from the shelf and advected by bottom currents (Mh, Ml, M_sr). Sediment-gravity flows (M_sg, M_sm) also contributed to mixed mud deposition. The existence of low levels of bioturbation (mean BI of 0.75) indicates deposition close to the distal limit of the oxycline, reflecting dominantly anoxic to dysoxic conditions.

4.4.2.4 Facies 2d (F2d): Bioclastic mixed mudstone and massive, calcareous to mixed mudstone

Description. This facies is dominated by bioclastic, mixed mudstone ($M_{bm}h$) and massive, calcareous to mixed mudstone ($M_{cm}b$) lithofacies (Figs. 4.9A, B, 4.16B). Very thin- to thick-bedded intervals consisting of fine mudstone with coarse mudstone laminae (Mh, Ml), current-ripple cross-laminated, fine to coarse mudstone (M_sr), massive, crinoidal mudstone ($M_{cr}b$), low-angle cross-bedded peloidal mudstone (M_pl, Fig. 4.11), sharp- to erosive-based, graded to massive, fine to coarse mudstone (M_sg, M_sm), hummocky cross-stratified intraclastic to bioclastic wackestone ($W_{ib}hcs$), and tuff to lapilli-ash tuff (Tm, Tg, Tr) lithofacies are less common (Fig. 4.13C).

Ichnology. This facies display variable intensities of bioturbation. BI is typically 1-4, with rare 5 or 6 intervals (mean BI of 2.29, n=1737), mean burrow diameter is 4.4 mm (n=27), and mean maximum bioturbation depth is 32.82 mm (n=34). Biodeformational structures occur in the massive lithofacies ($M_{cm}b$). Trace fossils are dominant in the tuffs, and include *Teichichnus rectus, Alcyonidiopsis longobardiae, Thalassinoides* isp., *Planolites* isp., *Nereites* isp., *Phycosiphon incertum, Teichichnus zigzag, Coprulus oblongus* and mantle and swirl structures (Table 4.2). *Diplocraterion* isp., *Zoophycos* isp., *Palaeophycus* isp., and pyrite-rich burrows are rare.

Interpretation. This facies has higher bioturbation levels, bioclastic-rich lithofacies, and carbonate content than F2c, suggesting deposition in a relatively oxic basin. Bottom current activity (Mh, Ml, M_sr, M_pl) occurred together with relatively minor sediment-gravity flows (M_sg, M_sm) and combined oscillatory and unidirectional flows during storms ($W_{ib}hcs$, Kietzmann and Palma, 2011). Oxygen fluctuated from lower dysoxic to oxic, to rarely anoxic depending on the activity of bottom currents and the position of the oxycline. Times of low hydrodynamic energy and intermittent current regimes allowed organisms to colonize the substrate and generate the highly bioturbated intervals (Paz *et al.*, in review b).

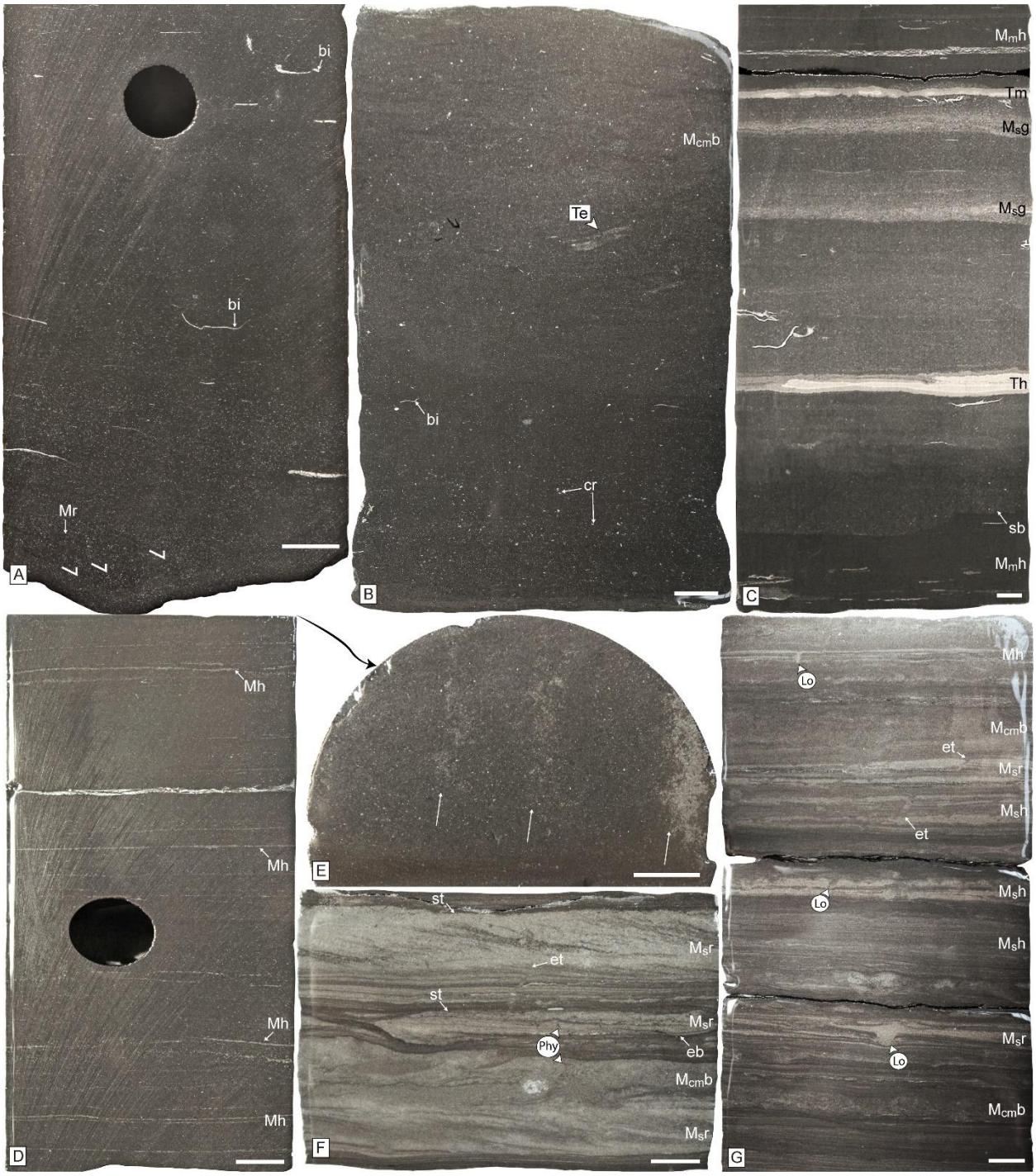

Fig. 4.9. Selected lithofacies of dysoxic and oxic basin (F2c, F2d) and drift facies associations (FA3). A) Bioclastic, mixed mudstone ($M_{bm}h$) showing bivalve bioclasts (bi) and intercalated rippled mudstone (Mr). B) Intensely bioturbated calcareous to mixed mudstone ($M_{cm}b$) with highly compressed *Teichichnus* isp. (Te). Body fossils include bioclasts (bi) and crinoids (cr). C) Intercalation of parallel-laminated mixed mudstone ($M_m h$), laminated and massive tuffs (Th, Tm) and normal graded coarse mudstone ($M_s g$). Note that the existence of calcareous mudstone with sharp bases (sb) is not associated with event beds but with

carbonate cementation. D) Fine mudstone with coarse mudstone laminae (Mh) associated with contour current activity. The laminae of coarse mudstone represents thin starved ripples, with the crests observed on top of the core (E, white arrows). F) Current-ripple cross-laminated coarse mudstone ($M_{s}r$), and intercalated bioturbated intervals ($M_{cm}b$). Some rippled beds show erosive bases (eb) and sharp tops (st). *Phycosiphon incertum* (Phy) and escape trace fossils (et) are observed. G) Fine mudstone with parallel coarse mudstone laminae (Mh), parallel- and current-ripple cross-laminated coarse mudstone ($M_{s}h$, $M_{s}r$), and bioturbated, calcareous to mixed mudstone ($M_{cm}b$) with escape traces (et) and ?*Lockeia* isp. (Lo). Scale bars are 1 cm.

4.4.3 Facies association 3 (FA3): Drift

FA3 groups facies deposited by contour currents in sediment drifts, below storm wave base. This facies association is located in both bottomset and lower foreset areas.

4.4.3.3 Facies 3a (F3a): Crinoidal mudstone

Description. This facies is dominated by massive and cross-bedded crinoidal mudstone ($M_{cr}b$, $M_{cr}t$) and crinoidal mudstone showing parallel-, low angle and minor wavy crinoid-rich laminae ($M_{cr}h$, $M_{cr}l$, $M_{cr}w$), and crinoid-rich lenses ($M_{cr}r$; Figs. 4.10, 4.16C). Very thin- to thin-bedded, graded to massive, fine to coarse mudstone ($M_{s}g$, $M_{s}m$), and thin- to thick-bedded, tuff to lapilli-ash tuff (Tm, Tg, Tr) lithofacies are locally observed.

Ichnology. Intervals sharply vary from unbioturbated to highly bioturbated (Fig. 4.10). BI is typically 3-6, or 0-1 in the areas with high preservation of sedimentary structures (mean BI of 1.78, n=462). Burrow diameter is *ca.* 6.24 mm and penetration depth is *ca.* 30-50 mm. Biodeformational structures, *Crininicaminus* isp., and *Planolites* isp. occur in the massive crinoidal mudstone ($M_{cr}b$, Fig. 4.16C). Locally, *Teichichus rectus, Phycosiphon incertum,* ?*Skolithos* isp., *Coprulus oblongus,* and uncompacted *Thalassinoides* isp. with sharp burrow boundaries occur.

Interpretation. This facies suggests areas of long-term, contour current activity of low sediment concentration in sediment drifts, reworking a pelagic crinoid community (Paz *et al.*, in review a). The microcrinoid belongs to the genus *Saccocoma* (Kietzmann and Palma, 2009a). Saccocomids have been interpreted as pelagic suspension feeders (Hess and Etter, 2011), which supports the idea of a continuous circulation system that maintained food in suspension and reworked the seafloor. Mesozoic crinoidal limestones with low-angle cross-lamination have been

also interpreted as storm deposits (Aigner, 1985; Jach, 2005), yet absence of structures such as gutter casts or hummocky cross-stratification, precludes a storm origin. Small burrow sizes and shallow penetration depth suggest upper dysoxic conditions, which prevailed during times of contour current activity. Hydrodynamic energy controlled infaunal colonization, with higher bioturbation intensity during low energy conditions (Paz *et al.*, in review b). As in F1b, *Thalassinoides* isp. with sharp burrow margins are associated with the local development of the *Glossifungites* Ichnofacies, indicating firmground conditions during high-energy current events.

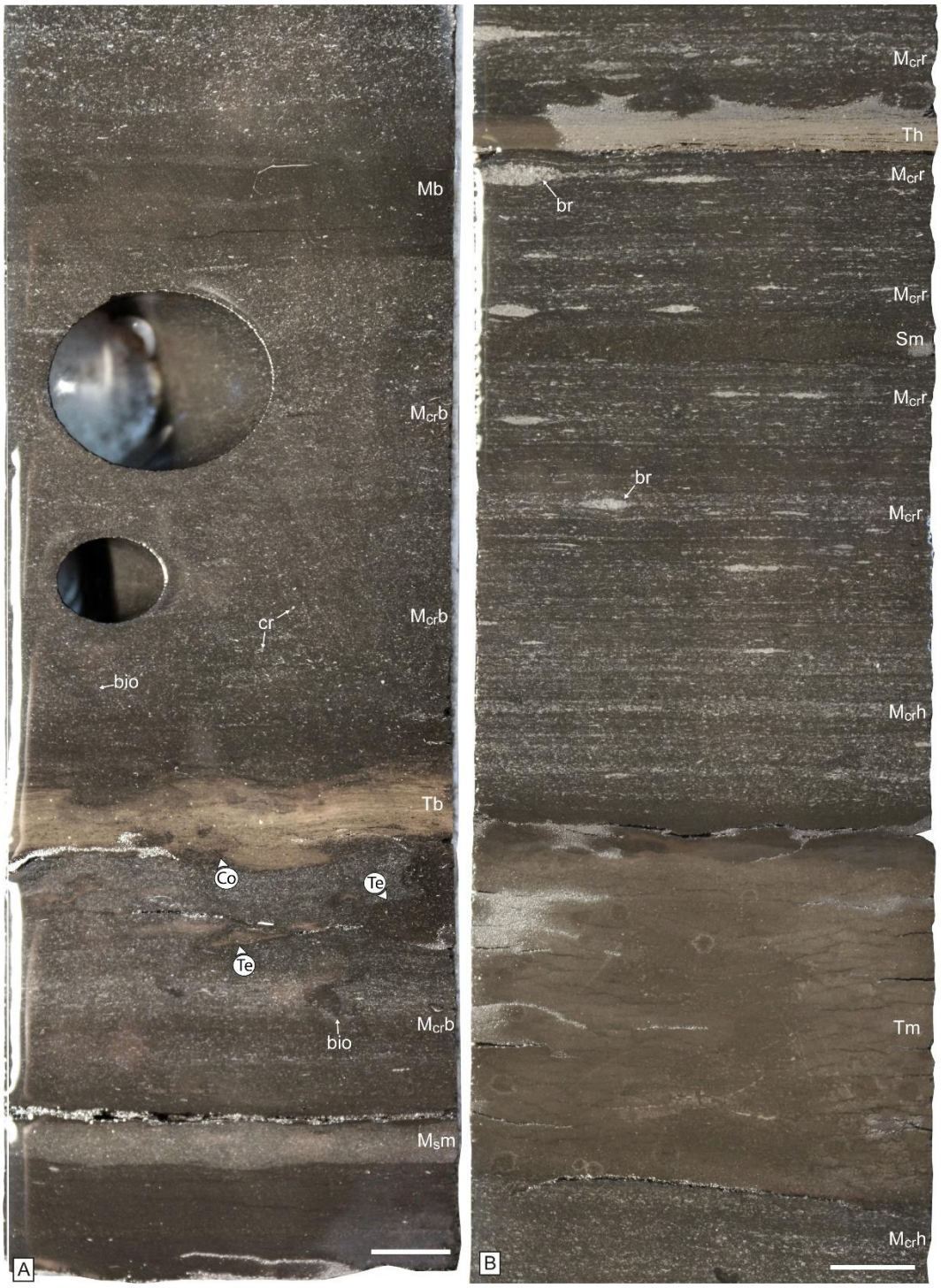

Fig. 4.10. Massive, crinoidal mudstone ($M_{cr}b$) and parallel- to ripple cross-laminated, crinoidal mudstone ($M_{cr}h$, $M_{cr}r$) of F3c. A) Bioturbated, massive crinoidal mudstone ($M_{cr}b$), with intercalated massive coarse mudstone (M_sm), bioturbated tuff (Tb), and mudstone (Mb). The tuff is bioturbated by *Teichichnus* isp. (Te). Biodeformational structures (bio), crinoids (cr), and *Coprulus oblongus* (Co) are delineated. B) Parallel-laminated to current ripple-cross laminated crinoidal mudstone ($M_{cr}h$, $M_{cr}r$) showing unbioturbated

massive and laminated tuff (Tm, Th), and massive sandstone (Sm). The lenticular structures are interpreted as bioclastic ripples (br). Scale bars are 1 cm.

Fig. 4.11. Low-angle cross-bedded peloidal mudstone of (M_pl). A) Core photograph and line drawing of the ripples observed, probably with associated bioturbation (bio?). B) Outcrop view and drawing of the low-angle cross-bedded mudstone, with ripples and trough cross-bedding on the surfaces (Mr/ Mt). S2 reactivation surfaces are delineated. Scales are 1 and 20 cm, respectively.

4.4.3.4 Facies 3b (F3b): Laminated, fine to coarse mudstone

Description. This facies consists dominantly of fine mudstone with parallel to low-angle, coarse mudstone laminae (Mh, Ml), parallel- to low-angle and current-ripple cross-laminated coarse mudstone (M_sh, M_sl, M_sr), and massive, calcareous to mixed mudstone (M_{cm}b) lithofacies (Figs. 4.9D, E, F, 16D). Thin-bedded, wave ripple cross-laminated coarse mudstone (M_sw), medium-bedded, low-angle cross-bedded peloidal mudstone (M_pl, Fig. 4.11) and very thin- to thin-bedded, graded to massive, fine to coarse mudstone (M_sg, M_sm) are less common lithofacies.

Ichnology. Bioturbation intensity is highly variable, and in some cases shows a decreasing to increasing BI pattern. BI is 0 to 2, with discrete, cm-thick intervals of 4-5 (M_{cm}b). Mean BI is 2.17 (n=193), mean burrow diameter is 3.57 mm (n=38) and penetration depth is approximately 20 mm. Biodeformational structures are common, whereas trace fossils consist of *Nereites* isp., *Phycosiphon incertum*, *Planolites* isp., *Palaeophycus* isp., and *Palaeophycus heberti* (Fig. 4.16D). Intervals with low bioturbation index show escape trace fossils. Locally, ?*Lockeia* isp., *Teichichus rectus, Alcyonidiopsis longobardiae, Coprulus oblongus,* and pyrite-rich burrows occur (Table 4.2). All trace fossils are present in the laminated, rippled and massive, fine to coarse mudstone lithofacies (Mh, Ml, M_sh, M_sl, M_sr, M_{cm}b).

Interpretation. This facies represents enhanced activity of long-term contour currents (Mh, Ml, M_sr, M_pl) loaded with silt and bioclasts, and depositing in sediment drifts (Paz *et al.*, in review a). Minor oscillatory flow reworking is observed during extreme storm events that were able to enhance current transport (M_sw). Low density flows (M_sg, M_sm) can be originated by resuspension events associated with the currents. Low energy currents delivered oxygen to the seafloor, generating upper dysoxic conditions. The decreasing to increasing BI pattern observed in some successions suggests an increased and then decreased hydrodynamic energy stress on the benthos (Paz *et al.*, in review b). This energy cyclicity resembles the typical contourite coarsening and fining upwards ("bigradational") cyclicity (Stow and Piper, 1984).

4.4.3.5 Facies 3c (F3c): Laminated, fine to coarse mudstone and massive calcareous mudstone

Description. This facies consists of thin-bedded, fine mudstone with coarse mudstone laminae (Mh, Ml), parallel to low angle, and current-ripple cross-laminated coarse mudstone (M_sh, M_sl, M_sr), massive, calcareous mudstone (M_cm), normal-graded, fine to coarse mudstone (M_sg)

and composite beds of fine to coarse mudstone (M_{comp}) (Figs. 4.9G, 4.16E). Bindstone (B_{m2}) is rare.

Ichnology. Bioturbation is highly variable, with typical BI of 0-3 and rarely 4 (mean BI of 1.75, n=239), Mean burrow diameter is 3.31 mm (n=130), and penetration depth is approximately 10 mm. The ichnofauna consists of equilibrium trace fossils, ?*Lockeia* isp. and *Lockeia siliquaria*, with minor escape trace fossils and ?*Skolithos* isp. (Table 2).

Interpretation. This facies is interpreted as a combination of contour current reworking (Mh, Ml, M_sh, M_sl, M_sr) and fluid mud and other sediment-gravity flow deposition (M_cm, M_sg, M_{comp}; Paz *et al.*, in review a). Seismic data related to this facies indicates the existence of elongated along-shore geobodies, suggesting contourite deposition (Reijenstein *et al.*, 2020). The dominance of trace fossils of suspension-feeding bivalves supports the idea of continuous currents maintaining food in suspension. In addition, fluid mud deposition probably was of low frequency to keep low turbidity levels and allow the establishment of suspension-feeding communities (Paz *et al.*, in review b).

4.4.4 Facies association 4 (FA4): Slope

FA4 represents slope environments migrating by deposition of hypopycnal and mesopycnal plumes and fluid mud flows originated in the mixed shelf. It represents the foreset of the clinoform system. Because the likely resuspension processes are storm or current events, the uppermost part of this area (upper foreset and topset) is close to the storm wave base.

4.4.4.1 Facies 4a (F4a): Mixed and calcareous mudstone

Description. This facies mostly consists of alternating parallel-laminated to -bedded, mixed (M_mh) and calcareous mudstone (M_ch) lithofacies (Figs. 4.12A, B, 4.17C). Intercalated are rare thin-bedded, massive calcareous mudstone (M_cm) and tuff to lapilli-ash tuff (Tm) lithofacies. Locally, mm-thick, discontinuous, bioclastic lags can be observed. Convolute laminae, slumped intervals, and synsedimentary normal faults are common (Fig. 4.12F), whereas subaqueous cracks are rare.

Ichnology. Beds are unbioturbated or rarely display low to moderate bioturbation indexes (BI= 1-2, mean BI of 0.90, n=488), burrow diameter is *ca.* 2.3 mm, and mean penetration depth is 11.4 mm (n=7). Trace fossils are represented by *Phycosiphon incertum, Nereites* isp., *Planolites*

isp., and ?*Skolithos* isp., associated with the calcareous mudstone (M_ch). Locally, tuffs contain *Alcyonidiopsis longobardiae*, *Teichichnus* isp., and *Coprulus oblongus* (Table 4.2).

Interpretation. This facies represents a distal slope affected by alternating pelagic (M_mh) and hemipelagic deposition from hypopycnal or mesopycnal plumes or low-density currents bringing mixed material from the shelf (M_ch). Oscillatory flow reworking in facies 4b (see below) indicates storm events generated the resuspension of mixed mud in proximal locations. In addition, the bioclastic lags are generated in situ by winnowing of fines and reworking by currents. Minor fluid-mud flows occurred (M_cm). Higher sedimentation rates, storm wave perturbation, and the existence of a slope induced the abundant slumps in this facies, and contributed to clinoform progradation (e.g. Denommee *et al.*, 2016). BI, burrow diameter and bioturbation depth are overall low, suggesting continuous dysoxic to anoxic conditions.

4.4.4.2 Facies 4b (F4b): Wavy to massive, calcareous mudstone

Description. This facies consists of wavy (M_cw) and massive, calcareous mudstone (M_cb) lithofacies (Figs. 4.13A, 4.17D). The tuff to lapilli-ash tuff lithofacies (Tm) is intercalated locally. Syn-sedimentary normal faults crosscut up to 5 cm-thick intervals. Minor subaqueous cracks and pressure dissolution seams are observed.

Ichnology. Beds are unbioturbated or display low to high bioturbation indexes (BI=2-4, mean BI of 2.48, n=824), mean burrow diameter is 2.74 mm (n=26), and mean penetration depth is 5.07 mm (n=7). *Phycosiphon incertum*, *Planolites* isp., *Thalassinoides* isp., and ?*Skolithos* isp. are common. *Nereites* isp., *Alcyonidiopsis longobardiae*, ?*Lockeia* isp., and mantle and swirl structures are rare.

Interpretation. This facies is interpreted as recording deposition in a middle slope area affected by oscillatory flow reworking during storm events (M_cw) that alternated with hemipelagic, carbonate mud deposition (M_cb). This environment is located at the upper foreset, suggesting that this was the seaward limit of the storm wave base. Higher intensities of bioturbation compared with F4a are due to an increase oxygen conditions in settings closer to the shore.

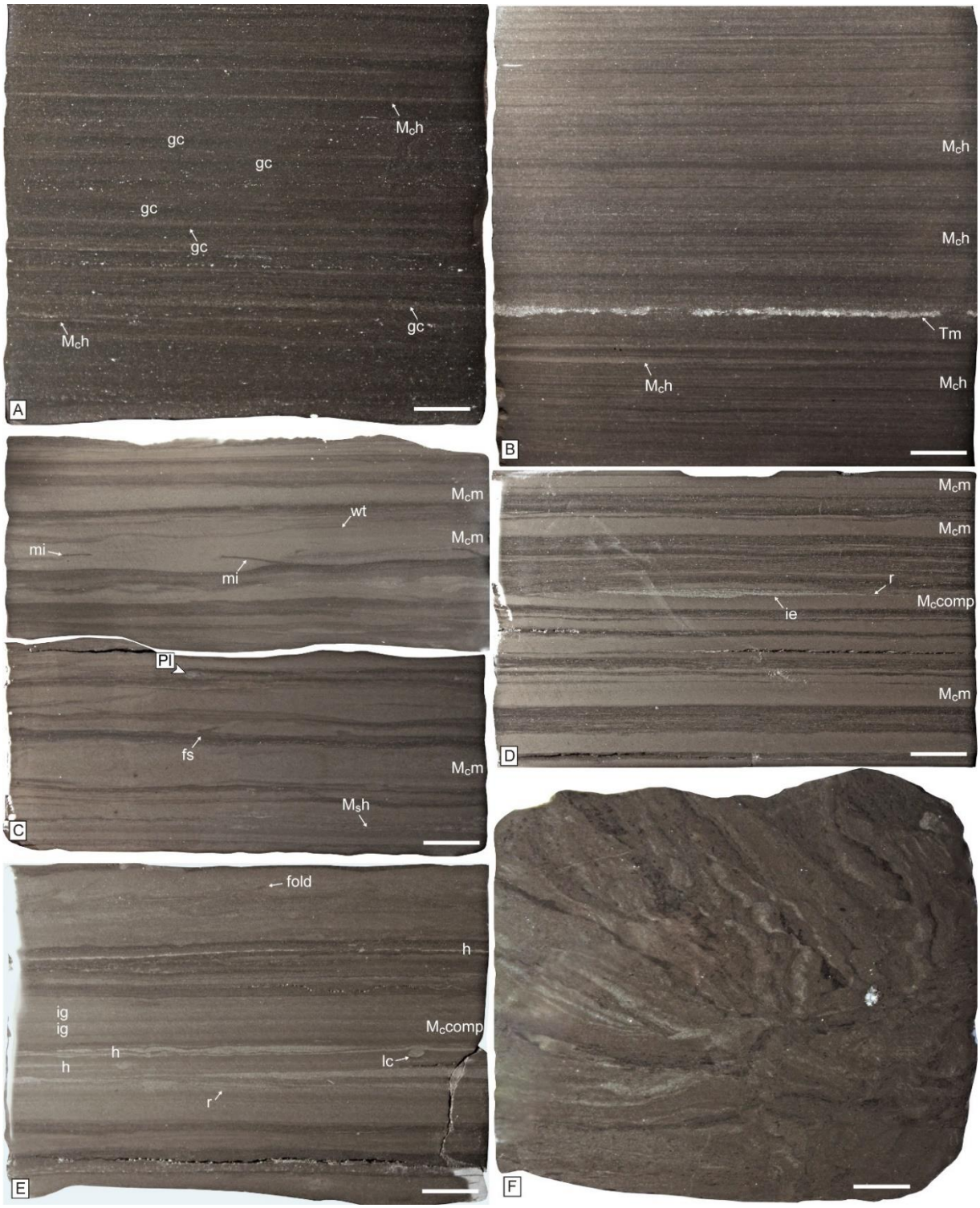

Fig. 4.12. Laminated, thin-bedded and massive calcareous mudstone (M_ch, M_cm) of the slope facies association (FA4). A) Heterolithic alternations of laminated calcareous mudstone (M_ch) and dark-colored fine mudstone, displaying gradational contacts (gc). B) Thinly laminated calcareous mudstone (M_ch) associated with unbioturbated tuff intervals (Tm). C) Massive calcareous mudstone (M_cm) with typical

features such as flame structures (fs), mudstone intraclasts (mi), parallel-lamination (M_sh), and wavy tops (wt). The beds are typically unbioturbated (BI 1-2) with minor *Planolites* isp. (Pl). D, E) Massive and composite calcareous mudstone (M_cm, $M_c$comp). Composite beds show massive structures associated with coarse mudstone ripples (r), parallel lamination (h) and inverse grading (ig), in some cases separated by intra-bed erosive surfaces (ie). Note also load casts (lc) and folds. F) Slumped intervals occurring in these lithofacies. Scale bars are 1 cm.

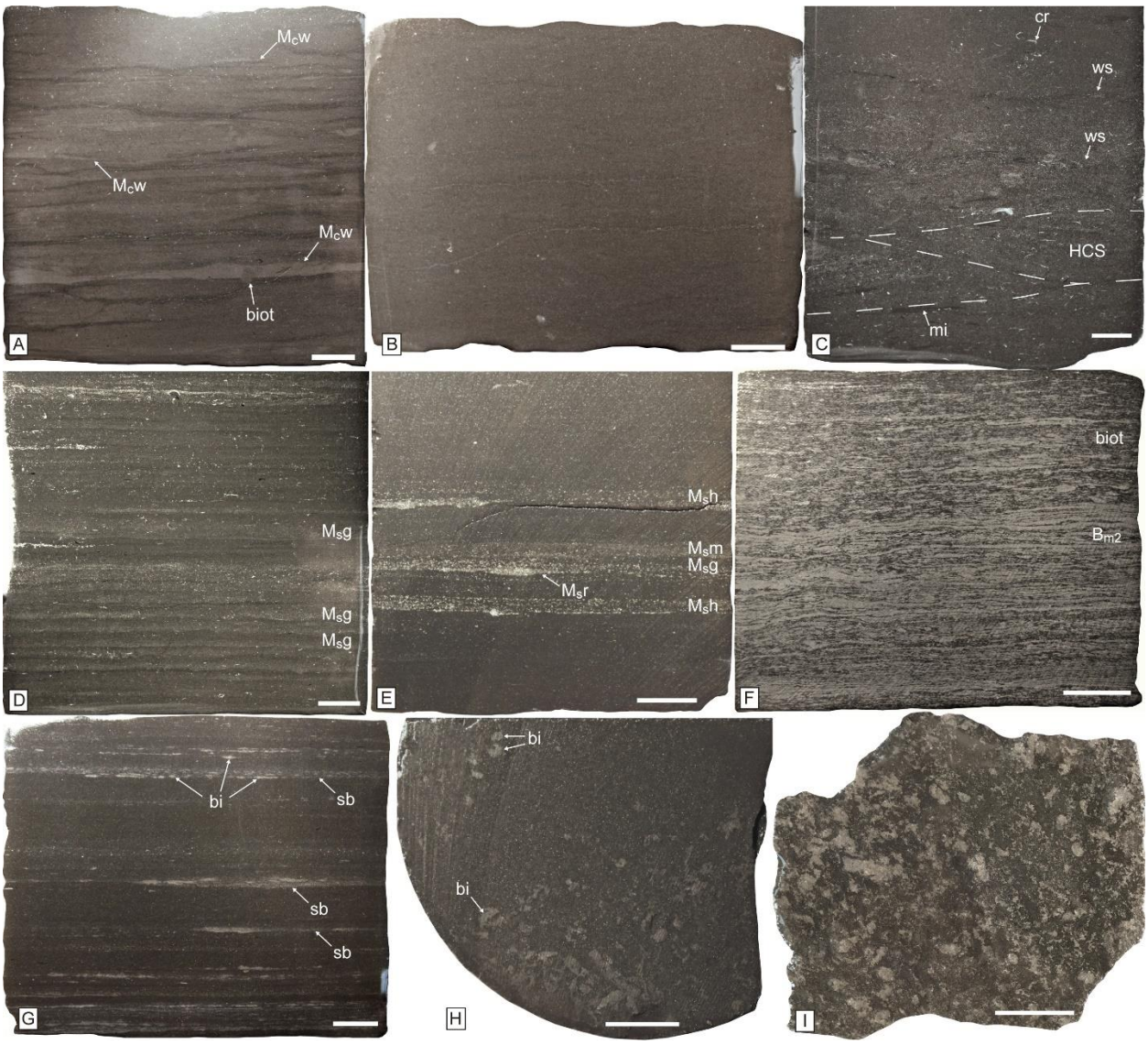

Fig. 4.13. Wavy to massive, calcareous mudstone (M_cw, M_cb) and other rare, intercalated lithofacies. A) Close-up of the wavy-bedded mudstone (M_cw) with minor bioturbation (biot). B) Massive calcareous mudstone with scattered carbonate intraclasts. C) Intraclastic to bioclastic wackestone (W_{ib}hcs), displaying hummocky cross-stratification (HCS, dashed lines delineating laminasets) and wavy surfaces (ws) on top

of an erosive base, and containing mudstone intraclasts (mi) and microcrinoids (cr). D) Thin-bedded, normal graded coarse to fine mudstone (M_sg). E) Composite beds showing alternations of parallel-laminated (M_sh), ripple cross-laminated (M_sr), and massive (M_sm) coarse mudstone. F) Dense, wavy and crinkly-laminated bindstone (B_{m2}), with areas disrupted by bioturbation (biot). G) Sharp-based (sb) mudstone with bindstone intraclasts (bi, lithofacies M_{bind}). H) Plan-view detail of the bindstone intraclasts (bi, from a different interval). I) Close-up of the base of a tuff (plan-view), with abundant pelagic aggregates, and benthic and planktonic pellets. The circular, elongated structures are pellet trails. Scales are 1 cm.

4.4.4.3 Facies 4c (F4c): Massive, calcareous mudstone

Description. This facies is mostly represented by massive, calcareous mudstone lithofacies (M_cb; Figs. 4.13B, 4.17E). Locally, wavy surfaces, bivalve and microcrinoids forming bioclastic lags, and tuff to lapilli-ash tuff (Tm) occur.

Ichnology. Beds are typically highly bioturbated (BI= 4-6, mean BI of 4.06, n=549), showing biodeformational structures. Mean burrow diameter is 4.96 mm (n=9), and mean penetration depth is 11.74 mm (n=4). Trace fossils include *Phycosiphon incertum*, *Thalassinoides* isp., *Planolites* isp., and rare *Nereites* isp.

Interpretation. This facies represents a proximal slope characterized by continuous hemipelagic sedimentation. High intensity of bioturbation in oxic environments completely homogenized the sediment, and precluded observations of primary sedimentary structures. The foraminifer *Epistomina* and ostracods have been found in similar intervals, indicating a low energy, anoxic to dysoxic environment (Ballent *et al.*, 2004, Pose *et al.*, 2014).

4.4.4.4 Facies 4d (F4d): Massive and composite beds of calcareous mudstone

Description. This facies is composed by a predominance of thin-bedded, massive calcareous mudstone lithofacies (M_cm) and composite beds of calcareous mudstone ($M_c$comp; Figs. 4.13D, E, 4.17F). Fine mudstone with parallel coarse mudstone laminae (Mh), and composite beds of fine to coarse mudstone (Mcomp) are less common. 0.3-1.6 m-thick slumped intervals are observed.

Ichnology. This facies is typically unbioturbated, with rare sparsely bioturbated intervals (BI= 1-3, mean BI of 0.95, n=335), mean burrow diameter is 2.57 mm (n=54) and bioturbation depth is *ca.* 4.62. Trace fossils are mostly biodeformational structures, with rare *Palaeophycus*

isp., *Phycosiphon incertum, Planolites* isp., *Nereites* isp., escape trace fossils, and ?*Skolithos* isp. Rare *Lockeia siliquaria* and ?*Lockeia* isp. occur in places (Table 4.2).

Interpretation. The area represents extensive fluid mud deposition in a slope (M_cm, $M_c$comp) generating progradation of the clinoforms. Modern fluid mud deposits show high to moderate levels of bioturbation (Bentley and Nittrouer, 2003); therefore, the typical low bioturbation intensity can be explained by a substrate consistency and low oxygen stress. Substrate consistency might have been a strong paleoenvironmental stress, as fluid mud deposits are unstable substrates for organisms (Aller and Aller, 1986). In addition, small burrow diameters point to upper dysoxic conditions. Minor bottom current reworking generated the traction current structures (Mh) and provided oxygen to support a low-diversity benthos. Similar fluid mud deposits with higher clay concentration were described in other locations (3-28%, Kietzmann *et al.*, 2020a; see also Lithofacies 7 of Minisini *et al.*, 2020a).

4.4.5 Facies association 5 (FA5): Outer ramp

This facies association includes facies displaying high bioturbation levels associated with an outer ramp, in localities without clinoform development.

4.4.5.1 Facies 5a (F5a): Massive, calcareous to mixed mudstone and minor intraclastic wackestone and bioclastic floatstone

Description. This facies is dominated by massive, calcareous to mixed mudstone (M_{cm}b), with minor intraclastic wackestone (W_ib, W_ih) and bioclastic floatstone (F_bb) lithofacies (Figs. 4.14, 4.17A). The tuff and lapilli-ash tuff lithofacies (Tm, Tg, Tr) are intercalated locally.

Ichnology. Bioturbation intensity is typically high (BI of 3-6, mean BI of 4.61, n=995), bioturbation diameter is 7.83 mm (n=9), and mean maximum bioturbation depth is 71.76 mm (n=11). Biodeformational structures are abundant in the massive lithofacies (M_{cm}b). Trace fossils mainly occur in tuffs and include *Teichichnus rectus, Teichichnus zigzag, Thalassinoides* isp., and *Phycosiphon incertum* (Table 4.2). *Planolites* isp., *Nereites* isp., *Alcyonidiopsis longobardiae,* and ?*Zoophycos* isp. are rare.

Interpretation. This facies suggests deposition in an outer ramp subject to continuous oxic conditions. The overall higher bioturbation intensity and the input of shallow-water intraclasts

compared with the regular basin facies (F2c and F2d) indicate an environment closer to the shore and with higher oxygenation.

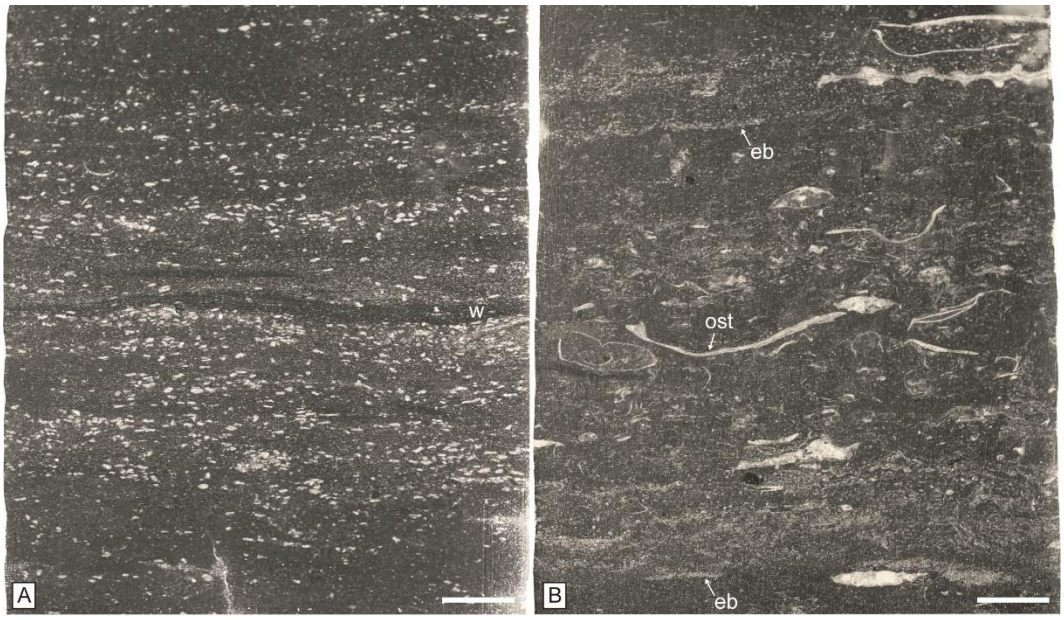

Fig. 4.14. Intraclastic wackestone (W_ib, W_ih) and bioclastic floatstone (F_bb) of the lower foreset (?) facies association (FA4). A) Close-up view of wavy surfaces (w) of the intraclastic mudstone containing rounded, very fine-grained to coarse-grained sand- and minor pebble-sized carbonate intraclasts. B) Bioclastic floatstone with ostreids (ost) and several erosive bases (eb) associated with lags. Scales are 1 cm.

4.4.5.2 Facies 5b (F5b): Intraclastic wackestone and bioclastic floatstone

Description. This facies is composed by intraclastic wackestone (W_ib, W_ih), bioclastic floatstone (F_bb), and massive, calcareous to mixed mudstone (M_{cm}b) lithofacies (Figs. 4.14, 4.17B).

Ichnology. Bioturbation intensity is high (BI= 4-6, mean BI of 4.54, n=265), bioturbation diameter is 13.27 mm (n=11), and mean maximum bioturbation depth is 89.44 mm (n=6). Trace-fossil content is represented by uncompacted *Teichichnus rectus* and *Thalassinoides* isp. with sharp burrow boundaries. Minor *Teichichnus rectus* and *Coprulus oblongus* occur as well (Table 4.2).

Interpretation. This facies is interpreted to be deposited in an outer ramp punctuated by high-energy currents. The sharp boundary and lack of compaction in *Teichichnus* and

Thalassinoides indicate that these suites represent firmground conditions typical of the *Glossifungites* Ichnofacies. Firmgrounds dominated in this facies and were produced by current erosion because energy was high enough to remove sediment and to exhume previously buried firmer substrates, therefore representing autogenic examples of this ichnofacies. Colonization of the firm surfaces took place at times of sediment by pass. The intense bioturbation in oxic environments erased physical sedimentary structures, precluding interpretation on the origin of the currents.

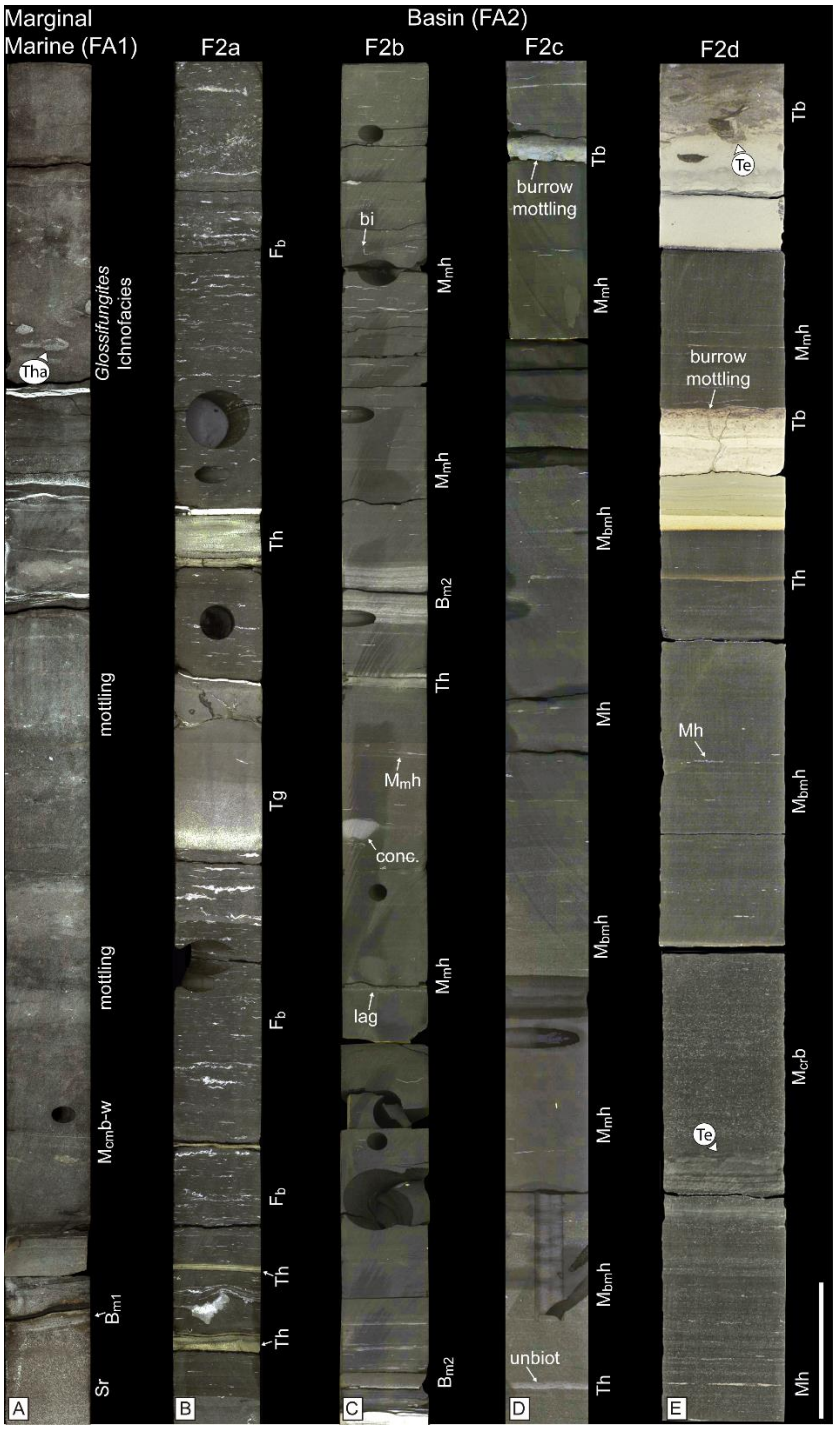

Fig. 4.15. Core photographs of the A) marginal marine (FA1) and B, C, D, E) basin (FA2) facies association, showing ripple cross-laminated sandstone (Sr), calcareous to mixed mudstone (M_{cm}b-w), parallel-laminated, normal graded or bioturbated tuff (Th, Tg, Tb), bioclastic floatstone (F_b), bindstone (B_{m1}, B_{m2}), parallel-laminated, bioclastic mixed and mixed mudstone (M_{bm}h, M_mh), fine mudstone with parallel coarse mudstone laminae (Mh) and bioturbated crinoidal mudstone (M_{cr}b). Bioclasts (bi), *Teichichnus* isp. (Te) and *Thalassinoides* isp. (Tha, white square) are observed. Scale bar is 10 cm.

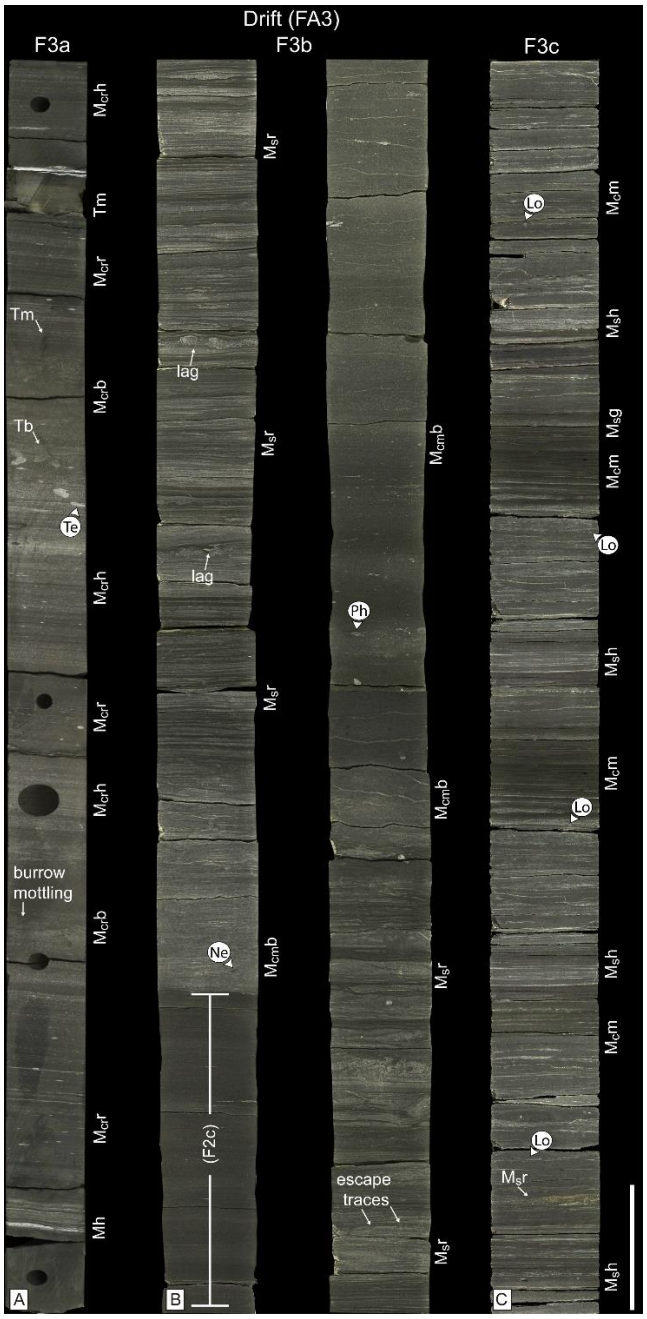

Fig. 4.16. Core photographs of the drift facies association (FA3). The succession consists of parallel-laminated, mixed mudstone (M_mh), bioturbated calcareous to mixed mudstone (M_{cm}b), fine mudstone with parallel coarse mudstone laminae (Mh), parallel- and ripple cross-laminated coarse mudstone (M_sh, M_sr), bioturbated and parallel- to ripple cross-laminated crinoidal mudstone (M_{cr}b, M_{cr}h, M_{cr}r), massive, calcareous mudstone (M_cm), normal-graded, coarse mudstone (M_sg), and bioturbated, parallel-laminated and massive tuff (Tb, Th, Tm). ?*Lockeia* isp. (Lo), *Nereites* isp. (Ne), *Palaeophycus heberti* (Ph), and *Teichichnus* isp. (Te) are observed. Scale bar is 10 cm.

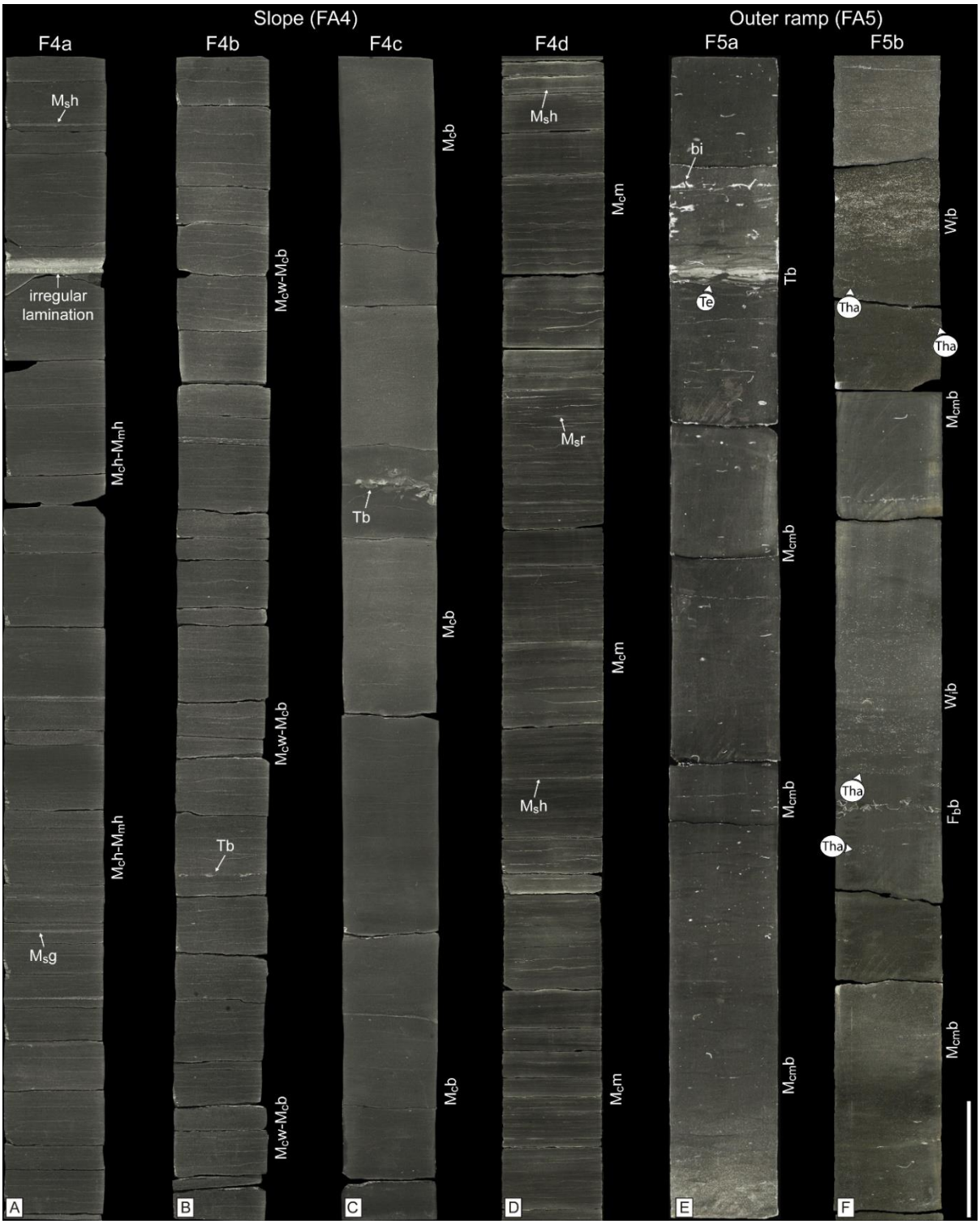

Fig. 4.17. Core photographs of the slope (FA4) and outer ramp (FA5) facies association. The succession comprises bioturbated, massive, laminated, and wavy calcareous mudstone (M_cb, M_cm, M_ch, M_cw), parallel-laminated mixed mudstone (M_mh), parallel- to ripple cross-laminated coarse mudstone (M_sh, M_sr),

bioturbated, calcareous to mixed mudstone ($M_{cm}b$), intraclastic wackestone ($W_i b$), bioclastic floatstone (F_b), and bioturbated tuff (Tb), with bioclasts (bi). *Teichichnus* isp. (Te) and *Thalassinoides* isp. (Tha) occur. Scale bar is 10 cm.

4.5 Geochemical data

Geochemical data of the mixed carbonate-siliciclastic clinoform facies associations (FA2, FA3, FA4 and FA5) is provided in the Appendix C, and was analyzed in terms of their composition and TOC (Fig. 4.18). FA2 shows a mixed to calcareous mudstone composition, with rare siliceous to argillaceous mudstone, displaying an increase in carbonate and clay composition onshore, towards more oxygenated facies (e.g. F2a and F2b compared with F2c and F2d; Fig. 4.18A). FA3 has a similar dominantly mixed to calcareous mudstone composition, with a trend to increasing carbonate content in the younger facies (F3c, Fig. 4.18B). FA4 is composed by calcareous to minor mixed mudstone, and has a clear landward increasing trend of carbonate (Fig. 4.18C). TOC displays higher values in FA2 than in FA3 (Av. TOC of 5.43%, 5.06%, 4.05%, and 4.77% in F2a, F2b, F2c, F2d, compared with 4.04% and 2.25% in F3a and F3b, respectively; Fig. 4.18D). However, the distal F2c shows a lower TOC than the proximal F2d in both cuttings and outcrop samples.

4.6 Depositional model: the interplay of processes in a clinoform system

The sedimentologic and ichnologic analysis allowed integration of sedimentary processes and environmental controls in a depositional model (Fig. 4.19). The Vaca Muerta Formation accumulated right after a sea-level rise which generated a transgression on top of the continental deposits of the coeval Tordillo and Catriel formations. Beach reworking is observed as a result of intermittent marine flooding upon eolian deposits (F1a). On top, when the sea completely covered the study area, a marginal-marine, bay environment showing wave activity and transgressive scouring was formed (F1b) (Paz *et al.*, 2021). Substrates were typically softgrounds switching to firmgrounds developed after high-energy erosive events associated with mudstone scouring and exhumation of compacted substrates. Oxygen conditions varied from typically oxic to rare dysoxic and anoxic due to an unstable oxycline. The characteristics of these marginal-marine deposits have

been analyzed in detail in the Picún Leufú area (south-western Neuquén Basin), where the thin TST and the reworked eolian relief preserved below indicate a rapid transgression caused by a sea-level rise (Paz *et al.*, 2021). The marginal-marine transition is comparable with the Holocene transgression of the carbonate coast of Abu Dhabi, United Arab Emirates, with a succession showing reworked eolian deposits overlain by microbial mats (Strohmenger *et al.*, 2010).

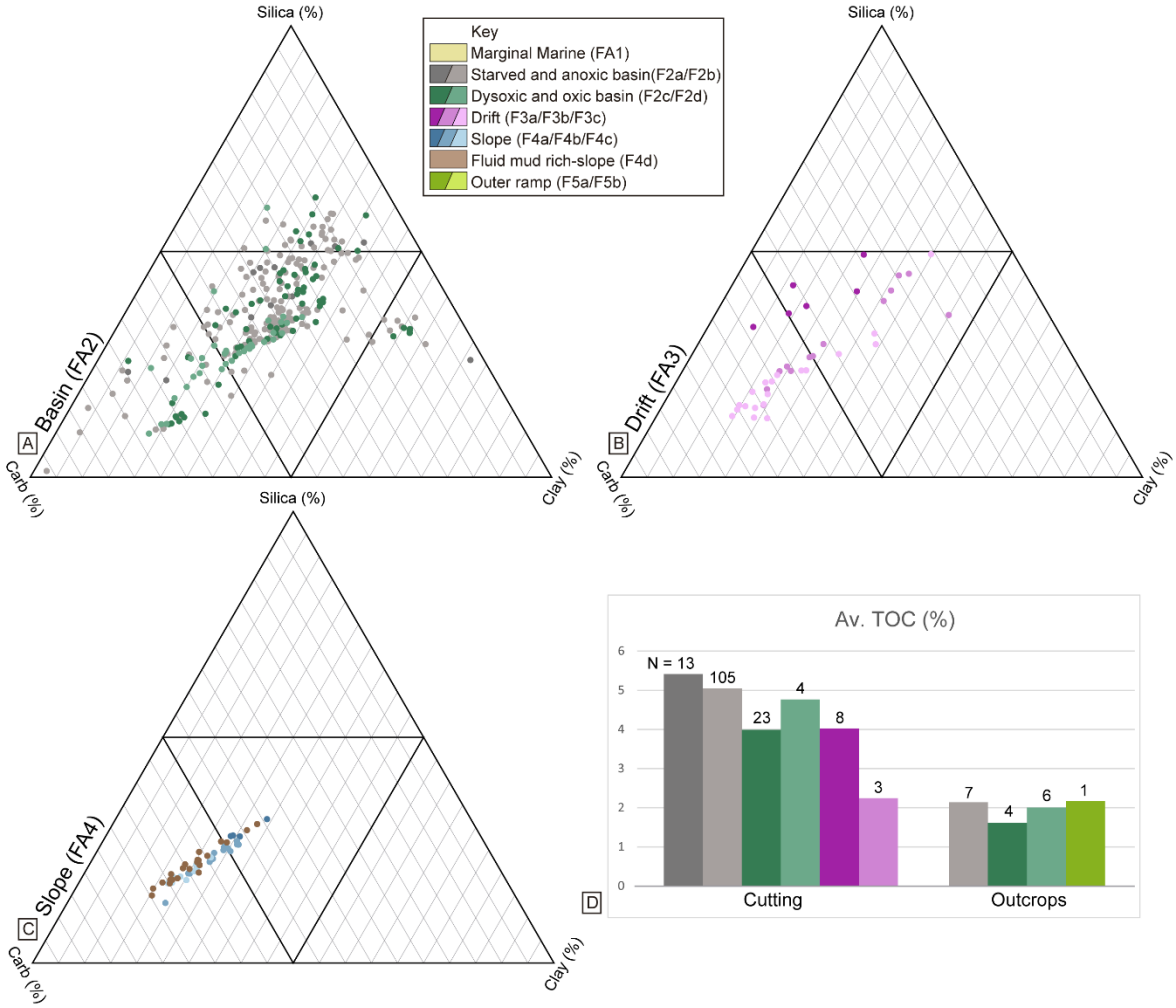

Fig. 4.18. Geochemical data of the different facies associations. Compositional data from XRD of the A) basin (FA2), B) drift (FA3) and C) slope (FA4) facies association. D) Average TOC content from cuttings and outcrop (Yesera del Tromen) samples.

On top of the transgressive, marginal-marine facies association, the Vaca Muerta Formation developed the regressive, subaqueous clinoform system. Migration rates, foreset vertical scale and bottomset bathymetry indicates that the clinoforms are of shelf-margin scale,

separating a bathymetric shelf with shallow-water deposits and slope and basin areas below storm wave base (Patruno *et al.*, 2015; Patruno and Helland-Hansen, 2018). The bottomset area was characterized by basin environments with low sedimentation rates, comprising pelagic and hemipelagic deposition below the oxycline (FA2, Fig. 4.19A). Very thin-bedded but conspicuous, bottom current deposits and quasi-steady or surge-like, sediment-gravity flow intervals derived from slope destabilization or hyperpycnal discharges occurred (Paz *et al.*, 2019; Otharán *et al.*, 2020). Oxygen conditions of bottom waters in the basin were typically anoxic to euxinic due to a stable oxycline, with very rare dysoxic conditions.

The bottomset was characterized by relatively shallow water depths and a stratified water column, generating a suitable environment for organic carbon enrichment (Tyson, 1995). Water depths of 270-400 m for the bottomset were obtained by backstripping analysis (Minisini *et al.*, 2020a). A sedimentation rate of 23-38 mm/kyr can be calculated for the basin to drift facies associations (FA2 and FA3), and absolute dating of volcanic tuffs suggests 20-80 mm/kyr (Minisini *et al.*, 2020a), indicating low siliciclastic dilution of organic matter. The location of the system in an area prone to wind-driven offshore Ekman transport (Hay, 1995) suggests mixing in the surface waters by upwelling, generating high organic carbon production. In addition, the proximity to the coast ensured a close and constant source of nutrients from rivers sourcing from the SW sector of the Basin (Picún Leufú, Leanza *et al.*, 2011), while shallow-water conditions enhanced the transport to the seafloor by a shortened degradation time in the water column (Berger *et al.*, 1989; Hay, 1995). The extensive volcanic activity recorded in the Vaca Muerta Formation may have also fueled high productivity waters, fertilizing the sea with nutrients (Frogner *et al.*, 2001). The area was located at the transition between arid and warm temperate climates during the Late Jurassic, with warm waters (water temperature typically >20 °C; Volkheimer *et al.*, 2008; Gómez-Dacal *et al.*, 2018) generating a relatively stable oxycline and basin-wide, estuarine circulation (deep watermass inflow and surface watermass outflow). These conditions allowed anoxic to euxinic bottom waters that promoted organic matter preservation at the sediment-water interface, while transgressions enriched the sea-floor with organic carbon by hampering offshore sediment delivery and consequently decreasing dilution effects.

The estuarine circulation of the Neuquén Basin with stable oxycline developed during starved and anoxic basin deposition (F2a, F2b), switched to a weakened estuarine or anti-estuarine circulation responsible for the sediment drifts (FA3) and oxygenated basin deposits (F2c, F2d; e.g.

Witzke, 1987; Stratford *et al.*, 2000). This switch in circulation system was triggered by the formation of cold, dense shelf waters in the south-western sector of the basin during times of winter cold fronts (Rodríguez Blanco *et al.*, 2020), that cascaded offshore and intensified a wind- and thermohaline-induced, contour current circulation system of relatively deep watermasses, similarly to that observed in the modern Mediterranean Sea (Verdicchio *et al.*, 2007, Verdicchio and Trincardi, 2008a; Lüdmann *et al.*, 2012; Miramontes *et al.*, 2016). Accordingly, FA3 represents the area of fine-grained sediment advection by contour currents and sediment-gravity flows, with rare influence of storm events. Considering the small number of erosive surfaces and lags, these areas comprise relatively low to moderate energy current reworking upon fine-grained sediments, generating ripple and dune accretion. Enhanced transport and reworking may had occurred where flow velocity increased due to presence of obstacles, channels producing flow constraint, or increase in slope stepness. The relatively high lateral continuity of F3a (*ca* 160 km from well 1 to outcrop YdT) suggests sustained current activity over wide areas. Substrates were typically soupy to soft, with firmer conditions during tuff deposition and after high-energy current events. Oxygen levels increased due to cascading of shelf (surface) waters, in a process similar to modern deep-water ventilation (e.g. Meier *et al.*, 2006; Coppola *et al.*, 2017). Moreover, oxygenation was controlled by the vertical and horizontal distance from the oxycline, because oxygen consumption by organic matter degradation increased offshore from the area of dense water production. Hence, dysoxic to anoxic conditions were observed in the bottomset to lower foreset locations of the basin environments (F2c), and dysoxic and oxic in the proper lower foreset (F2d). Ventilation of the seafloor in these environments generated higher organic matter remineralization and consequently lowered the TOC content, yet values remained high (e.g. Av. TOC of 4.04% in F3a, Fig. 4.18D).

The interval of increased contour current strength is associated with high carbonate deposition at a time of low sea-levels. Higher carbonate sedimentation was developed from the late Tithonian to the early Berrasian associated with arid climates, when the Picún Leufú carbonate shelf was active in SW Neuquén Basin (Rodríguez Blanco *et al.*, 2020). This carbonate and arid event is part of regional cooler climates and sea-level lowstands described in southern South America during the late Tithonian (Brysch, 2018). In the Vaca Muerta Formation, cooler waters calculated from bivalve oxygen isotope data were recorded in the south-western Neuquén Basin (Alberti *et al.*, 2020). This suggests that arid conditions associated with low riverine influence

might correlate with cooler climates and eustatic falls. Under Mesozoic greenhouse conditions, the subtropical arid belt might have expanded poleward during cooling trends (Hasegawa *et al.*, 2012), generating an increase in aridity in the Neuquén Basin (located at the southern tip of the arid belt) that decreased fluvial influence and triggered carbonate sedimentation (Sagasti, 2005).

After the weakened estuarine to anti-estuarine circulation event, the basin returned to estuarine conditions, generating a new stable oxycline that significantly reduced oxygenation and contour current reworking in the bottomset to lower foreset. These locations recorded pelagic, hemipelagic and minor bottom current and sediment-gravity flow events. In addition, the slope environments (FA4) record hemipelagic sedimentation from hypopycnal to mesopycnal plumes or low-density flows (M_ch), and rare fluid mud events (M_cm). In the study area, sabkha environments occur close to the shoreline (Leanza *et al.*, 2011), and thus, siliciclastic and carbonate constituents are derived from the SW Neuquén Basin, where fluvially influenced, shelf-margin clinoforms alternated with the development of a carbonate shelf (Zeller *et al.*, 2015; Paz *et al.*, 2019). NE-directed winds from the Kimmeridgian (Spalletti *et al.*, 2011) probably continued during the Tithonian, generating a wind-driven, counter-clockwise surface current that transported sediment to the clinoforms (Zeller *et al.*, 2015). The landward limit of the foreset is delineated by the storm wave base occurring at the upper foreset (F4b, F4c). Substrates were soft to soupy. Anoxic and rare dysoxic conditions dominated in the bottomset, whereas the lower foreset mainly documented dysoxic to anoxic conditions, with oxic conditions increasing towards the top, in the upper foreset (F4c).

A clear landward increase in carbonate composition suggests a carbonate mud source located in the upper foreset and topset that drove clinoform progradation (Fig. 4.18C). The carbonate-rich composition of the hypopycnal to mesopycnal plumes or low-density flows suggests that they were originated by cascading (e.g. Wilson and Roberts, 1995; Canals *et al.*, 2006; Palanques *et al.*, 2006; Eberli and Betzler, 2019), or nepheloid layers associated with other resuspension processes (e.g. Puig and Palanques, 1998; McPhee-Shaw *et al.*, 2004). Cascading has been also interpreted in the Vaca Muerta Formation from the coeval Los Catutos Member in the southern part of the basin (Rodríguez Blanco *et al.*, 2020). These plumes developed during times of estuarine circulation with stable density stratification and low contour current activity, suggesting that many may have cascaded from the shelf and continued along surfaces of density stratification as mesopycnal plumes (Rodríguez Blanco *et al.*, 2020). Hypopycnal and mesopycnal

sedimentation driving clinoform progradation highlights the importance of across- and along-shore advection of sediment in building-up clinoform systems, as observed in modern low-angle, muddy subaqueous clinoforms around the world (Cattaneo *et al.*, 2003; Liu *et al.*, 2007; Patruno *et al.*, 2015; Schattner *et al.*, 2020).

In the younger clinoforms, the foreset increased slope steepness (0.2-0.3° to 1-3°) because of shelf aggradation, and fluid-mud flows became more important (F3c, F4d, Fig. 4.19B). First, a short anti-estuarine event triggered contour current transport coupled with fluid mud events in the lower foreset (F3c), generating a sediment drift elongated along-shore (Notta *et al.*, 2017; Reijenstein *et al.*, 2020). Later, fluid muds and mass transport processes of slope environments dominated in the upper foreset (F4d, Notta *et al.*, 2017). Increments in oxygen levels are restricted to the contourite deposits (F3c), whereas dysoxic conditions and soupy substrate stress were common in the fluid mud deposits (F4d).

The abundance of intrabasinal components (Fe-dolomite grains, bivalve bioclasts, and radiolarians) in the fluid mud flows (M_cm) and its similar composition with the carbonate source area (F4c, Fig. 4.18C), suggest that they were triggered by bottom boundary processes inducing resuspension in the upper foreset to topset area (Ogston *et al.*, 2000; Traykovsky *et al.*, 2000; Hill *et al.*, 2007; Hale and Ogston, 2015). However, the high clay concentration measured by other authors in these deposits (Kietzmann *et al.*, 2020a; Minisini *et al.*, 2020a) indicates a fluvial influence in the shelf, contributing to the mixed composition of the resuspended flows. In muddy shelves, resuspension by storms alone may not leave an important sedimentary record if not coupled with sediment introduction, because consolidation and cohesion of mud deposits restrict reworking and resuspension (Wheatcroft *et al.*, 2007). For example, during an episode of combined storm and mud-rich river discharge, wave stress at the bottom boundary layer can sustain high-concentration layers of mud, suppressing turbulence and generating a dense fluid mud that can be transported downslope as a gravity flow (Ogston *et al.*, 2000; Traykovsky *et al.*, 2000; Hill *et al.*, 2007; Hale and Ogston, 2015). These fluid mud events lack evidence of oscillatory flow reworking, and are observed in the upper foreset. This supports the interpretation of a storm wave base located landwards, coincident roughly with the foreset to topset transition (i.e. shelf-break, 50 m water depth, Minisini *et al.*, 2020a) and resuspending carbonate mud to trigger the flows. The occurrence of such a shallow storm wave base is related with the reduced fetch of epicontinental basins, generating low wave energy (e.g. Palanques *et al.*, 2002; Ulses *et al.*, 2008).

The switch from an upper foreset storm wave base in younger clinoforms (F4b) to the foreset-topset transition might also be related with shelf aggradation or progradation of the clinoform into deeper basinal locations.

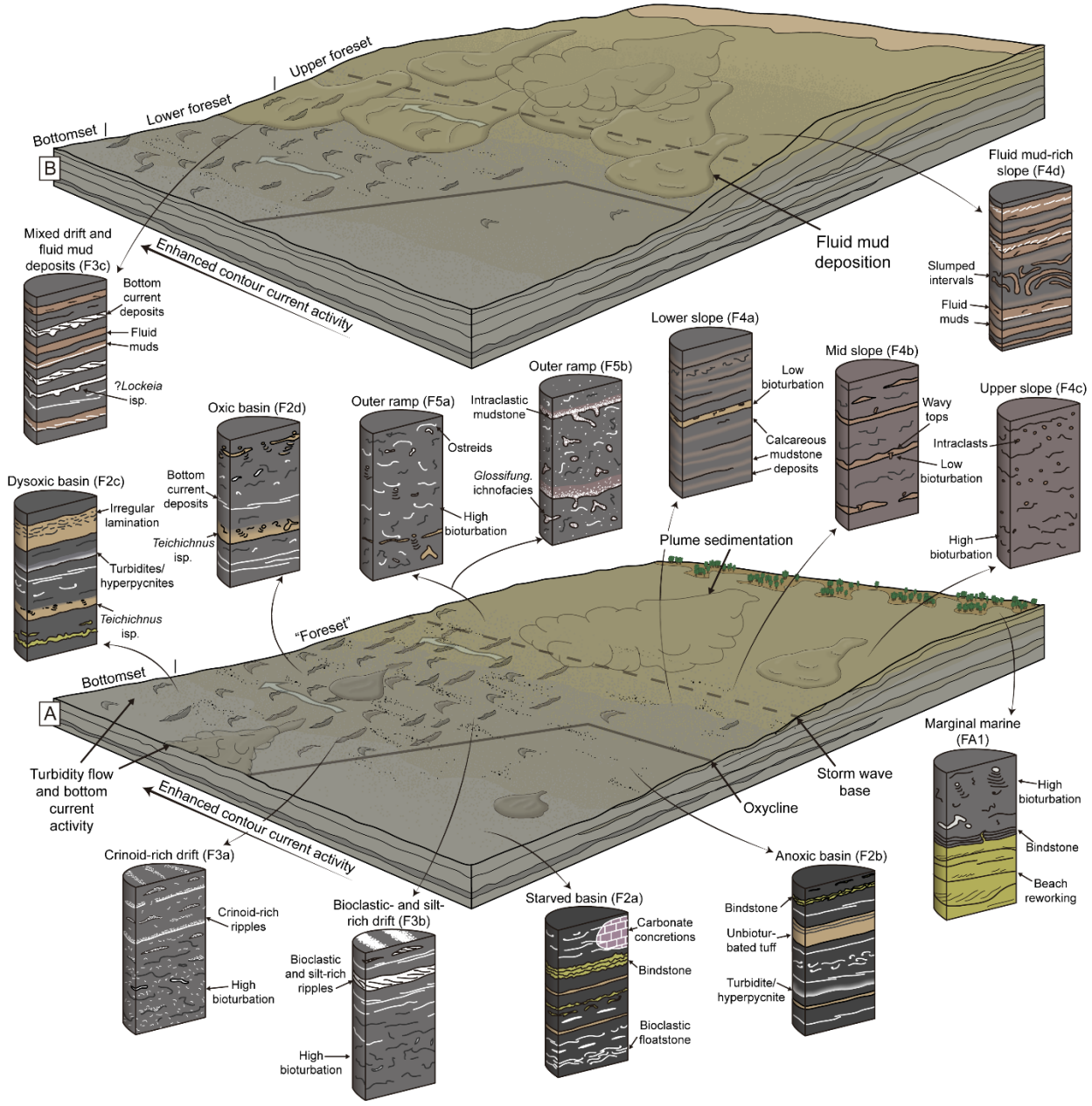

Fig. 4.19. Depositional model of the Vaca Muerta Formation for the A) low-angle older clinoforms, and B) higher angle clinoforms in younger successions. The clinoform anlge and contour current intensity controlled the oxycline position and the paleogeographic location of different facies.

The younger Unit 4 and Unit 5 lack sufficient core data to produce an analysis similar to the one dedicated to Units 1 to 3. The few inferences about Unit 4 and Unit 5 are that their outer ramp environments displayed alternating low-energy, hemipelagic-dominated conditions (F5a), and high-energy, current-dominated conditions with the occurrence of firmer substrates (F5b).

4.7 Sequence stratigraphy

Correlation of facies derived from cores and outcrop are presented in two NW-SE transects to understand lateral and vertical facies changes and to create a sequence-stratigraphic framework for the study area (Fig. 4.20). Units (1 to 5) and surfaces (B1 to B5) are derived from Minisini *et al.* (2020b) after González Tomassini *et al.* (2016) and Desjardins *et al.* (2018). The analysis mostly comprises Units 1 and 2, whereas data from Units 3 to 5 are fragmentary. In addition, some intervals (e.g. between surfaces B2 and B3) are missing. Three third-order sequences were defined in Units 1 to 3. The reduced data density in Units 4 and 5 only allowed the delineation of fourth-order sequences (i.e. parasequences).

4.7.1 Sequence 1 (S1)

This sequence developed from the early Tithonian to the early late Tithonian during Unit 1 (Fig. 4.20A, B, *Virgatosphinctes andesensis* to *Windhauseniceras internispinosum* ammonite zones; Riccardi, 2015; Desjardins *et al.*, 2018; Kietzmann *et al.*, 2018a; Minisini *et al.*, 2020b). The lower interval of S1 consists of a Transgressive Systems Tract (TST) above a Transgressive Surface (TS) developed on top of the Tordillo and Catriel formations. The TST is constituted by a retrogradational stacking pattern from continental deposits to marginal-marine (FA1) and basin (FA2) facies association. A condensed interval of 2-5 m comprising starved basin and anoxic basin facies (F2a and F2b) marks the Maximum Flooding Surface (MFS) 20-25 m above the base of the Vaca Muerta Formation. Above the MFS, a Highstand Systems Tract (HST) is developed. A progradational shift of facies from anoxic basin (F2b) to dysoxic and oxic basin (F2c, F2d) and drifts (FA3) represents a change towards anti-estuarine conditions occurring during low sea levels, defining one parasequence associated with the Falling Stage Systems Tract (FSST) above a Basal Surface of Forced Regression (BSFR).

4.7.2 Sequence 2 (S2)

This sequence was deposited during the late Tithonian, comprising Unit 2 and the top of Unit 1 (Fig. 4.20A, B, *Windhauseniceras internispinosum* to *Corongoceras alternans* ammonite zones; Riccardi, 2015; Kietzmann *et al.*, 2015; Desjardins *et al.*, 2018; Minisini *et al.*, 2020b). S2 rests on top of a Sequence Boundary (SB) representing a correlative conformity, where two parasequences are associated with a Lowstand Systems Tract (LST). A facies deepening from dysoxic basin (F2c) to anoxic basin facies (F2b) represents a retrogradational stacking pattern, yet the occurrence of contourite deposits and dysoxic evidence (F2d, F3b) indicates a continuation of anti-estuarine conditions during low sea levels, suggesting that the succession overlying the SB is part of an early TST, with a TS below correlated with surface T3. On top, anoxic basin facies clearly dominate the distal areas (F2b), and starved basin facies occur in wells 4 and 8 (F2a), indicating the highest sea level rise during late TST and the delineation of a MFS. Above, progradation of the clinoform system can be observed; however, a major switch to anti-estuarine circulation differentiating FSST and LST does not occur, and therefore the whole progradation occurs during a Regressive System Tract (RST). The SB delineating the top of S2 is amalgamated with a TS, likely equivalent to surface T5.

4.7.3 Sequences 3 and 4 (S3 and S4)

In this interval, the vertical relationship between sequences is poorly understood because data are few and sparse (only wells 6, 7 and 9 cored this succession). Nevertheless, two third-order sequences were deposited from late Tithonian to early Valanginian, included in Unit 3 (S3) and Units 4 and 5 (S4) (Fig. 4.20B, C, *Substeueroceras koeneni* to *Neocomites wichmanni* ammonite zones; Riccardi, 2015; Desjardins *et al.*, 2018; Kietzmann *et al.*, 2018a; Minisini *et al.*, 2020b). S3 consists of a TST displaying a shift from dysoxic and oxic basin facies (F2c, F2d) to starved basin facies (F2a), and continues with a RST comprising progradation of dysoxic and oxic basin facies (F2c, F2d). The overlying SB, amalgamated with a TS, is equivalent to surface B2. Sequence 4 (S4) is interpreted as a tentative third-order sequence because large-scale facies variations cannot be tracked laterally. In this succession, fourth-order sequences were observed, represented by the alternation of the facies associations belonging to basin (FA2), slope (FA4) and outer ramp (FA5).

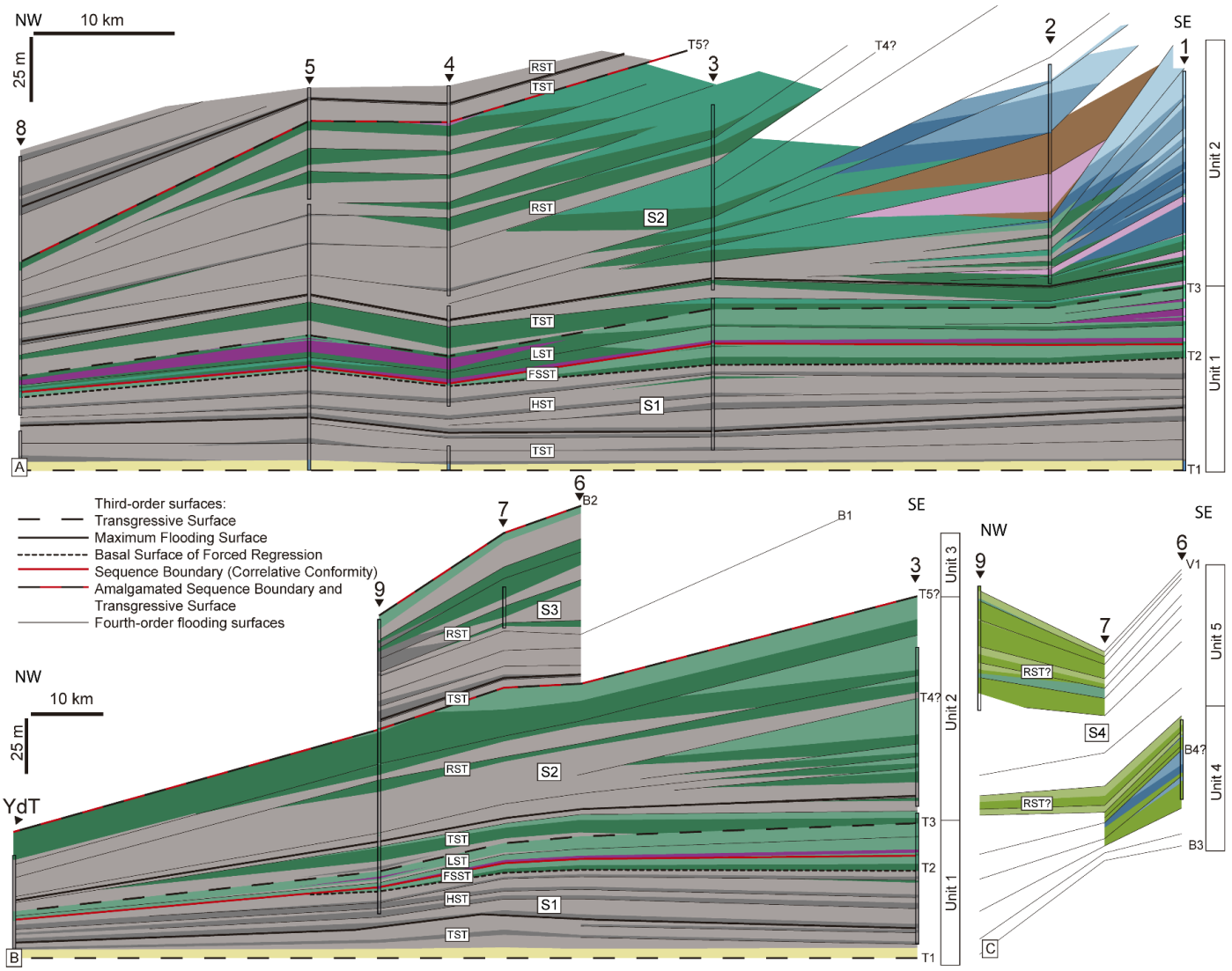

Fig. 4.20. NW-SE transects showing correlation of cores and outcrop analyzed, constrained by biostratigraphy and seismic data. The analysis of facies distribution (key in Fig. 4.18) provided the basis for the sequence-stratigraphic interpretation and the delineation of sequences 1 to 4 (S1-4). Stratigraphic surfaces and Unit nomenclature from Minisini *et al.* (2020b). Transect A shows Unit 1 and Unit 2, the transect B displays Unit 1 to Unit 3, the transect C shows Unit 4 and Unit 5. Location of transects in Fig. 4.1C. Transgressive Systems Tract (TST), Highstand Systems Tract (HST), Falling-stage Systems Tract (FSST), Lowstand Systems Tract (LST) and Regressive Systems Tract (RST) are delineated.

4.8 Discussion

4.8.1 Differentiating between muddy bottom currents and sediment-gravity flows

Bottom transport mechanisms in modern marine environments can be broadly subdivided into bottom currents and sediment gravity flows (Bouma and Hollister, 1973; Stow and Piper, 1984; Shanmugam, 2006). Bottom currents show "persistency" through time (Eberli and Betzler, 2019), and are typically of low sediment concentration. In contrast, sediment-gravity flows represent relatively short-term events primarily driven by excess density from high sediment concentration. In the lower density end of the sediment-gravity flow spectrum, flows may be deflected by Coriolis force to be transformed into bottom currents (Hill, 1984). Bottom current transport is developed by various mechanisms, such as wind- or thermohaline-driven contour currents and internal waves and tides (Shanmugam, 2006; Rebesco *et al.*, 2014). Density cascading may be considered a bottom current due to its low sediment concentration (Wilson and Roberts, 1995; Shapiro *et al.*, 2003), but it represents a hybrid because it is not continuous through time. The sediment-gravity flow concept refers to processes such as turbidity flows, concentrated density flows, hyperpycnal flows (river-derived flows, Bates, 1953), and wave or current-enhanced sediment-gravity flows.

In the Vaca Muerta Formation, evaluation of sediment concentration and the temporal scale of muddy sedimentary processes helped in recognition and differentiation between bottom currents and sediment-gravity flows (Paz *et al.*, in review a, see also Chapter 6). In addition, preservation of bottom current deposits was enhanced by oxygen deficiency during the early Tithonian, which prevented bioturbation. When passing the threshold for sediment resuspension and transport, bottom currents generate low sediment concentration suspended loads (in the order of mg/L, e.g. Hollister and McCave, 1984; Canals *et al.*, 2006; Puig *et al.*, 2013), producing extensive bedforms at the base of the flow due to dominant traction transport (e.g. Heezen and Hollister, 1964; Heezen *et al.*, 1966). The described contourite deposits (FA3) show considerable evidence of traction transport in coarse mudstone and crinoid-rich laminae (lithofacies Mh, Ml, M_{cr}h and M_{cr}l, e.g. Yawar and Schieber, 2017), parallel, low-angle, current- and wave-ripple cross-lamination mudstone and crinoidal mudstone (M_sh, M_sl, M_sr, M_sw, M_{cr}w, and M_{cr}r,), and low-angle and trough cross-bedded, crinoidal and peloidal mudstone (M_{cr}t, M_pl, Figs. 4.9, 4.10, 4.11) lithofacies. In contrast, muddy sediment-gravity flows need to sustain high sediment concentration in low angle shelves because excess density is necessary to generate gravitational forcing, contributing to a loss of turbulence in the flow (Baas and Best, 2002). Therefore, the deposit would display a massive or graded appearance with soft-sediment deformation structures due to the development

of upper transitional or quasi-laminar plug flows of high cohesive strength (Baas *et al.*, 2011), as recorded in modern muddy hyperpycnites (Ducassou *et al.*, 2008). Accordingly, the fluid mud deposits of the Vaca Muerta Formation (M_cm, $M_c$comp of F4d) show evidence of matrix strength associated with high-sediment loads, such as load casts, mudstone pseudonodules, flame structures, and pebble-sized deformed intraclasts (Figs. 4.12C, D, E). Identification of the different deposits of muddy sediment-gravity flows (e.g. turbidity flows, hyperpycnal flows and wave or current-enhanced sediment-gravity flows) is still an area to be refined with further work (Schieber, 2016).

Considering the temporal scale, recognizing the activity of sedimentary processes sustained through relatively long periods of time might help to distinguish bottom currents from sediment-gravity flows (Paz *et al.*, in review a). Sediment-gravity flows or downwelling currents associated with storm wave action do not persist in time, and cannot generate long-term sediment transport at the seafloor. In the Vaca Muerta Formation, the gradational alternation between highly bioturbated intervals and deposits with abundant traction transport structures suggests a continuous flow that controlled the establishment of the infauna by means of hydrodynamic energy (e.g. Fig. 4.10). Locally, successions showing decreasing to increasing bioturbation patterns (similar to bigradational successions; Gonthier *et al.*, 1984; Stow and Piper, 1984) indicate continuous, long-term currents occurring in the middle part of the successions preventing extensive bioturbation (Fig. 4.16D, Paz *et al.*, in review b). Also, the predominance of suspension-feeding organisms in F3c, suggests the existence of a continuous current maintaining sediment in suspension. Lastly, long-term activity of currents can be inferred from the highly bioturbated intervals observed in bottomset locations (Figs. 4.4, 4.9B, 4.10A), indicating sustained oxygen supply in typically anoxic environments. In contrast, sediment-gravity flows cannot maintain long-term oxygenation (e.g. Sholkovitz and Soutar, 1975), and may typically show top-down bioturbation patterns if generating short-term oxygen supply (e.g., Stow and Shanmugam, 1980; Ponce *et al.*, 2007; Buatois *et al.*, 2011).

The observed depositional and bioturbation pattern in the Vaca Muerta Formation suggests that sedimentary processes depended on basin circulation. During estuarine circulation, pelagic and hemipelagic conditions dominated in the bottomset to lower foreset, and hypopycnal to mesopycnal plumes and fluid mud flows in the upper foreset (FA4). However, during specific times of weakened estuarine or anti-estuarine circulation and relatively low sea levels, contour

currents reworked bottomset to lower foreset (FA3) and even probably to the foreset (the Los Catutos Member; Rodríguez Blanco *et al.*, 2020). Although the currents are likely to be intensified during storms, they do not produce tempestites themselves. The described contourite deposits do not grade landward into hummocky cross-stratified units, as observed with tempestites (Einsele and Seilacher, 1991), but into mud-rich deposits with current- and wave-ripple cross-lamination and silt laminae (Fig. 4.9F). In addition, the upper foreset during conditions of estuarine circulation lacks hummocky cross-stratification, and present only minor wave ripples (F4b, Fig. 4.13A). In the northern and south-western part of the basin, the Vaca Muerta Formation shows significant tempestite deposition in bottomset and foreset, due to clinoform migration in basin margin locations (Kietzmann and Palma, 2011; Paz *et al.*, 2019).

Wind- and thermohaline-driven contour currents constitute the best hypothesis to explain basin-wide, long-term changes in seafloor oxygenation recorded during the peak in current activity. Other forcing mechanisms are less likely, yet they are not discarded. They include tide-driven currents (Zeller *et al.*, 2015a), and internal wave or tides where the seafloor intersects the pycnocline (Cacchione and Drake, 1986). Considering tides, there is evidence of tidal transport in the shelf (Zeller *et al.*, 2015a), yet the existence of a volcanic arc in the west might have produced microtidal conditions in the Neuquén Basin (Canale *et al.*, 2020 and references therein). The large across-slope distance of some of the contourite facies (F3a, F3b, *ca* 160 km) precludes the idea of internal waves or tides, which are restricted to the area of pycnocline fluctuations. The core analysis does not allow paleocurrent measurements, thus more detailed work on this interval is needed to reveal the origin of the circulation system in the basin.

Contourite deposits have been described in other shallow-marine, organic-rich, fine-grained depositional environments. For instance, organic-rich, laminated or bioturbated, calcareous mudstone or mudstone clast-bearing calcareous coarse mudstone are known from the Upper Jurassic Haynesville Formations of USA, (Hammes and Frébourg, 2012; Frébourg *et al.*, 2013). These deposits indicate active traction transport interrupted by intense bioturbation, and are interpreted to have been accumulated as marine snow (pelagic) and later reworked into sedimentary drifts by contour currents (Frébourg *et al.*, 2013). Other examples are the Devonian Duvernay Formation and Horn River Group, Canada, both displaying abundant traction structures combined with moderate to minor bioturbation, and interpreted to have been deposited by contour currents (Knapp *et al.*, 2017; Ayranci *et al.*, 2018). The Cenomanian Eagle Ford Formation

characterized by organic-rich fine-grained marlstones is also deposited by bottom currents, which were weak (15-20 cm/s) to the point that they did not bring oxygen to the sea floor, thus maintaining the redox front at the sediment water interface and hampering bioturbation while preserving organic matter (Minisini *et al.*, 2018).

4.8.2 Environmental controls on trace fossils and their relationship with sedimentary processes and basin circulation

The ichnologic content of basin and slope deposits of the Vaca Muerta Formation records a combination of biodeformational structures, which are dominant, and discrete trace fossils. The later includes, in order of abundance, *Teichichnus rectus, Alcyonidiopsis longobardiae, Coprulus oblongus, Planolites* isp., *Thalassinoides* isp., *Teichichnus zigzag, Phycosiphon incertum, Palaeophycus* isp., ?*Lockeia* isp., *Lockeia siliquaria, Nereites* isp., *Palaeophycus heberti, Crininicaminus* isp., *Zoophycos* isp., *Teichichnus patens, Diplocraterion* isp., and ?*Skolithos* isp. Pellet trails, mantle and swirl structures, and escape and equilibrium structures also occur.

Integration of ichnologic, sedimentologic, and geochemical data suggests that the distribution of trace fossils was controlled by the interplay of substrate consistency, food, and oxygen in conjunction with sedimentary processes and basin circulation. The predominance of biodeformational structures generating parallel-bedded to massive fabrics (e.g. Fig. 4.9B, 4.10A) indicates that soft to soupy substrates were common, whereas soft to firmground conditions occurred after tuff deposition or high-energy current events that exhumed compacted sediments. Sediment contrast alone cannot account for the low number of discrete trace fossils, because, for example, sediment variations occur in the highly bioturbated crinoidal mudstone (Fig. 4.10A). The same situation can be observed in the Paleogene of Denmark (Pedersen, 1981). There, laminated diatomite composed of white, diatom-rich and brownish, clay-rich laminae represent hemipelagic, anoxic deposits, whereas bioturbated, massive (structureless) diatomite occur in direct association with tuff intervals displaying *Teichichnus, Planolites, Chondrites,* and *Taenidium* (Pedersen, 1981). Because the unbioturbated lithofacies has alternating white and brownish lamina, sediment contrast may have existed during deposition of the massive diatomite, and therefore it cannot be the only control generating massive fabrics.

As in other oxygen-deficient fossil successions, the decrease of BI, penetration depth, and burrow size observed in both mudstone and tuff is controlled by reduced bottom and pore water

oxygen levels (Savrda and Bottjer, 1986; Mángano, 2011). However, the present ichnologic dataset differs from other oxygen-deficient ichnofaunas in the paucity of *Chondrites* and *Zoophycos*, both ichnogenera typical of bottom water dysoxia (Bromley and Ekdale, 1984; Ekdale and Mason, 1988). *Chondrites* was not recorded in the study area, yet it was documented *ca* 250 km to the north, in the Mendoza Shelf (Doyle *et al.*, 2005), whereas *Zoophycos* is only locally present in F2d and F5a. This pattern most likely responds to the high food input, interpreted from the high TOC values (av. TOC of 5%; Minisini *et al.*, 2020b). High food scenarios tend to be associated with abundant biodeformational structures recording non-specialized feeding during exploitation of organic-rich, soft to soupy sediment (Wetzel, 1991; Wetzel *et al.*, 2011). In this sense, the Vaca Muerta ichnofauna is similar to the one recorded in the upwelling zone off Vietnam during glacial periods, where soft to soupy substrates, low oxygen, and high food conditions were conducive to the formation of biodeformational structures (Ichnofabric IV of Wetzel *et al.*, 2011).

The degree of oxygenation was affected by the distance from the oxycline and basin circulation. During estuarine conditions, strong water stratification generated anoxia to euxinia in the bottomset and anoxic to oxic conditions from lower foreset to upper foreset locations. In contrast, during weakened estuarine or anti-estuarine circulation, wind- and thermohaline-driven currents intensified by enhanced cascading of oxygenated, shelf dense waters, produced alternation of anoxic, dysoxic and oxic conditions in the bottomset at dm-scale intervals, whereas dysoxic to oxic levels occurred from lower foreset to probably foreset locations outside of the study area (Los Catutos Member, Rodríguez Blanco *et al.*, 2020). Suboxic conditions are typically delineated from geochemical evidence of nitrogenous, manganous, and/or ferruginous zones, and therefore, the present ichnological dataset cannot differentiate anoxia from suboxia. Spalletti *et al.* (2019) utilized Mo-U enrichment factor to show the influence of suboxic conditions in the Vaca Muerta Formation.

Basin-wide, upper dysoxic and oxic events have been detected in the Vaca Muerta Formation during FSST, LST of S1 and TST of S2 (*Windhauseniceras internispinosum* ammonite zone, Fig. 4.20). Some problems may have hampered the ability to recognize these events from an ichnologic perspective. Heterogeneities in the rock fabric in successions without sediment contrast (such as black shales) are difficult to visualize in outcrops, making virtually impossible a proper characterization of bioturbation structures. Moreover, geochemical analysis typically used to assess bottom water oxygen conditions have a lower time resolution compared with biofacies data,

because trace fossils are highly sensitive to short term (e.g. days to years) environmental changes (Wignall and Myers, 1988; Boyer and Droser, 2011). For example, the TOC-rich transgressive basal succession (Av. TOC of 3.03%, N=7) records anoxic to euxinic conditions based on trace element data (Spalletti *et al.*, 2014; Capelli *et al.*, 2018; Krim *et al.*, 2019), whereas trace fossils suggest mainly oxic conditions with relatively deep bioturbation (Figs. 4.4, 4.6B, C, D). Trace and body fossils analyzed from outcrops in the Mendoza Province indicate variations in bottom water oxygen levels (Doyle *et al.*, 2005). In the present study, fresh cross-sections obtained from cores and polished samples from outcrops, as well as detailed observations facilitated by sediment contrast provided by tuff intervals, allowed assessment of bioturbation structures and high-resolution delineation of oxic and dysoxic events.

4.8.3 Applications of the ichnofacies paradigm to the study of fine-grained depositional systems

The ichnofacies paradigm has been instrumental in refining the use of trace fossils in facies analysis and paleoenvironmental reconstructions (MacEachern *et al.*, 2007b). However, fine-grained depositional systems remain relatively underexplored from an ichnofacies perspective. The trace-fossil suites identified in the embayment deposits (F1b) (see also Paz *et al.*, 2021) favor comparisons with the depauperate expression of the *Cruziana* Ichnofacies, although this approach to marginal-marine environments has been criticized and their ichnofacies treatment is in a stage of flow (MacEachern and Bann, 2020). In addition, the suites of *Thalassinoides* isp. showing sharp boundaries, lack of compaction and passive infill, all features characteristic of firmground surfaces, clearly correspond to the *Glossifungites* Ichnofacies (MacEachern *et al.*, 1992, 2007c). This ichnofacies occurs locally during times of high-energy reworking of the sea floor that exhumed previously deposited sediment (F1b, F3a, F5a).

However, placing the typical softground ichnofaunas of the basin, slope, and outer ramp environments within the framework of the ichnofacies model is not straightforward. Basin and slope environments are traditionally recognized as being illustrated by the Seilacheran *Nereites* and *Zoophycos* Ichnofacies (MacEachern *et al.*, 2007b). However, the Vaca Muerta Formation is a shelf-margin clinoform system (e.g. Patruno and Helland-Hansen, 2018), separating a shallow-water shelf (topset) from slope and basin environments (foreset and bottomset) occurring mostly right below a storm wave base (located at the upper foreset or foreset-topset transition). Therefore,

the ichnofacies corresponding to the bathymetric range of these areas (right above or below storm wave base) are the *Cruziana* and *Zoophycos* Ichnofacies (MacEachern *et al.*, 2007b). The archetypal *Cruziana* Ichnofacies is characterized by high ichnodiversity and high abundance of trace fossils, representing a broad spectrum of ethologic categories, and dominated by horizontal traces produced by deposit and detritus feeding organisms. It occurs in settings located from slightly above the fair-weather wave base to the storm wave base (Seilacher, 1967; Pemberton *et al.*, 1992; MacEachern *et al.*, 2007b, Buatois and Mángano, 2011, 2021). The distal *Cruziana* Ichnofacies contains a higher number of grazing trails and specialized feeding structures, such as *Phycosiphon, Helminthopsis*, *Chondrites*, and *Zoophycos*, and is characteristic of the distal offshore (MacEachern *et al.*, 2007b, Buatois and Mángano, 2011, 2021). The *Zoophycos* Ichnofacies is represented by simple to complex feeding structures with spreite, low ichnodiversity and high abundance, typically comprising areas below storm wave base (Seilacher, 1967; MacEachern *et al.*, 2007b, Buatois and Mángano, 2011, 2021). This ichnofacies transitions into the distal *Cruziana* Ichnofacies to the point that distinguishing between the two may be difficult in some cases (MacEachern *et al.*, 2007b; Buatois and Mángano, 2011, 2021).

The mere use of a checklist approach would suggest that basin and slope deposits (FA2, FA4) present affinities with the *Cruziana* Ichnofacies. However, a more in-depth analysis shows that this is not correct. First, although taken as a whole, the Vaca Muerta Formation may be seen as relatively diverse, this is misleading because discrete assemblages are invariably of low diversity. The typical assemblage is mostly restricted to tuff intervals and comprises *Teichichnus rectus*, *Alcyonidiopsis longobardiae*, and *Phycosiphon incertum*. Second, whereas archetypal trace-fossil suites illustrating the *Cruziana* Ichnofacies represent mature benthic communities displaying relatively complex infaunal tiering structure, those from the Vaca Muerta Formation are very simple and represented dominantly by biodeformational structures, overprinted by a few shallow-tier discrete trace fossils emplaced in the tuffs. Third, the existence of an oxygenation stress associated with distal environments suggests some affinities with the *Zoophycos* Ichnofacies (MacEachern *et al.*, 2007b). However, this ichnofacies tends to be dominated by complex burrows (e.g. *Zoophycos*) that represent climax strategies, which is not the case of the Vaca Muerta Formation assemblages. In any case, the development of organic-rich seafloors such as in the Vaca Muerta Formation, has been interpreted to promote feeding strategies of ichnotaxa that are

characteristic of the *Zoophycos* Ichnofacies (Buatois and López Angriman, 1992), indicating that our assemblage may have more affinities with this ichnofacies than with the *Cruziana* Ichnofacies.

During contourite deposition (FA3), ichnodiversity and ethologic variability increased, recording a combination of suspension, deposit- and detritus-feeding strategies in heterolithic beds. However, these suites still constitute the record of poorly developed infaunal communities that represent colonization during brief times of environmental amelioration. Moreover, in the slope (FA4), lower dysoxic and anoxic conditions and hemipelagic and fluid mud deposition generated even less ichnodiversity and bioturbation index. The outer ramp succession (FA5) shows oxic conditions but low substrate consistency, recording low diversity communities.

4.8.4 Implications for sediment distribution, organic matter content, and sequence stratigraphy in mixed clinoform systems

The present analysis underscores the association of high carbonate production and basin-wide bottom water oxygenation during low sea level. The Vaca Muerta Formation constitutes a shelf-margin, subaqueous clinoform system where low-amplitude sea-level oscillations did not generate complete subaerial exposure of the shelf (e.g. karstification nor fluvial incision of the shelf; Reijenstein *et al.*, 2020). Stacking patterns, sediment composition and sediment partitioning are related with climatic oscillations associated with the migration of the arid belt under the influence of Milankovitch cycles (Sagasti, 2005; Kietzmann *et al.*, 2015). Therefore, sediment partitioning can be understood as depending on the predominant climate. During warmer climates and equatorward migration of the belt, high sea levels (late TST, HST and/or early FSST of third-order sequences) and humid conditions in the south produced high freshwater winter discharges. These conditions triggered stratification of the water column and estuarine circulation, causing organic matter enrichment in the bottomset and higher volumes of siliciclastics in the foreset. In contrast, during cooler climates and poleward migration of the belt, arid conditions and low sea levels (late FSST, LST and/or early TST of third-order sequences) prevailed in the basin, and cascading of dense, cold waters from the southern margin reached its peak (Rodríguez Blanco *et al.*, 2020), generating anti-estuarine circulation and strong contour current transport. Moreover, lowered sea levels probably affected carbonate build ups in the shelf due to the impingement of the photic zone, enhancing carbonate production (Reijenstein *et al.*, 2020). At these times, TOC

content decreased and carbonate composition increased due to higher organic matter remineralization and lower siliciclastic dilution.

This interpretation contrasts with sequence stratigraphic ideas related to subaerial clinoform systems, where progradation occurs during HST and retrogradation during TST. Zeller *et al.* (2015a) suggested increased siliciclastic transport during LST and TST because of intense continental erosion and subsequent flooding and redistribution of siliciclastic sediment in an area with increased space for sediment transport. In contrast, decreased siliciclastic transport was proposed to have occurred during HST due to a lack of accommodation space for current development and siliciclastic input (Zeller *et al.*, 2015a). However, this model may be inaccurate because HST are times of accommodation space creation (although at a lower rate than sedimentation rate), and accommodation space refers to the space available for sediments (and not for currents) to accumulate (Jervey, 1988). In addition, the model cannot explain the evidence of low sea levels at the peak of carbonate production, in the Picún Leufú Formation (e.g. root horizons, calcrete and coral bafflestone; Armella *et al.*, 2008; Zeller *et al.*, 2015a; Rodríguez Blanco *et al.*, 2020).

Subaqueous clinoforms such as the Vaca Muerta-Quintuco system maintain their shelf fully submerged during lowstands, and therefore, progradational cycles may occur anytime regressive conditions are created (HST, FSST and LST), and retrogradational cycles may develop during shutdown of both carbonate and siliciclastic sources, comparable to deep-water sequence stratigraphic models (Catuneanu, 2006). Therefore, a Transgressive-Regressive sequence stratigraphic approach is useful when HST, FSST and LST cannot be differentiated (e.g. González Tomassini *et al.*, 2014; Zeller *et al.*, 2015a; Krim *et al.*, 2017). Sediment partitioning during a Transgressive-Regressive cycle records increased siliciclastics and TOC during transgressions and increased carbonates during regressions (González Tomassini *et al.*, 2014; Kietzmann *et al.*, 2016), which is in clear agreement with higher siliciclastic export during high sea levels, and higher carbonate export by cascading during low sea-levels. Within this framework, the carbonate-rich top of third-order sequences displaying increased oxygenation from bottomset to foreset areas (weakened estuarine to anti-estuarine circulation) may represent FSST or LST conditions. However, it must be noted that the described partitioning is based on climate variability influencing precipitation patterns and low-amplitude eustatic variations, but the regional tectonic activity might have a stronger effect on relative sea-level changes. Moreover, the present analysis is

focused on the Tithonian succession of the Vaca Muerta-Quintuco system, where temperate to semi-arid conditions predominated, yet sediment partitioning can be different after the establishment of humid conditions in the Berriasian and Valanginian (Capelli *et al.*, 2021). In this sense, the Quintuco Formation parasequences have an upward increase in siliciclastics, coincident with progradation under a mixed, subaerial clinoform system (Kietzmann *et al.*, 2016). All the above highlights the need for further sedimentological and sequence stratigraphic analysis correlating bottomset to topset facies and improving the prediction of sediment partitioning in the Vaca Muerta-Quintuco system. These analysis might be important to evaluate the role of estuarine and anti-estuarine circulation as proposed in the present study.

Finally, concerning organic carbon enrichment, the present dataset suggests that anoxia and high productivity were common during estuarine circulation, indicating that dilution might have been the key controlling factor to generate enrichment in organic matter (low dilution during transgressions, Kietzmann *et al.*, 2016; Minisini *et al.*, 2020a). Organic matter production occurred as part of the pelagic rain. This is supported by the analysis of the upper part of unbioturbated tuffs (Tm) showing pelagic sedimentation consisting of radiolarians, coccolith-rich planktonic pellets, and pelagic aggregates (marine snow) with radiolarians and coccoliths (Fig. 4.8H, I, L), all materials that are found in abundance within the encasing mudstone (Fig. 4.8A, J, K). These components are important contributors to the particulate organic carbon flux in modern and ancient organic-rich deposits (Angel, 1984; Berger *et al.*, 1989; Lampitt *et al.*, 2009; Macquaker *et al.*, 2010a; Ghadeer and Macquaker, 2011), suggesting that the organic carbon was sourced from the water column. Radiolaria may be of special importance in the pelagic flux as indicated by their abundance in the diet of the *Coprulus oblongus* producers and by previous studies of organic-rich sediments (Xiang *et al.*, 2013; Khan *et al.*, 2019). Vertical transport through aggregation and formation of marine snow and production of planktonic fecal pellets rapidly transfers organic matter to the sea-floor, escaping the degradation process of the water column (McCave, 1975; Suess, 1980; Angel, 1984). Episodic bloom of autotrophs and a consequent deficient recycling process by heterotrophs and decomposers may have also promote efficient organic carbon transport (Berger *et al.*, 1989). In addition, a shallow oxycline during estuarine conditions generated anoxia and dysoxia from the bottomset to the middle foreset, and even in the lower foreset of basin-margin locations (e.g. Paz *et al.*, 2019), indicating a higher ability of the organic matter to escape the degradation process in the water column.

Bottomset and lower foreset locations, constituted by anoxic basin environments (F2a, F2b), represent the areas where the thickest TOC-rich intervals occur (Brisson *et al.*, 2020; Domínguez *et al.*, 2020; Tenaglia, 2020). Organic-rich deposits show a centripetal increment (Brisson *et al.*, 2020) typical of basins redistributing organic carbon by hydrodynamic sorting (Huc, 1988). Therefore, organic carbon was transported to basin environments by pelagic input, but also from hemipelagic sediment advection from productive areas towards the shore. The evidence that organic matter is produced from the water column and the fact that anoxic conditions occurred in the bottomset and lower foreset preclude interpretation of a model with oxygen minimum impinging on the upper slope and transporting organic matter downslope (e.g. Cornford, 1979; Rullkötter *et al.*, 1983). In contrast, both higher energy bottom currents and sediment-gravity flows generated dilution of organic carbon. Contourite deposits have a higher bioclastic content relative to the formation, whereas the slope displays extensive TOC-lean, carbonate-rich fluid mud deposits. Geochemical data shows a slight increase in carbonate minerals of the drifts (FA3) compared with the basin (FA2), and lower TOC values (Fig. 4.18).

Nevertheless, it must be noted that although contour currents lowered TOC content, these deposits show relatively high TOC (Av. TOC of 4.04% in F3a). This fact might be explained by a constant source of organic matter from upwelling, generating higher oxygen consumption at the sea-floor, and a relatively distal position from the shelf. Interestingly, TOC analysis of sediment-gravity flows in the bottomset locations has shown higher TOC content associated with traction structures compared with pelagic intervals (Otharán, 2020; Otharán *et al.*, 2020), suggesting that either hydraulic sorting contribute to organic carbon enrichment in specific laminae or that gravity flows were sourced from other basinal areas richer in TOC. Modern environments, such as the upwelling system off Peru, indicate that bottom currents have a direct impact on organic matter enrichment (Reimers and Suess, 1983). Lower organic carbon values are recorded in areas where bottom currents impinge a wide shelf or resuspend sediment in the mid slope. Moreover, fine-grained sediment advected by the Peru-Chile undercurrent and deposited where the current weakens, or derived from local river input or ephemeral runoff, may dilute organic matter accumulation generating low TOC values (Reimers and Suess, 1983). Bottom currents may also preclude organic carbon preservation due to resuspension of organic matter, increasing its exposure time to benthic decomposition (Reimers and Suess, 1983). Hence, an understanding of bottom and surface waters circulation is critical in this formation and other ancient successions in

order to evaluate sediment partitioning, sequence stratigraphic stacking patterns and construct robust depositional models.

4.9 Conclusions

The present integrated study investigates the sedimentary processes and the paleoenvironmental conditions in a fine-grained depositional system based on stratigraphic, sedimentologic, ichnologic, and sequence stratigraphic data. The Vaca Muerta Formation is part of a mixed carbonate-siliciclastic, shelf-margin, subaqueous clinoform system deposited during Late Jurassic to Early Cretaceous. This formation shows mixed, calcareous, siliceous and argillaceous mudstone, bioclastic to intraclastic wackestone, tuffs and rare sandstone and bindstone that were grouped into fifteen facies and five facies associations, namely marginal marine (FA1), basin (FA2), drift (FA3), slope (FA4), and outer ramp (FA5). FA1 represents marine reworking of the Catriel Formation eolian deposits in a beach area (F1a) and marginal-marine bay sedimentation (F1b), marking the onset of the Vaca Muerta deposition during a transgression. The following facies associations were intercalated depending on basin circulation and slope angle. During basin-wide, estuarine circulation, basin environments (FA2) record condensation (F2a) and pelagic and hemipelagic deposition under anoxia or euxinia, with rare sediment-gravity flows caused by slope destabilization and/or hyperpynal discharges and bottom currents (F2b) in bottomset locations. Foresets are represented by slope environments (FA4) documenting hemipelagic sedimentation under hypopycnal or mesopycnal plume and/or low-density flows generated by cascading events or other resuspension events. In younger clinoforms, shelf aggradation generated higher foreset slopes and FA4 is constituted by extensive fluid mud deposits generated by wave or current resuspension in the upper foreset and topset (F4d). Basin-wide, oxygenated events in the Neuquén Basin suggest a switch in circulation from estuarine to anti-estuarine or weakened estuarine circulation, associated with low-sea levels and arid and cooler climates. During these times, deposition in dysoxic to oxic basin (F2c, F2d) and sediment drift (FA3) environments was represented by pelagic and hemipelagic conditions and wind- and thermohaline-driven, contour current transport with rare sediment-gravity flows, at the bottomset to lower foreset locations. In the lower foreset of younger clinoforms, mixed drift and fluid mud deposits occurred (F3c). Data is fragmentary at the interval of FA5, but the succession shows outer

ramp environments affected by hemipelagic sedimentation and high-energy bottom currents. In the study area, the Vaca Muerta Formation comprises four third-order sequences. Each third-order sequence represents the progradation of a mixed clinoform system during HST, FSST and LST, whereas siliciclastics dominated during TST. The integrated sedimentological and ichnological analysis provides several insights to understand ancient fine-grained depositional environments: (1) bottom current can be differentiated from sediment-gravity flow deposits by their low sediment concentration and long-term duration, (2) trace-fossil analysis indicates the role of firm, soft and soupy substrates, oxygen-deficient conditions, and high food input in controlling the infauna of basin and slope environments, (3) wind- and thermohaline-driven, contour currents represent the best explanation for the basin-wide increase in oxygenation recorded from bottomset to foreset locations in the sediment drifts, (4) climate and associated basin circulation constitute a critical control on sediment partitioning, with warmer climates triggering equator-ward migration of the belt, humid conditions, high freshwater discharges and estuarine circulation causing in turn basin anoxia, and cooler climates generating pole-ward migration of the belt, arid conditions and anti-estuarine circulation prone to oxygenating deep waters by dense water cascading from the shelf, and (5) an evaluation of sedimentary processes and environmental controls indicates that organic matter was produced in the water column, preserved due to extensive anoxia and dysoxia (extending up to the middle foreset), and concentrated by low sediment dilution.

4.10 Acknowledgments

We thank Chevron, Shell, Tiser S.R.L., Total Austral S.A. and YPF for sharing core information with us. In addition, Germán Canto, Adrián Dolso, Sebastián J. Estrada, Sebastián Galeazzi, and Fabián Lamarque from Total Austral S.A. for sharing core information with us. This work was financially supported by the Natural Sciences and Engineering Research Council (NSERC) Discovery Grant [422931-20] to L.A. Buatois, and [311727–20] to M.G. Mángano, PI-UNRN 2017 [40-A-616], PIP-CONICET [11220170100129CO] to N.B. Carmona, PUE 0031CO to J.J. Ponce, and 2016 Student Research Grant from Society for Sedimentary Geology (SEPM), 2016 and 2018 Research Grant from the Geological Society of America (GSA), 2016 Grants-in-Aid Program of the American Association of Petroleum Geologists (AAPG), and 2018

Postgraduate Grant from the International Association of Sedimentologists (IAS) to Paz. M.G.M. thanks additional funding by the George J. McLeod Enhancement Chair in Geology.

TRANSITION

Chapter 4 deals with the sedimentological and sequence stratigraphic datasets of the Vaca Muerta Formation in the basin centre area, whereas Chapter 5 focuses on the ichnological content of that area. This study stresses the importance of oxygen and substrate consistency as the main controls for trace fossil distribution in fine-grained deposits. The studied ichnofauna differs from the typical oxygen-stressed ichnofauna showing abundant *Chondrites* or *Zoophycos*, probably due to abundant food resources.

CHAPTER 5: ICHNOLOGY OF AN ORGANIC-RICH, FINE-GRAINED DEPOSITIONAL SYSTEM: THE UPPER JURASSIC-LOWER CRETACEOUS VACA MUERTA FORMATION, ARGENTINA

Abstract

Over the past years, the interest in organic-rich, fine-grained depositional systems has been growing due to the increasing demand of unconventional shale reservoirs. However, ichnologic analysis in these systems is hindered by the scarcity of discrete trace fossils, small burrow sizes, and difficulty in obtaining fresh rock samples. The mixed carbonate-siliciclastic, subaqueous clinoform system of the Upper Jurassic-Lower Cretaceous, Vaca Muerta Formation is the most important unconventional reservoir in South America and an interesting example of a fine-grained depositional environment showing different trace fossils. An ichnologic analysis was carried on cores from nine wells and one outcrop to understand palaeoenvironmental controls on trace-fossil distribution. The Vaca Muerta Formation shows biodeformational structures, discrete trace fossils and biodepositional structures. Biodeformational structures are abundant in the mudstone lithologies, generating parallel-laminated, irregular-laminated, and massive fabrics. Discrete trace fossils and biodepositional structures are mainly observed in tuff intervals, and consist of (in order of abundance), *Teichichnus rectus*, *Alcyonidiopsis longobardiae*, *Coprulus oblongus*, *Phycosiphon incertum*, *Planolites* isp., *Teichichnus zigzag*, *Thalassinoides* isp., *Palaeophycus* isp., ?*Lockeia* isp., *Lockeia siliquaria*, *Nereites* isp., *Palaeophycus heberti*, *Crininicaminus* isp., *Zoophycos* isp., *Teichichnus patens*, *Diplocraterion* isp., and ?*Skolithos* isp. Pellet trails, mantle and swirl structures, and escape and equilibrium structures are also abundant. The analysis of tuffs reveals four distinct oxygen-related ichnocoenoses that illustrate the transition from anoxic to oxic conditions. Increased bioturbation index, penetration depth, burrow size, and ichnodiversity paralleled an increase in oxygenation. Biodeformational structures in mudstone are associated with soupy to very soft substrates, whereas a change to soft and stiffgrounds during ash deposition enhanced preservation of discrete traces. Other ichnocoenoses were described, illustrating the role of different paleoecological stress factors (substrate consistency, oxygen, and food) and sedimentary processes (hemipelagic, fluid mud, and contour current sedimentation) in controlling trace-fossil distribution. The Vaca Muerta ichnofauna differs from typical, oxygen-deficient

ichnofaunas in the virtual absence of *Chondrites*, the rarity of *Zoophycos*, and the presence of pellet-rich ichnocoenoses. These characteristics can be attributed to bioturbation in a food-rich environment, which precluded specialized feeding and the development of tiered communities. The analysis stresses the importance of rock fabric and bed disruption when evaluating ancient benthic oxygen levels.

5.1 Introduction

Fine-grained depositional systems make up most of the sedimentary record, and comprise a large volume of sediments in the world (Potter *et al.*, 1980). In recent years, an increasing interest in the development of unconventional reservoirs generated new data on fine-grained systems associated with organic carbon accumulations. Particularly, documentation of mud transport processes in shelves (Ogston *et al.*, 2000; Traykovski *et al.*, 2000) and the production of ripples composed by mud floccules in flume experiments (Schieber *et al.*, 2007) triggered new ideas and extensive research on sedimentology of fine-grained deposits.

However, the ichnologic data of fine-grained systems is not well understood, because many muddy substrates are soupy to soft with high water content, precluding preservation of discrete trace fossils after compaction (Wetzel and Uchman, 1998; Schieber, 2003). Consequently, the fossil record of these deposits is dominated by biodeformational structures or indistinct traces that cannot be classified ichnotaxonomically (e.g. pyrite burrows, mantle and swirl structures; Schieber, 2003). Another problem concerning organic-rich fine-grained deposits is their extensive palaeoxygenation stress, resulting in low bioturbation intensities and small-sized burrows (e.g. Savrda and Bottjer, 1989a; Wignall, 1991; Schieber, 2003; Mángano, 2011). Hence, cryptobioturbation occurs, and the definition of burrows is hindered by the difficulty of observing bed disruption in thin sections or homogeneous sedimentary successions (see discussion by Egenhoff and Fishman, 2013; Schieber, 2014; Schieber *et al.*, in press). Moreover, trace-fossil analysis in fine-grained systems is problematic due to the strong weathering of mudstone successions and the difficulty of acquiring fresh samples.

All of these problems are also characteristic of the fine-grained, Upper Jurassic-Lower Cretaceous Vaca Muerta Formation of Argentina, arguably the most important unconventional shale reservoir in South America (González *et al.*, 2018; Minisini *et al.*, 2020c). In this context,

the present analysis addresses many of these issues through a combined sedimentologic and ichnologic analysis of fresh, cross-section surfaces of muddy deposits provided by cores. The objectives of this study are to analyze the ichnologic dataset of cores from nine wells and the Yesera del Tromen outcrop, combine this information with a sedimentary facies framework, and evaluate the different paleoenvironmental controls on trace-fossil distribution.

5.2 Geologic Setting

The Vaca Muerta Formation occurs in the Neuquén Basin, western Argentina, a triangular-shaped basin encompassing approximately 7000 m of Jurassic and Cretaceous strata (Fig. 5.1A, B; Arregui *et al.*, 2011; Casadío and Montagna, 2015). The basin fill history can be subdivided into a syn-rift, back-arc, and foreland phase (Howell *et al.*, 2005). Syn-rift deposition began during the Late Triassic to Early Jurassic and comprise the Precuyano Cycle. The establishment of the Andean arc to the west started the back-arc phase during the Early Jurassic, generating alternation of continental and marine deposition caused by relative sea-level variations (Cuyo, Lotena, Mendoza and Bajada del Agrio groups; Arregui *et al.*, 2011). During the Late Cretaceous, a compressional regime produced the closure of the Pacific Ocean connection and a shift towards the foreland phase (Tunik *et al.*, 2010). Finally, a Late Cretaceous to early Paleogene Atlantic ocean transgression is recorded in the Malargüe Group (Arregui *et al.*, 2011).

The Vaca Muerta Formation is part of the Lower Mendoza Group, and represents shallow-marine, mixed carbonate-siliciclastic deposition from the early Tithonian to the early Valanginian (Fig. 5.2; Leanza *et al.*, 2011). Below, this formation has a sharp contact with the continental Tordillo Formation, whereas at the top it transitions gradually towards nearshore deposits of the Quintuco Formation. The Vaca Muerta Formation comprises mudstone, marl, limestone, and tuff with high organic carbon content, comprising a mixed carbonate-siliciclastic clinoform system (Spalletti *et al.*, 1999; Kietzmann *et al.*, 2014a). Sedimentologic and sequence stratigraphic analyses are vast due to its importance for the hydrocarbon industry and indicate that the Vaca Muerta Formation occurs at bottomset and foreset positions of a clinoform system (Mitchum and Uliana, 1985; Legarreta and Gulisano, 1989; Desjardins *et al.*, 2018; Domínguez *et al.*, 2020a).

The study area is of great interest for oil and gas companies, and many sedimentologic and sequence stratigraphic analyses have been performed in the analyzed cores (Fig. 5.1C; Fantín and

González, 2014; González Tomassini *et al.*, 2014; Pose *et al.*, 2014; Repol *et al.*, 2014; Notta *et al.*, 2017; Barredo *et al.*, 2018; Desjardins and Aguirre, 2018; Gómez Rivarola and Borgnia, 2018; Vallejo *et al.*, 2018; Minisini *et al.*, 2020a). In addition, the outcrop area is close to the core location and represents a well-studied succession from a sedimentologic perspective (Mitchum and Uliana, 1985; Spalletti *et al.*, 1999; Krim, 2015; Ponce *et al.*, 2015; Kietzmann *et al.*, 2016, 2018b; Rodriguez Blanco *et al.*, 2020), coupled with biostratigraphic and paleontologic studies (Leanza and Hugo, 1977; Leanza *et al.*, 1977; Leanza, 1993; Aguirre-Urreta *et al.*, 2014). Considering trace fossils, a single extensive ichnologic analysis was carried on the southern Mendoza Province (Doyle *et al.* 2015), yet from the study area some trace fossils were mentioned and figured (Kietzmann *et al.*, 2016; Ponce *et al.*, 2015; Desjardins and Aguirre, 2018; Kietzmann and Bressan, 2019; Leanza *et al.*, 2020b). Other studies have mentioned and analyzed trace fossils from the uppermost intervals, including the Quintuco and Picún Leufú Formations (Mángano and Buatois, 1991; Parada, 2019; Paz *et al.*, 2019).

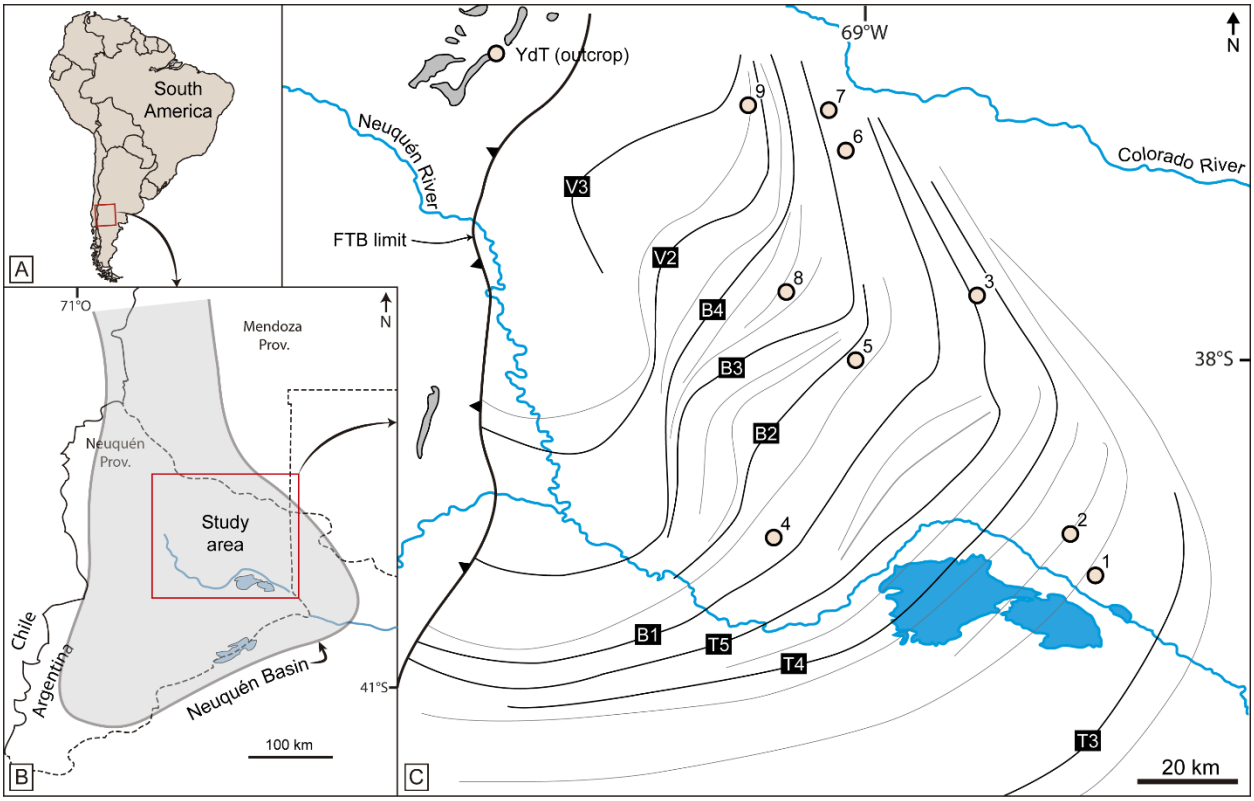

Fig. 5.1: Location maps. A, B) Location of the Neuquén Basin within Argentina. C) Study area showing the location of core sections (1-9) and the Yesera del Tromen section (YdT). Clinoform breaks from the different stratigraphic surfaces of the Vaca Muerta Formation were delineated (T2-T4, B1-B4, V2, V3;

from Domínguez *et al.*, 2020a). Grey areas are outcrops of the Vaca Muerta Formation, which are bounded at the east by the fold and thrust belt limit (FTB).

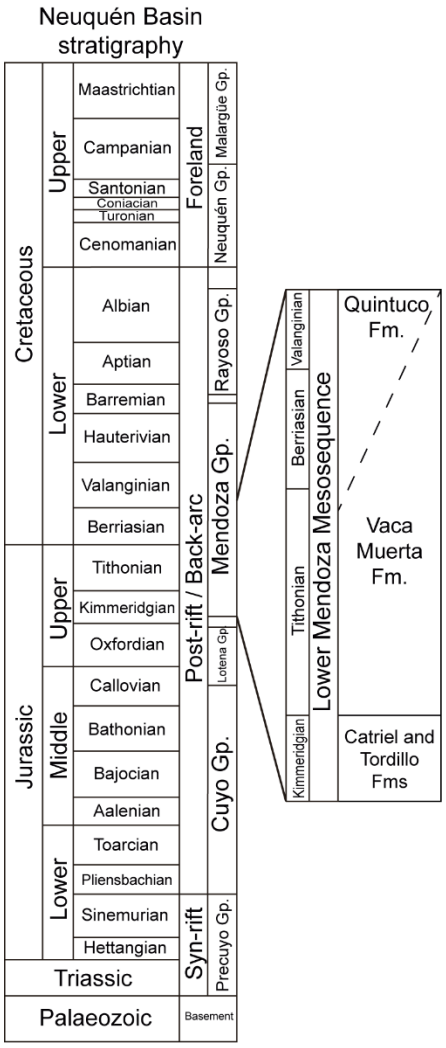

Fig. 5.2: Regional stratigraphy of the Neuquén Basin, displaying a detail of the stratigraphy in the study area.

5.3 Methodology

Cores (1031.5 m total) from nine wells and one outcrop (148 m, Yesera del Tromen) located in the Neuquén Basin Embayment were analyzed (Fig. 5.1C, 5.3). This outcrop section shows a fault at ~115 m that repeats the *W. internispinosum* ammonite zone (Aguirre-Urreta *et al.*, 2014). The sedimentologic analysis consisted of lithofacies characterization and interpretation in

terms of sedimentary processes (Paz *et al.*, in review c). Lithofacies information was integrated with trace-fossil data in order to define facies. Facies were grouped into facies associations corresponding to broad environments of deposition. Core visualization were improved using ethanol coating on the rocks and applying enhancement techniques to the photographs. Lithologies are characterized following Wright (1992) and Lazar *et al.* (2015b). Mudstone composition was described from thin section (N=59) and XRD analysis provided by companies owning the cores (YPF, Chevron, Total Austral, and Shell), and thin sections from outcrop samples (N=18). Three samples coated in 200Å of carbon were subject to backscattered electron (BSE) analysis. BSE images were obtained on a JEOL 8600 Superprobe electron microprobe analyzer using a Gellar Microanalytical dPict image adquisition system at the University of Saskatchewan Electron Microprobe Laboratory. Qualitative spot analyses were performed using energy dispersive spectrometry (EDS). The BSE and EDS data helped characterize mudstone and pellets composition.

The ichnologic study comprised the visual analysis of bioturbated intervals. In the case of discrete structures, a detailed description and identification of ichnotaxa was attempted. Additional metrics, such as ichnodiversity, bioturbation index, penetration depth, and reconstruction of tiering, and trace-fossil ethologies, were assessed. Bioturbation index (BI) was measured following the proposal of Taylor and Goldring (1993) after Reineck (1967). The index measures burrow overlap and loss of primary sedimentary structures due to the activity of infaunal macroburrowers. Penetration depth (PD) was only possible to be determined on intervals hosting tuff layers. In these cases, the distance between the top of the tuff layer (colonization surface) and the base of the deepest trace fossil can be roughly measured due to the strong sediment contrast exhibited between mudstone (black) and tuff (white) intercalations. Most of the trace fossils occur in shallow- to very-shallow tier, representing the activity of epifaunal to shallow infaunal organisms.

Environmental controls on the ichnofauna were inferred from trace-fossil analysis and sedimentary facies datasets. The bottom water oxygen content is described following Tyson and Pearson (1991) using the terms oxic (8-2 ml/l O_2), dysoxic (2-0.2 ml/l O_2), suboxic (0.2-0 ml/l O_2) and anoxic (0.0 ml/L, absence of any detectable O_2; Tyson and Pearson, 1991). However, palaeoxygen levels were likely fluctuating (Díaz and Rosenberg, 1995) and adaptations to cope with low oxygen environments might have evolved through time (Buatois and Mángano, 2011;

Mángano, 2011). Hence, oxygen levels provided above should be taken as approximations to mean values.

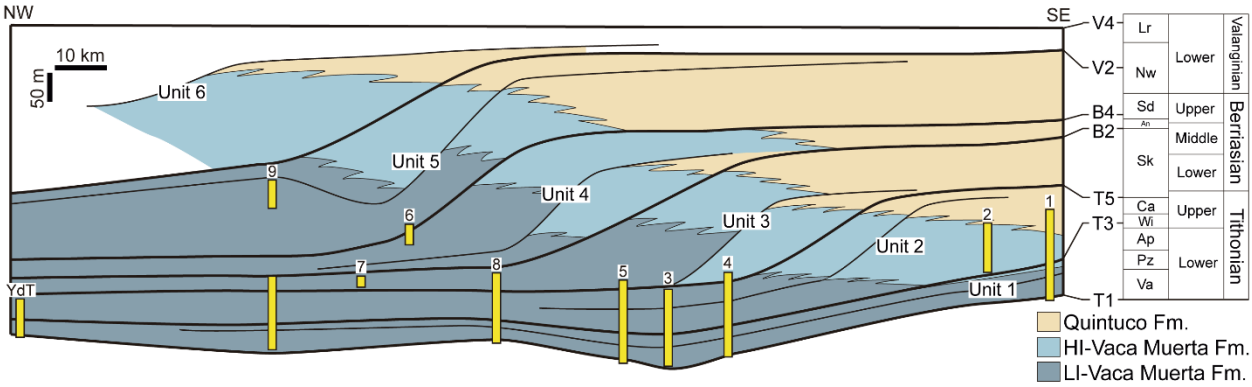

Fig. 5.3: NW-SE simplified cross-section of the Quintuco-Vaca Muerta system, showing the projected locations of the cores and outcrop analyzed (modified from Sattler *et al.*, 2018 and Reijenstein *et al.*, 2017b). The Vaca Muerta Formation is divided in a high acoustic impedance succession (HI, correlated with carbonate-rich rocks) and a low acoustic impedance succession (LI, correlated with organic-rich rocks). Units, stratigraphic surfaces and ages are from Desjardins *et al.* (2018), and Minisini *et al.* (2020b), and Andean ammonite zones (right) from Kietzmann *et al.* (2018a). Vm: *Virgatosphinctes andesensis*, Pz: *Pseudolissoceras zittelli*, Ap: *Aulacosphinctes proximus*, Wi: *Windhauseniceras internispinosum*, Ca: *Corongoceras alternans*, Sk: *Substeueroceras koeneni*, An: *Argentiniceras noduliferum*, Sd: *Spiticeras damesi*, Nw: *Neocomites wichmanni*, Lr: *Lissonia riveroi*).

5.3.1 Tuffs as taphonomic windows for the study of trace fossils in fine-grained deposits

Tuff intervals are exceptional beds to analyze trace fossils, because they represent new sediment available for bioturbation with a strong lithologic contrast. In addition, compaction is relatively inhibited by early diagenetic cements, which is crucial for trace-fossil visualization in fine-grained sediments. Most structures in ancient fine-grained successions, both biogenic and physical, suffered a significant thickness compaction. In particular, compaction in the Vaca Muerta Formation dramatically reduced the preservation potential of burrows (muds can be compacted up to 70%; see also Otharán *et al.*, 2020). The uppermost part of tuffs consists of an area of high biogenic mixing recording the activity of epifaunal and very shallow infaunal animals colonizing the new surface. This heterogenous, mottled bioturbated interval is interpreted as a mixed layer. Below, a transitional layer preserves most of the discrete trace fossils. Subsequent bioturbation related to sediment accretion will result on discrete trace fossils crosscutting the mixed layer due

to upward migration of the infaunal community, and they will become part of the historical layer. Depending on sedimentation rate (i.e. rate of ash fall), visible intervals with discrete trace fossils can occur below, within, or above the tuff.

In the Vaca Muerta Formation, tuffs and lapilli-ash tuffs are abundant in marginal-marine and basin facies associations (FA1 and FA2, see below). Bioturbation index, penetration depth, and burrow size in interbedded tuffs is typically consistent with the bioturbation index observed in the enclosing mudstone (Fig. 5.4, 5.5). In turn, bioturbation index generates different types of rock fabrics in the mudstone. We define three types of mudstone fabric: (1) parallel-laminated (BI 0), containing horizontal, parallel to irregular fractures and horizontal, undisturbed bed contacts (Fig. 5.4A), (2) irregular-laminated (BI 1-3), consisting of mudstone exhibiting horizontal to subhorizontal, irregular, parallel fractures and slightly disturbed bed contacts (Fig. 5.4B, 5.5A), and (3) massive mudstone (BI 4-6), showing a lack of any primary fabric and recognized by horizontal to oblique, irregular, planar to wavy fractures and bioturbated bed contacts (Fig. 5.5B). Similarities between bioturbation in the tuff and in the enclosing mudstone implies that oxygen levels and the benthos responsible for bioturbation were comparable in both the ash layer and the interbedded muds. Studies in modern environments also support the assumption of uniform oxygen levels after tuff deposition, with a decrease in oxygen pore waters only restricted to the pre-tuff deposits (Wetzel, 2009). In short, because the ichnotaxa identified in the tuffs are genetically related to organisms that are components of the mud community reworking the interbedded encasing mudstone, analysis of tuffs helps to track oxygen levels in the hosting mudstone where bioturbation is far harder to visualize. Therefore, trace fossils in tuff intervals, BI and mudstone fabric defined Oxygen-Related Ichnocoenoses (ORI; Savrda and Bottjer, 1986) that were used to delineate bottom water paleoxygen levels in the Vaca Muerta Formation.

In addition to trace fossils associated with dysoxic and oxic conditions, tuffs were critical to delineate unbioturbated successions depicting anoxic conditions, which are the most abundant at the Vaca Muerta Formation. In this sense, the occurrence of undisturbed, discrete mm-thick tuff and parallel-laminated hemipelagic deposits on top of tuff (Fig. 5.4A, 5.6) signal the absence of bioturbation. In environments with abundance of food, such as in the Vaca Muerta Formation, bioturbation mixing may completely rework tuff intervals (Wetzel, 2009). For example, very thin tuff intervals in well-oxygenated, bioturbated deep marine slope and abyssal plain deposits are only preserved where thickness exceed 0.62 cm (Lewis and Kohn, 1973; Sparks *et al.*, 1983).

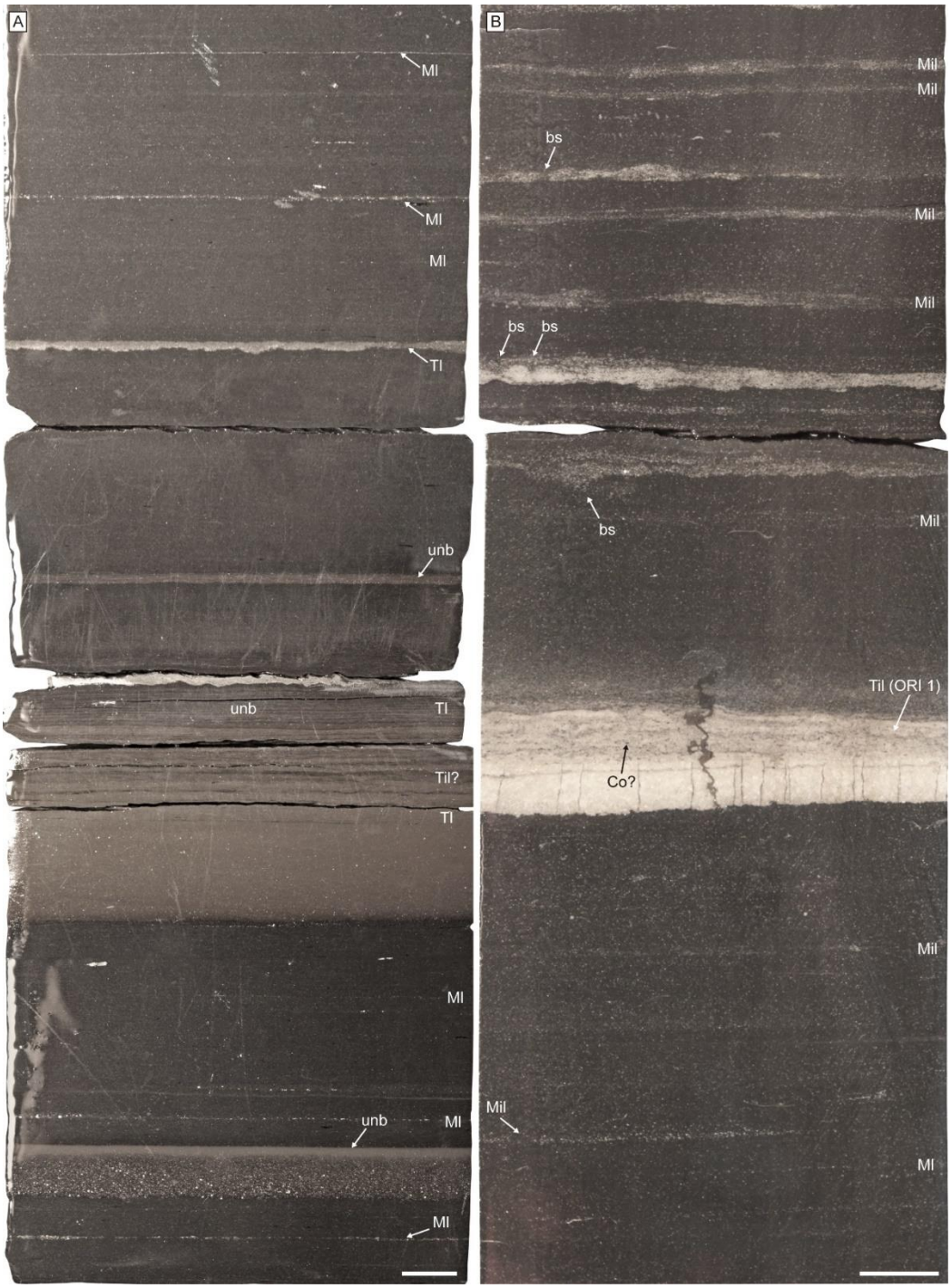

Fig. 5.4: Relationship between mudstone fabric and bioturbation in the tuff. A) Parallel-laminated mudstone (Ml) are associated with undisturbed bed contacts and unbioturbated (unb), parallel-laminated (Tl) to rare irregular-laminated (Til) tuff. B) Irregular-laminated mudstone (Mil) associated with the *Coprulus oblongus* ichnocoenosis (ORI 1, see below), showing small biodeformational structures (bs) and intercalated tuff with irregular lamination on top (Til) and possible *Coprulus oblongus* (Co?). Scale bars are 1 cm.

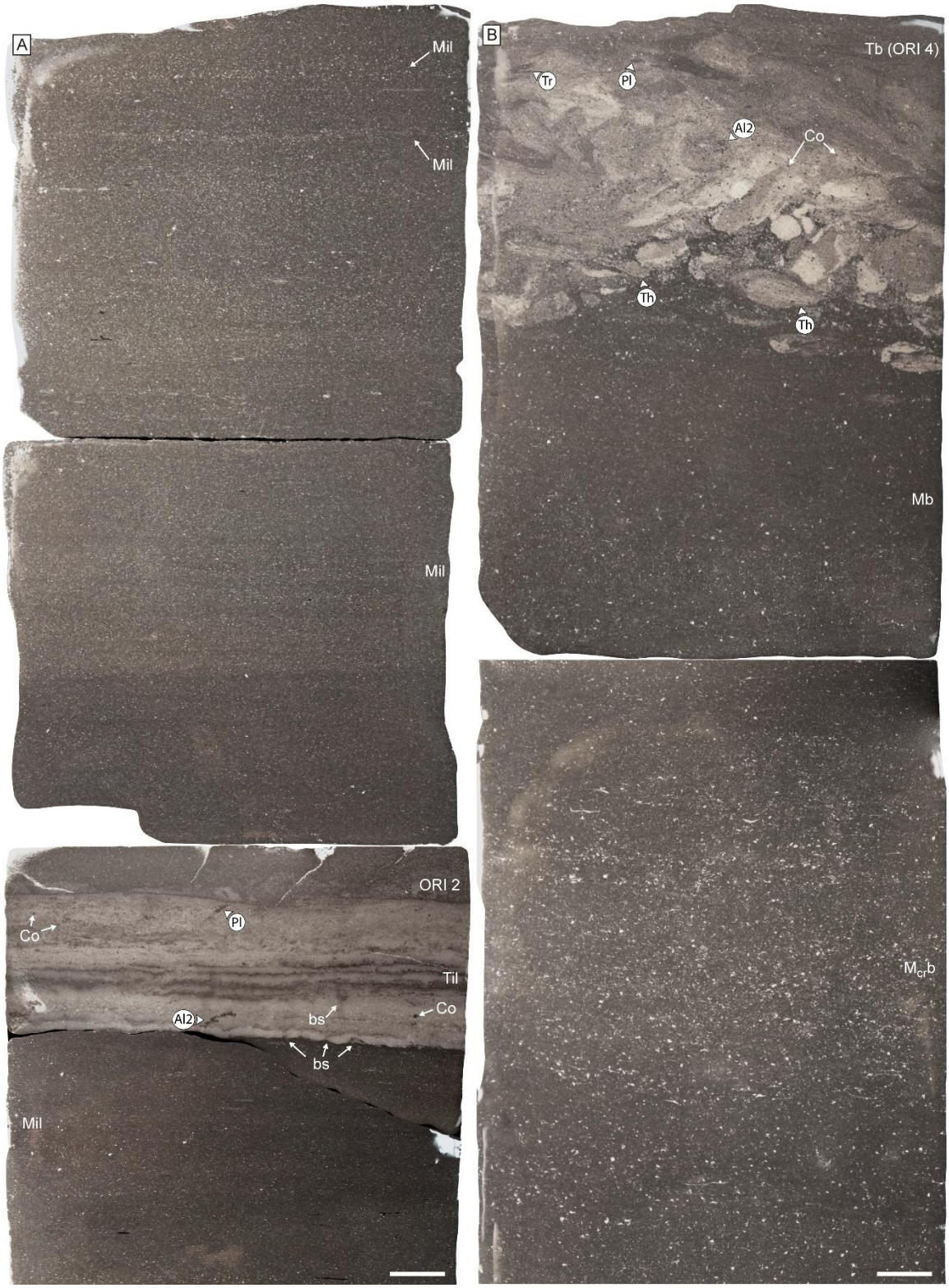

Fig. 5.5: Relationship between mudstone fabric and bioturbation in the tuff. A) Irregular-laminated mudstone (Mil) related to the development of the *Alcyonidiopsis longobardiae* ichnocoenosis (ORI 2, see below) in the tuffs. The tuffs display irregular lamination (Til), associated with *Alcyonidiopsis longobardiae*

type 2 (Al2), *Coprulus oblongus* (Co), and biodeformational structures (bs). B) Massive mudstone and crinoidal mudstone intervals (Mb, M_{cr}b) showing the *Teichichnus rectus-Phycosiphon incertum* ichnocoenosis (ORI 4, see below) in completely bioturbated tuff (Tb). *Alcyonidiopsis longobardiae* type 2 (Al2), *Coprulus oblongus* (Co), *Planolites* isp. (Pl), *Teichichnus rectus* (Tr) and *Thalassinoides* isp. (Th) occur. Scale bars are 1 cm.

Fig. 5.6: Unbioturbated successions of the Vaca Muerta Formation, characterized by parallel-laminated tuff (Tl), preserving tuff-mudstone intercalations towards its top. Scale bars are 1 cm.

5.4 Sedimentary Facies

The study area records a mixed carbonate-siliciclastic, subaqueous clinoform system developed during deposition of Units 1 to 5 of Desjardins *et al.* (2018; Fig. 5.3). The clinoform changes from a low angle slope (0.2-0.3°) during deposition of Unit 1 to higher angles in the following Units (0.5-2.3°, Reijenstein *et al.*, 2014). Fifteen facies were defined and grouped into five facies associations (see Chapter 4). Marginal-marine, basin, drift, and slope facies associations occur in Units 1 to 3 (Fig. 5.7; Paz *et al.*, in review c). An outer ramp facies association was poorly documented in Units 4 and 5 in an area without clinoform development (ramp-like), where less cores are available (Fig. 5.3).

The marginal-marine facies association (FA1, Fig. 5.7A) consists of massive, low-angle to ripple cross-laminated, medium- to coarse-grained sandstone with mudstone drapes, bindstone and calcareous to mixed mudstone. Common parallel lamination, wave ripples, and current-ripple

cross-lamination can be observed in the mudstone. Intercalated are thin- to thick-bedded, composite sandstone, peloidal mudstone, and tuff to lapilli-ash tuff. This facies occurs at the transgressive event of the transition between the eolian deposits observed below (Catriel Formation) and the Vaca Muerta Formation. It is interpreted as tidal flood and storm surge reworking (sandstone) and bay sedimentation (bindstone and mudstone) occurring during the transgressive phase of the base of the Vaca Muerta Formation (Paz *et al.*, 2021).

The basin facies association (FA2) comprises parallel-laminated, carbonaceous (av. TOC of 4.76%, N=182) mixed mudstone, parallel-laminated, bedded to masive, mixed to calcareous mudstone (Fig. 5.7B, C), bioclastic mixed mudstone, bioclastic floatstone to rudstone, parallel-, current-ripple to low-angle, cross-laminated peloidal mudstone, and crinoidal mudstone. Very thin- to thin-bedded, current-ripple cross-laminated, graded to massive, fine to coarse mudstone to coarse-grained sandstone, hummocky cross-stratified, intraclastic to bioclastic wackestone, bindstone, and tuff to lapilli-ash tuff occur. 5-30 cm-thick carbonate concretions are also observed. FA2 suggests low sedimentation rate in a pelagic-dominated basin environment, with rare deposition from sediment-gravity flows, bottom currents, and storms. Areas with a higher amount of carbonate concretions, bindstone, and bioclastic floatstone represent condensation events.

The drift facies association (FA3) consists of massive to cross-bedded, crinoidal mudstone, crinoidal mudstone showing parallel-, low angle and minor wavy crinoid-rich laminae and crinoid-rich lenses, fine mudstone with parallel to low-angle, coarse mudstone laminae, parallel-, low-angle to current-ripple cross-laminated coarse mudstone, and massive, calcareous to mixed mudstone (Fig. 5.7D). Very thin- to thin-bedded intervals showing graded to massive, fine to coarse mudstone, bindstone, and tuff to lapilli-ash tuff are also intercalated. FA3 comprises facies deposited by low-density contour currents, above or at the transition with the oxycline (see Chapter 6, Paz *et al.*, in review a). High ventilation of the seafloor suggests that intensification of the circulation system by cascading of dense, surface waters from the shelf is responsible for the currents (i.e. contourites; Paz *et al.*, in review a).

The slope facies association (FA4) comprises parallel-laminated to -bedded, wavy and massive, mixed to calcareous mudstone (Fig. 5.7E). Intercalated are thin-bedded, massive, calcareous mudstone, fine mudstone with parallel coarse mudstone laminae, and composite beds of fine to coarse mudstone (Fig. 5.7F). Slumps are observed. FA4 represents deposition in an area characterized by fair-weather pelagic sedimentation and high-energy events resuspending mud

from the shelf and transporting it by sediment plumes (hemipelagic) or low-density currents. The thin-bedded, massive calcareous mudstone represents fluid-mud flow deposits.

The outer ramp facies association (FA5) is dominated by massive, calcareous to mixed mudstone, intraclastic wackestone and bioclastic floatstone (Fig. 5.7G). Tuff and lapilli-ash tuff are present, but rare. FA5 represents hemipelagic deposition and bottom current reworking under oxic conditions.

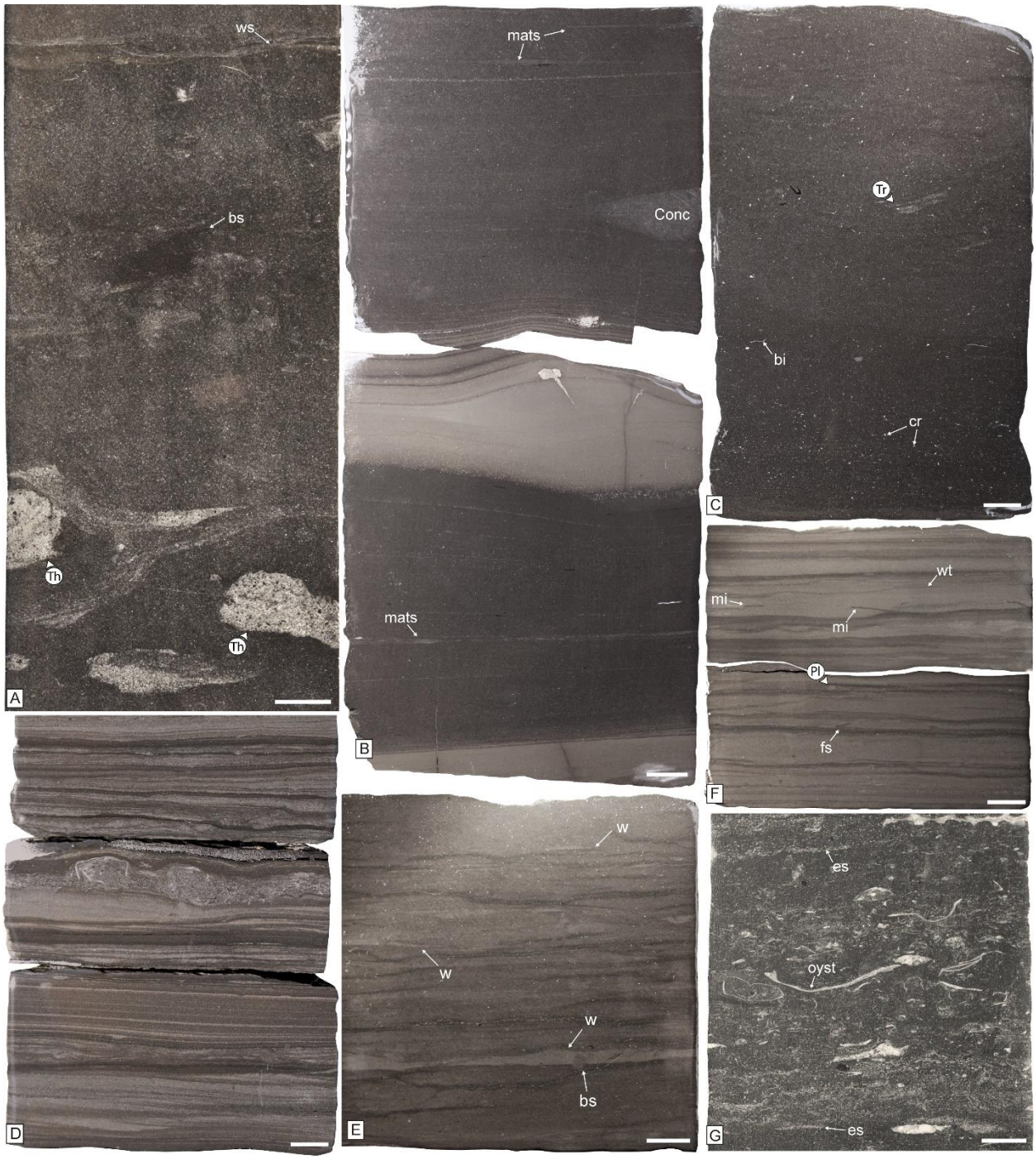

Fig. 5.7: General photographs of the sedimentary facies associations of the Vaca Muerta Formation. A) Marginal-marine facies association (FA1) showing calcareous coarse mudstone with wavy surfaces (ws), highly bioturbated by biodeformational structures (bs) and *Thalassinoides* isp. (Th). B) Basin facies association (FA2) comprising parallel-laminated fine mudstone with concretions (Conc) and mats, and intercalated parallel-laminated tuff. C) Example of basin facies association (FA2) consisting of highly bioturbated calcareous coarse mudstone, with bioclasts (bi) and crinoids (cr) and *Teichichnus rectus* (Tr).

D) Drift facies association (FA3) showing current ripple cross-laminated, coarse mudstone and parallel coarse mudstone laminae. E) Calcareous mudstone with wave ripples (w) and biodeformational structures (bs) of the slope facies association (FA4). F) Thin-bedded massive calcareous medium to coarse mudstone of FA4, locally displaying parallel lamination, flame structures (fs), mudstone intraclasts (mi), wavy tops (wt), and *Planolites* isp. (Pl). G) Bioclastic floatstone of the outer ramp facies association (FA5) showing oysters (oyst) and erosive surfaces (es). Scale bars are 1 cm.

5.5 Ichnology

The ichnologic content of the Vaca Muerta Formation consists of (in order of abundance), *Teichichnus rectus, Alcyonidiopsis longobardiae*, *Coprulus oblongus, Phycosiphon incertum, Planolites* isp., *Teichichnus zigzag, Thalassinoides* isp., *Palaeophycus* isp., ?*Lockeia* isp., *Lockeia siliquaria, Nereites* isp., *Palaeophycus heberti, Crininicaminus* isp., *Zoophycos* isp., *Teichichnus patens, Diplocraterion* isp., and ?*Skolithos* isp. Pellet trails, mantle and swirl structures, and escape and equilibrium structures are also abundant. Of these trace fossils, *Teichichnus rectus, Alcyonidiopsis longobardiae*, *Coprulus oblongus*, *Phycosiphon incertum*, *Planolites* isp., *Teichichnus zigzag,* and *Thalassinoides* isp. are the dominant components of the most abundant facies associations (basin, FA2). *Zoophycos* is present in tuff intervals from cores, but only a few specimens have been observed. *Chondrites* has been documented in the Mendoza shelf (Doyle *et al.*, 2005), but has not been recorded in the study area.

5.5.1 Indistinct and discrete bioturbation structures

Although traditionally considered an essentially unbioturbated unit, close examination of the Vaca Muerta Formation indicate variable bioturbation intensities. The most typical bioturbation is recorded by biodeformational structures (i.e. non discrete traces dominantly representing transient structures resulting in heterogenenous biogenic mixing). This style of bioturbation, commonly called “mottling” occurs in parallel-laminated, irregular-laminated and massive mudstone (Fig. 5.4, 5.5).

Discrete ichnotaxa in the Vaca Muerta Formation are typically restricted to tuff and lapilli-ash tuff, at lithologic interfaces, carbonate-rich intervals, contourite facies (FA3), or some thin-bedded, coarse mudstone to coarse-grained sandstone deposits.

Alcyonidiopsis longobardiae Massalongo, 1856 represents actively pellet-infilled, straight to slightly curved, seldom branching, unlined burrows. Three different forms can be differentiated. Type 1 comprises 1.3-2.3 mm wide and up to 20 mm long, horizontal, straight burrows (Fig. 5.8A). They contain closely packed *Coprulus oblongus* type B (see below), locally ordered in groups of four, aligned perpendicular to the burrow axis. Type 2 consists of 1-1.2 mm wide and 3-15 mm long, oblique to vertical burrows (Fig. 5.8B). They are filled with loosely packed *Coprulus oblongus* type B in places occurring in pairs. Locally, they are associated laterally or toward their tops with funnel-shaped biodeformational structures with a 5-mm diameter upper aperture. The biodeformational structures can be filled with type B pellets or material from above. Type 3 comprises 0.5-1 mm wide and 5-7 mm long oblique to vertical burrows (Fig. 5.8C). They contain loosely to closely packed *Coprulus oblongus* type A (see below). Locally, branching in type 2 and 3 burrows form Y-shaped structures. Preserved as full relief within tuff deposits or rarely in associated mudstone. *Alcyonidiopsis longobardiae* has been identified in both outcrop and core. *Syncoprulus* and *Halymenites* are its junior synonyms (Uchman 1995). *Tubotomaculum*, another similar actively pellet-infilled burrow, differs in its spindle-shaped morphology and sharp walls with scratch imprints suggestive of an open burrow (García-Ramos *et al.*, 2014). *Compaginatichnus* differs from *Alcyonidiopsis* due to the presence of menisci (Pickerill, 1989). *Phymatoderma* shows tree-like subhorizontal branching (Fu, 1991; Izumi, 2012). Disctinction between *Alcyonidiopsis* and *Tomaculum* has been debated. Some authors indicated that *Alcyonidiopsis* should be restricted to simple pellet-filled burrows and that *Tomaculum* should be used for isolated strands or clusters of pellets (Pickerill, 1989) or for surface fecal strings (Eiserhardt *et al.*, 2001). However, there is a growing consensus in considering *Alcyonidiopsis* as the senior synonym of *Tomaculum* (Chamberlain, 1977; Uchman, 1995; Buatois *et al*., 2017; Mángano *et al.*, 2019). In particular, *Alcyonidiopsis longobardiae* Massalongo, 1856, consists of simple, seldom branching, oblique to horizontal tubular burrows stuffed with fecal pellets (Chamberlain, 1977; Uchman, 1995). *Alcyonidiopsis pharmaceus* Richter and Richter, 1939 and *A. bavaricus* Uchman, 1999 are distinguished from *A. longobardiae* by their burrow and pellet size. However, size alone is not considered an appropiate ichnotaxobase (Bertling *et al.*, 2006). *Alcyonidiopsis* occurs in a wide variety of marine environments, and has been recorded in other oxygen-deficient successions similar to the described example (e.g. Mángano, 2011; Uchman *et al.*, 2013; Mángano *et al.*, 2019). It is interpreted as a feeding trace made by polychaetes

(Chamberlain, 1977; Gaillard *et al.*, 1994). Thin, pellet-filled, horizontal burrow networks made by the polychaete *Nereis diversicolor* in the Kundalika Estuary, India, were considered as modern analogues for *Alcyonidiopsis* (Kulkarni and Panchang, 2015). Considering its ethology, a cache model following the storage of bacterially enriched pellets to use during times of food shortage as in *Tubotomaculum* or *Tubulichnium* (García-Ramos *et al.*, 2014; Uchman and Wetzel, 2017) might be unlikely due to (1) the loose packing of pellets in burrows, suggesting burrows were not used for pellet storage, (2) the simple burrow morphology with typical short segments, precluding interpretation of a specialized farming technique, and (3) the abundance of organic matter in the Vaca Muerta Formation. The fact that fresh ash deposits constitute a relatively food-starved substrate (Wetzel, 2009) suggests epifaunal detritus feeders to shallow infaunal deposit feeders, using the tuff for waste disposal.

Crininicaminus isp. represents horizontal, passively infilled burrows showing 0.3-1 mm-thick bioclastic lining made up of crinoids (Fig. 5.8D). The burrow morphology can be discrete or irregular, with variations in lining thickness or areas with missing lining. Burrow cross-sections are oval-shaped, 5-6 mm wide, and 1-3 mm high. Preserved as full relief in crinoidal mudstone deposits (crinoids assigned to the genus *Saccocoma*; Kietzmann and Palma, 2009a). The specimens were only observed in cross-section views as transversal sections of the tube. *Crininicaminus* isp. has been identified only in core. Diameters of the burrow precludes its interpretation as a foraminifera tube, indicating they represent armored burrows instead. Lining constitutes the main ichnotaxobase for defining armored burrows at an ichnogeneric level (Belaústegui and Belaústegui, 2017; Mendoza-Rodriguez *et al*., 2020). Crinoid-rich linings in burrows were described as *Crininicaminus haneyensis* from the Upper Mississippian of Kentucky, USA (Ettensohn, 1981). In addition, Seike *et al.* (2014) erected *C. giberti* for crinoid-rich lining with a different arrangement of stem plates (vertical to the tube axis). The ossicle arrangement of the present example cannot be examined, and therefore the ichnospecies cannot be determined. The existence of only transversal section views and the fact that many tubes are irregularly preserved may indicate these specimens represent reworked, disaggregated tubes that laid flat on the sediment surface (e.g. Katto, 1976). These agglutinated worm tubes are commonly attributed to polychaete tube building (Ettensohn, 1981; Zatoń and Bond, 2016), recording both deposit- or suspension-feeding strategies (e.g. Finger *et al.*, 2008; Noffke *et al.*, 2009).

Diplocraterion isp. consists of a vertical, U-shaped, passively infilled burrow displaying protrusive and retrusive spreite (Fig. 5.8E). Locally, it contains a muddy, dark passive infill. The tube is 1-1.6 mm wide and 25-26 mm long, with a width between apertures of 8-10 mm. This trace fossil was observed in outcrop and cores, being preserved as full relief in two different tuff beds. In one of the occurrences, *Diplocraterion* is present in profuse densities. The small width size between apertures might be suggestive of *Diplocraterion habichi* (Fürsich, 1974), but affinities with *D. parallelum* are noted as well. However, more specimens may be needed to confirm ichnospecific assignment. *Diplocraterion* is interpreted as made by suspension-feeding organisms, typically associated with high-energy environments (Fürsich, 1974).

Lockeia siliquaria James, 1879 represents oval to almond-shaped structures in plan view (Fig. 5.8F), typically displaying displaying bowl-shaped or locally apparent cylindrical morphology in cross-section views (Fig. 5.8G). In bedding plane view, the oval structure shows one tapering and one rounded end, or locally both ends tapering. The burrows are 2-5 mm wide and 5-7 mm long. They are interfacial, preserved as negative epirelief or positive hyporelief passively infilled by the overlying sediment. *Lockeia siliquaria* has been identified only in core. *Lockeia siliquaria* James, 1879, *Lockeia ornata* Bandel, 1967 and *Lockeia cunctator* Schlirf *et al.*, 2001 are the current valid ichnospecies (Mángano *et al.*, 2002). *Lockeia gigantus* Kim and Kim, 2008 was differentiated by its size, which is not a proper ichnotaxobase (Bertling *et al.*, 2006). *Lockeia siliquaria* is distinguished from *L. ornata* due to the absence of ornamented surface (Mángano *et al.*, 2002). *Lockeia cunctator* can be differentiated by the arrangement of individual specimens of *Lockeia* into rows (Schlirf *et al.*, 2001). *Lockeia* is interpreted as resting traces (Seilacher and Seilacher, 1994) or semi-permanent domiciles (Mángano *et al.*, 2002) of bivalves, yet conchostracans and ostracodes are also potential producers (Bromley and Asgaard, 1979; Pollard and Hardy, 1991). Equilibrium structures suggesting stable positions with dominant vertical displacement indicate a suspension-feeding strategy (Mángano *et al.*, 1998).

In the same intervals where *Lockeia siliquaria* is observed, vertical to minor oblique, cylindrical and conical, passively infilled, structures with rounded bases occur (Fig. 5.8H, I). These structures are morphologic irregular variations of bivalve structures, and are here referred to as ?*Lockeia* isp. Burrow boundaries are smooth and sharp, although a serrated morphology can be recognized in some specimens towards the base of the burrows. The burrows are 1.3-9.5 mm wide and 0.5-6.1 mm high. They occur on bed bases and rarely on top of beds, showing passive fill from

the overlying bed, or from sediment that has been eroded away. They have only been observed in cores.?*Lockeia* isp. is observed as isolated specimens, in pairs or in groups of four to six specimens. In addition, they regularly display equilibrium behavior (Fig. 5.9A). Similarly, conical vertical burrows associated with *Lockeia* in the Lower Jurassic freshwater deposits from Poland were interpreted as bivalve dwelling structures (Pieńkowski and Niedźwiedzki, 2010).

Nereites isp. comprises horizontal burrows with an actively filled, muddy dark core and a white to gray mantle (Fig. 5.8J). Cross-sections are oval to elongated oval, with sharp to irregular burrow walls. The burrow cross-section is 2.5-15 mm wide and 1-4 mm high, with a core 1-11 mm wide and 0.5-2 mm high. *Nereites* isp. is preserved as full relief in tuffs and fine to coarse mudstone, and has been identified only in core. *Nereites* occurs in sparsely bioturbated, discrete beds with a few specimens, or in highly bioturbated, completely homogenized intervals. Restriction to core prevents to assess morphologic variability, and these trace fossils are classified only at ichnogenus level. *Nereites* represents a grazing trace of a worm-like organism (Mángano *et al.*, 2000; Fernández *et al.*, 2018), and indicates deposit or detritus feeding strategies (Wetzel, 2010).

Palaeophycus heberti de Saporta, 1872 is represented by horizontal to oblique, passively infilled burrows showing a 1 mm-thick white, muddy lining (Fig. 5.8K). Locally, pyrite cements the burrow lining. Burrow cross-sections are 4-8 mm wide and 1.5-3 high, with typical oval cross-sections and common burrow collapse. The specimens were only observed in core in cross-section view as transversal sections of the burrow, showing full relief preservation in fine to coarse mudstone deposits. The thick lining allows assignment to *P. heberti* (Pemberton and Frey, 1982). Morphology is similar to that of *Crininicaminus* isp., but the latter is distinguished by the presence of a wall made of crinoidal fragments. Some of the specimens studied occur in groups of two to three, resembling *Schaubcylindrichnus coronus*, but the common occurrence of single specimens with predominant horizontal orientation precludes assignment to the latter. Vermiform organisms, such as nereid (Dashtgard and Gingras, 2012) and terebellid (Bromley, 1996) polychaetes, have been shown to generate similar burrows with thick lining in modern environments. The structure corresponds to a dwelling burrow of a predaceous or suspension-feeding organism (Pemberton and Frey, 1982).

Palaeophycus isp. consists of horizontal, curved to straight, passively infilled, white core burrows with thin, dark mud lining (Fig. 5.8L). Burrows are 1-2.5 mm in diameter showing circular

to minor oval cross-sections. This ichnotaxon is preserved as full relief in tuffs and fine to coarse mudstone, and has only been observed in core. Locally, highly bioturbated beds display a subhorizontal to oblique, bead-shaped or anastomosed, irregular lamination, which resembles high-density populations of horizontal *Palaeophycus*. Core preservation does not allow to observe details of the lining and, accordingly, assignment at ichnospecies level is not possible. *Paleophycus* represents a dwelling structure produced by predator or suspension feeding vermiform organisms (Pemberton and Frey, 1982).

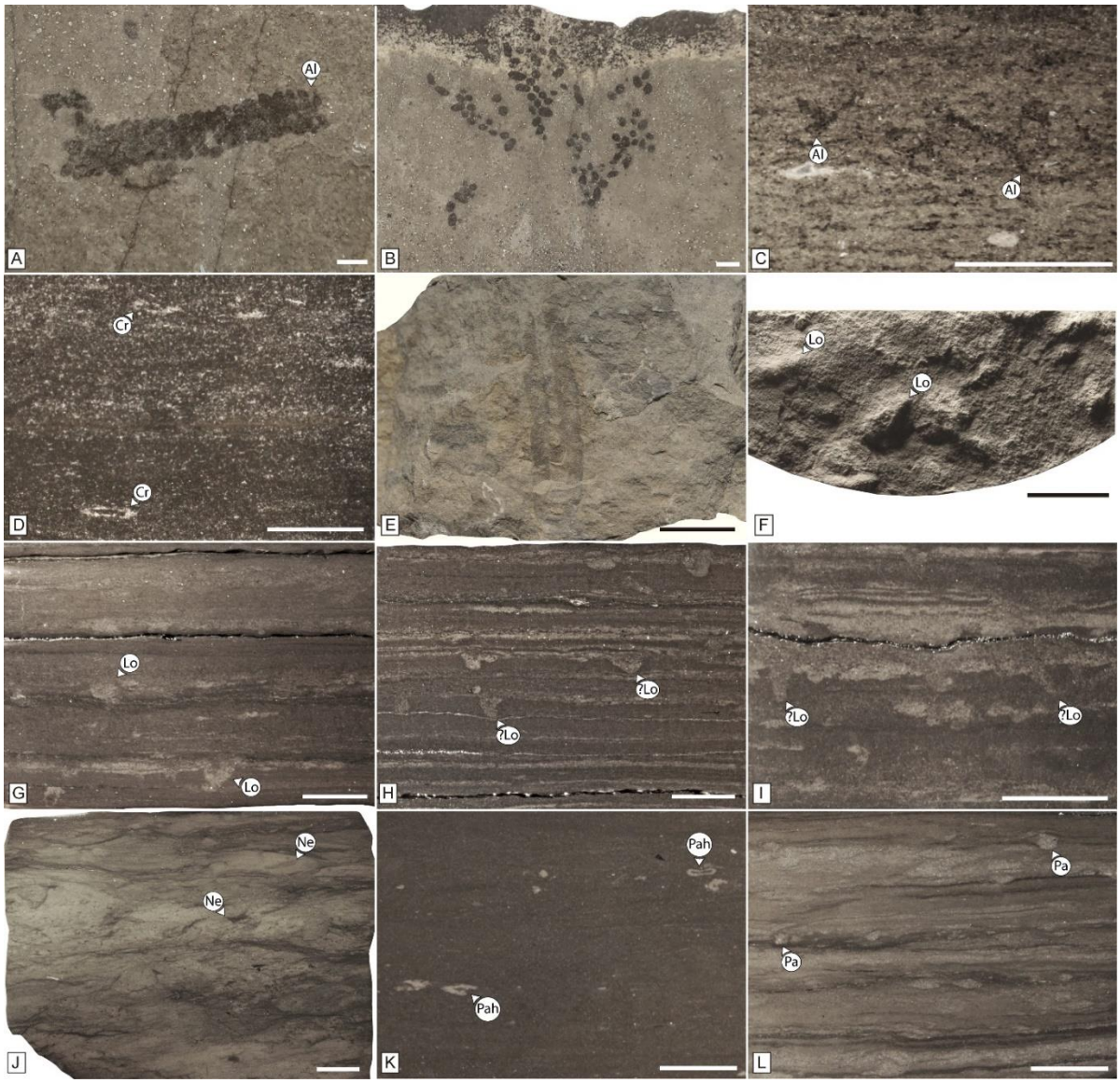

Fig. 5.8: Trace fossils of the Vaca Muerta Formation. A) Plan view of *Alcyonidiopsis longobardiae* (Al) type 1 in tuff. B, C) Core cross-section view of *Alcyonidiopsis longobardiae* type 2 and 3, respectively, in

tuff. D) Core cross-section view of *Crininicaminus* isp. (Cr) occurring in crinoidal mudstone. E) Cross-section of *Diplocraterion* isp. from tuff. F) Plan view of cores showing positive hyporelief *Lockeia siliquaria* (Lo) in calcareous mudstone. G) Cross-section view of *Lockeia siliquaria* (Lo). H, I) Cross-section of ?*Lockeia* isp., consisting of cylindrical and conical-shaped structures passively infilled by coarse mudstone in cores. J) Core cross-section of tuffs displaying *Nereites* (Ne). K, L) Cross-section of calcareous mudstone in cores, with *Palaeophycus heberti* (Pah) and *Palaeophycus* isp. (Pa). Scale bars are 1 mm in A and B, and 1 cm in C-L.

Phycosiphon incertum Fischer-Ooster, 1858 consists of oblique to horizontal, actively infilled burrows showing a dark, muddy core and white mantle (Fig. 5.9A). Cross-section views are tubular or rounded, with curved or straight forms, displaying 0.5 mm wide and 0.5-2 mm long core, and a 0.5-1 mm-thick mantle. This ichnotaxon is preserved as full relief in tuffs and fine to coarse mudstone deposits, and has been identified only in core. *Phycosiphon incertum* is the most common *Phycosiphon* ichnospecies. Locally, *Phycosiphon* occurs reworking several other burrows, such as *Teichichnus*, *Asterosoma* and *Nereites*. *Phycosiphon* represents selective deposit-feeding behavior of a vermiform organism exploiting organic-rich intervals (Wetzel, 2010; Izumi, 2014).

Planolites isp. consists of simple horizontal, straight to sinuous, unlined burrows displaying a dark, muddy or white, silty, active infill (Fig. 5.9B). Burrows show circular cross-sections that are 1-4 mm in diameter. *Planolites* isp. is preserved as full relief in tuffs and coarse mudstone deposits, and has been identified only in core. Core preservation does not allow assessing morphologic variability and, therefore, classification is only at ichnospecies level. This ichnotaxon occurs in sparsely to highly bioturbated intervals, locally generating a diffuse laminated fabric that mimics sedimentary lamination. *Planolites* is typically regarded as a deposit-feeding structure of a vermiform organism (Pemberton and Frey, 1982).

?*Skolithos* isp. is represented by vertical, straight, cylindrical, passively infilled burrows (Fig. 5.9C). Burrow diameter is 0.5-3 mm wide, whereas the structures are 3-7 m long. It is preserved as full relief in calcareous mudstone. Because a very few number of specimens were documented, assignment to *Skolithos* is tentatively. *Skolithos* comprise a dwelling structure produced by suspension feeding organisms or passive predators (phoronids or annelids, Bromley, 1996; Schlirf and Uchman, 2005).

Teichichnus is the most common discrete trace fossil found in the Vaca Muerta Formation, consisting of horizontal to oblique, passively infilled, arcuate-shaped burrows showing spreite. The spreite is typically vertical and retrusive, characterized by a convex-down laminae below the causative burrow. Three ichnospecies were identified, namely *Teichichnus patens, T. rectus* and *T. zigzag*. These traces are observed as full relief in both cores and outcrops.

Teichichnus patens Schlirf, 2000 consists of straight to minor curved, horizontal burrows with vertical spreite, in places showing secondary successive branching (Fig. 5.9D, E). Locally, a sinuous pattern can be observed (Fig. 5.9F). In plan-view, the burrows display a boxwork structure, with some paired burrows oriented parallel to each other. Branching occurs at angles of 15-20° or 60°. Causative burrow is 5-10 mm wide and up to 30 cm long. The spreite is vertical, with straight to minor zigzag patterns and occupies the whole vertical extension of tuffs, having a penetration depth of up to 40 cm (Fig. 5.9D). The sinuous shape and branching pattern support assignment to *T. patens*.

Teichichnus rectus Seilacher, 1955 shows a straight, vertical to minor oblique spreite (Fig. 5.9G). Causative burrow is 0.5-2 mm wide. *Coprulus oblongus* type A (see Biodeposition structures below) can occur loosely or closely packed within *Teichichnus rectus,* locally oriented parallel to burrow long axis.

Teichichnus zigzag Frey and Bromley, 1985 displays a vertical spreite that switch directions horizontally in a zigzag pattern, generating a causative burrow smaller than the spreite area (Fig. 5.9H, Frey and Bromley, 1985). Causative burrow is 0.5-1 mm wide.

Teichichnus patens was documented in one tuff interval of the transgressive facies of the Yesera del Tromen outcrop. Both *T. rectus* and *T. zigzag* occur in tuff, with rare specimens in mudstone or bioclastic mudstone. Penetration depth of *Teichichnus* is locally dependent on the tuff thickness, because deeper *Teichichnus* occur in thicker tuff deposits. Possible tracemakers of *Teichichnus* are polychaetes, echiurans, sipunculids, crustaceans, holothurians and, less likely, bivalves (Corner and Fjalstad, 1993; Bromley, 1996; Knaust, 2018). The common occurrence of *Teichichnus* in organic matter-poor intervals, such as sandstones (and tuffs in this case), and its passive infill indicate that this ichnotaxon might represent a dwelling or equilibrium structure (Domichnia, Equilibrichnia), sharing a similar interpretation with *Diplocraterion* (Corner and Fjalstad, 1993). The abundance of *Teichichnus* in tuff intervals (which comprises a food-starved substrate), and the local occurrence with *Diplocraterion*, supports this interpretation in the present

context. The organism could have been involved in surface-deposit, deposit, suspension, or re-suspension feeding (Leaman and McIlroy, 2017; Knaust, 2018). Tuff intervals restrict oxygen penetration due to oxygen consumption by reactive chemical components, generating a shallowing of the oxic-anoxic interface (Wetzel, 2009). Hence, *Teichichnus* deep penetration into tuffs and abundance of *Coprulus oblongus* within the burrow may suggest gardening activities associated with bacterial growth at the oxic-anoxic interfaces of the burrow wall.

Thalassinoides isp. comprises horizontal to oblique, unlined, passively infilled burrows (Fig. 5.9I). Burrow boundaries are typically sharp. Burrow cross-sections are rounded to slightly oval, 1-15 mm high and 3-40 mm wide. In some specimens, 1-2 mm wide draught fill canals are present. This ichnotaxon is preserved as full relief, in tuffs, sandstone, bioclastic and intraclastic wackestone, and mudstone in cores. *Thalassinoides* represents a dwelling structure made by suspension- or deposit-feeding callianassid or thalassinidean shrimps (Bromley and Frey, 1974).

Zoophycos isp. consists of horizontal to oblique, unlined burrows with lateral spreite (Fig. 5.9J). The spreite comprises elliptical- to round-shaped laminae showing intercalation of mud and ash. The burrow is 5-10 mm in diameter and locally crosscut the complete horizontal extension of the cores. *Zoophycos* isp. is preserved as full relief in tuffs, and has been identified only in core. In addition to uncertainties regarding the validity of its many ichnospecies, core preservation prevents evaluation of the overall burrow morphology and, accordingly, classification is done at ichnogeneric level. *Zoophycos* represent a vermiform organism structure probably produced by sipunculids, echiurans or other polychaetes (Wetzel and Werner, 1980; Kotake, 1992; Knaust, 2009).

Horizontal, unbranched, curved to straight pellet trails are also recognized (Fig. 5.9K). Trails are 0.3-0.7 mm wide and 2-4 mm long. The two types of pellets mentioned in connection to the infill of *Alcyonidiopsis longobardiae* and *Teichichnus rectus, Coprulus oblongus* type B and rarely type A, occur as part of the infill of these horizontal trails (see Biodeposition structures below). Preservation is as full relief at the base of tuff deposits. Eiserhardt *et al.* (2001) indicated that the name *Tomaculum* should be used for pellet traces occurring at the sediment surface, but *Tomaculum* is now regarded as a junior synonym of *Alcyonidiopsis* (Chamberlain, 1977; Uchman, 1995; Buatois *et al*., 2017; Mángano *et al.*, 2019). However, the stratinomic position of these pelletized structures at the base of ash layers strongly suggests an epibenthic or very shallow infaunal origin for these pellet strings rather than shallow, horizontal burrows. Although pellet

trails have low preservation potential, ash fallout could have aided in their preservation through sudden burial, avoiding biogenic reworking in the mixed layer. Fecal trails with pellets similar to *Coprulus oblongus* type A were produced by the polychaete *Nereis diversicolor* in the Kundalika Estuary, India (Kulkarni and Panchang, 2015).

Escape and equilibrium trace fossils comprise bowl-, U- and V-shaped, concave upwards, laminated structures oriented oblique to vertical (Fig. 5.9L, 5.10A). They are 0.5-3 mm wide and 1-15 mm long. Preserved as full relief in fine to coarse mudstone deposits, and only observed in cores. Locally, complete escape or equilibrium structures exhibit a predominant oblique orientation with heights of up to 2 cm, and in the case of specimens in current ripples, burrows point towards the direction of ripple migration. In many cases, these trace fossils are vertically associated with cylindrical and conical, passively infilled, structures assigned to *Lockeia* isp. Differentiation between escape and equilibrium structures has been problematic. Both types of trace fossils reflect the vertical adjustment of the organism to a sedimentation event, which can be either rapid (escape) or gradual (equilibrium; Bromley, 1996; Buatois and Mángano, 2011). Escape behavior was interpreted when inclined to vertical structures display deformed laminae crossing cm-thick deposits. Equilibrium adjustment was interpreted from either vertical, chevronated structures associated with thin (mm-thick) sedimentation events, or from vertically associated, sharp-lined burrows suggesting establishment of the organism in newly deposited sediment.

Mantle and swirl structures represent highly compacted, horizontal, oblique or vertical burrows showing irregular margins and locally an irregular concentric fill (Fig. 5.10B). Burrow cross sections are 1-3 mm high and 6-9 mm wide. These structures have only been observed in core, being preserved as full relief in tuffs and fine to coarse mudstone. The concentric fill, irregular boundaries, and compacted cross sections are typical of the mantle and swirl structures generated by the movement of vermiform organisms in soupy to soft substrates (Lobza and Schieber, 1999).

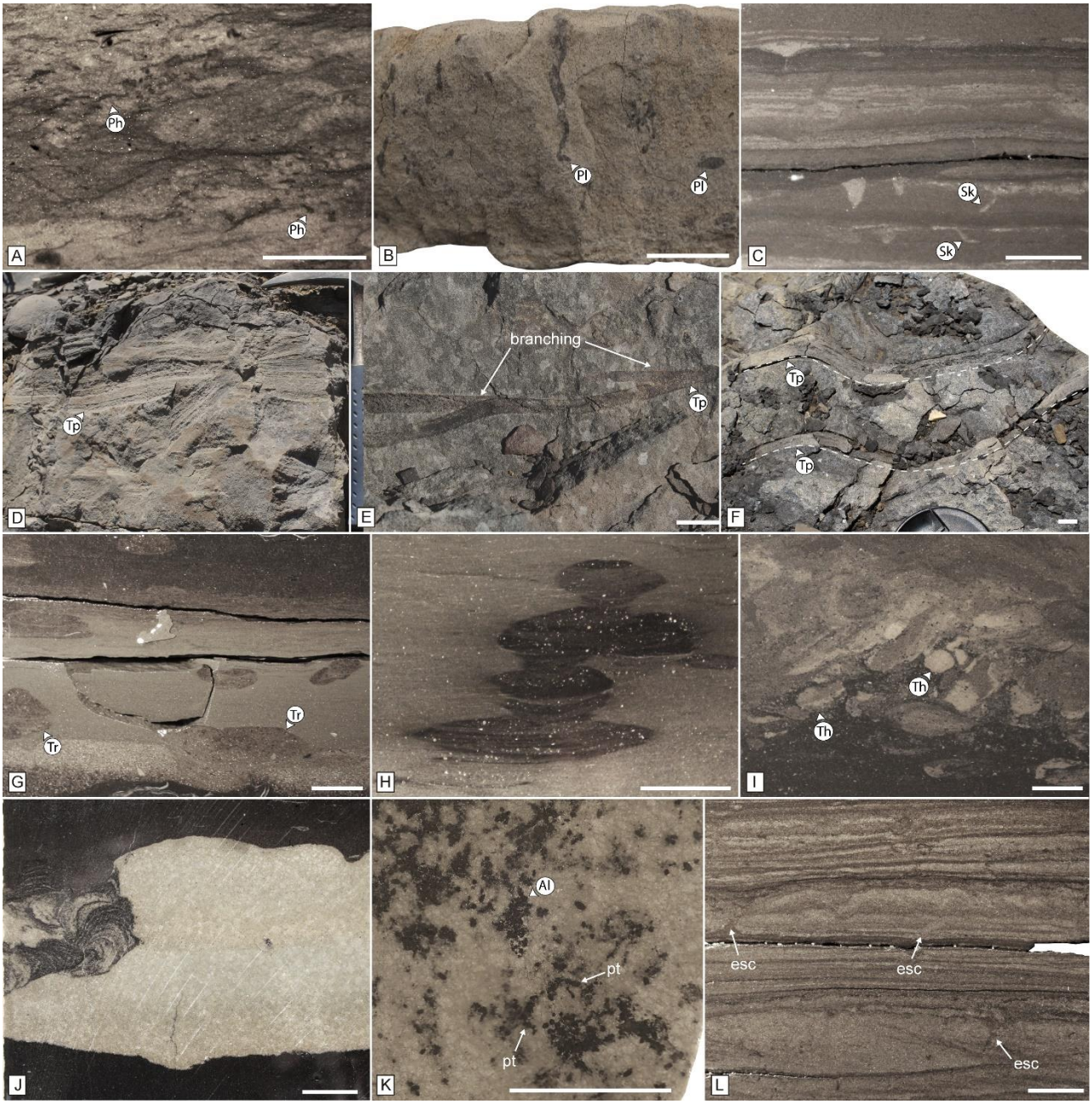

Fig. 5.9: Trace fossils of the Vaca Muerta Formation. A, B) Tuff cross-section in cores and outcrop, respectively, showing *Phycosiphon incertum* (Ph) and *Planolites* isp. (Pl). C) Cross-section of ?*Skolithos* isp. passively infilled by coarse mudstone in cores. D) Outcrop cross-section view of two crosscuting specimens of *Teichichnus patens* (Tp), located in the basal transgressive lithofacies of the Yesera del Tromen section. E, F) Plan view of *T. patens* (Tp), displaying the secondary successive branching and meandering morphologies (dashed lines). G, H) *Teichichnus rectus* (Tr) and *Teichichnus zigzag* (Tz) observed in cross-sections of tuff, in cores. I) *Thalassinoides* isp. (Th) in cross-section of tuffs. J) Cross-section of *Zoophycos* isp. crosscutting a tuff interval in cores. K) Plan view of a tuff, showing two curved

pellet trails (pt) associated with *Alcyonidiopsis longobardiae* (Al). L) Cores displaying cross-section of escape structures (esc) in ripple cross-laminated and laminated coarse mudstone. Scale bars are 1 cm.

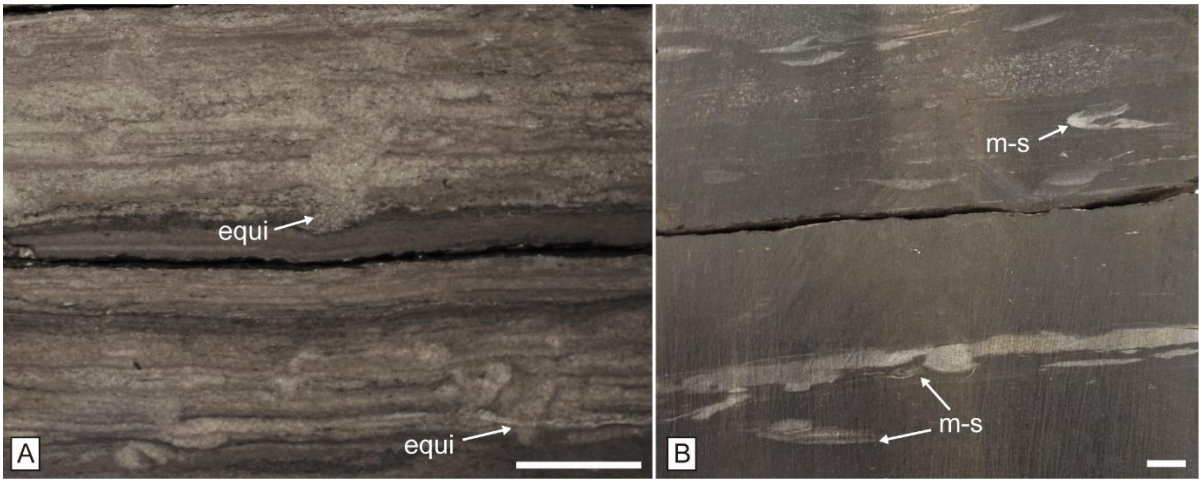

Fig. 5.10: Trace fossils of the Vaca Muerta Formation. A) Cross-section of equilibrium behavior (equi) of ?*Lockeia* isp., in cores. B) Cross-section of cores displaying irregular, mantle and swirl structures (m-s) in tuff, with concentric fills. Scales are 1 cm.

5.5.2 Biodeposition structures

Fecal pellets of benthic and planktonic organisms have been found (Fig. 5.11). Benthic pellets commonly form the fill of some discrete trace fossils (i.e. *Teichichnus rectus*, *Alcyonidiopsis longobardie*, and pellet strings), and they also appear disperse within the sediment as biodeposition structures. The benthic pellets are represented by ellipsoidal *Coprulus oblongus*, observed in tuffs and rarely in parallel-laminated mudstone (Fig. 5.11A, C, D, E). Their sizes show a continuum, yet they can be differentiated in two groups. *Coprulus oblongus* type A comprises 125-250 μm wide and 250-400 μm long structures. Average length to width ratio is 2.6. *Coprulus oblongus* type B are 250-500 μm wide and 400-800 μm long. Average length to width ratio is 2.01. *Coprulus oblongus* type A was only observed in cores, where thin sections to evaluate composition of these structures are unavailable. *Coprulus oblongus* type B shows a matrix with abundant microcrystalline quartz (60-80%) and minor framboidal pyrite (2%, Fig. 5.11D, E). It contains 45-175 μm calcite-replaced radiolarians (15-25%), silt-sized carbonate-replaced clasts, and clay floccules (<1%). Composition from EDS displays a predominance of Si related with the quartz occurrence (Fig. 5.11E). Carbonate sparite cementation replaces pellet matrix in different degrees (0-40% of the matrix).

The dense packing of the pellet infill and the occurrence of pellets as an active infill of *Alcyonidiopsis*, suggest production by a benthic organism (Cuomo and Bartholomew, 1991). The ellipsoidal shape, length to width ratio, size range, and homogeneous fill (Fig. 5.11E) of the pellets indicate that they can be assigned to *Coprulus oblongus* Mayer, 1952 (see Knaust, 2008, 2020). The producer cannot be inferred because ellipsoidal pellets are among the most typical shapes in fecal pellets (Moore, 1939; Schäfer, 1972). However, *Coprulus oblongus* and similar pellets were commonly assigned to polychaetes (e.g. Kraeuter and Haven, 1970; Arakawa, 1971; Cadeé, 1979; Bałuk and Radwański, 1979; Gaillard *et al.*, 1994). Other producers of benthic ellipsoidal pellets include bivalves, echiurans, and enteropneusts (Thomas, 1972; Wikander, 1981). The size of *Coprulus oblongus* type A is in the range of meiofauna to small macrofauna, whereas *C. oblongus* type B might have been produced by small macrofauna. The common occurrence of well-preserved radiolaria tests and microcrystalline quartz within pellets suggests a selective deposit feeder consuming the radiolarian-rich sediment. The difference in size between both pellet types can be explained by juvenile and adult populations (Cadeé, 1979). Other benthic pellets, such as crustacean microcoprolites, were also described in the Vaca Muerta Formation, yet they differ in their relative greater size (up to 1.5 mm in cross section) and the presence of longitudinal canals (Kietzmann and Palma, 2010a, b; Kietzmann *et al.*, 2010).

The planktonic pellets are easily distinguished in the tuff due to sediment contrast, although they occur in all the mudstone lithofacies. The pellets consist of 90-200 μm wide and 200-700 μm long structures with oval, elongated oval, rounded, square or irregular-shaped cross-sections (Fig. 5.11F, G). They can be observed concordant to bedding in the tuff topmost lamination, or randomly disposed within the tuff (Fig. 5.11B, F). Their matrix is mostly composed of coccoliths and carbonate clasts (80%), with minor clay floccules, microcrystalline quartz and illite coatings (<1%, Fig. 5.11H). Silt-sized grains within the pellets include quartz and volcanic glass shards (<1%). In contrast to benthic pellets, planktonic pellets from the tuffs show a predominance of coccoliths and are enriched in Ca.

The size and composition of these pellets suggest a planktonic origin. Planktonic pellets from various black shale deposits display an average of 65 μm width and 143 μm long (Porter and Robbins, 1981), being typically smaller than the benthic pellets observed here. These pellets shows a predominance of plankton food sources, such as biogenic debris and intact tests, pigments and organic materials, and minor clays (Hattin, 1975; Cuomo and Bartholomew, 1991). Particularly,

the abundance of coccoliths and Ca enrichnment suggest a predominant planktonic food source. Pellets of planktonic origin are easily degraded in the water column or by microbes in the seafloor (Honjo and Roman, 1978; Turner, 2002), yet intercalation with tuff material and local absence of bioturbation allowed rapid burial and preservation.

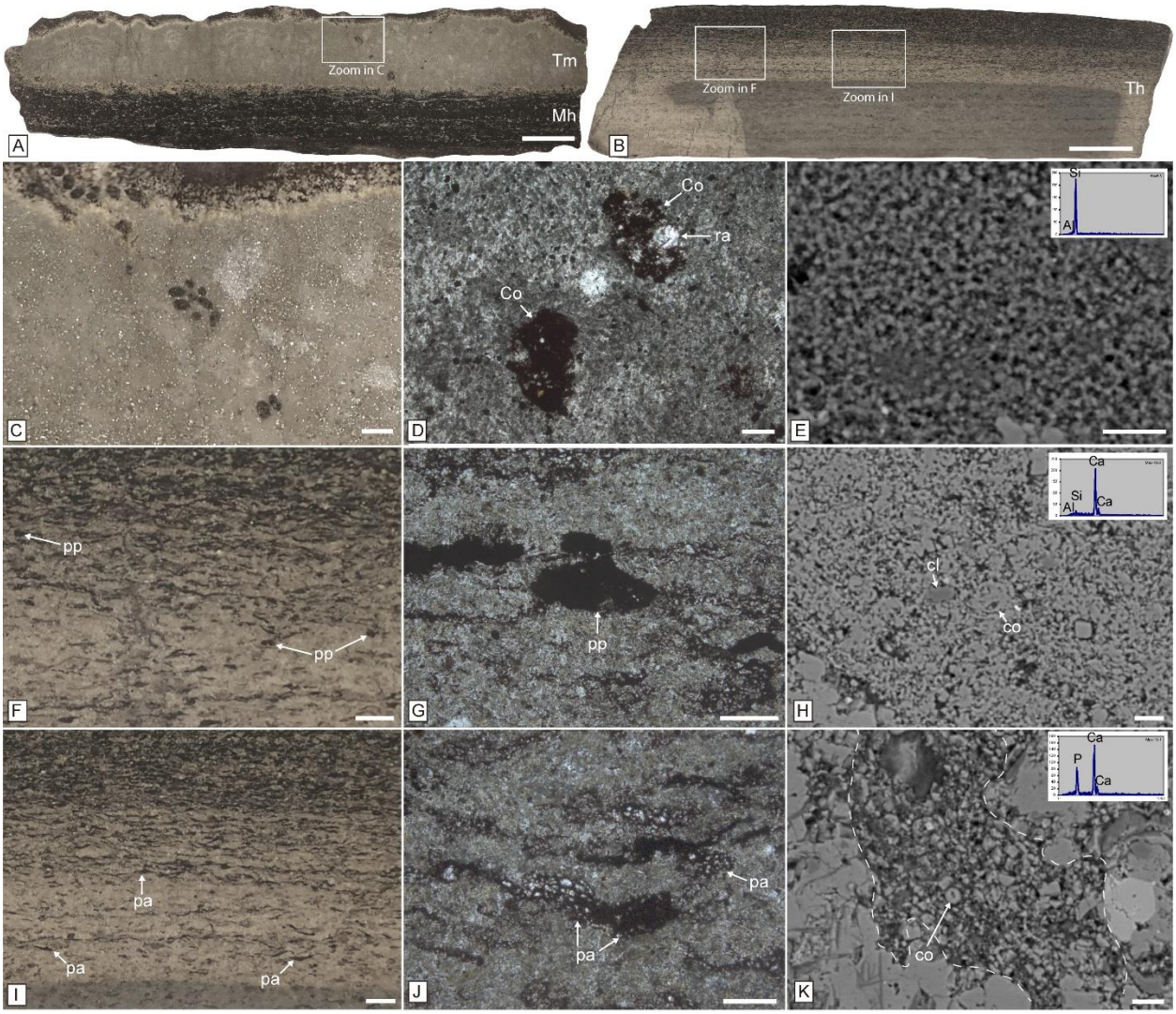

Fig. 5.11: Biodeposition structures and pelagic aggregates observed in tuff intervals. A, B) General view of the parallel-laminated and massive tuffs (Th, Tm) encased in parallel-laminated mudstone (Mh), with the location of close-up photos. C, D) Close-up sample and thin section photographs of the benthic pellet *Coprulus oblongus* (Co) composed of microcrystalline quartz and radiolarians (ra). E) BSE image and EDS composition of the fine-grained matrix of the benthic pellet. F, G) Sample and thin section photographs of the planktonic pellets (pp). H) BSE image and EDS composition of the planktonic pellets, with abundant coccoliths (co) and minor clay minerals (cl). I, J) Close-up outcrop sample and thin section photographs of

the pelagic aggregates. K) BSE images and EDS composition of the pelagic aggregates (delineated by dashed line), showing an abundance of calcite-rich coccoliths (co). Scale bars are 1 cm in A and B, 1 mm in C, F and I, 200 μm in D, G, J, and 10 μm in E, H, K.

Pelagic aggregates are also distinguished, associated with benthic and planktonic pellets on top of the tuffs (Fig. 5.11I). The aggregates comprise irregular, lenticular- to tabular-shaped, 50-100 μm wide and 0.5-2 mm long structures with indistinct boundaries. They are composed of radiolaria, plagioclase, volcanic glass, coccoliths, microsparite, illite floccules, and minor silica replacements (Fig. 5.11J, K). These aggregates of radiolaria and coccoliths are interpreted as marine snow flocs generated in the water column (Alldredge and Silver, 1988).

5.6 Ichnocoenoses

In order to characterize these deposits from an ichnologic perspective, we have grouped trace fossils into ichnocoenoses. Ichnocoenoses metrics are summarized in Table 5.1. An ichnocoenosis is defined as a group of trace fossils produced by a similar biological community (Buatois and Mángano, 2011). The ichnofauna of the Vaca Muerta Formation is subdivided into nine ichnocoenoses. Four of these ichnocoenoses are interpreted as oxygen-related ichnocoenoses (ORIs): the *Coprulus oblongus*, *Alcyonidiopsis longobardiae*, *Teichichnus rectus*, and *Techichnus rectus-Phycosiphon incertum* ichnocoenoses. ORIs represent ichnocoenoses that were deposited under approximately similar levels of bottom water oxygenation (Savrda and Bottjer, 1986). The other five ichnocoenoses comprise: *Palaeophycus heberti–Crininicaminus* isp., *Nereites* isp., and Equilibrichnia–Fugichnia ichnocoenoses, which are described in detail in Chapter 7, and the *Planolites* isp. and *Thalassinoides* isp. ichnocoenoses. Penetration depth was only measured in the ichnocoenoses associated with tuff intervals, where the colonization surface can be estimated. Mean burrow diameters are scarce in the *Alcyonidiopsis longobardiae* ichnocoenosis due to the difficulty in defining burrow boundaries in loosely packed *Alcyonidiopsis.*

Table 5.1: Summary of trace fossil metrics of the different ichnocoenoses.

	Average BI		Mean penetration depth		Mean burrow diameter	
		N	(mm)	N	(mm)	N
Coprulus oblongus ichnocoenosis (ORI 1)	0.7	80	5.83	10	-	-
Alcyonidiopsis longobardiae ichnocoenosis (ORI 2)	1.23	84	8.57	18	1.51	4
Teichichnus rectus ichnocoenosis (ORI 3)	1.6	168	11.45	42	3.50	18
Teichichnus rectus-Phycosiphon incertum ichnocoenosis (ORI 4)	3.53	243	41.56	37	5.05	36
	4.67	81	89.02	9	8.69	10
Palaeophycus heberti–Crininicaminus isp. ichnocoenosis	2.75	29	-	-	4.78	8
Nereites isp. ichnocoenosis	2.31	100	-	-	3.55	31
Equilibrichnia–Fugichnia ichnocoenosis	1.46	439	-	-	3.16	166
Planolites isp. ichnocoenosis	2.2	401	7.31	9	2.96	54
Thalassinoides isp. ichnocoenosis	2.57	68	89.15	9	15.08	12

5.6.1 *Coprulus oblongus* ichnocoenosis (ORI 1)

This ichnocoenosis is recorded by tuffs consisting of *Coprulus oblongus* type A, planktonic pellets and pelagic aggregates randomly disposed or intercalated in an irregular, faint lamination on top of tuff deposits (Fig. 5.12). Locally, a mm-scale gradation from undisturbed parallel laminae below to irregular laminae above can be observed (Fig. 5.12D). The penetration depth as measured on top of tuff is extremely shallow (mean PD of 5.83 mm, N=10, Table 5.1). Laminae preservation is moderate (BI 1-2). This ichnocoenosis occurs in tuffs. In the enclosing mudstone, the rock fabric is predominantly parallel-laminated (78.2%), and rarely irregular-laminated (17.4%, N=23), whereas massive, bioturbated fabrics are absent (Fig. 5.4B).

Abundance of chaotically distributed *Coprulus oblongus* type A within laminae suggests bioturbation by meiofauna (cryptobioturbation) to small macrofauna that generates a very thin

mixed layer under lower dysoxic bottom water conditions (comparable to quasi-anaerobic biofacies of Savrda and Bottjer, 1991). The preservation of lamination deeper into the tuff (Fig. 5.12D) points towards an epifaunal and probably shallow infaunal mode of life.

5.6.2 *Alcyonidiopsis longobardiae* ichnocoenosis (ORI 2)

This ichnocoenosis consists of shallow-tier *Alcyonidiopsis longobardiae*, *Coprulus oblongus*, and funnel-shaped biodeformational structures (<20 mm deep; BI 1-2, Fig. 5.13). At the base of tuff, sediment contrast allows identification of *Coprulus oblongus*, where they occur in high abundance (locally up to ~50 per cm^2, Fig. 5.13G). Rare very shallow-tier benthic pellet trails, and shallow-tier *Phycosiphon incertum*, *Planolites* isp., and ?*Teichichnus* isp. occur (Fig. 5.13C, D). In some cases, a thin (2-7 mm-thick) mottled interval on top is preserved. The trace fossils are shallow (mean PD of 8.57 mm, n=18, Table 5.1) and forming sparsely bioturbated intervals (BI 1-2). Mean diameter of burrows is 1.51 mm (n=4). This ichnocoenosis is delineated in tuffs. In the tuff, no parallel-lamination is preserved, whereas in the enclosing mudstone, parallel-laminated (58.1%) and irregular-laminated fabrics (39.5%) are observed, with minor massive fabrics (2.3%; n=43; Fig. 5.5A).

This ichnocoenosis represents bioturbation by dominantly meiofauna and small macrofauna (*Coprulus oblongus* type A and B) living at and/or very close to the sediment surface at lower dysoxic conditions. Small burrow size, scarcity of dwelling trace fossils (i.e. maintained structures), the existence of benthic pellet trails suggestive of epifaunal to very shallow infaunal feeding, and shallow tiers all point to low oxygen conditions at the time of emplacement of this community and anoxia or sulfur toxicity within the sediment.

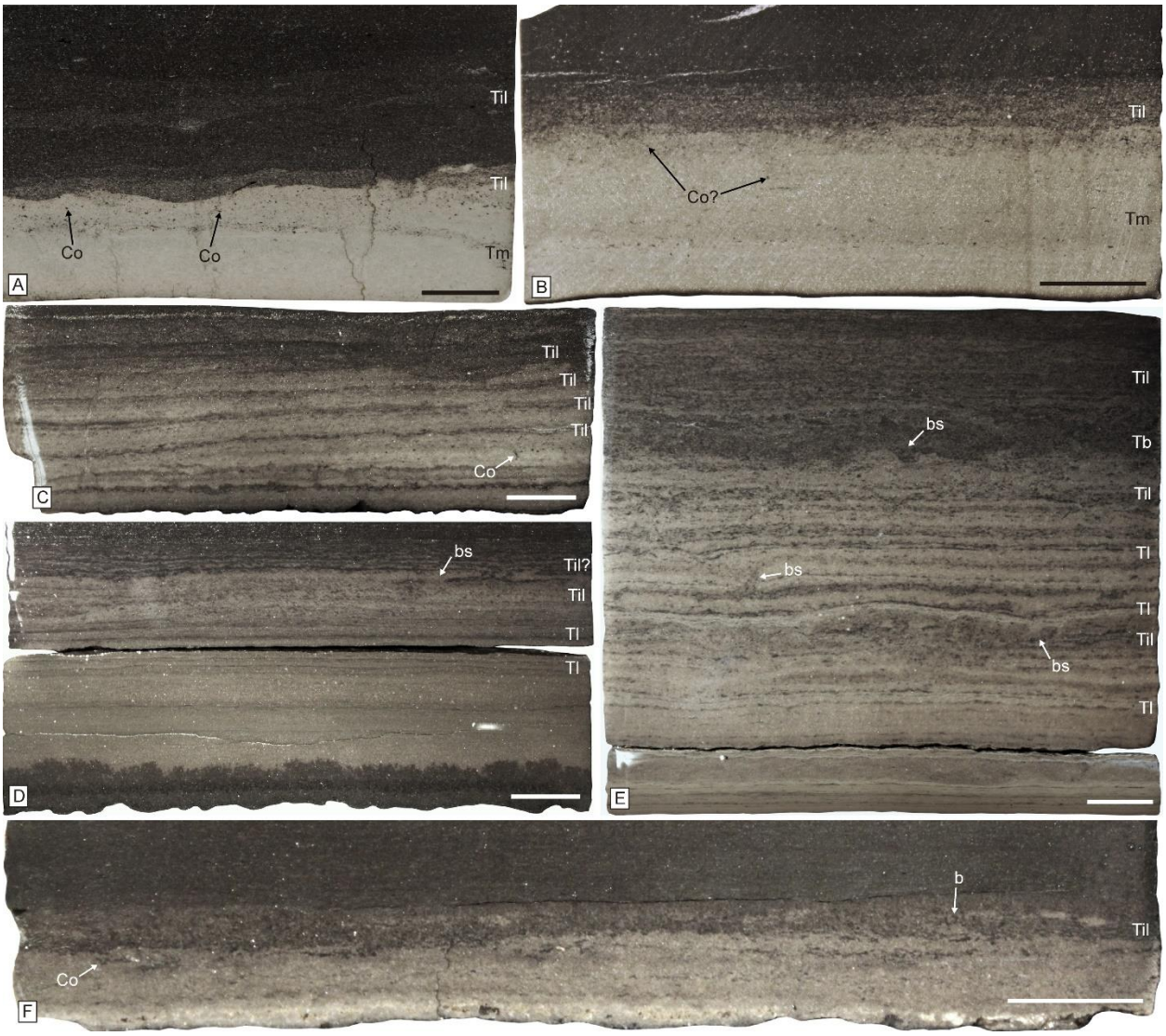

Fig. 5.12: Intervals hosting the *Coprulus oblongus* ichnocoenosis (ORI 1). A, B) Irregular lamination (Til) on top of a massive tuff (Tm, ORI 1). *Coprulus oblongus* (Co?) are delineated. C, D, E) Intercalated irregular (Til) and parallel-laminated tuff (Tl) with *Coprulus oblongus* (Co) and biodeformational structures (bs), interpreted as multiple colonization surfaces in a single volcanic event. F) *Coprulus oblongus* (Co) and small burrows (b) on top of an irregular-laminated tuff (Til). Scale bars are 1 cm.

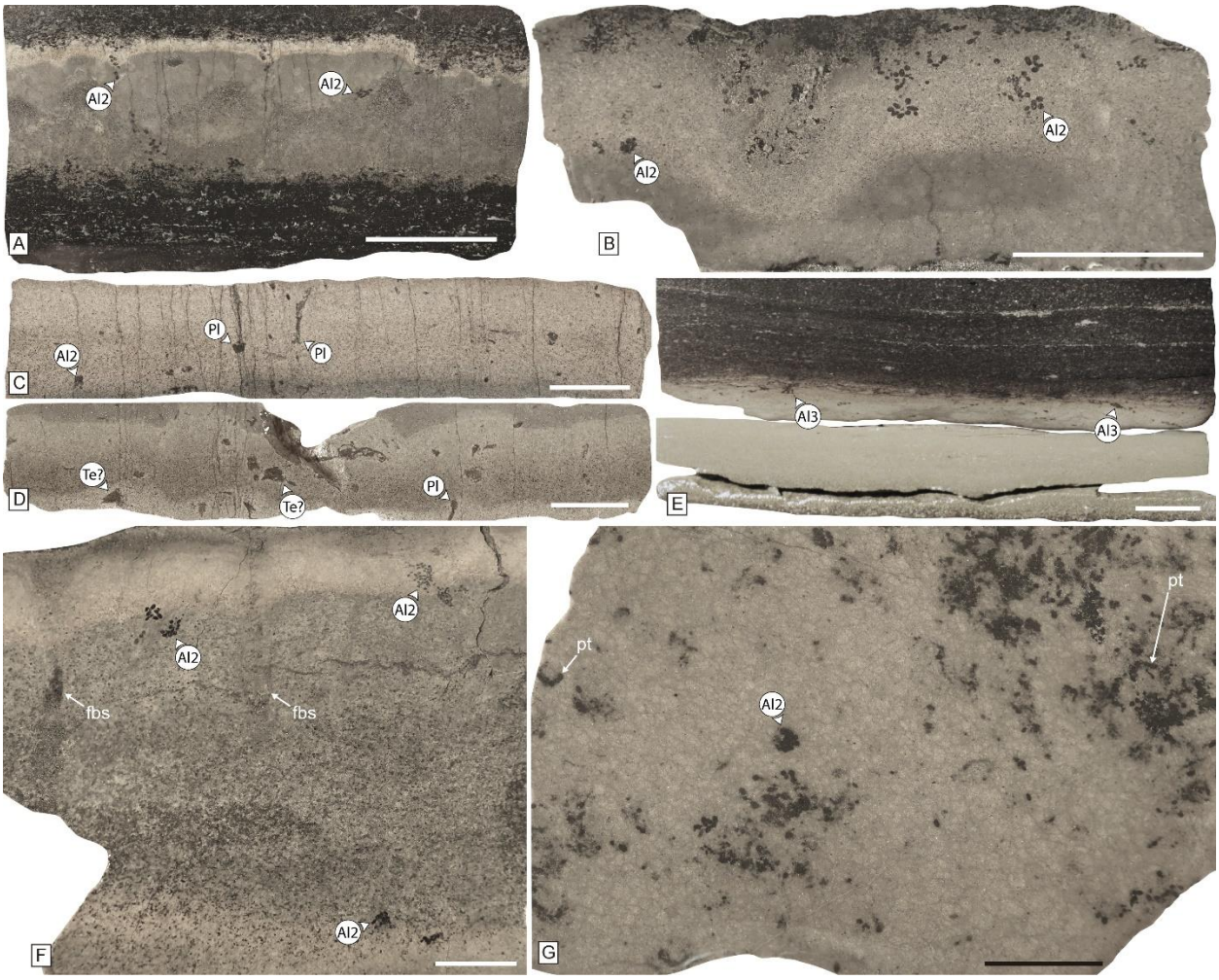

Fig. 5.13: *Alcyonidiopsis longobardiae* ichnocoenosis (ORI 2). A, B, C, D) Tuffs displaying *Alcyonidiopsis longobardiae* type 2 (Al2), *Planolites* isp. (Pl), and ?*Teichichnus* isp. (?Te). E) Core photograph of ORI 2, displaying *Alcyonidiopsis longobardiae* type 3 (Al3) towards the top of a tuff interval. F) *Alcyonidiopsis longobardiae* type 2 (Al2) in tuffs, associated with the funnel-shaped biodeformational structures (fbs). G) Plan-view photograph of a tuff interval, containing pellet trails (pt). Scale bars are 1 cm.

5.6.3 *Teichichnus rectus* ichnocoenosis (ORI 3)

It consists of tuffs showing shallow-tier *Teichichnus rectus*, *Planolites* isp., *Thalassinoides* isp., and *Coprulus oblongus* (<35 mm deep, BI 1-4, Fig. 5.14A), as well as biodeformational structures, such as mantle and swirl trace fossils (<30 mm deep, BI 1-3, Fig. 5.14B). Minor *Alcyonidiopsis longobardiae*, *Phycosiphon incertum*, *Nereites* isp., and *Palaeophycus* isp. also occur. A thin (3-9 mm-thick) mottled interval is rarely observed on top of the tuffs. Overall, the trace fossils occupy a shallow-tier (mean PD of 11.45 mm, n=42, Table 5.1) and are present in intervals of low to

moderate intensities of bioturbation (BI 2-3). Mean diameter of burrows is 3.5 mm (n=18). This ichnocoenosis can be observed in tuffs. In the enclosing mudstone, irregular-laminated (73.7%) fabrics are observed, with minor parallel-laminated (18.2%) and massive (9.1%; n=77) fabrics.

This ichnocoenosis comprises macrofaunal bioturbation in upper dysoxic environments that restricted burrowing to shallow zones within the sediment. However, higher burrow diameters, increased penetration depth, a wider range of morphologies, and the existence of open burrows (*Teichichnus, Thalassinoides,* and *Palaeophycus*) suggest higher bottom water oxygen levels compared with the *Coprulus oblongus* and *Alcyonidiopsis longobardiae* ichnocoenoses. This ichnocoenosis is similar to those from hemipelagic mud with remnants of lamination of the Santa Barbara Basin, showing 2-6 mm-diameter burrows and <1 cm of bioturbation depth, which was interpreted to lie close to the anoxic-dysoxic boundary (Behl, 1995).

5.6.4 *Teichichnus rectus-Phycosiphon incertum* ichnocoenosis (ORI 4)

This ichnocoenosis is typically composed by very shallow-tier *Alcyonidiopsis longobardiae, Coprulus oblongus, Phycosiphon incertum, Planolites* isp., and *Nereites* isp. (from 20 to 35 mm deep, BI 1-4), and shallow- to mid-tier *Teichichnus rectus, T. zigzag,* and *Thalassinoides* isp. (20-65 mm deep, BI 1-4; Fig. 5.15). Deep-tier *Teichichnus rectus* and *T. zigzag* are observed in places (120-150 mm deep, BI 1-2). Rare *Zoophycos* isp., *Palaeophycus* isp., and mantle and swirl structures also occur. A thin (5-45 mm-thick) mottled interval is observed on top of the tuffs. In most of the cases, the tiered community moved upwards in response to vertical aggradation of the sea floor, generating a composite ichnofabric (*sensu* Bromley and Ekdale, 1986). In a few cases, short-term deoxygenation events of local extent or burial by successive ash falls preserved the tiering of this ichnocoenosis (Fig. 5.16). Bioturbation metrics show two populations of PD and burrow diameter. The first one has mean PD of 41.56 mm (n=37), mean burrow diameter of 5.05 mm (n=36). The second one has a mean PD of 89.02 mm (n=9) and mean burrow diameter of 8.69 mm (n=10). This ichnocoenosis occur in tuff intervals, and rarely in mudstone. The host mudstone shows massive (79.8%) and, less commonly, irregular- (17.8%) and parallel-laminated (2.4%; N=84) fabrics (Fig. 5.5B).

A slightly higher ichnodiversity and mean burrow diameter compared with the *Teichichnus rectus* ichnocoenosis suggests amelioration of oxygen stress (Smith *et al.*, 2000). This ichnocoenosis represents more mature communities developing different tiers in environments

with background sediment deposition under more oxygenated bottom waters. The higher mean PD in the second population could be related to increased bottom water oxygen levels or changes in substrate consistency.

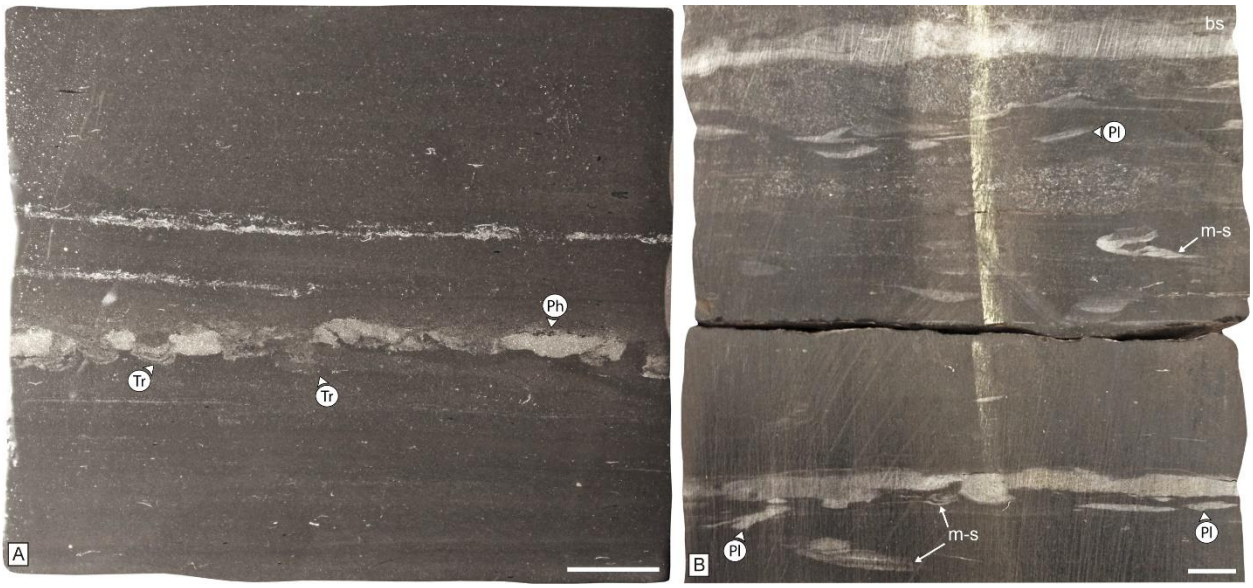

Fig. 5.14: *Teichichnus rectus* ichnocoenosis (ORI 3). A) Shallow bioturbation in tuff intervals represented by *Teichichnus rectus* (Tr) and *Phycosiphon incertum* (Ph). B) Tuff intervals displaying *Planolites* isp. (Pl), mantle and swirl structures (m-s) and biodeformational structures (bs). Scale bars are 1 cm.

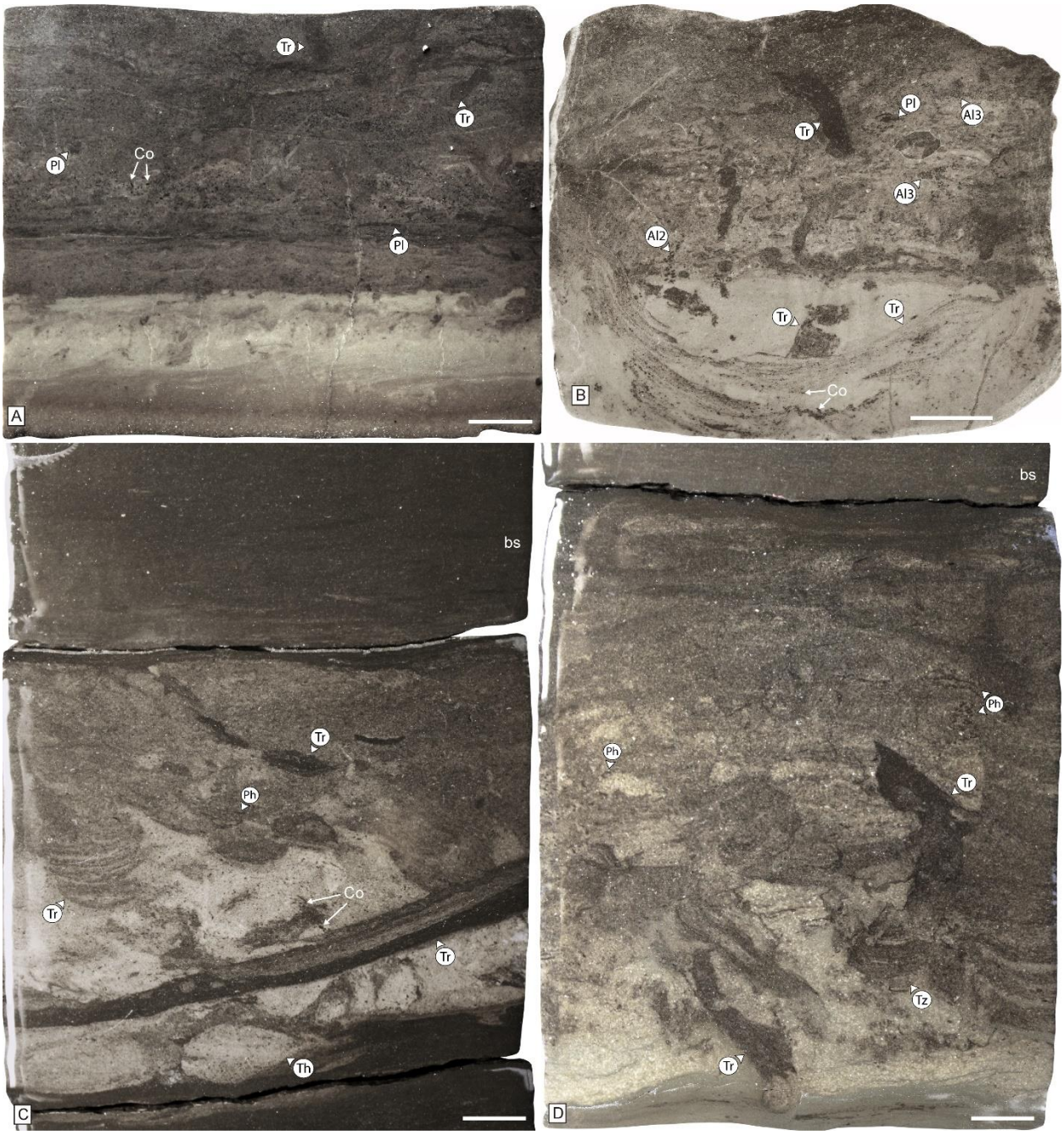

Fig. 5.15: *Teichichnus rectus-Phycosiphon incertum* ichnocoenosis (ORI 4). A, B, C, D) Core photographs of bioturbated tuff intervals, displaying *Alcyonidiopsis longobardiae* types 2 and 3 (Al2, Al3), *Coprulus oblongus* (Co), *Phycosiphon incertum* (Ph), *Planolites* isp. (Pl), *Teichichnus rectus* (Tr), *Teichichnus zigzag* (Tz), *Thalassinoides* isp. (Th), and biodeformational structures (bs). Scale bars are 1 cm.

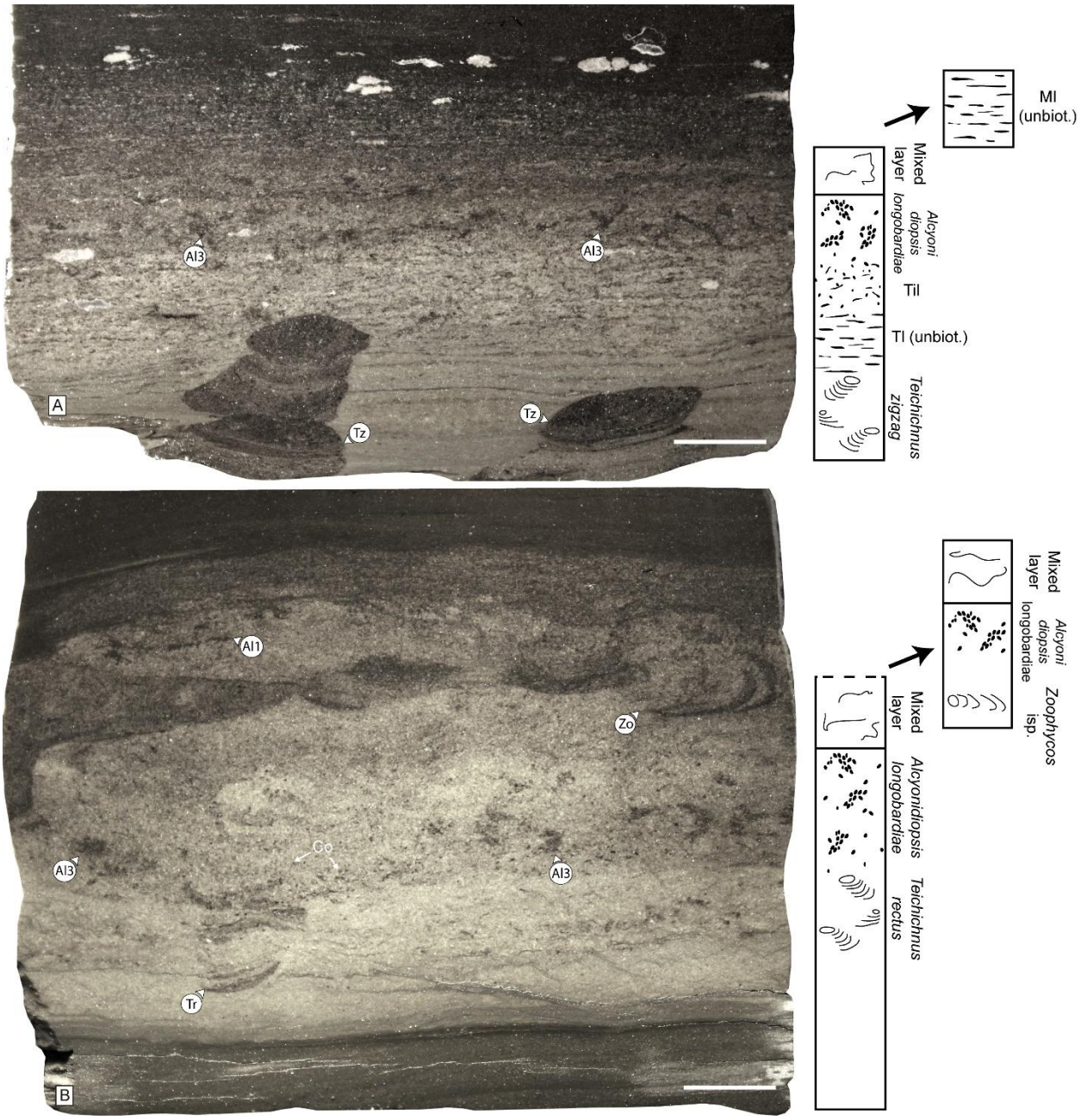

Fig. 5.16: Preservation of the tiering profile of the *Teichichnus rectus-Phycosiphon incertum* ichnocoenosis (ORI 4). A) Frozen tiered profile associated with a deoxygenation event of local extent. First, a mixed layer is established, with a transitional layer below preserving shallow-tier *Teichichnus zigzag* (Tz), and very shallow tier, irregular lamination (Til) associated with cryptobioturbation and *Alcyonidiopsis longobardiae* type 3 (Al3). Second, bottom water anoxia generates parallel-laminated mudstone on top (Ml), preserving the frozen tiered profile. B) Volcanic event comprising two tuff deposits, the first one developing shallow-tier *Teichichnus rectus* (Tr) and very shallow-tier *Alcyonidiopsis longobardiae* type 3 (Al3) and *Coprulus oblongus* (Co), with a diffuse mixed layer on top, and the second with shallow-tier *Zoophycos* isp. (Zo)

overprinting the sediment below, and very shallow tier *A. longobardiae* type 1 (Al1). In this case, a second high sedimentation volcanic event preserved the tiering profile of the ichnofauna established in the previous volcanic event. Scale bars are 1 cm.

5.6.5 *Palaeophycus heberti–Crininicaminus* isp. ichnocoenosis

It consists of shallow-tier, *Palaeophycus heberti*, *Palaeophycus* isp., *Crininicaminus* isp., and *Planolites* isp. (Fig. 5.17A). Bioturbation intensities are moderate to high (BI=4-6) and mean burrow diameter is 4.78 mm (n=8, Table 1). This ichnocoenosis observed in highly bioturbated, crinoidal mudstone and fine to coarse mudstone intervals.

This ichnocoenosis is present in the lithofacies of the drift facies association (FA3), indicating contour current activity during its formation. The common high bioturbation indexes observed support the idea of relatively lower-energy environments that allowed complete sediment homogenization by bioturbation, under upper dysoxic conditions (Paz *et al.*, in review b). The thick lining of *P. heberti* and *Crininicaminus* isp. represent a strategy to maintain open burrows in soft substrates, probably associated with suspension-feeding organisms.

5.6.6 *Nereites* isp. ichnocoenosis

It is represented by shallow-tier *Nereites* isp., *Phycosiphon incertum*, *Planolites* isp., *Palaeophycus isp.*, and rare *?Lockeia* isp. *Palaeophycus heberti*, and *?Skolithos* isp (Fig. 5.17B). Bioturbation intensity is either low (BI=1-2), showing an abundance of *Phycosiphon incertum*, or moderate to high (BI 3-5), displaying *Nereites* isp. Mean burrow diameter is 3.55 mm (n=31, Table 1). This ichnocoenosis occur in successions consisting of massive, current-ripple cross- or parallel-laminated, fine to coarse mudstone.

This ichnocoenosis is interpreted as opportunistic colonization by deposit-feeders during times of enhanced contour current activity (Paz *et al.*, in review b). Higher energy currents than in the *Palaeophycus heberti–Crininicaminus* isp. ichnocoenosis generated abundant traction structures, with the existence of low BI intervals. However, currents were low enough as to deliver organic matter to the sediment surface, estimulating the establishment of deposit feeders (Wetzel *et al.*, 2008).

5.6.7 Equilibrichnia–Fugichnia ichnocoenosis

It comprises very shallow tier *Lockeia siliquaria* and ?*Lockeia* isp. that are associated with equilibrium and escape structures. Rare ?*Skolithos* isp. can be observed. Bioturbation index is typically 1-2, whereas intervals associated with dense populations of equilibrium and/or escape structures show 3-4 (Fig. 5.17C). Mean burrow diameter is 3.16 mm (n=166, Table 5.1). This ichnocoenosis is observed in sparsely to moderately bioturbated, parallel-laminated fine to coarse mudstone.

This ichnocoenosis represents the activity of suspension feeding organisms (bivalves) in areas of continuous contour current and minor sediment-gravity flow deposition (Paz *et al.*, in review b). The small burrow sizes associated with this ichnocoenosis indicate long-term upper dysoxic conditions.

5.6.8 *Planolites* isp. ichnocoenosis

It comprises biodeformational structures, and rare shallow-tier *Planolites* isp., *Phycosiphon incertum*, *Nereites* isp., *Palaeophycus* isp., *Thalassinoides* isp., and ?*Skolithos* isp. (Fig. 5.17D, E). Bioturbation is shallow (mean PD of 7.31 mm, n=9, Table 5.1). Bioturbation intensity depends on the associated lithology, with massive to parallel-bedded, calcareous mudstone showing low to high indexes (BI 1-6, Fig. 5.17D), and thin-bedded calcareous mudstone displaying normally low indexes (BI 1, Fig. 5.17E). Mean burrow diameter is 2.96 mm (N=54).

Although calcareous mudstone beds were deposited in an area of higher sedimentation rate, biogenic structures can be established within weeks in fluid mud deposits (Bentley and Nittrouer, 2003), indicating other environmental stresses should occur to restrict bioturbation in this ichnocoenosis. The low number of discrete trace fossils indicates soupy to very soft substrates. The shallow bioturbation and small burrow sizes suggest low oxygenation. The areas with high bioturbation index points towards an environment with relatively low sedimentation rates and absence of event beds.

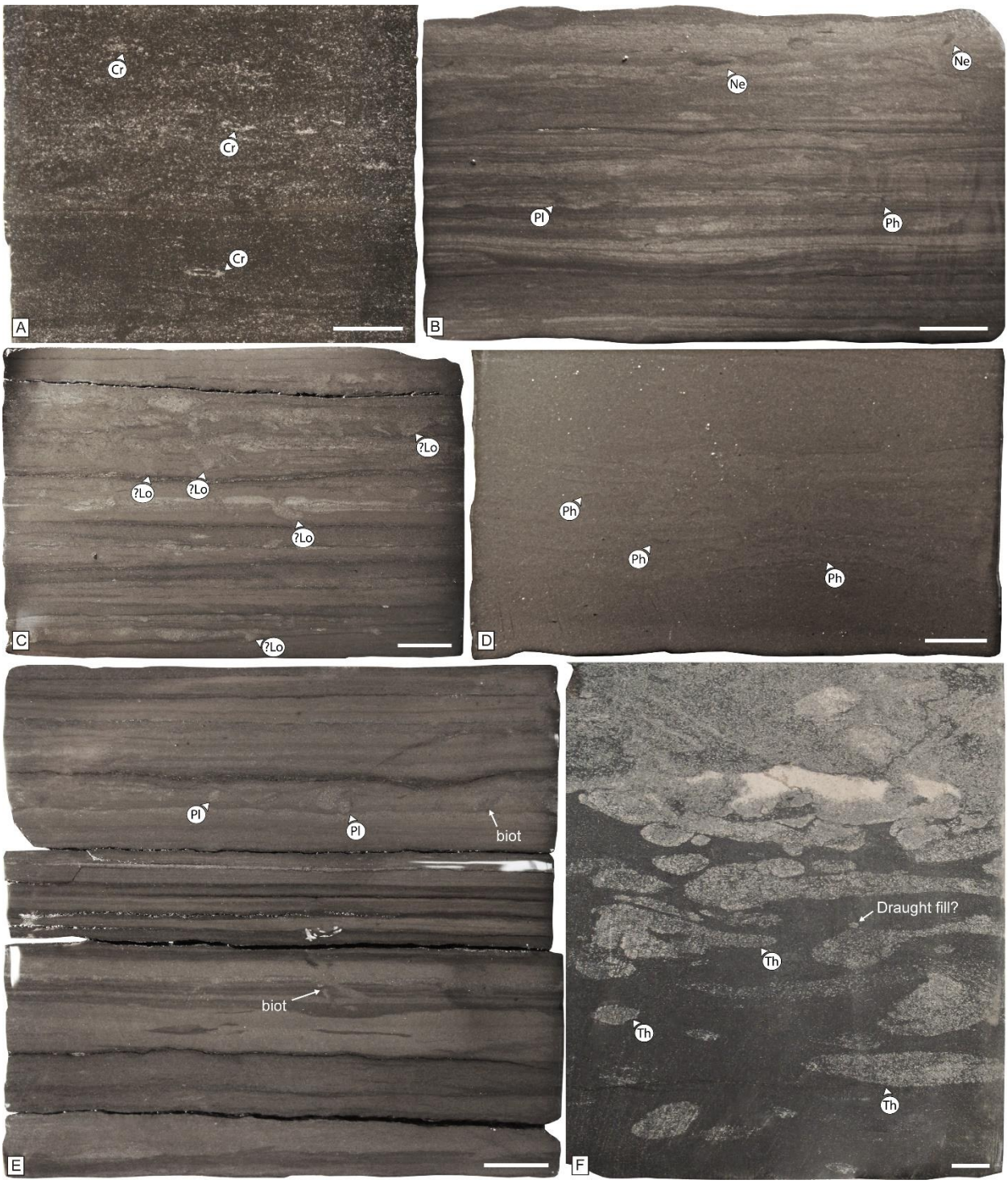

Fig. 5.17: Other ichnocoenoses of the Vaca Muerta Formation. A) Highly bioturbated intervals of the *Palaeophycus heberti-Crininicaminus* isp. ichnocoenosis, with *Crininicaminus* isp. (Cr). B) *Nereites* isp. ichnocoenosis characterized by *Nereites* isp. (Ne), *Phycosiphon incertum* (Ph), and *Planolites* isp. (Pl) in parallel-laminated calcareous mudstone. C) Equilibrichnia-Fugichnia ichnocoenosis displaying cylindrical and conical-shaped structures referred to as ?*Lockeia* isp. in thin-bedded calcareous mudstone. D)

Planolites isp. ichnocoenosis displaying *Phycosiphon incertum* (Ph), associated with hemipelagic deposits. E) *Thalassinoides* isp. ichnocoenosis (*Glossifungites* Ichnofacies) in massive mudstone passively infilled by overlying intraclastic mudstone. Note some possible draught fill canals within *Thalassinoides*. F) *Planolites* isp. ichnocoenosis showing *Planolites* isp. (Pl) and biodeformational structures (biot), associated with fluid mud deposits. Scale bars are 1 cm.

5.6.9 *Thalassinoides* isp. ichnocoenosis

It is composed by shallow to deep tier, sharp-walled, uncompacted *Thalassinoides* isp. (Fig. 5.17F). Bioturbation index is 2-3, mean PD is 89.15 mm (n=9), and mean burrow diameter is 15.08 mm (n=12). This ichnocoenosis has been observed at the base of sediment-gravity flow or lag deposits, encased in mixed mudstone or intraclastic wackestone.

The development of sharp walls and lack of compaction in burrows suggest firmground conditions associated with the development of the *Glossifungites* Ichnofacies. This occurs as a response of early cementation typical of carbonate depositional environments (Curran, 2007) or erosion and subsequent colonization of consolidated muds (MacEachern *et al*., 1992).

5.7 Paleoenvironmental distribution of ichnocoenoses

The ichnocoenoses are restricted to different facies associations depending on palaeoecological conditions associated with the different depositional environments (Fig. 5.18, 5.19). The marginal-marine facies association (FA1) shows trace fossils in the bay deposits, included in the *Teichichnus rectus-Phycosiphon incertum* (ORI 4) and the *Thalassinoides* isp. ichnocoenoses, with some occurrences of the *Alcyonidiopsis longobardiae* and *Teichichnus rectus* ichnocoenoses (ORIs 2 and 3, Fig. 5.19A). This indicates a dominantly oxic environment and soupy to very soft substrates, interrupted by high-energy events generating firmgrounds and rare dysoxic and anoxic conditions. The basin facies association (FA2) displays unbioturbated intervals interrupted by successions containing the *Coprulus oblongus*, *Alcyonidiopsis longobardiae*, *Teichichnus rectus*, and *Teichichnus rectus-Phycosiphon incertum* ichnocoenoses (ORIs 1 to 4), and minor *Palaeophycus heberti–Crininicaminus* isp. and *Thalassinoides* isp. ichnocoenoses (Fig. 5.19B, C). This suggests common anoxic conditions with soupy to very soft substrates that regularly switched to dysoxic and oxic, and the activity of high-energy events that exhumed previously deposited mud.

The drift facies association (FA3) has alternations of the *Palaeophycus heberti–Crininicaminus* isp., *Nereites* isp., and Equilibrichnia–Fugichnia ichnocoenoses (Fig. 5.19B, Paz *et al.*, in review b). Rare *Thalassinoides* isp. ichnocoenosis, and *Teichichnus rectus* and *Teichichnus rectus-Phycosiphon incertum* ichnocoenoses (ORIs 3 and 4) also occur. These characteristics points toward high contour current activity maintaining upper dysoxic to oxic conditions at the seafloor (Paz *et al.*, in review b). Soft substrates are suggested by the high preservation of discrete trace fossils. The slope facies association (FA4) shows dominantly unbioturbated beds in the most distal successions and the *Planolites* ichnocoenosis in the most proximal intervals. *Coprulus oblongus*, *Alcyonidiopsis longobardiae*, *Teichichnus rectus* (ORIs 1 to 3), and Equilibrichnia–Fugichnia ichnocoenoses are subordinate (Fig. 5.19C). This indicates a distal to proximal, anoxic to oxic gradient, and low sedimentation rates associated with hemipelagic and fluid mud sedimentation with soft to soupy substrates. The outer ramp facies association (FA5) comprises *Teichichnus rectus-Phycosiphon incertum* ichnocoenosis (ORI 4) and the *Thalassinoides* isp. ichnocoenosis, which suggests oxic environments and soft to soupy substrates interrupted by high-energy events producing firmgrounds (Fig. 5.19D).

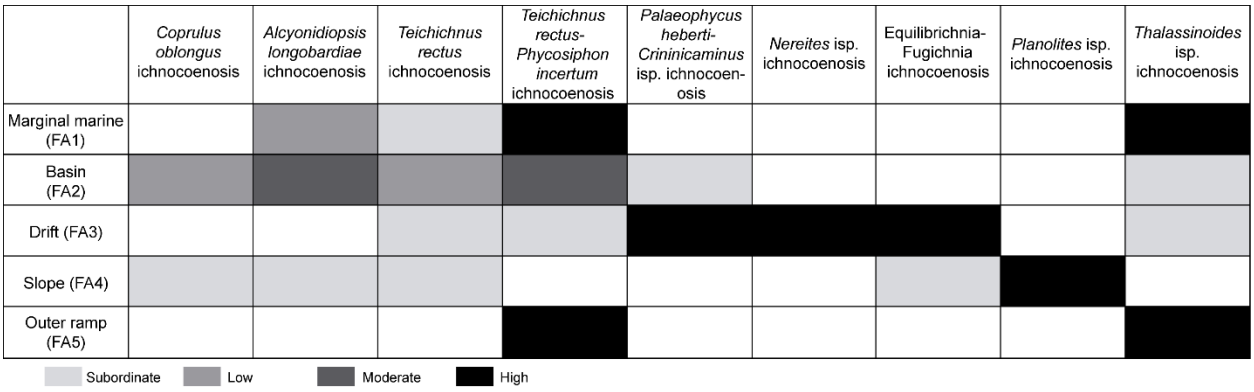

Fig. 5.18: Relative abundance of the ichnocoenoses within the different facies associations.

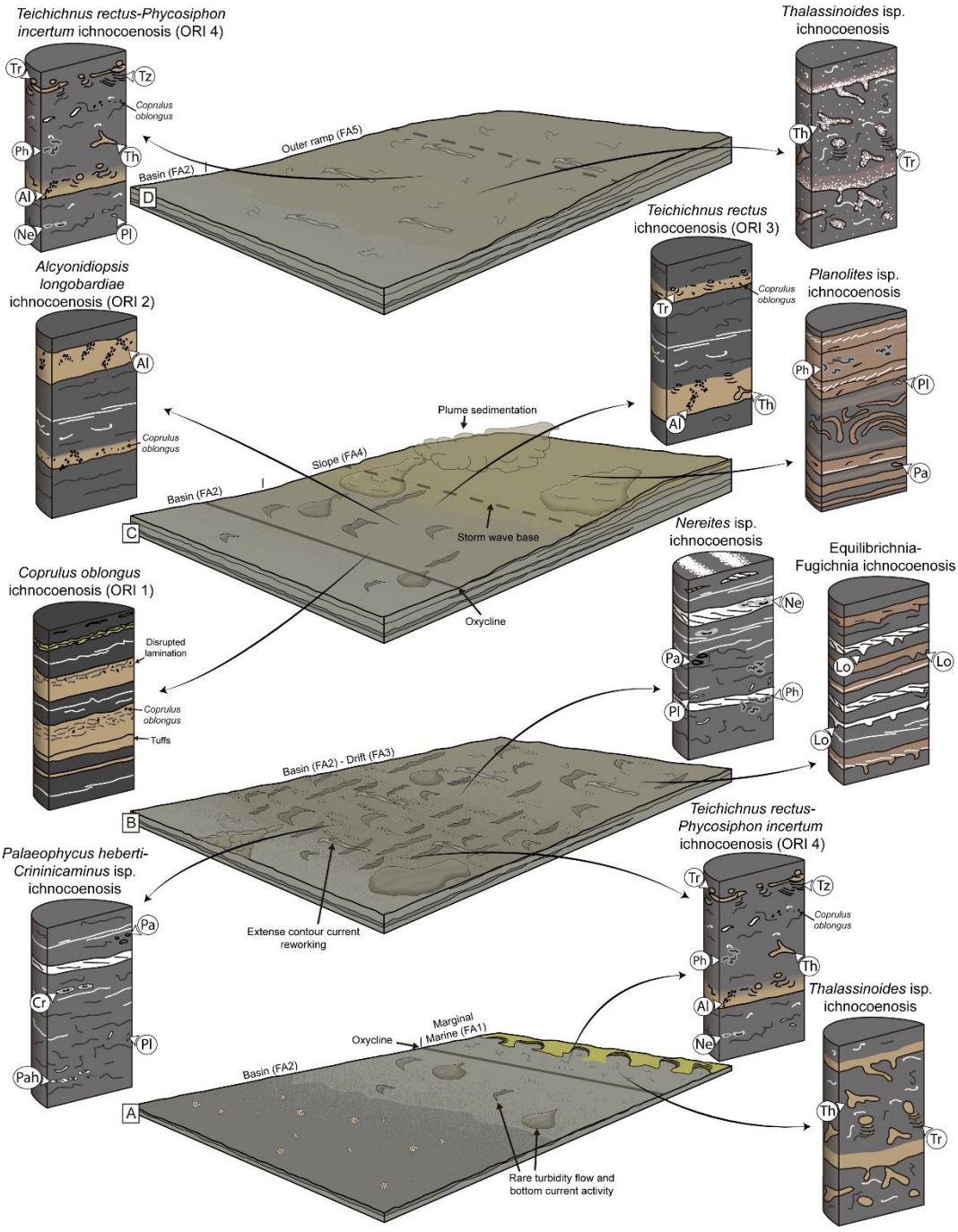

Fig. 5.19: Block diagram summarizing the environmental distribution of trace fossils during different stages of the clinoform. A) Transgressive hemicycle of the base of the Vaca Muerta Formation, associated with the development of marginal-marine facies associations (FA1). B) Times of weakened estuarine to anti-estuarine circulation in the Neuquén Basin, generating extensive ventilation and contour current reworking. C) Times of estuarine circulation, with the establishment of oxygen-deficient conditions. Slope environments are also observed due to progradation of the clinoform system. D) Ramp environments observed in the area without clinoform development. Ichnocoenoses show *Alcyonidiopsis longobardiae*

(Al), *Crininicaminus* isp. (Cr), ?*Lockeia* isp. (Lo), *Palaeophycus* isp. (Pa), *Palaeophycus heberti* (Pah), *Phycosiphon incertum* (Ph), *Planolites* isp. (Pl), *Nereites* isp. (Ne), *Teichichnus rectus* (Tr), *T. zigzag* (Tz), and *Thalassinoides* isp. (Th).

5.8 Paleoenvironmental Controls

Integration of sedimentologic and ichnologic datasets allowed delineation of paleoenvironmental controls along the clinoform system of the Vaca Muerta Formation. Substrate consistency, oxygen, food supply, and salinity are evaluated as controlling factors on trace-fossil distribution. For an in-depth explanation of paleoenvironmental implications associated with the drift deposits (FA3), see Chapter 7 and Paz *et al.* (in review b).

5.8.1 Substrate consistency

The overwhelming dominance of biodeformational structures and the paucity of discrete ichnotaxa in most of the mudstone lithologies of FA1, FA2 and FA5 suggests dominant soupgrounds or very softgrounds associated with pelagic and minor hemipelagic deposition in the clinoform bottomset. Thixotropy of the sediment and a lack of sediment contrast resulting in burrow mottling with no discrete traces have been recorded in modern fine-grained environments (e.g. California Borderland Basins, Edwards, 1985). In FA4, the occurrence of biodeformational structures also indicates soupy substrate consistency, yet in this case associated with hemipelagic and fluid mud sedimentation in the foreset of the clinoform. Studies on modern highly mobile fluid mud deposits suggest that unstable substrates in addition to low food availability are the main paleoecologic controls for organisms in these environments (Aller and Aller, 1986).

Departures of the typical soupgrounds occur during high-energy events and ash deposition. In the first case, reworking of the uppermost layers by autogenic processes resulted in erosional exhumation of previously buried and compacted sediment. Subsequent colonization of this exhumed sediment allows formation of trace-fossil suites representative of the firmground *Glossifungites* Ichnofacies (*Thalassinoides* isp. ichnocoenosis). In the second example, deposition of ash switched substrates to soft and stiffgrounds due to a coarser lithology and early cementation, promoting the emplacement of discrete trace fossils that delineate the ORIs (*Coprulus oblongus*,

Alcyonidiopsis longobardiae, Teichichnus rectus, and *Teichichnus rectus-Phycosiphon incertum* ichnocoenoses).

Although lithologic interfaces tend to enhance visibility, absence of discrete trace fossils in the Vaca Muerta Formation cannot be explained simply by the lack of adequate sediment contrast. Biodeformational structures are encountered in bioturbated crinoidal mudstone, where discrete trace fossils are also restricted to tuffs, suggesting that discrete trace fossils were not emplaced in intervals with contrasting sediment (crinoids). In the Paleogene of Denmark, a situation similar to the Vaca Muerta Formation has been recorded (Pedersen, 1981). There, parallel-laminated diatomites composed of alternating white, diatom-rich and brownish, clay-rich laminae are replaced by bioturbated, structureless diatomite. Trace fossils, such as *Teichichnus, Planolites, Chondrites* and *Taenidium*, occur in tuff deposits that are interbedded within the structureless diatomite (Pedersen, 1981). The fact that trace fossils are restricted to tuff intervals even though sediment contrasts existed in the primary deposit (laminated white and brown diatomite) precludes the idea of sediment contrast as a control on trace-fossil distribution (yet the contrary was interpreted, see Pedersen, 1981).

5.8.2 Oxygen

The increase in bioturbation index, penetration depth, burrow size, and ichnodiversity from ORIs 1 to 4 (*Coprulus oblongus, Alcyonidiopsis longobardiae, Teichichnus rectus,* and *Teichichnus rectus-Phycosiphon incertum* ichnocoenoses) indicates that oxygen controlled the development of these ichnocoenoses (Table 5.1). Because discrete trace fossils of the ORIs are correlated with the BI (and rock fabric) in the enclosing mudstone (Fig. 5.4, 5.5, Table 5.1), both ORIs and the BI can delineate oxygen levels along the sections. The model that follows is one of a single community of organisms generating biodeformational structures (without specialized behavior) in the mud-rich seafloor (soupgrounds), that produced discrete trace fossils after deposition of the ash layer (soft to stiffgrounds) under similar bottom water oxygen levels (Fig. 5.20). Consequently, the parallel-laminated fabrics depict the absence of bioturbation during times of anoxia. In the dysoxic intervals, the irregular-laminated fabric are generated by shallow-tier biodeformational structures followed by compaction and realignment of grains during diagenesis. Massive intervals indicate complete homogenization of the background sediment and dominance of biodeformational structures during upper dysoxic to oxic conditions (Fig. 5.20).

Similar to the Vaca Muerta Formation, ichnologic models from oxygen-deficient ancient successions record a decrease in burrow size and penetration (or bioturbation) depth as bottom water oxygen levels decrease (Savrda and Bottjer, 1986, 1991). Size reduction in animals represents a well-known strategy to cope with low oxygen levels (Forbes and Lopez, 1990; Rumohr *et al.* 1996; Levin, 2003) that has been also reported in trace fossils (Savrda *et al.*, 1984). In the case of penetration depth, organisms are restricted to live epifaunally to avoid burrowing due to a downward gradient of decreasing oxygenation and increasing toxicity caused by hydrogen sulphide in the sediment. A switch of infaunal organisms to epifaunal modes of life is a typical behavior of organisms to cope with decreasing oxygen levels observed in modern environments (Tyson and Pearson, 1991; Díaz and Rosenberg, 1995; Smith *et al.*, 2000).

Contrary to previous studies, we suggest that anoxic conditions of the Vaca Muerta Formation were punctuated by several dysoxic and oxic events. For example, geochemical data in the bay succession of the basal marginal-marine facies association (FA1) suggest deposition under anoxic to euxinic conditions (Spalletti *et al.*, 2014; Capelli *et al.*, 2018; Krim *et al.*, 2019), yet trace fossils indicate that oxic conditions dominated most of the time (47%), and dysoxic (33%) and anoxic (20%) were subordinate (Fig. 5.19A). After the deposition of FA1, the marine clinoform system was developed, and anoxia was dominant due to basin-wide estuarine circulation (Fig. 5.19C). Therefore, the basin (FA2) was mostly anoxic (93%), with rare dysoxic events (7%). Oxygenation in the slope (FA4) depended on the location within the foreset, with distal positions displaying dominantly dysoxic (60%) and anoxic (37%) conditions, and proximal areas mainly deposited under dysoxic (58%) and oxic (40%) conditions. However, basin-wide estuarine circulation was interrupted by times of bottom water ventilation caused by a switch to weakened estuarine or anti-estuarine circulation (Paz *et al.*, in review a). This switch was controlled by climatic oscillations, with cooler climates increasing the amount of dense water cascading from the shelf and generating extensive bottom (contour) current activity in the bottomset and foreset of the clinoform system (Paz *et al.*, in review a). Hence, during anti-estuarine circulation, oxygen content in the basin (FA2) increased, with a higher participation of dysoxic (47%) and oxic (10%) events, although anoxia was still pervasive (43%, Fig. 5.19B). Drift deposits (FA3) are difficult to evaluate in terms of oxygenation because many other paleoecological controls restricted trace fossil emplacement, yet most of these were deposited under upper dysoxic to oxic conditions. In

Units 4 and 5, the outer ramp facies association (FA5) was mainly affected by oxic (82%) and dysoxic (16%) conditions (Fig. 5.19D).

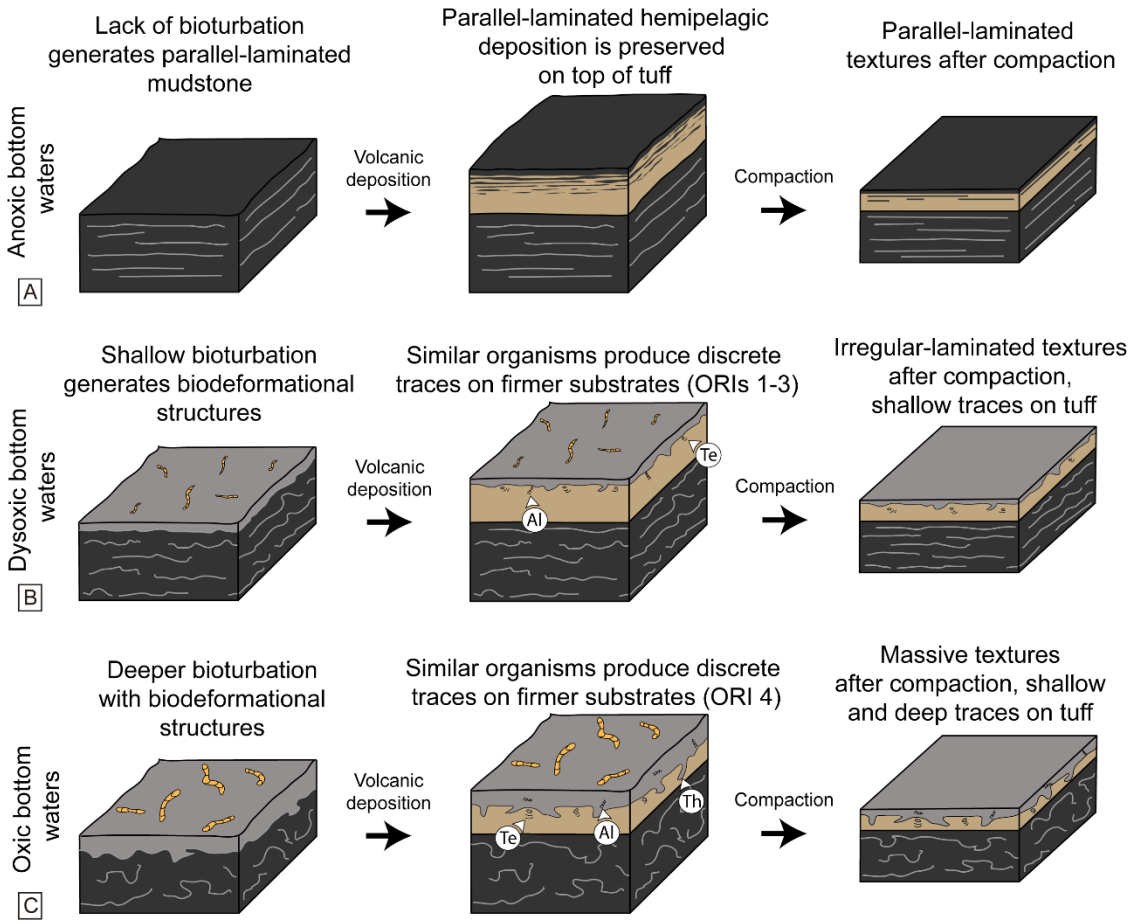

Fig. 5.20: Inferred mechanisms of trace-fossil preservation in tuffs of the Vaca Muerta Formation. Trace fossils are restricted to tuff intervals due to a change in substrate consistency. A) Anoxic bottom waters preclude bioturbation in both mudstone and tuff, generating preservation of parallel lamination on top of tuff and parallel-laminated fabrics after compaction. B) Shallow biodeformational structures are common in the mudstone deposited under dysoxic bottom waters due to a lack of specialized feeding in a food-rich environment. Organisms generate discrete traces (ORIs 1-3) in firmer deposits (tuffs). The rock lamination increases after compaction due to realignment of grains and the mudstone will show irregular-laminated fabrics. C) Biodeformational structures showing a deeper bioturbation depth occur under oxic conditions (ORI 4). Similarly, organisms produce discrete traces on firmer substrates, but compaction does not generate laminated fabrics. In this case, the mudstone preserve massive fabrics indicative of extensive bioturbation.

5.8.3 Food supply

The ichnologic content of the Vaca Muerta Formation in the study area differs from other oxygen-deficient ichnofaunas in the paucity of *Chondrites* and *Zoophycos* (Bromley and Ekdale, 1984; Savrda and Bottjer, 1986, 1991; Ekdale and Mason, 1988; Sageman 1989, Sageman *et al.*, 1991; Savrda, 1992). Both trace fossils represent typical elements of monospecific or low-diversity trace-fossil assemblages suggesting bottom water dysoxia (Bromley and Ekdale, 1984; Ekdale and Mason, 1988). A high food input throughout the deposition of the formation can explain the scarcity of these trace fossils. The high TOC content of the Vaca Muerta Formation (av. TOC of 4.76%, N=182 in FA2; general av. TOC of 5% to a maximum of 31%, Minisini *et al.*, 2020b), and the abundance of biodeformational structures and absence of a tiering structure in homogeneous mudstone, suggest a lack of specialized feeding strategies in food-rich environments (Wetzel, 1991). This agrees with the interpretation of *Zoophycos* as a cache trace fossil associated with fluctuating food content (Bromley, 1991; Löwemark, 2015; Dorador *et al.*, 2016), and *Chondrites* as a specialized feeding, chemosymbiotic or farming structure (Fu, 1991; Bromley, 1991; Baucon *et al.*, 2020). A similar ichnofauna has been recorded in the upwelling zone off Vietnam, where biodeformational structures dominated during glacial periods due to high food conditions (Wetzel, 1991; Wetzel *et al.*, 2011). The high-food conditions of the Formation were punctuated by times of food-starved conditions represented by the tuff intervals (Wetzel, 2009), in which case discrete trace fossils with tiering occur.

5.8.4 Salinity

Salinity is inferred to have been a limiting factor in the marginal-marine embayments represented in the lowermost strata of the Vaca Muerta Formation (FA1). In contrast, evidence for its role elsewhere is somewhat ambiguous. In the study area, a monospecific suite of *Teichichnus* is the most typical expression of the *Teichichnus rectus* and *Teichichnus rectus-Phycosiphon incertum* ichnocoenoses, with *Alcyonidiopsis*, *Planolites* and *Thalassinoides* being minor components. A relatively restricted connection with the Pacific Ocean could be responsible for the decrease in ichnodiversity and the replacement of typical open marine ichnogenera (*Chondrites*, *Zoophycos*) by facies-crossing trace fossils encountered in marginal-marine environments (e.g. *Teichichnus*, *Planolites*, *Thalassinoides*; MacEachern and Pemberton, 1994; Buatois and Mángano, 2011). Furthermore, river-derived hyperpycnites in distal environments may suggest decreased salinity

by fluvial input (Paz *et al.*, 2019; Otharán *et al.*, 2020). In contrast, Gasparini and Fernández (2005) suggested fully marine salinity levels for the Vaca Muerta Formation based on the high diversity of marine reptiles. Paleosalinities in the northern Neuquén Basin calculated from oxygen isotopes in oyster shells showed values of 31-35% (euhaline; Gómez-Dacal, 2017). Samples from the upper part of the Vaca Muerta Formation displayed values of 22-29%, yet they were attributed to a sea-level fall generating regression and a higher influence of marginal-marine environments (Lazo *et al.*, 2008). An explanation to the varied salinity interpretations might be the embayed morphology of the Neuquén Basin, which controls salinity depending on the proximity to the strait connecting to the Pacific Ocean. The present study is focused on the central Neuquén Basin, whereas the situation might be different with respect to those in the northern areas that are closer to the strait (Mendoza Province), where *Chondrites* has been described (Doyle *et al.*, 2005).

5.9 Discussion

5.9.1 Comparison with ichnologic datasets of other oxygen-deficient, fine-grained successions

As previously mentioned, the scarcity of *Chondrites* and *Zoophycos*, typical components of oxygen-deficient ichnofaunas (Bromley and Ekdale, 1984; Savrda and Bottjer, 1986, 1991; Ekdale and Mason, 1988; Sageman, 1989, Sageman *et al.*, 1991; Savrda, 1992), is striking in the Vaca Muerta Formation. By the Jurassic, a highly diverse ichnofauna associated with high levels of bioturbation occurred in offshore environments as part of the Mesozoic Marine Revolution (Buatois *et al.*, 2016). When observed in monospecific or low-diversity suites, *Chondrites* is regarded as a ubiquitous trace fossil of oxygen-deficient environments (Bromley and Ekdale, 1984). In particular, it has been recorded in several Jurassic, shallow-marine (~0-300 m water depth), fine-grained sedimentary environments (e.g. Savrda and Bottjer, 1989a; Wignall, 1991; Moghadam and Paul, 2000; Olóriz and Rodríguez-Tovar, 2002; Martin, 2004; Šimo and Tomašových, 2013; Leonowicz, 2015; Campetella *et al.*, 2020). *Zoophycos* is a less common component of oxygen-deficient ichnofaunas, probably due to a lower tolerance to anoxia (Bromley and Ekdale, 1984), occurring by the Jurassic in lower shelf and slope environments (Tyszka, 1994; Šimo and Tomašových, 2013; Zhang *et al.*, 2015; Mekki *et al.*, 2019). Similarly, during the Cretaceous, *Chondrites* and *Zoophycos* were described in oxygen-deficient, shallow to deep marine settings (Ekdale, 1985; Savrda and Bottjer, 1989b; Buatois and López Angriman, 1992;

Rodríguez-Tovar *et al.*, 2009; Monaco *et al.*, 2012; Uchman *et al.*, 2013; Richiano, 2014; Bayet-Goll *et al.*, 2016; Gilbert *et al.*, 2019), whereas in some cases oxygen-deficient environments lack *Zoophycos* but host *Chondrites* (e.g. Uchman *et al.*, 2008).

The ichnologic composition of the Vaca Muerta Formation supports the idea of an oxygen-controlled ichnofauna developed under a high food scenario, and favors comparison with modern examples showing abundant biodeformational structures (e.g. Behl, 1995; Wetzel *et al.*, 2011). A closer fossil counterpart would be the Paleogene of Denmark, where intercalated tuffs within homogeneous, bioturbated diatomites show *Teichichnus*, *Planolites*, *Chondrites*, and *Taenidium* (Pedersen, 1981). There is a clear need to evaluate fine-grained successions subject to oxygen deficiency with consideration of other paleoecologic controls (e.g. food, salinity, substrate consistency; e.g. Wignall, 1993) in order to understand the effect of each control on trace fossil distribution. On the other hand, the evolution of oxygen-depleted settings through time (Mángano, 2011; Buatois and Mángano, 2011; Mángano and Buatois, 2016) is a topic that has been poorly explored and might explain the distinct ichnologic model inferred for the Vaca Muerta Formation.

5.9.2 Pellet-rich ichnocoenoses in modern and ancient fine-grained successions

The Vaca Muerta Formation shows a clear oxygen gradient from anoxic to oxic conditions as revealed by the ORIs documenting this transition. Whereas ORIs 3 and 4 are characterized by several discrete trace fossils, ORIs 1 and 2 mostly comprise disorganized benthic pellets (*Coprulus oblongus*) and pellet-rich burrows (*Alcyonidiopsis longobardiae*). ORI 1 is interpreted as recording the activity of meiofauna to small macrofauna generating disturbed lamination at the top of tuffs (cryptobioturbation). The record of an upwards gradation at a mm-scale from undisturbed laminae, to disturbed irregular lamination (similar to ORI 1), to *Alcyonidiopsis longobardiae* (characteristic of ORI 2) in some tuff deposits showing frozen tier profiles (Fig. 5.16A), suggests that ORI 1 represents the most severe dysoxic conditions in the anoxic-dysoxic gradient. In Pliocene sapropels, Löhr and Kennedy (2015) have found a cm-scale, upward gradation from anoxic to dysoxic areas consisting of (1) parallel-laminated, unbioturbated deposits, (2) fragmented and deformed organic-rich laminae and less abundant benthic pellets produced by meiofauna to small macrofauna (comparable to ORI 1), and (3) pelletized intervals (comparable to ORI 2), indicating that the Vaca Muerta Formation might be similar to this example. Meiofauna thrives in dysoxic environments of modern basins, usually showing a higher tolerance to hypoxia than macrofauna

(Elmgren, 1975; Josefson and Widbom, 1988; Sergeeva and Zaika, 2013). Hence, they are expected to be the first organisms to occur in the transition from unbioturbated anoxic to bioturbated dysoxic sediments.

Less severe dysoxia is then represented by ORI 2, a pellet-rich ichnocoenosis produced by small macrofauna- to meiofauna-sized polychaetes. The fact that ORI 2 occurs under lower dysoxic conditions is supported by (1) irregular laminae preservation in the encasing, compacted mudstone, (2) the smallest trace-fossil diameters locally associated with *Alcyonidiopsis*, and (3) the epifaunal mode of life of the *Alcyonidiopsis* producer. The resilience of ORI 2 as expressed in most of the cores and through the succession may suggest persistent or periodic dysoxic conditions generating a reduced but stable, low oxygen-adapted community (Díaz and Rosenberg, 1995). However, the relative scarcity of ORI 2 compared with ORI 4 reflects the specific oxygen tolerance of this community at the edge of anoxic zones.

Cuomo and Rhoads (1987) and Cuomo and Bartholomew (1991) suggested that highly pelletized, sediments (coprolitic laminations) caused by benthic polychaete communities occur at the dysoxic-anoxic transition of modern and ancient environments. However, this ichnocoenosis has not been extensively recognized in later studies of fossil successions probably because of the difficulty of visualizing pellets in ancient black shales. Compaction typically precludes preservation of these pelletized beds (Friis, 1995). For example, a population of small (~2 cm long, 2 mm wide) surface feeding capitellid polychaetes can generate small-scale burrowing and bed pelletization in uncompacted strata, yet when thin sections of the same sediments are compacted and dewatered (40-60% decrease in volume), lamination is preserved with no bioturbation structures (Cuomo and Rhoads, 1987). Similar polychaete pellet-rich beds have been found in the oxygen-deficient Santa Barbara Basin of California (Emery and Hülsemann, 1962), in the Peruvian upwelling zone (Brodie and Kemp 1994, 1995), and in Pliocene sapropels from the Mediterranean Sea (Löhr and Kennedy, 2015; Löhr *et al.*, 2018). Frozen tier profiles of the Miocene Monterey Formation also suggest polychaete pelletization occur at the lower dysoxic end (Savrda and Ozalas, 1993). In the Vaca Muerta Formation, preservation within tuff intervals allowed identification of this ORI. *Coprulus oblongus* type A are in the size range of the fresh polychaete pellets of Cuomo and Rhoads (1987) and of the pellets type B of Löhr and Kennedy (2015), whereas *Coprulus oblongus* type B can be compared with the crushed diatom and clay pellets of Brodie and Kemp (1995).

Many of the ideas proposed by Cuomo and Rhoads (1987) are supported by our study. Compaction precludes preservation of the pellets in ancient deposits because pellets can be observed at the base of the tuff, but they cannot be delineated in the encasing mudstone. Moreover, the epifaunal to shallow infaunal mode of life proposed to enhance laminae preservation (Cuomo and Rhoads, 1987) is supported by the dump strategy of the *Alcyonidiopsis* producer. It is also confirmed that pellets occur in relatively high abundances (e.g. Fig. 5.13G), probably due to high reproduction of pioneering stage communities, as it has been shown in experiments (Cuomo and Rhoads, 1987) and studies of modern environments (Emery and Hülsemann, 1962; Nittrouer *et al.* 1998; Bentley and Nittrouer, 1999).

Although the response of benthic communities to dysoxia is highly variable, observations in modern oxygen-deficient environments support the idea of polychaetes as producers of the pellet-rich ichnocoenoses (Cuomo and Bartholomew, 1991; Diaz and Rosenberg, 1995). Polychaetes tolerate lower oxygen concentrations compared with normal macrofauna and occur in high abundances at the oxic-anoxic transitions of oxygen-deficient restricted basins (Baltic Sea, Rumohr *et al.* 1996; Black Sea, Zaika and Sergeeva, 2012; Santa Cruz Basin, USA, Edwards, 1985) and upwelling systems (California, USA, Mullins *et al.*, 1985; Thompson *et al.*, 1985; Chile and Peru, Rosenberg *et al.*, 1983; Gallardo *et al.*, 2004; Pakistan, Levin *et al.*, 2009). Ovoid pellet-rich beds attributed to polychaetes living at dysoxic conditions were recorded in restricted deep-marine basins (Emery and Hülsemann, 1962), upwelling systems (Bremner, 1983; Brodie and Kemp, 1995), and shallow bays (Nittrouer *et al.*, 1998; Bentley and Nittrouer, 1999), in many cases associated with low intensities of bioturbation. The polychaetes have many strategies to cope with low oxygen levels, such as cessation of feeding and burrowing, emergence from burrows, and switching to anaerobic respiration (Diaz and Rosenberg, 1995 and references therein).

5.9.3 Implications for ichnologic analyses in fine-grained successions

The present study highlights the need to understand the relationship between event beds and rock fabric in fine-grained successions, where the lack of sediment contrast, abundance of dark-colored, homogeneous successions and occurrence of poorly defined biodeformational structures may prevent interpretation of benthic oxygen levels. In the Vaca Muerta Formation, a direct correlation occurs between the trace fossils recorded in the tuff deposits and the BI (and rock fabric) of the encasing mudstone (Table 5.1), indicating that rock fabric evaluation is useful to delineate bottom

water paleoxygen. The fact that ash deposition was dominantly by suspension fallout supports the idea of the recovery of the resident ichnofauna rather than an alternative community colonizing the tuffs (Wetzel, 2009).

The existence of a lower dysaerobic community composed by meiofauna to small macrofaunal polychaetes generating disturbed lamination (ORIs 1 and 2), indicates that biogenic reworking by small-sized organisms can generate irregular-laminated or parallel-laminated mudstone fabrics (Fig. 5.4B, 5.5A, 5.20B), which after compaction may be indistinguishable from parallel-laminated, unbioturbated intervals (i.e. cryptobioturbation). In fact, in the Vaca Muerta Formation, ORI 1 and 2 occur 58-78% of the time in parallel-laminated intervals. Polychaete communities can preserve laminations in some modern environments (Calvert, 1964; Douglas, 1981; Levin *et al.*, 2009), and the creation of an irregular-laminated sediment fabric represents the transition between laminated and massive (bioturbated) fabrics (e.g. Behl, 1995; Bahk *et al.*, 2000). In other ancient deposits, this irregular-laminated mudstone has been recognized and assigned to dysoxic conditions (e.g. Wilson and Schieber, 2015).

Event bed and rock fabric evaluation may help in future ichnologic analyses of fine-grained successions, where the biogenicity criteria for meiofaunal trace fossils have been debated (cf. Egenhoff and Fishman, 2013; Schieber, 2014; Schieber *et al.*, in press). Because encasing beds are related with bioturbation in the homogeneous mudstone, an evaluation of the crosscutting relationships with intercalated laminae and beds should always be integrated to the analysis in order to claim biogenicity of burrows (e.g. Whitham, 1993; Brodie and Kemp, 1995; Löhr *et al.*, 2015; Wilson and Schieber, 2015). A similar statement could be said for the origin of pellets. For example, pellets of benthic origin described from thin sections are of organic matter- and clay-rich composition (e.g. Wilson and Schieber, 2015; Milliken *et al.*, 2019), yet *Coprulus oblongus* type B of the Vaca Muerta Formation show very low amounts of clays (minor mud floccules) and high concentration of microcrystalline quartz. Pellet origin should not be solely inferred from composition or shape (Cuomo and Bartholomew, 1991; Brodie and Kemp, 1995), because selective deposit feeders can show a preference for planktonic biogenic material, generating an enrichment in planktonic tests (Cuomo and Bartholomew, 1991), whereas zooplankton pellets could display high concentration of clays in areas of abundant suspended terrigenous sediment (Dunbar and Berger, 1981). Summarizing, evaluation of rock fabric can be a powerful tool to understand bioturbation in homogeneous mudstone successions that were typically out-of-reach in

ichnologic analyses due to the difficulty in delineating discrete trace fossils, and the existence of indistinct burrows of problematic ichnotaxonomic treatment.

5.10 Conclusions

The Vaca Muerta Formation comprises marginal-marine (FA1), basin (FA2), drift (FA3), slope (FA4), and outer ramp (FA5) environments of a mixed carbonate-siliciclastic, subaqueous clinoform system. The ichnologic analysis suggests the existence of discrete trace fossils, biodepositional structures and biodeformational structures. Trace fossils and biodepositional structures can be subdivided into nine ichnocoenoses, with four associated with an oxygen control (oxygen-related ichnocoenoses, ORI). In the ORIs, trace fossils are developed in tuff intervals, whereas the enclosing mudstone shows parallel-laminated, irregular-laminated, and massive fabrics produced by biodeformational structures. The *Coprulus oblongus* ichnocoenosis (ORI 1) is represented by randomly disposed *Coprulus oblongus,* planktonic pellets and pelagic aggregates. The *Alcyonidiopsis longobardiae* ichnocoenosis (ORI 2) comprises *Alcyonidiopsis longobardiae*, *Coprulus oblongus* and funnel-shaped biodeformational structures. The *Teichichnus rectus* ichnocoenosis (ORI 3) consists of *Teichichnus rectus, Planolites* isp., *Thalassinoides* isp., mantle and swirl structures and *Coprulus oblongus*. The *Teichichnus rectus-Phycosiphon incertum* ichnocoenosis (ORI 4) is represented by *Teichichnus rectus, Alcyonidiopsis longobardiae, Coprulus oblongus, Phycosiphon incertum, Planolites* isp., *Teichichnus zigzag, Thalassinoides* isp., and *Nereites* isp. Other ichnocoenoses are the *Palaeophycus heberti–Crininicaminus* isp., *Nereites* isp., Equilibrichnia–Fugichnia, *Planolites* isp., and *Thalassinoides* isp. ichnocoenoses.
The ichnologic analysis recognized different palaeoecological controls that affected the ichnofauna. Soupy to very soft substrates promoted the formation of biodeformational structures in the mudstone, whereas discrete trace fossils occur after emplacement of tuffs, in soft to stiffgrounds (ORIs). Exhumation of previously deposited sediment under autogenic, high-energy events produced firmgrounds (*Thalassinoides* isp. ichnocoenosis). The ORIs reflect an increasing bioturbation index, penetration depth, burrow size and ichnodiversity, as a response to increasing benthic oxygen. In turn, oxygen levels were associated with the circulation of the basin (estuarine vs. weakened estuarine or anti-estuarine), which in turn controls the ventilation generated by bottom (contour) currents, and the distance from the shore. The Vaca Muerta ichnofauna differs

from the typical trace fossil assemblages of oxygen-deficient environments by the absence of *Chondrites* and rarity of *Zoophycos*, suggesting colonization in a food-rich seafloor. Moreover, two pellet-rich ichnocoenoses are described (ORIs 1 and 2), depicting meiofauna to small macrofauna biogenic reworking generating parallel-laminated and irregular-laminated deposits (cryptobioturbation) under severe, lower dysoxic conditions. The present analysis stress out the importance of evaluating bed disruption and rock fabric evaluation in homogeneous mudstone succession to understand palaeoxygen variations and recognize biogenicity of burrows and pellets.

5.11 Acknowledgments

We thank Chevron, Shell, Tiser S.R.L., Total Austral S.A., YPF for sharing core information with us. This work was financially supported by the Natural Sciences and Engineering Research Council (NSERC) Discovery Grant [422931-20] to L.A. Buatois, and [311727–20] to M.G. Mángano, PI-UNRN 2017 [40-A-616] and PIP-CONICET [11220170100129CO] to N.B. Carmona, 2016 Student Research Grant from Society for Sedimentary Geology (SEPM), 2016 and 2018 Research Grant from the Geological Society of America (GSA), 2016 Grants-in-Aid Program of the American Association of Petroleum Geologists (AAPG), and 2018 Postgraduate Grant from the International Association of Sedimentologists (IAS). M.G. Mángano acknowledges additional funding provided by the George J. McLeod Enhancement Chair in Geology.

TRANSITION

Chapters 4 and 5 describe the sedimentological and ichnological datasets of the Vaca Muerta Formation in the basin centre location. These studies revealed the presence of contour current activity during specific intervals of time associated with weakened estuarine or anti-estuarine circulation. Chapter 6 focuses on these contourite deposits, describing their sedimentological characteristics, evaluating the evidence to discard other processes, and discussing the origin of the circulation system.

CHAPTER 6: ORGANIC-RICH, FINE-GRAINED CONTOURITES IN AN EPICONTINENTAL BASIN, THE UPPER JURASSIC-LOWER CRETACEOUS VACA MUERTA FORMATION, ARGENTINA

Paz, M., Buatois, L.A., Mángano, M.G., Desjardins, P.R., Notta, R., González Tomassini, F., Carmona, N.B. and Minisini, D. (in review). Bottom current activity within an organic-rich clinoform system, Upper Jurassic-Lower Cretaceous Vaca Muerta Formation, Argentina. *Marine and Petroleum Geology*.

Abstract

Over the last few years, recognition and characterization of sedimentary processes in fine-grained successions is receiving considerable attention in part due to the increased importance of unconventional reservoirs. Recent sedimentologic analyses of these successions has revealed abundant traction transport structures that suggest bottom current activity of different origins. The present study constitutes a detailed sedimentological analysis of contour current deposits from the shallow marine, mixed carbonate-siliciclastic Upper Jurassic-Lower Cretaceous Vaca Muerta Formation (Neuquén Basin, Argentina). The study area comprises the Neuquén Embayment, where organic-rich, mixed carbonate-siliciclastic deposits can be differentiated into fifteen lithofacies occurring within five facies, namely fine to coarse mudstone with bindstone intraclasts, peloidal mudstone, crinoidal mudstone, fine to coarse mudstone, and fine to coarse mudstone interbedded with calcareous mudstone. The deposits show traction structures such as parallel lamination, ripple cross-lamination and cross-bedding. These intervals were deposited or influenced by contour currents showing long-term activity, low sediment concentration and generating long-term oxygen supply to the seafloor. Locally, some successions display an increasing to decreasing bioturbation intensity pattern that may have a similar origin to the bi-gradational sequence of contourites. This analysis supports the idea that contour currents are associated with high bioturbation levels, which controls the degree of preservation of traction structures and consequently the possibility to delineate these processes within hemipelagic, fine-grained successions. These currents were probably along-shore, occurring in relatively shallow

water as part of a weakened estuarine or anti-estuarine, basin-wide circulation system, intensified by the enhanced action of dense water cascading during arid and cooler climate periods.

6.1 Introduction

Contour currents represent processes that occur in open oceans (Flemming, 1980, 1981; Ramsay, 1994; Viana *et al.*, 1998, 2002; Liu *et al.*, 2006) and epicontinental basins (Sivkov *et al.*, 2002; Cattaneo *et al.*, 2003; Verdicchio and Trincardi, 2008a; Vandorpe *et al.*, 2011; Pellegrini *et al.*, 2016; Moros *et al.*, 2020), associated with wind- and thermohaline-induced circulation. Contourites are increasingly being analyzed in modern environments due to their importance for hydrocarbon exploration, palaeoceanographic and palaeoclimatological studies, and assessment of slope stability (Rebesco *et al.*, 2014). However, contourites are hard to delineate in ancient successions because of the difficulty of establishing a concrete facies model. This issue stems from the complexity associated with bottom current transport ("bottom current" constitute a generic term that includes processes such as thermohaline- and wind-driven contour currents, cascading and internal waves). For example, bottom current forcing mechanism can be mixed, precluding the usage of a precise nomenclature associated with the origin of the currents (Shanmugam, 2017). In addition, currents can interact with other processes, such as turbidity flows, generating a continuum between different processes and facies (Stow and Smillie, 2020).

More than ten years have passed since the paradigm shifted from fine-grained sediment deposited by fallout in low-energy environments, to interpretations of more variable energetic conditions at the seafloor (Macquaker and Bohacs, 2007; Schieber *et al.*, 2007). Traction structures, represented by silt laminae encased in mudstone and muddy current ripples, have been observed in numerous fossil examples of fine-grained depositional systems and interpreted as produced by bottom currents of various origins (e.g., Pratt, 1984; Schieber, 1994, 1999a, 2016; O´Brien, 1996; Loucks and Ruppel, 2007; Singh *et al.*, 2008; Trabucho-Alexandre *et al.*, 2012; Egenhoff and Fishman, 2013; Leonowicz, 2013; Nyhuis *et al.*, 2014; Birgenheier *et al.*, 2017; Li and Schieber, 2018; Minisini *et al.*, 2018). Particularly, silt laminae structures have been reproduced in flume experiments, representing current-ripple cross-laminated deposits created by bedload traction transport of mixed silt-mud loads (Yawar and Schieber, 2017). Documentation of ancient examples of contour currents in shallow, epicontinental seas include the Middle and Upper

Devonian of Canada (Knapp *et al.*, 2017; Ayranci *et al.*, 2018) and the Upper Jurassic of Texas (Frébourg *et al.*, 2013). Most of these examples share several similarities with the fine-grained succession analyzed in this contribution: they are composed of fine-grained sediments with high organic matter content, and they were deposited in oxygen-deficient seafloors in shallow seas. However, there are still several questions regarding these sedimentary deposits and the associated environmental controls. For example, the role of bioturbation and oxygen supply is debated (Shanmugam, 2013), the facies model of these currents in the shallow-water realm is not well-constrained (Stow and Faugères, 2008), and the likely origin or triggering factors are relatively unknown (Schieber, 2016).

The example studied herein comes from the Vaca Muerta Formation (Neuquén Basin, Argentina, Fig. 6.1), the hottest unconventional play outside North America (Minisini *et al.*, 2020b). This formation represents a shallow-marine, mixed carbonate-siliciclastic muddy clinoform system developed during the Late Jurassic-Early Cretaceous (Stipanicic, 1969; Leanza, 1973). It comprises mixed and calcareous mudstone, limestone and volcaniclastic beds, and is characterized by high total organic carbon (av. 3.2%, Brisson *et al.*, 2020). Sedimentologic analyses of this formation are numerous, comprising outcrop studies (Spalletti *et al.*, 2000; Kietzmann *et al.*, 2014a; Zeller *et al.*, 2015a; Ponce *et al.*, 2015; Krim *et al.*, 2017; Paz *et al.*, 2019; Otharán *et al.*, 2020) and core investigations (González Tomassini *et al.*, 2014; Desjardins *et al.*, 2018; Minisini *et al.*, 2020a). In addition, sedimentologic analysis and reservoir characterization have been carried out in the cores from the study area (Pose *et al.*, 2014; Repol *et al.*, 2014; Notta *et al.*, 2017, 2020; Desjardins and Aguirre, 2018; Gómez Rivarola and Borgnia, 2018; Estrada *et al.*, 2020; Minisini *et al.*, 2020a). Several authors have interpreted the activity of bottom currents of different origins in distal environments of the Vaca Muerta Formation from other outcrop locations (e.g. Gasparini *et al.*, 1997; Spalletti *et al.*, 1999; Scasso *et al.*, 2002; Kietzmann *et al.*, 2008; 2014a; Kietzmann and Palma, 2009b; Zeller *et al.*, 2015a; Rodríguez Blanco *et al.*, 2020). However, a detailed sedimentologic and sequence stratigraphic analysis of bottom current deposits is currently lacking. In addition, an explanation of their origin and triggering mechanisms have been previously proposed (Zeller *et al.*, 2015a; Reijenstein *et al.*, 2020; Rodríguez Blanco *et al.*, 2020), yet the present analysis review and refines this interpretation. In this study, the analysis focuses on five facies displaying traction structures and variable bioturbation intensity attributable to contour current activity. The objectives of the study are to characterize lithofacies, combine it

with ichnologic data to characterize facies, and interpret sedimentary processes and paleoecological controls associated with contour current activity. All of this data is analyzed in order to explore several lines of evidence that can be used to suggest contour current activity in fine-grained depositional systems, and to characterize the origin of the circulation system associated with the currents.

6.2. Geologic setting

The Neuquén Basin represents a triangular-shaped depocenter whose infill history is subdivided into three stages: syn-rift, back-arc and foreland (Howell *et al.*, 2005; Casadío and Montagna, 2015). The first stage occurred during the Late Triassic to Early Jurassic, comprising volcaniclastic and epiclastic continental sedimentation in several rift depocenters (Carbone *et al.*, 2011). The back-arc stage showed the establishment of Andean volcanism and extensive subsidence since the Early Jurassic, with multiple transgressions and regressions (Howell *et al.*, 2005; Casadío and Montagna, 2015). Finally, the foreland phase started during the Late Cretaceous after the closure of the marine connection of the basin with the Pacific Ocean, and was dominated by continental sedimentation (Tunik *et al.*, 2010).

The Vaca Muerta Formation represents a marine episode of the back-arc stage developed from late early Tithonian to early Valanginian (Leanza, 1973; Leanza *et al.*, 2011). This formation overlies the Kimmeridgian eolian, lacustrine and fluvial deposits of the Tordillo Formation (Spalletti *et al.*, 2011), and is capped transitionally by the upper Tithonian to early Valanginian, carbonate and siliciclastic nearshore deposits of the Quintuco Formation (Mitchum and Uliana, 1985). The Vaca Muerta-Quintuco System forms a succession of NW-ward progradational clinoforms, up to 1800 m thick (Gulisano *et al.*, 1984; Legarreta and Gulisano, 1989), subdivided into six units (Desjardins *et al.*, 2018; Minisini *et al.*, 2020b; Fig. 6.2). The system shows a very high variability throughout the basin. In the north (Mendoza Province), shallower facies were deposited in a ramp rich in carbonate deposits (Kietzmann *et al.*, 2008; 2014a), whereas in the south, a higher siliciclastic composition can be observed, with the development of a mixed carbonate-siliciclastic shelf affected by tidal processes and hyperpycnal flows (Spalletti *et al.*, 2000; Zeller *et al.*, 2015a; Krim *et al.*, 2017; Paz *et al.*, 2019).

In the study area, biostratigraphic correlation using ammonites indicates that the Vaca Muerta Formation was deposited from late early Tithonian to late Tithonian-?early Berriasian (Desjardins and Aguirre, 2018; Desjardins *et al.*, 2018). The analyzed cores were recovered from the lower three units of the Vaca Muerta-Quintuco System, where a shallow marine mixed carbonate-siliciclastic clinoform system can be observed in seismic records (Desjardins *et al.*, 2018; Fig. 6.2). Core descriptions supported with Total Organic Carbon (TOC) and X-Ray Diffraction (XRD) analyses (silica, carbonate, clay ternary diagram) indicate that the lithologies are dominanted by mixed (siliceous-calcareous-argillaceous) mudstone, siliceous and calcareous mudstone, limestone, and argillaceous tuffs (aka ash beds, bentonites, tefras or volcaniclastic layers; Pose *et al.*, 2014; Repol *et al.*, 2014; Notta *et al.*, 2017, 2020; Desjardins and Aguirre, 2018; Gómez Rivarola and Borgnia, 2018; Reijenstein *et al.*, 2020).

6.3. Materials and methods

The studied material consists of cores (660.5 m) from five wells located in the Central Neuquén Basin (Figs. 6.1, 6.2). In addition, observations from the Yesera del Tromen outcrop (148 m thick, Northern Neuquén Province) were helpful to visualize the deposits at a mesoscale. Macroscopic observations, thin sections (59 sections from cores, 18 from outcrop samples) and mineralogical composition from XRD analysis on cores, were combined in order to define lithology. Lithology is described following Lazar *et al.* (2015b) for mudstone (where fine mud is <8 μm, medium mud is 8-32 μm, and coarse mud is 32-62.5 μm), and Wright (1992) for lithofacies rich in carbonate constituents. A lithological code was used only for the contour current lithofacies, following the proposal of Kietzmann *et al.* (2014a; referring to lithology, composition, and sedimentary structures). Paleocurrent directions are not provided because geographic orientation of cores was not recorded during the recovery process. Short-wave (254 nm) and long-wave (365 nm) UV light was utilized to delineate trace fossils in black mudstone lacking sediment contrast. Bioturbation index (BI) was determined following the scheme by Taylor and Goldring (1993; modified from Reineck, 1963), which comprises a zero to six scale that considers burrow density and overlap, and preservation of bedding boundaries (percentage of bioturbated area are 1-4% for BI 1, 5-30% for BI 2, 31-60% for BI 3, 61-90% for BI 4, 91-99% for BI 5 and 100% for BI 6). Additional unpublished data available from companies owning these cores was incorporated in the analysis

(i.e., electric logging data, X-Ray Fluorescence, XRD, TOC from cutting samples; see also Pose *et al.*, 2014; Repol *et al.*, 2014; Notta *et al.*, 2017, 2020; Desjardins and Aguirre, 2018; Gómez Rivarola and Borgnia, 2018; Estrada *et al.*, 2020; Minisini *et al.*, 2020a). Redox-sensitive elements (Mo and U) were evaluated to assess paleo-oxygen levels. U enrichment was calculated following its relationship with detrital U (Wignall and Myers, 1988). A scheme of lithofacies, facies and facies associations was used for the sedimentologic analysis (see also Paz *et al.*, in review c). Lithofacies were combined with ichnologic data to define facies characterizing depositional environments. Facies that show a genetical and spatial relationship were grouped into facies associations. The sequence stratigraphic analysis follows the proposal of Hunt and Tucker (1992) and Catuneanu (2006).

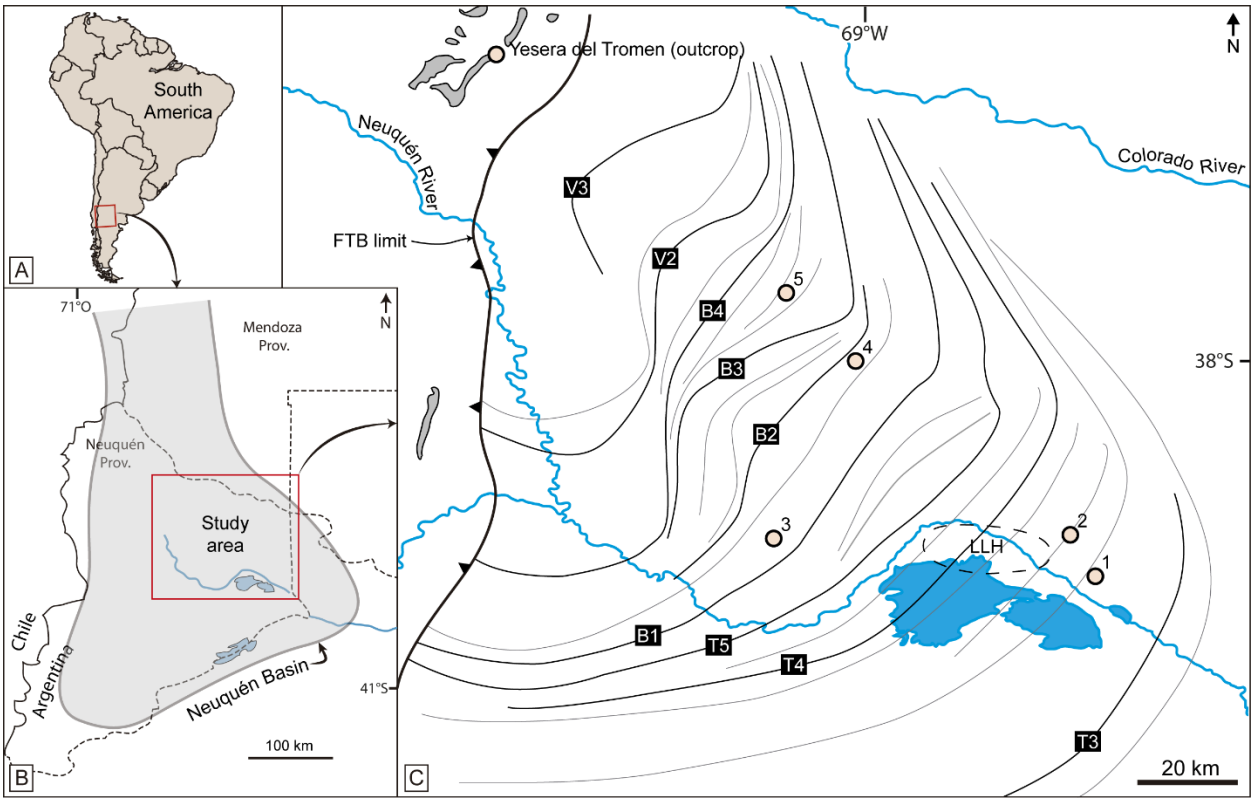

Fig. 6.1. Location maps. A, B) Map showing study area and Neuquen Basin location within a regional context. C) Study area showing the location of wells (1-5) and the outcrop section. Clinoform breaks from the different stratigraphic surfaces of the Vaca Muerta Formation were delineated (T2-T4, B1-B4, V2, V3; modified from Domínguez *et al.* 2020a). Grey areas are outcrops of the Vaca Muerta Formation, located West of the fold and thrust belt (FTB). Dashed line encloses the Loma La Lata High (LLH).

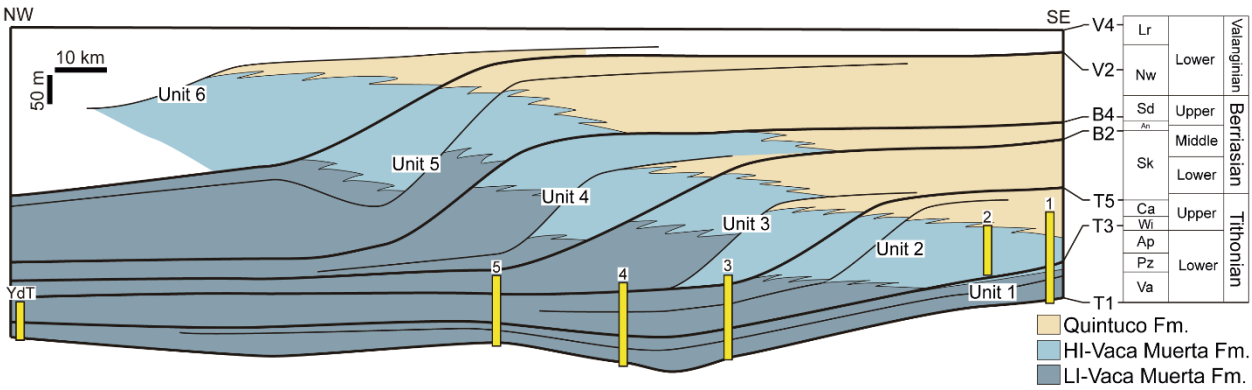

Fig. 6.2. Regional stratigraphic cross-section showing location of the studied cores and the Yesera del Tromen outcrop (YdT) within the Vaca Muerta-Quintuco system. The Vaca Muerta Formation is subdivided into a high (HI) and low (LI) impedance units. Adapted from Sattler *et al.* (2018) and Reijenstein *et al.* (2017b). Sequence-stratigraphic surfaces (T1, T3, T5, B2, B4, V2, V4) and Units (1 to 6) from Desjardins *et al.* (2018) and Domínguez *et al.* (2020a), and Andean ammonite zones (right) from Kietzmann *et al.* (2018a). Va = *Virgatosphinctes andesensis*, Pz = *Pseudolissoceras zitteli*, Ap = *Aulacosphinctes proximus*, Wi = *Windhauseniceras internispinosum*, Ca = *Corongoceras alternans*, Sk = *Substeueroceras koeneni*, An = *Argentiniceras noduliferum*, Sd = *Spiticeras damesi*, Nw = *Neocomites wichmanni*, Lr = *Lissonia riveroi*.

6.4 Facies and facies associations of the Vaca Muerta Formation

In the study area, Units 1 and 2 were mainly cored in their bottomset and foreset locations, whereas less cores are available in bottomset and lower foreset areas of Units 3, 4 and 5 (Fig. 6.2). Facies analysis laid down in Chapter 4 suggests that the Vaca Muerta Formation comprises five facies associations namely marginal marine, basin, drift, slope and outer ramp, which were subdivided into fifteen facies (Fig. 6.3, Paz *et al.*, in review c). Unit 1 shows the development of a low-angle clinoform system (0.2-0.3°), whereas higher angles are found in the following Units (1-3°, Minisini *et al.*, 2020b).

The transgressive, marginal marine facies association (FA1) is characterized by massive, parallel-, low-angle and current-ripple cross-laminated, medium- to coarse-grained sandstone with mud drapes, overlain by bindstone, and massive (bioturbated) to wavy, calcareous to mixed mudstone. Mean BI is 0.15 (n=58) and 3.04 (n=268) in the sandstone and mudstone, respectively. This facies association represents beach (sandstone, facies F1a), and bay facies (bindstone and mudstone, facies F1b, see also Paz *et al.*, 2021).

Basin facies association (FA2) consists of parallel-laminated, carbonaceous to bioclastic mixed mudstone, massive (bioturbated), calcareous to mixed mudstone, bioclastic floatstone to rudstone, tuffs, bindstone and carbonate concretions. Mean BI is 0.51 (n=13841). This facies association indicates dominantly pelagic and hemipelagic deposition and subordinate bottom currents, sediment-gravity flows and storm events. The association is subdivided into a starved basin showing evidence of sediment starvation (bindstone and carbonate concretions, facies F2a), and in anoxic (facies F2b), dysoxic (facies F2c) and oxic (facies F2d) basin depending on the degree of bioturbation (higher bioturbation associated with more oxygenated conditions).

Drift facies association (FA3) display massive (bioturbated), cross-bedded, parallel-, low angle- and wavy-laminated, crinoidal mudstone, crinoid-rich lenses, parallel to low angle coarse mudstone laminae encased in fine mudstone, massive (bioturbated), parallel-, low-angle and current-ripple cross-laminated, coarse mudstone, and thin-bedded, massive, normal-graded and composite beds of calcareous, fine to coarse mudstone. Mean BI is 1.86 (n=894). This association suggests bottom current deposition in sediment drifts of dominantly crinoid (facies F3a) and bioclastic to silt (facies F3b) composition, or drifts accumulated by combined contour current and fluid mud flow deposition (facies F3c).

The slope facies association (FA4), encompass parallel- to wavy-, laminated or bedded, and massive (bioturbated), mixed to calcareous mudstone, thin-bedded, massive and composite beds of calcareous mudstone, and m-thick slumped intervals. Mean BI is 2.29 (n=2196). This association formed by hemipelagic and fluid mud deposition below and near the storm wave-base, whereas a distal (facies F4a), mid (facies F4b), proximal (facies F4c) and fluid mud-rich (facies F4d) slope can be differentiated.

The outer ramp facies association (FA5) occurs in areas without clinoforms (ramp-like), and comprises massive, calcareous to mixed mudstone, intraclastic wackestone and bioclastic floatstone. Mean BI is 4.59 (n=1260). This association is interpreted to be deposited by hemipelagic and various current activity (low, facies F5a, and high, facies F5b) under oxic conditions. FA5 is not represented in the study area of this contribution.

The geochemical dataset indicates FA2 is rich in mixed mudstone, show a less amount of calcareous, siliceous and argillaceous mudstone, and has the highest TOC content, whereas FA3 and FA4 comprises calcareous and mixed mudstone (Fig. 6.4).

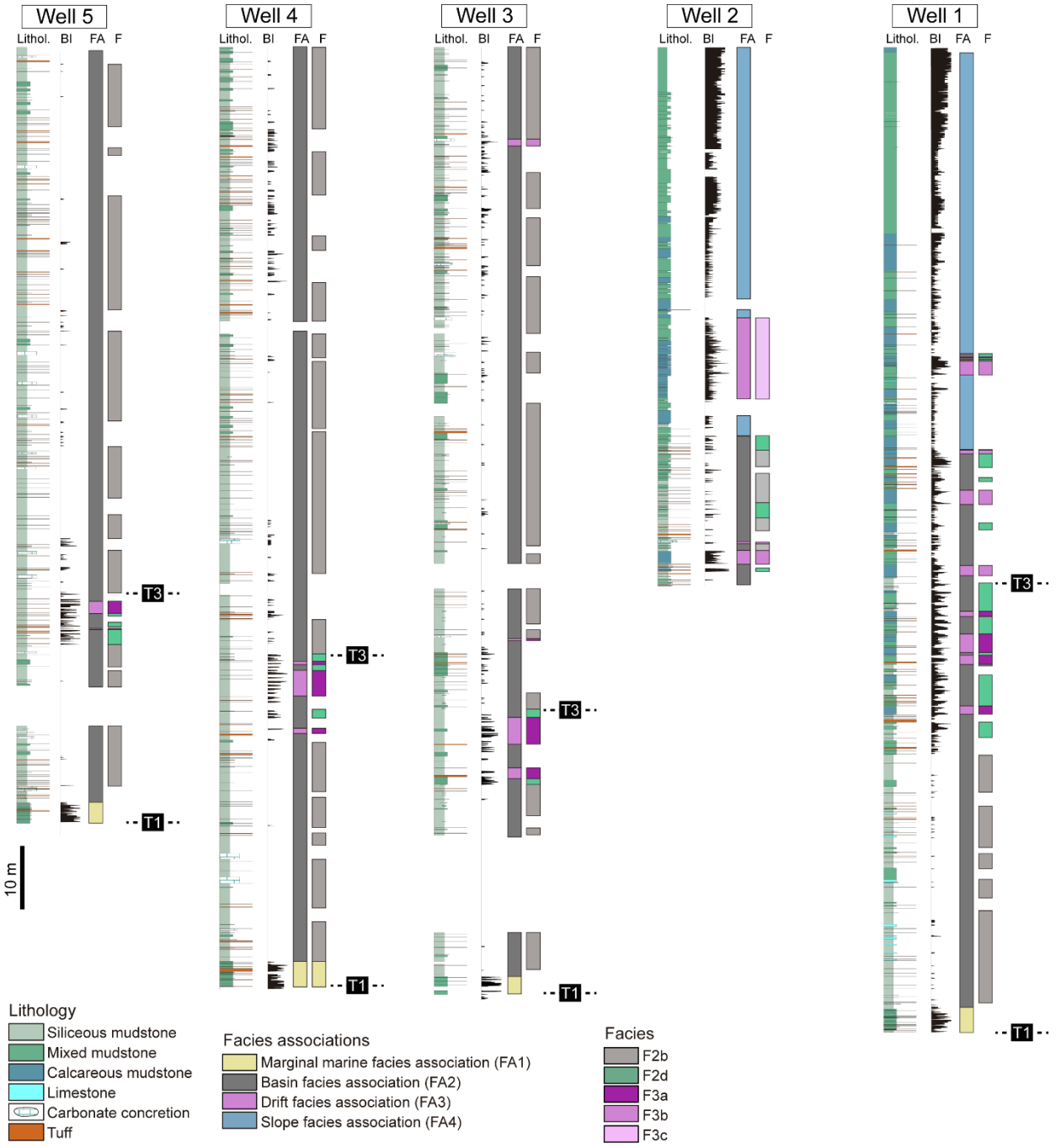

Fig. 6.3. Cores of the Vaca Muerta Formation with XRD analysis providing lithology, bioturbation index (BI), facies associations (FA) and facies (F). Facies associations based on the analysis provided in Chapter 4. Facies association 5 does not occur in the study area. Stratigraphic surfaces T1 and T3 define the bases of Unit 1 and Unit 2 of the Vaca Muerta-Quintuco clinoform system (Desjardins *et al.*, 2018; Minisini *et al.*, 2020b).

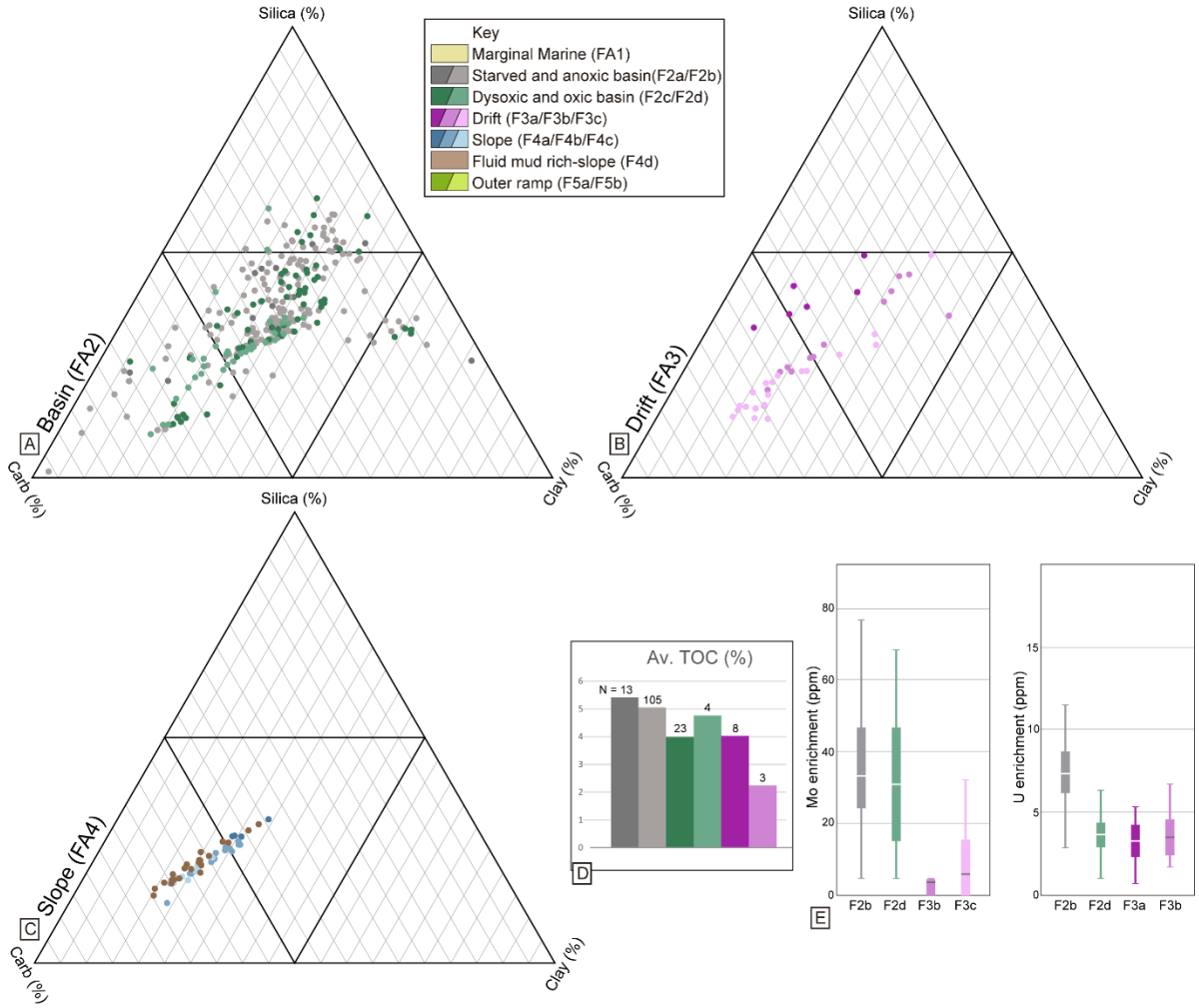

Fig. 6.4: Geochemical data of the different facies and facies associations (key from sedimentologic analysis of Chapter 4). Compositional data from XRD of the A) basin (FA2), B) drift (FA3) and C) slope (FA4) facies association. D) Average TOC content from cutting samples. E) Mo enrichment data provided by XRF, and U enrichment from spectral gamma ray data from wells 1 and 2, respectively. Median value indicated by a middle line in the box and whisker plot.

6.5 Facies indicating contour current activity

The present analysis focuses only on five facies showing evidence of bottom or contour current activity. These facies occur within basin (FA2) and drift (FA3) facies associations (Fig. 6.3). These facies derive from the previous sedimentological analysis laid down in Chapter 4, in which, F2b and F2d contain minor bottom current evidence, whereas F3a, F3b and F3c were dominantly

deposited by contour currents. A lithofacies code was used only for lithofacies produced by bottom or contour currents, and these are summarized in Fig. 6.5. Paleowater depth of the Vaca Muerta Formation varies between 50 to 400 m (Mitchum and Uliana, 1985; Kietzmann *et al.*, 2008; Kietzmann and Palma, 2009b; Minisini *et al.*, 2020a), and thus, contourite deposits can be considered mainly of shallow water (Stow *et al.*, 1998).

	Appearence in core	Size/ grain	Bed thickness	Description	Interpretation	Facies distribution
M_{bind}	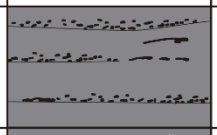	Pebble- to granule-sized bindstone clasts	2-10 mm	Sharp-based mudstone containing pebble- to granule-sized, tabular bindstone clasts	Bottom current reworking microbially stabilized sediments, that are transported as mat chips and concentrated in discrete beds	Subordinate in F2b
M_pl		Medium to coarse mud	20-70 cm	Ripple cross-laminated peloidal mudstone associated with low-angle cross-bedded surfaces	Migration of compound dunes due to high-energy unidirectional currents. Possible tidal influence?	Common in F2d, subordinate in F2b
M_cb	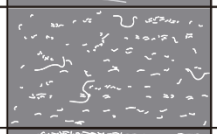	Fine to coarse mud and crinoids	5-50 cm	Completely bioturbated intervals, with rare bedding observed. Biodeformational structures are abundant, with minor discrete trace fossils	High abundance of organisms supported by high food and oxygen availability. Hydrodynamic energy remains low and burrowing infauna keeps pace with seafloor accretion	Dominant in F3a, subordinate in F2d
M_ch, M_cl, M_cw	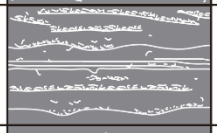	Fine to coarse mud and crinoids	2-15 cm	Discontinuous to continuous, planar, parallel-, low-angle to rare wavy-laminated crinoidal mudstone	Bedload traction transport in crinoid-rich sediments. Low-energy unidirectional currents associated with winnowing of muds	Dominant in F3a
M_cr	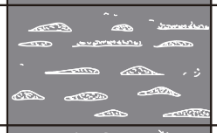	Crinoids	2-15 cm	Crinoidal mudstone with lenticular-shaped (0.5-3 mm-thick), crinoid-rich structures	Interpreted as starved ripples due to their common gradation from crinoid-rich laminae. Moderate energy conditions	Dominant in F3a
M_ct	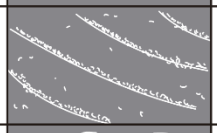	Crinoids, peloids	5-15 cm	Cross-bedded crinoidal-peloidal mudstone with sharp to erosive bases	Bioclastic dune migration affected by high energy unidirectional currents	Subordinate in F3a
$M_{cm}b$	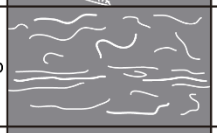	Fine to coarse mud	1-30 cm	Completely bioturbated intervals. Some remaining bedding can be recognized. Dominant biodeformational structures and rare discrete traces are distinguished	High abundance of organisms supported by high food and oxygen availability. Hydrodynamic energy remains low and the burrowing infauna keeps pace with seafloor accretion	Dominant in F3b, common in F2d
Mh, Ml		Fine to coarse mud	0.2-5 cm	Parallel to low-angle coarse mudstone laminae encased in fine mudstone	Silt and mud floccule segregation from bedload traction transport. Unidirectional currents associated with low energy and sedimentation rate	Dominant in F3b and F3c, subordinate in F2b and F2d
M_sh, M_sl	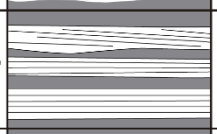	Coarse mud	0.2-5 cm	Lenticular to tabular, parallel- to low-angle cross-laminated coarse mudstone	Bedload traction transport under moderate energy and low sedimentation rate, above the threshold of mud floccule deposition	Dominant in F3b and F3c
M_sr, M_sw		Coarse mud to very fine-grained sand	0.2-5 cm	Lenticular to tabular, current- and wave-ripple cross-laminated coarse mudstone with black-colored laminae	Bed erosion and bedload traction transport under higher energy and sedimentation rate. Rare oscillatory current influence	Common in F3b and F3c subordinate in F2d

Fig. 6.5. Lithofacies codes and drawings used to describe and interpret contourite facies.

6.5.1 Facies 2b (F2b): Fine to coarse mudstone with bindstone intraclasts

6.5.1.1 Description

This facies consists of 0.2-1.0 cm thick intervals with sharp-based, fine to coarse mudstone with pebble- to granule-sized, tabular, light-colored, bindstone intraclasts (M_{bind}, Fig. 6.6A-D). Normal gradation is also observed. The mudstone is vertically associated with 0.5-30 cm-thick bindstone intervals composed of light-colored wavy and crinkly laminae (0.1-0.5 mm-thick), consisting of microsparite dolomite, minor organic matter and cubic pyrite. Moreover, this facies is dominated by parallel-laminated, carbonaceous, mixed to minor siliceous mudstone (av. TOC 5.06%, N=105). Rare cm-thick, bioclastic floatstone to rudstone, discontinuous, parallel-laminated peloidal packstone, and bioclastic mixed mudstone occur. Very thin- to thin-bedded and rare thick-bedded intervals showing fine mudstone with coarse mudstone laminae, sharp-to erosive-based, graded to massive, fine to coarse mudstone, and tuff to lapilli-ash tuff are interbedded. Locally, peloidal packstone with asymmetrical ripples occur. Carbonate concretions are observed (30-50 cm-thick). Although laminae is locally reworked by bioturbation (BI 1-2), this facies is typically unburrowed (BI 0). Locally, tuffs contain *Alcyonidiopsis longobardiae*, *Planolites* isp., *Coprulus oblongus*, pyrite-rich burrows, mantle and swirl structures, and biodeformational structures.

6.5.1.2 Interpretation

This facies was deposited in a basin environment dominated by organic-rich, pelagic deposition. Rare sediment-gravity flows are interpreted from the sharp- to erosive-based, fine to coarse mudstone. Bottom current activity is suggested by the fine mudstone with coarse mudstone laminae (see also F3b) and the mudstone with bindstone intraclasts (M_{bind}). The later is formed by the action of bottom currents reworking the microbially stabilized sea floor and generating “mat chips” (Noffke, 2010). The fact that these deposits are made solely of autochtonous sediment (bindstone intraclasts), precludes interpretation of sediment-gravity flows. The lower bioturbation intensity suggests microbial mats associated with oxygen-deficient environments, similar as in the Santa Barbara Basin (Soutar and Crill, 1977) or the coastal upwelling zone off central Chile (Fossing *et al.*, 1995).

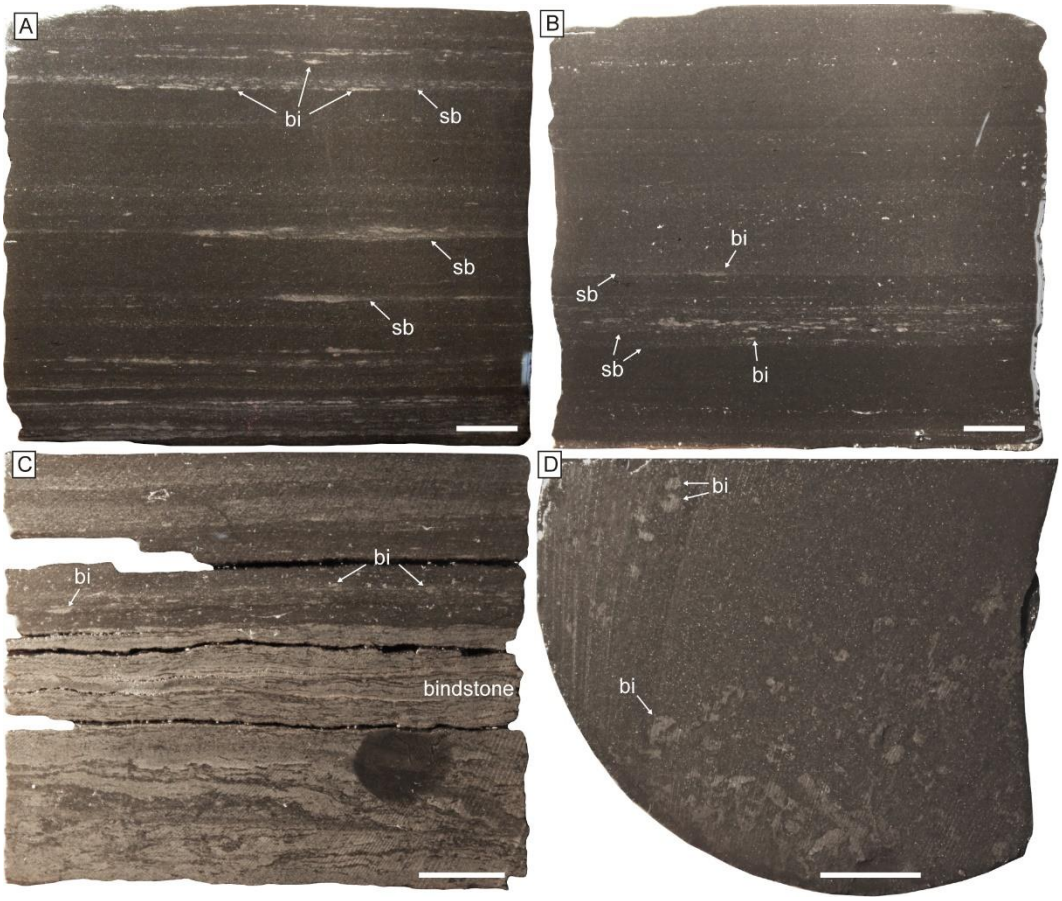

Fig. 6.6. Sharp-based mudstone composed of bindstone intraclasts (M_{bind}) of facies F2b. A, B) Sharp bases (sb) of lithofacies M_{bind}, showing tabular bindstone intraclasts (bi). C) Bindstone intervals associated with intraclasts on top. D) Plan view detail of the bindstone intraclasts (from a different interval). Scale bars are 1 cm.

6.5.2 Facies 2d (F2d): Peloidal mudstone

6.5.2.1 Description

This facies comprises 20-70 cm-thick intervals showing low-angle cross-bedded peloidal mudstone ($M_{p}l$), with 1-5 cm-thick current ripple cross-laminated intervals (Fig. 6.7A-C). Rare sinusoidal lamination, symmetrical ripples, and climbing ripples are also observed. Bases are typically sharp. Bidirectional ripples in outcrops suggest NE-SW orientation. In thin-section, silt-sized, lens-shaped clay peloids, quartz, plagioclase, and micas, and pebble-sized carbonate intraclasts are observed. Fossils comprise well-preserved to minor partially fragmented calcite-replaced radiolarians, gastropods, microcrinoids, ammonites and bivalves (1-5%) with random or concordant orientations to bedding. Extensive carbonate cementation affects this lithofacies. The

facies is also dominated by bioclastic, mixed mudstone, and massive, calcareous to mixed mudstone (av. TOC 4.77%, N=4). Very thin- to thick-bedded intervals of fine mudstone with coarse mudstone laminae, current-ripple cross-laminated, fine to coarse mudstone, massive crinoidal mudstone, sharp- to erosive-based, graded to massive, fine to coarse mudstone, hummocky cross-stratified, intraclastic to bioclastic wackestone and tuff to lapilli-ash tuff with rare wavy tops are intercalated. Lithofacies M_pl is typically unbioturbated, but variable bioturbation levels are observed in this facies (typically BI 1-4 with rare 5 or 6). Biodeformational structures are common. Trace fossils are observed in the tuffs and mainly include *Teichichnus rectus, Alcyonidiopsis longobardiae, Thalassinoides isp., Planolites isp., Nereites isp., Phycosiphon incertum, Teichichnus zigzag, Coprulus oblongus* and mantle and swirl structures with subordinate *Diplocraterion isp., Zoophycos isp., Palaeophycus isp.,* and pyrite-rich burrows.

6.5.2.2. Interpretation

This facies represents alternation of pelagic, hemipelagic deposition and contour current transport in an oxic basin. Rare oscillatory flow reworking during storms is inferred from the hummocky cross-stratification and the wavy tops in the tuffs. Bioturbation in the tuffs indicates higher oxygen levels in an area above the oxycline. Contour currents reworking mud floccules and peloids can produce the ripples in the low angle peloidal mudstone (Schieber *et al.*, 2007). Localized areas with high sedimentation rate combined with traction transport generated the minor sinusoidal lamination and climbing ripples (Martín-Chivelet *et al.*, 2003). Although bidirectional paleocurrents suggest tidal influence, the lack of slack-water mudstone intervals precludes its interpretation as a tidal deposit. Low-angle cross-bedding observed in outcrops with ripples on bedding surfaces can be interpreted as compound dunes, where cross-bedding represents second-order surfaces in which ripples and 3D dunes accrete (master bedding surfaces of Dalrymple, 2010).

Fig. 6.7. Peloidal mudstone with low-angle bedding (M_pl) of facies F2d, with current ripples and trough cross-bedding on bedding surfaces. A, B) Core photograph and drawing of the peloidal mudstone ripples

(M_pr), with undetermined burrows (b). Scale bars are 1 cm. C) Outcrop view and drawing of the peloidal mudstone, with ripples and trough cross-bedding on the surfaces (M_pr, M_pt). S2 reactivation surfaces are delineated. Scale is 20 cm.

6.5.3 Facies 3a (F3a): Crinoidal mudstone

6.5.3.1 Description

This facies consists of 5-50 cm-thick, massive crinoidal mudstone (M_cb, Fig. 6.8A), 2-15 cm-thick, crinoidal mudstone showing discontinuous to continuous, planar, parallel-, low-angle to rare wavy, crinoid-rich laminae (M_ch, M_cl, M_cw, Fig. 6.8B, C), lenticular-shaped (0.5-3 mm thick and 2-20 mm long), crinoid-rich structures (M_cr, Fig. 6.9A, B, C), and 5-15 cm-thick, cross-bedded crinoidal mudstone (M_ct, Fig. 6.9D; av. TOC 4.04%, N=8). Laminae are 1-2 mm thick. Lithofacies M_cb, M_ch, M_cl, and M_cw have transitional bases, whereas lithofacies M_cr and M_ct show sharp to erosive bases. In addition, very thin- to thin-bedded, sharp- to erosive-based, graded to massive, fine coarse mudstone, and thin- to thick-bedded tuff to lapilli-ash tuff, are intercalated. The fossil content predominantly consists of *Saccocoma* microcrinoids, with minor ammonites and bivalves, showing random orientations. Lithofacies M_cb and M_ct consist of loosely to densely packed (20-50%), fragmented to well-preserved (0.5-5 mm long) microcrinoids, whereas lithofacies M_ch, M_cl, M_cw and M_cr show densely packed (90-100%) fragmented (<2 mm diameter) microcrinoids. In thin section, the facies displays silt-sized, radiolarians, plagioclase, quartz and volcanic rock fragments.

Bioturbation intensity is high in M_cb (BI= 3-6) to absent or low in the rest of the lithofacies (BI= 0-1). Biodeformational structures are the most abundant biogenic structures, being locally associated with *Crininicaminus* isp. and *Planolites* isp., and rare *Teichichnus rectus*, *Phycosiphon incertum*, ?*Skolithos* isp., *Coprulus oblongus* and *Thalassinoides* isp.

6.5.3.2 Interpretation

This facies is interpreted as the product of long-term contour current activity in areas rich in pelagic crinoids (*Saccocoma*, Kietzmann and Palma, 2009a). The lenticular structures in M_cr are interpreted as starved ripples due to their common gradation from lenticular structures to laminae (Fig. 6.8C) and their erosive bases. The starved ripples and bioclastic laminae (M_ch, M_cl, M_cw) indicate bedload traction transport and winnowing of muds. In addition, bioclastic lineation in an

element map core image is observed in similar lithofacies (Gómez Rivarola and Borgnia, 2018, their Fig. 13.4.b), supporting the traction transport hypothesis. Lithofacies M_ct suggests bioclastic dune migration. In other areas, the pelagic crinoids have been interpreted as suspension feeders (Hess and Etter, 2011), suggesting the existence of a continuous current that maintained food in suspension and supporting the hypothesis of an active circulation system. High bioturbation intensity in M_cb indicates oxygenated environments. Hydrodynamic energy controlled lithofacies distribution: lithofacies M_cb was formed during times of low-velocity currents, whereas the other lithofacies record times of higher-energy currents.

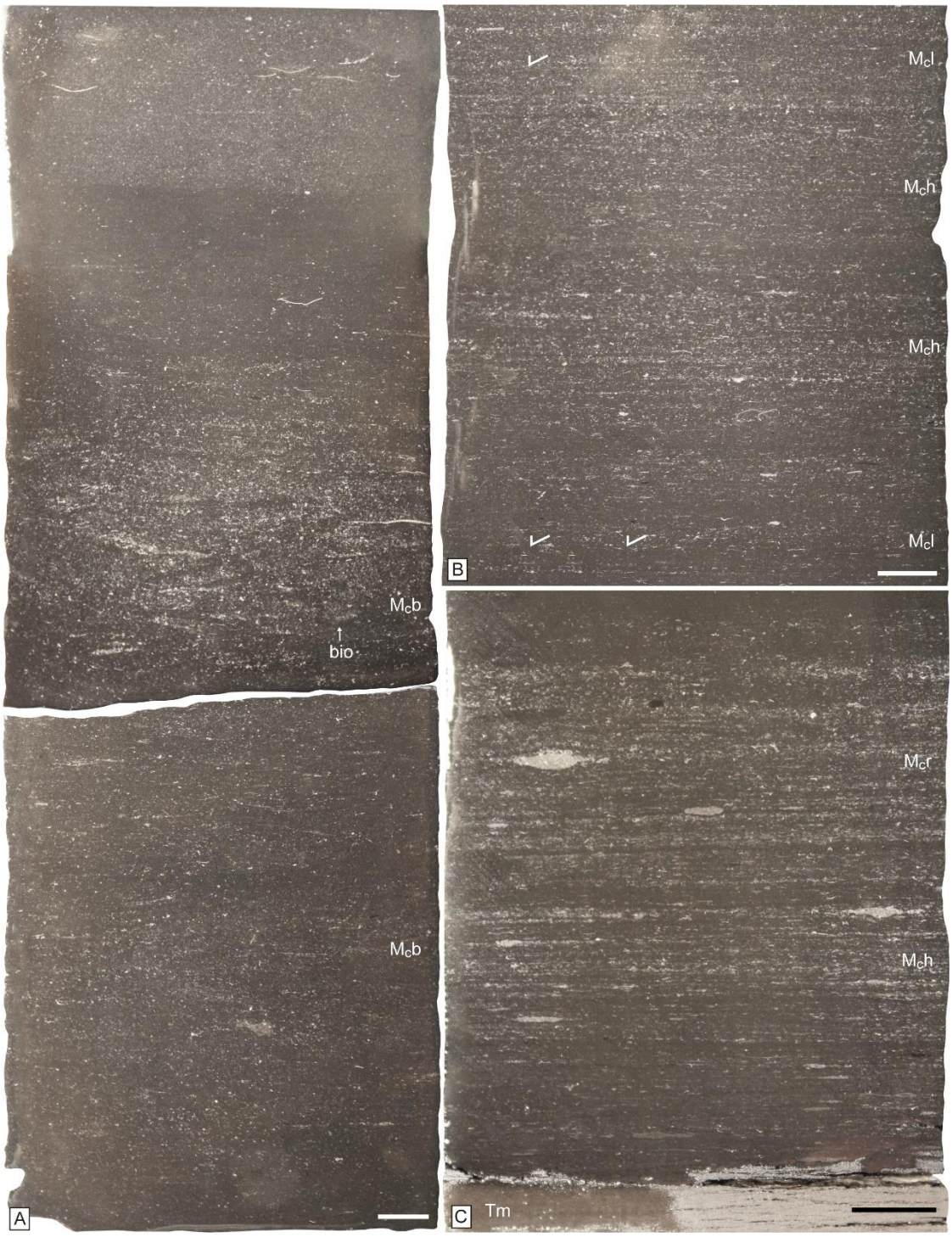

Fig. 6.8. Crinoidal mudstone of facies F3a. Scale bars are 1 cm. A) Bioturbated, massive crinoidal mudstone (M_cb), with biodeformational structures (bio) delineated in the image. B, C) Parallel- to low-angle cross-laminated crinoidal mudstone (M_ch, M_cl) and mudstone with lenticular structures interpreted as crinoidal ripples (M_cr) with associated unbioturbated massive tuff at the base (Tm).

Fig. 6.9. Crinoidal mudstone of facies F3a. Scale bars are 1 cm. A, B, C) The lenticular structures represent bioclastic ripples (br), representing ripple cross-laminated mudstone (M_cr). Note the ripple foresets in C. D) Trough cross-bedded crinoidal mudstone (M_ct) with erosive bases (eb).

6.5.4 Facies 3b (F3b): Fine to coarse mudstone

6.5.4.1 Description

This facies consists of 0.2-5 cm-thick, fine mudstone with parallel to low-angle coarse mudstone laminae (Mh, Ml), parallel- to low-angle and current-ripple cross-laminated coarse mudstone (M_sh, M_sl, M_sr), and 1-30 cm-thick, massive, calcareous to mixed mudstone (M_{cm}b, Fig. 6.10, 6.11; av. TOC 2.25%, N=3). The bases are sharp to erosive with wavy surfaces, or locally gradational. Beds are mostly tabular but occasionally lenticular, representing starved ripples. Laminae are 0.2-3.0 mm thick, showing black-colored, sand-sized, tabular to rounded mud intraclasts. The laminae in lithofacies Mh and Ml occur as tabular or lenticular, with a massive to rarely thinly laminated texture (Fig. 6.10B). Ml laminae can grade laterally to Mh (Fig. 6.10D). These lithofacies show several reactivation surfaces in a cm-scale, revealed by multiple erosive or sharp bases. Ripple cross-lamination shows one predominant orientation in the core (80.5 %, n=180), with minor ripples displaying an opposite direction (19.5 %). Moreover, thin-bedded, wave ripple cross-laminated coarse mudstone (M_sw), medium-bedded, low-angle cross-bedded peloidal mudstone (M_pl), and very thin- to thin-bedded, sharp- to erosive-based, normal-graded to massive, fine to coarse mudstone are minor constituents.

Petrographic analysis indicates a calcareous, siliceous to mixed, coarse to fine mudstone with minor very fine-grained sand-sized bioclasts and intraclasts. The grains are silt-sized plagioclase, calcite-replaced radiolarians, foraminifera, bivalves, carbonate intraclasts, undifferentiated skeletal fragments, mudstone intraclasts, and minor quartz, pellets and echinoderm fragments, occurring in a matrix with illite and coccoliths. The laminae consist of silt- to very fine sand-sized, demosponge *Rhaxella* fragments, foraminifera, calcite-replaced radiolarians, and mudstone intraclasts. The geochemical dataset shows lower Mo and U values compared with deposits from the basin (F2b, F2d; Fig. 6.5E).

Erosive structures, such as scour marks, gutter casts, and intraclastic and bioclastic lags, also occur. Minor soft-sediment deformation structures include small-sized load casts at the base of beds, syneresis cracks, pseudonodules, and normal synsedimentary microfaults. Degree of bioturbation varies from absent to intense, reaching a BI of 4-5 in lithofacies M_{cm}b. Common trace fossils are *Nereites* isp., *Phycosiphon incertum, Planolites* isp., *Palaeophycus* isp., *Palaeophycus heberti* and escape trace fossils, whereas ?*Lockeia* isp., *Teichichnus rectus, Alcyonidiopsis*

longobardiae, Coprulus oblongus and pyrite-rich burrows are minor constituents. Locally, the facies is arranged in four discrete 1.7-2.2 m-thick successions showing, bottom up, a decreasing and then an increasing BI. These bigradational successions can be subdivided into two types: type A shows lithofacies Mh and Ml and a high percentage of M_{cm}b over total thickness (~50-60 %), type B shows lithofacies Mh, Ml, M_sh, M_sl and M_sr, a low percentage of M_{cm}b (~15-30 %), local presence of M_sw, and intraclastic and bioclastic lags (Fig. 6.12).

6.5.4.2 Interpretation

This facies represents enhanced contour current activity generating fine-grained sediment drifts. Following terminology from the literature (e.g. Stow and Bowen, 1980; Stow and Shanmugam, 1980), Mh is comparable to the silt laminae encased in fine mud, the minor discontinuous laminae grouped in lithofacies Mh can be correlated with the "wispy lamination", Ml is similar to the "low-amplitude ripples", and M_sr represents current ripples. All the traction structures were generated during bedload sediment segregation from mixed clay-silt suspensions and consequent floccules and silt ripple formation, similarly as in flume experiments (Schieber, 2011; Yawar and Schieber, 2017). Periodic introduction of different sediment grain sizes into the current produced the mixed suspensions that were subsequently sorted during bedload transport (Kuenen, 1966). Lithofacies Mh is laterally associated with current ripples of lithofacies Ml (Fig. 6.10D) or shows downlap laminae relationships (Fig. 6.10C), supporting the origin as a low-relief, bedload traction structure compacted during diagenesis (Schieber *et al.*, 2007). Velocities below 25 cm/s are responsible for lithofacies Mh and Ml deposition, whereas above 25 cm/s, lithofacies M_sh, M_sl and M_sr were produced due to transport above the threshold for clay floccule accumulation (Yawar and Schieber, 2017). This hydrodynamic energy gradation change occurs in tandem with increased bed erosion and the amount of sharp to erosive bases. Intraclastic and bioclastic lags reflect periods of increased flow velocity and erosion. The facies display multiple recurrence of the traction structure deposits alternating with colonization surfaces, indicative of fluctuating current velocity (Rodríguez-Tovar *et al.*, 2019). The occurrence of lithofacies M_sw suggests oscillatory flow reworking in the coarser-grained facies (type B successions), associated with long wavelength waves during storms. Alternatively, lithofacies M_sw could be the result of unidirectional, transitional flows rich in clays developing irregular bedforms (Baas *et al.*, 2016).

Lithofacies $M_{cm}b$ is generated due to high bioturbation during low energy current activity. A moderately diverse trace-fossil assemblage, highly bioturbated intervals in comparison with basin deposits, and low values of redox-sensitive trace elements suggest oxygen and food increments associated with the currents. Moreover, hydrodynamic energy increased from successions type A to type B, characterized by an increase of traction structures and a decrease in the thickness of bioturbated bed ($M_{cm}b$).

Hydrodynamic energy constitutes the prime control for bioturbation in this facies, i.e. the higher the hydrodynamic energy, the higher the stress over the benthos and the lower the bioturbation intensity. This is exemplified by the type A and B successions. At the base of the successions, an intermittent current regime and low flow velocities promoted extensive bioturbation and beds were completely homogenized. The middle part records steady currents and higher flow velocities that inhibited bioturbation allowing preservation of sedimentary structures. Locally, colonization surfaces and escape trace fossils indicate current velocity variations (e.g. Rodríguez-Tovar *et al.*, 2019). The top records a new decrease of energetic conditions allowing organisms to completely rework the sediment. Although grain size trends within the type A and B successions were not observed, these successions are similar to the documented cyclicity of contourite deposits, where an increasing to decreasing grain size pattern is produced by fluctuations in hydrodynamic energy (Gonthier *et al.*, 1984; Stow and Faugères, 2008).

The role of oxygenation on the development of the bigradational BI successions needs to be addressed. In the California Continental Borderland, high oxygenation associated with increased bioturbation during inter-glacial events and high hydrodynamic energy during glacial times were interpreted as factors controlling the preservation/destruction of traction structures (Robinson *et al.*, 2007). In the present case, deposition of the drifts may have been under oxygen-deficient conditions due to the high organic carbon content of the deposits and the dominance of relatively small sizes of burrows. Therefore, upper dysoxic conditions may have been a background control during deposition of each succession, overprinted by hydrodynamic energy which, in contrast, fluctuated in intensity. Hence, dysoxia combined with high hydrodynamic energy may explain the preservation of sedimentary structures in the present contourite example.

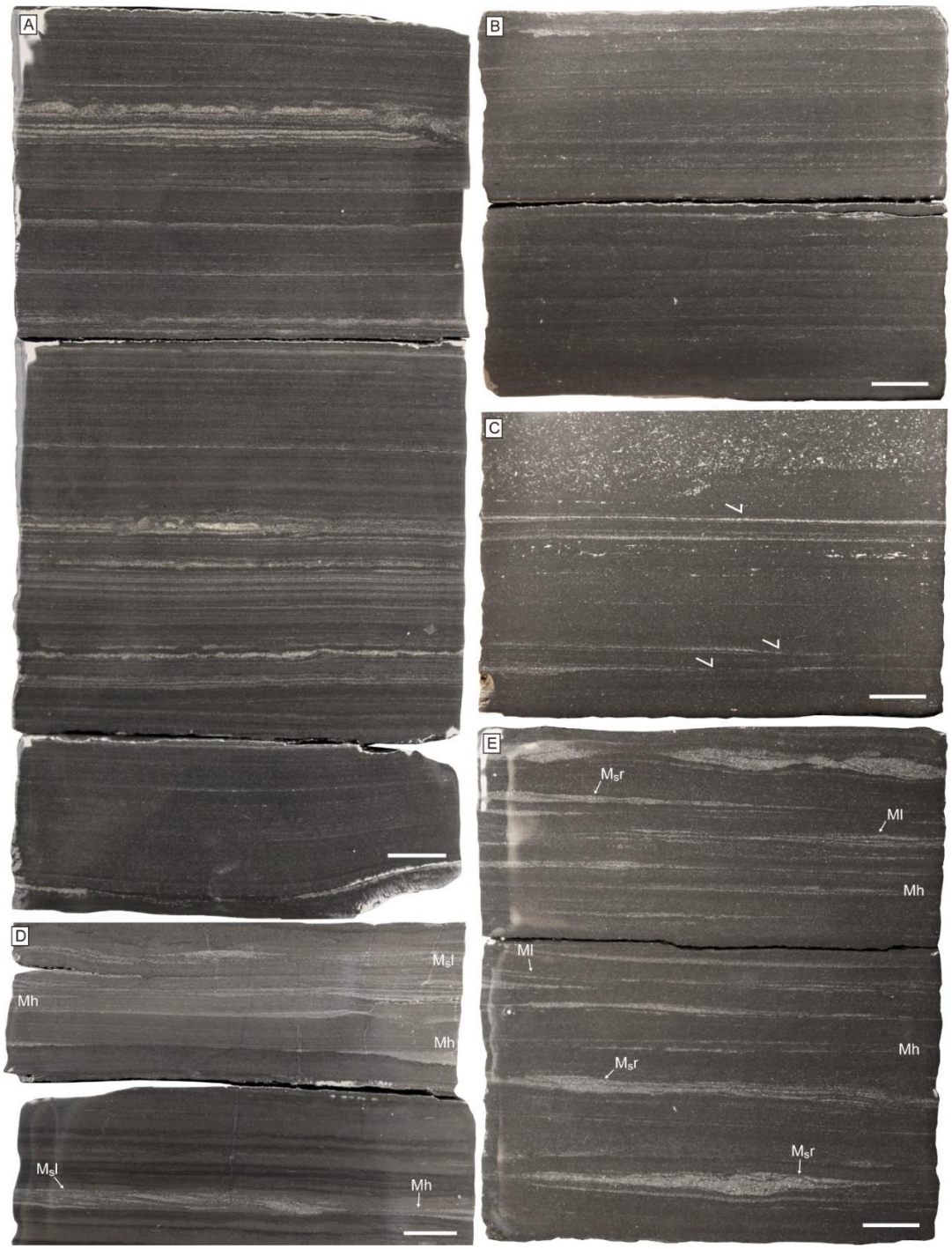

Fig. 6.10. Core photographs of parallel- to low-angle cross-laminated coarse mudstone laminae encased on fine mudstone (Mh, Ml), and low-angle to ripple cross-laminated coarse mudstone (M_sl, M_sr) of facies F3b. A) Lithofacies Mh showing small trace fossils. B) Thinly laminated, discontinuous, laminae of lithofacies Mh. C) Downlapping relationships in coarse mudstone laminae (Mh). D, E) Lithofacies Mh, Ml, M_sl and M_sr interbedded with fine mudstone. Note the lateral and vertical association of the four lithofacies. Scale bars are 1 cm.

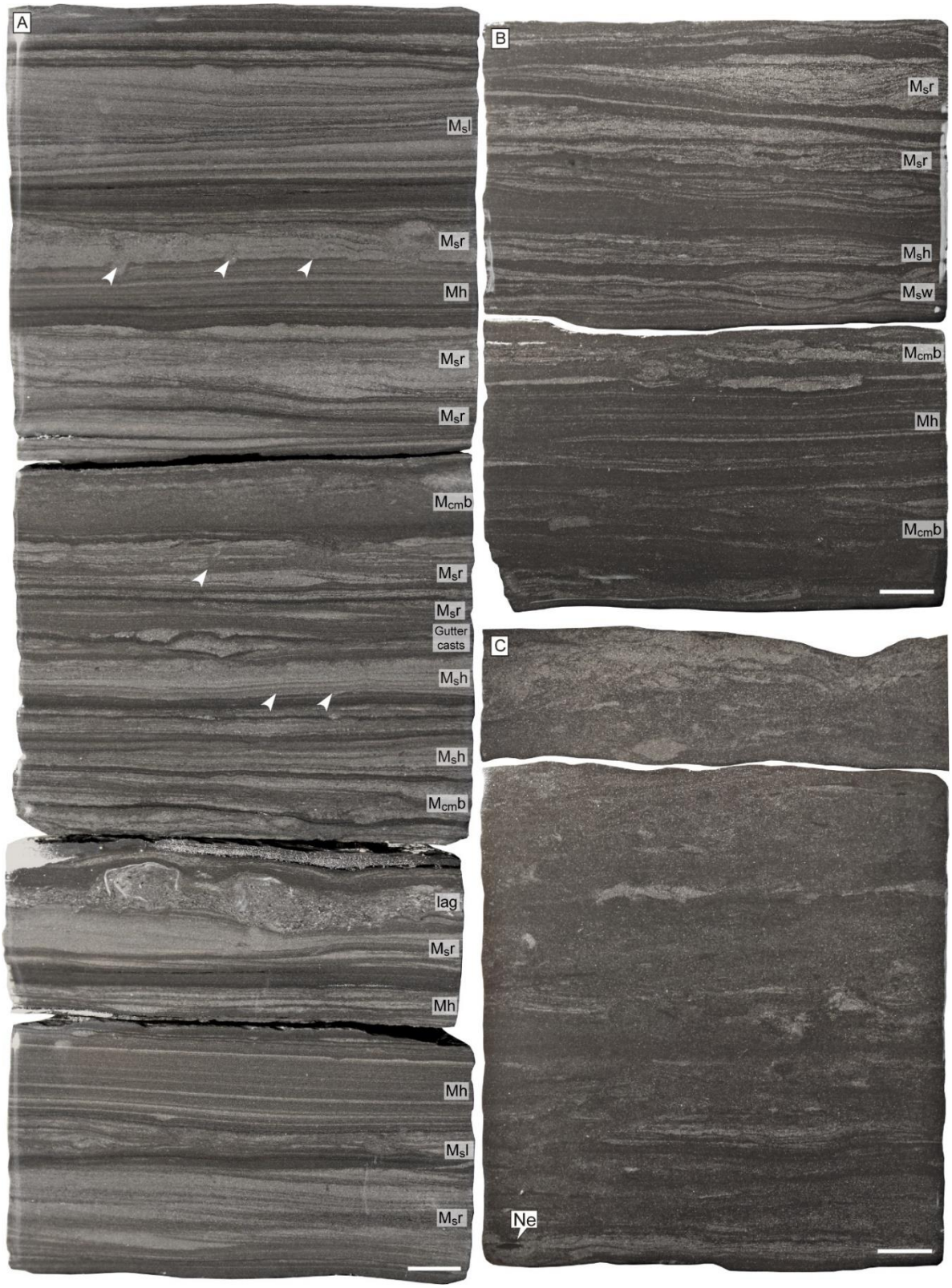

Fig. 6.11. A, B) Core photograph of facies F3b, showing parallel coarse mudstone laminae encased in fine mudstone (Mh), parallel-, low-angle and ripple cross-laminated coarse mudstone (M_sh, M_sl, M_sr),

intercalated with bioturbated mudstone ($M_{cm}b$), and minor small gutter casts and lags. Escape and undetermined trace fossils are indicated with white arrows. C) Highly bioturbated intervals, showing biodeformational structures and *Nereites* isp. (Ne). Scale bars are 1 cm.

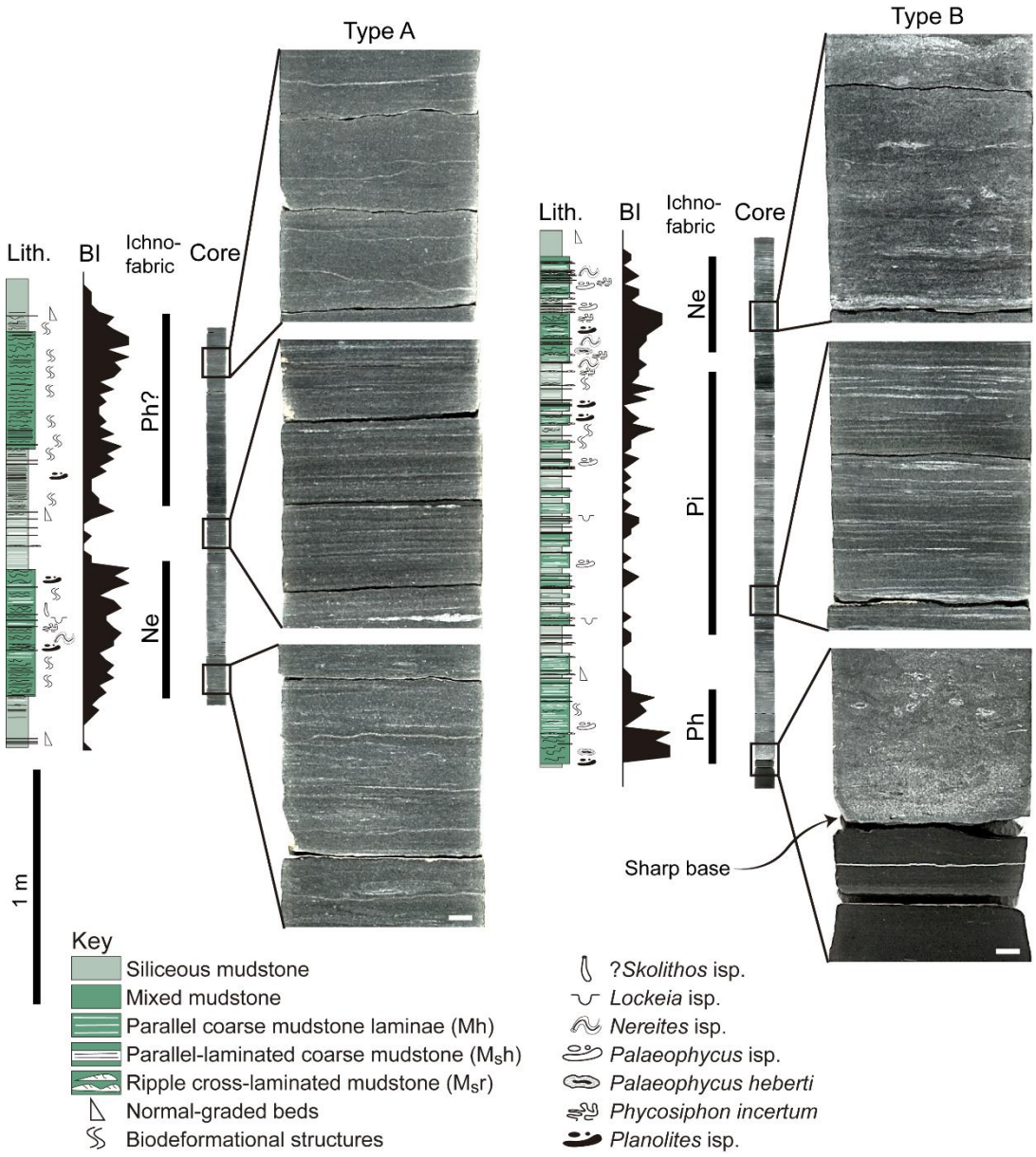

Fig. 6.12. Facies F3b characterized by two upwards successions of decreasing to increasing bioturbation index (BI). Note that the low BI in the middle of both Type A and Type B successions allows the preservation of sedimentary structures. Scale bars at the bottom right of the cores are 1 cm.

6.5.5 Facies 3c (F3c): Laminated, fine to coarse mudstone and massive calcareous mudstone

6.5.5.1 Description

This facies comprises 0.2-5 cm-thick, fine mudstone with parallel- to low-angle coarse mudstone laminae (Mh, Ml), and parallel to low angle, and current-ripple cross-laminated coarse mudstone (M_sh, M_sl, M_sr; Fig. 6.13). In addition, 1-3 cm-thick, massive calcareous mudstone, normal-graded, fine to coarse mudstone, and composite beds of fine to coarse mudstone are intercalated. Minor dark, crinkly-laminated, bindstone occurs. Sharp to erosive bases are common in all these lithologies. The composite mudstone is represented by erosively based, thin-bedded, intraclastic coarse mudstone, followed by parallel-laminated coarse and medium mudstone (Fig. 6.13A). Lithofacies Mh, Ml, M_sh, M_sl and M_sr in this facies show the same composition as in F3b. The normal-graded, massive and composite mudstone shows a mud matrix composed of clays and carbonate mud, and contains tabular, dark bindstone intraclasts, pebble-size, carbonate and mudstone intraclasts, fine-grained sand-sized skeletal and intraclast grains, and silt-sized, quartz, plagioclase, and Fe-dolomite grains. Fossils include bivalves and calcite-replaced radiolarians. Local convolute bedding and centimetre-scale synsedimentary normal faults occur.

Variable bioturbation index is observed (BI 0-3 and rarely 4). The trace-fossil content is represented by equilibrium trace fossils, ?*Lockeia* isp., and *Lockeia siliquaria* with minor escape trace fossils and ?*Skolithos* isp.

6.5.5.2 Interpretation

This facies is interpreted as deposited by a combination of low to moderate energy contour currents (Mh, Ml, M_sh, M_sl, M_sr) and fluid mud flows (massive and composite mudstone) and turbidity flows (graded mudstone) generating a sediment drift (see also Notta *et al.*, 2017; Reijenstein *et al.*, 2020). The massive and composite mudstone reflects deposition from concentrated density flows to debris flows, whereas the normal-graded mudstone was deposited by mud-rich waning turbidity currents (Otharán *et al.*, 2020). Bindstone intraclasts in the composite mudstone are restricted to the areas with bindstone, representing a distinct sedimentary structure attributed to erosion and redeposition of bindstone fragments as intraclasts by density flows. Microbial communities generating the bindstone thrived because of a higher sand-sized clasts in some areas, which constitute a favorable substrate for their growth (Noffke, 2010). Equilibrium structures suggest suspension feeding organisms (Mángano *et al.*, 1998), supporting the existence of contour current activity in this facies.

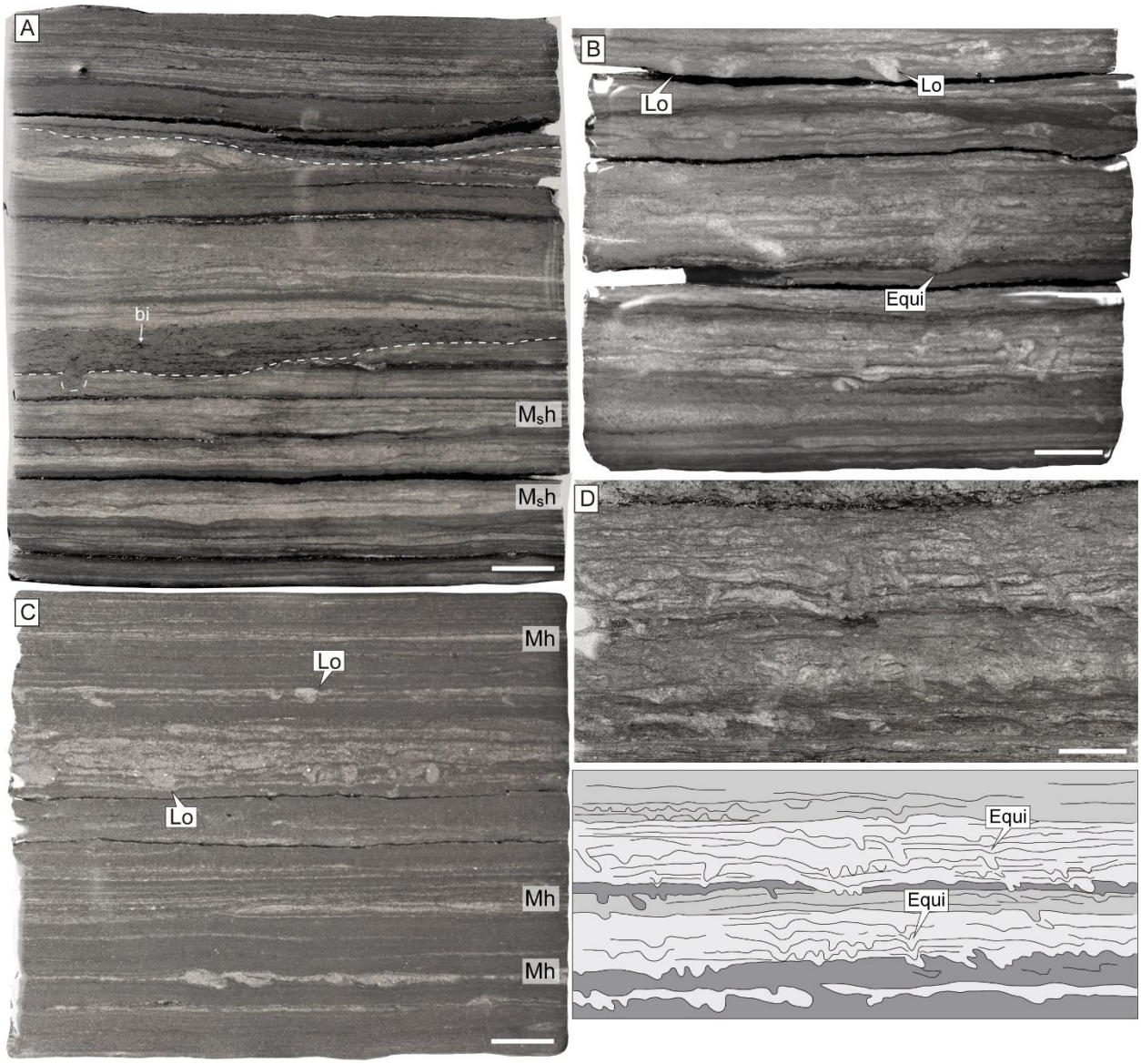

Fig. 6.13. Photographs of facies F3c showing mixed contour current (M_sh, Mh) and fluid mud flow (composite mudstone) sedimentation. A) Composite mudstone beds (bed bases delineated with a dashed line) comprising a basal, intraclastic mudstone, parallel-laminated coarse mudstone and normal-graded mudstone, containing bindstone intraclasts (bi). Contour current lithofacies, such as parallel-laminated coarse mudstone (M_sh), are intercalated. B) *Lockeia* isp. (Lo), locally displaying equilibrium structures (Equi). C) Coarse mudstone laminae encased in fine mudstone (Mh), with *Lockeia* isp. (Lo). D) Photograph and drawing of intervals with dense occurrence of equilibrium structures (Equi). Scale bars are 1 cm.

6.6 Paleoenvironmental and stratigraphic distribution of contourite facies

The Vaca Muerta Formation carbonate-siliciclastic clinoform system can be differentiated into basin (FA2), drift (FA3) and slope (FA4) facies associations. When these associations are projected on the seismic sections, they can calibrate the acoustic impedance, allowing to derive sedimentary environments in areas where neither cores, nor logs are available. This integration of sedimentology, stratigraphy, and seismic attributes represents a powerful tool to predict rock characteristics. In our case, this correlation highlights that the landward decrease of organic matter and increase of carbonate content is associated with an increase in acoustic impedance from basin to drift to slope environments (Reijenstein *et al.*, 2020; Fig. 6.3, 6.14A, B).

The stratigraphic distribution of contourite facies can be contextualized within the sequence stratigraphic study of Well 1 and Well 2 laid down in Chapter 4 and proposed by other authors that analyzed the study area (Fig. 6.14; e.g., Repol *et al.*, 2014; Notta *et al.*, 2017; Desjardins and Aguirre, 2018; Minisini *et al.*, 2020a). The succession shows three fourth-order sequences developed during deposition of Units 1 and 2 (Desjardins *et al.*, 2018; Minisini *et al.*, 2020b; Fig. 6.14C). The first sequence develops a Transgressive Systems Tract (TST) deepening towards starved basin conditions (F2a) and a Highstand Systems Tract (HST) within anoxic basin deposits (F2b). A sharp sea-level fall generating oxic basin (F2d) and drift deposits (F3a) above anoxic basin facies (F2b) characterized a Falling Stage Systems Tract (FSST). On top, the succession shows an aggradational pattern with a repetition of F2d and F3a, indicating a Lowstand Systems Tract (LST). The second sequence shows a TST characterized by the development of dysoxic basin deposits (F2c) on top of oxic basin facies (F2d), a HST comprising the progradation of the clinoform system, and a FSST triggering extensive contour current activity (F3c of Well 2). The third sequence developed a LST consisting of aggradation of fluid mud-rich, slope facies (F4d), whereas above, shutdown of fluid mud activity (F4b) represented deepening conditions of a TST.

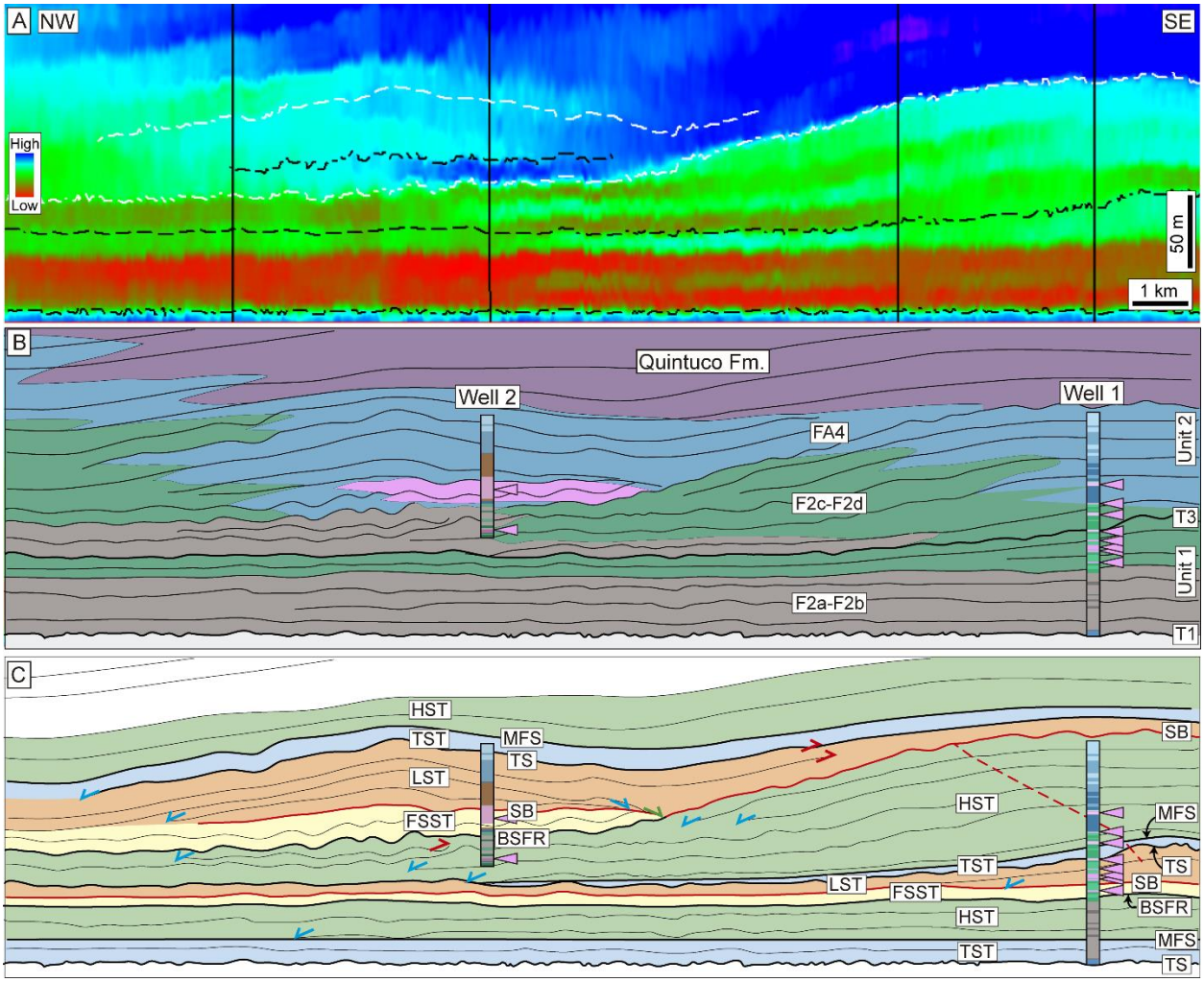

Fig. 6.14. Stratigraphic analysis of the Vaca Muerta Formation and stratigraphic position of the contourite facies from seismic data correlating Well 1 and Well 2. A) NW-SE acoustic impedance cross section (from Repol *et al.*, 2014; see location of wells in fig. 6.1). Lower impedance correlates with organic-rich mudstone, whereas higher impedance with carbonate-rich mudstone. B) Facies interpretation derived from sedimentologic analysis in core and impedance from image above. See fig. 6.4 for facies key. The starved and anoxic basin (F2a-F2b, grey) correlates with red colors in the impedance image A, the dysoxic and oxic basin (F2c-F2d, green) and drift (FA3, pink) facies with green and blue impedance colors, and the slope (FA4, light blue) with blue and light blue impedance colors. Pink arrows show facies dominated by contour current deposition (F3a, F3b, F3c) in the wells. C) Sequence-stratigraphic interpretation based on stratal termination analysis and facies evolution. Blue arrows = downlap, red arrows = truncation, green arrows = offlap, TS = Transgressive Surface, MFS = Maximum Flooding Surface, SB = Sequence Boundary, BSFR = Basal Surface of Forced Regression, TST = Transgressive Systems Tract, HST = Highstand Systems Tract, FSST = Falling Stage Systems Tract, LST = Lowstand Systems Tract.

6.7 Discussion

6.7.1 Evidence supporting a bottom/contour current origin

Differentiation between the depositional products of bottom currents and sediment-gravity flows has been a matter of debate for a long time because of the interplay of these two oceanographic processes in deep-marine environments and many shared characteristics (Heezen and Hollister, 1964; Heezen *et al.*, 1966; Hollister and Heezen, 1972; Stow and Lovell, 1979; Shanmugam *et al.*, 1993a, 1993b; Stanley, 1993; Stow *et al.*, 1998; Shanmugam, 2006, 2017; Hüneke and Stow, 2008; Mulder *et al.*, 2008; Stow and Faugères, 2008; Mulder, 2011; Rebesco *et al.*, 2014; Alonso *et al.*, 2016). Episodic turbidity and hyperpycnal flows are responsible for the most common gravity-flow deposits that may be confused with bottom currents. For instance, both low-density turbidity flows (*sensu* Stow and Shanmugam, 1980) and bottom currents (Shanmugam *et al.*, 1993a, 1993b; Shanmugam, 2006) record traction transport at the base of the flow. The associated deposits differ by the vertical arrangement of sedimentary structures: turbidites show traction structures from a waning flow, whereas bottom current deposits do not (Martín-Chivelet *et al.*, 2003). Hyperpycnal flow deposits share an additional characteristic with bottom currents: inverse-to-normally graded beds due to waxing-to-waning flows that can be confused with the similar bi-gradational energy profile of contourites (Mulder, 2011).

In Unit 1 of the Vaca Muerta Formation, most of the bottomset and foreset locations comprise pelagic and hemipelagic sedimentation, with minor sediment-gravity flow deposits in the bottomset (Paz *et al.*, 2019; Otharán *et al.*, 2020), and bottom current deposits in the bottomset to foreset. In Unit 2, sediment-gravity flows are dominant in the foreset due to higher angles. In this section, the evidence favoring a bottom current explanation for the lithofacies described in Fig. 6.5 and 6.15 is summarized (for an alternative interpretation of F3c, see Kietzmann *et al.*, 2020a). The list of processes that are not bottom currents include wave- or current-enhanced sediment gravity flows, quasy-steady turbidity currents (producing hyperpycnites), and surge-like turbidity or concentrated density flows (producing turbidites; Shanmugam, 2006). In addition, the observed dataset cannot be interpreted as downwelling, storm-induced return flows (producing tempestites) because these deposits are too deep (200-400 m; Minisini *et al.*, 2020b) to be considered above storm wave base of an epicontinental sea (<50 m, Schieber, 2016). However,

rare storm influence and symmetrical ripples are observed in F2d and F3b, respectively, indicating a higher contribution of storms towards shallower areas.

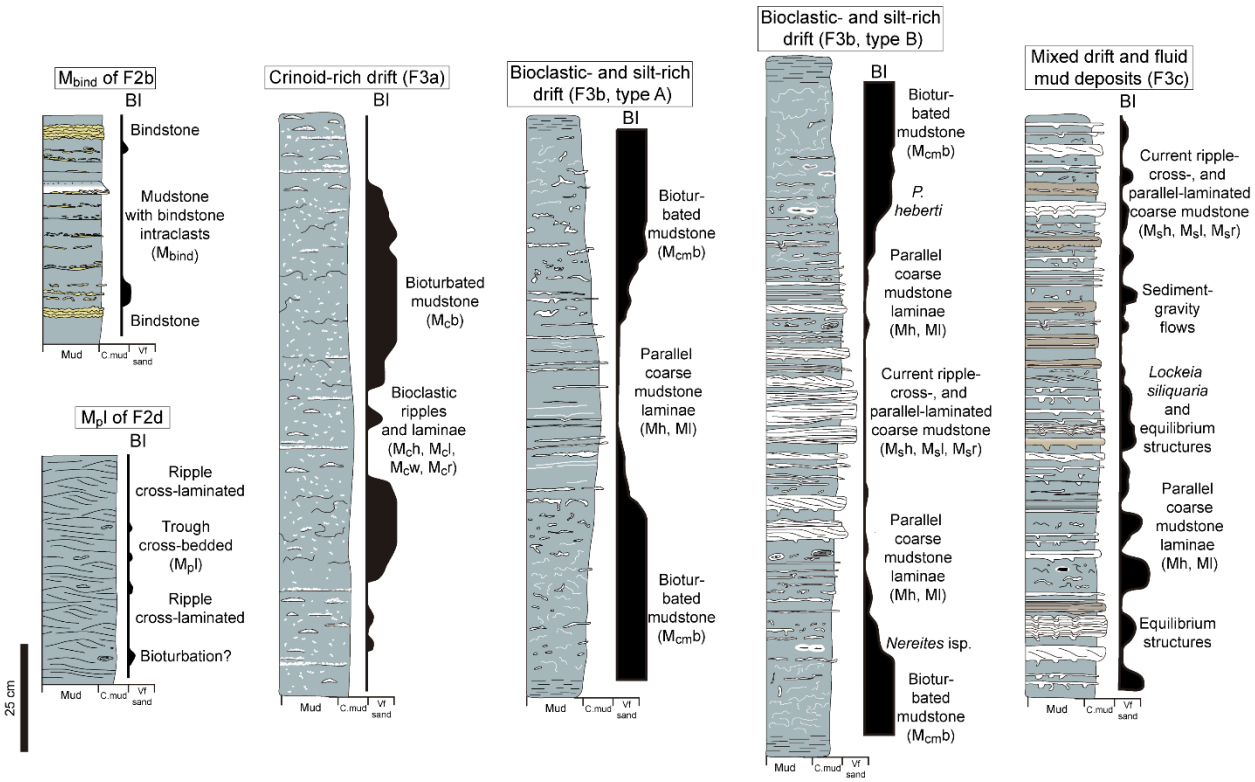

Fig. 6.15. Idealized facies succession for bottom/contour currents documented from the Vaca Muerta Formation displaying lithology, sedimentary structures, trace fossil content, and bioturbation index (BI).

6.7.1.1 Evidence of long-term current activity

In modern environments, bottom currents of contour-current type affect the seafloor during long periods of time (kyr to Myr; Stow and Faugères, 2008), depending on latitude, seafloor morphology, climate, or eustatic changes. This is in clear contrast with episodic sedimentation resulting in deposition of event beds (e.g. turbidites, tempestites, hyperpycnites). For instance, turbidites have a recurrence of 1 event per 1-150 ky (Talling, 2014 and references therein). However, other processes may have a higher recurrence in the rock record (gravity flows associated with failures of delta fronts or canyon heads, 0.1-5 events per year, Talling, 2014 and references therein; hyperpycnal flows, 1 event per 1-10 years, Johnson *et al.*, 2001; Warrick and Milliman, 2003).

Event beds display a bioturbated top that is developed during flow pauses (e.g., Stow and Shanmugam, 1980; Ponce *et al.*, 2007; Buatois *et al.*, 2011), whereas beds recording bottom current activity show traction structures with an unbioturbated sharp upper contact (Shanmugam *et al.*, 1993a, 1993b; Ito, 2002; Martín-Chivelet *et al.*, 2003; Shanmugam, 2006). Accordingly, the absence of normally-graded or bioturbated tops suggests a lack of post-event bed, hemipelagic sedimentation. Therefore, sharp upper contacts associated with many of the contour current lithofacies in our dataset indicate a continuous current of long-term duration (e.g. Figs. 6.8B, C, 6.9, 6.10, 6.11).

In addition, the occurrence of low bioturbation intensity in the middle of the type A and type B bi-gradational successions supports the idea of long-term currents, due to a continuous hydrodynamic energy stress on the ichnofauna (Fig. 6.12). In other words, the intervals rich in traction structures (represented by lithofacies Mh, Ml, M_sh, M_sl, M_sr, M_ch, and M_cr) are interpreted as deposited by long-term current activity that precluded the establishment of an infauna associated with background, post-event (fair-weather) deposition, as most traces can be emplaced within days after deposition (Wheatcroft *et al.*, 1989). A single event explanation for the type A and B bi-gradational successions is rejected due to the existence of a few colonization surfaces (Fig. 6.11) and the intercalation of tuffs (Fig. 6.8C).

From palaeontological and ichnological datasets, long-term current activity can be inferred from the presence of suspension feeding organisms, which can take advantage of subhorizontal currents delivering food. Equilibrium structures in facies F3c (Fig. 6.13B, D) are interpreted as produced by bivalves keeping pace with sedimentation, establishing a connection with the seafloor to feed from suspended food (Mángano *et al.*, 1998). *Crininicaminus* isp. and *Palaeophycus heberti* (observed in F3a and F3b) have been interpreted as domiciles of suspension feeders, although they can also be associated with detritus-feeding or predatory organisms (Ettensohn, 1981; Pemberton and Frey, 1982). In addition, although other modes of life have been proposed (e.g. benthic, Milsom, 1994), the *Saccocoma* crinoids were interpreted in other areas as pelagic suspension feeders, indicating the existence of a current system in the water column associated with F3a (Hess and Etter, 2011). This interpretation agrees with the local preferential occurrence of cold-water corals (sessile suspension feeders) on the path of contour currents of the Atlantic Ocean, Gulf of Mexico, and Mediterranean Sea (Hübscher *et al.*, 2010; Hebbeln *et al.*, 2016), although these type of corals have not been reported for the Vaca Muerta Formation.

6.7.1.2 Evidence of low sediment concentration

Bottom currents represent flows with low sediment concentration. For example, contour currents show concentrations of <0.01 to 10 mg/L (Hollister, 1993; Tucholke, 2002), cascading events display concentrations of 40 to more than 68 mg/L (Canals *et al.*, 2006, Palanques *et al.*, 2006), and internal tides develop peaks of ~200 mg/L (Puig *et al.*, 2013). Abundant traction structures are encountered in modern examples of deep-marine seafloors affected by bottom currents, due to dominant traction transport at the base of the flow (e.g., Heezen and Hollister, 1964; Heezen *et al.*, 1966). Mud floccule ripples created in flume experiments were produced under suspended sediment concentration of tens of mg/L (Schieber and Southard, 2009). Therefore, bottom-current reworked deposits show rare massive (by *en masse* deposition) or graded beds (Shanmugam *et al.*, 1993a, 1993b; Shanmugam, 2017; Martín-Chivelet *et al.*, 2003; 2008), and common laminated and rippled lithofacies, as found in facies F3a, F3b and F3c. Although laminated and rippled lithofacies are also common in turbidites, in our dataset they are not part of the typical Bouma sequence (Tc; Figs. 6.10, 6.11).

In contrast, sediment-gravity flows are characterized by high sediment concentration because excess density is necessary to generate gravitational forcing in the case of a low-angle seafloor, such as the Vaca Muerta foresets and bottomsets in Unit 1 (0.1-0.3° angles, Desjardins *et al.*, 2018; Minisini *et al.*, 2020b). For example, flood waters require high sediment concentrations to plunge and trigger a river-derived, hyperpycnal flow (1 g/L, Parsons *et al.*, 2001), and fluid mud flows and storm surge return flows need to overcome Coriolis forces deflecting transport along-shore (>1 g/L, Myrow and Southard, 1996; >10 g/L, Traykovski *et al.*, 2000). Modern observations of wave- and current-enhanced sediment gravity flows in low-angle slopes suggest depth-averaged sediment concentrations of 8-150 g/L for flows to be transported offshore, depending on ambient currents (Wright *et al.*, 2001). For instance, concentration values of up to 6 g/L were recorded during wave resuspension events in low angle shelves (*ca* 0.25°), but these suspensions were transported by shelf currents, not downslope (Traykovski *et al.*, 2000). Moreover, if compared with sand-rich flows, these high concentration, mud-rich flows present minor turbidity restricted to the base and a dominance of laminar conditions due to the high cohesiveness of the mud (Baas and Best, 2002; Baas *et al.*, 2011). The final deposit may be massive

or graded with soft-sediment deformation structures due to the development of upper transitional or quasi-laminar plug flows of high cohesive strength (e.g. Baas *et al.*, 2011).

Sediment-gravity flow deposits in the Vaca Muerta Formation comprise very thin to thin-bedded, massive calcareous medium to coarse mudstone, showing load casts, mudstone pseudonodules, flame structures, and pebble-sized, deformed intraclasts indicating soft-sediment deformation (Fig. 6.16). Muddy hyperpycnites in the SW Neuquén Basin contain deformed mudstone intraclasts (Paz *et al*., 2019). All these deformation structures suggest high sediment concentration and laminar flow transport in high cohesive strength flows, contrasting with the characteristics of low-concentration bottom currents (Shanmugam, 2006). The fine-grained turbidite model (*sensu* Stow and Shanmugam, 1980) and several muddy hyperpycnite examples (Bhattacharya and MacEachern, 2009; Wilson and Schieber, 2014) show an abundance of soft-sediment deformation structures, such as convolute lamination, load casts and pseudonodules, as well as mantle and swirl structures representative of bioturbation in soupy substrate conditions (Lobza and Schieber, 1999). In addition, sandy hyperpycnites display evidence of soft to soupy substrate conditions, including compacted *Thalassinoides* in distal delta front and proximal prodelta facies (Buatois *et al.*, 2011). Sandy hyperpycnites encased in deep-water heterolithic levees and in distal lobes contain biodeformational structures and *Tasselia* (Olivero and Lopez-Cabrera, 2010; Carmona and Ponce, 2011), a trace fossil associated with soupground conditions (Wetzel and Bromley, 1996). The soft to soupy sediment consistency is related to the liquefied nature of sediment-gravity flows due to water trapping at high sediment concentrations. All these characteristics can be used to infer high sediment concentration in sediment-gravity flows, which clearly contrast with the sediment loads of bottom currents.

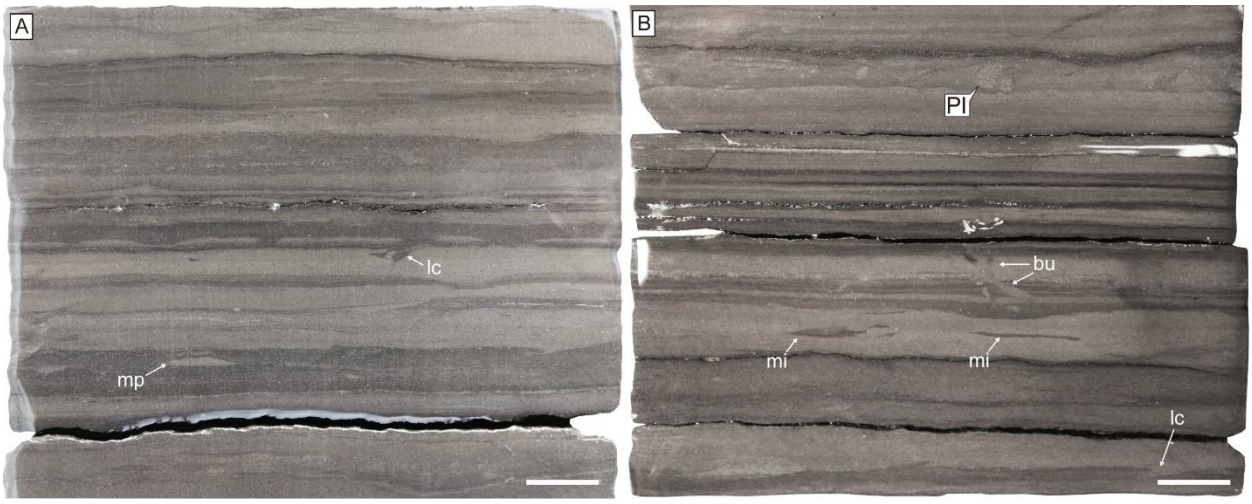

Fig. 6.16. A, B) Examples of sediment-gravity flows observed in the Vaca Muerta Formation (not analyzed in the present study). White beds are rich in coarse, calcareous mudstone whereas dark beds consists of fine mudstone. Massive and graded mudstone with minor silt laminae is common, displaying mudstone pseudonodules (mp), load casts (lc), mudstone intraclasts (mi), unidentified burrows (bu) and *Planolites* isp. (Pl). Scale bars are 1 cm.

6.7.1.3 Evidence of long-term oxygen supply

In areas with background anoxic to dysoxic conditions, oxygen and food supplied by bottom currents can generate highly bioturbated intervals (Wetzel *et al.*, 2008), whereas sediment-gravity flows cannot sustain long-term oxygenation and would produce the "doomed pioneer" ichnofabric (i.e., isolated *Thalassinoides* and *Gyrolithes* encased in unbioturbated laminated dark mudstone; Föllmi and Grimm, 1990). For example, in the Santa Barbara Basin, USA, turbidity currents were able to introduce oxygen in the deeper, oxygen-deficient areas, but the basin chemistry was restored after one month (Sholkovitz and Soutar, 1975). In the Vaca Muerta Formation, wave-influenced, sandy and muddy hyperpycnal lobes, channels and overbanks encased in anoxic, hemipelagic deposits are completely unbioturbated, suggesting sediment-gravity flows were not able to modify oxygen levels at the seafloor (Paz *et al.*, 2019).

Therefore, the association of traction structures with dm-scale, highly bioturbated intervals (Fig. 6.8A, 6.11C), in some cases sharply overlying parallel-laminated dark mudstone reflecting anoxic conditions (Fig. 6.12), suggests oxygen supply by bottom currents. This is reflected in the BI of drift deposits (1.86, n=894), compared with the BI of anoxic basin deposits (0.09, n=9110) or facies rich in fluid mud flows (0.95, n=335). Redox-sensitive elements and average TOC

decreasing during bottom current activity also indicates an increase in oxygen (Fig. 6.4D, E), however, small burrow diameters suggest upper dysoxic conditions. Unbioturbated and sparsely bioturbated intervals may occur in these deposits (e.g. the middle part of type A and type B successions), yet they are caused by long-term, hydrodynamic stress and/or local dysoxic to completely anoxic conditions.

6.7.2 Origin of the currents

The cores described were not oriented when retrieved, hence there is no paleocurrent data to understand the direction of current transport. The existence of some shelf-derived sediments in the higher-energy lithofacies of F3b and F3c (e.g. *Rhaxella* fragments and carbonate intraclasts) indicates an across-shore flow component shedding material from the shelf (Rodríguez Blanco *et al.*, 2020). Nevertheless, plan-view seismic amplitude extraction of the sedimentary body associated with F3c shows an along-slope elongation (5 km wide and 20 km long), suggestive of along-shore transport (Reijenstein *et al.*, 2020). Rock magnetic analysis to determine paleocurrents are currently under study and may shed light on the paleocurrent directions in the future (e.g. Kohan Martínez *et al.*, 2018).

During deposition of the contourite facies of the top of Unit 1 and base of Unit 2 (*A. proximus* to *W. internispinosum* ammonite zones), coeval landward deposits in the foresets of the clinoform are represented by the Los Catutos Member of the Vaca Muerta Formation, which are host to highly fossiliferous limestones interbedded with marlstones and mudstones deposited during the Tithonian (upper *A. proximus* to *W. internispinosum* ammonite zones; Rodríguez Blanco *et al.*, 2020). In turn, this Member was developed while a pure carbonate interval in the topsets (shelf) occurred (*W. internispinosum* ammonite zone interval of the Picún Leufú Formation), displaying wackestone-packstone intercalated with bivalve-oyster floatstone and cross-bedded oolitic grainstone of tidal or bay origin (Zeller *et al.*, 2015a; Parada, 2019; Rodríguez Blanco *et al.*, 2020). High bioturbation, heterolithic bedding, the existence of *Palaeophycus heberti*, and bivalve trace fossils in Los Catutos Member (Kietzmann *et al.*, 2014b; Rodríguez Blanco *et al.*, 2020; M. Paz unpublished data) indicate that this unit may be related to the contourites described in the present study.

The circulation system generating enhanced contour current activity during the time interval associated with the described contourites and the development of the Los Catutos Member

(Fig. 6.2, 6.3, 6.14) was influenced by atmospheric circulation (wind stress) and buoyancy forces (thermohaline drivers). NE-trending winds during the Kimmeridgian (Spalletti *et al.*, 2011) probably continued into the Tithonian, due to the existence of monsoonal wind patterns (Scherer *et al.*, 2020). Hence, in the study area, NE-directed winds generated counterclockwise surface circulation that affects water depths associated with the topset to upper foreset of the subaqueous clinoform system (Zeller *et al.*, 2015a). At deeper water depths, intermediate water masses producing clockwise circulation may have reworked lower foreset and bottomset locations. This circulation system may have been similar to, or fed by, low-oxygen paleo-poleward undercurrents such as those observed at Eastern Boundary Upwelling Systems (e.g. Peru-Chile Undercurrent, Fonseca, 1989; or the California Undercurrent, Lynn and Simpson, 1990). The more vigorous circulation of this time interval is provided by increased or higher density cascading of high salinity and low temperature, dense waters from shelf areas (topset), originated during times of cold fronts or storms (Eberli and Betzler, 2019; Minisini *et al.*, 2020a; Rodriguez Blanco *et al.*, 2020). NE winds may have acted as cold dry fronts that lowered the temperature of shelfal waters, for instance, in the Picún Leufú shelf. Cascading of surface watermasses change the chemistry of deep waters, producing the oxygen increase recorded in the studied dataset (e.g. Meier *et al.*, 2006; Coppola *et al.*, 2017). These currents cascaded deeper than during previous warmer periods due to higher density. Once reaching intermediate waters, they were deflected to the left by the Coriolis force, feeding the clockwise circulation system. Higher density intermediate water masses may have changed the outflow pattern of the Neuquén Basin, switching towards a stage of deep outflow associated with anti-estuarine (or probably weakened estuarine), basin-wide circulation. Higher current velocity in wells 1 and 2 may have been augmented by the close location to a strait, evidenced by local subsidence associated with normal faults (during deposition of Unit 1) and the activation of the Loma La Lata high (Fig. 6.1, during deposition of Unit 2; Domínguez *et al.*, 2020b). Similar successions deposited by contour currents occur in marginal seas such as the Adriatic Sea (Verdicchio and Trincardi, 2008b) or the Western Mediterranean Sea (Lüdmann *et al.*, 2012).

Although processes such as tides are unlikely to be amplified enough to trigger basin-wide, long-term changes in seafloor oxygenation, these processes are not completely excluded as possible drivers for bottom current transport (e.g. Kietzmann *et al.*, 2014b; Zeller *et al.*, 2015a; Schieber, 2016). Zeller *et al.* (2015a) considered tides as a driver for basin circulation in the Vaca

Muerta Formation, based on the evidence of tidal transport on the shelf (Picún Leufú Formation), such as sigmoidal cross-bedding with mud drapes, herringbone cross-bedding and inclined heterolithic stratification (Spalletti *et al.*, 2000; Kietzmann *et al.*, 2014b). Nonetheless, Parada (2019) analyzed the same interval and pointed out the absence of tidal sedimentary structures. In our dataset, the black laminae in F3b are composed of mud intraclasts and do not represent mud drapes of tidal origin (e.g. massive mud layers with local flame structures; Sato *et al.*, 2011), indicating traction processes of a bimodal, non-pulsating flow (Fig. 6.11; Baas *et al.*, 2016; Yawar and Schieber, 2017; Canale *et al.*, 2020). The volcanic arc with islands to the west might have attenuated the tidal effects in the Neuquén Basin, similar to what is observed today in the Gulf of Mexico or the Japan Sea (Canale *et al.*, 2020 and references therein). Indeed, tidal modelling of epicontinental basins indicates that the existence of islands greatly affects the tidal range values of the basin (Wells *et al*., 2005). However, the tidal effects on the Vaca Muerta Formation might be confined to the topsets (shelf) where tidal wave shoaling or resonance might took place.

An additional process that can resuspend sediment and maintain bedforms are internal waves, which propagate along a pycnocline and rework sediment on sloping surfaces (Cacchione and Drake, 1986). The interval containing *Saccocoma* mudstone (F3a) in the Vaca Muerta Formation shows an alternation of oxic and anoxic conditions, suggesting a paleo water depth close to the fluctuating paleo-oxycline (a probable area of density stratification). Deposits from internal waves have been reported in the Upper Jurassic Rosso Ammonitico Formation in the Betic Cordillera (Spain), where cross-bedded peloidal grainstone and *Saccocoma* packstone with hummocky cross-stratification (HCS) are interbedded with bioturbated, bioclastic wackestone (Pomar *et al.*, 2019). This alternation is interpreted as shifts from anoxic and high-energy conditions, to dysaerobic and calm, to aerobic and calm (Pomar *et al.*, 2019). In our case, no HCS were observed neither in the Yesera del Tromen outcrop, nor in core (where narrow samples may hamper visualization of larger scale bedding surfaces). Nevertheless, internal waves producing sediment wave fields have an across-slope extension of tens of km, restricted by the range of pycnocline oscillations, which contrasts with the deposits of our dataset (Puig *et al.*, 2007; Ribó *et al.*, 2016). During the end of Unit 1 deposition, contour currents occurred in bottomset to foreset areas (extending to the outcrop section), indicating an across-slope distance of *ca* 160 km. Ultimately, future paleocurrent measurements may help to understand the role of internal waves

in sedimentation, as these currents may show across-shore orientation that contrasts with the along-shore orientation of contour currents (Urgeles *et al.*, 2011).

In conclusion, the deposits from our dataset can be interpreted as produced by contour currents intensified by enhanced cascading of dense, shelf waters. However, it must be noted that some of the discussed evidence cannot be attributed to lithofacies M_{bind} of F2b. For example, lithofacies M_{bind} does not have evidence of long-term duration or long-term oxygen introduction, yet it was produced by a current showing low sediment concentration and reworking authochtonous material. Therefore, other short-term processes, such as internal solitary waves or deep-water flushing reworking, can also explain lithofacies M_{bind} occurrence.

6.7.3 Sedimentologic implications for the Vaca Muerta Formation

An integrated sedimentologic model for the contourites of the Vaca Muerta Formation is proposed in this study (Figs. 6.15, 6.17). These deposits have been described before from this Formation, yet their origin has been unknown (e.g. Gasparini *et al.*, 1997; Spalletti *et al.*, 1999; Scasso *et al.*, 2002; Kietzmann *et al.*, 2008; 2014a; Kietzmann and Palma, 2009b). Seismic and backstripping analyses estimate a depositional water depth of 200-400 m for the bottomset (Mitchum and Uliana, 1985; Minisini *et al.*, 2020a). The low fetch of the basin might have generated a shallow storm wave base (<50 m water depth for epicontinental seas; Schieber, 2016; see also Kietzmann and Palma, 2009b). Rivers and eolian input from the south provided siliciclastics that mixed with benthic and pelagic carbonate production and volcaniclastic material (Leanza *et al.*, 2011; Minisini *et al.*, 2020a). Towards the shelf, wind effects might have been dominant, generating a wind-driven, counterclockwise surface current system that drove clinoform progradation by lateral sediment advection in the slope (Zeller *et al.*, 2015a). Offshore, cascading water masses, clockwise contour currents, and sediment-gravity flows likely transported sediment and reworked bottomset and foreset locations.

In our scheme, contourites are abundant in FSST and LST of the first sequence and FSST of the second sequence, although they are also identified in HST and TST (Fig. 6.14, 6.17). Both contourite intervals were interpreted in regional seismic data as FSST or LST based on acoustic impedance and stratal terminations (Notta *et al.*, 2017; Domínguez *et al.*, 2020a). These intervals of low sea-levels are associated with carbonate-rich deposition. In turn, carbonate-rich intervals are bracketed between the siliciclastic-rich to mixed, early Tithonian (*Virgatosphinctes andesensis*

and *Pseudolissoceras zitteli* ammonite zones in Picún Leufú, Paz *et al.*, 2019) and late Tithonian to late Berriasian (*Substeueroceras koeneni* and *Spiticeras damesi* ammonite zones in Sierra de la Vaca Muerta, Zeller, 2013) or early Berrasian (Capelli *et al.*, 2021), suggesting a decrease of riverine input generating enhanced carbonate formation. In fact, in the SW Neuquén Basin, Krim *et al.* (2017) analyzed clay minerals and interpreted reduced terrigenous supply for the carbonate interval, associated with either establishment of arid conditions or a decreased size of fluvial catchment areas due to tectonic reconfiguration. However, data from basin centre locations indicate temperate, semi-arid conditions for the whole Tithonian interval (Capelli *et al.*, 2021).

Moreover, times of carbonate deposition might be associated with cooler climates. For instance, during deposition of inner to outer shelf carbonates of the Picún Leufú Formation in the southern part of the basin (late Tithonian-early Berrasian, Leanza *et al.*, 2020), Alberti *et al.* (2020) recorded a cold snap (18°C) using bivalve oxygen isotope data. However, Gómez-Dacal *et al.* (2018) calculated relatively warm temperatures (~25°C) in the northern Neuquén Basin at the same time. Regional paleoclimatic analysis of southern South America and western Antarctica suggests cool climates and sea-level lowstands during the late Tithonian (Brysch, 2018). An increase in aridity has been documented in Tethyan and Boreal domains for the Tithonian (Hesselbo *et al.*, 2009), in some cases associated with cooler surface waters (Ruffell *et al*., 2002).

The model that follows is that the contour currents were probably intensified during FSST and LST (Notta *et al.*, 2017; Domínguez *et al.*, 2020a), when sea-level was low enough to enhance bioclastic carbonate production in the topset (Reijenstein *et al.*, 2020), and arid and cooler climates increased the rate and density of cascading events. This is exemplified by the upward increase in carbonate content, current strength, and oxygenation in the Vaca Muerta Formation shallowing upward parasequences. Zeller *et al.* (2015a) suggested increased carbonate deposition and low current activity during HST due to a lack of accommodation space for current development that decreases siliciclastic input (Zeller *et al.*, 2015a). However, the model might be innaccurate because HST are times of accommodation space creation (although at a lower rate than sedimentation rate), and accommodation space refers to the space available for sediments (and not for currents) to accumulate (Jervey, 1988). It is likely that the issue resides in using a sequence stratigraphic approach for carbonate deposition (HST carbonates vs. LST and TST siliciclastic) for a subaqueous clinoform system that lacks a siliciclastic-rich LST associated with complete topset subaerial exposure (Reijenstein *et al.*, 2020). Therefore, as observed in our dataset, HST

successions are associated with siliciclastic- and organic-rich intervals, whereas FSST and LST show carbonate-rich deposition (Fig. 15). Brackenridge *et al.* (2011) suggested a contourite sequence-stratigraphic model of enhanced current activity during first- or second-order LST associated with enhanced erosion in the shelf. Although the present sequences are of third- or fourth-order, the Vaca Muerta Formation departs from this model in that arid and cooler climates increased winter convection and were the cause of more vigorous contour current circulation during low sea-levels.

The eight successions of F3a and F3b in Well 1 span a minimum of *ca* 1.21 My (from T2, base of *Aulacosphinctes proximus,* to lower Unit 2, lower *Windhauseniceras internispinosum* ammonite zone; Desjardins and Aguirre, 2018; Kietzmann *et al.*, 2018a; Minisini *et al.*, 2020b), hence implying a *ca.* 152 ky minimum recurrence for the intensification of contour currents and indicating a probable control by high-frequency eccentricity cycles (Kietzmann *et al.*, 2015; 2020b). In modern environments, contour currents can be intensified during cooler periods at a kyr scale, due to more vigorous circulation associated with enhanced deep convection (e.g. Baltic Sea, Moros *et al.*, 2020; Mediterranean Sea, Cacho *et al.*, 2000).

In the southern part of the Neuquén Basin, Rodríguez Blanco *et al.* (2020) have interpreted shelf-sourced carbonates in the Vaca Muerta Formation generated by density cascading. This mechanism is effective in providing oxygen to deeper watermasses (e.g. Meier *et al.*, 2006; Coppola *et al.*, 2017) and allows explaining the complete, basin-wide bottom water oxygenation recorded during the development of F2d, F3a, F3b and F3c (Fig. 6.3). Alternation between basin-wide anoxic and more oxygenated conditions was probably controlled by changes in the rate and density of winter cascading, which can modify the general circulation pattern of the Neuquén Basin. During times of estuarine circulation, anoxic bottom waters were sluggish and dense, and the surface waters constituted the typical basin outflow. During times of weakened estuarine or anti-estuarine circulation, a higher rate and density of cascading events increased the density and oxygen content of deep waters, generating a deep outflow of the basin (Witzke, 1987; Stratford *et al.*, 2000). Alternation of these two systems is controlled by the density differences between surface and bottom waters, which is mainly affected by riverine input and temperature.

The Vaca Muerta Formation occurs at the boundary between mid-latitude arid conditions to the north and warm moist climates to the south (Volkheimer *et al.*, 2008). Therefore, a poleward shift of the arid belt may have triggered arid conditions in the Southern Neuquén Basin, generating

a decrease in fluvial input from the North Patagonian Massif, less stable pycnoclines, contraction of anoxic zones and increased carbonate production and exportation from shallower areas (Sagasti, 2005; Kietzmann *et al.*, 2020b). In turn, the poleward migration of the arid belt might be associated with cooler stages, due to the evidence of lowering water temperatures. The idea of a poleward expansion of the arid belt during cooler climates goes against the fact that the belt is currently migrating poleward under modern global warming. However, Hasegawa *et al.* (2012) suggested the contrary for the Cretaceous greenhouse climate, with an equatorward shift of the arid belt during warming events when certain CO_2 levels are surpassed (but see Wagner *et al.*, 2013), which may represent an explanation for the increase in aridity in tandem with cooling during the late Tithonian.

The present sedimentologic model explains the enigmatic occurrence of bottom current activity in relatively deep, basinal locations of the Vaca Muerta Formation, which were previously described as "outer ramp" environments, a depositional setting characterized by infrequent storm reworking (Burchette and Wright, 1992). Backstripping analysis suggests water depths considerably deeper than the location of the storm wave base (200-350 m for the proximal bottomset, Minisini *et al.*, 2020b), and the evidence presented herein precludes the idea of storm-generated sediment-gravity flows. Storms were probably the trigger of cascading events originating from the shelf, although cascading was controlled by climatic conditions. Therefore, the model is able to explain both the upwards increase of carbonate deposition in parasequences and the climatic control generating rhythmicity in the Vaca Muerta Formation (e.g. Kietzmann et al., 2020b). Relatively shallower areas such as the Mendoza shelf or Picún Leufú record clear HCS structures in peloidal mudstone and sandstone (Kietzmann and Palma, 2011; Paz *et al.*, 2019), indicating a storm wave base associated with basin margin locations.

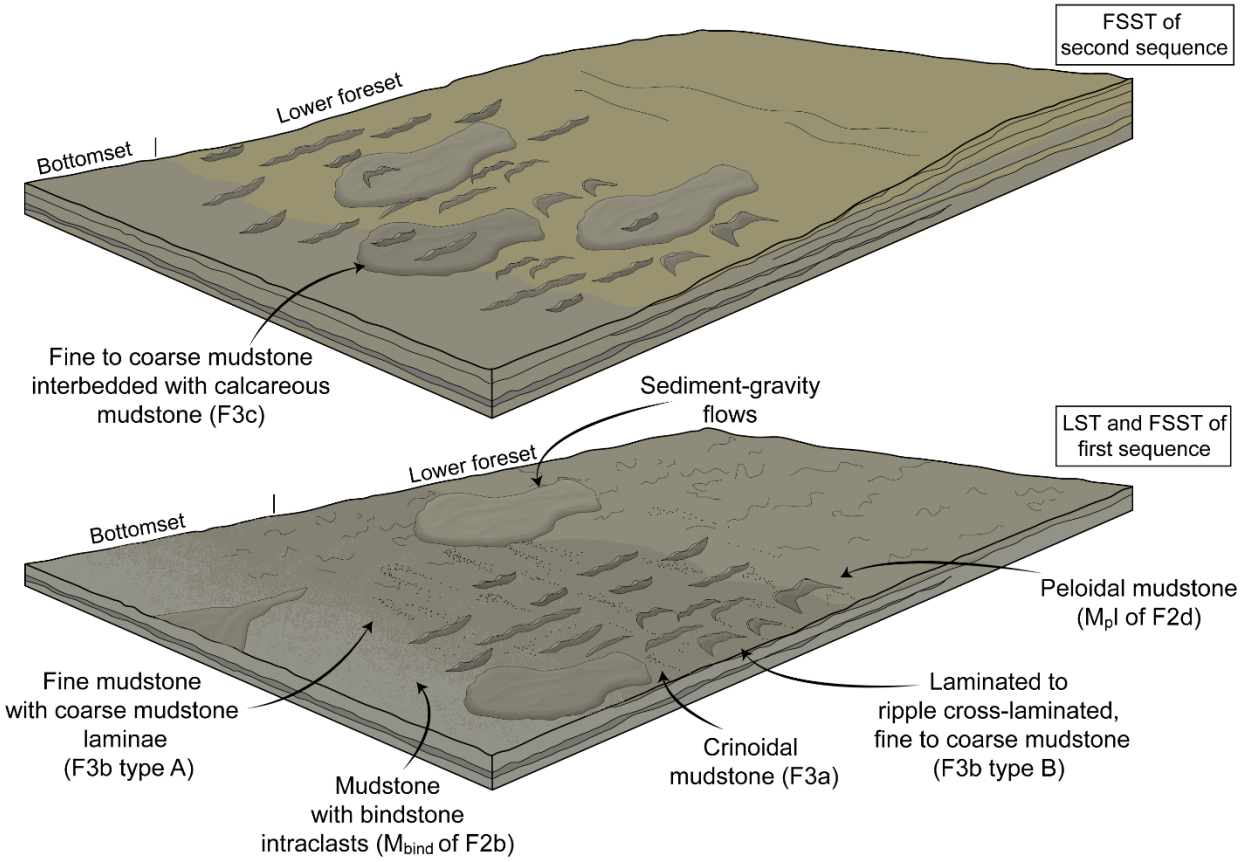

Fig. 6.17. Block diagram showing the location of bottom/contour current deposits in the mixed carbonate-siliciclastic clinoform system of the Vaca Muerta Formation.

6.7.4 Sedimentologic implications for a broader analysis of fine-grained successions

The present study generates different lines of evidence to interpret sedimentary features in fine-grained successions as deposited by contour currents. Where traction structures are abundant and low slope angles preclude sediment-gravity flow transport, the bottom current forcing mechanism represents a plausible process to redistribute mud in distal locations (Schieber, 2016). Moreover, in successions affected by background oxygen deficiency, the presence of highly bioturbated beds are indeed an evidence of contour current reworking and deep-water oxygen renewal (Stow and Faugères, 2008; Wetzel *et al.*, 2008; Rodríguez-Tovar and Hernandez-Molina, 2018; Birgenheier and Moore, 2018). In addition, it must be noted that the evidence of currents with long-term duration, low sediment concentration, and long-term oxygen introduction is not a prerequisite to suggest bottom current activity. Bottom currents can be of short-term duration (e.g. cascading, flushing of deep waters), may support high sediment loads due to entrainment

(Shanmugam, 2013), be composed of mixed planktonic and neritic sediment (Eberli and Betzler, 2019), and show low oxygen content (e.g. Sivkov *et al.*, 2002). Minor graded and massive beds with load casts and pseudonodules were also recorded in F3b, implying that high-concentration suspensions can be achieved by these currents.

Interbedded contour current and sediment-gravity flow deposits occur in F3c (Fig. 6.13). Reworking of sediment-gravity flow deposits by contour currents constitutes a process documented in modern (Mulder *et al.*, 2008 and references therein) and ancient examples (e.g., Stanley, 1993; Ito, 2002), although debate persists regarding its recognition in the case of ancient deposits (cf., Stanley, 1993; Stow *et al.*, 1998). Sharp upper bed contacts with overlying hemipelagites, better-sorted rippled sands, and a different paleocurrent direction contrasting with the gravity-flow paleocurrent, are evidence used in fossil examples to determine contour current activity (Ito, 2002). In our case, current ripples atop and within massive beds indicate contour current reworking, superimposed to gravity flow deposits.

Furthermore, analysis and delineation of these deposits have industry applications, as TOC is typically less in the facies recording contour current activity (F3a and F3b; av. TOC of 4.04% and 2.25%, respectively) than in facies recording hemipelagic deposition (F2b and F2d; av. TOC of 5.06% and 4.77%, respectively; Fig. 6.4D). This fact is related to the enhanced organic carbon remineralization due to bioturbation associated with the oxygenation events of the currents (Aller, 1994; Wetzel *et al.*, 2008) and with a high content of carbonate grains and skeletal components generating TOC dilution. The oxygen content of the along-shore system is influenced by the rate and density of shelf water cascading and the distance from the shelf, because currents decrease their oxygen content as they travel through the organic matter-rich seafloor. Hence, relatively high TOC intervals in F3a are related with anoxic contour currents in distal positions. The geochemical data also supports the idea of less reducing conditions in the contourite deposits (Fig. 6.4E). In addition to low TOC, these lithofacies have low porosity (mainly interparticle) and high water saturation (Lithofacies 3 of Minisini *et al.*, 2020a).

Contouritic deposition can be sumarized in two facies models: (1) a model that implies high bioturbation index due to food- and oxygen-rich environments (Faugères *et al.*, 1984; Gonthier *et al.*, 1984; Stow and Lovell, 1979; Stow and Faugères, 2008; Rodríguez-Tovar and Hernandez-Molina, 2018; Dorador *et al.*, 2019), and (2) a model characterized by the abundance of traction structures (Shanmugam *et al.*, 1993a, 1993b; Martín-Chivelet *et al.*, 2003, 2008;

Shanmugam, 2006, 2017). This discrepancy was explained due to contrasting energy conditions between low-energy, bioturbated muddy contourites, and high-energy, unbioturbated sandy contourites (Stow and Faugères, 2008; Rebesco *et al.*, 2014). However, the present contribution shows highly bioturbated intervals and successions with relatively well-preserved traction structures in a muddy to bioclastic deposit (Fig. 6.15), unifying both facies models and demonstrating that sedimentary structures could be preserved in fine-grained depositional environments when stress factors (hydrodynamic energy and oxygen deficiency) limit bioturbation.

The documented deposits constitute an additional example to the growing list of fine-grained successions where traction structures are considered the product of current reworking (e.g., Pratt, 1984; Schieber 1994, 1999a, 2016; O´Brien, 1996; Loucks and Ruppel, 2007; Singh *et al.*, 2008; Trabucho-Alexandre *et al.*, 2012; Egenhoff and Fishman, 2013; Frébourg *et al.*, 2013; Leonowicz, 2013; Nyhuis *et al.*, 2014; Birgenheier *et al*., 2017; Knapp *et al.*, 2017; Ayranci *et al.*, 2018; Li and Schieber, 2018; Minisini *et al.*, 2018). Surprisingly, many of these fine-grained deposits also occur in epicontinental basins affected by oxygen deficiency and showing high organic matter content. The Vaca Muerta Formation differs from other records of bottom current activity mainly by the existence of bioturbation and, in particular, its bigradational bioturbation pattern. In addition, the sharp boundaries at the base and top of some successions with unbioturbated dark mudstone constitute an exceptional preservation of these deposits, as they delineate the beginning and end of the currents or shifts in the current axis, and facilitated a detailed description of sedimentary processes and environmental controls.

6.8 Conclusions

In the study area (Neuquén Embayment, Neuquén Basin, Argentina), the Lower Jurassic-Upper Cretaceous Vaca Muerta Formation comprises a mixed carbonate-siliciclastic clinoform system showing basin, drift and slope environments. The sedimentologic analysis focused on fine to coarse mudstone with bindstone intraclasts, cross-bedded, peloidal mudstone, bioturbated, laminated and cross-bedded crinoidal mudstone, and bioturbated, laminated and rippled, fine to coarse mudstone observed in cores from five wells. These deposits can be subdivided into fifteen lithofacies encased in facies affected or dominated by contour current transport. The evidence

supporting a contour current hypothesis can be summarized as follows: (1) the absence of normal-graded or bioturbated caps, the continuous high hydrodynamic stress observed in the middle of the decreasing to increasing bioturbation index successions, and the suspension feeding organisms, which indicate the existence of long-term current activity, (2) the high amount of traction structures ,point towards a flow of low sediment concentration capable of moving sediment across low angle slopes (bottomset and foreset), and (3) the existence of highly bioturbated intervals, which suggests sustained oxygen introduction to benthic environments by currents. Due to the correlation with the Los Catutos Member and modern analogs, we propose that cascading of cold, dense shelf waters triggered the intensification of an along-shore, contour current system that reworked bottomset to foreset locations. This process represents the most plausible explanation to generate a switch in basin circulation (from estuarine circulation, to weakened estuarine or anti-estuarine circulation) and oxygenate distal areas of the system. The present study supports previous interpretations of sedimentary features, such as traction structures and high bioturbation, as produced by contour current transport. Differentiation from hyperpycnites, turbidites, and wave- and current-enhanced sediment gravity flows represent a real challenge because bottom/contour currents can be of short-term duration, contain high-sediment concentration, show mixed composition, and low oxygen content. These difficulties suggest that more work is needed in this area to expand our understanding of sediment transport processes in fine-grained sediments.

6.9 Acknowledgments

We thank Shell and Tiser S.R.L., and Germán Canto, Adrián Dolso, Sebastián J. Estrada, Sebastián Galeazzi, and Fabián Lamarque from Total Austral S.A. for sharing core information with us. Special thanks to Andreas Wetzel for his valuable comments on an early draft of the manuscript. This work was financially supported by the Natural Sciences and Engineering Research Council (NSERC) Discovery Grant [422931-20] to L.A. Buatois, [311727–20] and the George McLeod Enhancement Chair in Geology to M.G. Mángano, PI-UNRN 2017 [40-A-616] and PIP-CONICET [129] to N.B. Carmona, 2016 Student Research Grant from Society for Sedimentary Geology (SEPM), 2016 and 2018 Research Grant from the Geological Society of America (GSA), 2016 Grants-in-Aid Program of the American Association of Petroleum Geologists (AAPG), and 2018 Postgraduate Grant from the International Association of Sedimentologists (IAS).

TRANSITION

Chapter 6 comprises a sedimentological analysis of the bottom current deposits of the Vaca Muerta Formation located in the basin centre area. Chapter 7 focuses on the ichnological dataset of these deposits. An ichnofabric analysis was conducted, and the role of different stress factors is evaluated in order to understand palaeocological controls on bioturbation.

CHAPTER 7: ICHNOLOGY OF MUDDY SHALLOW-WATER CONTOURITES FROM THE UPPER JURASSIC-LOWER CRETACEOUS VACA MUERTA FORMATION, ARGENTINA: IMPLICATIONS FOR TRACE-FOSSIL MODELS

Paz, M., Mángano, M.G., Buatois, L.A., Desjardins, P.R., Notta, R., González Tomassini, F., and Carmona, N.B. (in review). Ichnology of muddy shallow-water bottom current deposits from the Upper Jurassic-Lower Cretaceous Vaca Muerta Formation, Argentina: Implications for trace-fossil models. *Palaios*.

Abstract

Contour current activity is increasingly being recognized in ancient fine-grained depositional environments. However, detailed ichnological analysis focused on shallow-water examples of these deposits are scarce. The Upper Jurassic-Lower Cretaceous Vaca Muerta Formation from Argentina constitutes an important unconventional reservoir that displays dm- to m-thick, laminated, rippled and bioturbated, crinoidal mudstone and fine to coarse mudstone deposited by wind- and thermohaline-driven contour currents. Four ichnofabrics were recognized in three facies. The *Palaeophycus heberti* ichnofabric is the dominant one in facies 3a (crinoidal mudstone), forming highly bioturbated intervals. The *Palaeophycus heberti*, *Nereites* isp. and *Phycosiphon incertum* ichnofabrics are present in facies 3b (fine to coarse mudstone), typically forming highly, moderately and sparsely bioturbated intervals, respectively. In this facies, m-thick successions comprising an upward decrease and then increase in bioturbation index occur. The Equilibrichnia-Fugichnia ichnofabric was mostly recorded in facies 3c (fine to coarse mudstone and calcareous mudstone) and less commonly in facies 3b, forming distinctive bioturbated intervals within scarcely bioturbated successions. Benthic activity was controlled by food distribution, oxygenation, hydrodynamic energy, and water turbidity. Food was delivered at the surface or in suspension, promoting deposit- or suspension-feeding strategies in the infauna, respectively. Oxygen levels increased during contour current activity, yet remained relatively low (upper dysoxic). Hydrodynamic energy controlled bioturbation intensity, resulting in lower degrees of bioturbation during high-energy events. Suspension feeding strategies suggest that water turbidity was relatively low during current transport. The present example increases our

understanding of environmental controls of shallow-water contour currents, supporting the fact that high bioturbation levels are typical of contourite deposits, and providing an example of muddy contourites showing a high preservation of sedimentary structures due to oxygen deficiency in bottom waters.

7.1 Introduction

Shallow-water contour currents occur within 50-300 m of water depth (Stow *et al.*, 1998), and are induced by thermo-haline, wind-, or tide-driven circulation. The action of currents generates abundant traction structures at the seafloor owing to the constant transport of sediment by water masses movement. During the last two decades, special attention has been paid to traction structures, such as silt laminae and current ripples, in fine-grained depositional systems (Schieber, 1994, 2016; Macquaker and Bohacs, 2007; Schieber *et al.*, 2007), and they were in many cases interpreted as produced by bottom currents of thermohaline forcing origin (e.g., Frébourg *et al.*, 2013; Knapp *et al.*, 2017; Ayranci *et al.*, 2018). These deposits share many characteristics with the present example, because they comprise fine-grained sediments with high organic matter content, formed under oxygen-deficient conditions.

Trace-fossil analysis represents a useful tool to unravel environmental controls on bioturbated contourites (see reviews by Wetzel *et al.*, 2008, and Rodriguez-Tovar and Hernández-Molina, 2018). However, ichnologic studies of shallow-water ancient and modern contourites are scarce and insufficient to illustrate the whole range of ecologic constrains of these systems (e.g., Virtasalo *et al.*, 2011; Ayranci *et al.*, 2018). One of the most important problems to describe trace fossils in these deposits is the difficulty to detect contour current transport in areas with tidal, storm and wave action such as the shallow-water realm, which can be superimposed to ambient currents and modify the sedimentary deposit. In this sense, most ichnologic studies available focus on ancient and modern mid- and deep-water contourites (Fu and Werner, 1994; Baldwin and McCave, 1999; Savrda *et al.*, 2001; Löwemark *et al.*, 2004, Wetzel *et al.*, 2008; Rasmussen and Surlyk, 2012; Rodríguez-Tovar and Hernandez-Molina, 2018; Míguez-Salas and Rodríguez-Tovar, 2019; Rodríguez-Tovar *et al.*, 2019; Reolid and Betzler, 2019; Dorador *et al.*, 2019; Hovikoski *et al.*, 2020). Other ichnological analyses were made on shallow-water marine straits and corridors, where current activity is intensified due to flow constraint (Miguez-Salas and Rodríguez-Tovar,

2021). Regardless, these studies documenting contour current deposits in deep-marine environments serve as the basis for comparison with the present example in terms of both physical and biologic processes.

This paper documents the trace fossil dataset of a muddy, bioclastic-rich, intensely bioturbated succession with abundant traction structures, interpreted to be deposited by shallow-marine contour currents (Paz *et al.*, in review a; see also Chapter 6), from the Upper Jurassic-Lower Cretaceous Vaca Muerta Formation of the Neuquén Basin, Argentina (Fig. 7.1). This formation represents an important unconventional resource, which has triggered a growing interest in the oil and gas industry (González *et al.*, 2018; Minisini *et al.*, 2020c). Several authors have suggested the activity of bottom currents in this Formation in previous studies (Spalletti *et al.*, 1999; Scasso *et al.*, 2002; Kietzmann *et al.*, 2008; 2014; Zeller *et al.*, 2015; Reijenstein *et al.*, 2020; Rodríguez Blanco *et al.*, 2020), yet detailed sedimentologic and ichnological analyses of these deposits are currently lacking. The objectives of this study are to: (1) document in detail the ichnology of shallow-water contourites, (2) infer potential environmental controls on the benthos, and (3) compare with other trace-fossil assemblages from ancient and modern contourites.

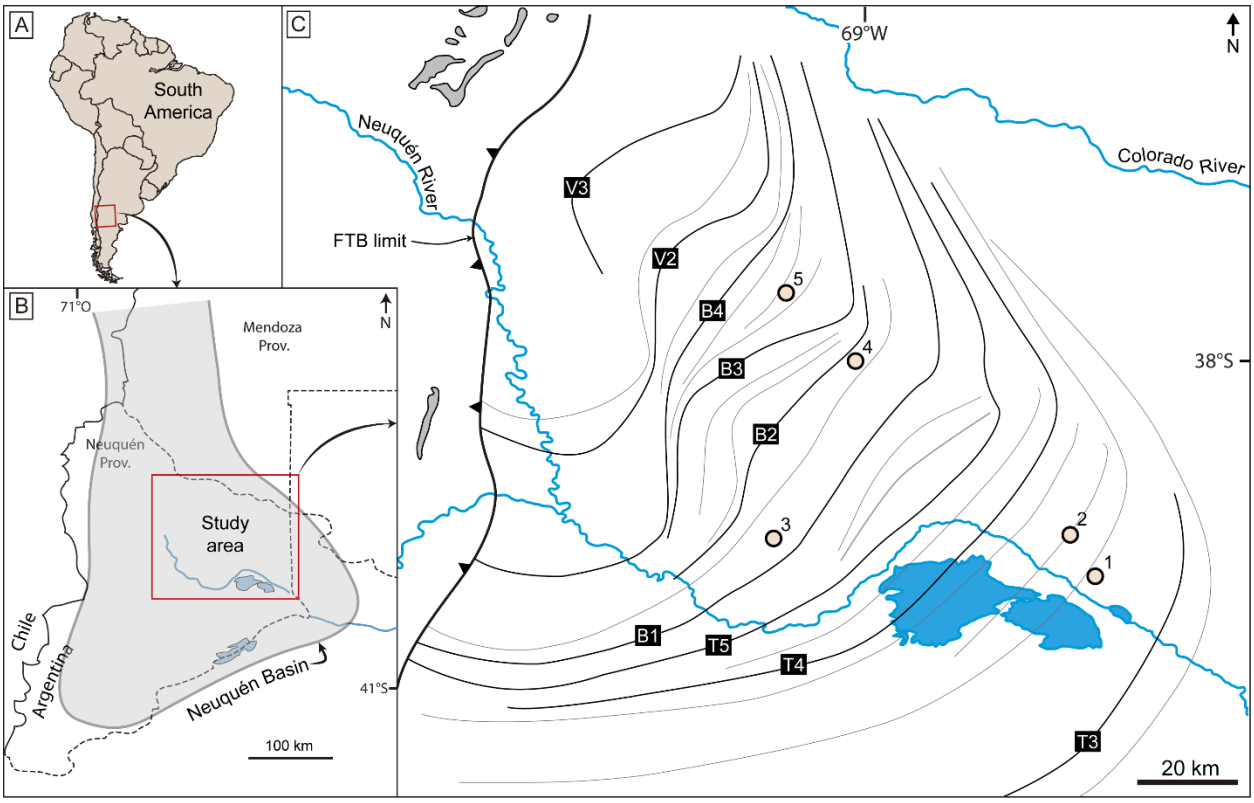

Fig. 7.1. Location maps. A, B) Maps showing location of the study area and the Neuquén Basin within a regional context. C) Location of the five wells analyzed in the present study and of clinoform breaks from the different stratigraphic surfaces of the Vaca Muerta Formation (T3-T4, B1-B4, V2, V3; modified from Domínguez *et al.*, 2020a). Grey areas are outcrops of the Vaca Muerta Formation, located west of the fold and thrust belt (FTB).

7.2 Materials and methods

Sedimentologic descriptions and interpretations of intervals attributable to contour current deposition were based on core observations from five wells (660.5 m) located in the Central Neuquén Basin (Paz *et al.*, in review a, Figs. 7.1, 7.2, 7.3, Table 7.1). Macroscopic observations, thin sections (59 sections from cores, 18 from outcrop samples) and mineralogical composition from X-Ray Diffraction (XRD) analysis on cores, were combined in order to define lithology. Lithology is described following Lazar *et al.* (2015) for mudstone (where fine mud is <8 μm, medium mud is 8-32 μm, and coarse mud is 32-62.5 μm). The present analysis focused on ichnologic descriptions of these intervals. The ichnologic study consists of the characterization of ichnotaxa, bioturbation index, ichnodiversity, tiering, ichnofabrics, and inferred ethologies, trophic types and producers. Burrow size was recorded where burrow cross-section views were available. Description of core samples was improved spraying samples with ethanol and applying image enhancement techniques to photographs, such as brightness, contrast and level adjustment. Short-wave (254 nm) and long-wave (365 nm) UV light was utilized to delineate trace fossils in monotonous black mudstone. The Vaca Muerta Formation is predominantly dominated by mudstone successions lacking sediment contrast and showing biodeformational structures, and hence measuring bioturbation index (BI) was challenging, yet it was done following the proposal of Taylor and Goldring (1993) after Reineck (1963), focusing on recording bed preservation. In addition to this general BI, an estimation of the bioturbated area corresponding to specific ichnotaxa were made for intervals containing discrete ichnotaxa. Trace fossils were classified following conventional practice in ichnotaxonomy, such as the use of ichnotaxobases (see below for details) and they are briefly described and discussed in Table 7.2. Ichnofabrics were defined and characterized in order to interpret environmental factors affecting the benthos.

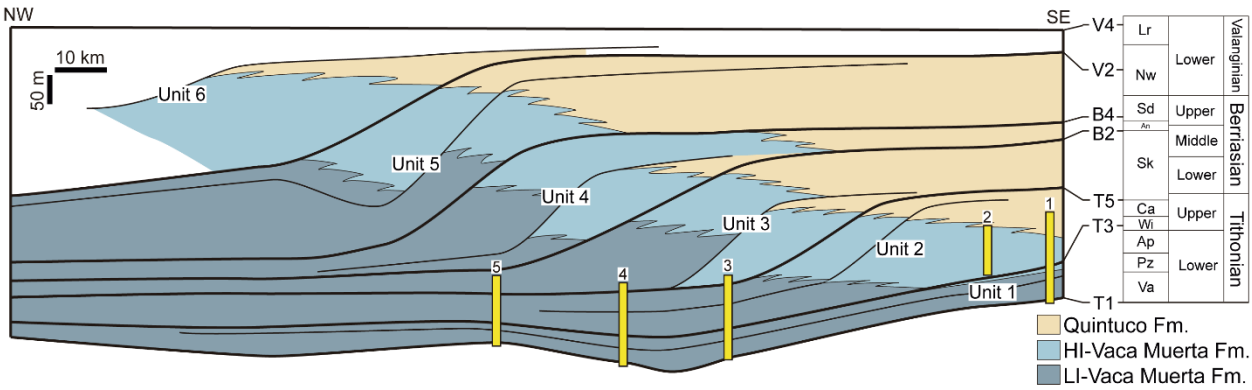

Fig. 7.2. Regional stratigraphic cross-section showing location of the studied cores within the Vaca Muerta-Quintuco system. The Vaca Muerta Formation is subdivided into a high (HI) and low (LI) impedance units. Adapted from Sattler *et al.* (2018) and Reijenstein *et al.* (2017b). Sequence-stratigraphic surfaces (T1, T3, T5, B2, B4, V2, V4) and Units (1 to 6) from Desjardins *et al.* (2018) and Domínguez *et al.* (2020a), and Andean ammonite zones (right) from Kietzmann *et al.* (2018a). Va = *Virgatosphinctes andesensis*, Pz = *Pseudolissoceras zitteli*, Ap = *Aulacosphinctes proximus*, Wi = *Windhauseniceras internispinosum*, Ca = *Corongoceras alternans*, Sk = *Substeueroceras koeneni*, An = *Argentiniceras noduliferum*, Sd = *Spiticeras damesi*, Nw = *Neocomites wichmanni*, Lr = *Lissonia riveroi*.

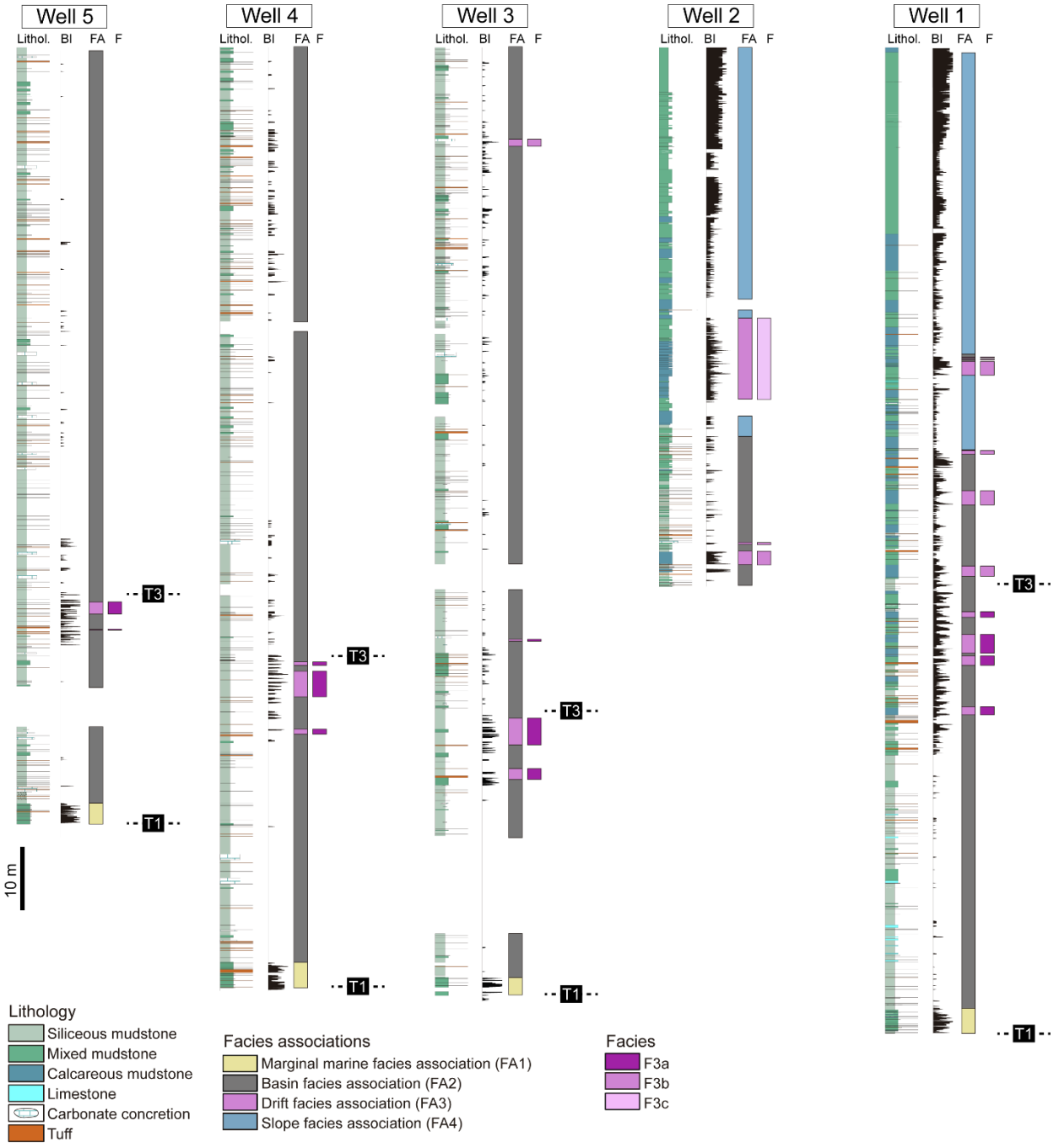

Fig. 7.3. Lithologies from XRD analysis, spectral gamma ray (SGR), bioturbation index (BI), facies associations (FA) and facies (F) described in the five wells, with the location of contourite facies (F3a, F3b, F3c). T1 and T3 stratigraphic surfaces are from Desjardins *et al.*, (2018).

Table 7.1. Description and interpretation of the contourite lithofacies derived from sedimentological analysis of Chapters 4 and 6.

Lithofacies	Description	Composition	Interpretation
M_ch, M_cl, M_cw	2-15 cm-thick intervals showing discontinuous to continuous, planar, parallel-, low-angle to rare wavy-laminated crinoidal mudstone (Fig. 7.4C)	Silt-sized plagioclase, quartz, and volcanic rock fragments. Fossils: dominant *Saccocoma* microcrinoids and minor radiolarians, ammonites and bivalves.	Bedload traction transport in crinoid-rich sediments. Low energy unidirectional currents associated with winnowing of muds
M_cr	2-15 cm-thick intervals of crinoidal mudstone with lenticular-shaped (0.5-3 mm-thick), crinoid-rich structures (Fig. 7.4C)		Interpreted as starved bioclastic ripples due to their common gradation from crinoid-rich laminae. Moderate energy conditions
M_ct	5-15 cm-thick, cross-bedded crinoidal mudstone with sharp to erosive bases		Bioclastic dune migration affected by high energy unidirectional currents
M_cb	5-50 cm-thick, completely bioturbated intervals, with rare bedding observed. Biodeformational structures are abundant, with minor discrete trace fossils		High abundance of organisms supported by high food and oxygen availability. Hydrodynamic energy remains low and the burrowing infauna keeps pace with seafloor accretion
Mh, Ml	0.2-5 cm-thick intervals of parallel- to low-angle coarse mudstone encased in fine mudstone (Fig. 7.4A)	Silt-sized plagioclase, carbonate intraclasts, undifferentiated skeletal fragments, mudstone intraclasts, quartz, pellets,	Silt and mud floccule segregation from bedload traction transport. Unidirectional currents

		and echinoderm fragments. Fossils: calcite-replaced radiolarians, forams and bivalves. Laminae composed of silt- to very fine-grained sand-sized fragments of *Rhaxella*, forams, calcite-replaced radiolarians and mudstone intraclasts. Illitic and coccolith-rich matrix.	associated with low energy and sedimentation rate
M_sh, M_sl	0.2-5 cm-thick, lenticular to tabular, parallel- to low-angle cross-laminated coarse mudstone (Fig. 7.4B, D)		Bedload traction transport under moderate energy and low sedimentation rate, above the threshold of mud floccule deposition
M_sr, M_sw	0.2-5 cm-thick, lenticular to tabular, current- and wave-ripple cross-laminated coarse mudstone with black-colored laminae (Fig. 7.4B)		Bed erosion and bedload traction transport under higher energy and sedimentation rate. Rare oscillatory current influence
M_{cm}b	1-30 cm-thick, completely bioturbated intervals. Some remaining bedding can be recognized. Dominant biodeformational structures and rare discrete traces are distinguished		Similar as M_cb but of silty and bioclastic composition
M_pl	20-70 cm-thick, low-angle cross-bedded peloidal mudstone with ripple cross-lamination and cross-bedding on bedding surfaces	Silt-sized, lens-shaped peloids, quartz, plagioclase and micas, and pebble-sized carbonate intraclasts. Fossils: calcite-replaced radiolarians, gastropods, microcrinoids, ammonites and bivalves. Gastropod and bivalve shell cavities typically filled with sparite.	Migration of compound dunes due to high-energy unidirectional currents. Possible tidal influence?

M_{bind}	2-10 mm-thick, sharp-based mudstone containing pebble- to granule-sized, tabular to rounded bindstone clasts	Bindstone laminae composed by microsparite dolomite and minor organic matter and cubic pyrite	Unidirectional currents reworking microbially stabilized sediments, that are transported as mat chips and concentrated in discrete beds

Table 7.2. Description of the ichnotaxa from the contourite deposits.

Ichnotaxa	Characteristics	Remarks	Ethology	Trophic type
Crininicaminus isp.	Horizontal, passively infilled burrows with bioclastic lining made up of crinoids. Burrows are 5-6 mm wide.	Specimens were only observed in cross-section views as strongly compacted full reliefs.	Domichnia	Predation/suspension feeding
Lockeia siliquaria	Passively infilled, oval- shaped structures with rounded bases. Locally, one end with a straight tapering and another rounded end. Burrows are 2-5 mm wide and 5-7 mm long.	Occurrence of typically more than one positive hyporelief and negative epirelief. Specimens are observed on bedding planes within intervals containing other structures seen in cross-section and inferred to have been produced by the same maker (e.g. *?Lockeia* isp., escape and equilibrium structures).	Domichnia-Cubichnia	Suspension feeding
?Lockeia isp.	Passively infilled, bowl-shaped structures with	Specimens only observed in cross-section. Present in	Domichnia-Cubichnia	Suspension feeding

	rounded bases. Burrows are 1.3-9.5 mm wide.	intervals that show *Lockeia siliquaria* on bedding-plane views.		
Nereites isp.	Horizontal burrows with an actively filled, muddy dark core and a white to gray mantle. Burrows are 2.5-10 mm wide.	Classified at ichnogenus rank as details of overall morphology and mantle are not possible to observe in cross-section.	Fodinichnia	Deposit/detritus feeding
Palaeophycus isp.	Horizontal, curved to straight, passively infilled, typically lighter core and thin dark lined burrows. Burrows are 1-2.5 mm diameter.	Classified at ichnogenus rank as details of overall morphology and wall are not possible to observe in cross-section.	Domichnia	Predation/suspension feeding
Palaeophycus heberti	Horizontal to oblique, passively infilled burrows with a 1 mm-thick white muddy wall. Burrows are 4-8 mm wide.	Presence of thick lined walls supports ichnospecific assignment.	Domichnia	Predation/suspension feeding
Phycosiphon incertum	Oblique to horizontal, actively infilled burrows with a dark muddy core and white mantle.	Ichnotaxonomic assignment based on diagnostic features of the mantle as spreite is not possible to detect in core.	Fodinichnia	Deposit feeding

	Burrows are 0.5 mm wide.			
Planolites isp.	Simple, dominantly horizontal, unlined, straight to curved burrows with a dark or white infill. Burrows are 1-4 mm wide.	Classified at ichnogenus rank as details of overall morphology and fill are not possible to observe in cross-section.	Fodinichnia	Deposit feeding
?Skolithos isp.	Vertical, tube-shaped, passively infilled structures. Burrows are 3-7 mm long and 0.5-3 mm wide.	Ichnogeneric assignment cannot be fully confirmed due to a low number of specimens.	Domichnia	Suspension feeding
Escape trace fossils	Oblique to vertical U- and V-shaped, nested structures.	Differentiated from equilibrium structures by their occurrence in cm-thick deposits indicating rapid sedimentation. However, this distinction is not always possible.	Fugichnia	Suspension feeding
Equilibrium trace fossils	Oblique to vertical, U- and V-shaped, nested, vertically aligned, sharp-lined structures.	Differentiated from escape traces by their sharp-lined burrow boundaries indicating re-establishment of the organism into a new colonization surface.	Equilibrichnia	Suspension feeding

	Locally ?*Lockeia* isp. is present at interfacial basal surfaces.	Present in layers interpreted as formed under low sedimentation rates rather that event deposition. However, distinction from escape trace fossils is not always possible.		

7.3 Geologic setting

7.3.1 The Neuquen Basin and the Vaca Muerta Formation

The Neuquén Basin of western central Argentina constitutes a triangular-shaped basin hosting a more than 6000-m-thick sedimentary succession (Fig. 7.1, Howell *et al.*, 2005; Casadío and Montagna, 2015). A syn-rift phase associated with extensional regime due to Pangea break-up marked the beginning of the basin during the Late Triassic. Volcanic and epiclastic deposits are grouped into the Precuyano cycle (Gulisano *et al.*, 1984). The re-establishment of a subduction regime in the western margin of Gondwana generated a volcanic arc and a shift towards a back-arc basin stage during the Early Jurassic (Casadío and Montagna, 2015). The back-arc phase showed multiple marine transgressions and regressions documented in the Cuyo, Lotena, Mendoza and Bajada del Agrio groups (Arregui *et al.*, 2011). The Upper Cretaceous recorded extensive continental deposits associated with a foreland basin and the end of the connection with the Pacific Ocean (Casadío and Montagna, 2015).

The Vaca Muerta Formation represents a marine event developed during the back-arc stage from the early Tithonian to the early Valanginian (Leanza, 1973; Leanza *et al.*, 2011). This formation is bounded at the base and top by the Tordillo and Quintuco formations, respectively, constituting the Lower Mendoza Mesosequence of Legarreta and Gulisano (1989). The Tordillo Formation consists of a Kimmeridgian continental phase composed by eolian, lacustrine, and fluvial deposits (Spalletti *et al.*, 2011). On top, the Vaca Muerta Formation comprises marine deposits characterized by the development of a mixed carbonate-siliciclastic clinoform system of up to 1800 m thick (Spalletti *et al.*, 2000), showing a clear progradational pattern towards the NW

in the southern margin, and W and SW in the northern margin (Gulisano *et al.*, 1984; Legarreta and Gulisano, 1989). The bottomset and lower foreset of the clinoform system correspond to the Vaca Muerta Formation, whereas the nearshore upper foreset and topset correspond to the Quintuco Formation (Mitchum and Uliana, 1985).

The study area is in the Neuquen Embayment area, 70 km northwest of Neuquén city (Fig. 7.1), and the analyzed interval comprises Unit 1 and 2 of the Vaca Muerta Formation (Fig. 7.2; Desjardins *et al.*, 2018). Biostratigraphic correlation based on ammonite zones suggests a late early Tithonian to late Tithonian stratigraphic range for the studied wells (Riccardi, 2015; Desjardins and Aguirre, 2018; Desjardins *et al.*, 2018). Seismic, core descriptions, and XRD mineralogy in the study area indicate the existence of a low angle (0.2-0.3°) mixed carbonate-siliciclastic clinoform system during Unit 1, that changed to higher angles during the following Units (1-3°; Minisini *et al.* 2020a), consisting of mixed (siliceous-calcareous-argillaceous) mudstone, calcareous mudstone, and argillaceous ash beds (tuffs). These lithologies occur with different arrangements recording marginal marine, basin, drift and slope environments (Fig. 7.3, Paz *et al.*, in review c). High productivity in the water column generated organic-rich mudstone in the basin environments (3–8% TOC with upper values of 10–12%, Uliana *et al.*, 1999), which represent important unconventional reservoirs. Sedimentologic aspects of the Vaca Muerta Formation have been extensively documented based on both outcrop studies (e.g., Spalletti *et al.*, 2000; Kietzmann *et al.*, 2014a; Zeller *et al.*, 2015a; Ponce *et al.*, 2015; Paz *et al.*, 2019; Otharán *et al.*, 2020) and core investigations (e.g., González Tomassini *et al.*, 2014; Repol *et al.*, 2014; Notta *et al.*, 2017, 2020; Desjardins and Aguirre, 2018; Desjardins *et al.*, 2018, Gómez Rivarola and Borgnia, 2018; Estrada *et al.*, 2020; Minisini *et al.*, 2020a). Contrastingly, ichnologic studies of this formation are very rare, being restricted to outcrops in southern Mendoza Province (Doyle *et al.*, 2005); or local trace-fossil identifications in cores and outcrops (Kietzmann *et al.*, 2014a; Ponce *et al.*, 2015; Desjardins and Aguirre, 2018; Paz *et al.*, 2019, 2021; see also Leanza *et al.*, 2020).

7.3.2 The contourite deposits

Sedimentologic analysis of the contourite deposits has been laid down in Chapter 6. These deposits were grouped into basin and drift successions, and can be subdivided into fifteen lithofacies (Table 7.1). Laminated and current-rippled lithofacies include parallel-, low-angle to wavy-laminated crinoidal mudstone (M_ch, M_cl, M_cw), and mudstone showing crinoid-rich lenses

(M_cr), parallel- to low-angle to wavy-laminated crinoidal mudstone (M_ch, M_cl, M_cw), and mudstone showing crinoid-rich lenses (M_cr), parallel- to low-angle cross-laminated, coarse mudstone laminae encased in fine mudstone (Mh, Ml), and parallel-, low-angle, current- and wave-ripple cross-laminated coarse mudstone (M_sh, M_sl, M_sr, M_sw; Fig. 7.4A-C). These lithofacies are interpreted as produced by long-term activity of contour currents reworking crinoid-rich or silt- and bioclastic-rich deposits (Paz *et al.*, in review a). The laminated coarse mudstone is produced by bedload segregation under low velocity currents, whereas the ripple cross-laminated mudstone represents increasing velocity and sedimentation rate (Schieber, 2011; Yawar and Schieber, 2017).

Intercalated with the laminated and current-rippled lithofacies are bioturbated or massive lithofacies consisting of fine to coarse mudstone (M_{cm}b) or crinoidal mudstone (M_cb). These deposits are interpreted as produced by low-energy contour currents under more oxygenated conditions, allowing for extensive reworking by the infauna (Paz *et al.*, in review a). Other lithofacies include cross-bedded crinoidal mudstone (M_ct), low-angle cross-bedded peloidal mudstone, showing current-ripple cross-lamination and trough cross-bedding on stratification surfaces (M_pl), and sharp-based mudstone containing pebble-to granule-sized, light colored bindstone clasts (M_{bind}). Lithofacies M_ct and M_pl are interpreted as forming compound dunes, whereas lithofacies M_{bind} represents the action of currents reworking microbially stabilized sediments (Paz *et al.*, in review a).

Contourite deposits are locally interbedded with lithofacies formed by sediment gravity flows. These include normal-graded to massive, fine to coarse mudstone (M_sg, M_sm), composite beds of fine to coarse mudstone (Mcomp), and massive, calcareous mudstone (M_cm, Fig. 4D). Lithofacies Mcomp is composed by an alternation of intervals with massive, parallel-laminated and intraclastic coarse mudstone. Lithofacies M_cm shows erosive to sharp bases with minor small scour marks, load casts, mudstone pseudonodules, and flame structures. These beds are interpreted as produced by high-density, fluid mud flows suffering *en masse* deposition (M_cm), and transitional or turbidity flows (M_sg, M_sm, Mcomp) associated with downslope transport originated after resuspension events (Paz *et al.*, in review a).

Contourite lithofacies containing trace fossils have been grouped into three facies that correspond to the drift facies association (FA3) of the Vaca Muerta Formation, located in bottomset and lower foreset locations of the clinoform (see Chapter 6). Following the nomenclature of Chapter 6, facies 3a (F3a) is composed of an alternation of bioturbated (M_cb),

laminated and rippled (M_ch, M_cl, M_cw, M_cr), crinoidal mudstone lithofacies. Mean BI is 1.78 (n=462). In addition, lithofacies M_ct, M_sm, and M_sg are minor components. Facies 3b (F3b) consists of an alternation of bioturbated (M_{cm}b), laminated and rippled (Mh, Ml, M_sh, M_sl, M_sr), coarse to fine mudstone lithofacies, generating heterolithic bedding. Mean BI is 2.17 (n=193). Lithofacies M_sw, M_pl, M_sm and M_sg are rare. This facies records sedimentation in a more proximal position than F3a (Paz *et al.*, in review a). Facies 3c (F3c) comprises laminated and rippled, fine to coarse mudstone lithofacies (Mh, Ml, M_sh, M_sl, M_sr), intercalated with sediment gravity flow deposits represented by massive calcareous mudstone (M_cm), normal-graded coarse mudstone (M_sg) and composited mudstone (Mcomp) (Fig. 7.4D). Mean BI is 1.75 (n=239). M-thick slumped intervals also occur. F3c is the most landward of the three (Paz *et al.*, in review a).

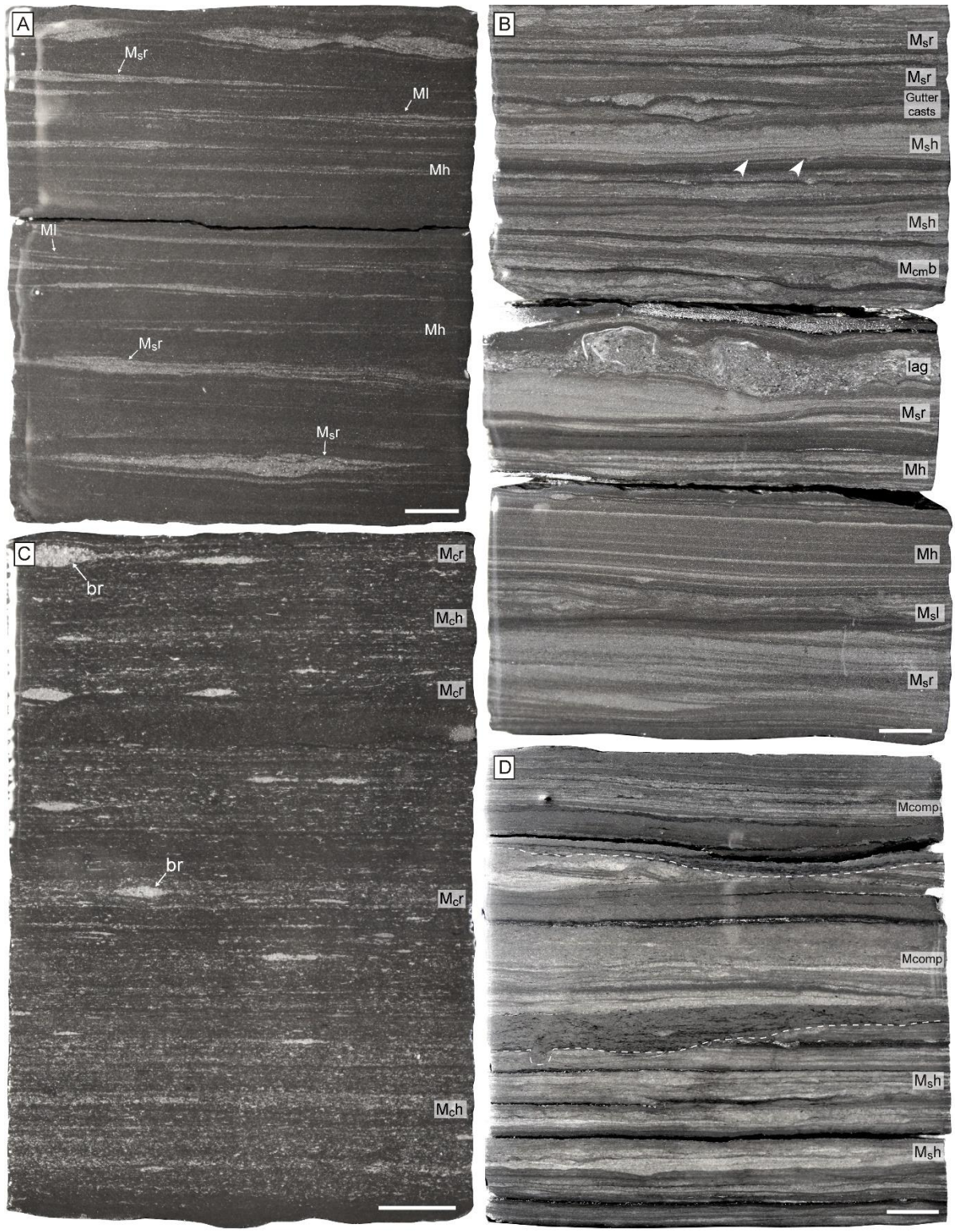

Fig. 7.4. Core photographs of the contour current lithofacies. A, B) Parallel- to low-angle coarse mudstone laminae encased in fine mudstone (Mh, Ml), parallel-laminated to current ripple-cross laminated mudstone (M_sh, M_sr) and bioturbated, calcareous to mixed mudstone (M_{cm}b) lithofacies. C) Current-rippled (M_cr) and

parallel-laminated (M_ch) crinoidal mudstone lithofacies. Bioclastic ripples (br) are delineated. D) Parallel-laminated coarse mudstone (M_sh), and composite mudstone beds (Mcomp). Bed bases are delineated with dashed lines. Scale bars are 1 cm.

The circulation system generating the contourite deposits is likely wind- and thermohaline-driven, enhanced during times of arid and cool climates and low sea-levels (Chapter 6, Paz *et al.*, in review a). Generation of high salinity and low temperature dense waters cascading from the shelf, during deposition of carbonate-rich intervals (e.g. Rodríguez Blanco *et al.*, 2020), intensified the current and provided oxygen to deeper watermasses. NE-directed winds might have occurred in the Neuquén Basin during the Tithonian, suggesting that wind forcing probably affected the shallow shelf areas, originating a counterclockwise circulation (Zeller *et al.*, 2015a). Currents of intermediate waters reworked bottomset and lower foreset areas with a clockwise circulation. Other processes such as tidal currents or internal waves or tides affecting the contour currents are disregarded. Tidal currents represent a mechanism in shelf areas that may rework fine-grained depositional systems (Schieber, 2016), however a volcanic arc to the west might have produced microtidal conditions in the Neuquén Basin (Canale *et al.*, 2020). Internal waves or tides may be involved because of a position close to a density stratification surface (oxycline), but the high across-shore extension of the contourite deposits (*ca* 160 km in bottomset and foreset locations) indicates a process that is not restricted to the area where the pycnocline intersects the seafloor (Paz *et al.*, in review a).

7.4 Results

7.4.1 Remarks on the classification of trace fossils

Biogenic structures in fine-grained deposits are notoriously difficult to identify and classify (see Schieber *et al.*, in press). Also, identifying trace fossils in core presents its own challenges (see Pemberton *et al.*, 2001). In spite of these difficulties, we follow the recommendation of Bromley (1990), and attempt to classify ichnotaxa at ichnospecific rank wherever possible (Table 7.2). In addition, special effort has been made to analyze available horizontal views in order to support ichnotaxonomic determinations that are otherwise only based on 2D vertical cross-sections. This has been instrumental, for example, to identify the diagnostic morphology of the ichnospecies

Lockeia siliquaria when horizontal preservation is available in beds hosting the Equilibrichnia-Fugichnia ichnofabric.

Irregular-shaped structures showing evidence of vertical adjustment after sedimentation events are abundant. They occur on bed bases and rarely on top of beds, showing passive fill from the overlying bed, or recording sediment that has been eroded. In cross-sectional views, apparent small bowl-shaped forms resemble *Bergaueria* and *Conichnus,* ichnogenera that are typically assigned to burrowing anemones (Pemberton *et al.*, 1988). However, where bedding planes are available for analysis, oval-shaped, positive hyporeliefs or negative epireliefs identical to *Lockeia siliquaria* occur. This observation suggests that the structures seen in cross-sectional views are most likely bivalve structures, although the connection to *Lockeia siliquaria* cannot be confirmed. We adopt, however, a parsimonius decision and refer to all these structures as ?*Lockeia* isp. Following this line of reasoning, the associated biodeformational structures indicating vertical adjustment are regarded as equilibrium (Equilibrichnia) or escape trace fossils (Fugichnia) produced by bivalves.

Differentiation between equilibrium and escape trace fossils is not always possible. Both behaviors are relatively similar, as they indicate the vertical adjustment of an organism either under high and rapid, or low and background sedimentation rates. In principle, however, we can distinguish two distinct end members recording normal versus rapid adjustments. Normal adjustment is interpreted to record equilibrium structures in those cases in which (1) vertical, chevronated structures illustrate migration after deposition of a thin sediment layer, and (2) vertically associated, sharp-lined basal boundaries suggest re-establishment of the organism in the newly deposited substrate. In contrast, escape behavior is interpreted when inclined to vertical structures display deformed laminae crossing thicker (cm-thick) deposits, representing rapid adjustment synchronous with rapid deposition (Bromley, 1990; Buatois and Mángano, 2011). Differentiation between rapid and background sedimentation, which is relatively straightforward in settings affected by sediment gravity flows or storms, is difficult in environments influenced by contour currents. Accordingly, in the cases in which such distinction is not possible, we refer to these structures as Equilibrichnia-Fugichnia.

7.4.2 Ichnofabric analysis

Our ichnofabric analysis is focused on the contourite deposits (Table 7.1), where four ichnofabrics have been recognized: *Palaeophycus heberti*, *Phycosiphon incertum*, *Nereites* isp., and Equilibrichnia-Fugichnia ichnofabrics. In addition to the trace fossils present in these ichnofabrics, other biogenic structures (e.g., *Teichichnus rectus, Alcyonidiopsis longobardiae, Planolites* isp., *Phycosiphon incertum, Coprulus oblongus*, rare *Thalassinoides* isp.) occur locally in associated intervals dominated by hemipelagic deposits. These intervals, typical of basin environments of the Vaca Muerta Formation, are not addressed in the present study (see Chapter 4 for a complete sedimentologic analysis of the study area).

7.4.2.1 Description and interpretation of ichnofabrics

The *Palaeophycus heberti* ichnofabric consists of discrete, shallow-tier *Palaeophycus heberti*, *Planolites* isp., *Crininicaminus* isp., and rare *Palaeophycus* isp. (Fig. 7.5A-C) overprinted onto a mottled background recording irregular biodeformational structures. BI is typically 4-6, with mean burrow diameter of 4.8 mm. This ichnofabric forms 10-50 cm-thick, highly bioturbated, crinoidal mudstone or fine to coarse mudstone intervals. Discrete trace fossils occur in highly variable densities. Although the sedimentary fabric is typically obliterated by bioturbation in most instances (Fig. 7.5A, 7.5B), a relict primary lamination may be preserved in some cases (Fig. 7.5C). Dominant superimposed discrete structures may represent the domiciles of passive predators, and/or suspension feeders (Ettensohn, 1981; Pemberton and Frey, 1982). Deposit feeding is represented by *Planolites*. Density of bioturbation suggests higher oxygenation and food availability. Completely bioturbated background texture most likely records foraging in a soft to soupy sediment. Association with traction structures implies low-energy contour currents that allowed sediment homogenization by bioturbation. The thick lining of *P. heberti* and agglutinated lining of *Crininicaminus* isp. represent a strategy for maintaining open burrows in soft substrates. The epibenthic tube may work as a strategy to raise the organism head over the sediment surface and access the low energy flow on top with high suspended food concentration (Ettensohn, 1981).

The *Phycosiphon incertum* ichnofabric is represented by shallow-tier *Phycosiphon incertum*, *Nereites* isp., *Planolites* isp., *Palaeophycus* isp., and rare ?*Lockeia* isp. (Fig. 7.6A-C). BI is mostly 1, with a few intervals showing 2, and mean burrow diameter of 3.0 mm, except for *Phycosiphon incertum,* which is 0.2-0.5 mm. The *Phycosiphon incertum* ichnofabric forms 1-10 cm-thick, sparsely bioturbated, current-ripple cross- and parallel-laminated, fine to coarse

mudstone intervals. This ichnofabric represents opportunistic colonization and selective deposit-feeding upon the organic matter-rich lamination (Wetzel, 2010).

The *Nereites* isp. ichnofabric is dominated by shallow-tier structures, such as *Nereites* isp., *Phycosiphon incertum, Planolites* isp., and *Palaeophycus* isp. (Fig. 7.6D, 7.6E). *Palaeophycus heberti, ?Skolithos isp.* and ?*Lockeia* are rare. Small patches of burrow mottling recording biodeformational structures are also present. BI is 3-5, and mean burrow diameter is 3.6 mm. The *Nereites* isp. ichnofabric forms 1-10 cm-thick, dominantly moderately bioturbated, fine to coarse mudstone intervals. Primary fabric is partially preserved in most instances. This ichnofabric consists of structures of deposit- and detritus-feeders in soft substrates, most likely indicating times of current pauses or decreased current velocity and consequent food accumulation at the sediment surface. Suspension feeding or predation are only represented by rare *Palaeophycus heberti* and *Palaeophycus* isp. *Nereites* and *Phycosiphon* are typical trace fossils associated with abundant food input, which is also characteristic of areas affected by bottom currents (Thistle *et al.*, 1985; Wetzel, 2010; Hovikoski *et al.*, 2020). Some elements of the *Nereites* isp. ichnofabric have been commonly recorded in the literature as post-depositional trace fossils on top of turbidites (Uchman and Wetzel 2011); yet in the present example they are part of the drift facies association, and they do not occur in the sediment gravity flow deposits of the Vaca Muerta Formation. Other environmental stressors, such as low substrate consistency, may have also played a role during deposition of the latter (Paz et al. in review).

The Equilibrichnia-Fugichnia ichnofabric is characterized by very shallow tier, bowl-shaped structures referred to as ?*Lockeia* isp., U- and V-shaped, nested vertical to highly inclined structures, interpreted as equilibrium and escape structures, and rare ?*Skolithos* isp. (Fig. 7.7A-E). In several fortuite instances, *Lockeia siliquaria* has been identified on bedding planes, in both bases and tops (Fig. 7.7C). BI is typically 1-2, with dense populations of equilibrium and/or escape structures forming more pervasively bioturbated intervals (BI 3-4; Fig. 7.7E). Burrow mean maximum diameter is 3.2 mm. Locally, vertical axis of burrows displays a preferred orientation, dipping in a direction opposite to current direction inferred from the presence of unidirectional current ripples (Fig. 7.7A). This ichnofabric forms 1-30 cm-thick, sparsely to moderately bioturbated, parallel-laminated fine to coarse mudstone intervals. Primary fabric is well preserved in most intervals. Common equilibrium behavior is inferred from the successive vertical association of these structures, with vertical movements through 0.1-2.0 cm of sediment. Based on

the identification of *Lockeia siliquaria* on numerous bedding planes, this ichnofabric is interpreted as most likely produced by suspension-feeding bivalves. The equilibrichnia strategy reflects an animal able to respond and adjust its position to keep pace with sedimentation and maintain the connection to the seafloor in order to access suspended food particles (Mángano *et al.*, 1998). A similar burrow size for individual colonization surface suggests a single population recording the activity of an opportunistic species. Burrow orientation can be caused by the alignment of suspension feeders with respect to a constant current (Over 1988). Times of low sedimentation rate coupled with sufficient suspended food are inferred from the densely populated chevron equilibrium structures indicating retrusive burrowing (Hanken *et al.*, 2001). Higher and rapid sedimentation rates are recorded from the escape structures. Irregular burrow boundaries suggest soft substrates associated with mud-rich sediment, whereas in some cases, well-defined burrow boundaries indicate development of relatively stiff substrates.

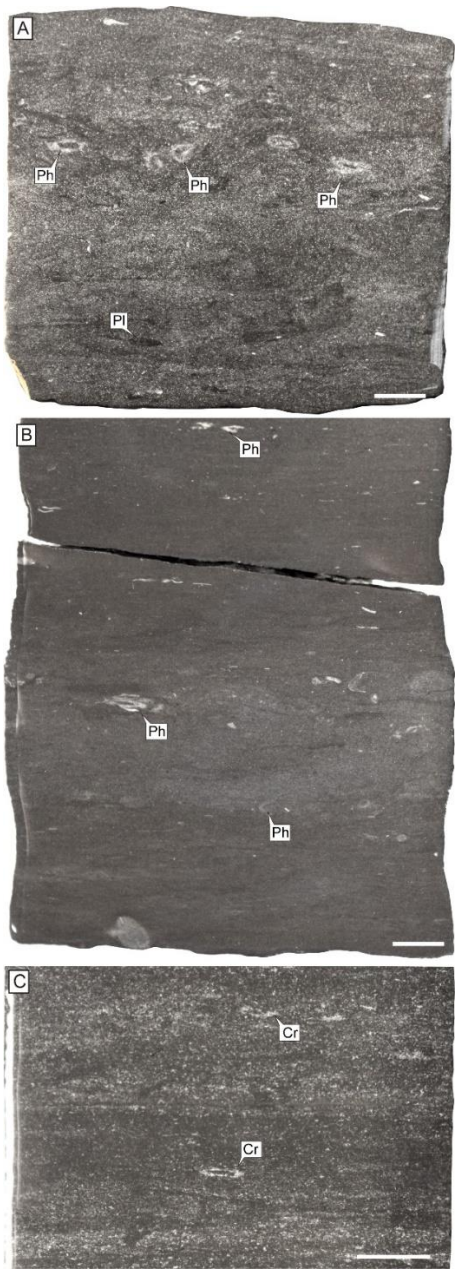

Fig. 7.5. Core photographs of the *Palaeophycus heberti* ichnofabric. A, B) *Palaeophycus heberti* (Ph) and *Planolites* (Pl) in highly bioturbated intervals with massive appearance. C) *Crininicaminus* isp. (Cr) from bioturbated crinoidal mudstone showing relatively good preservation of the primary fabric. Scale bars are 1 cm.

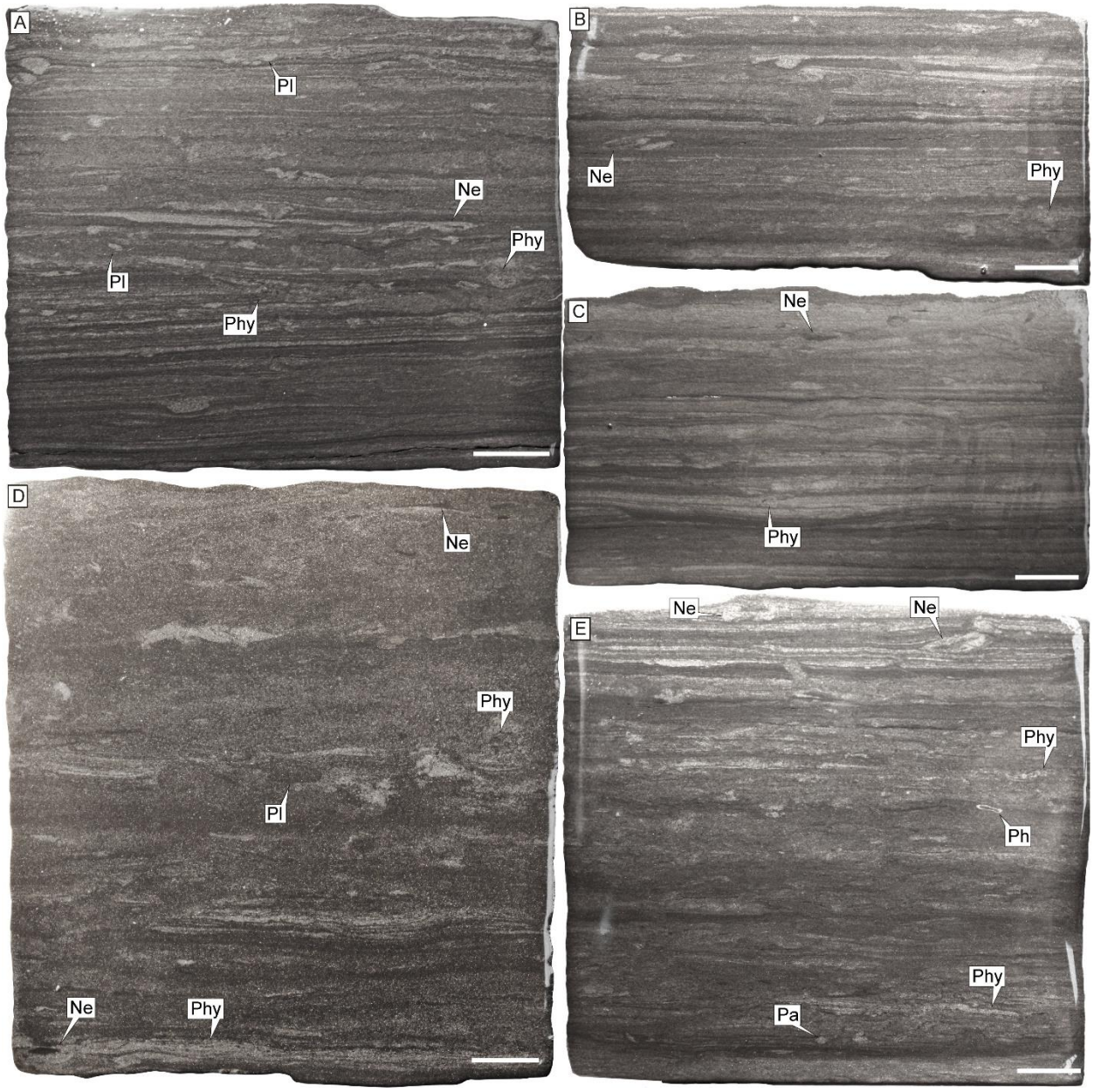

Fig. 7.6. Sparsely to moderately bioturbated intervals of the *Phycosiphon incertum* and *Nereites* isp. ichnofabrics, scale bars are 1 cm. A, B, C) Sparsely bioturbated intervals of the *Phycosiphon incertum* ichnofabric with *Nereites* isp. (Ne), *Phycosiphon incertum* (Phy) and *Planolites* isp. (Pl). D, E) Moderately bioturbated intervals of the *Nereites* isp. ichnofabric, displaying *Nereites* isp. (Ne), *Palaeophycus* isp. (Pa), *Palaeophycus heberti* (Ph), *Phycosiphon incertum* (Phy) and *Planolites* isp. (Pl).

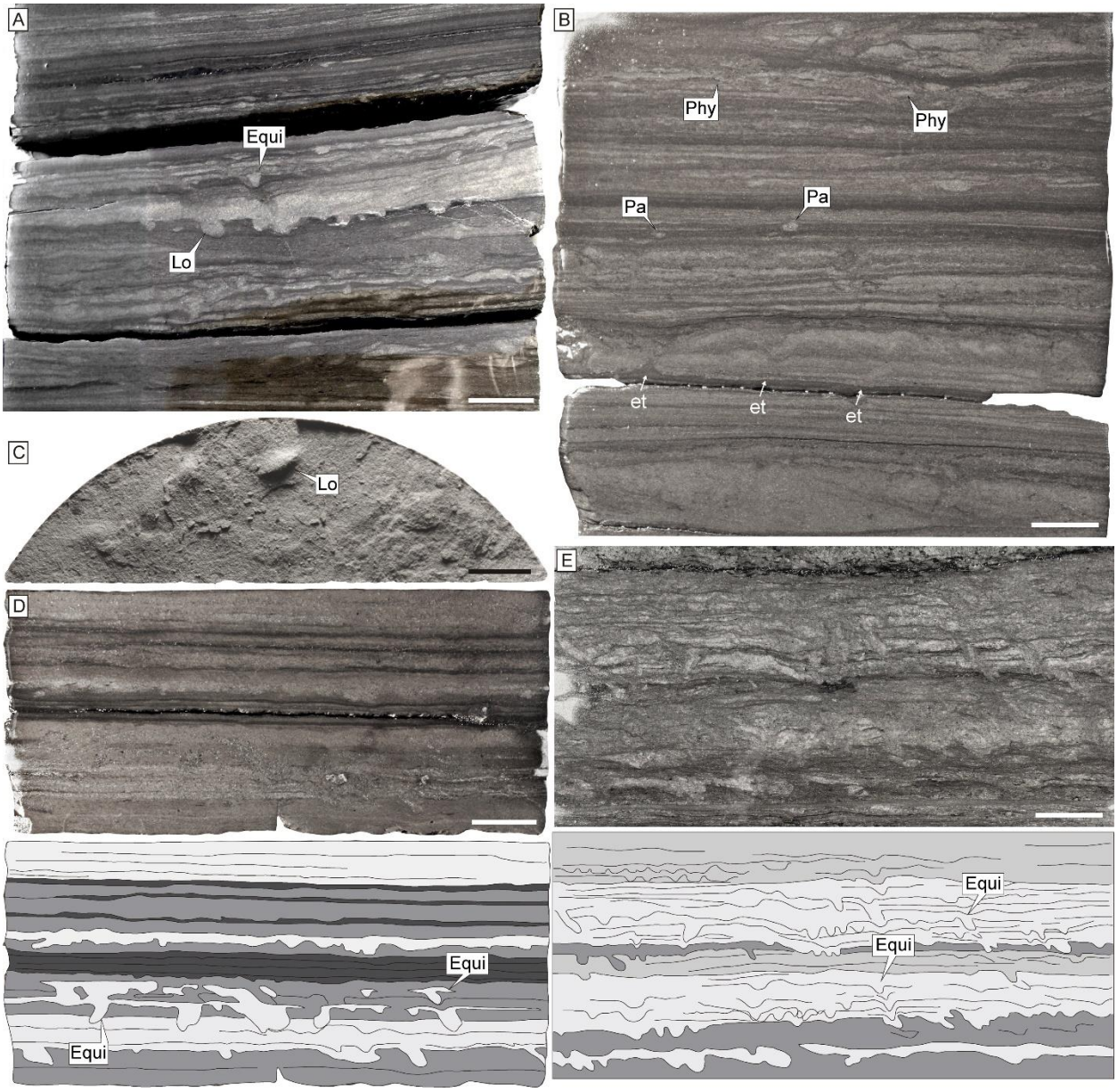

Fig. 7.7. Equilibrichnia-Fugichnia ichnofabric, scale bars are 1 cm. A) Sparsely bioturbated intervals with ?*Lockeia* isp. (Lo) in beds with equilibrium structures. B) Escape trace fossils (et) of the Equilibrichnia-Fugichnia ichnofabric. On top, moderately bioturbated intervals with *Palaeophycus* isp. (Pa) and *Phycosiphon incertum* (Phy) are part of the *Nereites* isp. ichnofabric C) Positive hyporelief preservation of *Lockeia siliquaria* (Lo). D, E) Moderately to highly bioturbated intervals showing equilibrium structures (Equi, see drawing below for delineation of structures). Contrast in D has been manipulated to enhance visibility of structures.

7.4.2.2 Patterns of ichnofabric and trace-fossil distribution

The ichnofabrics display a pattern of distribution in relation with contourite deposits (represented by both lithofacies and facies) that reflects spatial trends in bioturbation in drift environments (FA3) located in bottomset and lower foreset locations of the clinoform (Figs. 7.8, 7.9). F3a is host to the *Palaeophycus heberti* ichnofabric, showing a predominance of *Crininicaminus* isp. over other discrete trace fossils and high intensities of bioturbation (Fig. 7.5C).

F3b, located in a shallower-water position than F3a, shows sparsely bioturbated intervals hosting the *Phycosiphon incertum* ichnofabric, moderately bioturbated intervals comprising the *Nereites* isp. ichnofabric, and highly bioturbated intervals with the *Palaeophycus heberti* ichnofabric. The Equilibrichnia-Fugichnia ichnofabric is a minor component, except for well 2, where it occurs forming sparsely to moderately bioturbated successions. Locally, this facies shows m-thick intervals displaying a decreasing and then increasing BI, which can be differentiated into types A and B successions (Figs. 7.8, 7.10). Type A has a high percentage of highly bioturbated intervals ($M_{cm}b$, ~50-60 %) and dominance of Mh and Ml. Type B exhibits less percentage of highly bioturbated intervals ($M_{cm}b$, ~15-30 %), and has a higher participation of M_sh, M_sl and M_sr.

F3c is the most landward facies of the three. This facies shows a dominance of the Equilibrichnia-Fugichnia ichnofabric, displaying low to moderate intensities of bioturbation.

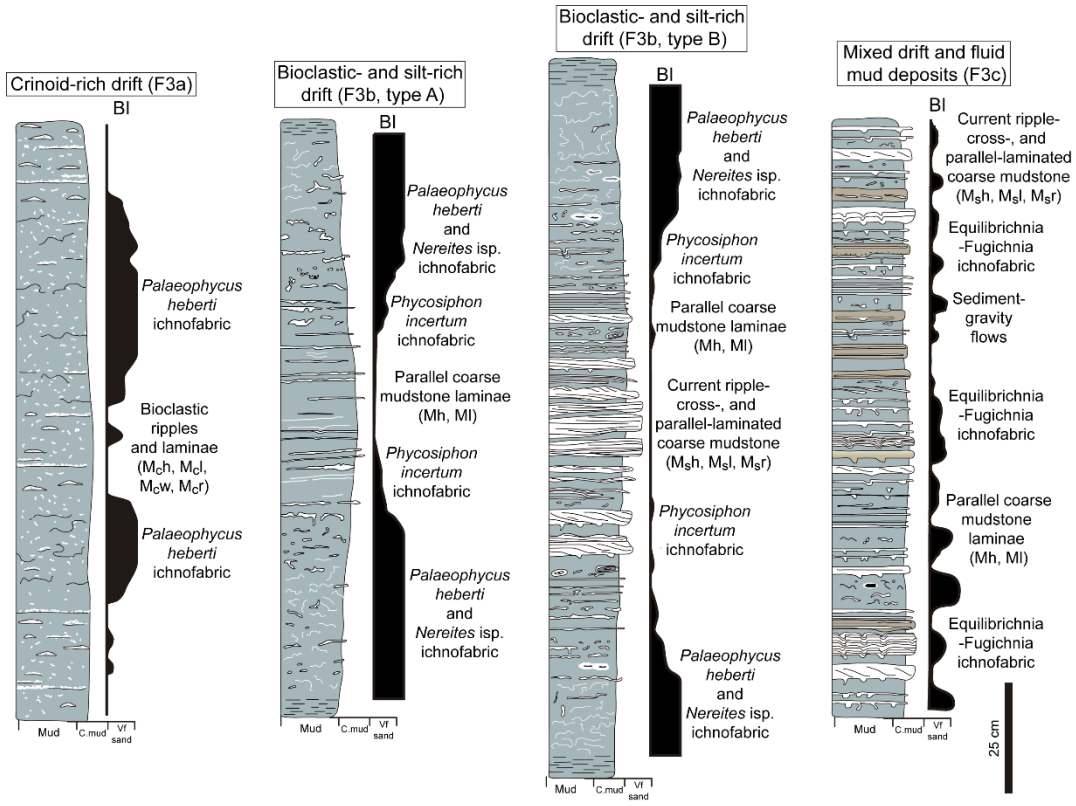

Fig. 7.8. Idealized facies succession for shallow-water contour currents documented from the Vaca Muerta Formation displaying lithology, sedimentary structures, ichnofabrics, and bioturbation index.

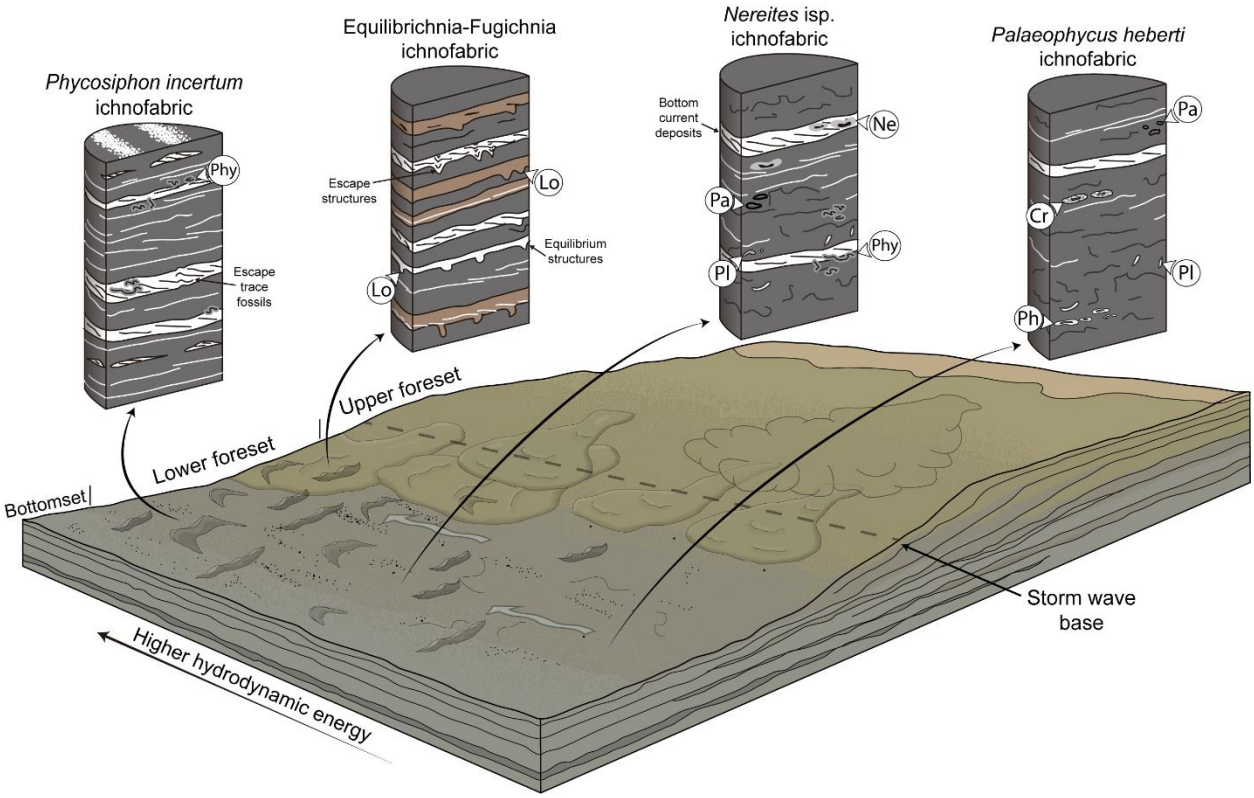

Fig. 7.9. Block diagram showing the environmental distribution of the ichnofabrics depending on the clinoform location and hydrodynamic energy of the contour currents. Cr = *Crininicaminus* isp., Lo = *Lockeia siliquaria,* Ne = *Nereites* isp., Pa = *Palaeophycus* isp., Pl = *Planolites* isp., Ph = *Palaeophycus heberti*, Phy = *Phycosiphon incertum*. See text for explanation.

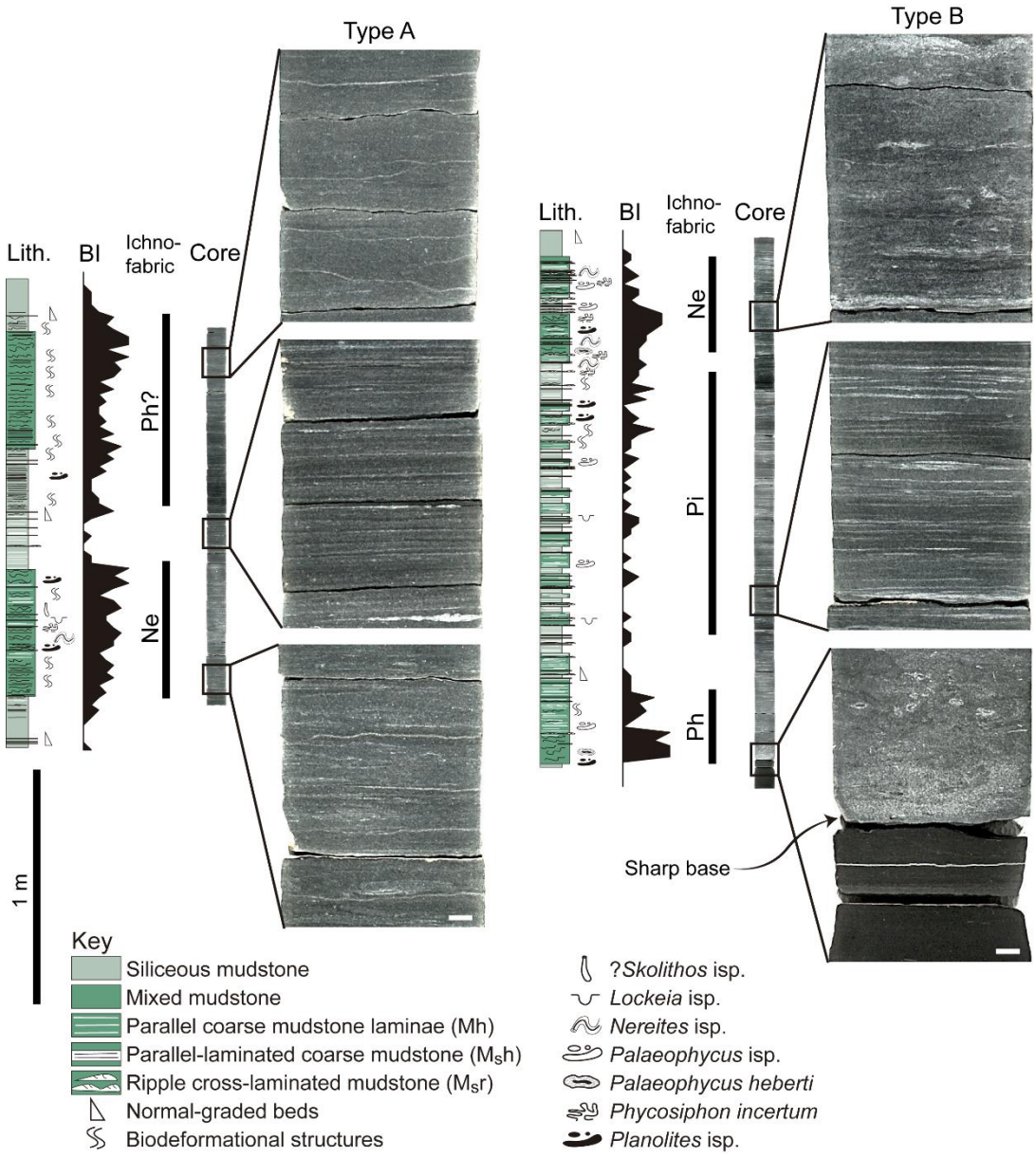

Fig. 7.10. Examples of the contourite successions showing decreasing and then increasing BI (F3b type A and B), with distribution of the *Palaeophycus heberti* (Ph), *Nereites* isp. (Ne) and *Phycosiphon incertum* (Pi) ichnofabrics and close-up images. Scale bars at the bottom right of the cores are 1 cm.

7.4.3 Paleoenvironmental implications

Environmental controls on bioturbation can be summarized through the integration of the available sedimentologic and ichnologic datasets (Fig. 7.11). Food, oxygenation, hydrodynamic energy, and water turbidity are suggested to have been the main controlling factors on trace-fossil distribution

in the studied deposits. Extensive documentation on the effects of deep-water contour currents on benthic ecology serve for comparison with benthic communities affected by shallow contour currents (cf. Thistle *et al.*, 1985, 1991; Aller, 1989, 1997; Flach *et al.*, 1998; Lavaleye *et al.*, 2002; Wetzel *et al.*, 2008).

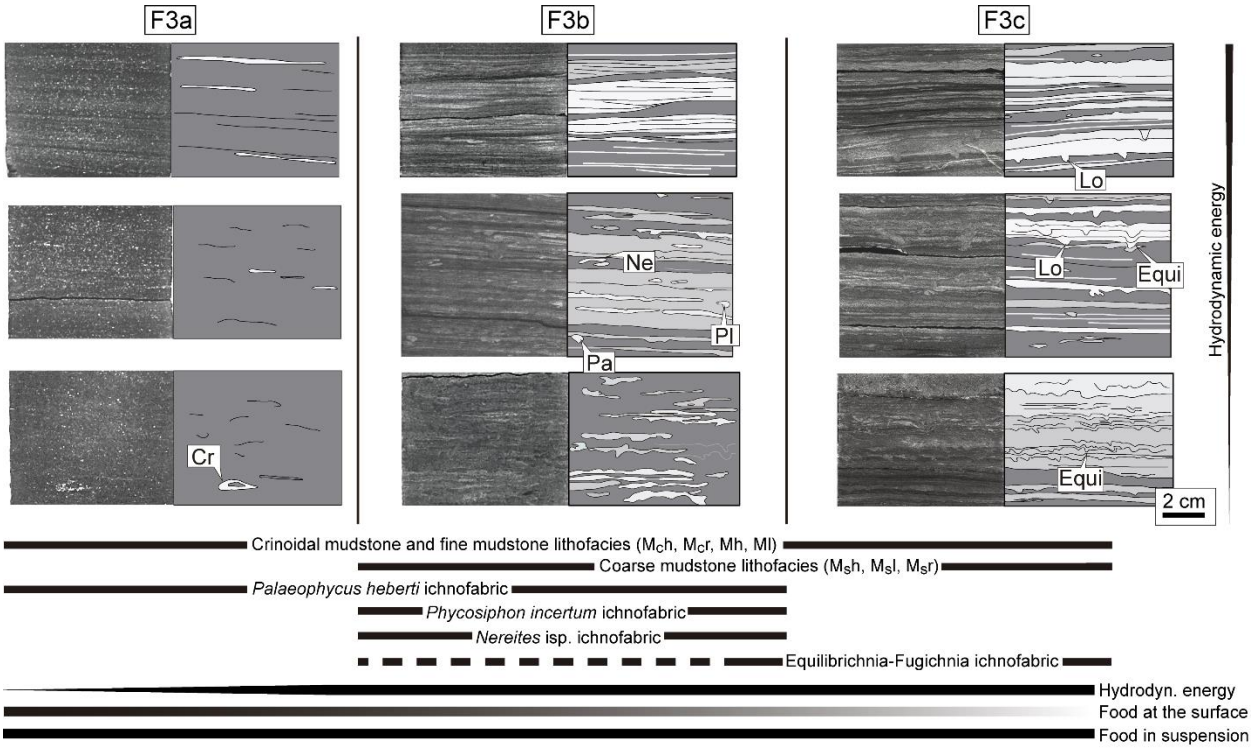

Fig. 7.11. Summary of environmental factors controlling ichnofabric distribution in the different contourite facies. Cr = *Crininicaminus* isp., Equi = equilibrium structures, Lo = *Lockeia siliquaria*, Ne = *Nereites* isp., Pa = *Palaeophycus* isp., Pl = *Planolites* isp.

7.4.3.1 Food

In contour current-affected areas, benthic standing stock and biologic mixing is fuelled by a higher food input compared with areas of continental slope or abyssal plain (DeMaster *et al.*, 1985; Thistle *et al.*, 1985). The different intensities in current speed generate distinctive scenarios of benthic responses to food distribution. High velocity currents of >25 cm/s promote removal of metabolites, organic matter, microorganisms, larvae and juveniles (Aller, 1989), and an increase in suspension-feeding and, to a lesser extent, surface-feeding organisms (Flach *et al.*, 1998; Flach, 2003; Wetzel *et al.*, 2008). In particular, suspension feeders benefit from food becoming enriched at the boundary layer (Rosenberg, 1995; Flach and Thomsen, 1998; Lavaleye *et al.*, 2002). In contrast,

slower currents (<10 cm/s) make organic matter available at the sediment surface, and deposit feeders tend to be dominant (Flach and Thomsen, 1998; Lavaleye *et al.*, 2002; Wetzel *et al.*, 2008). A switch between these two feeding strategies may also be adopted by the same organism (namely deposit-suspension feeders) when flow conditions change (e.g., bivalves, Olafsson, 1989; polychaetes, Taghon and Greene, 1992).

The high productivity suggested by the high TOC content of the Vaca Muerta Formation indicates that food was not a limiting factor. However, the contourite deposits in this unit imply a complex mosaic of feeding strategies in response to variable types of food available for the benthos, namely suspended food for the Equilibrichnia-Fugichnia ichnofabric, food on the surface and within the sediment in association with the *Nereites* isp. and *Phycosiphon incertum* ichnofabrics, and mixed suspended and surface-deposited food for the *Palaeophycus heberti* ichnofabric. The predominance of *Nereites* isp. and *Palaeophycus heberti* ichnofabrics associated with intensely to moderately bioturbated intervals suggests lower energy or intermittent currents with food delivered at the sediment surface and subsequently shallowly buried. The presence of suspension-feeding structures in the latter is also suggestive of some participation of food particles kept in suspension in the water column. The *Phycosiphon incertum* ichnofabric reflects opportunistic colonization of areas with benthic food affected by moderate energy currents during short colonization periods.

The Equilibrichnia-Fugichnia ichnofabric, with its dominance of vertical structures produced by suspension-feeding bivalves and the absence of deposit-feeding traces, indicates abundant organic particles in the water column. This ichnofabric occurs in deposits formed in the most landward environments affected by contour currents (F3c), where coarse mudstone deposits indicate velocities above the threshold of mud accumulation (>25 cm/s, Yawar and Schieber, 2017). Thus, this area is envisaged as having high content of suspended organic matter transported by high-energy currents closer to the shore. The organisms probably presented an exposed body area for suspension feeding that was adjusted to the surface after sedimentation events. The contour current direction may have influenced the orientation of burrows (Fig. 7.7A). Similar small (0.2-0.5 cm wide, 1-2 cm long) cone-shaped *Lingulichnus* in the Silurian Delorme Group of Canada shows orientations that were caused by bottom current transport in a shelf-slope transition (Over, 1988). Suspension feeders orientate their burrows in an opposite direction to the dominant flow to prevent filling of their burrows with fine-grained material and blocking of their feeding apparatus,

to optimize feeding surfaces and respiration avoiding interference with other organisms and to passively remove waste materials (Over, 1988; Zonneveld and Pemberton, 2003). However, the occurrence of slump structures (F3c) and the accumulation of these deposits on areas with slope indicate that burrow orientation could also be an artifact of sediment creeping or current-induced sediment shearing generating burrow deformation (Gingras and Bann, 2006).

7.4.3.2 Oxygenation

Contour currents provided oxygen to the generally oxygen-deficient Vaca Muerta Formation seafloor and pore waters, generating an environment suitable for the establishment of a low to moderately diverse benthic fauna. The oxygen supply in bottom waters is evidenced by the high bioturbation observed in the drifts (mean BI of 1.78 in F3a, 2.17 in F3b and 1.75 in F3c), that contrasts with the otherwise parallel-laminated basin deposits of this Formation (mean BI of 0.09, n=9110). Deep water renewal by cascading of dense, surface watermasses contributes to increase oxygen levels at the seafloor (Meier *et al.*, 2006; Coppola *et al.*, 2017).

However, shallow-tier bioturbation and small burrow sizes (mean burrow diameter of 3.47 mm, n=174) are characteristic of all the facies, and clearly contrasts with modern examples of areas oxygenated by contour currents (e.g., Fu and Werner, 1994; Reolid and Betzler, 2019), where high oxygen and food levels allow the establishment of a diverse, deep-burrowing infauna with normal sizes that completely homogenize the successions. Oxygenation is regarded as one of the main controlling factors on bioturbator body size and burrowing depth, with decreasing oxygen producing a gradational decrease of burrow size and depth (Savrda *et al.*, 1984). Current speed could not have controlled burrow size, because highly bioturbated intervals also display small sizes. Therefore, relatively low-oxygen levels, probably in the range of upper dysoxia, might be the cause of size reduction, constituting an environmental stress that aided in preservation of sedimentary structures (e.g. Robinson *et al.*, 2007). Similarly, the existence of trace fossil restricted to shallow-tiers indicate oxygen-deficient conditions. For example, bottom water ventilation in oxygen-deficient basins generates thin (up to 1 cm) bioturbated intervals dominated by shallow-tier trace fossils (Virtasalo *et al.*, 2011). Oxygen-deficient contour currents can occur in glaciated margins (e.g., Antarctic Peninsula margin; Lucchi and Rebesco, 2007) or in basins affected by anoxic-dysoxic conditions (e.g., Baltic Sea, Sivkov *et al.*, 2002; Virtasalo *et al.*, 2011; California Continental Borderland, Robinson *et al.*, 2007).

7.4.3.3 Hydrodynamic energy

Hydrodynamic energy controlled bioturbation and the preservation of traction structures. The pattern of decreasing-to-increasing BI in the successions types A and B of F3b indicates an increasing to decreasing effect of hydrodynamic stress over the benthos. At the base, low energy and probably intermittent currents promoted extensive biogenic reworking and beds were completely homogenized (*Nereites* isp. and *Palaeophycus heberti* ichnofabrics). The middle part represents the core of the current, constituting areas with high-energy and more continuous currents that preserved physical sedimentary structures and the *Phycosiphon incertum* ichnofabric, characterized by sparse bioturbation. However, a few colonization surfaces suggest current intermittency (e.g. Rodríguez-Tovar *et al.*, 2019). The top displays a decrease in energy at the edges of the current, where organisms completely reworked the sediment during low-energy conditions (*Nereites* isp. and *Palaeophycus heberti* ichnofabrics). Oxygen controlled bioturbation in these successions by restricting bioturbation depth, but anoxia cannot account for the high-energy, middle parts because sparse discrete burrows occur.

The increasing-to-decreasing energy gradation resembles the bi-gradational sequence characteristic of the contour current facies model (Gonthier *et al.*, 1984; Stow and Faugères, 2008). The bi-gradational pattern demonstrates the shifting of the current from the slower velocity marginal areas affected by eddies to the higher velocity core and viceversa. The described patterns are developed in 0.2-3 m thick intervals (Stow and Faugères, 2008), similar to the successions documented in this study (Figs. 7.3, 7.10). Moreover, the rise in hydrodynamic energy from type A to type B, is recorded by an increase in the abundance and thickness of current-ripple cross- and parallel-laminated beds, and by a decrease in the abundance and thickness of bioturbated beds. A similar gradation in sedimentary structures has been documented in ancient examples (Martín-Chivelet *et al.*, 2008 and references therein).

7.4.3.4 Water Turbidity

The suspension-feeding strategy inferred for the burrows present in the Equilibrichnia-Fugichnia ichnofabric and the abundance of current ripples indicate low levels of water turbidity during deposition of F3c and some intervals of F3b. Substrates showing high turbidity and surface water content typically exclude suspension-feeding organisms, because of the clogging of their filtering

structures and inability to attach to the bottom (Rhoads and Young, 1970). It is noticeable, however, that this ichnofabric occurs in the facies that shows deposition of sediment gravity flows. In addition, irregular burrow boundaries in the Equilibrichnia-Fugichnia ichnofabric suggest soft substrates associated with moderate water content. A rapid alternation between high-turbidity flow events and low-turbidity, current-dominated times after deposition may be the explanation for the occurrence of Equilibrichnia-Fugichnia ichnofabric in F3c.

7.5 Discussion: Implications for the analysis of shallow-water contourite deposits

The present analysis represents a special case of shallow-water contour currents within an oxygen-deficient, epicontinental basin, where different paleoenvironmental factors may have played a role. The highly bioturbated intervals associated with traction structures suggest contour currents can supply oxygen to environments with background anoxic to dysoxic conditions (Reolid and Betzler, 2019), in contrast with other processes such as sediment-gravity flows which rarely show complete bioturbation (Wetzel *et al.*, 2008). Sediment-gravity flows (e.g., wave- and current-enhanced sediment gravity flows, turbidity currents, hyperpycnal flows) cannot sustain long-term oxygenation, and most likely result in "doomed pioneer" ichnofabrics (i.e., discrete occurrences of *Thalassinoides* and *Gyrolithes* encased in unbioturbated laminated dark mudstone; Föllmi and Grimm, 1990). For example, in the Santa Barbara Basin, USA, turbidity currents were able to introduce oxygen in the deeper, oxygen-deficient areas, but the basin chemistry was restored after one month (Sholkovitz and Soutar, 1975). This pattern can also be detected in the Vaca Muerta Formation, where bioturbation index in the contourite deposits show values of 0-5 (mean BI of 1.85, n=894), controlled by hydrodynamic energy, dropping to 0-2 in the sediment-gravity flow-rich areas (mean BI of 0.95, N = 336). However, absent to intense bioturbation in other muddy contourite deposits indicates variable oxygen levels and the existence of contour currents that do not supply oxygen to the seafloor (Frébourg *et al.*, 2013; Knapp *et al.*, 2017; Ayranci *et al.*, 2018). In the Vaca Muerta Formation, unbioturbated contourite deposits are also observed in basin environments (M_{bind}), which supports the idea of anoxic currents.

Moreover, this study suggests that bioturbation can be suppressed in contourites when different environmental stresses are combined, increasing the chance of preserving sedimentary structures. In the present case, it is suggested that the sparsely bioturbated intervals of F3b resulted

from the combined effects of deposition under upper dysoxic conditions and high hydrodynamic energy.

Analyses of similar muddy contourite deposits pointed out the role of sedimentation rate in the preservation of sedimentary structures (Frébourg *et al.*, 2013; Knapp *et al.*, 2017). However, the long-term character of contour currents and their low sediment concentration suggest variable degrees of sediment erosion and bypass indicative of relatively low sedimentation rate. In addition, the higher accumulation areas within modern silty and muddy contourite drifts are highly bioturbated (Faugères *et al.*, 1984; Wetzel *et al.*, 2008), indicating that sedimentation rate cannot restrict bioturbation. In the Vaca Muerta Formation, colonization surfaces within the sparsely bioturbated intervals suggest that traction structures did not form during a single, high sedimentation rate event, but by successive discrete episodes. This pattern highlights the role of hydrodynamic energy (instead of sedimentation rate *per se*) in suppressing bioturbation. Moreover, the evidence of suspension feeding organisms in environments below storm wave base suggests the long-term duration of intense hydrodynamic energy conditions, indicating relatively continuous, contour current activity at the seafloor that maintained food in suspension.

The extent of bioturbation in contourites is still a topic of disagreement. Some studies have incorporated biogenic structures in contourite facies models, suggesting that a highly bioturbated, coarsening and then fining upward, bigradational succession is typical of these deposits (Faugères *et al.*, 1984; Gonthier *et al.*, 1984; Stow and Piper, 1984; Stow and Faugères, 2008; Rodríguez-Tovar and Hernandez-Molina, 2018; Reolid and Betzler, 2019). However, the paucity of bioturbation structures and the abundance of traction structures in deposits attributable to contour current activity have been underscored in other studies (e.g., Hollister and Heezen, 1972; Shanmugam *et al.*, 1993a, 1993b; Martín-Chivelet *et al.*, 2003, 2008; Shanmugam, 2017, 2018). Some studies outline that this discrepancy may reflect contrasting energy conditions between muddy and sandy contourites, precluding bioturbation in the later case (Stow and Faugères, 2008; Rebesco *et al.*, 2014; Rodríguez-Tovar and Hernández-Molina, 2018). The muddy contourite deposits of the Vaca Muerta Formation reveal both intensely bioturbated intervals interbedded with deposits displaying extensive preservation of traction structures. In addition, the observed upward decreasing and then increasing bioturbation index pattern can be interpreted as similar to the bigradational succession of contourites (Fig. 7.8, Stow and Faugères, 2008). Hence, the present analysis agrees with both facies models and demonstrate that sedimentary structures could be

preserved in fine-grained depositional environments when stress factors (dysoxia and high hydrodynamic energy in the present case) limit bioturbation.

7.6 Conclusions

The ichnologic content from contourite deposits of the Upper Jurassic-Lower Cretaceous Vaca Muerta Formation was analyzed to assess environmental controls on the benthos. These deposits occur in drift environments of a mixed carbonate-siliciclastic clinoform system, and comprise laminated, rippled and bioturbated, crinoidal mudstone and fine to coarse mudstone. The ichnofauna consists of *Crininicaminus* isp., *Lockeia siliquaria*, ?*Lockeia* isp., *Nereites* isp., *Palaeophycus* isp., *Palaeophycus heberti*, *Phycosiphon incertum*, *Planolites* isp., ?*Skolithos* isp., and escape and equilibrium trace fossils. Four ichnofabrics, namely *Palaeophycus heberti, Phycosiphon incertum, Nereites* isp., and Equilibrichnia-Fugichnia ichnofabrics, have been characterized. A pattern of ichnofabric distribution in the lithofacies and facies defined is apparent. Facies 3a comprises crinoidal mudstone lithofacies and hosts the *Palaeophycus heberti* ichnofabric forming highly bioturbated intervals. Facies 3b comprises fine to coarse mudstone lithofacies, with the *Phycosiphon incertum, Nereites* isp. and *Palaeophycus heberti* ichnofabrics in sparsely, moderately and highly bioturbated intervals, respectively; and rare Equilibrichnia-Fugichnia ichnofabric forming sparsely to moderately bioturbated intervals. Locally, facies 3b shows m-thick successions with a decreasing and then increasing bioturbation index pattern. Facies 3c consists of fine to coarse mudstone lithofacies, recording not only deposition from contour currents but from sediment gravity flows as well. This facies displays a predominance of the Equilibrichnia-Fugichnia ichnofabric. The most likely environmental controls on benthos included food distribution, oxygenation, hydrodynamic energy, and water turbidity. Food was delivered in suspension or at the sediment surface depending on the current energy and regime, generating a switch between the Equilibrichnia-Fugichnia (suspension-feeding dominant), the *Nereites* isp. and *Phycosiphon incertum* (deposit-feeding dominant), and *Palaeophycus heberti* (a mixed of suspension- and deposit-feeding structures) ichnofabrics. Suspension feeding strategies (Equilibrichnia-Fugichnia ichnofabric) are abundant in the most landward facies (F3c), indicating higher energy currents generating a constant source of suspended organic matter. Oxygenation provided by the contour currents supported a moderately diverse benthos that contrasts with the

typical unbioturbated intervals of the Vaca Muerta Formation, yet small burrow diameters and shallow penetration depths indicate oxygen levels were not in excess (upper dysoxic conditions), as recorded in modern contourite deposits. Hydrodynamic energy controlled biogenic reworking and preservation of sedimentary structures, particularly in the successions with decreasing-to-increasing bioturbation index. Water turbidity remained low during contour current development, supporting a community of suspension feeders, but alternated with high turbidity during sediment-gravity flow deposition. The present analysis supports the fact that high bioturbation levels are common in contourites, highlights their role in ventilating bottom waters, and provides an example of a muddy contourite deposits with high preservation of sedimentary structures.

7.7 Acknowledgments

We thank Shell and Tiser S.R.L., and Germán Canto, Adrián Dolso, Sebastián Estrada, Sebastián Galeazzi, and Fabián Lamarque from Total Austral S.A. for sharing core information with us. We also appreciate the valuable comments of Andreas Wetzel, Juan José Ponce, and an anonymous reviewer on an early draft of the manuscript. This work was financially supported by the Natural Sciences and Engineering Research Council of Canada (NSERC Discovery Grants 311727–20 to MGM), PI-UNRN 2017 40-A-616 and PIP-CONICET 11220170100129CO to NBC, 2016 Student Research Grant from Society for Sedimentary Geology (SEPM), 2016 and 2018 Research Grant from the Geological Society of America (GSA), 2016 Grants-in-Aid Program of the American Association of Petroleum Geologists (AAPG), and 2018 Postgraduate Grant from the International Association of Sedimentologists (IAS). MGM also acknowledges support by the George McLeod Enhancement Chair in Geology.

CHAPTER 8: CONCLUSIONS

The Vaca Muerta Formation represents a mixed carbonate-siliciclastic, shelf-margin, subaqueous clinoform system subdivided into six units by previous authors (Unit 1 to 6, Desjardins *et al.*, 2018), showing a different sedimentologic and sequence stratigraphic evolution depending on the position within the basin. In the basin margin area (Picún Leufú), marine reworking of the underlying eolian dune-field relief (Quebrada del Sapo Formation) during the Vaca Muerta Formation transgressive event and delineation of marginal marine deposits reject the current paradigm of a catastrophic flooding. A rapid transgression with Holocene-like rates of sea-level rise is proposed as an alternative to catastrophic and gradual scenarios of eolian to marine transitions. The fact that the global eustatic sea-level curve predated the transgression indicates that thermal and tectonic subsidence played a major role to generate such high rates of sea-level rise. Progradation of a clinoform system occurred during deposition of two third-order sequences included in Unit 1. At the base, the transgressive succession starts with beach, bay margin, proximal bay and distal bay environments. On top, the regressive interval shows a sediment-starved basin punctuated by wave-influenced, hyperpycnal lobe and lobe fringe sedimentation. Shallower waters, proximity to the coast, and estuarine circulation generated the hyperpycnal flows and storm wave reworking. During lowstand conditions, wave-influenced, hyperpycnal channel-fill complex, lobe and lobe fringe facies occur. The foreset and topset prograded during regression, comprising mud belt, mixed slope, sand bodies, sandy shoal, sand bar, and lagoonal deposits. Organic matter was produced in the water column, and hyperpycnal flows contributed to its dilution.

In the basin centre location (Embayment and Yesera del Tromen areas), a low- to moderate-angle clinoform system evolved during four third-order sequences recorded in Units 1 to 5. The first sequence shows a transgressive basal section represented by beach and open bay marginal marine deposits. On top, it comprises a regressive basin succession with dominantly pelagic and hemipelagic sedimentation and rare sediment-gravity flow and bottom current deposits in the bottomset. At the end of the first sequence, enhanced cascading of dense waters from the shelf, oxygenated bottom waters and intensified deep water circulation, switching the (anoxia-prone) basin estuarine circulation to an anti-estuarine to weakened estuarine circulation. Therefore, hemipelagic, pelagic and contour current sedimentation occurred in upper dysoxic to oxic basin

and sediment drift environments at bottomset and lower foreset locations. The second sequence records bottomset pelagic and hemipelagic sedimentation similarly as the first, whereas foreset areas show hemipelagic-rich sedimentation caused by hypopycnal and mesopycnal plume or low-density flows generated by cascading events or other resuspension processes in a low-angle slope. In younger clinoforms, topset aggradation generated higher foreset slopes that triggered extensive fluid mud deposition during estuarine circulation, or drift and fluid mud deposits during anti-estuarine to weakened estuarine circulation. Fluid mud flows were originated by wave or current resuspension in the shelf, with a storm wave-base located close to the upper foreset or topset. This analysis indicates that climate and basin circulation affected by migration of the subtropical arid belt constituted an important control on sediment partitioning. Thus, warmer climates triggered an equatorward migration of the belt, humid conditions, freshwater discharges and estuarine circulation that produced bottom water anoxia, whereas cooler climates generated poleward migration of the belt, arid conditions and anti-estuarine to weakened estuarine circulation that oxygenated deep locations by water mass renewal from cascading of dense, surface waters. In addition, the contourite deposits are abundant at times of eustatic fall (Lowstand Systems Tract and Falling Stage Systems Tract). This study supports previous assumptions indicating a carbonate increase towards the regressive top of sequences and organic matter enrichment in transgressive successions that lowered dilution effects by sediment condensation and increased water column productivity due to enhanced riverine input.

The ichnologic content of this succession consists of (in order of abundance) *Teichichnus rectus*, *Alcyonidiopsis longobardiae*, *Coprulus oblongus*, *Phycosiphon incertum*, *Planolites* isp., *Teichichnus zigzag*, *Thalassinoides* isp., *Palaeophycus* isp., ?*Lockeia* isp., *Lockeia siliquaria*, *Nereites* isp., *Palaeophycus heberti*, *Crininicaminus* isp., *Zoophycos* isp., *Teichichnus patens*, *Diplocraterion* isp., and ?*Skolithos* isp. Pellet trails, mantle and swirl structures, and escape and equilibrium structures are also common. The analysis of oxygen-deficient ichnocoenoses indicates that increased bioturbation index, penetration depth, burrow size, and ichnodiversity paralleled an increase in bottom water oxygenation. This ichnofauna differs from the typical, oxygen-deficient ichnofaunas by the absence or scarcity of the classic *Chondrites* and *Zoophycos* ichnoguild, dominance of cryptobioturbation, pellet-rich ichnocoenoses and biodeformational structures, recording bioturbation in a food-rich environment where specialized feeding or the development of tiered communities were precluded. Visualization of trace fossils represent a real challenge in

homogeneous mudstone successions that lack sediment contrast. A correlation between the trace fossils recorded in tuff intervals and the fabric of the enclosing mudstone indicates that organisms bioturbated a soupy to very soft, muddy substrate and switched to soft and stiffgrounds after ash deposition. Consequently, paleo-oxygen levels were recorded from discrete trace fossils in the tuff and the mudstone fabric, revealing the importance of rock fabric and bed disruption when evaluating the biogenicity of trace fossils or benthic oxygen levels.

The contourite deposits from the Vaca Muerta Formation mainly comprise laminated, rippled and bioturbated, fine to coarse mudstone and crinoidal mudstone. These deposits represent a particular succession previously described as tempestite, sediment-gravity flow or tidal deposits. Hence, a comprehensive discussion on the sedimentologic and ichnologic evidence was needed, which can be summarized as follows: (1) the relative absence of normal-graded or bioturbated tops, the continuous hydrodynamic stress at the middle of the decreasing to increasing bioturbation index successions, and the suspension feeding strategies indicate the existence of a current of long-term duration (yr to kyr), (2) the dominance of traction structures suggest a current of low sediment concentration, and (3) the highly bioturbated intervals point towards long-term oxygen introduction. All these characteristics are common for bottom current deposits (such as contourites), but are inconsistent with sediment-gravity flow deposits (e.g. hyperpycnites, turbidites, wave- and current-enhanced sediment gravity flow deposits). A wind- and thermohaline-driven circulation system may have originated the contour currents, yet other processes are not completely disregarded. The paleowater depth of these deposits is too deep to consider them as tempestites, whereas tide-driven circulation is probably unlikely due to the presence of an island arc to the west that attenuated tidal effects. The high across-slope extension of the deposits (*ca* 160 km) suggests a circulation process that is not restricted to the area of pycnocline variations, precluding interpretation of internal waves or tides. Cascading of dense, shelf waters, similar as observed in the present-day Mediterranean Sea, may have intensified the circulation system and oxygenated distal locations of the basin during arid and cooler climates. Contourite deposits show four ichnofabrics that were controlled by food distribution, oxygenation, hydrodynamic energy, and water turbidity. Food was delivered at the surface or in suspension, triggering deposit- or suspension-feeding strategies. Oxygen levels increased yet remained upper dysoxic, probably due to high remineralization in an organic-rich benthic environment. Hydrodynamic energy controlled biogenic reworking and consequently the preservation of

sedimentary structures. Water turbidity remained low, supporting a community of suspension feeders. Differentiating bottom currents from sediment-gravity flows can be challenging because bottom currents may be of short-term duration, contain high sediment concentration and low oxygen content, which highlights the need to expand our understanding of sediment transport processes in muddy successions.

REFERENCES

Abril, J.M. and Periáñez, R. (2016). Revisiting the time scale and size of the Zanclean flood of the Mediterranean (5.33 Ma) from CFD simulations. *Marine Geology*, 382, 242–256.

Acevedo, H. and Bande, A. (2018). Characterization of lower Vaca Muerta at Fortín de Piedra in Neuquén Basin, Argentina. *The Leading Edge*, 37, 255–260.

Aguirre-Urreta, M.B. and Vennari, V.V. (2009). On Darwin's footsteps across the Andes: Tithonian-Neocomian fossil invertebrates from the Piuquenes pass. *Revista de la Asociación Geológica Argentina*, 64, 32–42.

Aguirre-Urreta, B., Vennari, V.V., Lescano, M., Naipauer, M., Concheyro, A., and Ramos, V.A. (2014). Bioestratigrafía y geocronología de alta resolución de la Formación Vaca Muerta, Cuenca Neuquina. In *IX Congreso de Exploración y Desarrollo de Hidrocarburos, Simposio de Recursos No Convencionales* (p. 245–268), Abstract, Mendoza.

Aguirre-Urreta, B., Naipauer, M., Lescano, M., López-Martínez, R., Pujana, I., Vennari, V., De Lena, L.F., Concheyro, A. and Ramos, V.A. (2019). The Tithonian chrono-biostratigraphy of the Neuquén Basin and related Andean areas: A review and update. *Journal of South American Earth Sciences*, 92, 350–367.

Ahlbrandt, T.S. and Fryberger, S.G. (1981). Sedimentary features and significance of interdune deposits. In F.G. Ethridge and R.M. Flores (Eds.), *Recent and Ancient Nonmarine Depositional Environments: Models for Exploration* (p. 293–314). SEPM Special Publication v. 31.

Ahmed Benan, C.A. and Kocurek, G. (2000). Catastrophic flooding of an aeolian dune field: Jurassic Entrada and Todilto formations, Ghost Ranch, New Mexico, USA. *Sedimentology*, 47, 1069–1080.

Aigner, T. (1985). An ancient storm depositional system: Dynamic stratigraphy of intracratonic carbonates, Upper Muschelkalk (Middle Triassic), South-German Basin. In T. Aigner (Ed.), *Storm Depositional Systems: Dynamic Stratigraphy in Modern and Ancient Shallow-Marine Sequences* (p. 51–158). Lecture Notes in Earth Sciences 3.

Al-Hinai, K.G., Moore, J.M. and Bush, P.R. (1987). LANDSAT image enhancement study of possible submerged sand-dunes in the Arabian Gulf. *Int. J. Remote Sens.*, 8, 251–258.

Alberti, M., Parent, H., Garrido, A.C., Andersen, N., Garbe-Schönberg, D. and Danise, S. (2020). Stable isotopes ($\delta^{13}C$, $\delta^{18}O$) and element ratios (Mg/Ca, Sr/Ca) of Jurassic belemnites, bivalves and brachiopods from the Neuquén Basin (Argentina): challenges and opportunities for palaeoenvironmental reconstructions. *Journal of the Geological Society*, 178, jgs2020-163.

Alldredge, A.L. and Silver, M.W. (1988). Characteristics, dynamics and significance of marine snow. *Progress in Oceanography*, 20, 41–82.

Aller, J.Y. (1989). Quantifying sediment disturbance by bottom currents and its effect on benthic communities in a deep-sea western boundary zone. *Deep Sea Research Part A, Oceanographic Research Papers*, 36, 901–934.

Aller, R.C. (1994). Bioturbation and remineralization of sedimentary organic matter: effects of redox oscillation. *Chemical Geology*, 114, 331–345.

Aller, J.Y. (1997). Benthic community response to temporal and spatial gradients in physical disturbance within a deep-sea western boundary region. *Deep Sea Research Part I: Oceanographic Research Papers*, 44, 39–69.

Aller, J.Y. and Aller, R.C. (1986). General characteristics of benthic faunas on the Amazon inner continental shelf with comparison to the shelf off the Changjiang River, East China Sea. *Continental Shelf Research*, 6, 291–310.

Allmon, W.D. (1988). Ecology of Recent turritelline gastropods (Prosobranchia, Turritellidae): Current knowledge and paleontological implications. *Palaios*, 3, 259.

Alonso, B., Ercilla, G., Casas, D., Stow, D.A.W, Rodríguez-Tovar, F.J., Dorador, J. and Hernández-Molina, F.J. (2016). Contourite vs gravity-flow deposits of the Pleistocene Faro Drift (Gulf of Cadiz): Sedimentological and mineralogical approaches. *Marine Geology*, 377, 77–94.

Angel, M.V. (1984). Detrital organic fluxes through pelagic ecosystems. In M.J.R. Fasham (Ed.), Flows of Energy and Materials in Marine Ecosystems (p. 475–516). Springer, Boston.

Aplin, A.C., and Macquaker, J.H. (2011). Mudstone diversity: Origin and implications for source, seal, and reservoir properties in petroleum systems. *AAPG Bulletin*, 95, 2031–2059.

Arakawa, K.Y. (1971). Studies on the faecal pellets of marine invertebrates (excluding molluscs) I. *Publications of the Seto Marine Biological Laboratory*, 19, 231–241.

Argüello Scotti, A. and Veiga, G.D. (2015). Morphological characterization of an exceptionally preserved eolian system: The Cretaceous Troncoso Inferior Member in the Neuquén Basin (Argentina). *Lat. Am. J. Sedimentol. Basin Anal.*, 22, 29–46.

Armella, C., Cabaleri, N., and Leanza, H.A. (2007). Tidally dominated, rimmed-shelf facies of the Picún Leufú Formation (Jurassic/Cretaceous boundary) in southwest Gondwana, Neuquén Basin, Argentina. *Cretaceous Research*, 28, 961–979.

Armella, C., Cabaleri, N. and Leanza, H. (2008), Facies de patch reefs en la Formación Picún Leufú (límite Jurásico/Cretácico) en la región de Zapala, Cuenca Neuquina. *Revista del Museo Argentino de Ciencias Naturales*, 10, 63–70.

Arregui, C. (2014). Ciclos deposicionales de las Fms Quintuco y Vaca Muerta: Génesis y evolución. Área Central - Cuenca Neuquina. In *IX Congreso de Exploración y Desarrollo de Hidrocarburos* (pp. 189–207). Mendoza, Argentina.

Arregui, C., Carbone, O., and Leanza, H.A. (2011). Contexto tectosedimentario. In H.A. Leanza, C. Arregui, O. Carbone, J.C. Danieli, and J.M. Vallés (Eds.), *Geología y Recursos Naturales de la Provincia del Neuquén* (p. 29–36). Asociación Geológica Argentina.

Ayranci, K., Harris, N.B. and Dong, T. (2018). Sedimentological and ichnological characterization of the Middle to Upper Devonian Horn River Group, British Columbia, Canada: insights into mudstone depositional conditions and processes below storm wave base. *Journal of Sedimentary Research*, 88, 1–23.

Baas, J.H. and Best, J.L. (2002). Turbulence modulation in clay-rich sediment-laden flows and some implications for sediment deposition. *Journal of Sedimentary Research*, 72, 336–340.

Baas, J.H., Best, J.L. and Peakall, J. (2011). Depositional processes, bedform development and hybrid bed formation in rapidly decelerated cohesive (mud–sand) sediment flows. *Sedimentology*, 58, 1953–1987.

Baas, J.H., Best, J.L. and Peakall, J. (2016). Predicting bedforms and primary current stratification in cohesive mixtures of mud and sand. *Journal of the Geological Society*, 173, 12–45.

Bahk, J.J., Chough, S.K. and Han, S.J. (2000). Origins and paleoceanographic significance of laminated muds from the Ulleung Basin, East Sea (Sea of Japan). *Marine Geology*, 162, 459–477.

Baldwin, C.T. and McCave, I.N. (1999). Bioturbation in an active deep-sea area: implications for models of trace fossil tiering. *Palaios*, 14, 375–388.

Ball, M.M. (1967). Carbonate sand bodies of Florida and the Bahamas. *Journal of Sedimentary Petrology*, 37, 556–591.

Ballent, S.C., Ronchi, D.I., and Angelozzi, G.N. (2004). Microfósiles calcáreos tithonianos (Jurásico superior) en el sector oriental de la cuenca Neuquina, Argentina. *Ameghiniana*, 40, 13–24.

Bałuk, W. and Radwański, A. (1979). Polychaete-attributable faecal pellets, *Tibikoia sanctacrucensis* ichnosp. n., from the Korytnica Clays (Middle Miocene; Holy. Cross Mountains, Central Poland). *Acta Geologica Polonica*, 29, 335–344.

Barredo, S., Speranza, T., Massaro, A.S., Foschiatti, I., and Párica, A. (2018). Análisis geológico integral de los controles en la acumulación y preservación de la materia orgánica de la Formación Vaca Muerta en el sector norte de la Cuenca Neuquina. In *X Congreso de Exploración y Desarrollo de Hidrocarburos, Simposio de Recursos No Convencionales* (p. 193–211). Mendoza, Argentina.

Bates, C.C. (1953). Rational theory of delta formation. *AAPG Bulletin*, 37, 2119–2162.

Baucon, A., Bednarz, M., Dufour, S., Felletti, F., Malgesini, G., de Carvalho, C.N., Niklas, K.J., Wehrmann, A., Batstone, R., Bernardini, F. and Briguglio, A. (2020). Ethology of the trace fossil *Chondrites*: form, function and environment. *Earth-Science Reviews*, 202, 102989.

Bayet-Goll, A., Monaco, P., Jalili, F. and Mahmudy-Gharaie, M.H. (2016). Depositional environments and ichnology of Upper Cretaceous deep-marine deposits in the Sistan Suture Zone, Birjand, Eastern Iran. *Cretaceous Research*, 60, 28–51.

Behl, R.J. (1995). Sedimentary facies and sedimentology of the Late Quaternary Santa Barbara Basin, site 893. In Kennett, J.P., Baldauf, J.G. and Lyle, M. (Eds.), *Proceedings of the Ocean Drilling Program*, Scientific Results, v. 146 (p. 295–308).

Belaústegui, Z. and Belaústegui, A. (2017). Modernist architecture in Barcelona reveals a new trace fossil from the Miocene of Montjuïc (NE Spain). *Geologica Acta*, v. 15, p. 169–186.

Belknap, D.F. and Kraft, J.C. (1981). Preservation potential of transgressive coastal lithosomes on the U.S. Atlantic shelf. *Marine Geology*, 42, 429–442.

Bennett, R.H., Bryant, W.R. and Hulbert, M.H. (1991). *Microstructures in Fine-Grained Sediments: From Mud to Shale*. Springer, 582 p.

Bentley, S.J. and Nittrouer, C.A. (1999). Physical and biological influences on the formation of sedimentary fabric in an oxygen-restricted depositional environment; Eckernförde Bay, southwestern Baltic Sea. *Palaios*, 14, 585–600.

Bentley, S.J. and Nittrouer, C.A. (2003). Emplacement, modification, and preservation of event strata on a flood-dominated continental shelf: Eel shelf, Northern California. *Continental Shelf Research*, 23, 1465–1493.

Berger, W.H., Smetacek, V.S., and Wefer, G. (1989). Ocean productivity and paleoproductivity—an overview. In Berger, W.H., Smetacek, V.S., and Wefer, G. (Eds.), *Productivity of the Ocean: Present and Past* (p. 1–34). Wiley New York, v. 44.

Berne, S., Lericolais, G., Marsset, T., Bourillet, J.F., De Batist, M. (1998). Erosional offshore sand ridges and lowstand shorefaces; examples from tide- and wave-dominated environments of France. *Journal of Sedimentary Research*, 68, 540–555.

Bertling, M., Braddy, S.J., Bromley, R.G., Demathieu, G.R., Genise, J., Mikuláš, R., Nielsen, J.K., Nielsen, K.S., Rindsberg, A.K., Schlirf, M. and Uchman, A. (2006). Names for trace fossils: a uniform approach. *Lethaia*, 39, 265–286.

Bhattacharya, J.P. and MacEachern, J.A. (2009). Hyperpycnal rivers and prodeltaic shelves in the Cretaceous seaway of North America. *Journal of Sedimentary Research*, 79, 184–209.

Bilmes, J. (2018). Apuesta por la recuperación de YPF (2012-2015): diseño, desempeño e implicancias. *Cuestiones de Sociología*, 19, e063.

Birgenheier, L.P. and Moore, S.A. (2018). Carbonate mud deposited below storm wave base. *The Sedimentary Record*, 16, 4–10.

Birgenheier, L.P., Horton, B., McCauley, A.D., Johnson, C.L. and Kennedy, A. (2017). A depositional model for offshore deposits of the lower Blue Gate Member, Mancos Shale, Uinta Basin, Utah, USA. *Sedimentology*, 64, 1402–1438.

Blakey, R.C., Peterson, F., Caputo, M.V., Geesaman, R.C. and Voorhees, B.J. (1983). Paleogeography of Middle Jurassic continental, shoreline and shallow marine sedimentation, Southern Utah. In M.W. Reynolds and E.D. Dolly (Eds.), *Mesozoic Paleogeography of West-Central United States* (p. 77–100). Rocky Mountain Paleogeography Symposium 2, SEPM.

Blakey, R.C., Havholm, K.G. and Jones, L.S. (1996). Stratigraphic analysis of eolian interactions with marine and fluvial deposits, Middle Jurassic Page Sandstone and Carmel Formation, Colorado Plateau, U.S.A. *J. Sediment. Res.*, 66, 324–342.

Blanc, P.-L. (2002). The opening of the Plio-Quaternary Gibraltar Strait: assessing the size of a cataclysm. *Geodin. Acta*, 15, 303–317.

Blaszczyk, J.K. (1981). Palaeomorphology of Weissliegendes top as the control on facies variability in ore-bearing series of Lubin copper-field, Southwestern Poland. *Geol. Sudetica*, 16, 195–217.

Boll, A. and Valencio, D. (1996). Relación estratigráfica entre las formaciones Tordillo y Vaca Muerta en el sector central de la Dorsal de Huincul, Provincia del Neuquén. In *13º Congreso Geológico Argentino y 3º Congreso de Exploración de Hidrocarburos* (p. 205–223). Asociación Geológica Argentina, Buenos Aires, Argentina.

Borbolla, M.C., Cruz, C.E., Villar, H.J., Annizzotto, N., D'Odorico Benites, P. and Cattaneo, D. (2014). Formación Vaca Muerta: variación lateral de facies y su implicancia en los cambios de espesor hacia el borde se cuenca. Perspectivas exploratorias en shale oil en la Plataforma de Catriel, Cuenca Neuquina, Argentina. In *IX Congreso de Exploracion y Desarrollo de Hidrocarburos* (p. 315–339). IAPG, Mendoza, Argentina.

Borcovsky, D., Egenhoff, S., Fishman, N., Maletz, J., Boehlke, A. and Lowers, H. (2017). Sedimentology, facies architecture, and sequence stratigraphy of a Mississippian black

mudstone succession—The upper member of the Bakken Formation, North Dakota, United States. *AAPG Bulletin*, 101, 1625–1673.

Boulesteix, K., Poyatos-Moré, M., Flint, S.S., Taylor, K.G., Hodgson, D.M. and Hasiotis, S.T. (2019). Transport and deposition of mud in deep-water environments: Processes and stratigraphic implications. *Sedimentology*, 66, 2894–2925.

Bouma, A. H. (1962). *Sedimentology of some Flysch Deposits: A Graphic Approach to Facies Interpretation*. Elsevier, Amsterdam, Netherlands, 168 pp.

Bouma, A.H. and Hollister, C.D. (1973). Deep ocean basin sedimentation. In Middleton, G.V., and Bouma, A.H. (Eds.), *Turbidites and Deep Water Sedimentation* (p. 79–118). SEPM Pacific Section Short Course, Anaheim.

Boyer, D.L. and Droser, M.L. (2011). A combined trace-and body-fossil approach reveals high-resolution record of oxygen fluctuations in Devonian seas. *Palaios*, 26, 500–508.

Boyer, C., Clark, B., Jochen, V., Lewis, R., and Miller, C.K. (2011). Shale gas: A global resource. *Oilfield Review*, 23, 28–39.

Brackenridge, R., Stow, D.A. and Hernández-Molina, F.J. (2011). Contourites within a deep-water sequence stratigraphic framework. *Geo-Marine Letters*, 31, 343–360.

Bremner, J. M. (1983). Biogenic sediments on the South West African (Namibian) continental margin. In Thiede, J., and Suess, E. (Eds.), *Coastal Upwelling, its Sediment Record, Part B* (p. 73–103). Sedimentary Records of Ancient Coastal Upwelling, Plenum Press.

Brisson, I.E., Fasola, M.E. and Villar, H.J. (2020). Organic geochemical patterns of the Vaca Muerta Formation. In Minisini, D., Fantín, M, Lanusse Noguera, I., and Leanza, H. (Eds.), *Integrated Geology of Unconventionals: The Case of the Vaca Muerta Play, Argentina* (p. 297–328). AAPG Memoir, v. 121.

Brodie, I. and Kemp, A.E.S., (1994). Variation in biogenic and detrital fluxes and formation of laminae in late Quaternary sediments from the Peruvian coastal upwelling zone. *Marine Geology*, 116, 385–398.

Brodie, I. and Kemp, A.E.S. (1995). Pelletal structures in Peruvian upwelling sediments. *Journal of the Geological Society*, 152, 141–150.

Bromley, R.G. (1990). *Trace Fossils. Biology and Taphonomy*. Unwin Hyman, London, 280 p.

Bromley, R.G. (1991). *Zoophycos*: strip mine, refuse dump, cache or sewage farm?. *Lethaia*, 24, 460–462.

Bromley, R.G. (1996). *Trace Fossils, Biology, Taphonomy and Applications*. Springer Science, 361 p.

Bromley, R.G. and Frey, R.W. (1974). Redescription of the trace fossil *Gyrolithes* and taxonomic evaluation of *Thalassinoides*, *Ophiomorpha* and *Spongeliomorpha*. *Bulletin of the Geological Society of Denmark*, 23, 311–335.

Bromley, R.G. and Asgaard, U. (1979). Triassic freshwater ichnocoenoses from Carlsberg Fjord, east Greenland. *Palaeogeography, Palaeoclimatology, Palaeoecology*, 28, 39–80.

Bromley, R.G. and Ekdale, A.A. (1984). *Chondrites*: a trace fossil indicator of anoxia in sediments. *Science*, 224, 872–874.

Bromley, R.G. and Ekdale, A.A. (1986). Composite ichnofabrics and tiering of burrows. *Geological Magazine*, 123, 59–65.

Bromley, R.G. and Uchman, A. (2003). Trace fossils from the Lower and Middle Jurassic marginal marine deposits of the Sorthat Formation, Bornholm, Denmark. *Bull. Geol. Soc. Denmark*, 50, 185–208.

Brysch, S. (2018). *Changes in Climate and Palaeoenvironment During the Late Jurassic–Early Cretaceous in Southern South America and Western Antarctica*. PhD dissertation, der Ruprecht-Karls-Universität, Heidelberg, 233 p.

Buatois, L.A. and López Angriman, A.O. (1992). The ichnology of a submarine braided channel complex: the Whisky Bay Formation, Cretaceous of James Ross Island, Antarctica. *Palaeogeography, Palaeoclimatology, Palaeoecology*, 94, 119–140.

Buatois, L.A. and Mángano, M.G. (2011). *Ichnology: Organism-Substrate Interactions in Space and Time*. Cambridge University Press, 358 p.

Buatois, L.A. and Mángano, M.G. (2021). Ichnofacies. In Alderton, D. and Elias, S.D. (Eds.), *Encyclopedia of Geology* (Second Edition, p. 511–519). Elsevier.

Buatois, L.A., Gingras, M.K., MacEachern, J.A., Mángano, M.G., Zonneveld, J.-P., Netto, R.G. and Martin, A. (2005). Colonization of brackish-water systems through time: Evidence from the trace-fossil record. *Palaios*, 20, 321–347.

Buatois, L. A., Saccavino, L. L. and Zavala, C. (2011). Ichnologic signatures of hyperpycnal flow deposits in Cretaceous river-dominated deltas, Austral Basin, southern Argentina. In Slatt, R.M., and Zavala, C. (Eds.), *Sediment Transfer from Shelf to Deep Water—Revisiting the Delivery System* (p. 153–170). AAPG Studies in Geology, v. 61.

Buatois, L.A., Carmona, N.B., Curran, H.A., Netto, R.G., Mángano, M.G., and Wetzel, A. (2016). The Mesozoic Marine Revolution. In Mángano, M.G., and Buatois, L.A. (Eds.), *The Trace-Fossil Record of Major Evolutionary Events Volume 2: Mesozoic and Cenozoic* (p. 19–134). Topics in Geobiology, v. 40.

Buatois, L.A., Wisshak, M., Wilson, M.A. and Mangano, M.G. (2017). Categories of architectural designs in trace fossils: a measure of ichnodisparity. *Earth-Science Reviews*, 164, 102–181.

Buatois, L.A., Mángano, M.G., Pattison, S.A. (2019). Ichnology of prodeltaic hyperpycnite-turbidite channel complexes and lobes from the Upper Cretaceous Prairie Canyon Member of the Mancos Shale, Book Cliffs, Utah, USA. *Sedimentology*. doi:10.1111/sed.12560

Cacchione, D.A. and Drake, D.E. (1986). Nepheloid layers and internal waves over continental shelves and slopes. *Geo-Marine Letters*, 6, 147–152.

Cacho, I., Grimalt, J.O., Sierro, F.J., Shackleton, N. and Canals, M. (2000). Evidence for enhanced Mediterranean thermohaline circulation during rapid climatic coolings. *Earth and Planetary Science Letters*, 183, 417–429.

Cadée, G.C. (1979). Sediment reworking by the polychaete Heteromastus filiformis on a tidal flat in the Dutch Wadden Sea. *Netherlands Journal of Sea Research*, 13, 441–456.

Calvert, S.E. (1964). Factors affecting distribution of laminated diatomaceous sediments in Gulf of California. In van Andel, T.H., and Shor, G.G. Jr. (Eds.), *Marine Geology of the Gulf of California: A Symposium* (p. 311–330). AAPG Memoir, v. 3.

Campetella, D.M., Carmona, N.B., Ponce, J.J., Wetzel, A., Rodríguez, M. and Parada, M.N. (2020). Trace fossils as tools to unravel oxygen conditions: A case study from Los Molles

Formation (Toarcian-lower Callovian). *Revista de la Asociacón Geológica Argentina*, 77, 463–477.

Canale, N., Ponce, J.J., Carmona, N.B., Parada, M.N. and Drittanti, D.I. (2020). Sedimentología e icnología de un delta fluvio-dominado, Formación Lajas (Jurásico Medio), Cuenca Neuquina, Argentina. *Andean Geology*, 47, 179–206.

Canals, M., Puig, P., de Madron, X.D., Heussner, S., Palanques, A. and Fabres, J. (2006). Flushing submarine canyons. *Nature*, 444, 354–357.

Capelli, I.A., Scasso, R.A., Kietzmann, D.A., Cravero, M.F., Minisini, D., and Catalano, J.P. (2018). Mineralogical and geochemical trends of the Vaca Muerta-Quintuco system in the Puerta Curaco section, Neuquén Basin. *Revista de la Asociación Geológica Argentina*, 75, 210–228.

Capelli, I.A., Scasso, R.A., Spangenberg, J.E., Kietzmann, D.A., Cravero, F., Duperron, M. and Adatte, T. (2021). Mineralogy and geochemistry of deeply-buried marine sediments of the Vaca Muerta-Quintuco system in the Neuquén Basin (Chacay Melehue section), Argentina: Paleoclimatic and paleoenvironmental implications for the global Tithonian-Valanginian reconstructions. *Journal of South American Earth Sciences*, 107, 103103.

Carbone, O., Franzese, J., Limeres, M., Delpino, D., and Martínez, R. (2011). El Ciclo Precuyano (Triásico Tardío-Jurásico Temprano) en la Cuenca Neuquina. In Leanza, H.A., Arregui, C., Carbone, O., Danieli, J.C., and Vallés, J.M. (Eds.), *Geología y Recursos Naturales de la Provincia del Neuquén* (p. 63–76). Asociación Geológica Argentina.

Carmona, N.B. and Ponce, J.J. (2011). Ichnology and sedimentology of Miocene hyperpycnites of the Austral Foreland Basin (Tierra del Fuego, Argentina): Trace fossil distribution and paleoecological implications. In Slatt, R.M. and Zavala, C.A. (Eds.), *Sediment Transfer from Shelf to Deep Water–Revisiting the Delivery System* (p. 171–192). AAPG Studies in Geology, v. 61.

Carmona, N., Bornoud, C., Ponce, J.J. and Cuadrado, D.G. (2011). The role of microbial mats in the preservation of bird footprints: a case study from the mesotidal Bahia Blanca Estuary (Argentina). In N. Noffke and H. Chafetz (Eds.), *Microbial Mats in Siliciclastic Depositional Systems Through Time* (p. 37–45). SEPM Special Publication.

Carmona, N.B., Ponce, J.J., Wetzel, A., Bournod, C.N. and Cuadrado, D.G. (2012). Microbially induced sedimentary structures in Neogene tidal flats from Argentina: Paleoenvironmental, stratigraphic and taphonomic implications. *Palaeogeogr. Palaeoclimatol. Palaeoecol.*, 353–355, 1–9.

Casadío, S., and Montagna, A.O. (2015). Estratigrafía de la Cuenca Neuquina. In Ponce, J.J., Montagna, A.O. and Carmona, N. (Eds.), *Geología de la Cuenca Neuquina y sus Sistemas Petroleros* (p. 8–21). Fundación YPF, Buenos Aires,.

Catalano, J.P., Scasso, R.A., Kietzmann, D., Föllmi, K., Spangenberg, J., and Capelli, I. (2018). Carbonate sedimentology and diagenesis of the Vaca Muerta Formation at Puerta Curaco, Neuquén Basin, Argentina. In *X Congreso de Exploración y Desarrollo de Hidrocarburos, Simposio de Recursos No Convencionales* (p. 481–501). IAPG, Mendoza, Argentina.

Cattaneo, A. and Steel, R.J. (2003). Transgressive deposits: A review of their variability. *Earth-Science Rev.*, 62, 187–228.

Cattaneo, A., Correggiari, A., Langone, L. and Trincardi, F. (2003). The late-Holocene Gargano subaqueous delta, Adriatic shelf: sediment pathways and supply fluctuations. *Marine Geology*, 193, 61–91.

Catuneanu, O. (2006). *Principles of Sequence Stratigraphy*. Elsevier, 388 p.

CEPAL (2015). *Impacto Socioeconómico de YPF desde su Renacionalización (Ley 26.741): Desempeño Productivo e Implicancias sobre los Mercados Laborales y el Entramado de Proveedores. Volumen I*. Comisión Económica para América Latina y el Caribe, Serie Documentos de Proyectos, 107 p.

Cevallos, M. (2005). Análisis estratigráfico de alta frecuencia del límite kimmeridgiano-tithoniano en el subsuelo de la Dorsal de Huincul, Cuenca Neuquina. In *VI Congreso de Exploración y Desarrollo de Hidrocarburos* (Actas CD). Mar del Plata, Argentina.

Chamberlain, C.K. (1977). *Ordovician and Devonian Trace Fossils from Nevada*. Nevada Bureau of Mines and Geology Bulletin, v. 90, 24 p.

Chan, M.A. and Kocurek, G. (1988). Complexities in eolian and marine interactions: processes and eustatic controls on erg development. *Sedimentary Geology*, 56, 283–300.

Collinson, J.C. (1994). Sedimentary deformational structures. In A. Maltman (Ed.), *The Geological Deformation of Sediments* (p. 95–125). Chapman and Hall, London.

Coppola, L., Prieur, L., Taupier-Letage, I., Estournel, C., Testor, P., Lefevre, D., Belamari, S., Lereste, S. and Taillandier, V. (2017). Observation of oxygen ventilation into deep waters through targeted deployment of multiple Argo-O_2 floats in the north-western Mediterranean Sea in 2013. *Journal of Geophysical Research, Oceans*, 122, 6325–6341.

Cornée, J.-J., Münch, P., Achalhi, M., Merzeraud, G., Azdimousa, A., Quillévéré, F., Melinte-Dobrinescu, M., Chaix, C., Moussa, A. Ben, Lofi, J., Séranne, M. and Moissette, P. (2016). The Messinian erosional surface and early Pliocene reflooding in the Alboran Sea: New insights from the Boudinar basin, Morocco. *Sediment. Geol.*, 333, 115–129.

Corner, G.D. and Fjalstad, A. (1993). Spreite trace fossils (*Teichichnus*) in a raised Holocene fjord-delta, Breidvikeidet, Norway. *Ichnos*, 2, 155–164.

Cornford, C. (1979). Organic deposition at a continental rise: organic geochemical interpretation and synthesis at DSDP Site 397, eastern North Atlantic. In von Rad, U., *et al.* (Eds.), *Initial Reports of the Deep-Sea Drilling Project* (p. 503-510). US Government Printing Office, Washington, v. 47.

Cuomo, M.C. and Bartholomew, P.R. (1991). Pelletal black shale fabrics: their origin and significance. In Tyson, R.V. and Pearson, T.H. (Eds.), *Modern and Ancient Continental Shelf Anoxia* (p. 221–232). Geological Society of London, Special Publications, v. 58.

Cuomo, M.C. and Rhoads, D.C. (1987). Biogenic sedimentary fabrics associated with pioneering polychaete assemblages; modern and ancient. *Journal of Sedimentary Research*, 57, 537–543.

Curran, H.A. (2007). Ichnofacies, ichnocoenoses, and ichnofabrics of Quaternary shallow-marine to dunal tropical carbonates: A model and implications. In Miller, W. (Ed.), *Trace Fossils, Concepts, Problems, Prospects* (p. 232–247). Elsevier.

Dalrymple, R.W. (2010). Tidal Depositional Systems. In James, N.P. and Dalrymple R.W. (Eds.), *Facies Models 4* (p. 201–232). Geological Association of Canada.

Dalrymple, R. W., Mackay, D. A., Ichaso, A. A., Choi, K. S. (2012). Processes, morphodynamics, and facies of tide-dominated estuaries. In Davis, R.A., Dalrymple, R.W. (Eds.), *Principles of Tidal Sedimentology* (p. 79–107). Springer, Dordrecht.

Damborenea, S.E. and Leanza, H.A. (2016). *Huncalotis*, an enigmatic new pectinoid genus (Bivalvia, Late Jurassic) from South America. *Pal Z*, 90, 449–468.

Dashtgard, S.E. and Gingras, M.K. (2012). Marine invertebrate neoichnology. In Knaust, D., and Bromley, R.G. (Eds.), *Trace Fossils as Indicators of Sedimentary Environments* (p. 273–295). Developments in Sedimentology, v. 64.

De, C. (2019). *Mangrove Ichnology of the Bay of Bengal Coast, Eastern India*. Springer, 347 pp.

De, C. (2000). Neoichnological activities of endobenthic invertebrates in Downdrift Coastal Ganges Delta Complex, India: Their significance in trace fossil interpretations and Paleoshoreline reconstructions. *Ichnos*, 7, 89–113.

del Rosario Lanz, M., Azmy, K., Cesaretti, N.N. and Fortunatti, N.B. (2021). Diagenesis of the Vaca Muerta Formation, Neuquén Basin: Evidence from petrography, microthermometry and geochemistry. *Marine and Petroleum Geology*, 124, 104769.

DeMaster, D.J., McKee, B.A., Nittrouer, C.A., Brewster, D.C. and Biscaye, P.E. (1985). Rates of sediment reworking at the HEBBLE site based on measurements of Th-234, Cs-137 and Pb-210. *Marine Geology*, 66, 133–148.

Denommee, K.C., Bentley, S.J., Harazim, D. and Macquaker, J.H. (2016). Hydrodynamic controls on muddy sedimentary-fabric development on the Southwest Louisiana subaqueous delta. *Marine Geology*, 382, 162–175.

DeReuil, A.A., Birgenheier, L.P. (2019). Sediment dispersal and organic carbon preservation in a dynamic mudstone-dominated system, Juana Lopez Member, Mancos Shale. *Sedimentology*, 66, 1002–1041.

Desjardins, P. and Aguirre, H. (2018), Chapter 7: Sierras Blancas. In González, G., Vallejo, M.D., Kietzmann, D.A., Marchal, D., Desjardins, P.R., González Tomassini, F., Gómez Rivarola, L., Domínguez, R.F. and Fantín, M.A. (Eds.), *Regional Cross Section of the Vaca Muerta Formation, Integration of Seismic, Well Logs, Cores and Outcrops* (p. 71–82). Special Publication of IAPG, Buenos Aires.

Desjardins, P., Fantín, M., González Tomassini, F., Reijenstein, H., Sattler, F., Domínguez, F., Kietzmann, D., Bande, A., Benoit, S., Borgnia, M., Vittore, F., Simo, T. and Minisini, D., (2018). Chapter 2: Regional seismic stratigraphy. In González, G., Vallejo, M.D., Kietzmann, D.A., Marchal, D., Desjardins, P.R., González Tomassini, F., Gómez Rivarola, L., Domínguez, R.F. and Fantín, M.A. (Eds.), *Regional Cross Section of the Vaca Muerta Formation, Integration of Seismic, Well Logs, Cores and Outcrops* (p. 5–22). Special Publication of IAPG, Buenos Aires.

Desmond, R.J., Steidtmann, J.R. and Cardinal, D.F. (1984). Stratigraphy and depositional environments of the middle member of the Minnelusa Formation, central Powder River Basin, Wyoming. In *Wyoming Geological Association 35th Annual Field Conference Guidebook* (p. 213–239).

Diaz, R.J. and Rosenberg, R. (1995). Marine benthic hypoxia: a review of its ecological effects and the behavioural responses of benthic macrofauna. *Oceanography and Marine Biology: An Annual Review*, 33, 245–303.

Díez-Canseco, D., Buatois, L.A., Mángano, M.G., Rodriguez, W. and Solorzano, E. (2015). The ichnology of the fluvial-tidal transition: Interplay of ecologic and evolutionary controls. In P.J. Ashworth, J.L. Best, and D.R. Parsons (Eds.), *Fluvial-Tidal Sedimentology* (p. 283–321). Developments in Sedimentology, v. 68.

Digregorio, J.H. (1972). Neuquén. In Leanza, A.F. (Ed.), *Geología Regional Argentina* (p. 439–505). Academia Nacional de Ciencias, Córdoba.

Dimroth, E. and Yamagishi, H. (1987). Criteria for the recognition of ancient subaqueous pyroclastic rocks. *Rep. Geol. Surv. Hokkaido*, 58, 55–88.

Doe, T.W. and Dott, R.H.J. (1980). Genetic significance of deformed cross bedding–with examples from the Navajo and Weber Sandstones of Utah. *J. Sediment. Petrol.*, 50, 793–812.

Domínguez, R.F., Paulin, S., Continanzia, M.J., Askenazi, A.D., Seoane, F.N. (2014). Estratigrafía del intervalo Vaca Muerta–Quintuco en el sector central de la Cuenca Neuquina. In *IX Congreso de Exploración y Desarrollo de Hidrocarburos* (p. 231–250). Mendoza, Argentina.

Domínguez, R.F., Reijenstein, H., Kohler, G., Sattler, F., Moreno, M., Gómez Rivarola, L., Borgnia, M. (2017). Distribución regional de quiebres de clinoformas del sistema Vaca Muerta-Quintuco. In *XX Congreso Geológico Argentino, Geología de la Formación Vaca Muerta* (p. 38–45). San Miguel de Tucumán, Argentina.

Domínguez, R.F., Catuneanu, O., Reijenstein, H.M., Notta, R. and Posamentier, H.W. (2020a). Sequence stratigraphy and the three-dimensional distribution of organic-rich units. In Minisini, D., Fantin, M., Lanusse Noguera, I. and Leanza, H.A. (Eds.), *Integrated Geology of Unconventionals: The Case of the Vaca Muerta Play, Argentina* (p. 163–200). AAPG Memoir, v. 121.

Domínguez, R.F., Leanza, H.A., Fantín, M., Marchal, D. and Cristallini, E. (2020b). Basin configuration during the Vaca Muerta times. In Minisini, D., Fantín, M., Lanusse Noguera, I. and Leanza, H.A. (Eds.), *Integrated geology of unconventionals: The case of the Vaca Muerta play, Argentina* (p. 141–162). AAPG Memoir, v. 121.

Dorador, J., Wetzel, A. and Rodríguez-Tovar, F.J. (2016). *Zoophycos* in deep-sea sediments indicates high and seasonal primary productivity: Ichnology as a proxy in palaeoceanography during glacial–interglacial variations. *Terra Nova*, 28, 323–328.

Dorador, J., Rodríguez-Tovar, F.J., Mena, A. and Francés, G. (2019). Lateral variability of ichnological content in muddy contourites: Weak bottom currents affecting organisms' behavior. *Nature Sci. Rep.*, 9, 17713.

Douglas, R.G. (1981). Paleoecology of continental margin basins: a modern case history from the borderland of southern California. In Douglas, R.G., Colburn, I.P. and Gorsline, D.S. (Eds.), *Depositional Systems of Active Continental Margin Basins* (p. 121–156). SEPM Short Course Notes, Pacific Section.

Doyle, P., Poiré, D.G., Spalletti, L.A., Pirrie, D., Brenchley, P., and Matheos, S.D. (2005). Relative oxygenation of the Tithonian—Valanginian Vaca Muerta—Chachao formations of the Mendoza Shelf, Neuquén Basin, Argentina. In Veiga, G.D., Spalletti, L.A., Howell, J.A., and Schwarz, E. (Eds.), *The Neuquén Basin, Argentina: A Case Study in Sequence Stratigraphy and Basin Dynamics* (p. 185–206). Geological Society of London Special Publications, v. 252.

Ducassou, E., Mulder, T., Migeon, S., Gonthier, E., Murat, A., Revel, M., Capotondi, L., Bernasconi, S.M., Mascle, J. and Zaragosi, S. (2008). Nile floods recorded in deep Mediterranean sediments. *Quaternary Research*, v. 70, p. 382–391.

Duke, W.L., Arnott, R.W.C. and Cheel, R.J. (1991). Shelf sandstones and hummocky cross-stratification: new insights on a stormy debate. *Geology*, 19, 625–628.

Dunbar, R.B. and Berger, W.H. (1981). Fecal pellet flux to modern bottom sediment of Santa Barbara Basin (California) based on sediment trapping. *Geological Society of America Bulletin*, 92, 212–218.

Eberli, G.P. and Betzler, C. (2019). Characteristics of modern carbonate contourite drifts. *Sedimentology*, 66, 1163–1191.

Edwards, B.D. (1985). Bioturbation in a dysaerobic, bathyal basin: California Borderland. In Curran, H.A. (Ed.), *Biogenic Structures: Their Use in Interpreting Depositional Environments* (p. 309–331). SEPM Special Publication, v. 35.

Edwards, D.A., Leeder, M.R., Best, J.L., Pantin, H.M. (1994). On experimental reflected density currents and the interpretation of certain turbidites. *Sedimentology*, 41, 437–461.

Egenhoff, S.O. and Fishman, N.S. (2013). Traces in the dark—Sedimentary processes and facies gradients in the upper shale member of the Upper Devonian–Lower Mississippian Bakken Formation, Williston Basin, North Dakota, USA. *Journal of Sedimentary Research*, 83, 803–824.

Eiserhardt, K.H., Koch, L. and Eiserhardt, W.L. (2002). Revision of the ichnotaxon *Tomaculum* Groom, 1902. *Neues Jahrbuch fur Geologie und Palâontologie Abhandlungen*, 221, 325–358.

Ekdale, A.A. (1985). Trace fossils and mid-Cretaceous anoxic events in the Atlantic Ocean. In Curran, H.A. (Ed.), *Biogenic Structures: Their Use in Interpreting Depositional Environments* (p. 333–342). SEPM Special Publication, v. 35.

Ekdale, A.A. and Mason, T.R. (1988). Characteristic trace-fossil associations in oxygen-poor sedimentary environments. *Geology*, 16, 720–723.

Elmgren, R. (1975). Benthic meiofauna as indicator of oxygen conditions in the northern Baltic proper. *Merentutkimuslait. Julk./Havsforskningsinst. Skr.*, 239, 265–271.

Embry, A. F., and Johannessen, E. P. (1992). T–R sequence stratigraphy, facies analysis and reservoir distribution in the uppermost Triassic-Lower Jurassic succession, western Sverdrup Basin, Arctic Canada. In Vorren, T.O., Bergsager, E., Dahl-Stamnes, O.A., Holter, E., Johansen, B., Lie, E., and Lund, T.B. (Eds.), *Arctic Geology and Petroleum Potential* (p. 121–146). Norwegian Petroleum Society Special Publication, v. 2.

Emery, K.O. and Hülsemann, J. (1962). The relationships of sediments, life and water in a marine basin. *Deep-Sea Research*, 8, 165–180.

Eschner, T.B., Kocurek, G. (1986). Marine destruction of eolian sand seas: Origin of mass flows. *J. Sediment. Petrol.*, 56, 401–411.

Eschner, T.B. and Kocurek, G. (1988). Origins of relief along contacts between eolian sandstones and overlying marine strata. *Am. Assoc. Pet. Geol. Bull.*, 72, 932–943.

Estrada, E.J., Raverta, M.F., Coloma, M.S., Torres, J.P., and Galeazzi, S. (2020). Pilot phase of the Aguada Pichana Este block, gas window. In Minisini, D., Fantin, M., Lanusse Noguera, I. and Leanza, H.A. (Eds.), *Integrated Geology of Unconventionals: The Case of the Vaca Muerta Play, Argentina* (p. 497–514). AAPG Memoir, v. 121.

Ettensohn, F.R., (1981). *Crininicaminus haneyensis*, a new agglutinated worm tube from the Chesterian of East-Central Kentucky. *Journal of Paleontology*, 55, 479–482.

Fantín, M.A., and González, R.I. (2014). Primeros pasos en la evaluación de la Formación Vaca Muerta como reservorio no convencional en el bloque El Trapial. In *IX Congreso de Exploración y Desarrollo de Hidrocarburos, Simposio de Recursos No Convencionales* (p. 631–652). Mendoza, Argentina.

Faugères, J.-C., Gonthier, E. and Stow, D.A.V. (1984). Contourite drift molded by deep Mediterranean outflow. *Geology*, 12, 296–300.

Fenchel, T. (1998). Formation of laminated cyanobacterial mats in the absence of benthic fauna. *Aquatic Microbial Ecology*, 14, 235–240.

Fernández, D.E., Comerio, M. and Pazos, P.J. (2018). *Nereites* in Lower Cretaceous marginal-marine facies from Patagonia: Ichnotaxonomic and ethological implications. *Cretaceous Research*, 81, 51–63.

Finger, K.L., Flenniken, M.M. and Lipps, J.H. (2008). Foraminifera used in the construction of Miocene polychaete worm tubes, Monterey Formation, California, USA. *The Journal of Foraminiferal Research*, 38, 277–291.

Fiske, R.S. and Matsuda, T. (1964). Submarine equivalents of ash flows in the Tokiwa Formation, Japan. *American Journal of Science*, 262, 76–106.

Flach, E.C. (2003). Factors controlling soft bottom macrofauna along and across European continental margins. In Wefer, G., Billett, D., Hebbeln, D., Jorgensen, B.B., Schlüter, M. and Van Weering, T. (Eds.), *Ocean Margin Systems* (p. 351–363). Springer-Verlag, Berlin.

Flach, E.C. and Thomsen, L. (1998). Do physical and chemical factors structure the 341xploración341 community at a continental slope in the NE Atlantic?. In Baden, S., Pihl, L., Rosenberg, R., Strömberg, J.-O., Svane, I. and Tiselius, P. (Eds.), *Recruitment, Colonization and Physical-Chemical Forcing in Marine Biological Systems* (p. 265–285). Developments in Hydrobiology, Springer, v. 132.

Flach, E., Lavaleye, M., De Stigter, H. and Thomsen, L. (1998). Feeding types of the benthic community and particle transport across the slope of the N.W. European Continental Margin (Goban Spur). *Progress in Oceanography*, 42, 209–231.

Flemming, B.W. (1980). Sand transport and bedform patterns on the continental shelf between Durban and Port Elizabeth (southeast African continental margin). *Sedimentary Geology*, 26, 179–205.

Flemming, B.W. (1981). Factors controlling shelf sediment dispersal along the Southeast African Continental Margin. *Marine Geology*, 42, 259–277.

Föllmi, K.B. and Grimm, K.A. (1990). Doomed pioneers: Gravity-flow deposition and bioturbation in marine oxygen-deficient environments. *Geology*, 18, 1069–1072.

Fonseca, T.R. (1989). An overview of the poleward undercurrent and upwelling along the Chilean coast. In Neshyba, S.J., Mooers, Ch.N.K., Smith, R.L. and Barber, R.T. (Eds.), *Poleward*

Flows along Eastern Ocean Boundaries (p. 203–228). Coastal and Estuarine Studies, v. 34.

Forbes, T.L. and Lopez, G.R. (1990). The effect of food concentration, body size, and environmental oxygen tension on the growth of the deposit-feeding polycheate, *Capitella* species 1. *Limnology and Oceanography*, 35, 1535–1544.

Fossing, H., Gallardo, V.A., Jorgensen, B.B., Hüttel, M., Nielsen, L.P., Schulz, H., Canfield, D.E., Forster, S., Glud, R.N., Gundersen, J.K., Küver, J., Ramsing, N.B., Teske, A., Thamdrup, B. and Ulloa, A. (1995). Concentration and transport of nitrate by the mat-forming sulphur bacterium *Thioploca*. *Letters to Nature*, 374, 713–715.

Frébourg, G., Ruppel, S.C. and Rowe, H. (2013). Sedimentology of the Haynesville (Upper Kimmeridgian) and Bossier (Tithonian) Formations, in the Western Haynesville Basin, Texas, U.S.A. In Hammes, U. and Gale, J. (Eds.), *Geology of the Haynesville Gas Shale in East Texas and West Louisiana* (p. 47–67). AAPG Memoir, v. 105.

Freije, H., Azúa, G., González, R., Ponce, J.J., Zavala, C.A. (2002). Actividad tectónica sinsedimentaria en el Jurásico del sur de la Cuenca Neuquina. In *V Congreso de Exploración y Desarrollo de Hidrocarburos* (p. 17). Mar del Plata, Argentina.

Frey, R.W. and Bromley, R.G. (1985). Ichnology of American chalks: the Selma Group (Upper Cretaceous), western Alabama. *Canadian Journal of Earth Sciences*, 22, 801–828.

Friis, H. (1995). The role of fecal pellets in deposition of marine muddy sediments–examples for Danish Tertiary. *Bulletin of the Geological Society of Denmark*, 42, 68–73.

Frogner, P., Gíslason, S.R. and Óskarsson, N. (2001). Fertilizing potential of volcanic ash in ocean surface water. *Geology*, 29, 487–490.

Fryberger, S.G. (1984). The Permian Upper Minnelusa Formation, Wyoming: ancient example of an offshore-prograding eolian sand sea with geomorphic facies, and system-boundary traps for petroleum. In *Wyoming Geological Association 35th Annual Field Conference Guidebook* (p. 241–271).

Fryberger, S.G. (1986). Stratigraphic traps for petroleum in wind-laid rocks. *Am. Assoc. Pet. Geol. Bull.*, 70, 1765–1798.

Fryberger, S.G., Schenk, C.J. and Krystinik, L.F. (1988). Stokes surfaces and the effects of near-surface ground-water-table on eolian deposition. *Sedimentology*, 35, 21–41.

Fryberger, S.G., Krystinik, L.F. and Schenk, C.J. (1990). Tidally flooded back-barrier dunefield, Guerrero Negro area, Baja California, Mexico. *Sedimentology*, 37, 23–43.

Fu, S. (1991). *Funktion, Verhalten und Einteilung fucoider und lophocteniider Lebensspuren*. Courier Forschungsinstitut Senckenberg, v. 135, 64 p.

Fu, S. and Werner, F. (1994). Distribution and composition of biogenic structures on the Iceland-Faeroe Ridge: relation to different environments. *Palaios*, 9, 92–101.

Fürsich, F.T. (1974). On *Diplocraterion* Torell 1870 and the significance of morphological features in vertical, spreiten-bearing, U-shaped trace fossils. *Journal of Paleontology*, 48, 952–962.

Gabbott, S.E., Zalasiewicz, J., Aldridge, R.J., Theron, J.N. (2010). Eolian input into the Late Ordovician postglacial Soom Shale, South Africa. *Geology*, 38, 1103–1106.

Gaillard, C., Bernier, P., Gall, J.C., Gruet, Y. and Barale, G. (1994). Ichnofabric from the Upper Jurassic lithographic limestone of Cerin, southeast France. *Palaeontology*, 37, 285–304.

Gallardo, V.A., Palma, M., Carrasco, F.D., Gutiérrez, D., Levin, L.A. and Cañete, J.I. (2004). Macrobenthic zonation caused by the oxygen minimum zone on the shelf and slope off central Chile. *Deep Sea Research Part II*, 51, 2475–2490.

Garcia-Castellanos, D., Estrada, F., Jiménez-Munt, I., Gorini, C., Fernàndez, M., Vergés, J. and De Vicente, R. (2009). Catastrophic flood of the Mediterranean after the Messinian salinity crisis. *Nature*, 462, 778–781.

García-Ramos, J.C., Mángano, M.G., Piñuela, L., Buatois, L.A. and Rodríguez-Tovar, F.J. (2014). The ichnogenus *Tubotomaculum*: an enigmatic pellet-filled structure from Upper Cretaceous to Miocene deep-marine deposits of southern Spain. *Journal of Paleontology*, 88, 1189–1198.

Gasparini, Z. and Fernández, M. (2005). Jurassic marine reptiles of the Neuquén Basin: records, faunas and their palaeobiogeographic significance. In Veiga, G.D., Spalletti, L.A., Howell, J.A. and Schwarz, E. (Eds.), *The Neuquén Basin, Argentina: A Case Study in Sequence*

Stratigraphy and Basin Dynamics (p. 279–294). Geological Society, London, Special Publications, v. 252.

Gasparini, Z., Spalletti, L. and De la Fuente, M. (1997). Tithonian marine reptiles of the Western Neuquén Basin, Argentina. Facies and palaeoenvironments. *Geobios*, 30, 701–712.

Ghadeer, S.G., and Macquaker, J.H. (2011). Sediment transport processes in an ancient mud-dominated succession: a comparison of processes operating in marine offshore settings and anoxic basinal environments. *Journal of the Geological Society*, 168, 1121–1132.

Ghinassi, M. (2007). The effects of differential subsidence and coastal topography on high-order transgressive-regressive cycles: Pliocene nearshore deposits of the Val d'Orcia Basin, Northern Apennines, Italy. *Sediment. Geol.*, 202, 677–701.

Gilbert, G.K. (1885). The topographic features of lake shores. *U.S. Geol. Surv. Annu. Rep.*, 5, 104–108.

Gilbert, M.M., Buatois, L.A. and Renaut, R.W. (2019). Ichnology and depositional environments of the Upper Cretaceous Dinosaur Park–Bearpaw formation transition in the Cypress Hills region of Southwestern Saskatchewan, Canada. *Cretaceous Research*, 98, 189–210.

Gingras, M.K. and Bann, K.L. (2006). The bend justifies the leans: interpreting recumbent ichnofabrics. *Journal of Sedimentary Research*, 76, 483–492.

Glennie, K.W. and Buller, A.T. (1983). The Permian Weissliegend of NW Europe: The partial deformation of aeolian dune sands caused by the Zechstein transgression. *Sediment. Geol.*, 35, 43–81.

Gómez Rivarola, L., and Borgnia, M. (2018). Chapter 13: San Roque. In González, G., Vallejo, M.D., Kietzmann, D.A., Marchal, D., Desjardins, P.R., González Tomassini, F., Gómez Rivarola, L., Domínguez, R.F. and Fantín, M.A. (Eds.), *Regional Cross Section of the Vaca Muerta Formation, Integration of Seismic, Well Logs, Cores and Outcrops* (p. 143–153). Special Publication of IAPG, Buenos Aires.

Gómez-Dacal, A.R. (2017). *Petrología, geoquímica y diagénesis de sedimentitas y fósiles carbonáticos del Jurásico Superior-Cretácico Inferior de las cuencas Neuquina y Austral, Argentina.* Universidad Nacional de La Plata, PhD Thesis, 269 p.

Gómez-Dacal, A.R., Gómez Peral, L.E., Spalletti, L.A., Sial, A.N., Siccardi, A. and Poiré, D.G., (2018). First record of the Valanginian positive carbon isotope anomaly in the Mendoza shelf, Neuquén Basin, Argentina: palaeoclimatic implications. *Andean Geology*, 45, 111–129.

Gonthier, E.G., Faugeres, J.-C. and Stow, D.A.V. (1984). Contourite facies of the Faro Drift, Gulf of Cadiz. In Stow, D.A.V. and Piper, D.J.W. (Eds.), *Fine-grained sediments: Deep-water processes and facies* (p. 275–292). Geological Society of London Special Publications, v. 15.

González, G., Vallejo, M.D., Kietzmann, D.A., Marchal, D., Desjardins, P.R., González Tomassini, F., Gómez Rivarola, L., Domínguez, R.F. and Fantín, M.A. (2018). *Regional Cross Section of the Vaca Muerta Formation. Integration of Seismic, Well Logs, Cores and Outcrops.* Special Publication of IAPG, Buenos Aires, p. 252.

González Tomassini, F., Kietzmann, D.A., Fantín, M.A., Crousse, L.C. and Reijenstein, H.M. (2014). Estratigrafía y análisis de facies de la Formación Vaca Muerta en el área de El Trapial, Cuenca Neuquina, Argentina. In *IX Congreso de Exploracion y Desarrollo de Hidrocarburos, Simposio de Recursos No Convencionales* (p. 587–611). IAPG, Mendoza, Argentina.

González Tomassini, F., Fantín, M., Desjardins, P., Vallejo, M.D., Kietzmann, D., Marchal, D., Leanza, H., González, G., Sattler, F., Gómez Rivarola, L., Domínguez, R.F., Reijenstein, H., Kohler, G., Santiago, M., Jait, D., Minisini, D., Aguirre-Urreta, B., Bande, A., Simo, T., Vittore, F., Crousse, L., Rodriguez Schelotto, M.L., Aguirre, H., Feinstein, E., Liberman, A., Cuervo, S., Depine, G., Sylwan, C., Guerberoff, D., De la Cal, H., Alonso, S., Suriano, J., Ambrosio, A., Lanusse Noguera, I. (2016). 'Co-opetition': a game-changing synergy among operators. A case delivering a Rosetta Stone for the Vaca Muerta Stratigraphy (Argentina). In *Unconventional Resources Technology Conference (URTeC)* (n. 2461073, doi 10.15530). San Antonio, USA.

Gorsline, D.S. (1984). A review of fine-grained sediment origins, characteristics, transport and deposition. In Stow, D.A.V. and Piper, D.J.W. (Eds.), *Fine-grained Sediments: Deep-Water Processes and Facies* (p. 17–34). Geological Society, London, Special Publications, v. 15.

Gründel, J. and Parent, H. (2001). Lower and Middle Tithonian marine gastropods from the Neuquén-Mendoza Basin, Argentina. *Bol. del Inst. Fisiogr. y Geol.*, 71, 13–18.

Gründel, J. and Parent, H. (2006). Marine Jurassic gastropods of Argentina. III. Lower and Middle Tithonian of Picún Leufú and Cerro Lotena. *N. Jb. Geol. Paläont. Mh.*, 2006, 503–512.

Gulisano, C. (1981). El ciclo Cuyano en el norte de Neuquén y sur de Mendoza. In. *8º Congreso Geológico Argentino, Actas 3* (p. 579–592). San Luis, Argentina.

Gulisano, C.A., Gutiérrez Pleimling, A.R. and Digregorio, R.E. (1984). Análisis estratigráfico del intervalo Tithoniano-Valanginiano (Formaciones Vaca Muerta, Quintuco y Mulichinco) en el suroeste de la provincia de Neuquén. In *IX Congreso Geológico Argentino, Actas I* (p. 221–235). Asociación Geológica Argentina, Bariloche.

Hale, R.P. and Ogston, A.S. (2015). In situ observations of wave-supported fluid-mud generation and deposition on an active continental margin. *Journal of Geophysical Research: Earth Surface*, 120, 2357–2373.

Hammes, U. and Frébourg, G. (2012). Haynesville and Bossier mudrocks: A facies and sequence stratigraphic investigation, East Texas and Louisiana, USA. *Marine and Petroleum Geology*, 31, 8–26.

Hanebuth, T., Stattegger, K. and Grootes, P.M. (2000). Rapid flooding of the Sunda Shelf: A Late-Glacial sea-level record. *Science*, 288, 1033–1035.

Hanebuth, T.J.J., Stattegger, K. and Bojanowski, A. (2009). Termination of the Last Glacial Maximum sea-level lowstand: The Sunda-Shelf data revisited. *Glob. Planet. Change*, 66, 76–84.

Hanebuth, T.J.J., Mersmeyer, H., Kudrass, H.R. and Westphal, H. (2013). Aeolian to shallow-marine shelf architecture off a major desert since the Late Pleistocene (northern Mauritania). *Geomorphology*, 203, 132–147.

HANKEN, N.M., BROMLEY, R.G. and THOMSEN, E. (2001). Trace fossils of the bivalve *Panopea faujasi*, Pliocene, Rhodes, Greece. *Ichnos*, 8, 117–130.

Haq, B.U. (2018). Jurassic Sea-Level Variations: A Reappraisal. *GSA Today*, 28, 4–10.

Harazim, D., Callow, R.H. and Mcilroy, D. (2013). Microbial mats implicated in the generation of intrastratal shrinkage ('synaeresis') cracks. *Sedimentology*, 60, 1621–1638.

Harris, P.T. and Macmillan-Lawler, M. (2016). Seafloor mapping along continental shelves. In C.W. Finkl and C. Makowski (Eds.), *Seafloor Mapping along Continental Shelves: Research and Techniques for Visualizing Benthic Environments* (p. 69–104). Springer International Publishing, Cham, v. 13.

Hasegawa, H., Tada, R., Jiang, X., Suganuma, Y., Imsamut, S., Charusiri, P., Ichinnorov, N. and Khand, Y. (2012). Drastic shrinking of the Hadley circulation during the mid-Cretaceous Supergreenhouse. *Climate of the Past*, 8, 1323–1337.

Hattin, D.E. (1975). Petrology and origin of fecal pellets in Upper Cretaceous strata of Kansas and Saskatchewan. *Journal of Sedimentary Research*, 45, 686–696.

Havholm, K.G. and Kocurek, G. (1994). Factors controlling aeolian sequence stratigraphy: clues from super bounding surface features in the Middle Jurassic Page Sandstone. *Sedimentology*, 41, 913–934.

Hay, W.W. (1995). Paleoceanography of marine organic-carbon-rich sediments. In Huc, A.-Y. (Ed.), *Paleogeography, Paleoclimate, and Source Rocks* (p. 21–59). AAPG Studies in Geology, v. 40.

Hebbeln, D., Van Rooij, D. and Wienberg, C. (2016). Good neighbours shaped by vigorous currents: Cold-water coral mounds and contourites in the North Atlantic. *Marine Geology*, 378, 171–185.

Hedges, J.I., Keil, R.G. (1995). Sedimentary organic matter preservation: an assessment and speculative synthesis. *Mar. Chem.*, 49, 81–115.

Heezen, B.C. and Hollister, C. (1964). Deep-sea current evidence from abyssal sediments. *Marine Geology*, 1, 141–174.

Heezen, B.C., Hollister, C.D. and Ruddiman, W.F. (1966). Shaping of the continental rise by deep geostrophic contour currents. *Science*, 152, 502–508.

Helland-Hansen, W., Hampson, G.J. (2009). Trajectory analysis: Concepts and applications. *Basin Res.*, 21, 454–483.

Hess, H., and Etter, W. (2011). Life and death of *Saccocoma tenella* (Goldfuss). *Swiss Geological Society*, doi: 10.1007/s00015-011-0059-z

Hesselbo, S.P., Deconinck, J.F., Huggett, J.M. and Morgans-Bell, H.S. (2009). Late Jurassic palaeoclimatic change from clay mineralogy and gamma-ray spectrometry of the Kimmeridge Clay, Dorset, UK. *Journal of the Geological Society*, 166, 1123–1133.

Higgs, R. (2004). Ross and Bude Formations (Carboniferous, Ireland and England): Reinterpreted as lake-shelf turbidites. *J. Pet. Geol.*, 27, 47–66.

Hill, P.R. (1984). Facies and sequence analysis of Nova Scotian Slope muds: turbidite vs "hemipelagic" deposition. In Stow, D.A.V., and Piper, D.J.W. (Eds.), *Fine-Grained Sediments: Deep-Water Processes and Facies* (p. 311–318). Geological Society of London Special Publications, v. 15.

Hill, P.S., Fox, J.M., Crockett, J.S., Curran, K.J., Friedrichs, C.T., Geyer, W.R., Milligan, T.G., Ogston, A.S., Puig, P., Scully, M.E., Traykovski, P.A. (2007). Sediment delivery to the seabed on continental margins. In Nittrouer, C.A., Austin, J.A., Field, M.E., Kravitz, J.H., Syvitski, J.P.M and Wiberg, P.L. (Eds.), *Continental Margin Sedimentation: From Sediment Transport to Sequence Stratigraphy* (p. 49–99). International Association of Sedimentologists, Special Publications, v. 37.

Hine, A.C. (1977). Lily Bank, Bahamas: History of an active oolite sand shoal. *J. Sediment. Res.*, 47, 1554–1581.

Hollister, C.D. (1993). The concept of deep-sea contourites. *Sedimentary Geology*, 82, 5–11.

Hollister, C.D. and Heezen, B.C. (1972). Geologic effects of ocean bottom currents: Western North Atlantic. In Gordon, A.L. (Ed.), *Studies in Physical Oceanography* (p. 37–66). Gordon and Breach, New York.

Hollister, C.D. and McCave, I.N. (1984). Sedimentation under deep-sea storms. *Nature*, 309, 220–225.

Honjo, S. and Roman, M.R. (1978). Marine copepod fecal pellets: production, preservation and sedimentation. *Journal of Marine Research*, 36, 45–57.

Hovikoski, J., Uchman, A., Weibel, R., Nohr-Hansen, H., Sheldon, E., Ineson, J., Bjerager, M., Therkelsen, J., Olivarius, M., Larsen, M., Alsen, P. and Bojesen-Koefoed, J. (2020). Upper Cretaceous bottom current deposits, north-east Greenland. *Sedimentology*, 67, 3619–3654.

Howell, J.A., Schwarz, E., Spalletti, L.A. and Veiga, G.D. (2005). The Neuquén Basin: an overview. In Veiga, G.D., Spalletti, L.A., Howell, J.A. and Schwarz, E. (Eds.), *The Neuquén Basin, Argentina: A Case Study in Sequence Stratigraphy and Basin Dynamics* (p. 1–14). Geological Society of London Special Publications, London, v. 252.

Hübscher, C., Dullo, C., Flögel, S., Titschack, J. and Schönfeld, J. (2010). Contourite drift evolution and related coral growth in the eastern Gulf of Mexico and its gateways. *International Journal of Earth Sciences*, 99, 191–206.

Huc, A.Y. (1988). Aspects of depositional processes of organic matter in sedimentary basins. *Organic Geochemistry*, 13, 263–272.

Hummel, G. and Kocurek, G. (1984). Interdune areas of the back-island dune field, north Padre Island, Texas. *Sediment. Geol.*, 39, 1–26.

Hüneke, H. and Stow, D.A.V. (2008). Identification of ancient contourites: problems and palaeoceanographic significance. In Rebesco, M. and Camerlenghi, A. (Eds.), *Contourites* (p. 323–344). Developments in Sedimentology, Elsevier, v. 60.

Hunt, D. and Tucker, M.E. (1992). Stranded parasequences and the forced regressive wedge systems tract: deposition during base-level fall. *Sedimentary Geology*, 81, 1–9.

Huntoon, J.E. and Chan, M.A. (1987). Marine origin of paleotopographic relief on eolian White Rim Sandstone (Permian), Elaterite Basin, Utah. *Am. Assoc. Pet. Geol. Bull.*, 71, 1035–1045.

Immenhauser, A. (2005). High-rate sea-level change during the Mesozoic: New approaches to an old problem. *Sediment. Geol.*, 175, 277–296.

Inman, D.L., Ewing, G.C. and Corliss, J.B. (1966). Coastal sand dunes of Guerrero Negro, Baja California, Mexico. *Geological Society of America Bulletin*, 77, 787–802.

Ito, M. (2002). Kuroshio Current-influenced sandy contourites from the Plio-Pleistocene Kazusa forearc basin, Boso Peninsula, Japan. In Stow, D.A.V., Pudsey, C.J., Howe, J.A., Faugères,

J.-C. and Viana, A.R. (Eds.), *Deep-Water Contourite Systems: Modern Drifts and Ancient Series, Seismic and Sedimentary Characteristics* (p. 421–432). Geological Society of London Memoirs, London, v. 22.

Izumi, K. (2012). Formation process of the trace fossil Phymatoderma granulata in the Lower Jurassic black shale (Posidonia Shale, southern Germany) and its paleoecological implications. *Palaeogeography, Palaeoclimatology, Palaeoecology*, 353, 116–122.

Izumi, K. (2014). Utility of geochemical analysis of trace fossils: Case studies using Phycosiphon incertum from the Lower Jurassic shallow-marine (Higashinagano Formation, southwest Japan) and Pliocene deep-marine deposits (Shiramazu Formation, central Japan). *Ichnos*, 21, 62–72.

Jach, R. (2005). Storm-dominated deposition of the Lower Jurassic crinoidal limestones in the Krížna unit, Western Tatra Mountains, Poland. *Facies*, 50, 561–572.

Jennings, J.N. (1975). Desert dunes and estuarine fill in the Fitzroy estuary (North-Western Australia). *Catena*, 2, 215–262.

Jervey, M.T. (1988). Quantitative geological modeling of siliciclastic rock sequences and their seismic expression. In Wilgus, C.K., Hastings, B.S., Posamentier, H., Van Wagoner, J., Ross, C.A., and Kendall, C.G. (Eds.), *Sea-Level Changes—An Integrated Approach* (p. 47–69). SEPM Special Publication, v. 42.

Joeckel, R.M. and Korus, J.T. (2012). Bayhead delta interpretation of an upper Pennsylvanian sheetlike sandbody the broader understanding of transgressive deposits in cyclothems. *Sediment. Geol.*, 274–275, 22–37.

Johnson, K.S., Paull, C.K., Barry, J.P. and Chavez, F.P. (2001). A decadal record of underflows from a coastal river into the deep sea. *Geology*, 29, 1019–1022.

Jordan, O.D. and Mountney, N.P. (2010). Styles of interaction between aeolian, fluvial and shallow marine environments in the Pennsylvanian to Permian lower Cutler beds, south-east Utah, USA. *Sedimentology*, 57, 1357–1385.

Jordan, O.D. and Mountney, N.P. (2012). Sequence stratigraphic evolution and cyclicity of an ancient coastal desert system: The Pennsylvanian-Permian Lower Cutler Beds, Paradox Basin, Utah, U.S.A. *J. Sediment. Res.*, 82, 755–780.

Josefson, A.B. and Widbom, B. (1988). Differential response of benthic macrofauna and meiofauna to hypoxia in the Gullmar Fjord basin. *Marine Biology*, 100, 31–40.

Katto, J. (1976). Additional problematica from southwest Japan. *Res. Rep., Kochi Univ.*, 25, 17–24.

Katz, B.J. (2005). Controlling factors on soure rock development - a review of productivity, preservation, and sedimentation rate. In Harris, N.B. (Ed.), *The Deposition of Organic-Carbon-Rich Sediments: Models, Mechanisms, and Consequences* (p. 7–16). SEPM Special Publication, v. 82.

Kendall, C.G.S.C. and Schlager, W. (1981). Carbonates and relative changes in sea level. *Mar. Geol.*, 44, 181–212.

Khan, M.Z., Feng, Q., Zhang, K. and Guo, W. (2019). Biogenic silica and organic carbon fluxes provide evidence of enhanced marine productivity in the Upper Ordovician-Lower Silurian of South China. *Palaeogeography, Palaeoclimatology, Palaeoecology*, 534, 109278.

Kidwell, S.M. and Aigner, T. (1985). Sedimentary dynamics of complex shell beds: implications for ecologic and evolutionary patterns. In Bayer, U., and Seilacher, A. (Eds.), *Sedimentary and Evolutionary Cycles* (p. 382–395). Lecture Notes in Earth Sciences, v. 1.

Kietzmann, D.A. and Palma, R.M. (2009a). Microcrinoideos saccocómidos en el Tithoniano de la Cuenca Neuquina. ¿Una presencia inesperada fuera de la región del Tethys?. *Ameghiniana*, 46, 695–700.

Kietzmann, D.A., and Palma, R.M. (2009b). Tafofacies y biofacies de Formación Vaca Muerta en el sector surmendocino de la Cuenca Neuquina: implicancias paleoecológicas, sedimentológicas y estratigráficas. *Ameghiniana*, 46, 321–343.

Kietzmann, D.A. and Palma, R.M. (2010a). New crustacean microcoprolites from the Lower Cretaceous (middle Berriasian–lower Valanginian) of the Neuquén Basin, southern Mendoza, Argentina. *Journal of South American Earth Sciences*, 30, 58–64.

Kietzmann, D.A. and Palma, R.M. (2010b). Primer registro de microcoprolitos de crustáceos de la Cuenca Neuquina: el icnogénero *Palaxius* en el Tithoniano de la Formación Vaca Muerta, Mendoza. *Ameghiniana*, 47, 257–261.

Kietzman, D.A. and Palma, R.M. (2011). Las tempestitas peloidales de la Formación Vaca Muerta (Tithoniano-Valanginiano) en el sector surmendocino de la Cuenca Neuquina, Argentina. *Latin American Journal of Sedimentology and Basin Analysis*, 18, 121–149.

Kietzmann, D.A., and Rodríguez Schelotto, M.L. (2018). Chapter 3: Lithologic classifications. In González, G., Vallejo, M.D., Kietzmann, D.A., Marchal, D., Desjardins, P.R., González Tomassini, F., Gómez Rivarola, L., Domínguez, R.F. and Fantín, M.A. (Eds.), *Regional Cross Section of the Vaca Muerta Formation, Integration of Seismic, Well Logs, Cores and Outcrops* (p. 23–31). Special Publication of IAPG, Buenos Aires.

Kietzmann, D.A. and Bressan, G.S. (2019). The coprolite *Lumbricaria* Münster in the Early Tithonian of the Neuquén Basin, Argentina: new evidence for a holothurian producer. *PalZ*, 2, 357–369.

Kietzmann, D.A., Palma, R.M. and Bressan, G.S. (2008). Facies y microfacies de la rampa tithoniana-berriasiana de la Cuenca Neuquina (Formación Vaca Muerta) en la sección del Arroyo Loncoche-Malargüe, provincia de Mendoza. *Revista de la Asociación Geológica Argentina*, 63, 696–713.

Kietzmann, D.A., Blau, J., Fernandez, D.E. and Palma, R.M. (2010). Crustacean microcoprolites from the Upper Jurassic—Lower Cretaceous of the Neuquén Basin, Argentina: systematics and biostratigraphic implications. *Acta Palaeontologica Polonica*, 55, 277–284.

Kietzmann, D.A., Palma, R.M., Riccardi, A.C., Martín-Chivelet, J. and López-Gómez, J. (2014a). Sedimentology and sequence stratigraphy of a Tithonian–Valanginian carbonate ramp (Vaca Muerta Formation): A misunderstood exceptional source rock in the Southern Mendoza area of the Neuquén Basin, Argentina, Mendoza. *Sedimentary Geology*, 302, 64–86.

Kietzmann, D.A., Ambrosio, A.L., Suriano, J., Alonso, S., Vennari, V.V., Aguirre-Urreta, M.B., Depine, G. and Repol. D. (2014b). Variaciones de facies de las secuencias basales de la Formación Vaca Muerta en su localidad tipo (Sierra de la Vaca Muerta), Cuenca Neuquina. *In IX Congreso de Exploración y Desarrollo de Hidrocarburos* (p. 299–317). IAPG, Mendoza.

Kietzmann, D.A., Palma, R.M., and Iglesia Llanos, M.P. (2015). Cyclostratigraphy of an orbitally-driven Tithonian–Valanginian carbonate ramp succession, Southern Mendoza, Argentina: implications for the Jurassic–Cretaceous boundary in the Neuquén Basin. *Sedimentary Geology*, 315, 29–46.

Kietzmann, D.A., Ambrosio, A.L., Suriano, J., Alonso, M.S., González Tomassini, F., Depine, G. and Repol, D. (2016). The Vaca Muerta–Quintuco system (Tithonian–Valanginian) in the Neuquén Basin, Argentina: A view from the outcrops in the Chos Malal fold and thrust belt. *AAPG Bulletin*, 100, 743–771.

Kietzmann, D.A., Iglesia Llanos, M.P., Ivanova, D.K., Kohan Martínez, M. and Sturlesi, M.A. (2018a). Toward a multidisciplinary chronostratigraphic calibration of the Jurassic-Cretaceous transition in the Neuquén Basin. *Revista de la Asociación Geológica Argentina*, 75, 175–187.

Kietzmann, D.A., Ambrosio, A.L., Alonso, M.S., and Suriano, J. (2018b). Chapter 20: Puerta Curaco. In González, G., Vallejo, M.D., Kietzmann, D.A., Marchal, D., Desjardins, P.R., González Tomassini, F., Gómez Rivarola, L., Domínguez, R.F. and Fantín, M.A. (Eds.), *Regional Cross Section of the Vaca Muerta Formation, Integration of Seismic, Well Logs, Cores and Outcrops* (p. 219–232). Special Publication of IAPG, Buenos Aires.

Kietzmann, D.A., González Tomassini, F., and Smith, T. (2020a). Grain association, petrography, and lithofacies. In Minisini, D., Fantín, M., Lanusse Noguera, I. and Leanza, H.A. (eds.), *Integrated Geology of Unconventionals: The Case of the Vaca Muerta Play, Argentina* (p. 267–296). AAPG Memoir, v. 121.

Kietzmann, D.A., Iglesia Llanos, M.P. and Kohan Martínez, M. (2020b). Orbital controls and high-resolution cyclostratigraphy of Late Jurassic–Early Cretaceous in the Neuquén Basin. In Kietzmann, D.A. and Folguera, A. (Eds.), *Opening and Closure of the Neuquén Basin in the Southern Andes* (p. 211–235). Springer.

Knapp, L.J., McMillan, J.M. and Harris, N.B. (2017). A depositional model for organic-rich Duvernay Formation mudstones. *Sedimentary Geology*, 347, 160–182.

Knaust, D. (2008). *Balanoglossites* Mägdefrau, 1932 from the Middle Triassic of Germany: part of a complex trace fossil probably produced by burrowing and boring polychaetes. *Paläontologische Zeitschrift*, 82, 347–372.

Knaust, D. (2009). Complex behavioural pattern as an aid to identify the producer of *Zoophycos* from the Middle Permian of Oman. *Lethaia*, 42, 146–154.

Knaust, D. (2018). The ichnogenus *Teichichnus* Seilacher, 1955. *Earth-Science Rev.*, 177, 386–403.

Knaust, D. (2020). Invertebrate coprolites and cololites revised. *Papers in Palaeontology*, 6, 385–423.

Kneller, B. (1995). Beyond the turbidite paradigm: physical models for deposition of turbidites and their implications for reservoir prediction. *Geol. Soc. London, Spec. Publ.*, 94, 31–49.

Kneller, B.C., Bennett, S.J., McCaffrey, W.D. (1997). Velocity and turbulence structure of density currents and internal solitary waves: potential sediment transport and the formation of wave ripples in deep water. *Sediment. Geol.*, 112, 235–250.

Kocurek, G. (1981). Significance of interdune deposits and bounding surfaces in aeolian dune sands. *Sedimentology*, 28, 753–780.

Kocurek, G. and Nielson, J. (1986). Conditions favourable for the formation of warm-climate aeolian sand sheets. *Sedimentology*, 33, 795–816.

Kocurek, G., Robinson, N.I. and Sharp, J.M. (2001). The response of the water table in coastal aeolian systems to changes in sea level. *Sediment. Geol.*, 139, 1–13.

Kocurek, G., Martindale, R.C., Day, M., Goudge, T.A., Kerans, C., Hassenruck-Gudipati, H.J., Mason, J., Cardenas, B.T., Petersen, E.I., Mohrig, D., Aylward, D.S., Hughes, C.M. and Nazworth, C.M. (2019). Antecedent aeolian dune topographic control on carbonate and evaporite facies: Middle Jurassic Todilto Member, Wanakah Formation, Ghost Ranch, New Mexico, USA. *Sedimentology*, 66, 808–837.

Kohan Martínez, M., Kietzmann, D.A., Llanos, M.I., Leanza, H.A. and Luppo, T. (2018). Magnetostratigraphy and cyclostratigraphy of the Tithonian interval from the Vaca Muerta

Formation, southern Neuquén Basin, Argentina. *Journal of South American Earth Sciences*, 85, 209–228.

Könitzer, S.F., Davies, S.J., Stephenson, M.H., Leng, M.J. (2014). Depositional controls on mudstone lithofacies in a basinal setting: Implications for the delivery of sedimentary organic matter. *J. Sediment. Res.*, 84, 198–214.

Kotake, N. (1992). Deep-sea echiurans: possible producers of *Zoophycos*. *Lethaia*, 25, 311–316.

Kraeuter, J. and Haven, D.S. (1970). Fecal pellets of common invertebrates of lower York River and lower Chesapeake Bay, Virginia. *Chesapeake Science*, 11, 159–173.

Kranck, K. (1981). Particulate matter grain-size characteristics and flocculation in a partially mixed estuary. *Sedimentology*, 28, 107–114.

Krim, N. (2015). *Architecture Stratigraphique, Dynamique Sédimentaire et Distribution de la Matière Organique de la Formation de la Vaca Muerta (Bassin de Neuquén, Argentine)*. Ph.D. tesis, Université de Pau et des Pays de l'Adour, p. 428.

Krim, N., Bonnel, C., Tribovillard, N., Imbert, P., Aubourg, C., Riboulleau, A., Bout-Roumazeilles, V., Hoareau, G. and Fasentieux, B. (2017). Paleoenvironmental evolution of the southern Neuquén basin (Argentina) during the Tithonian-Berriasian (Vaca Muerta and Picún Leufú Formations): a multi-proxy approach. *Bulletin de la Société Géologique de France*, 188, art. 34.

Krim, N., Tribovillard, N., Riboulleau, A., Bout-Roumazeilles, V., Bonnel, C., Imbert, P., Aubourg, C., Hoareau, G. and Fasentieux, B. (2019). Reconstruction of palaeoenvironmental conditions of the Vaca Muerta formation in the southern part of the Neuquén Basin (Tithonian-Valanginian): evidences of initial short-lived development of anoxia. *Marine and Petroleum Geology*, 103, 176–201.

Kuenen, P. (1960). Experimental abrasion 4: Eolian action. *J. Geol.*, 68, 427–449.

Kuenen, P.H. (1966). Experimental turbidite lamination in a circular flume. *The Journal of Geology*, 74, 523–545.

Kulkarni, K.G. and Panchang, R. (2015). New insights into polychaete traces and fecal pellets: another complex ichnotaxon?. *PloS one*, 10, p.e0139933.

Lamb, M.P. and Mohrig, D. (2009). Do hyperpycnal-flow deposits record river-flood dynamics?. *Geology*, 37, 1067–1070.

Lamb, M.P., Myrow, P.M., Lukens, C., Houck, K., Strauss, J. (2008). Deposits from wave-influenced turbidity currents: Pennsylvanian Minturn Formation, Colorado, U.S.A. *J. Sediment. Res.*, 78, 480–498.

Lampitt, R.S., Salter, I. and Johns, D. (2009). Radiolaria: Major exporters of organic carbon to the deep ocean. *Global Biogeochemical Cycles*, 23, GB1010.

Lash, G.G. (2016). Hyperpycnal transport of carbonaceous sediment–example from the Upper Devonian Rhinestreet Shale, western New York, USA. *Palaeogeography, Palaeoclimatology, Palaeoecology*, 459, 29–43.

Lavaleye, M.S.S., Duineveld, G.C.A., Berghuis, E.M., Kok, A. and Witbaard, R. (2002). A comparison between the megafauna communities on the N.W. Iberian and Celtic continental margins – Effects of coastal upwelling?. *Progress in Oceanography*, 52, 459–476.

Lazar, O.R., Bohacs, K.M., Schieber, J., Macquaker, J.H. and Demko, T.M. (2015a). *Mudstone Primer: Lithofacies Variations, Diagnostic Criteria, and Sedimentologic-Stratigraphic Implications at Lamina to Bedset Scales*. Society for Sedimentary Geology Special, Concepts in Sedimentology and Paleontology, v. 12, 198 p.

Lazar, O.R., Bohacs, K.M., Macquaker, J.H.S., Schieber, J. and Demko, T.M. (2015b). Capturing key attributes of fine-grained sedimentary rocks in outcrops, cores, and thin sections: Nomenclature and description guidelines. *Journal of Sedimentary Research*, 85, 230–246.

Lazo, D.G., Aguirre-Urreta, M.B., Price, G.D., Rawson, P.F., Ruffell, A.H. and Ogle, N. (2008). Palaeosalinity variations in the Early Cretaceous of the Neuquén Basin, Argentina: Evidence from oxygen isotopes and palaeoecological analysis. *Palaeogeography, Palaeoclimatology, Palaeoecology*, 260, 477–493.

Leaman, M. and McIlroy, D. (2017). Three-dimensional morphological and permeability modelling of *Diplocraterion*. *Ichnos*, 24, 51–63.

Leanza, H.A. (1973). Estudio sobre los cambios faciales de los estratos limitrofes Jurasico-Cretacicos entre Loncopue y Picun Leufu, provincia de Neuquen, Republica Argentina. *Revista de la Asociación Geológica Argentina*, 28, 97–132.

Leanza, H.A. (1993). *Jurassic and Cretaceous Trigoniid Bivalves from West-Central Argentina*. Bulletins of American Paleontology, v. 343, p. 95.

Leanza, H.A. (2012). The Vaca Muerta Formation (Late Jurassic-Early Cretaceous): History, stratigraphic context and events of this emblematic unit of the Neuquén basin, Argentina. In AAPG GTW, December 2-4, Buenos Aires, Argentina.

Leanza, H.A., and Hugo, C.A. (1977). Sucesión de ammonites y edad de la Formación Vaca Muerta y sincrónicas entre los paralelos 35° y 40° l.s. Cuenca Neuquina-Mendocina. *Revista de la Asociación Geológica Argentina*, 32, 248–264.

Leanza, H.A. and Hugo, C.A. (1997). *Hoja Geológica 3969-III, Picún Leufú*. Instituto de Geología y Recursos Minerales, Servicio Geológico Minero Argentino, 135 p.

Leanza, H.A., Marchese, H.G., and Riggi, J.C. (1977). Estratigrafía del Grupo Mendoza con especial referencia a la Formación Vaca Muerta y sincrónicas entre los paralelos 35º y 40º L.S., Cuenca Neuquina – Mendocina. *Revista de la Asociación Geológica Argentina*, 32, 190–208.

Leanza, H.A., Sattler, F., Martinez, R.S., and Carbone, O. (2011). La Formación Vaca Muerta y equivalentes (Jurásico Tardío-Cretácico Temprano) en la Cuenca Neuquina. In Leanza, H.A., Arregui, C., Carbone, O., Danieli, J.C., and Vallés, J.M. (Eds.), *Geología y Recursos Naturales de la Provincia del Neuquén* (p. 113–130). Asociación Geológica Argentina.

Leanza, H.A., Kietzmann, D.A., Iglesia Llanos, M.P. and Kohan Martínez, M. (2020a). Stratigraphic context: Cyclostratigraphy, magnetostratigraphy, and seismic stratigraphy. In Minisini, D., Fantin, M., Lanusse Noguera, I. and Leanza, H.A. (Eds.), *Integrated Geology of Unconventionals: The Case of the Vaca Muerta Play, Argentina* (p. 39–60). AAPG Memoir, v. 121.

Leanza, H.A., Vennari, V.V., Aguirre-Urreta, M.B., Concheyro, A., Lescano, M., Ivanova, D., Kietzmann, D.A., López-Martínez, R., Martz, P.A., Paolillo, M.A., Guler, M.V., Pujana, I. and Paz, M. (2020b). Relevant marine paleobiological markers of the Vaca Muerta

Formation. In Minisini, D., Fantin, M., Lanusse Noguera, I. and Leanza, H.A. (Eds.), *Integrated geology of unconventionals: The case of the Vaca Muerta play, Argentina* (p. 61–98). AAPG Memoir, v. 121.

Legarreta, L. (2001). Desiccation events and non-marine clastic lowstands in the Neuquina Basin: Stratigraphy, facies and hydrocarbon distribution. In *Hedberg Conference, American Association of Petroleum Geologists* (p. 28–29). Mendoza, Argentina.

Legarreta, L. (2002). Eventos de desecación en la Cuenca Neuquina: depósitos continentales y distribución de hidrocarburos. In *5º Congreso de Exploración y Desarrollo de Hidrocarburos* (Actas CD). Mar del Plata, Argentina.

Legarreta, L., and Gulisano, C. (1989). Análisis estratigráfico secuencial de la Cuenca Neuquina (Triásico Superior-Terciario Inferior), Argentina. In Chebli, G.A., and Spalletti, L.A. (Eds.), *Cuencas Sedimentarias Argentinas* (p. 221–243). Serie Correlación Geológica, v. 6.

Leonowicz, P. (2013). The significance of mudstone fabric combined with palaeoecological evidence in determining sedimentary processes–An example from the Middle Jurassic of southern Poland. *Geological Quaterly*, 57, 243–260.

Leonowicz, P. (2015). Ichnofabrics of shallow-marine mudstone, the result of changing environmental conditions: an example from the Middle Jurassic ore-bearing clay from southern Poland. *Facies*, 61, 11.

Levin, L.A. (2003). Oxygen minimum zone benthos: adaptation and community response to hypoxia. *Oceanography and Marine Biology: An Annual Review*, 41, 1–45.

Levin, L.A., Whitcraft, C.R., Mendoza, G.F., Gonzalez, J.P. and Cowie, G. (2009). Oxygen and organic matter thresholds for benthic faunal activity on the Pakistan margin oxygen minimum zone (700–1100 m). *Deep Sea Research Part II*, 56, 449–471.

Lewis, K.B. and Kohn, B.P. (1973). Ashes, turbidites, and rates of sedimentation on the continental slope off Hawkes Bay. *New Zealand Journal of Geology and Geophysics*, 16, 439–454.

Li, Z. and Schieber, J. (2018). Detailed facies analysis of the Upper Cretaceous Tununk Shale Member, Henry Mountains Region, Utah: Implications for mudstone depositional models in epicontinental seas. *Sedimentary Geology*, 364, 141–159.

Lin, W. and Bhattacharya, J.P. (2021). Storm-flood-dominated delta: A new type of delta in stormy oceans. *Sedimentology*, 68, 1109–1136.

Liu, J.P., Li, A.C., Xu, K.H., Velozzi, D.M., Yang, Z.S., Milliman, J.D. and DeMaster, D.J. (2006). Sedimentary features of the Yangtze River-derived along-shelf clinoform deposit in the East China Sea. *Continental Shelf Research*, 26, 2141–2156.

Liu, J.P., Xu, K.H., Li, A.E.A., Milliman, J.D., Velozzi, D.M., Xiao, S.B. and Yang, Z.S. (2007). Flux and fate of Yangtze River sediment delivered to the East China Sea. *Geomorphology*, 85, 208–224.

Lobza, V. and Schieber, J. (1999). Biogenic sedimentary structures produced by worms in soupy, soft muds; observations from the Chattanooga Shale (Upper Devonian) and experiments. *Journal of Sedimentary Research*, 69, 1041–1049.

Löhr, S.C. and Kennedy, M.J. (2015). Micro-trace fossils reveal pervasive reworking of Pliocene sapropels by low-oxygen-adapted benthic meiofauna. *Nature Communications*, 6, 1–8.

Löhr, S.C., Kennedy, M.J., George, S.C., Williamson, R.J. and Xu, H. (2018). Sediment microfabric records mass sedimentation of colonial cyanobacteria and extensive syndepositional metazoan reworking in Pliocene sapropels. *The Depositional Record*, 4, 293–317.

Loucks, R.G. and Ruppel, S.C. (2007). Mississippian Barnett Shale: Lithofacies and depositional setting of a deep-water shale-gas succession in the Fort Worth Basin, Texas. *AAPG Bulletin*, 91, 579–601.

Löwemark, L. (2015). Testing ethological hypotheses of the trace fossil *Zoophycos* based on Quaternary material from the Greenland and Norwegian Seas. *Palaeogeography, Palaeoclimatology, Palaeoecology*, 425, 1–13.

Löwemark, L., Schönfeld, J., Werner, F. and Schäfer, P. (2004). Trace fossils as a paleoceanographic tool: Evidence from Late Quaternary sediments of the southwestern Iberian margin. *Marine Geology*, 204, 27–41.

Lucchi, R.G. and Rebesco, M. (2007). Glacial contourites on the Antarctic Peninsula margin: insight for palaeoenvironmental and palaeoclimatic conditions. In Viana, A.R. and Rebesco, M. (Eds.), *Economic and Palaeoceanographic Significance of Contourite*

Deposits (p. 111–127). Geological Society of London Special Publications, London, v. 276.

Lüdmann, T., Wiggershaus, S., Betzler, C., and Hübscher, C. (2012). Southwest Mallorca Island: a cool-water carbonate margin dominated by drift deposition associated with giant mass wasting. *Marine Geology*, 307, 73–87.

Lynn, R.J. and Simpson, J.J. (1990). The flow of the undercurrent over the continental borderland off southern California. *Journal of Geophysical Research, Oceans*, 95, 12995–13008.

Ma, Y., Wright, L.D., Friedrichs, C.T. (2008). Observations of sediment transport on the continental shelf off the mouth of the Waiapu River, New Zealand: Evidence for current-supported gravity flows. *Cont. Shelf Res.*, 28, 516–532.

MacEachern, J.A. and Pemberton, S.G. (1994). Ichnological aspects of incised-valley fill systems from the Viking Formation of the Western Canada Sedimentary Basin, Alberta, Canada. In Dalrymple, R.W., Boyd, R. and Zaitlin, B. (Eds.), *Incised-Valley Systems: Origin and Sedimentary Sequences* (p. 129–157). SEPM Special Publication, v. 51.

MacEachern, J.A., and Gingras, M.K. (2007). Recognition of brackish-water trace-fossil suites in the Cretaceous Western Interior Seaway of Alberta, Canada. In Bromley, R.G., Buatois, L.A., Mángano, G., Genise, J.F., and Melchor, R.N., (Eds.), Sediment-Organism Interactions: A Multifaceted Ichnology (p. 149–193). SEPM Special Publication, v. 88.

MacEachern, J.A. and Bann, K.L. (2020). The *Phycosiphon* Ichnofacies and the *Rosselia* Ichnofacies: Two new ichnofacies for marine deltaic environments. *Journal of Sedimentary Research*, 90, 855–886.

MacEachern, J.A., Raychaudhuri, I. and Pemberton, S.G (1992). Stratigraphic applications of the *Glossifungites* ichnofacies: delineating discontinuities in the rock record. In Pemberton, S.G. (Ed.), Applications of Ichnology to Petroleum Exploration: A Core Workshop (p. 169–198). SEPM Core Workshop, v. 17.

MacEachern, J. A., Pemberton, S. G., Bann, K. L. and Gingras, M. K. (2007a). Departures from the archetypal Ichnofacies: Effective recognition of physico-chemical stresses in the rock record. In J.A. MacEachern, K.L. Bann, M.K. Gingras, and S.G. Pemberton (Eds.), *Applied Ichnology* (p. 65–93). SEMP Short Courses, v. 52.

MacEachern, J.A., Pemberton, S.G., Gingras, M.K. and Bann, K.L. (2007b). The ichnofacies paradigm: a fifty-year retrospective. In Miller, W. (Ed.), *Trace Fossils, Concepts, Problems, Prospects* (p. 52–77). Elsevier.

MacEachern, J.A., Pemberton, S.G., Gingras, M.K., Bann, K.L. and Dafoe, L.T. (2007c). Uses of trace fossils in genetic stratigraphy. In Miller, W. (Ed.), *Trace Fossils, Concepts, Problems, Prospects* (p. 110–134). Elsevier.

MacEachern, J. A., Dashtgard, S.E., Knaust, D., Catuneanu, O., Bann, K.K. and Pemberton, S. G. (2012). Sequence stratigraphy. In D. Knaust and R.G. Bromley (Eds.), *Trace Fossils as Indicators of Sedimentary Environments* (p. 157–195). Developments in Sedimentology, v. 64.

Macquaker, J.H.S. and Bohacs, K.M. (2007). On the accumulation of mud. *Science*, 318, 1734–1735.

Macquaker, J.H., Taylor, K.G. and Gawthorpe, R.L. (2007). High-resolution facies analyses of mudstones: implications for paleoenvironmental and sequence stratigraphic interpretations of offshore ancient mud-dominated successions. *Journal of Sedimentary Research*, 77, 324–339.

Macquaker, J.H., Keller, M.A. and Davies, S.J. (2010a). Algal blooms and "marine snow": Mechanisms that enhance preservation of organic carbon in ancient fine-grained sediments. *Journal of Sedimentary Research*, 80, 934–942.

Macquaker, J.H., Bentley, S.J. and Bohacs, K.M. (2010b). Wave-enhanced sediment-gravity flows and mud dispersal across continental shelves: Reappraising sediment transport processes operating in ancient mudstone successions. *Geology*, 38, 947–950.

Mángano, M.G. (2011). Trace-fossil assemblages in a Burgess Shale-type deposit from the Stephen Formation at Stanley Glacier, Canadian Rocky Mountains: unraveling ecologic and evolutionary controls. *Palaeontographica Canadiana*, 31, 89–107.

Mángano, M.G. and Buatois, L.A. (1991). Discontinuity surfaces in the Lower Cretaceous of the High Andes (Mendoza, Argentina): trace fossils and environmental implications. *Journal of South American Earth Sciences*, 4, 215–229.

Mángano, M.G., Buatois, L.A., West, R.R. and Maples, C.G. (1998). Contrasting behavioral and feeding strategies recorded by tidal-flat bivalve trace fossils from the Upper Carboniferous of eastern Kansas. *Palaios*, 13, 335–351.

Mángano, M.G., Buatois, L.A., Maples, C.G. and West, R.R. (2000). A new ichnospecies of *Nereites* from Carboniferous tidal-flat facies of eastern Kansas, USA: implications for the *Nereites–Neonereites* debate. *Journal of Paleontology*, 74, 149–157.

Mángano, M.G., Buatois, L.A., West, R.R., and Maples, C.G. (2002). *Ichnology of a Pennsylvanian Equatorial Tidal Flat: The Stull Shale Member at Waverly, Eastern Kansas*. Kansas Geological Survey, 245, 133 p.

Mángano, M.G., Hawkes, C.D. and Caron, J.B. (2019). Trace fossils associated with Burgess Shale non-biomineralized carapaces: bringing taphonomic and ecological controls into focus. *Royal Society Open Science*, 6, 172074.

Maretto, H., and Pángaro, F. (2005). Edad de formación de algunas de las grandes estructuras del engolfamiento de la Cuenca Neuquina: Actividad tectónica durante la depositación de la Fm. Quintuco. In *6° Congreso de Exploración y Desarrollo de Hidrocarburos* (Actas CD-ROM). Mar del Plata, Argentina.

Martin, K.D. (2004). A re-evaluation of the relationship between trace fossils and dysoxia. In McIlroy, D. (Ed.), *The Application of Ichnology to Palaeoenvironmental and Stratigraphic Analysis* (p. 141–156). Geological Society, London, Special Publications, v. 228.

Martín-Chivelet, J., Fregenal-Martínez, M.A. and Chacón, B. (2003). Mid-depth calcareous contourites in the latest Cretaceous of Caravaca (Subbetic Zone, SE Spain). Origin and palaeohydrological significance. *Sedimentary Geology*, 163, 131–146.

Martín-Chivelet, J., Fregenal-Martínez, M.A. and Chacón, B. (2008). Traction structures in contourites. In Rebesco, M. and Camerlenghi, A. (Eds.), *Contourites* (p. 159–182). Developments in Sedimentology, v. 60.

Massaferro, J.L., Zeller, M., Giunta, D.L., Sagasti, G., and Eberli, G.P. (2014). Evolución del sistema mixto Tithoniano-Valanginiano (Formaciones Vaca Muerta, Quintuco y equivalentes) a partir de estudios de afloramientos y subsuelo, centro-sur de la Cuenca

Neuquina. In *IX Congreso de Exploración y Desarrollo de Hidrocarburos* (p. 251–274). Mendoza, Argentina.

McCave, I.N. (1972). Transport and escape of fine-grained sediment from shelf areas. In Swift, D.J.P., Duane, D.B. and Pilkey, O.H. (Eds.), *Shelf sediment transport: process and pattern* (p. 225–248).

McCave, I.N. (1975). Vertical flux of particles in the ocean. *Deep-Sea Research*, 22, 491–502.

McPhee-Shaw, E.E., Sternberg, R.W., Mullenbach, B. and Ogston, A.S. (2004). Observations of intermediate nepheloid layers on the northern California continental margin. *Continental Shelf Research*, 24, 693–720.

Meier, H.E.M., Feistel, R., Piechura, J., Arneborg, L., Burchard, H., Fiekas, V., Golenko, N., Kuzmina, N., Mohrholz, V., Nohr, C. and Paka, V.T. (2006). Ventilation of the Baltic Sea deep water: A brief review of present knowledge from observations and models. *Oceanologia*, 48, 133–164.

Mekki, F., Zhang, L.J., Vinn, O., Toom, U., Benyoucef, M., Bendella, M., Bouchemla, E., Bensalah, M. and Adaci, M. (2019). Middle Jurassic *Zoophycos* and *Chondrites* from the Mélah Formation of Saharan Atlas, Algeria. *Estonian Journal of Earth Sciences*, 68, 190–198.

Mendoza-Rodríguez, G., Buatois, L.A., Rincón-Martínez, D., Mángano, M.G. and Baumgartner-Mora, C. (2020). The armored burrow *Nummipera eocenica* from the upper Eocene San Jacinto Formation, Colombia: morphology and paleoenvironmental implications. *Ichnos*, 27, 81–91.

Míguez-Salas, O. and Rodríguez-Tovar, F.J. (2019). Ichnofacies distribution in the Eocene-Early Miocene Petra Tou Romiou outcrop, Cyprus: sea level dynamics and palaeoenvironmental implications in a contourite environment. *International Journal of Earth Sciences*, 108, 2531–2544.

Míguez-Salas, O. and Rodríguez-Tovar, F.J. (2021). Trace fossil analysis of sandy clastic contouritic deposits in the late Miocene Rifian Corridor (Morocco): Ichnotaxonomical and palaeoenvironmental insights. *Journal of African Earth Sciences*, 174, 104054.

Milliken, K.L., Reed, R.M., McCarty, D.K., Bishop, J., Lipinski, C.J., Fischer, T.B., Crousse, L. and Reijenstein, H. (2019). Grain assemblages and diagenesis in the Vaca Muerta Formation (Jurassic-Cretaceous), Neuquén Basin, Argentina. *Sedimentary Geology*, 380, 45–64.

Milsom, C.V. (1994). *Saccocoma*: a benthic crinoid from the Jurassic Solnhofen Limestone, Germany. *Palaeontology*, 37, 121–129.

Minisini, D., Eldrett, J., Bergman, S.C., and Forkner, R. (2018). Chronostratigraphic framework and depositional environments in the organic-rich, mudstone-dominated Eagle Ford Group, Texas, USA. *Sedimentology*, 65, 1520–1557.

Minisini D., Desjardins, P., Otharán, G., Paz, M., Kietzmann, D., Eberli, E., Zavala, C., Simo, T., Macquaker, J.H. and Heine, C. (2020a). Sedimentology, depositional model, and implications for reservoir quality. In Minisini, D., Fantín, M., Lanusse Noguera, I. and Leanza, H. A. (Eds.), *Integrated Geology of Unconventionals: The Case of the Vaca Muerta Play, Argentina* (p. 201-236). AAPG Memoir, v. 121.

Minisini, D., Fryklund, B., Gerali, F. and Fantín, M. (2020b). The first economical unconventional play outside North America: Context, history, and "coopetition". In Minisini, D., Fantín, M., Lanusse Noguera, I. and Leanza, H.A. (Eds.), *Integrated geology of unconventionals: The case of the Vaca Muerta play, Argentina* (p. 1–24). AAPG Memoir, v. 121.

Minisini, D., Fantin, M., Lanusse Noguera, I. and Leanza, H.A. (2020c). *Integrated Geology of Unconventionals: The Case of the Vaca Muerta Play, Argentina*. AAPG Memoir, v. 121, 554 p.

Miramontes, E., Cattaneo, A., Jouet, G., Thereau, E., Thomas, Y., Rovere, M., Cauquil, E. and Trincardi, F. (2016). The Pianosa contourite depositional system (northern Tyrrhenian Sea): Drift morphology and Plio-Quaternary stratigraphic evolution. *Marine Geology*, 378, 20–42.

Mitchum, R.M.J., Uliana, M.A. (1985). Seismic stratigraphy of carbonate depositional sequences, Upper Jurassic-Lower Cretaceous, Neuquén Basin, Argentina. In Berg, O., and Woolverton, D. (Eds.), *Seismic Stratigraphy II: An Integrated Approach to Hydrocarbon Exploration* (p. 255–274). AAPG Memoir, v. 39.

Moghadam, H.V. and Paul, C.R.C. (2000). Trace fossils of the Jurassic, Blue Lias, Lyme Regis, southern England. *Ichnos*, 7, 283–306.

Monaco, P., Rodríguez-Tovar, F.J. and Uchman, A. (2012). Ichnological analysis of lateral environmental heterogeneity within the Bonarelli Level (uppermost Cenomanian) in the classical localities near Gubbio, Central Apennines, Italy. *Palaios*, 27, 48–54.

Moore, W.R. (1983). The nature of the Minnelusa-Opeche contact in the Halverson field area, Powder River basin, Wyoming. *Mt. Geol.*, 20, 113–120.

Moros, M., Kotilainen, A.T., Snowball, I., Neumann, T., Perner, K., Meier, H.M., Leipe, T., Zillén, L., Damste, J.S.S. and Schneider, R. (2020). Is 'deep-water formation'in the Baltic Sea a key to understanding seabed dynamics and ventilation changes over the past 7,000 years?. *Quaternary International*, 550, 55–65.

Mosquera, A., Silvestro, J., Ramos, V.A., Alarcón, M. and Zubiri, M. (2011). La estructura de la Dorsal de Huincul. In H.A. Leanza, C. Arregui, O. Carbone, J.C. Danieli, and J.M. Vallés (Eds.), *Relatorio del XVIII Congreso Geológico Argentino* (p. 385–398). Buenos Aires, Argentina.

Mpodozis, C., Ramos, V.A. (2008). Tectónica jurásica en Argentina y Chile: extensión, subducción oblicua, rifting, deriva y colisiones? *Rev. Asoc. Geol. Argentina*, 63, 481–497.

Mulder, T. (2011). Gravity processes and deposits on continental slope, rise and abyssal plains. In Hüneke, H. and Mulder, T. (Eds.), *Deep-Sea Sediments* (p. 25–148). Developments in Sedimentology, Elsevier, v. 63.

Mulder, T. and Syvitski, J.P.M. (1995). Turbidity currents generated at river mouths during exceptional discharges to the world oceans. *J. Geol.*, 103, 285–299.

Mulder, T. and Alexander, J. (2001). The physical character of subaquaeous sedimentary density flows and their deposits. *Sedimentology*, 48, 269–299.

Mulder, T. and Chapron, E. (2011). Flood deposits in continental and marine environments: character and significance. In Slatt, R.M., Zavala, C.A. (Eds.), *Sediment Transfer from Shelf to Deep Water-Revisiting the Delivery System* (p. 1–30). AAPG Studies in Geology, v. 61.

Mulder, T., Syvitski, J.P.M., Migeon, S., Faugeres, J.C. and Savoye, B. (2003). Marine hyperpycnal flows: initiation, behavior and related deposits. A review. *Mar. Pet. Geol.*, 20, 861–882.

Mulder, T., Faugères, J.-C. and Gonthier, E. (2008). Mixed turbidite-contourite systems. In Rebesco, M. and Camerlenghi, A. (Eds.), *Contourites* (p. 435–456). Developments in Sedimentology, v. 60.

Mullins, H.T., Thompson, J.B., McDougall, K. and Vercoutere, T.L. (1985). Oxygen-minimum zone edge effects: evidence from the central California coastal upwelling system. *Geology*, 13, 491–494.

Mutti, E. and Sonnino, M. (1981). Compensation cycles: a diagnostic feature of turbidite sandstone lobes. In *International Association of Sedimentologists, 2nd European Regional Meeting* (p. 120–123). Bologna, Italy.

Mutti, E. and Normark, W.R. (1991). An integrated approach to the study of turbidite systems. In Weimer, P., Link, M.H., (Eds.*), Seismic Facies and Sedimentary Processes of Submarine Fans and Turbidite Systems* (p. 75–106). Springer-Verlag, New York.

Mutti, E., Gulisano, C.A. and Legarreta, L. (1994). Anomalous systems tracts stacking patterns within 3rd. order depositional sequences (Jurassic–Cretaceous backarc Neuquén Basin, Argentina Andes. In H.W. Posamentier and E. Mutti (Eds.), *Second High Resolution Sequence Stratigraphy Conference, Abstracts* (p. 137-143). Tremp.

Mutti, E., Davoli, G., Tinterri, R. and Zavala, C.A. (1996). The importance of ancient fluvio-deltaic systems dominated by catastrophic flooding in tectonically active basins. *Mem. di Sci. Geol.*, 48, 223–291.

Myrow, P.M. and Southard, J.B. (1996). Tempestite deposition. *Journal of Sedimentary Research*, 66, 875–887.

Myrow, P.M., Fischer, W., Goodge, J.W. (2002). Wave-modified turbidites: Combined-flow shoreline and shelf deposits, Cambrian, Antarctica. *J. Sediment. Res.*, 72, 641–656.

Myrow, P.M., Lukens, C., Lamb, M.P., Houck, K., Strauss, J. (2008). Dynamics of a transgressive prodeltaic system: Implications for geography and climate within a Pennsylvanian intracratonic basin, Colorado, U.S.A. *J. Sediment. Res.*, 78, 512–528.

Naipauer, M., García Morabito, E., Marques, J.C., Tunik, M., Rojas Vera, E.A., Vujovich, G.I., Pimentel, M.P., Ramos, V.A. (2012). Intraplate Late Jurassic deformation and exhumation in western central Argentina: Constraints from surface data and U-Pb detrital zircon ages. *Tectonophysics*, 524–525, 59–75.

Neumeier, U. (1998), Tidal dunes and sand waves in deep outer-shelf environments, Bajocian, SE Jura, France. *Journal of Sedimentary Research*, 68, 507–514.

Newport, S.M., Jerrett, R.M., Taylor, K.G., Hough, E. and Worden, R.H. (2017). Sedimentology and microfacies of a mud-rich slope succession: in the Carboniferous Bowland Basin, NW England (UK). *Journal of the Geological Society*, 175, 247–262.

Nichols, M.M. (1989). Sediment accumulation rates and relative sea-level rise in lagoons. *Mar. Geol.*, 88, 201–219.

Nichols, G. (2009). *Sedimentology and Stratigraphy*. John Wiley & Sons, 419 p.

Nittrouer, C.A., Lopez, G.R., Wright, L.D., Bentley, S.J., D'Andrea, A.F., Friedrichs, C.T., Craig, N.I. and Sommerfield, C.K. (1998). Oceanographic processes and the preservation of sedimentary structure in Eckernförde Bay, Baltic Sea. *Continental Shelf Research*, 18, 1689–1714.

Nittrouer, C.A., Austin, J.A., Field, M.E., Kravitz, J.H., Syvitski, J.P. and Wiberg, P.L. (2007). *Continental Margin Sedimentation: From Sediment Transport to Sequence Stratigraphy*. International Association of Sedimentologists, v. 25, 560 p.

Noffke, N. (2010). *Geobiology: Microbial Mats in Sandy Deposits from the Archaean Era to Today*. Springer, Heidelberg, 194 p.

Noffke, A., Hertweck, G., Kröncke, I. and Wehrmann, A. (2009). Particle size selection and tube structure of the polychaete *Owenia fusiformis*. *Estuarine, Coastal and Shelf Science*, 81, 160–168.

Notta, R., Davogustto, O., Desjardins, P. and Williams, B. (2017). Slumps deposits identification in low angle carbonate ramp settings, Cruz de Lorena (Neuquen Basin, Argentina): Towards an integrated model explaining anomalous water recovery and poor well performance. In *XX Congreso Geológico Argentino, Simposio 5 Geología de la Formación Vaca Muerta* (p. 91–96). Asociación Geológica Argentina, Tucumán.

Notta, R., Kruijs, E., Jain, V., Diaz-Perez, G. and Mandler, H. (2020). De-risking the Sierras Blancas and Cruz de Lorena blocks, black-oil window. In Minisini, D., Fantín, M., Lanusse Noguera, I. and Leanza, H.A. (Eds.), *Integrated geology of unconventionals: The case of the Vaca Muerta play, Argentina* (p. 445–468). AAPG Memoir, v. 121.

Nummedal, D. and Swift, D.J.P. (1987). Transgressive stratigraphy at sequence-bounding unconformities: some principles derived from Holocene and Cretaceous examples. In D. Nummedal, O.H. Pilkey, and J.D. Howard (Eds.), *Sea-Level Fluctuation and Coastal Evolution* (p. 241–260). SEPM Special Publication, v. 41.

Nyhuis, C.J., Rippen, D. and Denayer, J. (2014). Facies characterization of organic-rich mudstones from the Chokier Formation (lower Namurian), south Belgium. *Geologica Belgica*, 17, 311–322.

O'Brien, N.R. (1996). Shale lamination and sedimentary processes. In Kemp, A.E.S. (Ed.), *Palaeoclimatology and Palaeoceanography from Laminated Sediments* (p. 23–36). Geological Society of London Special Publications, London, v. 116.

O'Brien, N.R. and Slatt, R.M. (1990). *Argillaceous Rock Atlas*. Springer, Berlin, Heidelberg, New York, 141 p.

Ogston, A.S., Cacchione, D.A., Sternberg, R.W., Kineke, G.C. (2000). Observations of storm and river flood-driven sediment transport on the northern California continental shelf. *Continental Shelf Research*, 20, 2141–2162.

Olafsson, E.B. (1989). Contrasting influences of suspension-feeding and deposit-feeding populations of *Macoma balthica* on infaunal recruitment. *Marine Ecology Progress Series*, 55, 171–179.

Olivero, E.B. and López-Cabrera, M.I. (2010). *Tasselia ordamensis*: A biogenic structure of probable deposit-feeding and gardening maldanid polychaetes. *Palaeogeography, Palaeoclimatology, Palaeoecology*, 292, 336–348.

Olivo, M.S., Schwarz, E. and Veiga, G.D. (2016). Modelo de acumulación y evolución secuencial del intervalo cuspidal de la Formación Quintuco en su área tipo: implicancias para las reconstrucciones paleogeográficas del margen austral de la Cuenca Neuquina durante el Valanginiano. *Andean Geology*, 43, 215–239.

Olóriz, F. and Rodríguez-Tovar, F.J. (2002). Trace-fossils and minor discontinuities in a marl limestone rhythmite, Lower–Middle Kimmeridgian, southern Spain. *Geobios*, 35, 581–593.

Oschmann W. (2000). Microbes and Black Shales. In Riding, R.E. and Awramik, S.M. (Eds.), *Microbial Sediments* (p. 137–148). Springer.

Otharán, G.A. (2020). *Sedimentología y Análisis de Facies de la Formación Vaca Muerta (Jurásico-Cretácico), Cuenca Neuquina. El rol de los Flujos de Fango en la Depositación de Espesas Sucesiones de Lutitas*. Ph.D. tesis, Universidad Nacional del Sur, Bahía Blanca, Argentina, 421 p.

Otharán, G.A., Zavala, C., Arcuri, M. (2017). Las turbiditas de la Formación Vaca Muerta (Tithoniano) en la subcuenca de Picún Leufú, Cuenca Neuquina, Argentina. In *XX Congreso Geológico Argentino, Geología de la Formación Vaca Muerta* (p. 103–109). San Miguel de Tucumán, Argentina.

Otharán, G.A., Zavala, C., Arcuri, M., Di Meglio, M., Zorzano, A., Marchal, D., and Köhler, G. (2020). Facies analysis of organic-rich fluid mud flow deposits. The lower section of the Vaca Muerta Formation (Tithonian) at basinal positions, Neuquén Basin, Argentina. *Andean Geology*, 47, 384–417.

Over, D.F. (1988). Lingulid brachiopods and *Lingulichnus* from a Silurian shelf-slope carbonate sequence, Delorme Group, Mackenzie Mountains, Northwest Territories. *Canadian Journal of Earth Sciences*, 25, 465–471.

Paim, P.S.G., Correa, E.L.C., Faccini, U.F. (2011). Fluvial-derived turbidites in the Los Molles Formation (Jurassic of the Neuquén Basin): Initiation, transport, and deposition. In Slatt, R.M., Zavala, C.A. (Eds.), *Sediment Transfer from Shelf to Deep Water-Revisiting the Delivery System* (p. 95–116). AAPG Studies in Geology, v. 61.

Palanques, A., Puig, P., Guillén, J., Jiménez, J., Gràcia, V., Sánchez-Arcilla, A. and Madsen, O. (2002). Near-bottom suspended sediment fluxes on the microtidal low-energy Ebro continental shelf (NW Mediterranean). *Continental Shelf Research*, 22, 285–303.

Palanques, A., Durrieu de Madron, X., Puig, P., Fabres, J., Guillén, J., Calafat, A., Canals, M., Heussner, S. and Bonnin, J. (2006). Suspended sediment fluxes and transport processes in

the Gulf of Lions submarine canyons. The role of storms and dense water cascading. *Marine Geology*, 234, 43–61.

Paola, C., Wiele, S.M. and Reinhardt, M.A. (1989). Upper-regime parallel lamination as the result of turbulent sediment transport and low-amplitude bedforms. *Sedimentology*, 36, 47–59.

Parada, M.N. (2019). *Análisis Sedimentológico e Icnológico de la Sección Basal de la Formación Picún Leufú (Tithoniano-Berriasiano) en su Localidad Tipo, Cuenca Neuquina, Argentina*. Bachelor's tesis, Universidad Nacional de Río Negro, General Roca, 48 p.

Parent, H., Garrido, A.C., Schweigert, G., Scherzinger, A. (2011). The Tithonian ammonite fauna and stratigraphy of Picún Leufú, southern Neuquén Basin, Argentina. *Rev. Paleobiol.*, 30, 45–104.

Parker, G. (1965). *Relevamiento Geológico Escala 1:100.00 – Hoja 4169-3*. I.G.M. Lonco Vaca. Provincia de Río Negro. YPF unpublished report, Buenos Aires.

Parsons, J.D., Bush, J.W.M., and Syvitski, J.P.M. (2001). Hyperpycnal plume formation from riverine outflows with small sediment concentrations. *Sedimentology*, 48, 465–478.

Patruno, S. and Helland-Hansen, W. (2018). Clinoforms and clinoform systems: Review and dynamic classification scheme for shorelines, subaqueous deltas, shelf edges and continental margins. *Earth-Science Reviews*, 185, 202–233.

Patruno, S., Hampson, G.J. and Jackson, C.A. (2015). Quantitative characterisation of deltaic and subaqueous clinoforms. *Earth-Science Reviews*, 142, 79–119.

Pattison, S. (2005). Storm-influenced prodelta turbidite complex in the Lower Kenilworth Member at Hatch Mesa, Book Cliffs, Utah, U.S.A.: Implications for shallow marine facies models. *J. Sediment. Res.*, 75, 420–439.

Pattison, S.A., Hoffman, T. A. (2008). Sedimentology, architecture and origin of shelf turbidite bodies in the Upper Cretaceous Kenilworth Member, Book Cliffs, Utah, USA. In G.J. Hampson (Ed.), *Recent Advances in Models on Siliciclastic Shallow-marine Stratigraphy* (p. 391–420). SEPM Spec. Publ., v. 90.

Pattison, S.A.J., Ainsworth, R.B., Hoffman, T.A. (2007). Evidence of across-shelf transport of fine-grained sediments: Turbidite-filled shelf channels in the Campanian Aberdeen Member, Book Cliffs, Utah, USA. *Sedimentology*, 54, 1033–1063.

Paz, M., Ponce, J.J., Buatois, L.A., Mángano, M.G., Carmona, N.B., Pereira, E. and Desjardins, P.R (2019). Bottomset and foreset sedimentary processes in the mixed carbonate-siliciclastic Upper Jurassic-Lower Cretaceous Vaca Muerta Formation, Picún Leufú Area, Argentina. *Sedimentary Geology*, 389, 161–185.

Paz, M., Ponce, J.J., Mángano, M.G., Buatois, L.A., Carmona, N.B., Wetzel, A., Pereira, E. and Rodríguez, M.N. (2021). The Vaca Muerta transgression (Upper Jurassic), Neuquén Basin, Argentina: Insights into the evolution and timing of aeolian-marine transitions. *Sedimentology*, doi: 10.1111/sed.12872.

Paz, M., Buatois, L.A., Mángano, M.G., Desjardins, P.R., Notta, R., González Tomassini, F., Carmona, N.B. and Minisini, D. (in review a). Shallow-water bottom current activity within an organic-rich clinoform system, Upper Jurassic-Lower Cretaceous Vaca Muerta Formation, Argentina. *Marine and Petroleum Geology*.

Paz, M., Mángano, M.G., Buatois, L.A., Desjardins, P.R., Notta, R., González Tomassini, F. and Carmona, N.B. (in review b). Ichnology of muddy shallow-water bottom current deposits from the Upper Jurassic–Lower Cretaceous Vaca Muerta Formation, Argentina: Implications for trace-fossil models. *Palaios*.

Paz, M., Buatois, L.A., Mángano, M.G., Desjardins, P.R., Rodríguez, M.N., Ponce, J.J., Minisini, D., González Tomassini, F., Pereira, E., Carmona, N.B., Fantín, M. and Vallejo, M.D. (in review c). Interplay of sedimentary processes in a fine-grained carbonate-siliciclastic, subaqueous clinoform: The Upper Jurassic-Lower Cretaceous Vaca Muerta Formation, Neuquén Basin, Argentina. *GSA Bulletin*.

Pedersen, G.K. (1981). Anoxic events during sedimentation of a Palaeogene diatomite in Denmark. *Sedimentology*, 28, 487–504.

Pedersen, G.K. and Surlyk, F. (1977). Dish structures in Eocene volcanic ash layers, Denmark. *Sedimentology*, 24, 581–590.

Pellegrini, C., Maselli, V. and Trincardi, F. (2016). Pliocene–Quaternary contourite depositional system along the south-western Adriatic margin: changes in sedimentary stacking pattern and associated bottom currents. *Geo-Marine Letters*, 36, 67–79.

Pemberton, S.G. and Frey, R.W. (1982). Trace fossil nomenclature and the *Planolites-Palaeophycus* dilemma. *Journal of Paleontology*, 56, 843–881.

Pemberton, S.G. and Frey, R.W. (1985). The *Glossifungites* Ichnofacies: Modern Examples from the Georgia Coast, U.S.A. In H.A. Curran (Ed.), *Biogenic Structures: Their Use in Interpreting Depositional Environments* (p. 237–259). SEPM Spec. Publ., v. 35.

Pemberton, S.G., Frey, R.W. and Bromley, R.G. (1988). The ichnotaxonomy of *Conostichus* and other plug-shaped ichnofossils. *Canadian Journal of Earth Sciences*, 25, 866–892.

Pemberton, S.G., MacEachern, J.A. and Frey, R.W. (1992). Trace fossil facies models: environmental and allostratigraphic significance. In Walker, R.G. and James, N.P. (Eds.), *Facies Models: Response to Sea Level Change* (p. 47–72). Geological Association of Canada.

Pemberton, S.G., Spila, M., Pulham, A.J., Saunders, T., MacEachern, J.A., Robbins, D. and Sinclair, I.K. (2001). *Ichnology & Sedimentology of Shallow to Marginal Marine Systems. Ben Nevis and Avalon Reservoirs, Jeanne d'Arc Basin*. Geological Association of Canada Short Course Notes, v. 15, St. John's, 343 p.

Petersen, H.I., Andsbjerg, J., Bojesen-Koefoed, J.A., Nytoft, H.P. and Rosenberg, P. (1998). *Petroleum Potential and Depositional Environments of Middle Jurassic Coals and Non-Marine Deposits, Danish Central Graben, with Special Reference to the Søgne Basin*. Geological Survey of Denmark Bulletin, v. 36, 78 pp.

Pickerill, R.K. (1989). *Compaginatichnus*: a new ichnogenus from Ordovician flysch of eastern Canada. *Journal of Paleontology*, 63, 913–919.

Pieńkowski, G. and Niedźwiedzki, G. (2008). Invertebrate trace fossil assemblages from the lower Hettangian of Sołtyków, Holy Cross Mountains, Poland. *Volumina Jurassica*, 6, 109–132.

Pirmez, C., Pratson, L.F., Steckler, M.S. (1998). Clinoform development by advection-diffusion of suspended sediment: Modeling and comparison to natural systems. *J. Geophys. Res.*, 103, 24141–24157.

Playton, T., Janson, X., Kerans, C. (2010). Carbonate Slopes. In James, N.P., Dalrymple, R.W., (Eds.), *Facies Models 4* (p. 449–476). Geological Association of Canada.

Plink-Björlrklund, P., Steel, R.J. (2004). Initiation of turbidity currents: Outcrop evidence for Eocene hyperpycnal flow turbidites. *Sediment. Geol.*, 165, 29–52.

Plint, A.G. (2010). Wave-and storm-dominated shoreline and shallow-marine systems. In James, N.P., Dalrymple, R.W. (Eds.), *Facies Models 4* (p. 167–200). Geological Association of Canada.

Pollard, J.E. and Hardy, P.G. (1991). Trace fossils from the Westphalian D of Writhlington Geological Nature Reserve, nr. Radstock, Avon. *Proceedings of the Geologists' Association*, 102, 169–178

Pomar, L., Molina, J.M., Ruiz-Ortiz, P.A. and Vera, J.A. (2019). Storms in the deep: Tempestite- and beach-like deposits in pelagic sequences (Jurassic, Subbetic, South of Spain). *Marine and Petroleum Geology*, 107, 365–381

Ponce, J.J., Olivero, E.B., Martinioni, D.R. and López Cabrera, M.I. (2007). Sustained and episodic gravity-flow deposits and related bioturbation patterns in Paleogene turbidites (Tierra del Fuego, Argentina). In Bromley, R.G., Buatois, L.A., Mángano, M.G., Genise, J.F. and Melchor, R.N. (Eds.), *Sediment-Organism Interactions: A Multifaceted Ichnology* (p. 253–266). SEPM Special Publication, v. 88.

Ponce, J.J., Olivero, E.B., Martinioni, D.R. (2008). Upper Oligocene-Miocene clinoforms of the foreland Austral Basin of Tierra del Fuego, Argentina: Stratigraphy, depositional sequences and architecture of the foredeep deposits. *J. South Am. Earth Sci.*, 26, 36–54.

Ponce, J.J., Carmona, N.B. (2011a). Coarse-grained sediment waves in hyperpycnal clinoform systems, Miocene of the Austral foreland basin, Argentina. *Geology*, 39, 763–766.

Ponce, J. J., Carmona, N. B. (2011b). Miocene deep-marine hyperpycnal channel levee complexes, Tierra del Fuego, Argentina: Facies associations and architectural elements. In Slatt, R.M., Zavala, C.A., (Eds.), *Sediment Transfer from Shelf to Deep Water-Revisiting the Delivery System* (p. 75–93). AAPG Studies in Geology, v. 61.

Ponce, J.J., Carmona, N. B., Montagna, A., Canale, N. (2015). *Sedimentología e Icnología de los Sistemas Petroleros no Convencionales de la Cuenca Neuquina*. Guia de Campo. Universidad Nacional de Río Negro - Fundación YPF, 112 p.

Ponce, J.J, Carmona, N., Wetzel, A., Paz, M. (2016). Sedimentología e Icnología del tramo basal de la Formación Vaca Muerta, Cuenca Neuquina, Argentina: Implicancias en el análisis de la transgresión del Tithoniano. In *7° Latin American Congress of Sedimentology and 15th Argentinean Meeting of Sedimentology* (p. 136). Santa Rosa, Argentina.

Porębski, S.J. and Steel, R.J. (2003). Shelf-margin deltas: their stratigraphic significance and relation to deepwater sands. *Earth-Science Reviews*, 62, 283–326.

Porter, K.G. and Robbins, E.I. (1981). Zooplankton fecal pellets link fossil fuel and phosphate deposits. *Science*, 212, 931–933.

Posamentier, H.W. and Vail, P.R. (1988). Eustatic controls on clastic deposition II-Sequence and Systems Tract models. In Wilgus, C.K., Hastings, B.S., Posamentier, H., Van Wagoner, J., Ross, C.A., Kendall, C.G.St.C., (Eds.), *Sea-Level Changes - An Integrated Approach* (p. 125–154). SEPM Special Publication, v. 42.

Posamentier, H.W., Jervey, M.T. and Vail, P.R. (1988). Eustatic controls on clastic deposition I—conceptual framework. In Wilgus, C.K., Hastings, B.S., Posamentier, H., Van Wagoner, J., Ross, C.A., Kendall, C.G.St.C., (Eds.), *Sea-Level Changes - An Integrated Approach* (p. 109–124). SEPM Special Publication, v. 42.

Pose, F., Gangui, A. and Galeazzi, S. (2014). Estratigrafía secuencial del intervalo Quintuco-Vaca Muerta en el Engolfamiento Neuquino, Cuenca Neuquina, Argentina. In *Simposio de Recursos No Convencionales, IX Congreso de Exploración y Desarrollo de Hidrocarburos* (p. 211-229). IAPG, Mendoza, Argentina.

Potter, P.E., Maynard, J.B. and Pryor, W.A. (1980). *Sedimentology of Shale*. Springer-Verlag, New York, 306 p.

Poyatos-Moré, M., Jones, G.D., Brunt, R.L., Hodgson, D.M., Wild, R.J. and Flint, S.S. (2016). Mud-dominated basin-margin progradation: processes and implications. *Journal of Sedimentary Research*, 86, 863–878.

Pratt, L.M. (1984). Influence of paleoenvironmental factors on preservation of organic matter in Middle Cretaceous Greenhorn Formation, Pueblo, Colorado. *AAPG Bulletin*, 68, 1146–1159.

Prélat, A. and Hodgson, D.M. (2013). The full range of turbidite bed thickness patterns in submarine lobes: controls and implications. *J. Geol. Soc. London.*, 170, 209–214.

Puig, P. and Palanques, A. (1998). Nepheloid structure and hydrographic control on the Barcelona continental margin, northwestern Mediterranean. *Marine Geology*, 149, 39–54.

Puig, P., Ogston, A.S., Guillén, J., Fain, A.M.V. and Palanques, A. (2007). Sediment transport processes from the topset to the foreset of a crenulated clinoform (Adriatic Sea). *Continental Shelf Research*, 27, 452–474.

Puig, P., Greenan, B.J.W., Li, M.Z., Prescott, R.H. and Piper, D.J.W. (2013). Sediment transport processes at the head of Halibut Canyon, eastern Canada margin: An interplay between internal tides and dense shelf-water cascading. *Marine Geology*, 341, 14–28.

Pye, K. (1983). Early post-depositional modification of aeolian dune sands. In M.E. Brookfield and T.S. Ahlbrandt (Eds.), *Eolian Sediments and Processes, Developments in Sedimentology* (p. 197–221). Elsevier, Amsterdam.

Raiswell, R. and Fisher, Q.J. (2004). Rates of carbonate cementation associated with sulphate reduction in DSDP/ODP sediments: implications for the formation of concretions. *Chemical Geology*, 211, 71–85.

Ramos, V.A. and Folguera, A. (2005). Tectonic evolution of the Andes of Neuquén: Constraints derived from the magmatic arc and foreland deformation. In Veiga, G.D., Spalletti, L.A., Howell, J.A. and Schwarz, E. (Eds.), *The Neuquén Basin, Argentina: A Case Study in Sequence Stratigraphy and Basin Dynamics* (p. 15–35). Geological Society of London, Special Publications, v. 252.

Ramsay, P.J. (1994). Marine geology of the Sodwana Bay shelf, southeast Africa. *Marine Geology*, 120, 225–247.

Rasumssen, S.L. and Surlyk, F. (2012). Facies and ichnology of an Upper Cretaceous chalk contourite drift complex, eastern Denmark, and the validity of contourite facies models. *Journal of the Geological Society*, 169, 435–447.

Rebesco, M., Hernández-Molina, F.J., Van Rooij, D. and Wåhlin, A. (2014). Contourites and associated sediments controlled by deep-water circulation processes: State-of-the-art and future considerations. *Marine Geology*, 352, 111–154.

Reijenstein, H.M., Posamentier, H.W., Fantin, M., González Tomassini, F., and Lipinski, C. (2014). Vaca Muerta seismic stratigraphy and geomorphology: Regional architectural trends for unconventional exploration. In *IX Congreso de Exploración y Desarrollo de Hidrocarburos* (p. 211–220). Mendoza, Argentina.

Reijenstein, H., Lanusse, I., Oviedo, P., Licitra, D., Sotelo, D., Vittore, F., Quiroga, J., González Tomassini, F. (2017a). ¿Deslizamientos en Vaca Muerta? Observaciones e integración de datos sísmicos, pozos y coronas en el yacimiento Loma Campana, Cuenca Neuquina, Argentina. In *XX Congreso Geológico Argentino, Geología de la Formación Vaca Muerta* (p. 122–129). San Miguel de Tucumán, Argentina.

Reijenstein, H.M., Domínguez, R.F., Bande, A., Vallejo, M.D., Notta, R., Guerberoff, D., Lanusse, I., Köhler, G., Borgnia, M., Benoit, S., Leanza, H.A., Gómez Rivarola, L., Weger, R., González Tomassini, F., Kietzmann, D., Rodríguez Schelotto, M.L., Desjardins, P., Marchal, D., Martínez, A., Vittore, F., Fantín, M., Depine, G., Sattler, F. and Rosemblat, A. (2017b). Transecta sísmica regional del sistema Vaca Muerta – Quintuco: Interpretación de facies sísmicas basada en impedancia acústica y litofacies dominantes. In *XX Congreso Geológico Argentino, Simposio 5 Geología de la Formación Vaca Muerta* (p. 130–134). Asociación Geológica Argentina, Tucumán.

Reijenstein, H.M., Posamentier, H.W., Bande, A., Lozano, F.P., Domínguez, R.F., Wilson, R., Catuneanu, O. and Galeazzi, S. (2020). Seismic geomorphology, depositional elements, and clinoform sedimentary processes: Impact on unconventional reservoir prediction. In Minisini, D., Fantín, M., Lanusse Noguera, I. and Leanza, H.A. (Eds.), *Integrated geology of unconventionals: The case of the Vaca Muerta play, Argentina* (p. 237–266). AAPG Memoir, v. 121.

Reimers, C.E. and Suess, E. (1983). Spatial and temporal patterns of organic matter accumulation on the Peru continental margin. In Thiede, J., and Suess, E. (Eds.), *Coastal Upwelling, its Sediment Record, Part B: Sedimentary Records of Ancient Coastal Upwelling* (p. 311–346). Plenum Press.

Reineck, H.E. (1963). Sedimentgefüge im Bereich der südlichen Nordsee. *Abhandlungen der Senckenbergischen Naturforschenden Gesellschaft*, 505, 1–138.

Reineck, H.-E. (1967). Parameter von Schichtung und Bioturbation. *Geologisches Rundschau*, 56, 420–438.

Reineck, H.E. and Wunderlich, F. (1968). Classification and origin of flaser and lenticular bedding. *Sedimentology*, 11, 99–104.

Reolid, J. and Betzler, C. (2019). The ichnology of carbonate drifts. *Sedimentology*, 66, 1427–1448.

Repol, D., Desjardins, P.R., Buenafama, P., Li, X., Depine, G., Thompson, M., Rucci, F., Veldkamp, J. and Smith, P. (2014). Vaca Muerta liquid-rich shale: Key properties and insights towards a predictive geological model, Sierras Blancas block, Neuquen Basin. In *IX Congreso de Exploracion y Desarrollo de Hidrocarburos, Simposio de Recursos No Convencionales* (p. 567–586). IAPG, Mendoza, Argentina.

Rhoads, D.C. and Young, D.K. (1970). The influence of deposit-feeding organisms on sediment stability and community trophic structure. *Journal of Marine Research*, 28, 150–178.

Ribó, M., Puig, P., Muñoz, A., Iacono, C.L., Masqué, P., Palanques, A., Acosta, J., Guillén, J. and Ballesteros, M.G. (2016). Morphobathymetric analysis of the large fine-grained sediment waves over the Gulf of Valencia continental slope (NW Mediterranean). *Geomorphology*, 253, 22–37.

Riccardi, A.C. (2008). El Jurásico de la Argentina y sus amonites. *Rev. la Asoc. Geol. Argentina*, 63, 625–643.

Riccardi, A.C. (2015). Remarks on the Tithonian–Berriasian ammonite biostratigraphy of west central Argentina. *Volumina Jurassica*, 13, 23–52.

Richiano, S. (2014). Lower Cretaceous anoxic conditions in the Austral basin, south-western Gondwana, Patagonia Argentina. *Journal of South American Earth Sciences*, 54, 37–46.

Robinson, R.S., Murillo de Nava, J.M. and Gorsline, D.S. (2007). Slope currents and contourites in an eastern boundary current regime: California Continental Borderland. In Viana, A.R.

and Rebesco, M. (Eds.), *Economic and Palaeoceanographic Significance of Contourite Deposits* (p. 155–169). Geological Society of London Special Publications, v. 276.

Rodríguez Blanco, L.R., Eberli, G.P., Weger, R.J., Swart, P.K., Tenaglia, M., Sanchez, L.E.R. and McNeill, D.F. (2020). Periplatform ooze in a mixed siliciclastic-carbonate system-Vaca Muerta Formation, Argentina. *Sedimentary Geology*, 396, 105521.

Rodríguez-López, J.P., Meléndez, N., de Boer, P.L. and Soria, A.R. (2012). Controls on marine-erg margin cycle variability: Aeolian-marine interaction in the mid-Cretaceous Iberian Desert System, Spain. *Sedimentology*, 59, 466–501.

Rodríguez-Tovar, F.J. and Hernández-Molina, F.J. (2018). Ichnological analysis of contourites: Past, present and future. *Earth-Science Reviews*, 182, 28–41.

Rodríguez-Tovar, F.J., Uchman, A. and Martín-Algarra, A. (2009). Oceanic Anoxic Event at the Cenomanian–Turonian boundary interval (OAE-2): ichnological approach from the Betic Cordillera, southern Spain. *Lethaia*, 42, 407–417.

Rodríguez-Tovar, F.J., Hernández-Molina, F.J., Hüneke, H., Llave, E. and Stow, D. (2019). Contourite facies model: Improving contourite characterization based on the ichnological analysis. *Sedimentary Geology*, 384, 60–69.

Röhl, H.J., Schmid-Röhl, A., Oschmann, W., Frimmel, A., Schwark, L. (2001). The Posidonia Shale (Lower Toarcian) of SW Germany: an oxygen depleted ecosystem controlled by sea level and paleoclimate. *Palaeogeography, Palaeoclimatology, Palaeoecology*, 165, 27–52.

Rosenberg, R. (1995). Benthic marine fauna structured by hydrodynamic processes and food availability. *Netherlands Journal of Sea Research*, 34, 303–317.

Rosenberg, R., Arntz, W.E., de Flores, E.C., Flores, L.A., Carbajal, G., Finger, I. and Tarazona, J. (1983). Benthos biomass and oxygen deficiency in the upwelling system off Peru. *Journal of Marine Research*, 41, 263–279.

Ruffell, A.H., Price, G.D., Mutterlose, J., Kessels, K., Baraboshkin, E. and Gröcke, D.R. (2002). Palaeoclimate indicators (clay minerals, calcareous nannofossils, stable isotopes) compared from two successions in the late Jurassic of the Volga Basin (SE Russia). *Geological Journal*, 37, 17–33.

Rullkötter, J., Vuchev, V., Hinz, K., Winterer, E.L., Baumgartner, P.O., Bradshaw, M.L., Channel, J.E.T., Jaffrezo, M., Jansa, L.F., Leckie, R.M. and Moore, J.M. (1983). Potential deep sea petroleum source beds related to coastal upwelling. In Thiede, J. and Suess, E. (Eds.), *Coastal Upwelling, its Sedimentary Record, Part B: Sedimentary Records of Ancient Coastal Upwelling* (p. 467–483). Plenum Press.

Rumohr, H., Bonsdorff, E. and Pearson, T.H. (1996). Zoobenthic succession in Baltic sedimentary habitats. *Archive of Fishery and Marine Research*, 44, 179–214.

Ryan, W. and Pitman, W. (1998). *Noah's Flood: The New Scientific Discoveries about the Event that Changed History*. Simon & Schuster, New York, 320 p.

Ryan, W.B.F., Pitman, W.C., Major, C.O., Shimkus, K., Moskalenko, V., Jones, G.A., Dimitrov, P., Gorür, N., Sakinç, M. and Yüce, H. (1997). An abrupt drowning of the Black Sea shelf. *Mar. Geol.*, 138, 119–126.

Sagasti, G. (2005). Hemipelagic record of orbitally-induced dilution cycles in Lower Cretaceous sediments of the Neuquén Basin. In Veiga, G.D., Spalletti, L.A., Howell, J.A. and Schwarz, E. (Eds.), *The Neuquén Basin, Argentina: A Case Study in Sequence Stratigraphy and Basin Dynamics* (p. 231–250). Geological Society of London, Special Publications, v. 252.

Sageman, B.B. (1989). The benthic boundary biofacies model: Hartland Shale Member, Greenhorn Formation (Cenomanian), Western Interior, North America. *Palaeogeography, Palaeoclimatology, Palaeoecology*, 74, 87–110.

Sageman, B.B., Wignall, P.B. and Kauffman, E.G. (1991). Biofacies models for oxygen-deficient facies in epicontinental seas: Tool for paleoenvironmental analysis. In Einsele, G., Ricken, W., and Seilacher, A. (Eds.), *Cycles and Events in Stratigraphy* (p. 542–564). Springer-Verlag.

Sageman, B.B., Murphy, A.E., Werne, J.P., Ver Straeten, C.A., Hollander, D.J. and Lyons, T.W., (2003). A tale of shales: The relative roles of production, decomposition, and dilution in the accumulation of organic-rich strata, Middle-Upper Devonian, Appalachian basin. *Chem. Geol.*, 195, 229–273.

Santiago, M.F., Rauzi, R.S., Laffitte, G.A. and Alvarado, O.A. (2014). La Formación Vaca Muerta como objetivo exploratorio no convencional en la subcuenca de Picún Leufú. Neuquén,

Argentina. In *IX Congreso de Exploración y Desarrollo de Hidrocarburos, Simposio de Recursos No Convencionales* (p. 275–314). Mendoza, Argentina.

Sato, T., Taniguchi, K., Takagawa, T. and Masuda, F. (2011). Generation of tidal bedding in a circular flume experiment: Formation process and preservation potential of mud drapes. *Geo-Marine Letters*, 31, 101–108.

Sattler, F., Domínguez, R.F., Benoit, S., and Denis, M. (2018). Enclosure 1: Regional cross-section A-A'. In González, G., Vallejo, M.D., Kietzmann, D.A., Marchal, D., Desjardins, P.R., González Tomassini, F., Gómez Rivarola, L., Domínguez, R.F. and Fantín, M.A. (Eds.), *Regional Cross Section of the Vaca Muerta Formation, Integration of Seismic, Well Logs, Cores and Outcrops.* Special Publication of IAPG, Buenos Aires.

Savrda, C.E. and Bottjer, D.J. (1986). Trace-fossil model for reconstruction of paleo-oxygenation in bottom waters. *Geology*, 14, 3-6.

Savrda, C.E. and Bottjer, D.J. (1987). The exaerobic zone, a new oxygen-deficient marine biofacies. *Nature*, 327, 54–56.

Savrda, C.E. and Bottjer, D.J. (1989a). Anatomy and implications of bioturbated beds in" black shale" sequences; examples from the Jurassic Posidonienschiefer (southern Germany). *Palaios*, 4, 330–342.

Savrda, C.E. and Bottjer, D.J. (1989b). Trace fossil model for reconstructing oxygenation histories of ancient marine bottom waters: application to Upper Cretaceous Niobrara Formation, Colorado. *Palaeogeography, Palaeoclimatology, Palaeoecology*, 74, 49–74

Savrda, C.E. and Bottjer, D.J. (1991). Oxygen-related biofacies in marine strata: an overview and update. In Tyson, R.V. and Pearson, T.H. (Eds.), *Modern and Ancient Continental Shelf Anoxia* (p. 201–219). Geological Society, London, Special Publications, v. 58.

Savrda, C.E. and Ozalas, K. (1993). Preservation of mixed-layer ichnofabrics in oxygenation-event beds. *Palaios*, 8, 609–612.

Savrda, C.E., Bottjer, D.J. and Gorsline, D.S. (1984). Development of a comprehensive oxygen-deficient marine biofacies model: evidence from Santa Monica, San Pedro, and Santa Barbara Basins, California Continental Borderland. *AAPG Bulletin*, 68, 1179–1192.

Savrda, C.E., Krawinkel, H., McCarthy, F.M.G., McHugh, C.M.G., Olson, H.C. and Mountain, G. (2001). Ichnofabrics of a Pleistocene slope succession, New Jersey margin: Relations to climate and sea-level dynamics. *Palaeogeography, Palaeoclimatology, Palaeoecology*, 171, 41–61.

Schattner, U., Lobo, F.J., López-Quirós, A., dos Passos Nascimento, J.L. and de Mahiques, M.M. (2020). What feeds shelf-edge clinoforms over margins deprived of adjacent land sources? An example from southeastern Brazil. *Basin Research*, 32, 293–301.

Scherer, C.M., Mello, R.G., Ferronatto, J.P., Amarante, F.B., Reis, A.D., Souza, E.G. and Goldberg, K. (2020). Changes in prevailing surface-palaeowinds of western Gondwana during Early Cretaceous. *Cretaceous Research*, 116, 104598.

Schieber, J. (1986). The possible role of benthic microbial mats during the formation of carbonaceous shales in shallow Mid-Proterozoic basins. *Sedimentology*, 33, 521–536.

Schieber, J. (1994). Evidence for high-energy events and shallow-water deposition in the Chattanooga Shale, Devonian, central Tennessee, USA. *Sedimentary Geology*, 93, 193–208.

Schieber, J. (1999a). Distribution and deposition of mudstone facies in the Upper Devonian Sonyea Group of New York. *Journal of Sedimentary Research*, 69, 909–925.

Schieber, J. (1999b). Microbial mats in terrigenous clastics: The challenge of identification in the rock record. *Palaios*, 14, 3–12.

Schieber, J. (2003). Simple gifts and buried treasures—implications of finding bioturbation and erosion surfaces in black shales. *The Sedimentary Record*, 1, 4–8.

Schieber, J. (2007). Microbial mats on muddy substrates – Examples of possible sedimentary features and underlying processes. In J. Schieber, P.K. Bose, P.G. Eriksson, S. Banerjee, S. Sarkar, W. Altermann, O. Catuneanu (Eds.), *Atlas of Microbial Mat Features Preserved within the Siliciclastic Rock Record* (p. 117–134). Elsevier.

Schieber, J. (2011). Reverse engineering mother nature - Shale sedimentology from an experimental perspective. *Sedimentary Geology*, 238, 1–22.

Schieber, J. (2014). Traces in the dark—Sedimentary processes and facies gradients in the upper shale member of the Upper Devonian–Lower Mississippian Bakken Formation, Williston Basin, North Dakota, USA—Discusion. *Journal of Sedimentary Research*, 84, 837–838.

Schieber, J. (2016). Mud re-distribution in epicontinental basins - Exploring likely processes. *Marine and Petroleum Geology*, 71, 119–133.

Schieber, J., and Zimmerle, W. (1998). The history and promise of shale research. In Schieber, J., Zimmerle, W. and Sethi, P., (Eds.), *Shales and Mudstones (vol. 1): Basin Studies, Sedimentology and Paleontology* (p. 1–10). Schweizerbart'sche Verlagsbuchhandlung, Stuttgart.

Schieber, J., and Wilson, R.D. (2021). Burrows without a trace—How meioturbation affects rock fabrics and leaves a record of meiobenthos activity in shales and mudstones. *PalZ*, doi: 10.1007/s12542-021-00590-7.

Schieber, J. and Southard, J.B. (2009). Bedload transport of mud by floccule ripples—direct observation of ripple migration processes and their implications. *Geology*, 7, 483–486.

Schieber, J., Zimmerle, W. and Sethi, P.S. (1998). *Shales and Mudstones, I. Basin Studies, Sedimentology and Paleontology.* E. Schweizerbart'sche Verlagsbuchhandlung, Stuttgart, 384 p.

Schieber, J., Southard, J.B. and Thaisen, K.G. (2007). Accretion of mudstone beds from migrating floccule ripples. *Science*, 318, 1760–1763.

Schieber, J., Southard, J.B., Kissling, P., Rossman, B. and Ginsburg, R. (2013). Experimental deposition of carbonate mud from moving suspensions: importance of flocculation and implications for modern and ancient carbonate mud deposition. *J. Sediment. Res.*, 83, 1025–1031.

Schieber, J., Shao, X., Yawar, Z. and Liu, B. (in press). Cryptic burrow traces in black shales – a petrographic Rorschach test or the real thing?. *Sedimentology*, doi: 10.1111/sed.12870.

Schlager, W. (2005). *Carbonate Sedimentology and Sequence Stratigraphy*. SEPM, Concepts in Sedimentology and Paleontology, v. 8, 200 pp.

Schlirf, M. (2000). Upper Jurassic trace fossils from the Boulonnais (northern France). *Geologica et Palaeontologica*, 34, 145–213.

Schlirf, M. and Uchman, A. (2005). Revision of the ichnogenus *Sabellarifex* Richter, 1921 and its relationship to *Skolithos* Haldeman, 1840 and *Polykladichnus* Fürsich, 1981. *Journal of Systematic Palaeontology*, 3, 115–131.

Schlirf, M., Uchman, A. and Kümmel, M. (2001). Upper Triassic (Keuper) non-marine trace fossils from the Haßberge area (Franconia, south-eastern Germany). *Paläontologische Zeitschrift*, 75, 71–96.

Scott, E. and Bouma, A.H. (2004). *Depositional Processes and Reservoir Characteristics of Siltstones, Mudstones and Shales*. SEPM Miscellaneous Publication, v. 2, CD-ROM.

Seike, K., Shiino, Y. and Suzuki, Y. (2014). *Crininicaminus giberti* isp. nov.: Tubular trace fossil armored with crinoid stem plates from the Upper Permian Kamiyasse Formation, northeastern Japan. *Spanish Journal of Palaeontology*, 29, 45–50.

Seilacher, A. (1967). Bathymetry of trace fossils. *Marine Geology*, 5, 413–428.

Seilacher, A.T., and Seilacher, E. (1994). Bivalvian trace fossils: a lesson from actuopaleontology. *Courier Forschungs-Institute Senckenberg*, 169, 5–15.

Sergeeva, N.G. and Zaika, V.E. (2013). The Black Sea meiobenthos in permanently hypoxic habitat. *Acta Zoologica Bulgarica*, 65, 139–150.

Shanmugam, G. (2006). *Deep-Water Processes and Facies Models: Implications for Sandstone Petroleum Reservoirs.* Elsevier, Amsterdam, 476 p.

Shanmugam, G. (2013). Comment on "Internal waves, an under-explored source of turbulence events in the sedimentary record" by L. Pomar, M. Morsilli, P. Hallock, and B. Bádenas [Earth-Science Reviews, 111 (2012), 56–81]. *Earth-Science Reviews*, 116, 195–205.

Shanmugam, G. (2017). The contourite problem. In Mazumder, R. (Ed.), *Sediment Provenance: Influences on Compositional Change from Source to Sink* (p. 183–254). Elsevier, Cambridge.

Shanmugam, G. (2018). Comment on “Ichnological analysis of contourites: Past, present and future” by Francisco J. Rodríguez-Tovar and F. Javier Hernández-Molina [EarthScience Reviews, 182 (2018), 28–41]. *Earth-Science Reviews*, 184, 46–49.

Shanmugam, G., Spalding, T.D. and Rofheart, D.H. (1993a). Traction structures in deep-marine, bottom-current-reworked sands in the Pliocene and Pleistocene, Gulf of Mexico. *Geology*, 21, 929–932.

Shanmugam, G., Spalding, T.D. and Rofheart, D.H. (1993b). Process sedimentology and reservoir quality of deep-marine bottom- current reworked sands (sandy contourites): an example from the Gulf of Mexico. *AAPG Bulletin*, 77, 1241–1259.

Shapiro, G.I., Huthnance, J.M. and Ivanov, V.V. (2003). Dense water cascading off the continental shelf. *Journal of Geophysical Research*, 108, 3390.

Shinn, E. A. (1973). Sedimentary Accretion along the Leeward, SE Coast of Qatar Peninsula, Persian Gulf. In B.H. Purser (Ed.) *The Persian Gulf* (p. 199–210). Springer-Verlag.

Sholkovitz, E. and Soutar, A. (1975). Changes in the composition of the bottom water of the Santa Barbara Basin: effect of turbidity currents. *Deep-sea Research*, 22, 13–21.

Šimo, V. and Tomašových, A. (2013). Trace-fossil assemblages with a new ichnogenus in “spotted” (Fleckenmergel—Fleckenkalk) deposits: a signature of oxygen-limited benthic communities. *Geologica Carpathica*, 64, 355–374.

Singh, P., Slatt, R.M. and Coffey, W. (2008). Barnett Shale - unfolded: sedimentology, sequence stratigraphy, and regional mapping. *Gulf Coast Association of Geological Societies Transactions*, 58, 777–795.

Sivkov, V., Gorbatskiy, V., Kuleshov, A. and Zhurov, Y. (2002). Muddy contourites in the Baltic Sea: an example of a shallow-water contourite system. In Stow, D.A.V., Pudsey, C.J., Howe, J.A., Faugères, J.-C. and Viana, A.R. (Eds.), *Deep-Water Contourite Systems: Modern Drifts and Ancient Series, Seismic and Sedimentary Characteristics* (p. 121–136). Geological Society of London Memoirs, London, v. 22.

Smith, D.B. (1979). Rapid marine transgressions and regressions of the Upper Permian Zechstein Sea. *J. Geol. Soc. London*, 136, 155–156.

Smith, C.R., Levin, L.A., Hoover, D.J., McMurtry, G. and Gage, J.D. (2000). Variations in bioturbation across the oxygen minimum zone in the northwest Arabian Sea. *Deep Sea Research Part II: Topical Studies in Oceanography*, 47, 227–257.

Snedden, J.W. and Nummedal, D. (1990). Coherence of surf zone and shelf current flow on the Texas (USA) coastal margin: implications for interpretation of paleo-current measurements in ancient coastal sequences. *Sed. Geol.*, 67, 221–236.

Snedden J.W. and Dalrymple R.W. (1999). Modern shelf sand bodies: from historical perspective to a unified theory for sand body genesis and evolution. In Bergman, K.M., Snedden, J.D., (Eds.), *Isolated Shallow Marine Sand Bodies: Sequence Stratigraphic Analysis and Sedimentologic Interpretation* (p. 13–28). SEPM Spec. Publ., v. 64.

Soutar, A. and Crill, P.A. (1977). Sedimentation and climatic patterns in the Santa Barbara Basin during the 19th and 20th centuries. *Geological Society of America Bulletin*, 88, 1161–1172.

Spalletti, L.A. and Colombo Piñol, F. (2005). From alluvial fan to playa: An Upper Jurassic ephemeral fluvial system, Neuquen Basin, Argentina. *Gondwana Res.*, 8, 363–383.

Spalletti, L.A. and Veiga, G.D. (2007). Variability of continental depositional systems during lowstand sedimentation: An example from the Kimmeridgian of the Neuquén Basin, Argentina. *Lat. Am. J. Sedimentol. Basin Anal.*, 14, 85–104.

Spalletti, L.A., Gasparini, Z., Veiga, G., Schwarz, E., Fernandez, M. and Matheos, S. (1999). Facies anóxicas, procesos deposicionales y herpetofauna de la rampa marina Titoniano-Berriasiana en la Cuenca Neuquina (Yesera del Tromen), Neuquén, Argentina. *Revista Geológica de Chile*, 26, 109–123.

Spalletti, L.A., Franzese, J.R., Matheos, S.D. and Schwarz, E. (2000). Sequence stratigraphy of a tidally dominated carbonate-siliciclastic ramp; the Tithonian-Early Berriasian of the Southern Neuquén Basin, Argentina. *Journal of the Geological Society of London*, 157, 433–446.

Spalletti, L.A., Arregui, C.D. and Veiga, G.D. (2011). La Formación Tordillo y equivalentes (Jurásico Tardío) en la cuenca Neuquina. In Leanza, H.A., Arregui, C.D., Carbone, O.C., Danieli, J.C. and Vallés, J. (Eds.), *Relatorio del XVIII Congreso Geológico Argentino* (p. 99–112). Asociación Geológica Argentina, Buenos Aires.

Spalletti, L.A., Schwarz, E. and Veiga, G.D. (2014). Geoquímica inorgánica como indicador de procedencia y ambiente sedimentario en sucesiones de lutitas negras: los depósitos transgresivos titonianos (Formación Vaca Muerta) de la Cuenca Neuquina, Argentina. *Andean Geology*, 41, 401–435.

Spalletti, L.A., Remírez, M.N. and Sagasti, G. (2019). Geochemistry of aggradational-Progradational sequence sets of the Upper Jurassic–Lower Cretaceous Vaca Muerta shales (Añelo area, Neuquén Basin, Argentina): Relation to changes in accommodation and marine anoxia. *Journal of South American Earth Sciences*, 93, 495–509.

Sparks, R.S.J., Brazier, S., Huang, T.C. and Muerdter, D. (1983). Sedimentology of the Minoan deep-sea tephra layer in the Aegean and Eastern Mediterranean. *Marine Geology*, 54, 131–167.

Sparks, R.S.J., Bonnecaze, R.T., Huppert, H.E., Lister, J.R., Hallworth, M.A., Mader, H., Phillips, J. (1993). Sediment-laden gravity currents with reversing buoyancy. *Earth Planet. Sci. Lett.*, 114, 243–257.

Stanley, D.J. (1993), Model for turbidite-to-contourite continuum and multiple process transport in deep marine settings: examples in the rock record. *Sedimentary Geology*, 82, 241–255.

Steel, R. and Olsen, T. (2002). Clinoforms, clinoform trajectories and deepwater sands. In *22nd Annual Gulf Coast Section* (p. 367–380).

Steel, E., Simms, A.R., Warrick, J. and Yokoyama, Y. (2016). Highstand shelf fans: The role of buoyancy reversal in the deposition of a new type of shelf sand body. *Geological Society of America Bulletin*, 128, 1717–1724.

Steele, R.P. (1983). Longitudinal draa in the Permian Yellow Sands of north-fast England. In M.E. Brookfield and T.S. Ahlbrandt (Eds.), *Eolian Sediments and Processes* (p. 543–550). Developments in Sedimentology, v. 38.

Sternberg, R.W., Cacchione, D.A., Paulso, B., Kineke, G.C. and Drakez, D.E. (1996). Observations of sediment transport on the Amazon subaqueous delta. *Continental Shelf Research*, 16, 697–715.

Stipanicic, P.N. (1969). El avance en los conocimientos del Jurásico argentino a partir del esquema de Groeber. *Revista de la Asociación Geológica Argentina*, 24, 367-388.

Stipanicic, P. N., Rodrigo, F., Baulies, O.L., Martínez, C.G. (1968). Las Formaciones presenonianas en el denominado Macizo Nordpatagónico y regiones adyacentes. *Rev. Asoc. Geol. Argentina*, 23, 67–98.

Stow, D.A.V. and Lovell, J.P.B. (1979), Contourites: Their recognition in modern and ancient sediments. *Earth Science Reviews*, 14, 251–291.

Stow, D.A.V. and Bowen, A.J. (1980). A physical model for the transport and sorting of fine-grained sediment by turbidity currents. *Sedimentology*, 27, 31–46.

Stow, D.A.V. and Shanmugam, G. (1980). Sequence of structures in fine-grained turbidites: Comparison of recent deep-sea and ancient flysch sediments. *Sedimentary Geology*, 25, 23–42.

Stow, D.A.V. and Piper, D.J.W. (1984). Deep-water fine-grained sediments: facies models. In Stow, D.A.V., Piper, D.J.W. (Eds.), *Fine-Grained Sediments: Deep-Water Processes and Facies* (p. 611–646). Geological Society of London Special Publication, v. 15.

Stow, D.A.V. and Faugères, J.-C. (2008). Contourite facies and the facies model. In Rebesco, M. and Camerlenghi, A. (Eds.), *Contourites* (p. 223–256). Developments in Sedimentology, v. 60.

Stow, D. and Smillie, Z. (2020). Distinguishing between deep-water sediment facies: Turbidites, contourites and hemipelagites. *Geosciences*, 10, 68.

Stow, D.A.V., Faugères, J.-C., Viana, A.R. and Gonthier, E. (1998). Fossil contourites: A critical review. *Sedimentary Geology*, 115, 3–31.

Stratford, K., Williams, R.G. and Myers, P.G. (2000). Impact of the circulation on sapropel formation in the eastern Mediterranean. *Global Biogeochemical Cycles*, 14, 683–695.

Strohmenger, C.J., Al-Mansoori, A., Al-Jeelani, O., AlShamry, A., Al-Hosani, I., Al-Mehsin, K. and Shebl, H. (2010). The sabkha sequence at Mussafah Channel (Abu Dhabi, United Arab Emirates): Facies stacking patterns, microbial-mediated dolomite and evaporite overprint. *GeoArabia*, 15, 49–90.

Strömbäck, A. and Howell, J.A. (2002). Predicting distribution of remobilized aeolian facies using sub-surface data: the Weissliegend of the UK Southern North Sea. *Petroleum Geoscience*, 8, 237–249.

Strömbäck, A., Howell, J.A. and Veiga, G.D. (2005). The transgression of an erg - sedimentation and reworking/soft-sediment deformation of aeolian facies: The Cretaceous Troncoso Member, Neuquén Basin, Argentina. In G.D. Veiga, L.A. Spalletti, J.A. Howell, and E. Schwarz (Eds.), *The Neuquén Basin, Argentina: A Case Study in Sequence Stratigraphy and Basin Dynamics* (p. 163–183). Geological Society, London, Special Publications, v. 252.

Suess, E. (1980). Particulate organic carbon flux in the oceans—surface productivity and oxygen utilization. *Nature*, 288, 260–263.

Swenson, J.B., Paola, C., Pratson, L., Voller, V.R., Murray, A.B. (2005). Fluvial and marine controls on combined subaerial and subaqueous delta progradation: Morphodynamic modeling of compound-clinoform development. *J. Geophys. Res. Earth Surf.*, 110, 1–16.

Swift, D.J.P. (1968). Coastal erosion and transgressive stratigraphy. *J. Geol.*, 76, 444–456.

Swift, D.J.P., Han, G., Vincent, C.E. (1986). Fluid processes and sea-floor response on a modern storm-dominated shelf: middle Atlantic Shelf of North America. Part I: the storm-current regime. In Knight, R.J., Ross Mclean, J., (Eds.), *Shelf Sands and Sandstones* (p. 99–119). AAPG Memoir, v. 11.

Szczuciński, W., Jagodziński, R., Hanebuth, T. J. J., Stattegger, K., Wetzel, A., Mitręga, M., Unverricht, D., and Van Phach, P. (2013). Modern sedimentation and sediment dispersal pattern on the continental shelf off the Mekong River delta, South China Sea. *Global Planetary Change*, 110, 195–213.

Taghon, G.L. and Greene, R.R. (1992). Utilization of deposited and suspended particulate matter by benthic “interface” feeders. *Limnology and Oceanography*, 37, 1370–1391.

Talling, P.J. (2014). On the triggers, resulting flow types and frequencies of subaqueous sediment density flows in different settings. *Marine Geology*, 352, 155–182.

Tanner, W.F. (1967). Ripple mark indices and their uses. *Sedimentology*, 9, 89–104.

Tanner, W.F. (1970). Triassic-Jurassic lakes in New Mexico. *Mt. Geol.*, 7, 281–289.

Taylor, A.M. and Goldring, R. (1993). Description and analysis of bioturbation and ichnofabric. *Journal of the Geological Society*, 150, 141–148.

Tenaglia, M. R., 2020, Depositional Partitioning of Organic Material in a Mixed Carbonate-Siliciclastic System, Controls on Production, Preservation and Dilution: The Vaca Muerta Formation, Neuquén Argentina [Ph.D Thesis]: University of Miami, Coral Gables, USA, 160 pp.

Thistle, D., Yingst, J.Y. and Fauchald, K. (1985). A deep-sea benthic community exposed to strong near-bottom currents on the Scotian Rise (western Atlantic). *Marine Geology*, 66, 91–112.

Thistle, D., Ertman, S.C. and Fauchald, K. (1991). The fauna of the HEBBLE site: patterns in standing stock and sediment-dynamic effects. *Marine Geology*, 99, 413–422.

Thomas, I.M. (1972). Action of the gut in Saccoglossus otagoensis (Hemichordata: Enteropneusta). *New Zealand Journal of Marine and Freshwater Research*, 6, 560–569.

Thompson, J.B., Mullins, H.T., Newton, C.R., and Vercoutere, T.L. (1985). Alternative biofacies model for dysaerobic communities. *Lethaia*, 18, 167–179.

Trabucho-Alexandre, J., Dirkx, R., Veld, H., Klaver, G. and de Boer, P.L. (2012). Toarcian black shales in the Dutch Central Graben: Record of energetic, variable depositional conditions during an Oceanic Anoxic Event. *Journal of Sedimentary Research*, 82, 104–120.

Traykovski, P., Geyer, W.R., Irish, J.D., and Lynch, J.F. (2000). The role of wave-induced density-driven fluid mud flows for cross-shelf transport on the Eel River continental shelf. *Continental Shelf Research*, 20, 2113–2140.

Tucholke, B.E. (2002). The Greater Antilles Outer Ridge: development of a distal sedimentary drift by deposition of fine-grained contourites. In Stow, D.A., Pudsey, C.J., Howe, J.A., Faugeres, J.-C. and Viana, A.R. (Eds.), *Deep-Water Contourite Systems: Modern Drifts and Ancient Series, Seismic and Sedimentary Characteristics* (p. 39–55). The Geological Society of London, v. 22.

Tucker, M. E. and Wright, V. P. (1990). *Carbonate Sedimentology*. John Wiley & Sons, 482 p.

Tunik, M., Folguera, A., Naipauer, M., Pimentel, M. and Ramos, V.A. (2010). Early uplift and orogenic deformation in the Neuquén Basin: Constraints on the Andean uplift from U-Pb and Hf isotopic data of detrital zircons. *Tectonophysics*, 489, 258–273.

Turner, J.T. (2002). Zooplankton fecal pellets, marine snow and sinking phytoplankton blooms. *Aquatic Microbial Ecology*, 27, 57–102.

Tyson, R.V. (1995). *Sedimentary Organic Matter, Organic Facies and Palynofacies*. Chapman and Hall, 615 p.

Tyson, R. V. (2005). The "productivity versus preservation" controversy: cause, flaws, and resolution. In Harris, N.B., (Ed.), *The Deposition of Organic-Carbon-Rich Sediments: Models, Mechanisms, and Consequences* (p. 17–33). SEPM Special Publication, v. 82.

Tyson, R.V. and Pearson, T.H. (1991). Modern and ancient continental shelf anoxia: an overview. In Tyson, R.V. and Pearson, T.H. (Eds.), *Modern and Ancient Continental Shelf Anoxia* (p. 1–24). Geological Society, London, Special Publications, v. 58.

Tyszka, J. (1994). Paleoenvironmental implications from ichnological and microfaunal analyses of Bajocian spotty carbonates, Pieniny Klippen Belt, Polish Carpathians. *Palaios*, 9, 175–187.

Uchman, A. (1995). Taxonomy and palaeoecology of flysch trace fossils: the Marnoso arenacea formation and associated facies (Miocene, Northern Apennines, Italy). *Beringeria*, 15, 3–115.

Uchman, A., and Wetzel, A. (2011). Deep-sea ichnology: The relationships between depositional environments and endobenthic organisms. In Hüneke, H., and Mulder, T. (Eds.), *Deep-Sea Sediments* (p. 517–556). Developments in Sedimentology, v. 63.

Uchman, A. and Wetzel, A. (2017). Hidden subsurface garden on own faeces: the trace fossil Tubulichnium rectum (Fischer-Ooster, 1858) from the Cretaceous-Palaeogene deep-sea sediments. *Palaeontologia Electronica*, 20.2.40A.

Uchman, A., Bąk, K. and Rodríguez-Tovar, F.J. (2008). Ichnological record of deep-sea palaeoenvironmental changes around the Oceanic Anoxic Event 2 (Cenomanian–Turonian boundary): an example from the Barnasiówka section, Polish Outer Carpathians. *Palaeogeography, Palaeoclimatology, Palaeoecology*, 262, 61–71.

Uchman, A., Rodríguez-Tovar, F.J., Machaniec, E. and Kędzierski, M. (2013). Ichnological characteristics of Late Cretaceous hemipelagic and pelagic sediments in a submarine high around the OAE-2 event: A case from the Rybie section, Polish Carpathians. *Palaeogeography, Palaeoclimatology, Palaeoecology*, 370, 222–231.

Uliana, M.A., Legarreta, L., Laffitte, G.A., Villar, H. (1999). Estratigrafía y geoquímica de las facies generadoras de hidrocarburos en las Cuencas Petrolíferas de Argentina. In *4º Congreso de Exploración y Desarrollo de Hidrocarburos*. *Simposio de Sistemas Petroleros de las Cuencas Argentinas* (Actas CD ROM). Mar del Plata, Argentina.

Ulses, C., Estournel, C., De Madron, X.D. and Palanques, A. (2008). Suspended sediment transport in the Gulf of Lions (NW Mediterranean): Impact of extreme storms and floods. *Continental Shelf Research*, 28, 2048–2070.

Urgeles, R., Cattaneo, A., Puig, P., Liquete, C., De Mol, B., Amblàs, D., Sultan, N. and Trincardi, F. (2011). A review of undulated sediment features on Mediterranean prodeltas: distinguishing sediment transport structures from sediment deformation. *Marine Geophysical Research*, 32, 49–69.

Vallejo, M.D., González Tomassini, F., Fantín, M., Reijenstein, H., Cuervo, S., and Crousse, L. (2018). Chapter 19: El Trapial. In González, G., Vallejo, M.D., Kietzmann, D.A., Marchal, D., Desjardins, P.R., González Tomassini, F., Gómez Rivarola, L., Domínguez, R.F. and Fantín, M.A. (Eds.), *Regional Cross Section of the Vaca Muerta Formation, Integration of Seismic, Well Logs, Cores and Outcrops* (p. 205–218). Special Publication of IAPG, Buenos Aires.

Van West, F.P. (1972). Trapping mechanism of Minnelusa oil accumulations, Northeastern Powder River basin, Wyoming. *Mt. Geol.*, 9, 3–20.

Vandorpe, T.P., van Rooij, D., Stow, D.A.V. and Henriet, J.P. (2011). Pliocene to Recent shallow-water contourite deposits on the shelf and shelf edge off south-western Mallorca, Spain. *Geo-Marine Letters*, 31, 391–403.

Varban, B.L. and Plint, G. (2008). Palaeoenvironments, palaeogeography, and physiography of a large, shallow, muddy ramp: Late Cenomanian-Turonian Kaskapau Formation, Western Canada foreland basin. *Sedimentology*, 55, 201–233.

Veiga, G.D. and Spalletti, L.A. (2007). The Upper Jurassic (Kimmeridgian) fluvial-aeolian systems of the southern Neuquén Basin, Argentina. *Gondwana Res.*, 11, 286–302.

Vennari, V. V., Lescano, M., Naipauer, M., Aguirre-Urreta, M.B., Concheyro, A., Schaltegger, U., Armstrong, R., Pimentel, M. and Ramos, V.A. (2014). New constraints on the Jurassic-Cretaceous boundary in the High Andes using high-precision U-Pb data. *Gondwana Res.*, 26, 374–385.

Verdicchio, G. and Trincardi, F. (2008a). Shallow-water contourites. In Rebesco, M. and Camerlenghi, A. (Eds.), *Contourites* (p. 409–433). Developments in Sedimentology, v. 60.

Verdicchio, G. and Trincardi, F. (2008b). Mediterranean shelf-edge muddy contourites: Examples from the Gela and South Adriatic basins. *Geo-Marine Letters*, 28, 137–151.

Verdicchio, G., Trincardi, F. and Asioli, A. (2007). Mediterranean bottom-current deposits: an example from the Southwestern Adriatic Margin. In Viana, A.R and Rebesco, M. (Eds.), *Economic and Palaeoceanographic Significance of Contourite Deposits* (p. 199–224). Geological Society of London, Special Publication, v. 276.

Vergani, G.D., Tankard, A.J., Belotti, H.J. and Welsink, H.J. (1995). Tectonic evolution and paleogeography of the Neuquén Basin, Argentina. In A.J. Tankard, R. Suarez Soruco and H.J. Welsink (Eds.), *Petroleum Basins of South America* (p. 383–402). AAPG Memoir, v. 62.

Viana, A.R., Faugères, J.C., Kowsmann, R.O., Lima, J.A.M., Caddah, L.F.G. and Rizzo, J.G. (1998). Hydrology, morphology and sedimentology of the Campos continental margin, offshore Brazil. *Sedimentary Geology*, 115, 133–157.

Viana, A.R., De Almeida, W. and De Almeida, C.W. (2002). Upper slope sands: Late Quaternary shallow-water sandy contourities of Campos Basin, SW Atlantic Margin. In Stow, D.A.V, Pudset, C.J., Howe, J.A., Faugères, J.-C. and Viana, A.R. (Eds.), *Deep-Water Contourite Systems: Modern Drifts and Ancient Series* (p. 261–270). Geological Society of London Memoirs, London, v. 22.

Vincelette, R.R. and Chittum, W.E. (1981). Exploration for oil accumulations in Entrada Sandstone, San Juan Basin, New Mexico. *AAPG Bulletin*, 65, 2546–2570.

Virtasalo, J.J., Leipe, T., Moros, M. and Kotilainen, A.T. (2011). Physicochemical and biological influences on sedimentary-fabric formation in a salinity and oxygen-restricted semi-enclosed sea: Gotland Deep, Baltic Sea. *Sedimentology*, 58, 352–375.

Volkheimer, W., Rauhut, O.W., Quattrocchio, M.E. and Martinez, M.A. (2008). Jurassic paleoclimates in Argentina, a review. *Revista de la Asociación Geológica Argentina*, 63, 549–556.

Wagner, T., Hofmann, P. and Flögel, S. (2013). Marine black shale deposition and Hadley Cell dynamics: A conceptual framework for the Cretaceous Atlantic Ocean. *Marine and Petroleum Geology*, 43, 222–238.

Waite, R. and Strasser, A. (2011). A comparison of recent and fossil large, high-spired gastropods and their environments: The Nopparat Thara tidal flat in Krabi, South Thailand, versus the Swiss Kimmeridgian carbonate platform. *Facies*, 57, 223–248.

Wang, H., Ma, F., Tong, X., Liu, Z., Zhang, X., Wu, Z., Li, D., Wang, B., Xie, Y. and Yang, L. (2016). Assessment of global unconventional oil and gas resources. *Pet. Explor. Dev.*, 43, 925–940.

Warrick, J.A. and Milliman, J.D. (2003). Hyperpycnal sediment discharge from semiarid southern California rivers: Implications for coastal sediment budgets. *Geology*, 31, 781–784.

Warrick, J.A., Simms, A.R., Ritchie, A., Steel, E., Dartnell, P., Conrad, J.E., Finlayson, D.P. (2013). Hyperpycnal plume-derived fans in the Santa Barbara Channel, California. *Geophys. Res. Lett.*, 40, 2081–2086.

Weaver, C.E. (1931). *Paleontology of the Jurassic and Cretaceous of West Central Argentina.* Memoirs of the University of Washington, v. 1, 469 p.

Weaver, C.E. (1989). *Clays, Muds, and Shales*. Elsevier, New York, 819 p.

Wells, M.R., Allison, P.A., Hampson, G.J., Piggott, M.D. and Pain, C.C. (2005). Modelling ancient tides: the Upper Carboniferous epi-continental seaway of Northwest Europe. *Sedimentology*, 52, 715–735.

Westphal, H., Munnecke, A., Böhm, F. and Bornholdt, S. (2008). Limestone–marl alternations in epeiric sea settings–witnesses of environmental changes or diagenesis?. *Special Paper–Geological Association of Canada*, 389, 389–406.

Wetzel, A. (1991). Ecologic interpretation of deep-sea trace fossil communities. *Palaeogeography, Palaeoclimatology, Palaeoecology*, 85, 47–69.

Wetzel, A. (2009). The preservation potential of ash layers in the deep-sea: The example of the 1991-Pinatubo ash in the South China Sea. *Sedimentology*, 56, 1992–2009.

Wetzel, A. (2010). Deep-sea ichnology: observations in modern sediments to interpret fossil counterparts. *Acta Geologica Polonica*, 60, 125–138.

Wetzel, A. and Werner, F. (1980). Morphology and ecological significance of *Zoophycos* in deep-sea sediments off NW Africa. *Palaeogeography, Palaeoclimatology, Palaeoecology*, 32, 185–212.

Wetzel, A. and Bromley, R.G. (1996). The ichnotaxon *Tasselia ordamensis* and its junior synonym *Caudichnus annulatus*. *Journal of Paleontology*, 70, 523–526.

Wetzel, A. and Uchman, A. (1998). Biogenic sedimentary structures in mudstones - an overview. In J. Schieber, W. Zimmerle and P. Sethi (Eds.), *Shales and Mudstones I* (p. 351–369). Schweizerbart, Stuttgart.

Wetzel, A. and Allia, V. (2000). The significance of hiatus beds in shallow-water mudstones: an example from the Middle Jurassic of Switzerland. *Journal of Sedimentary Research*, 70, 170–180.

Wetzel, A., Werner, F. and Stow, D.A.V. (2008). Bioturbation and biogenic sedimentary structures in contourites. In Rebesco, M. and Camerlenghi, A. (Eds.), *Contourites* (p. 183–202). Developments in Sedimentology, v. 60.

Wetzel, A., Tjallingii, R. and Wiesner, M.G. (2011). Bioturbational structures record environmental changes in the upwelling area off Vietnam (South China Sea) for the last 150,000 years. *Palaeogeography, Palaeoclimatology, Palaeoecology*, 311, 256–267.

Wetzel, A., Szczygielski, A., Unverricht, D. and Stattegger, K. (2017). Sedimentological and ichnological implications of rapid Holocene flooding of a gently sloping mud-dominated

incised valley – an example from the Red River (Gulf of Tonkin). *Sedimentology*, 64, 1173–1202.

Wheatcroft, R.A., Smith, C.R. and Jumars, P.A. (1989). Dynamics of surficial trace assemblages in the deep sea. *Deep Sea Research Part A, Oceanographic Research Papers*, 36, 71–91.

Wheatcroft, R.A., Wiberg, P.L., Alexander, C.R., Bentley, S.J., Drake, D.E., Harris, C.K. and Ogston, A.S. (2007). Post-depositional alteration and preservation of sedimentary strata. In Nittrouer, C.A., Austin, J.A., Field, M.E., Kravitz, J.H., Syvitski, J.P.M., Wiberg, P.L. (Eds.), *Continental Margin Sedimentation: From Sediment Transport to Sequence Stratigraphy* (p. 101–155). Special Publication of the International Association of Sedimentologists, v. 37.

Whitham, A.G. (1993). Facies and depositional processes in an Upper Jurassic to Lower Cretaceous pelagic sedimentary sequence, Antarctica. *Sedimentology*, 40, 331–349.

Wignall, P.B. (1991). Dysaerobic trace fossils and ichnofabrics in the Upper Jurassic Kimmeridge Clay of southern England. *Palaios*, 6, 264–270.

Wignall, P.B. (1993). Distinguishing between oxygen and substrate control in fossil benthic assemblages. *Journal of the Geological Society*, 150, 193–196.

Wignall, P.B. and Myers, K.J. (1988). Interpreting benthic oxygen levels in mudrocks: a new approach. *Geology*, 16, 452–455.

Wikander, P.B. (1981). Quantitative aspects of deposit feeding in Abra nitida (Müller) and A. longicallus (Scacchi) (Bivalvia, Tellinacea). *Sarsia*, 66, 35–48.

Williams, H.D., Burgess, P.M., Wright, V.P., Della Porta, G., Granjeon, D. (2011). Investigating Carbonate Platform Types: Multiple Controls and a Continuum of Geometries. *J. Sediment. Res.*, 81, 18–37.

Wilson, P.A. and Roberts, H.H. (1995). Density cascading; off-shelf sediment transport, evidence and implications, Bahama Banks. *Journal of Sedimentary Research*, 65, 45–56.

Wilson, R.D. and Schieber, J. (2014). Muddy prodeltaic hyperpycnites in the Lower Genesee Group of Central New York, USA: Implications for mud transport in epicontinental seas. *Journal of Sedimentary Research*, 84, 866–874.

Wilson, R.D. and Schieber, J. (2015). Sedimentary facies and depositional environment of the Middle Devonian Geneseo Formation of New York, USA. *Journal of Sedimentary Research*, 85, 1393–1415.

Witzke, B.J. (1987). Models for circulation patterns in epicontinental seas applied to Paleozoic facies of North America craton. *Paleoceanography*, 2, 229–248.

Wright, V.P. (1992). A revised classification of limestones. *Sediment. Geol.*, 76, 177–185.

Wright, L.D. (2012). Recent advances in understanding continental shelf sediment transport. In Li, M.Z, Sherwood, C.R., Hill, P.R. (Eds.), *Sediments, Morphology and Sedimentary Processes on Continental Shelves* (p. 159–172). International Association of Sedimentologists, Special Publication, v. 44.

Wright, A.L.D. and Nittrouer, C.A. (1995). Dispersal of river sediments in coastal seas: six contrasting cases. *Estuaries*, 18, 494–508.

Wright, L.D. and Friedrichs, C.T. (2006). Gravity-driven sediment transport on continental shelves: A status report. *Cont. Shelf Res.*, 26, 2092–2107.

Wright, L.D., Friedrichs, C.T., Kim, S.C. and Scully, M.E. (2001). Effects of ambient currents and waves on gravity-driven sediment transport on continental shelves. *Marine Geology*, 175, 25–45.

Xiang, Y., Feng, Q., Shen, J. and Zhang, N. (2013). Changhsingian radiolarian fauna from Anshun of Guizhou, and its relationship to TOC and paleo-productivity. *Science China Earth Sciences*, 56, 1334–1342.

Yanko-Hombach, V., Gilbert, A.S., Panin, N. and Dolukhanov, P.M. (2007). *The Black Sea Flood Question: Changes in Coastline, Climate and Human Settlement*. Springer, Dordrecht, The Netherlands, 971 p.

Yawar, Z. and Schieber, J. (2017). On the origin of silt laminae in laminated shales. *Sedimentary Geology*, 360, 22–34.

Yokoyama, Y., De Deckker, P., Lambeck, K., Johnston, P. and Fifield, L. (2001). Sea-level at the Last Glacial Maximum: evidence from northwestern Australia to constrain ice volumes for oxygen isotope stage 2. *Palaeogeogr. Palaeoclimatol. Palaeoecol.*, 165, 281–297.

Yose, L.A. and Heller, P.L. (1989). Sea-level control of mixed-carbonate-siliciclastic, gravity-flow deposition: lower part of the Keeler Canyon Formation (Pennsylvanian), southeastern California. *Geological Society of America Bulletin*, 101, 427–439.

Zaika, V. and Sergeeva, N. (2012). Deep-water benthic polychaetes (*Vigtorniella zaikai* and *Protodrilus* sp.) in the Black Sea as indicators of the hydrogen sulfide zone boundary. *Vestnik zoologii*, 46, 19–27.

Zanettini, J.C.M. (1979). Geología de la comarca de Campana Mahuida (Provincia del Neuquén). *Rev. Asoc. Geol. Argentina*, 34, 61–68.

Zatoń, M. and Bond, D.P. (2016). Insight into tube-building behaviour and palaeoecology of some agglutinating worms from the Upper Devonian of Nevada, USA. *Palaeogeography, Palaeoclimatology, Palaeoecology*, 445, 138–146.

Zavala, C.A. and Freije, H. (2002). Cuñas clásticas jurásicas vinculadas a la Dorsal de Huíncul. Un ejemplo del area de Picun Leufu. Cuenca Neuquina, Argentina. In *V Congreso de Exploración y Desarrollo de Hidrocarburos* (Actas CD). Mar del Plata, Argentina.

Zavala, C.A. and Arcuri, M. (2016). Intrabasinal and extrabasinal turbidites: Origin and distinctive characteristics. *Sediment. Geol.*, 337, 36–54.

Zavala, C.A., Maretto, H. and Di Meglio, M. (2005). Hierarchy of bounding surfaces in aeolian sandstones of the Jurassic Tordillo Formation (Neuquén Basin, Argentina). *Geol. Acta*, 3, 133–145.

Zavala, C.A., Lampe, J.M.M., Fernández, M., Di Meglio, M., Arcuri, M. (2008). El diacronismo entre las formaciones Tordillo y Quebrada del Sapo (Kimeridgiano) en el sector sur de la cuenca Neuquina. *Rev. la Asoc. Geol. Argentina*, 63, 754–765.

Zavala, C.A., Arcuri, M., Di Meglio, M., Gamero Diaz, H., Contreras, C. (2011). A Genetic Facies Tract for the Analysis of Sustained Hyperpycnal Flow Deposits. In Slatt, R.M., Zavala, C.A. (Eds.), *Sediment Transfer from Shelf to Deep Water-Revisiting the Delivery System* (p. 31–51). AAPG Studies in Geology, v. 61.

Zavala, C.A., Arcuri, M. and Blanco Valiente, L. (2012). The importance of plant remains as diagnostic criteria for the recognition of ancient hyperpycnites. *Rev. Paleobiol. Vol. spec.*, 11, 457–469.

Zavala, C., Arcuri, M., Di Meglio, M., Zorzano, A., Otharán, G., Irastorza, A. and Torresi, A. (in press). Deltas: a new classification expanding Bates's concepts. *Journal of Palaeogeography*, doi: 10.1186/s42501-021-00098-w

Zeller, M. (2013). *Facies, Geometries and Sequence Stratigraphy of the Mixed Carbonate - Siliciclastic Quintuco - Vaca Muerta System in the Neuquén Basin, Argentina: An Integrated Approach*. PhD Thesis, University of Miami, 206 pp.

Zeller, M., Eberli, G.P., Weger, R.J., Giunta, D.L., Massaferro, J.L. (2014). Seismic expressions of the Quintuco-Vaca Muerta system based on outcrop facies and geometry. In *IX Congreso de Exploración y Desarrollo de Hidrocarburos* (p. 209–224). Mendoza, Argentina.

Zeller, M., Verwer, K., Eberli, G.P., Massaferro, J.L., Schwarz, E., Spalletti, L.A. (2015a). Depositional controls on mixed carbonate-siliciclastic cycles and sequences on gently inclined shelf profiles. *Sedimentology*, 62, 2009–2037.

Zeller, M., Reid, S.B., Eberli, G.P., Weger, R.J., Massaferro, J.L. (2015b). Sequence architecture and heterogeneities of a field - scale Vaca Muerta analog (Neuquén Basin, Argentina) - From outcrop to synthetic seismic. *Mar. Pet. Geol.*, 66, 829–847.

Zhang, L.J., Fan, R.Y. and Gong, Y.M. (2015). *Zoophycos* macroevolution since 541 Ma. *Scientific Reports*, 5, 1–10.

Zonneveld, J.P., and Pemberton, S.G. (2003). Ichnotaxonomy and Behavioral Implications of Lingulide-Derived Trace Fossils from the Lower and Middle Triassic of Western Canada. *Ichnos*, 10, 25–39.

APPENDIX A

Stratigraphic sections of the study area. See Fig. 2.1 and 2.3 for location of the sections. Next to the sections is the facies (F) and facies association (FA) interpretation.

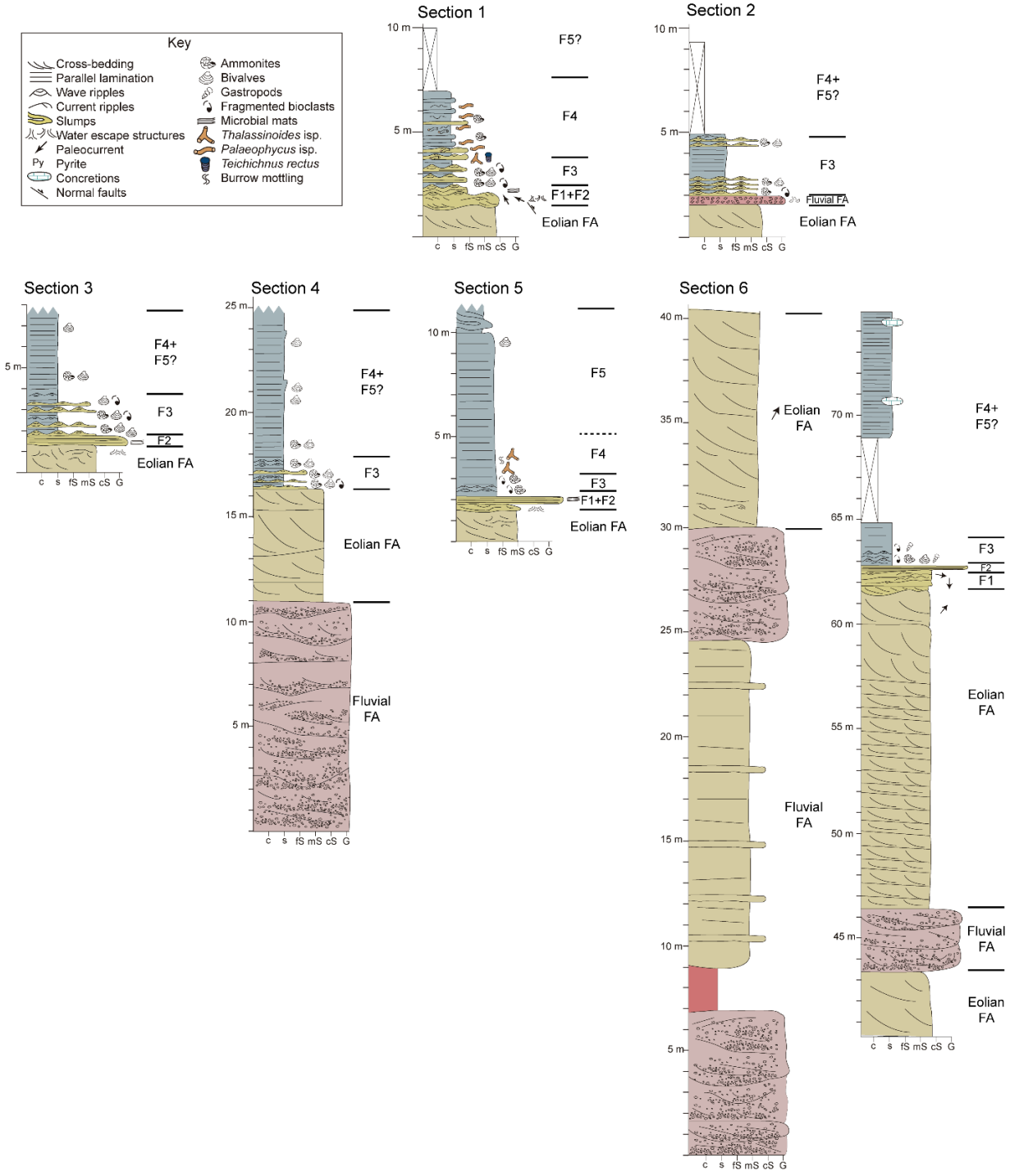

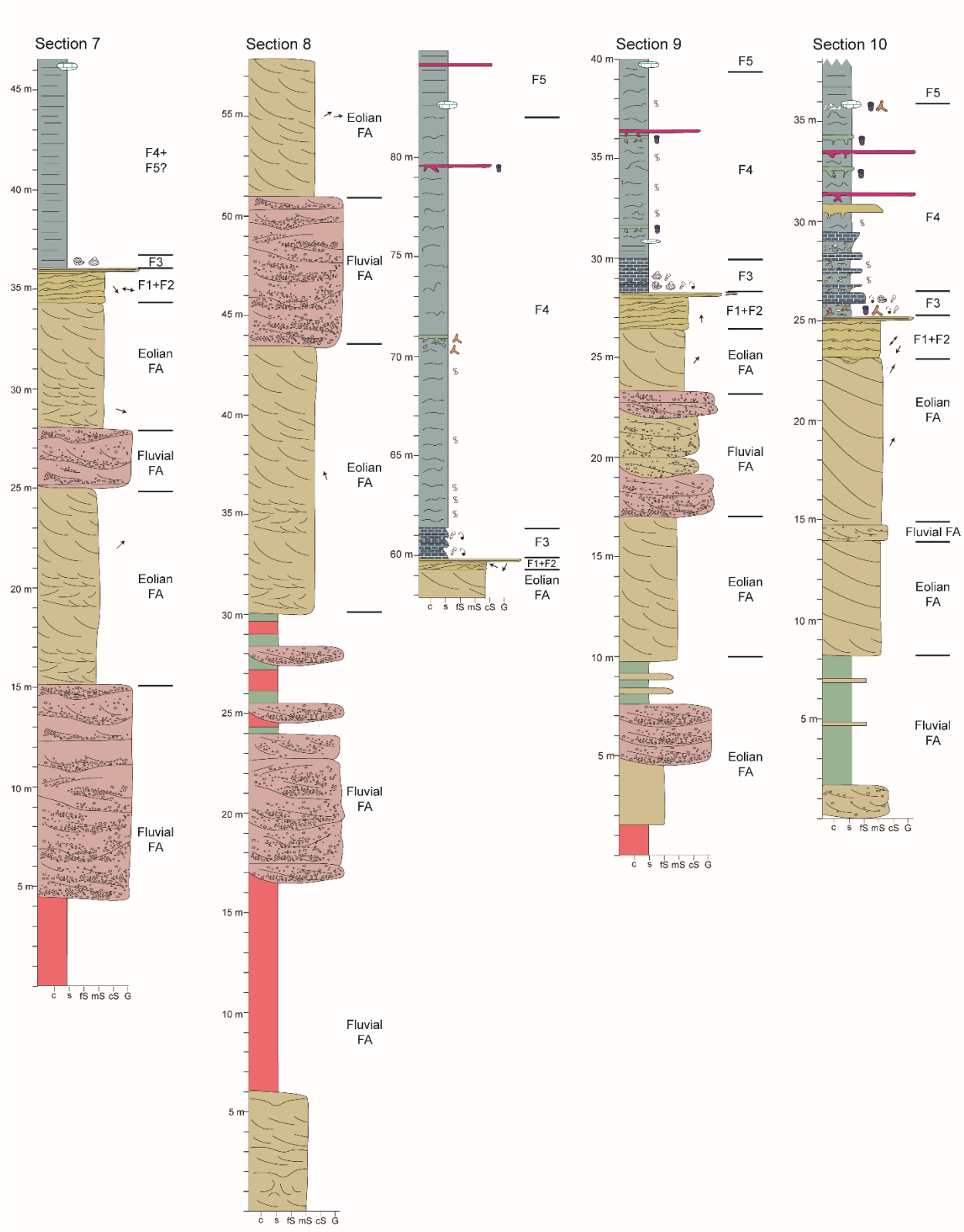
Section 7
45 m
40 m
35 m
30 m
25 m
20 m
15 m
10 m
5 m
F4+
F5?
F3
F1+F2
Eolian
FA
Fluvial
FA
Eolian
FA
Fluvial
FA
c s fS mS cS G
Section 8
55 m
50 m
45 m
40 m
35 m
30 m
25 m
20 m
15 m
10 m
5 m
Eolian
FA
Fluvial
FA
Eolian
FA
Fluvial
FA
Fluvial
FA
c s fS mS cS G
80 m
75 m
70 m
65 m
60 m
F5
F4
F3
F1+F2
Eolian
FA
c s fS mS cS G
Section 9
40 m
35 m
30 m
25 m
20 m
15 m
10 m
5 m
F5
F4
F3
F1+F2
Eolian
FA
Fluvial
FA
Eolian
FA
Eolian
FA
c s fS mS cS G
Section 10
35 m
30 m
25 m
20 m
15 m
10 m
5 m
F5
F4
F3
F1+F2
Eolian
FA
Fluvial FA
Eolian
FA
Fluvial
FA
c s fS mS cS G

APPENDIX B

Sedimentary logs of the basin centre study area. BI=Bioturbation index, F=Facies.

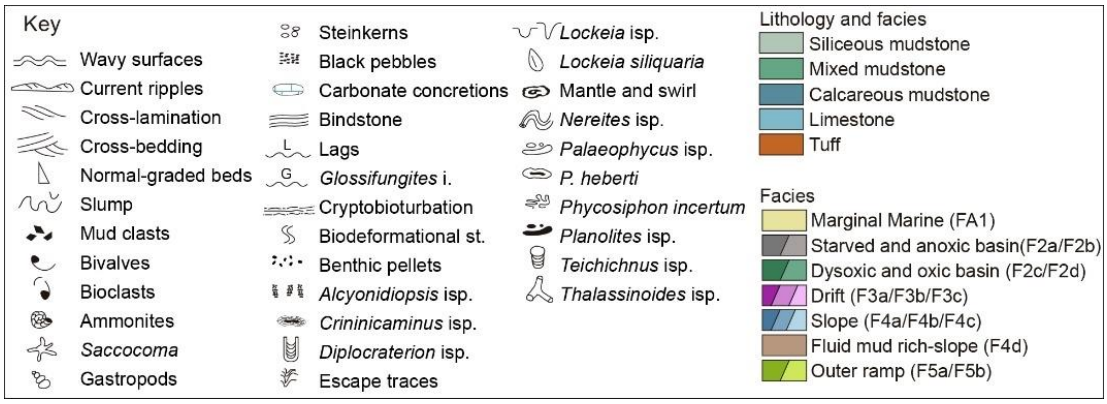

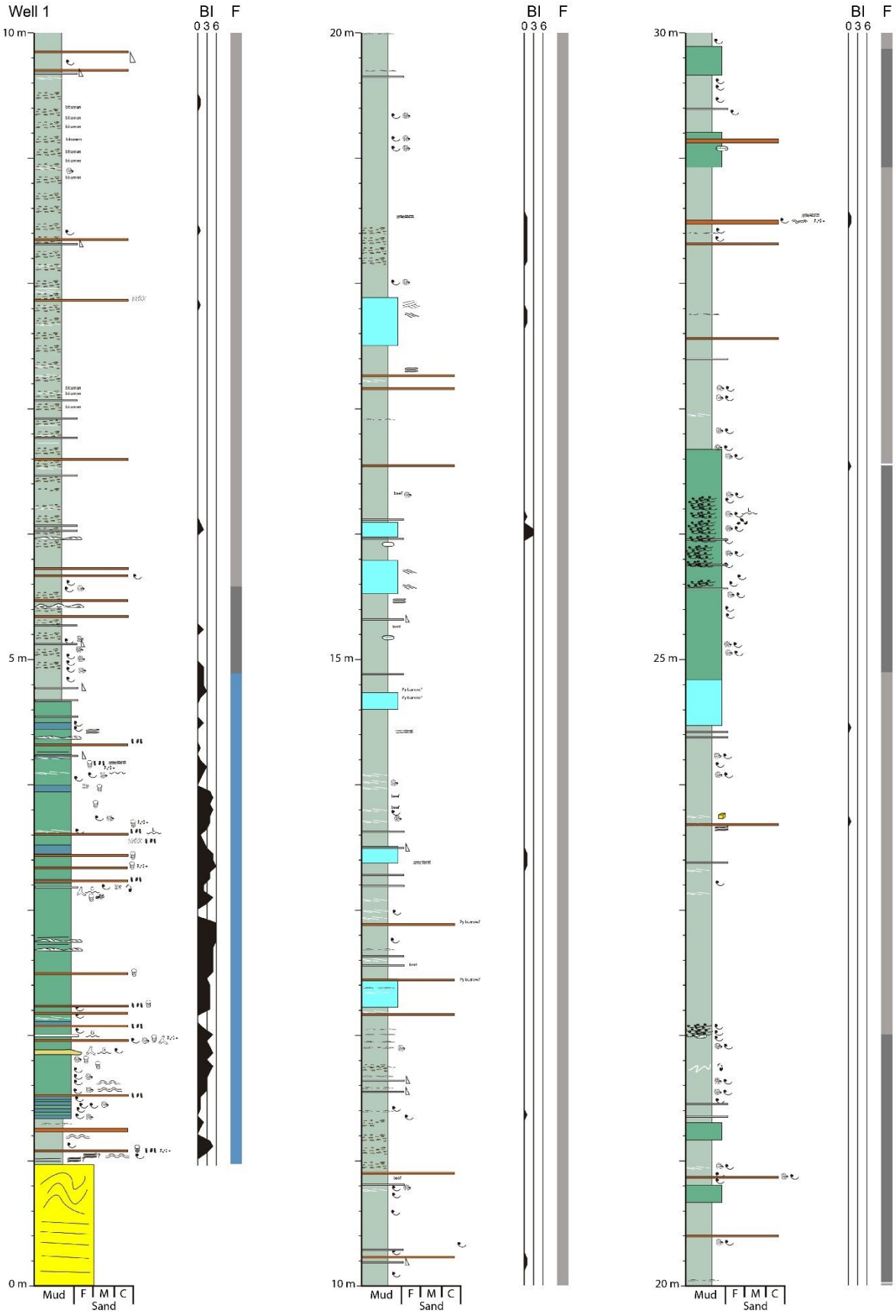
Well 1
BI
0 3 6
F
10 m
5 m
0 m
Mud
F
M
C
Sand
20 m
15 m
10 m
30 m
25 m
20 m

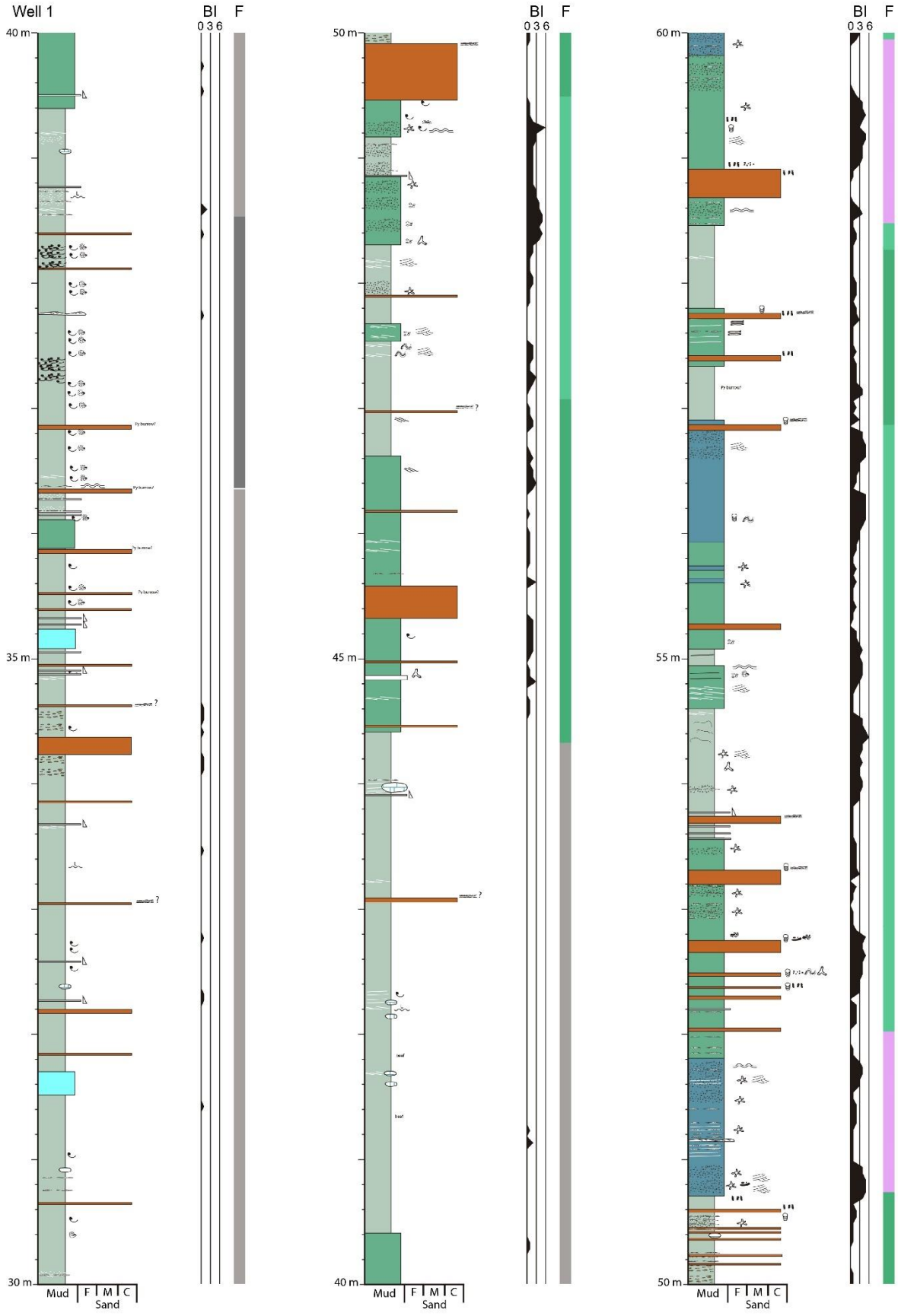
Well 1
BI
0 3 6
F
40 m
35 m
30 m
50 m
45 m
40 m
60 m
55 m
50 m
Mud
F
M
C
Sand

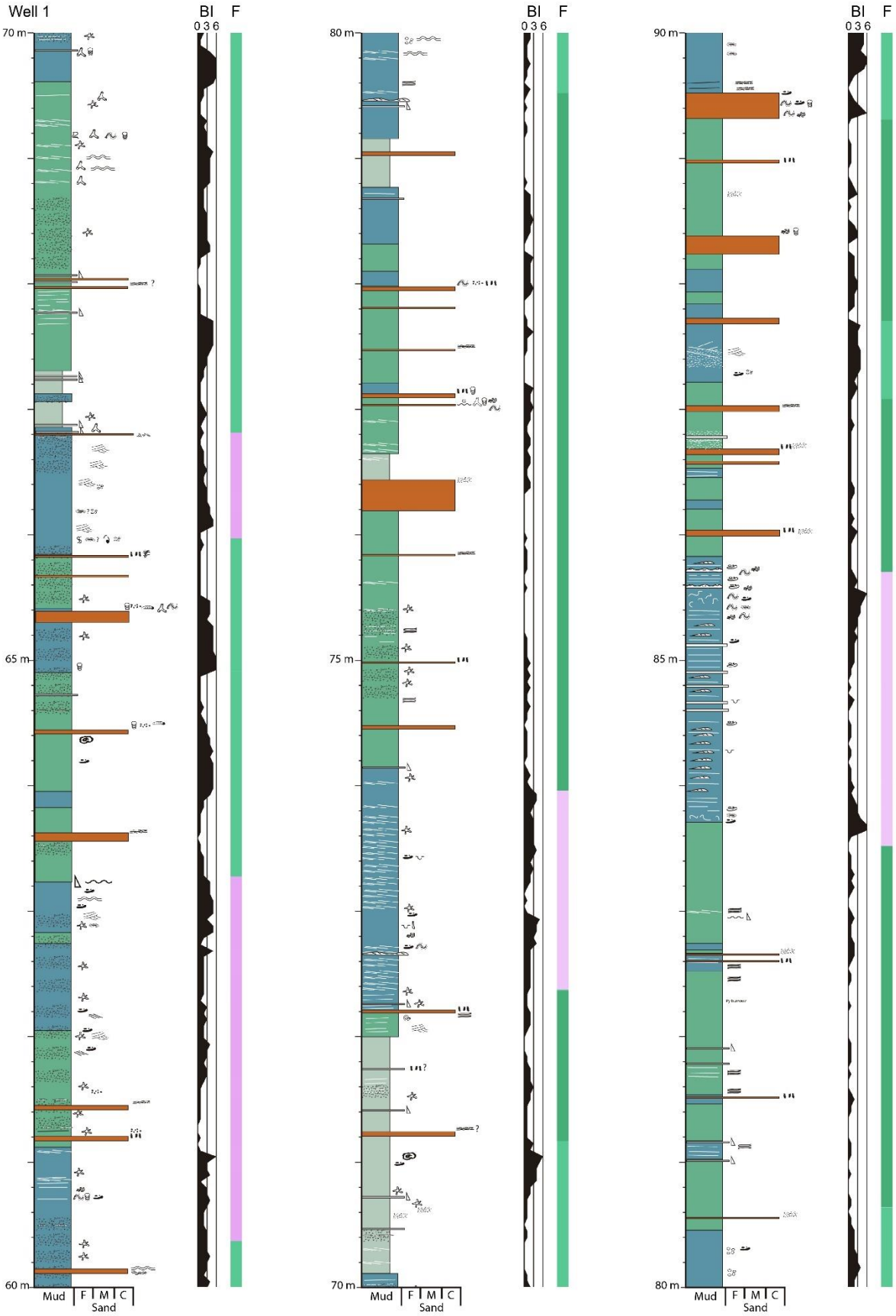
Well 1
BI
0 3 6
F
70 m
65 m
60 m
80 m
75 m
70 m
90 m
85 m
80 m
Mud
F
M
C
Sand

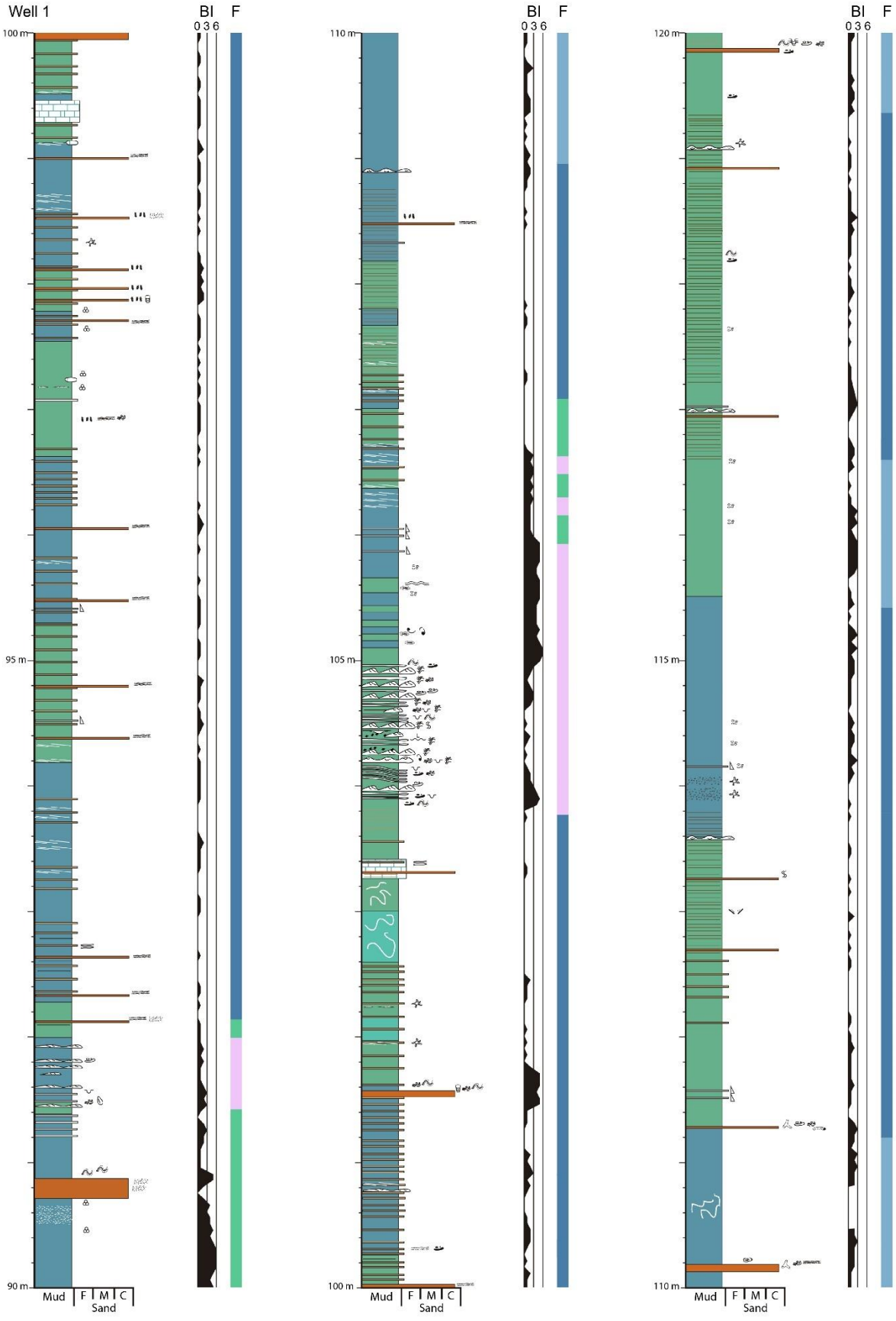
Well 1
BI
0 3 6
F
100 m
95 m
90 m
Mud
F
M
C
Sand
110 m
105 m
100 m
120 m
115 m
110 m

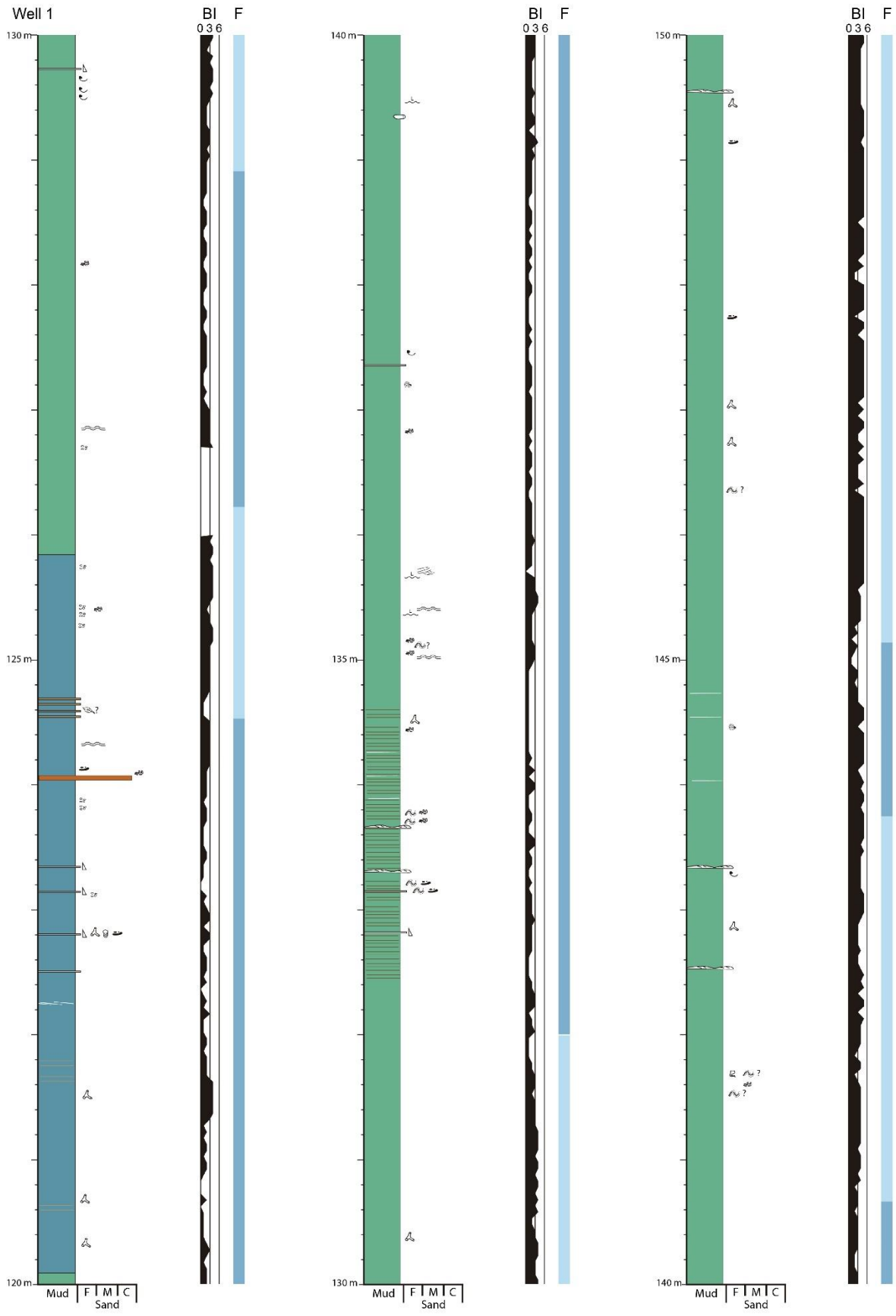
Well 1
BI
0 3 6
F
130 m
125 m
120 m
Mud
F
M
C
Sand
140 m
135 m
130 m
150 m
145 m
140 m

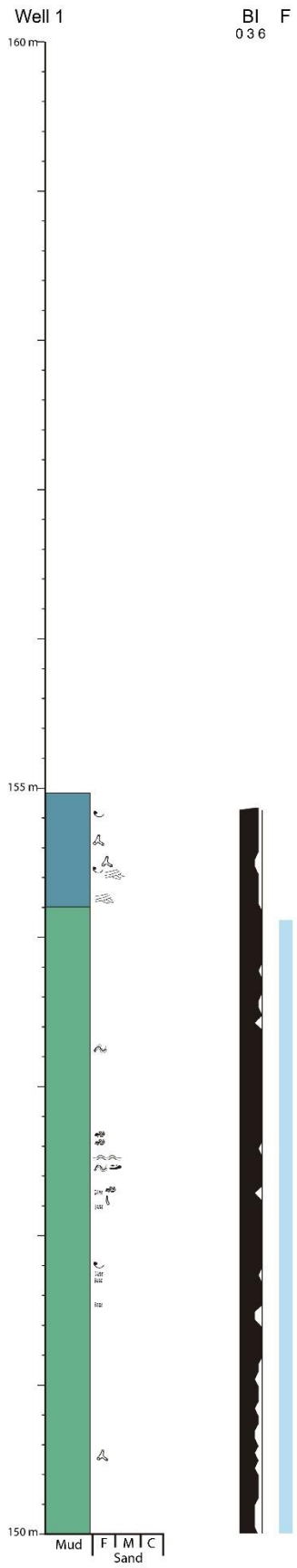
Well 1
BI F
0 3 6
160 m
155 m
150 m
Mud
F
M
C
Sand

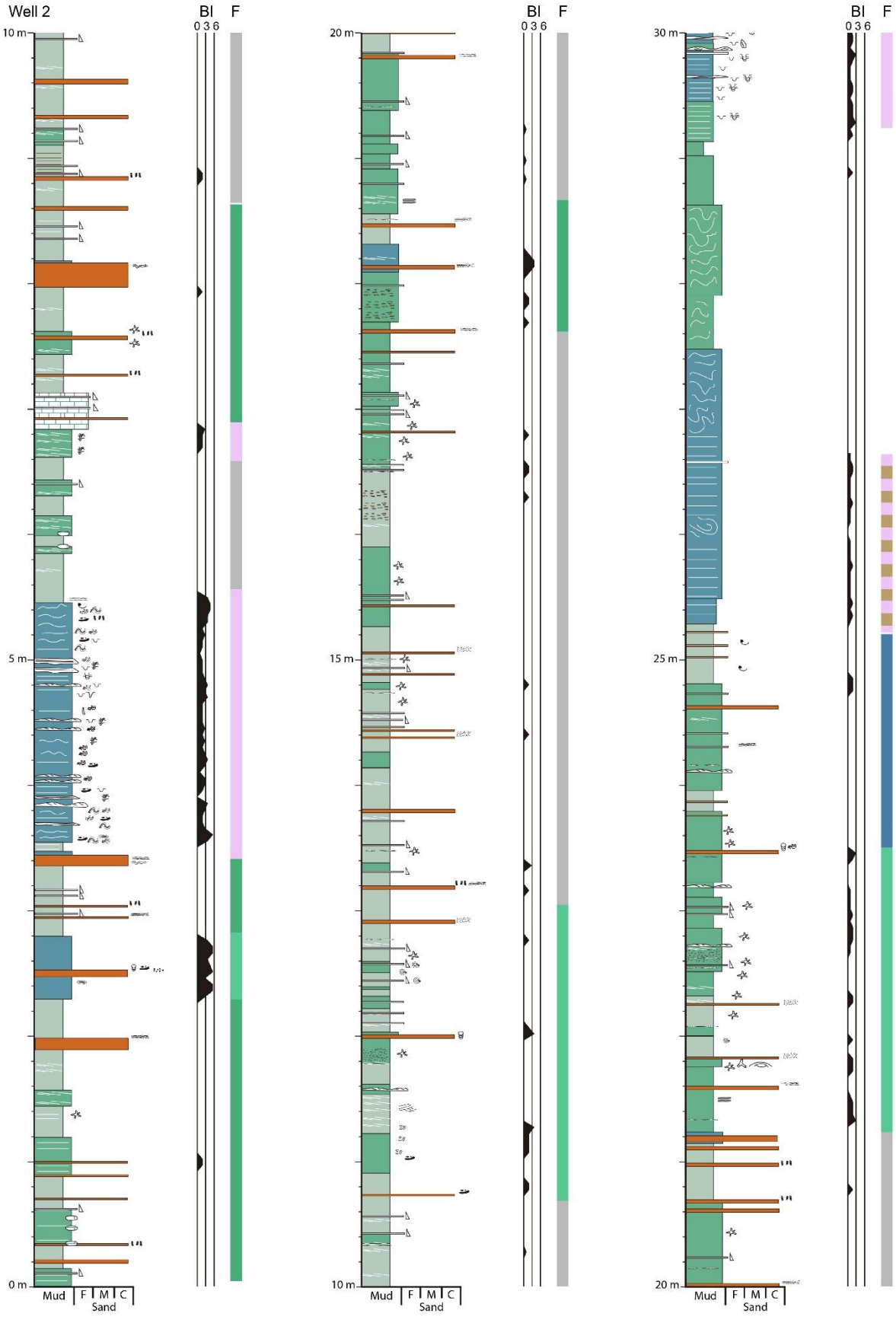
Well 2
BI
0 3 6
F
10 m
5 m
0 m
Mud
F
M
C
Sand
20 m
15 m
10 m
30 m
25 m
20 m

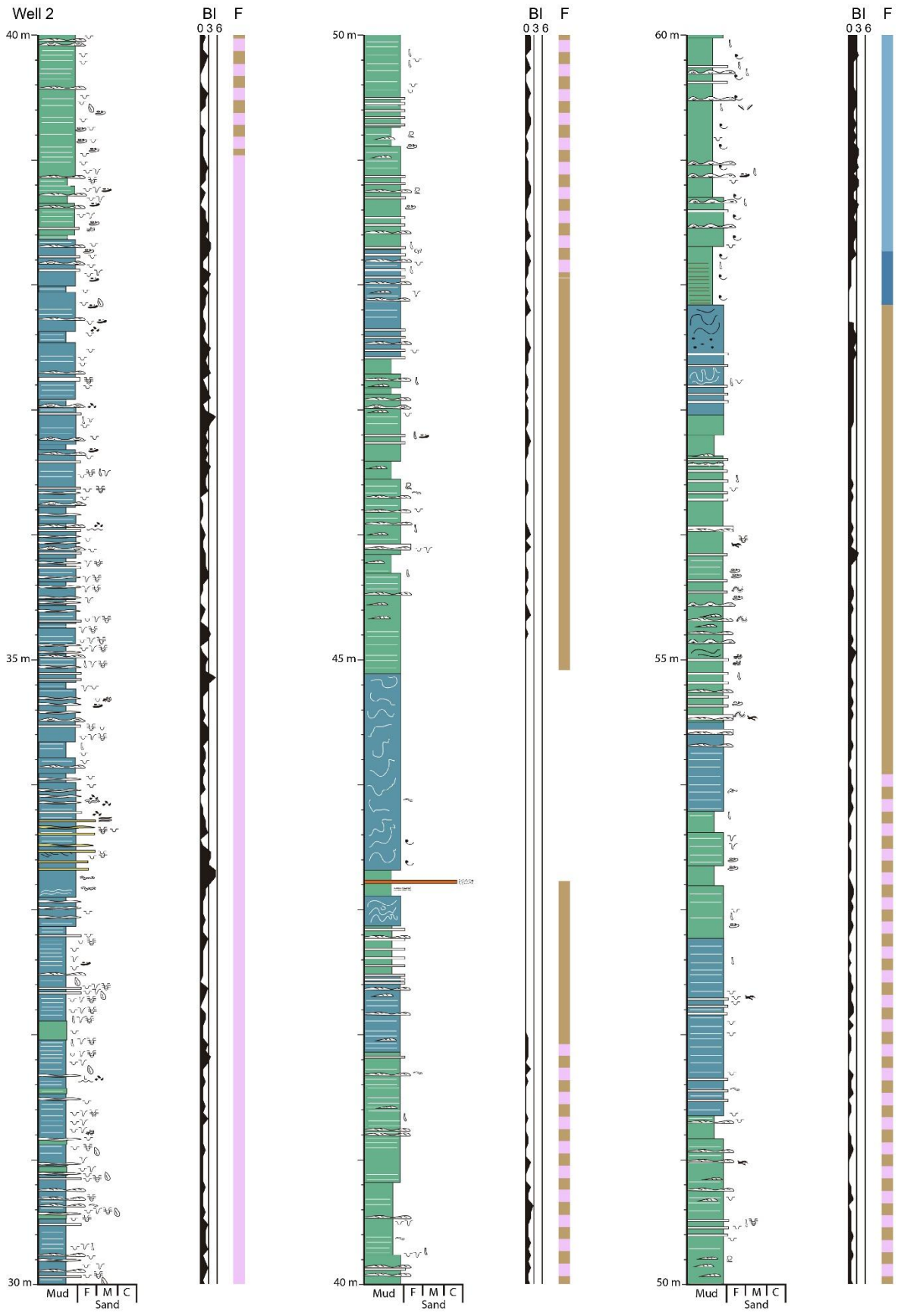
Well 2
BI
0 3 6
F
40 m
35 m
30 m
Mud
F
M
C
Sand
50 m
45 m
40 m
60 m
55 m
50 m

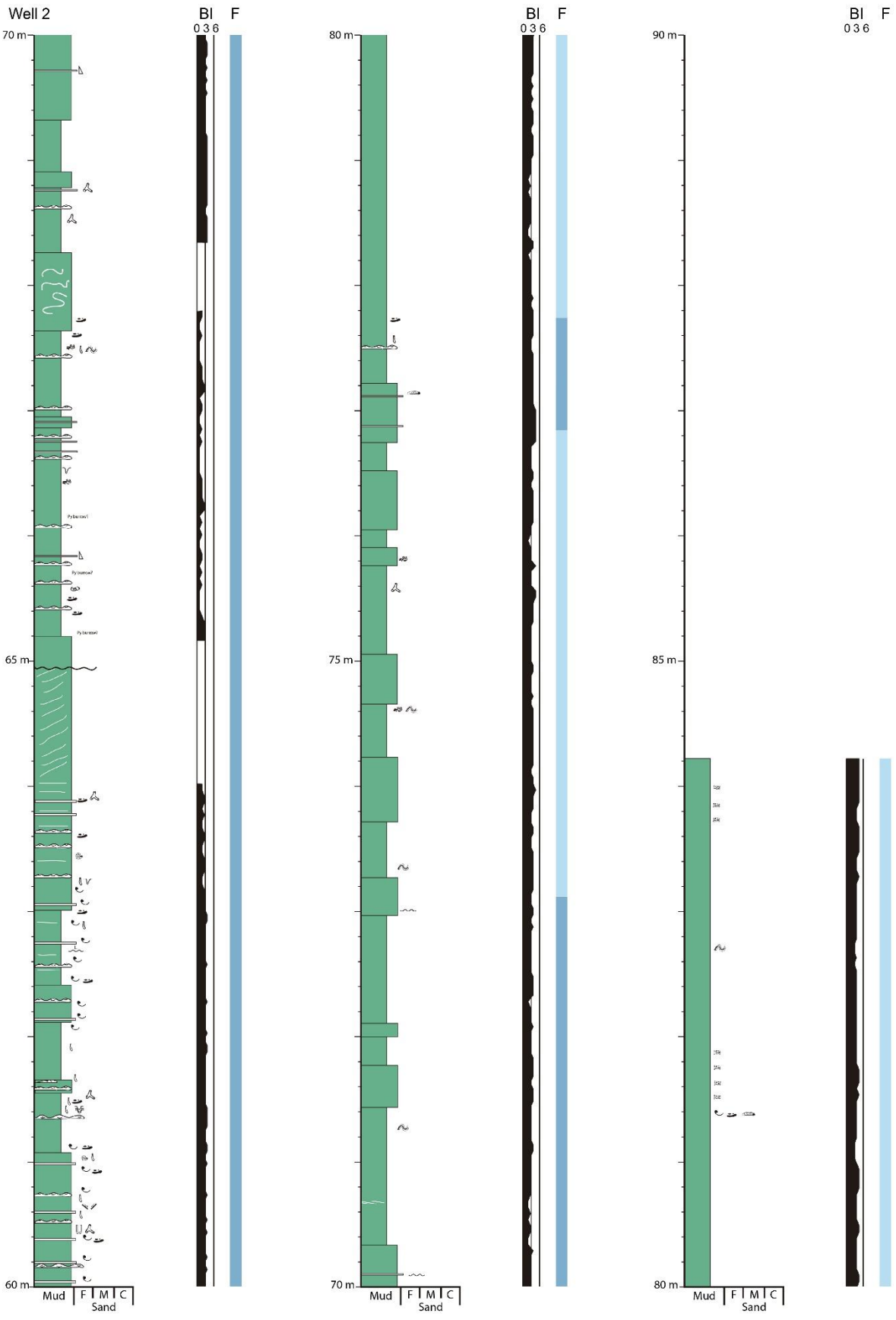
Well 2
Bl
0 3 6
F
70 m
65 m
60 m
Mud
F
M
C
Sand
80 m
75 m
70 m
90 m
85 m
80 m

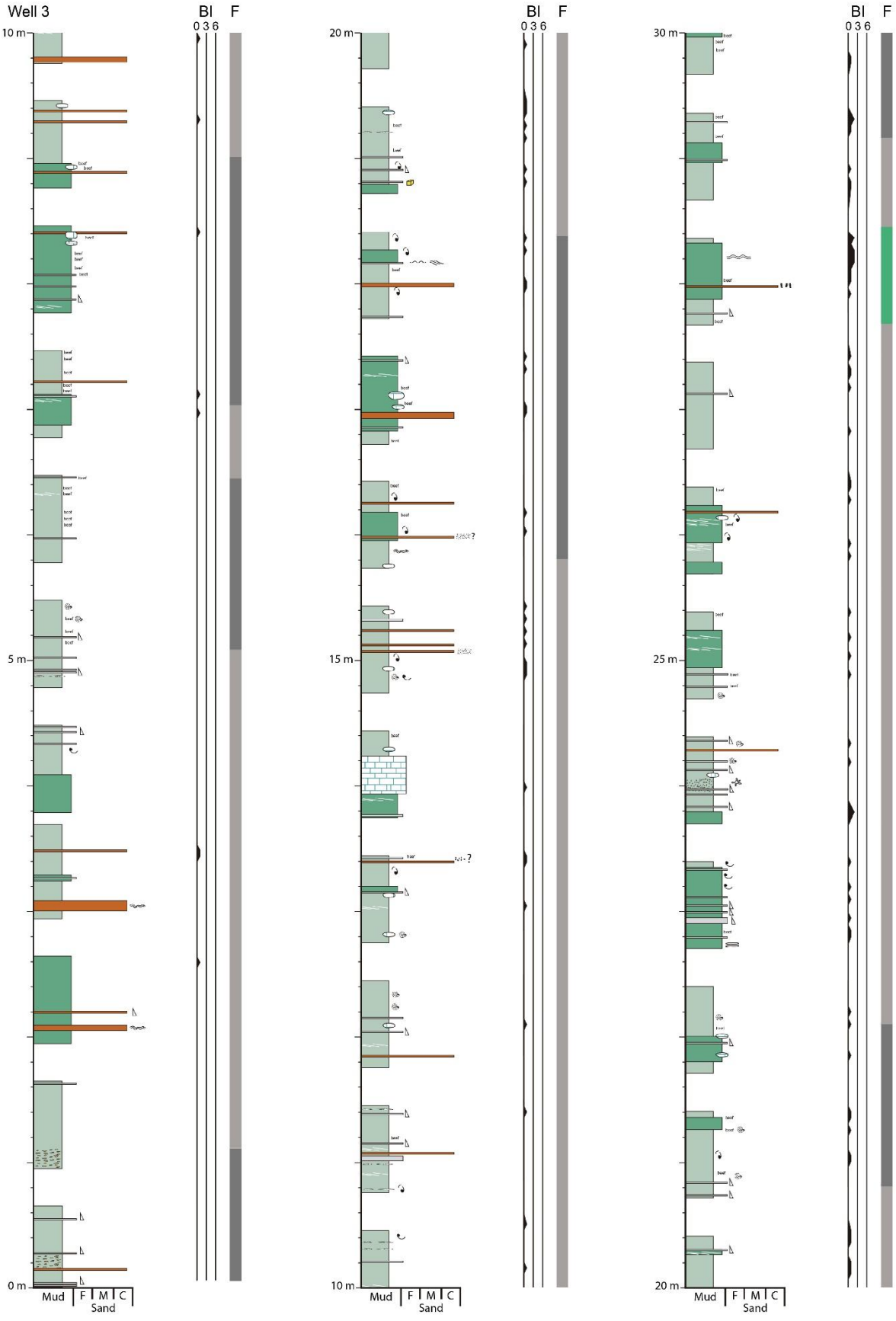
Well 3
Bl
F
0 3 6
10 m
5 m
0 m
20 m
15 m
10 m
30 m
25 m
20 m
Mud
F
M
C
Sand

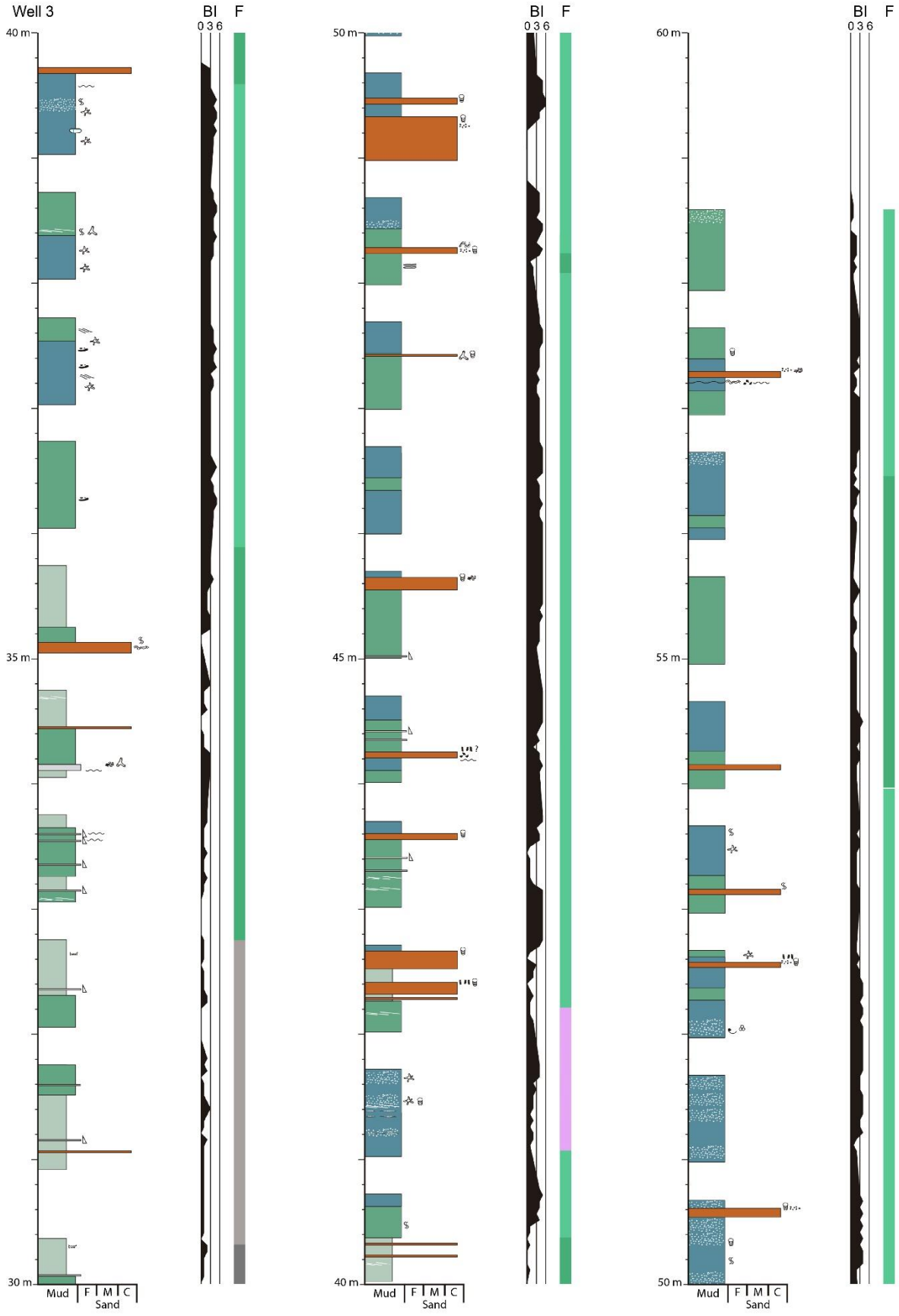
Well 3
BI
0 3 6
F
40 m
35 m
30 m
Mud
F
M
C
Sand
50 m
45 m
40 m
60 m
55 m
50 m

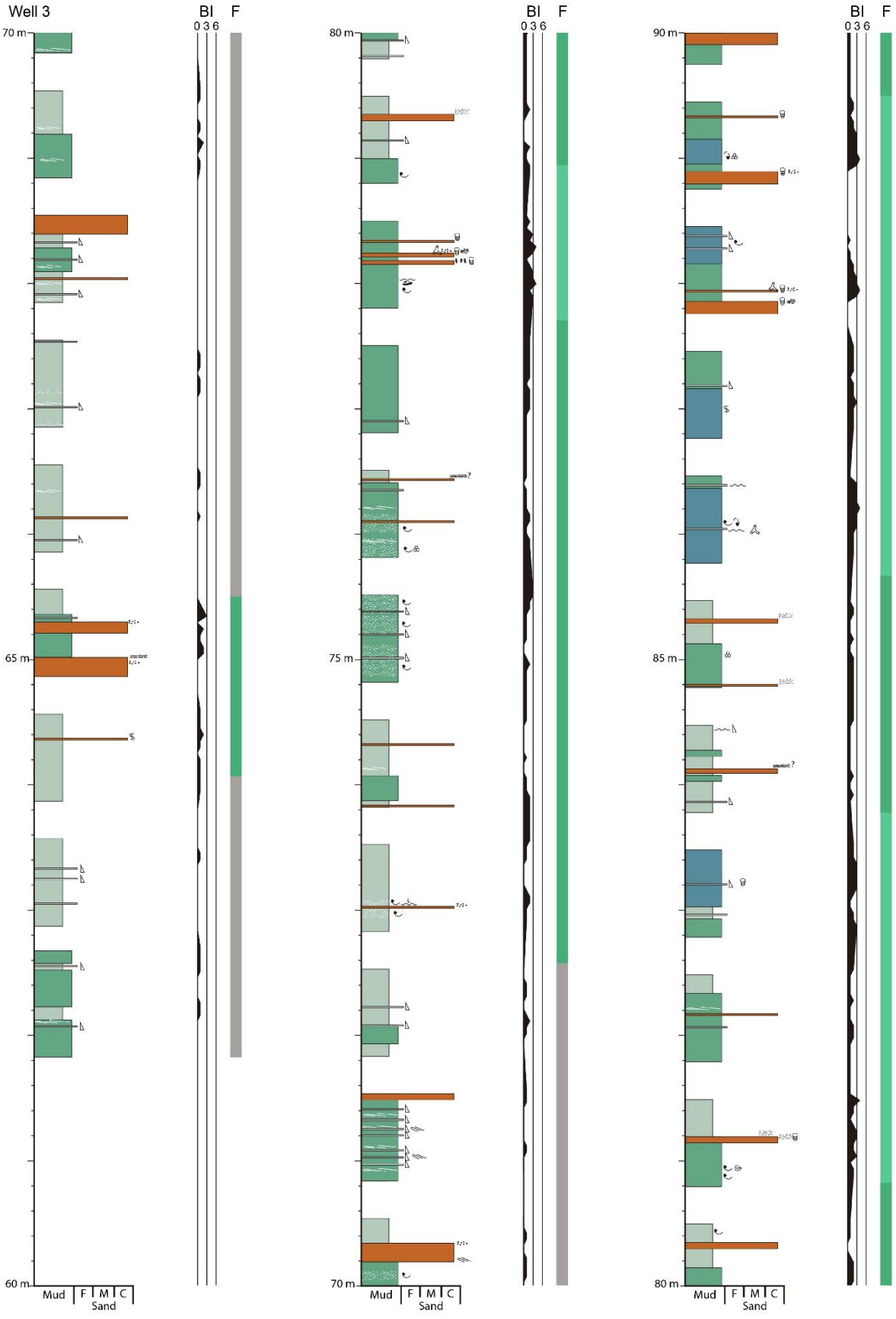
Well 3
BI
0 3 6
F
70 m
65 m
60 m
80 m
75 m
70 m
90 m
85 m
80 m
Mud
F
M
C
Sand

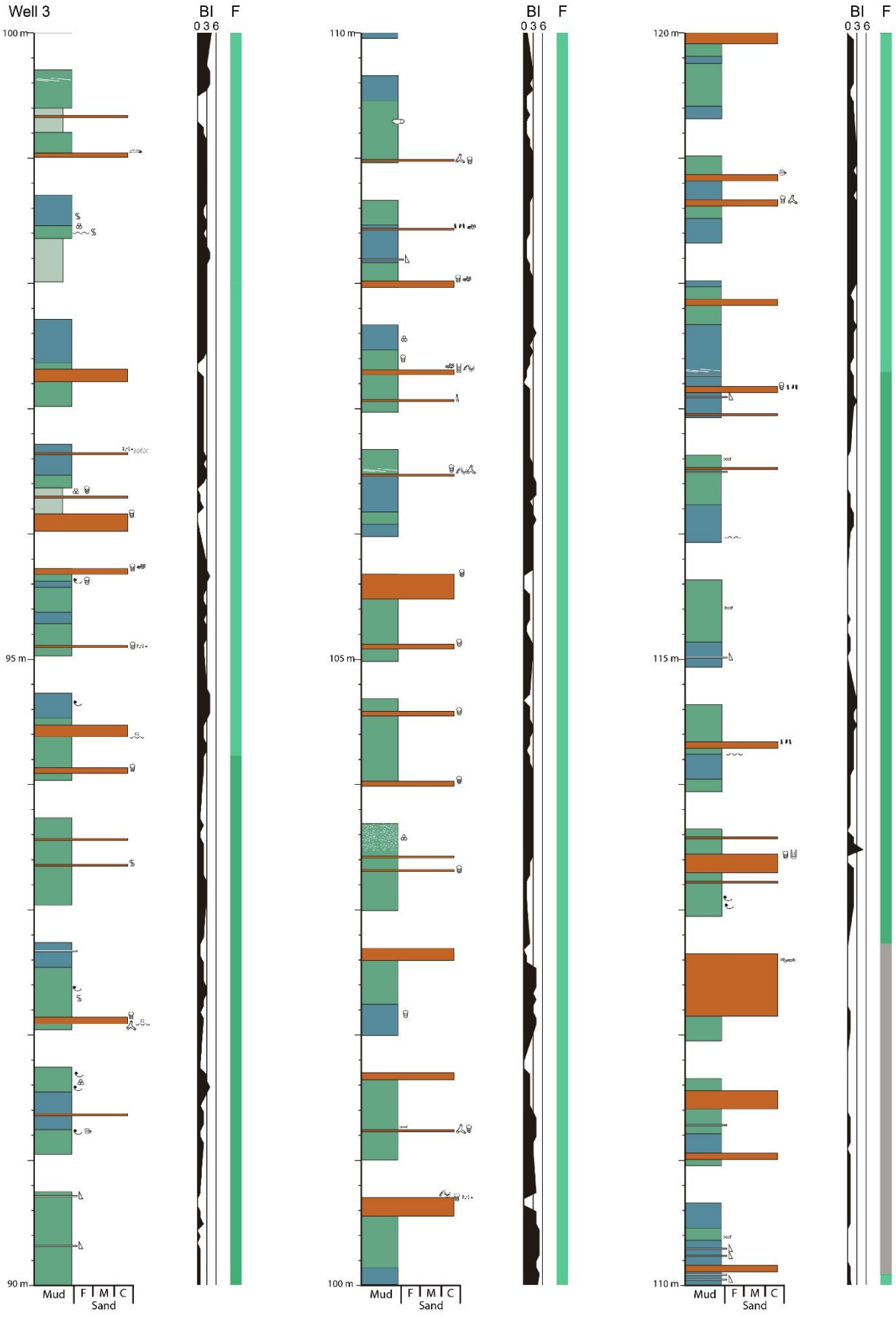
Well 3
BI
0 3 6
F
100 m
95 m
90 m
Mud
F
M
C
Sand
110 m
105 m
100 m
120 m
115 m
110 m

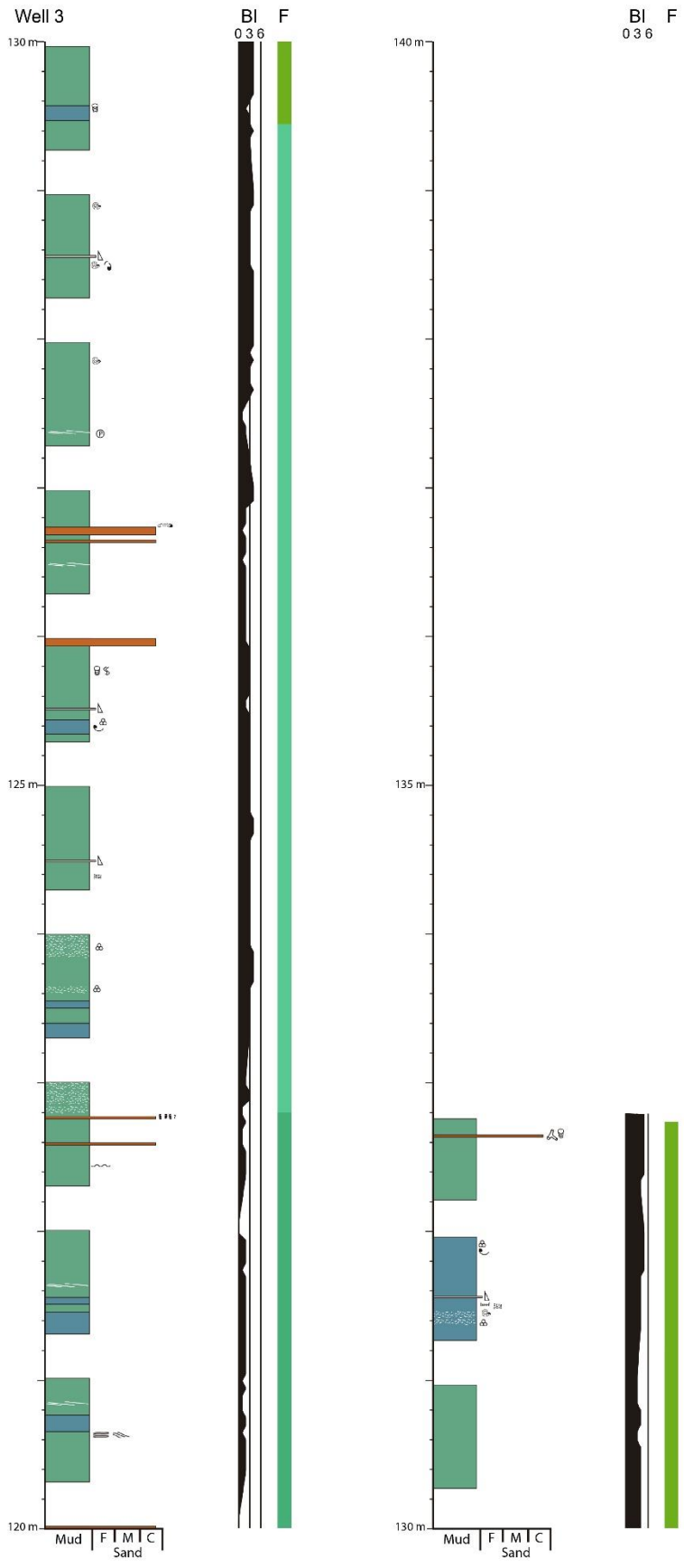
Well 3
BI
0 3 6
F
130 m
125 m
120 m
Mud
F
M
C
Sand
BI
0 3 6
F
140 m
135 m
130 m
Mud
F
M
C
Sand

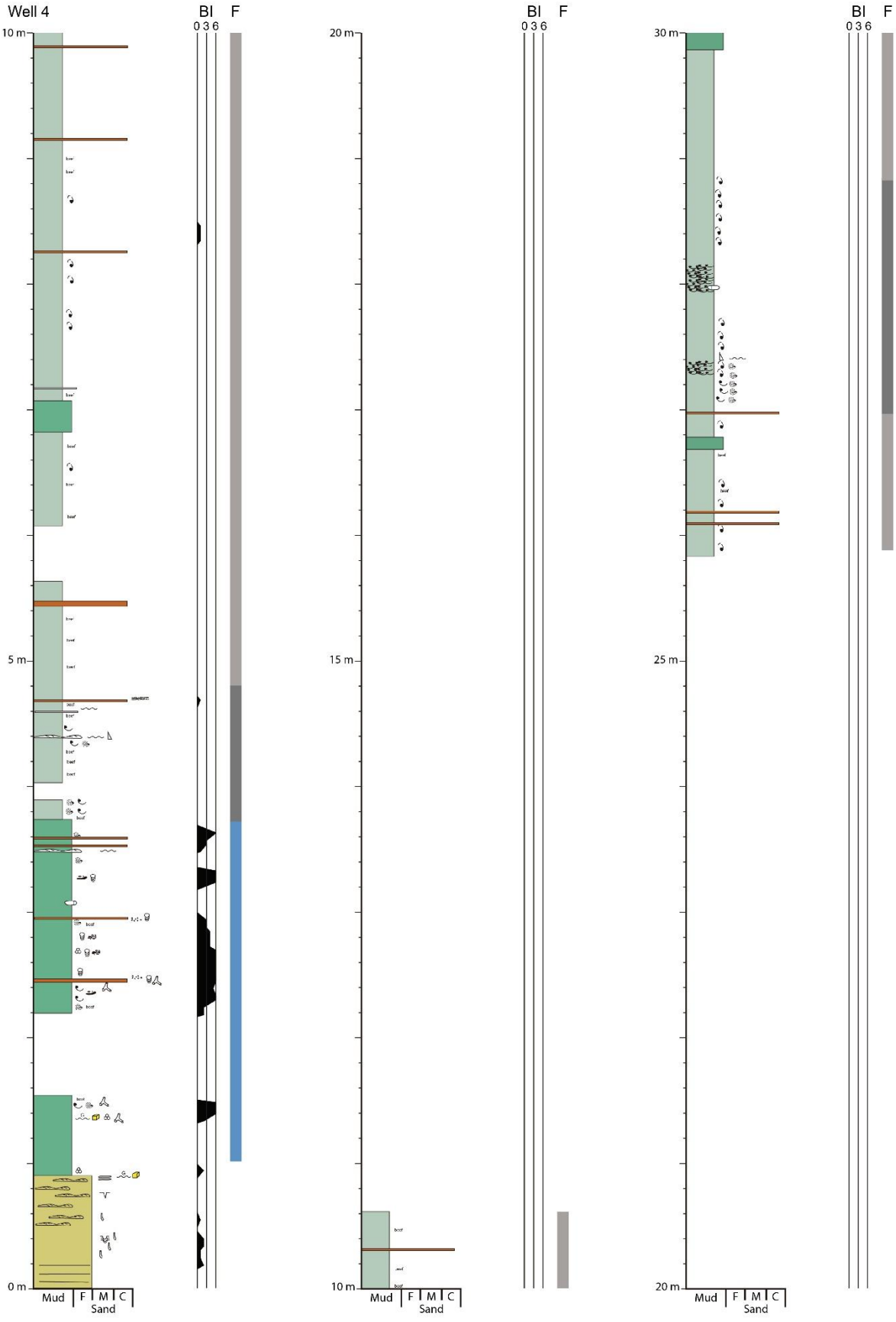
Well 4
BI
F
0 3 6
10 m
5 m
0 m
Mud
F
M
C
Sand
20 m
15 m
10 m
30 m
25 m
20 m

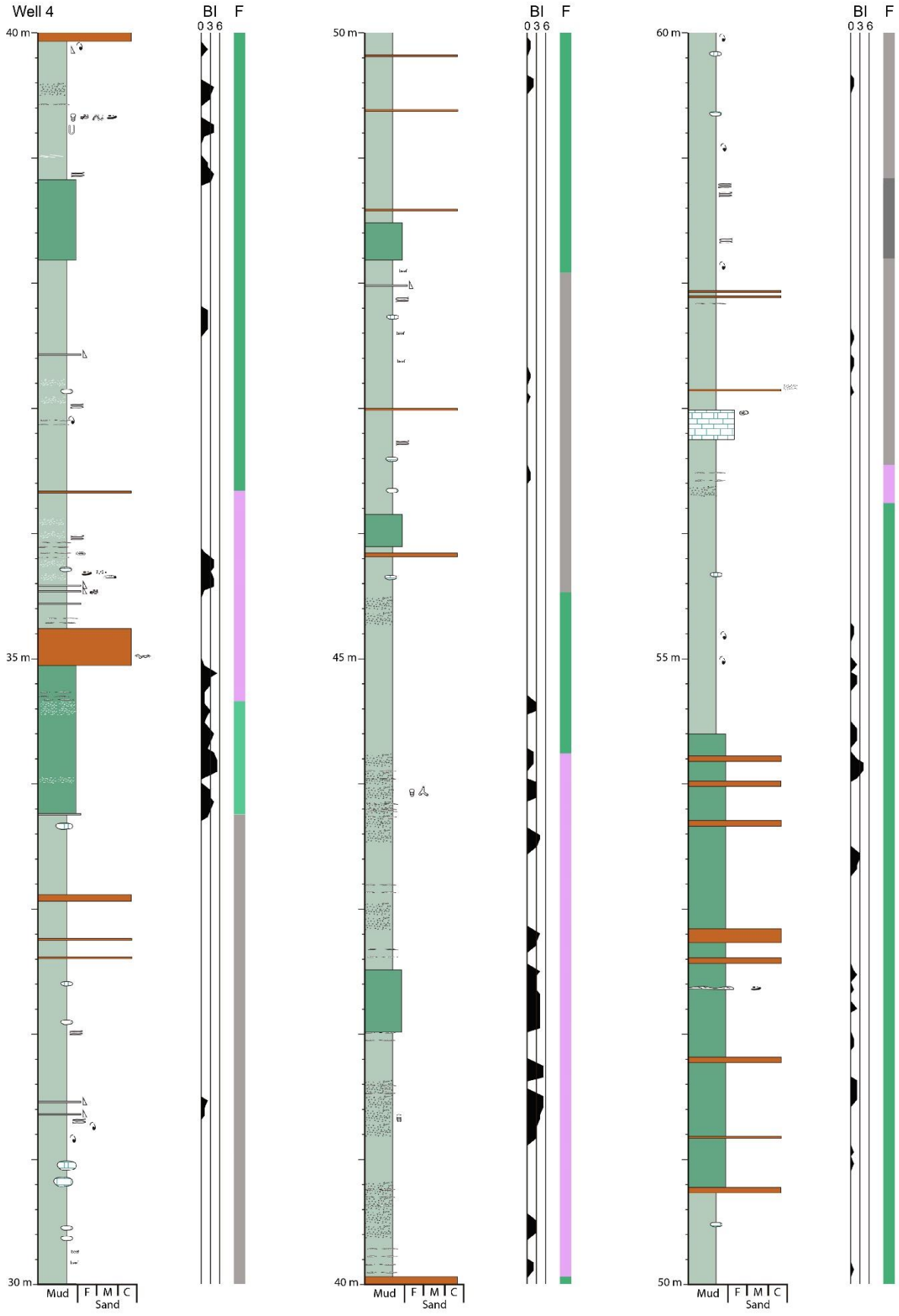
Well 4
BI
0 3 6
F
40 m
35 m
30 m
Mud
F
M
C
Sand
50 m
45 m
40 m
60 m
55 m
50 m

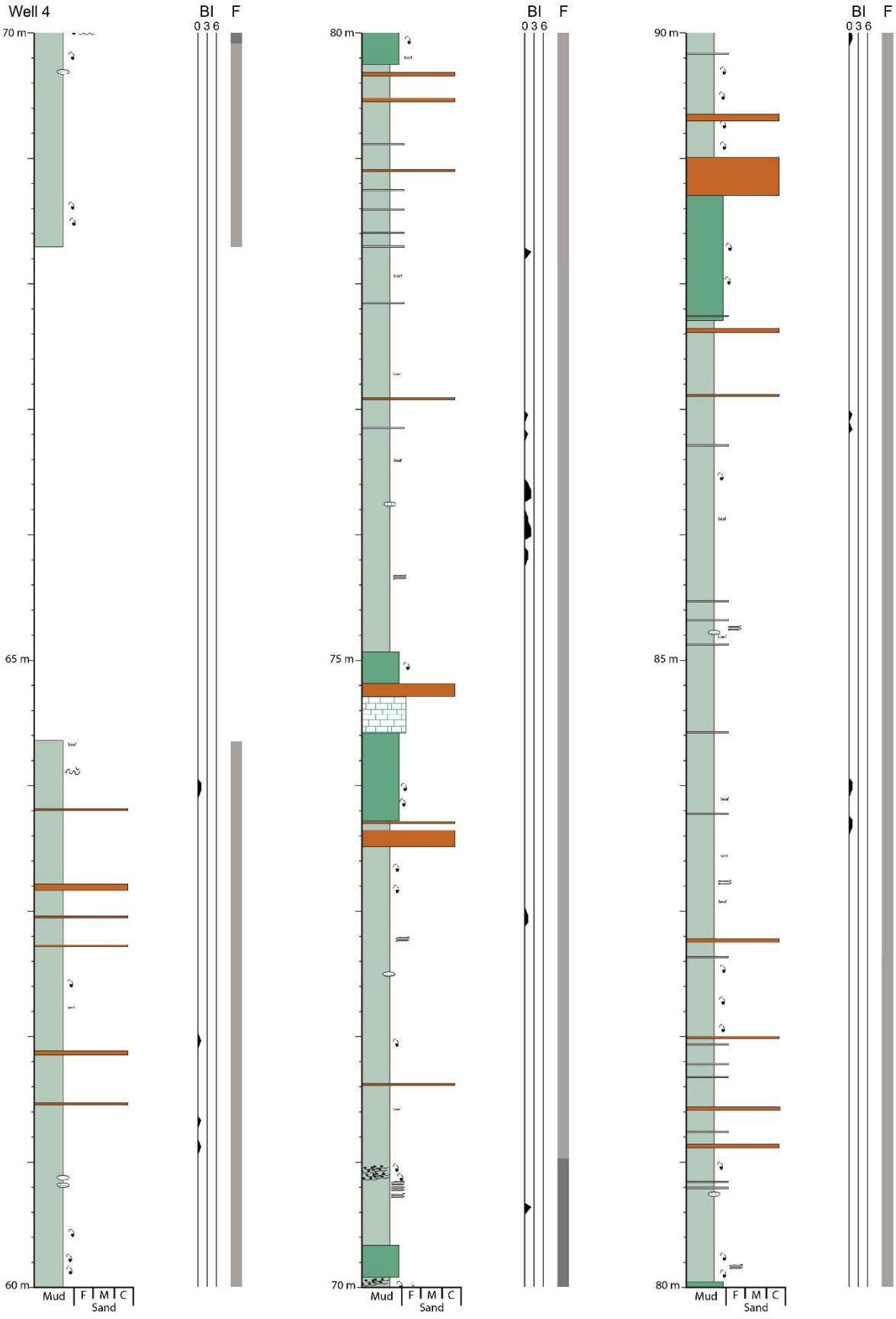
Well 4
BI
0 3 6
F
70 m
65 m
60 m
Mud
F
M
C
Sand
80 m
75 m
70 m
90 m
85 m
80 m

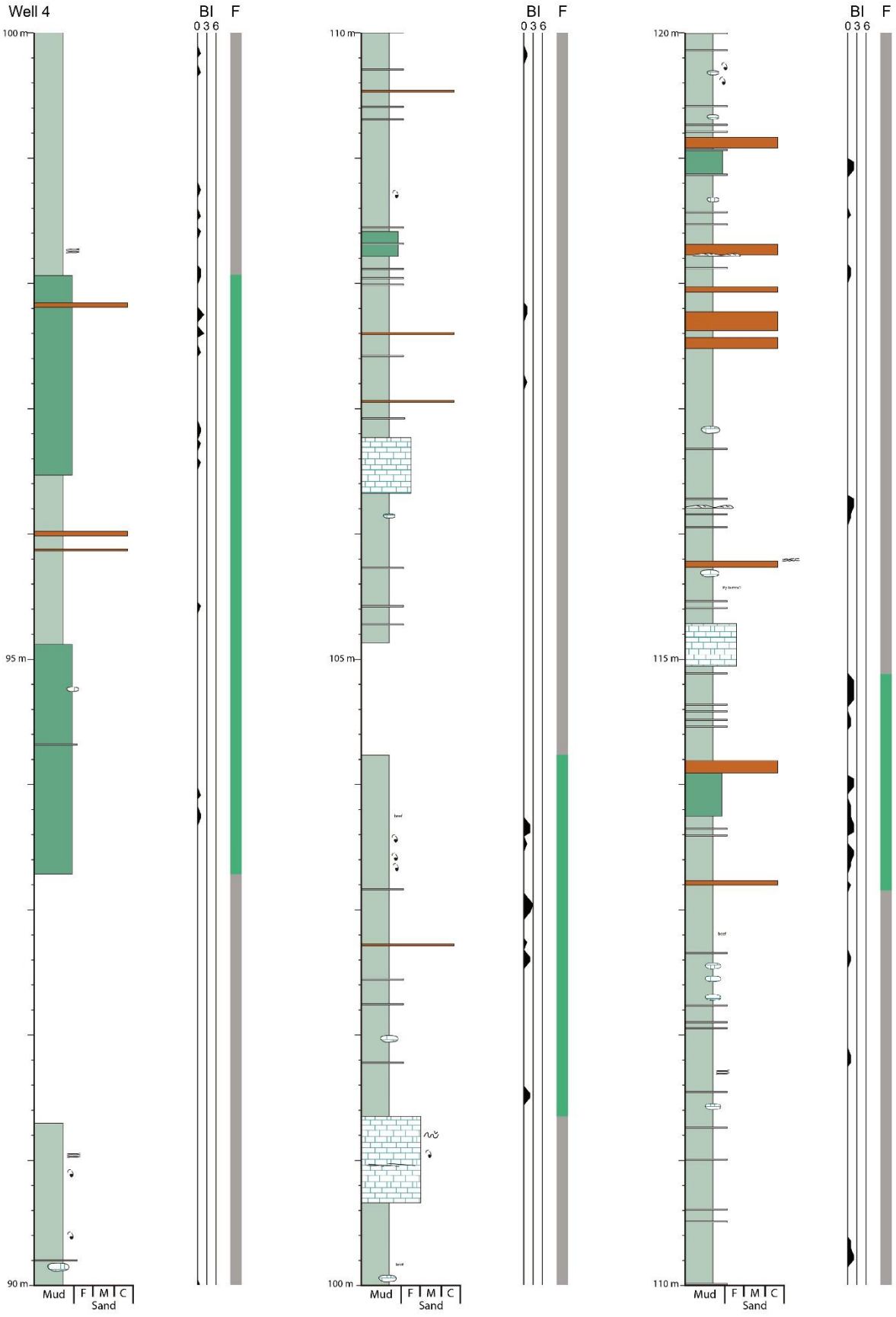
Well 4
BI
0 3 6
F
100 m
95 m
90 m
Mud
F
M
C
Sand
110 m
105 m
100 m
120 m
115 m
110 m

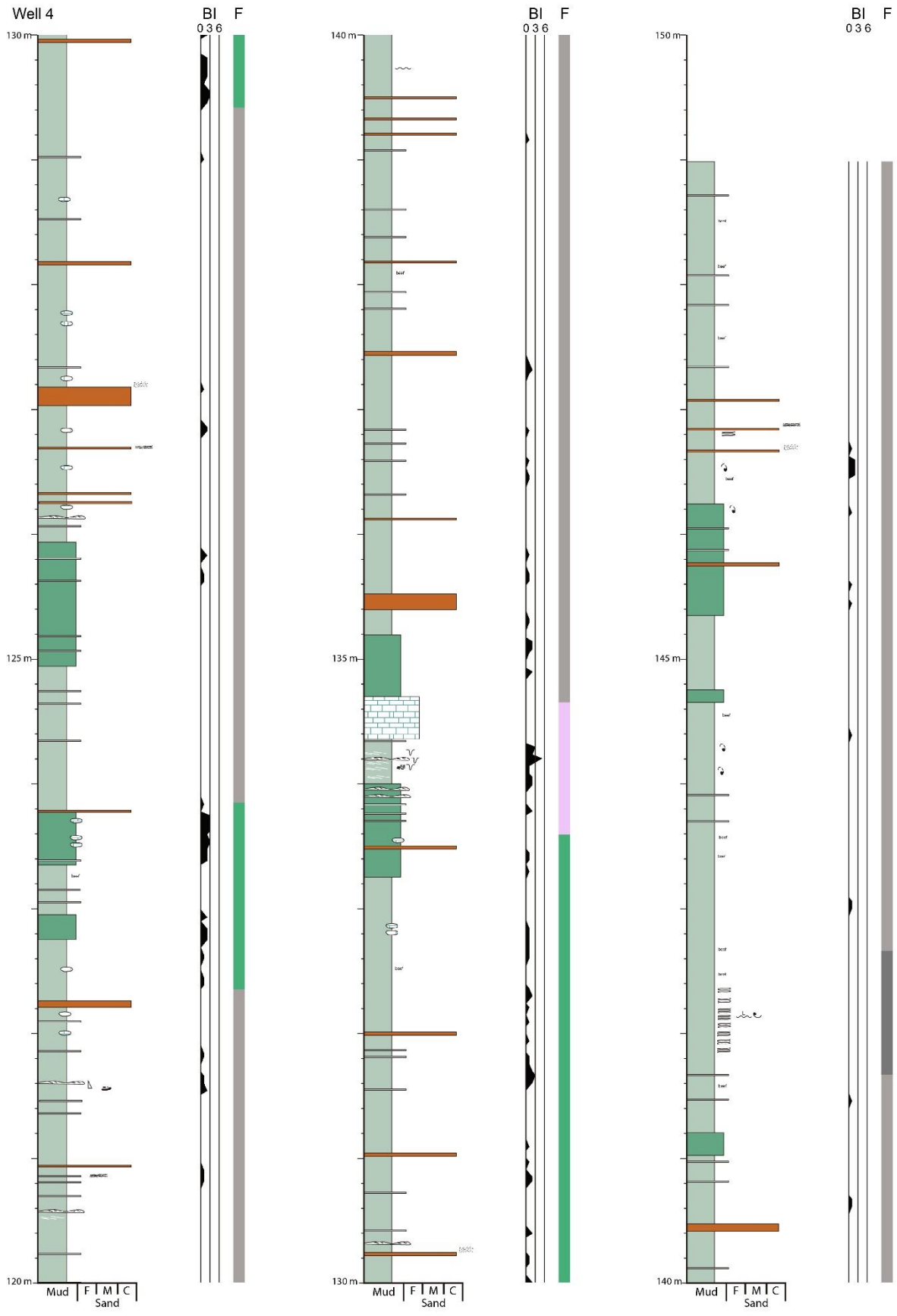
Well 4
BI
0 3 6
F
130 m
125 m
120 m
Mud
F
M
C
Sand
140 m
135 m
130 m
150 m
145 m
140 m

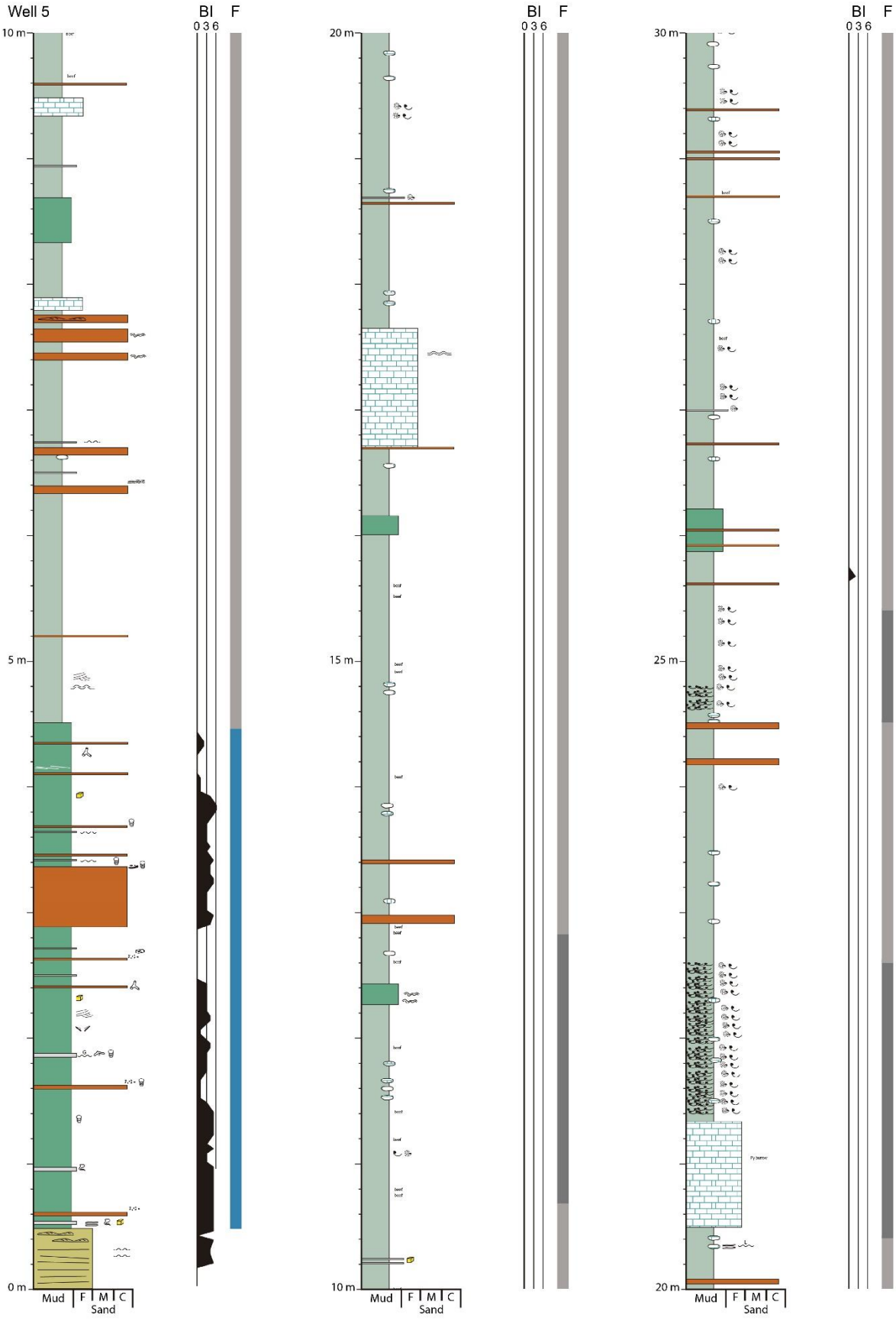
Well 5
BI
F
0 3 6
10 m
5 m
0 m
15 m
20 m
25 m
30 m
Mud
F
M
C
Sand

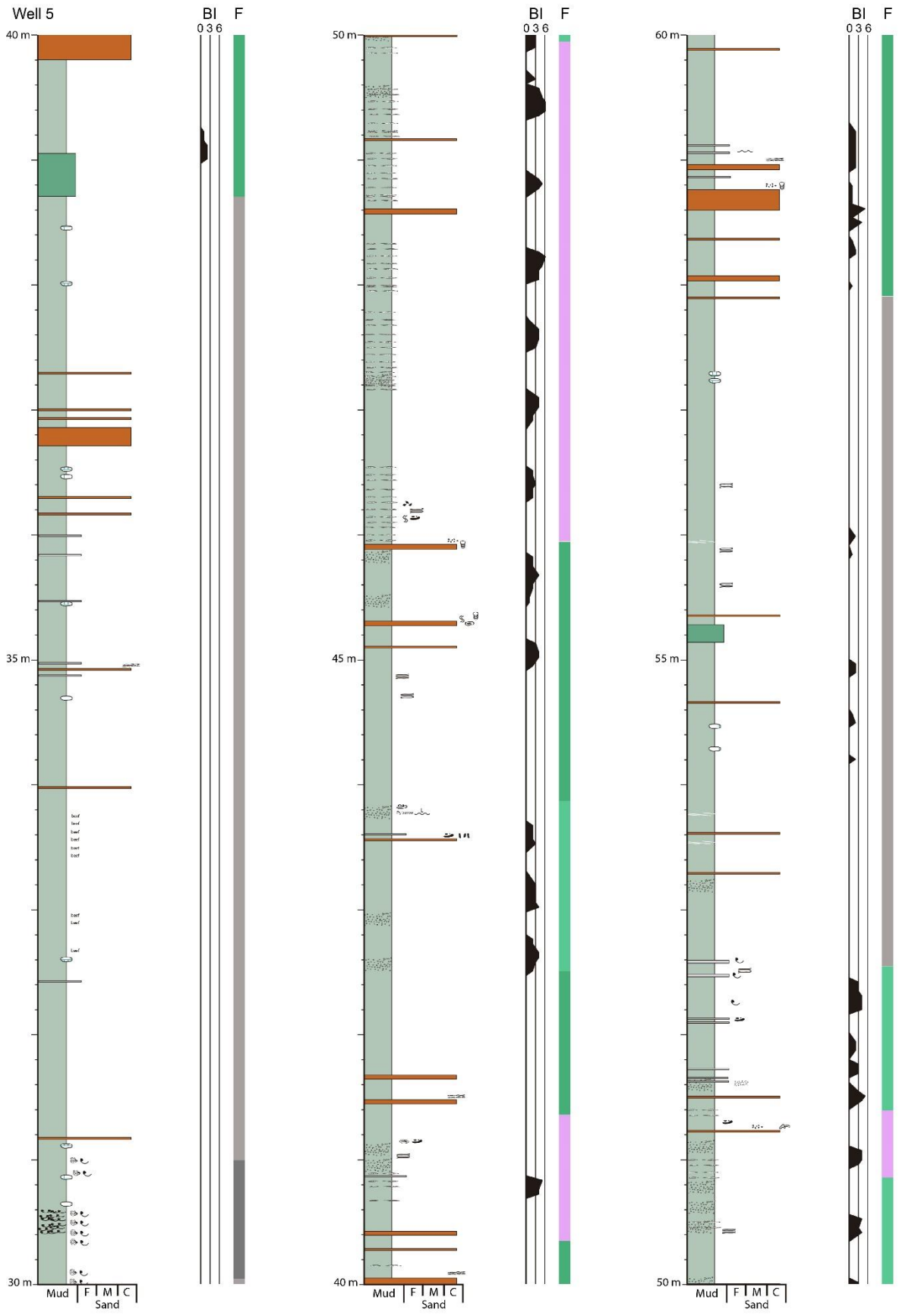
Well 5
BI
0 3 6
F
40 m
35 m
30 m
50 m
45 m
40 m
60 m
55 m
50 m
Mud
F
M
C
Sand

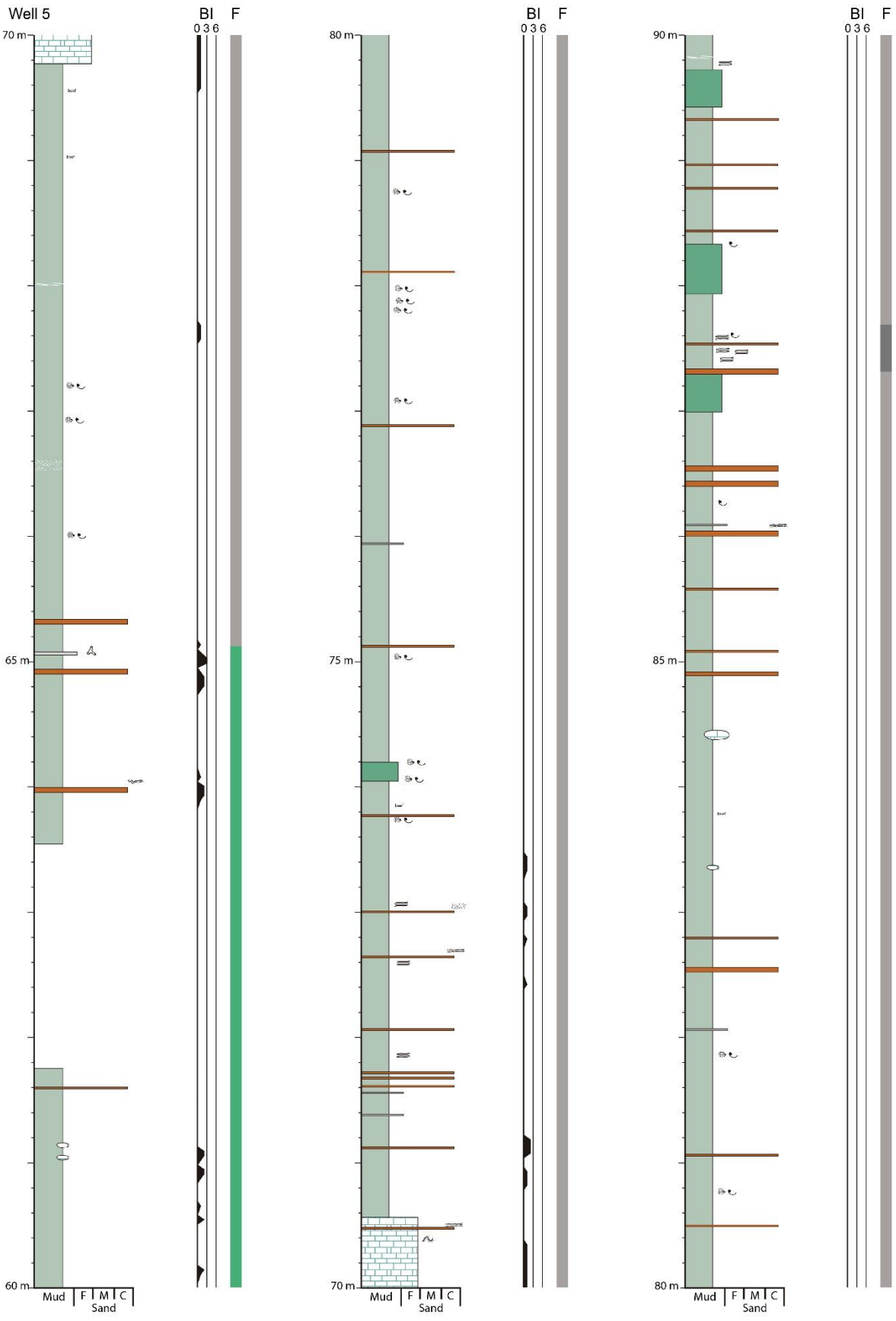
Well 5
BI
0 3 6
F
70 m
65 m
60 m
Mud
F
M
C
Sand
80 m
75 m
70 m
90 m
85 m
80 m

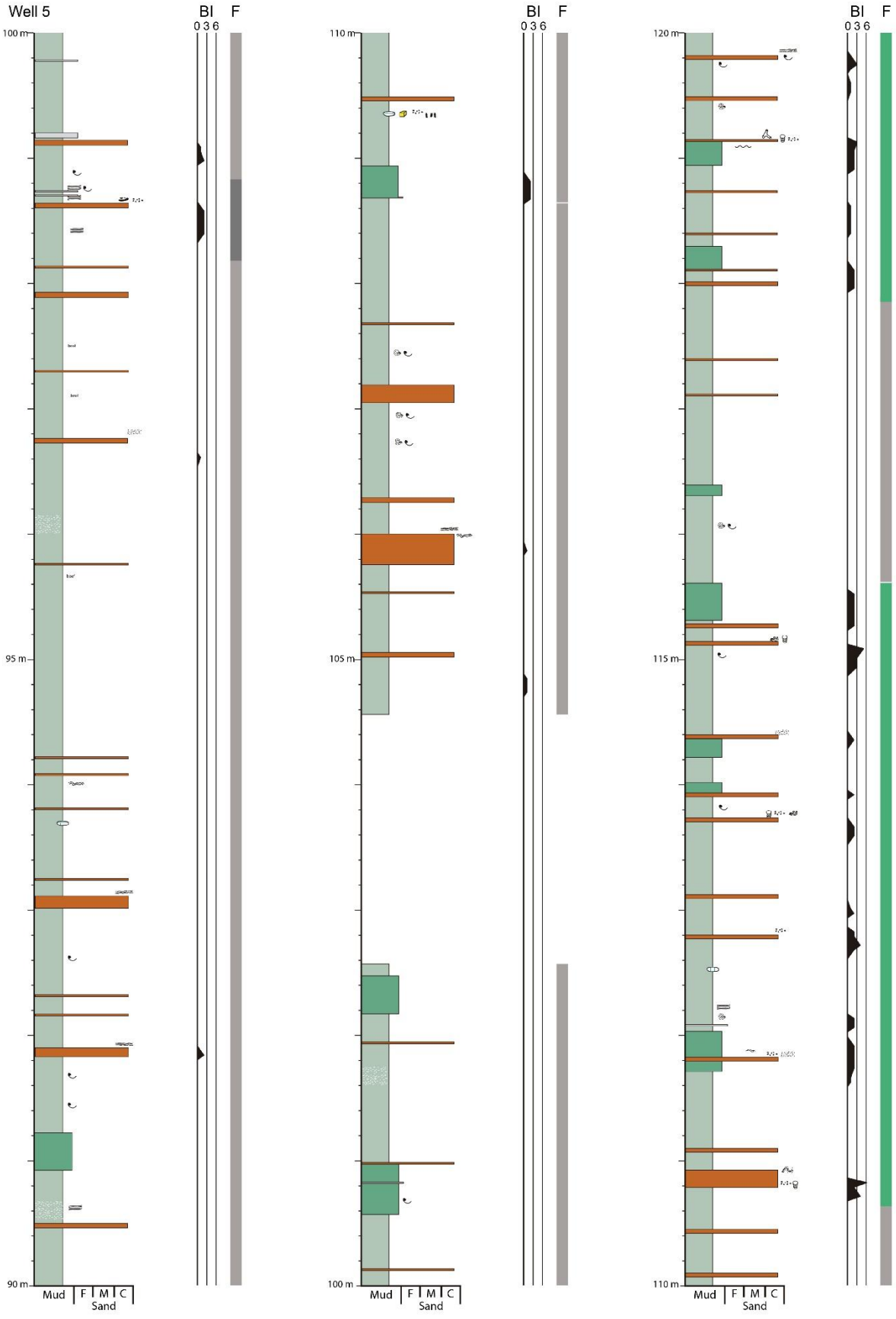
Well 5
BI
0 3 6
F
100 m
95 m
90 m
Mud
F
M
C
Sand
110 m
105 m
100 m
120 m
115 m
110 m

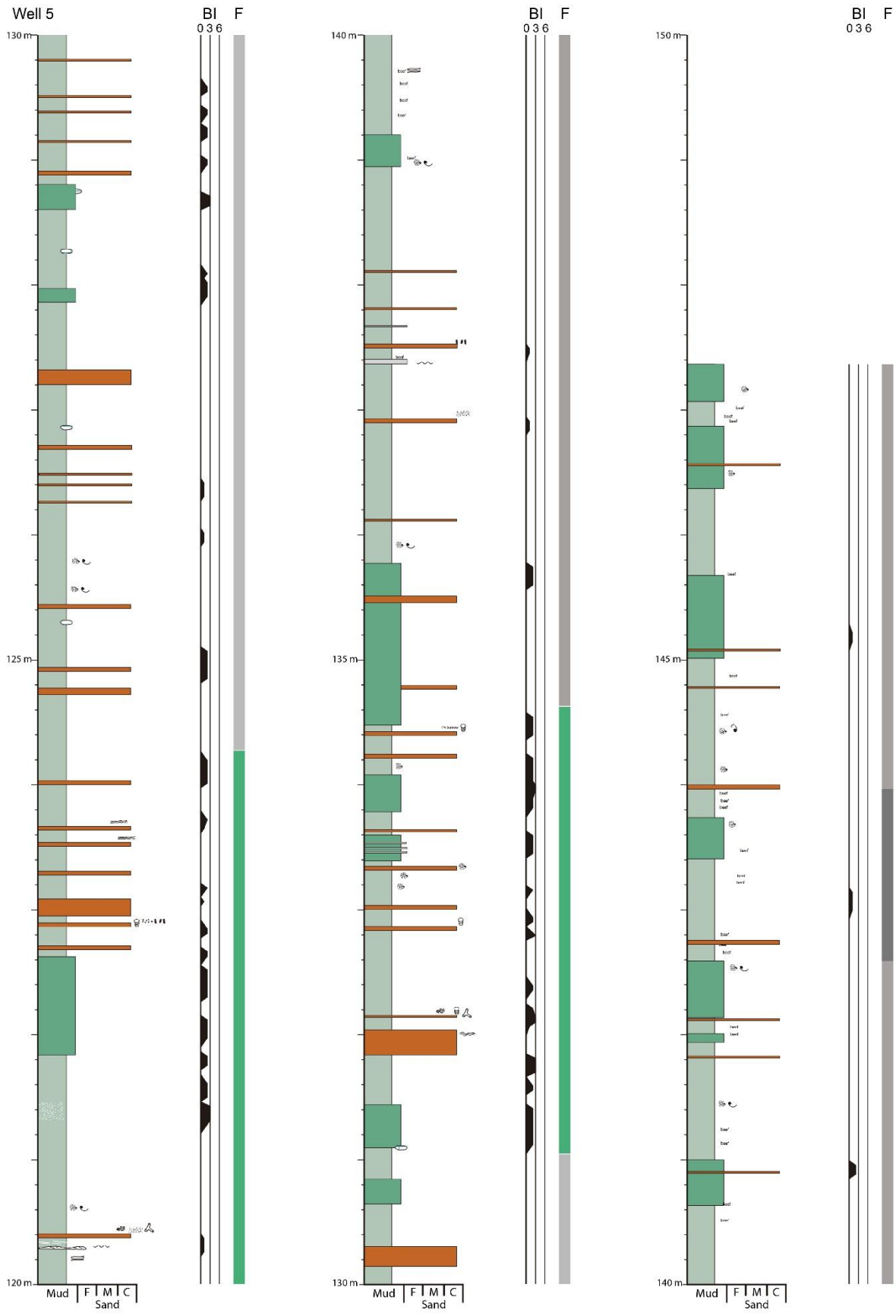
Well 5
BI
F
0 3 6
130 m
125 m
120 m
Mud
F
M
C
Sand
140 m
135 m
130 m
150 m
145 m
140 m

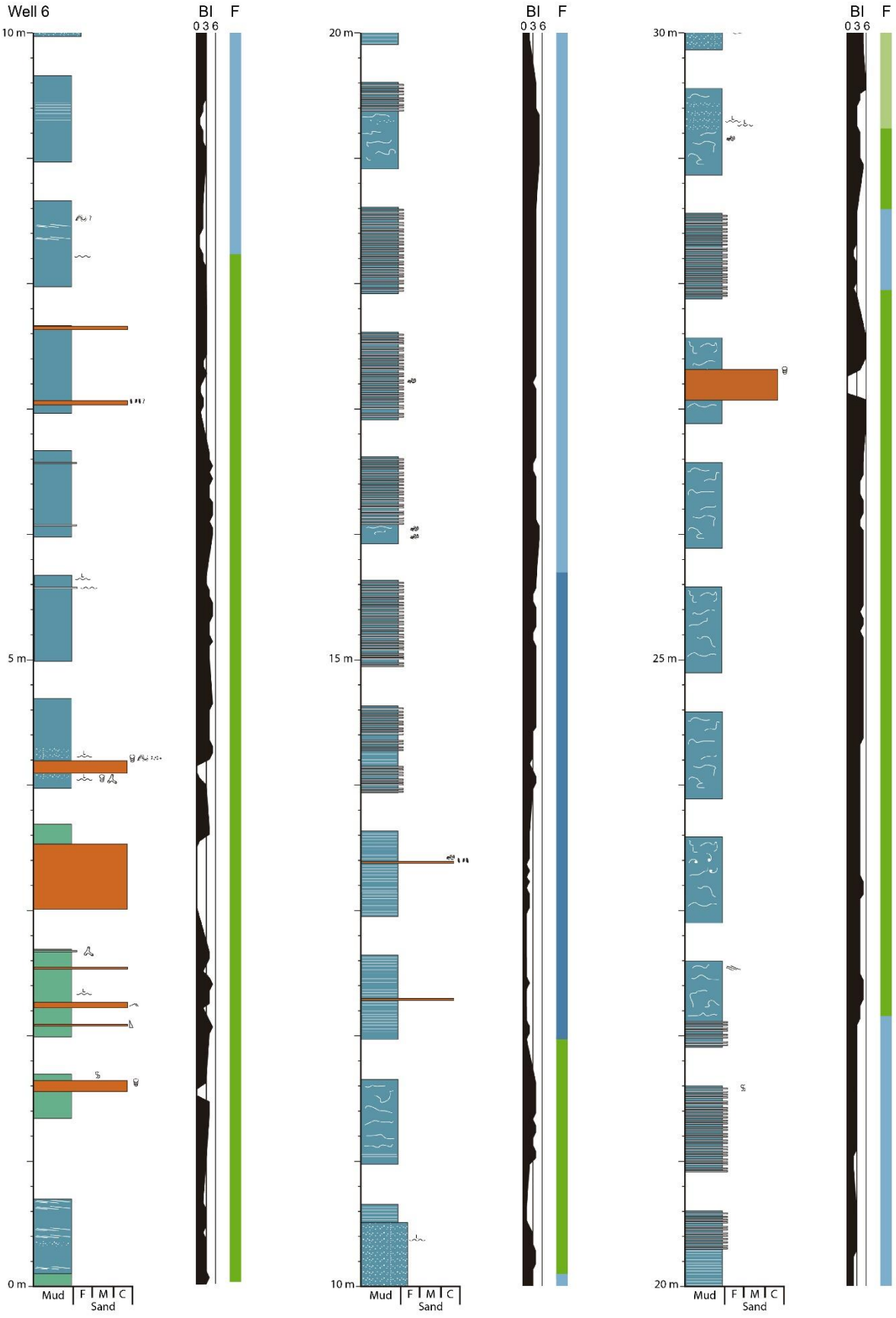
Well 6
BI
0 3 6
F
10 m
5 m
0 m
Mud
F
M
C
Sand
20 m
15 m
10 m
30 m
25 m
20 m

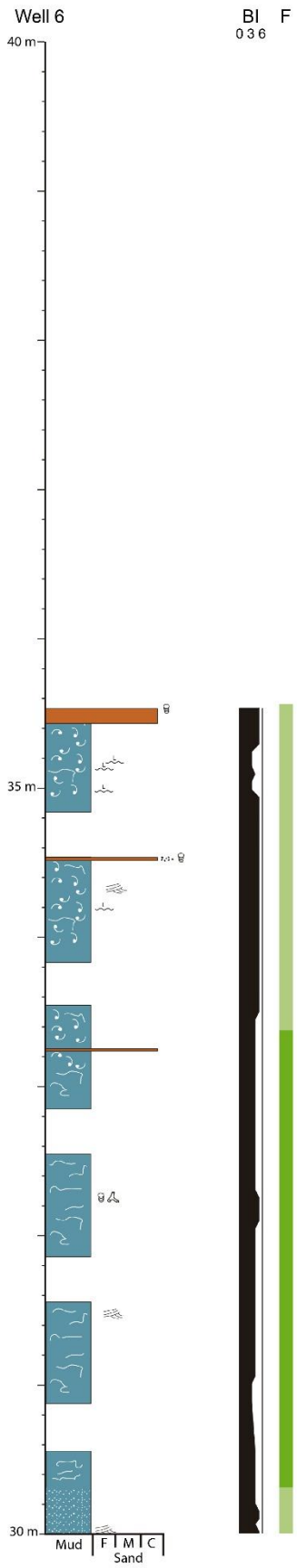
Well 6
BI F
0 3 6
40 m
35 m
30 m
Mud
F
M
C
Sand

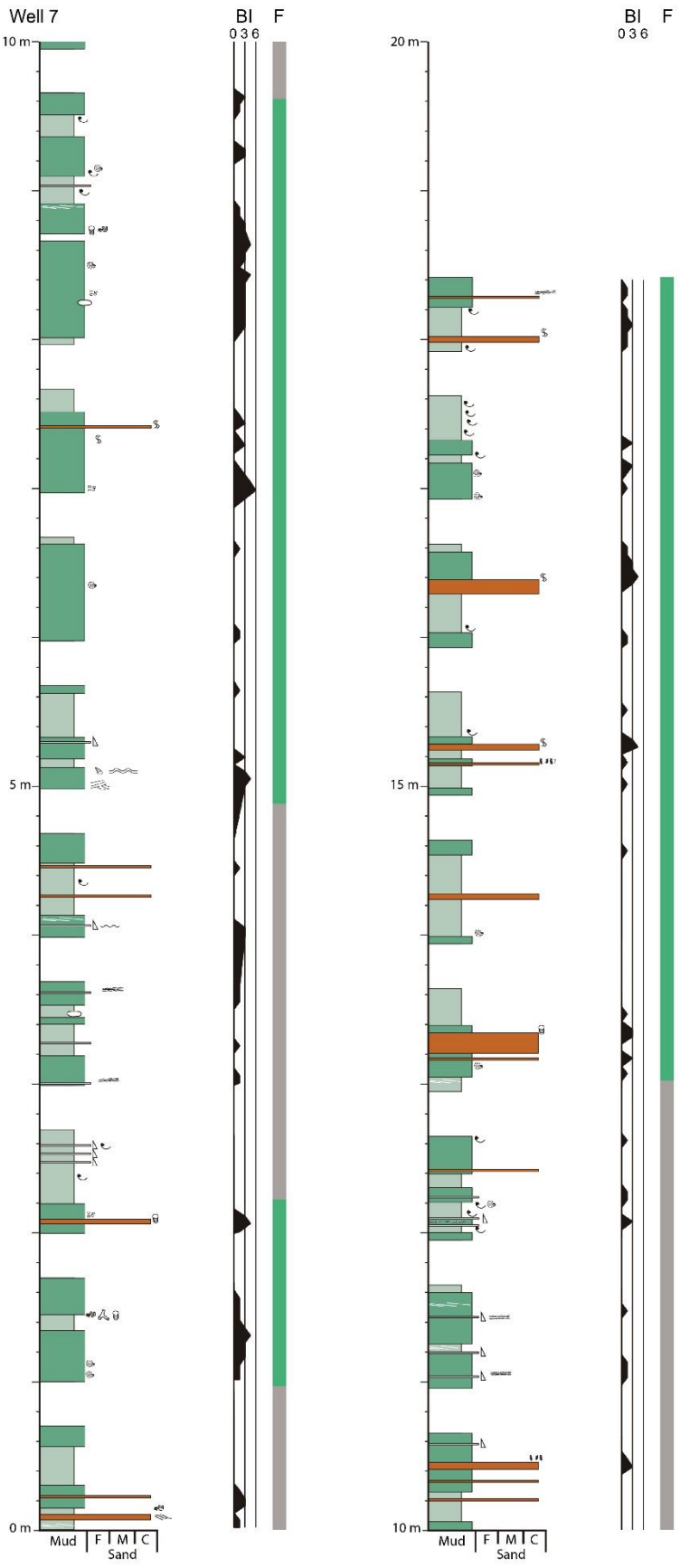
Well 7
BI
0 3 6
F
10 m
5 m
0 m
Mud
F
M
C
Sand
20 m
15 m
10 m

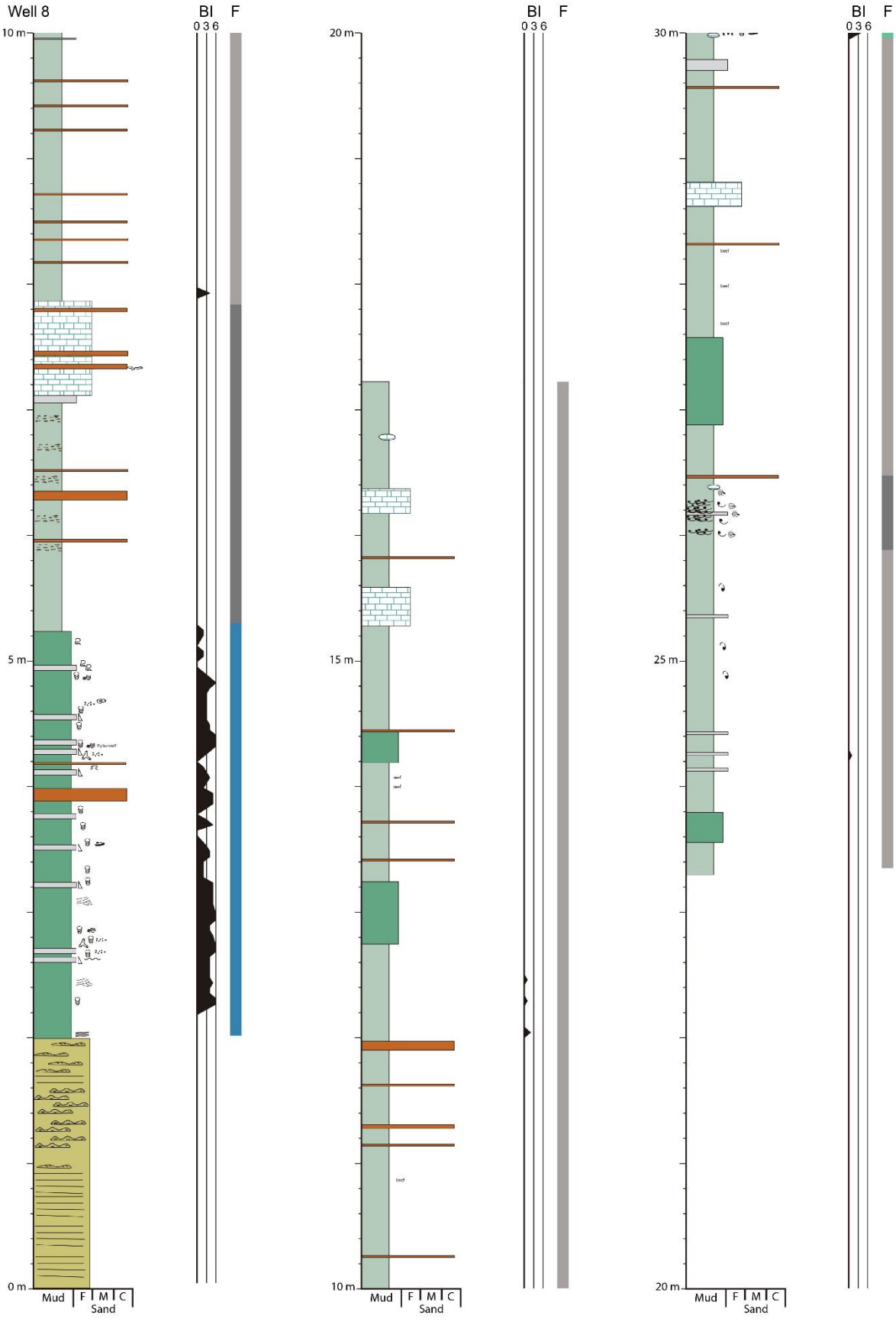
Well 8
BI
0 3 6
F
10 m
5 m
0 m
Mud
F
M
C
Sand
20 m
15 m
10 m
30 m
25 m
20 m

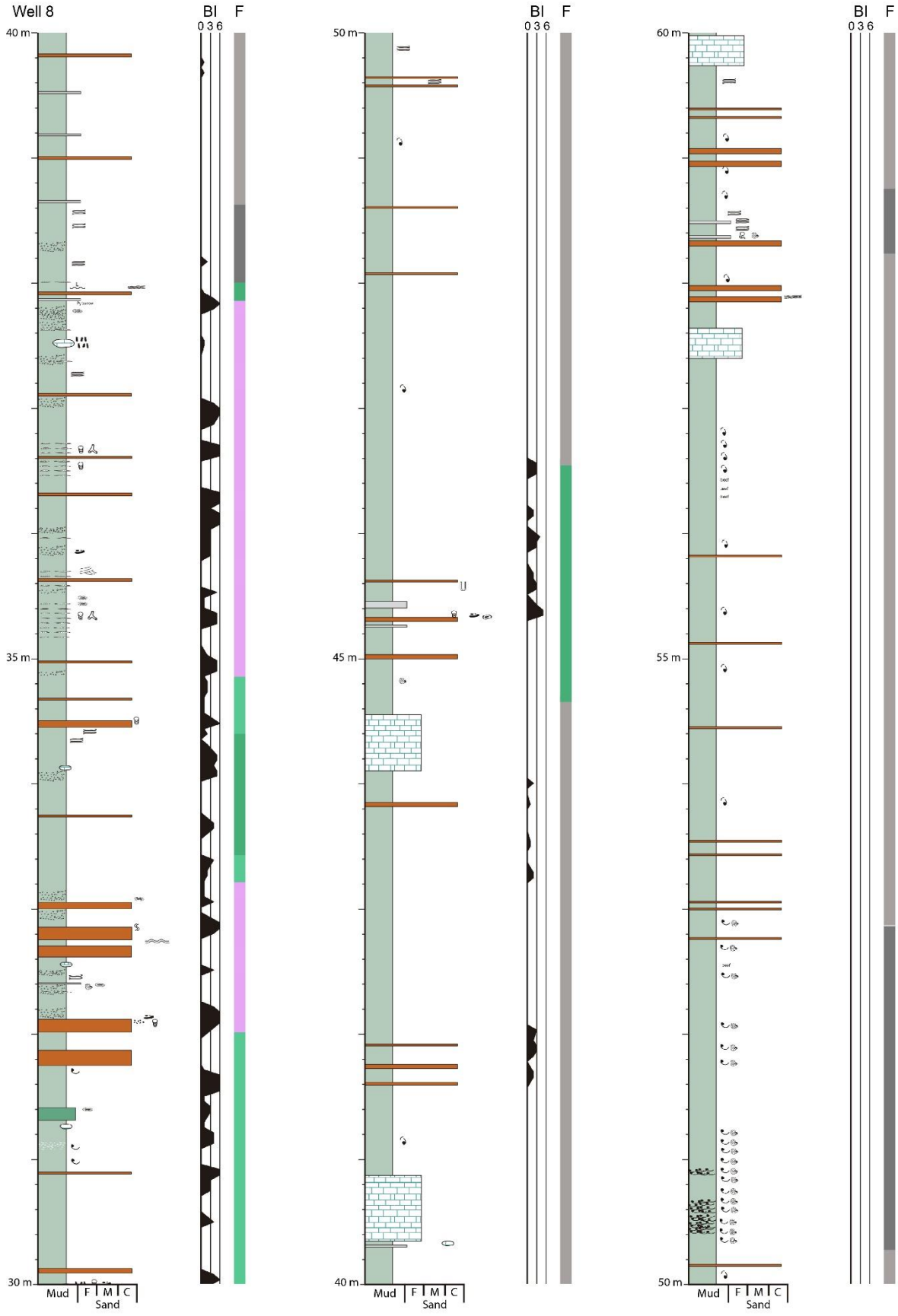
Well 8
BI
0 3 6
F
40 m
35 m
30 m
Mud
F
M
C
Sand
50 m
45 m
40 m
60 m
55 m
50 m

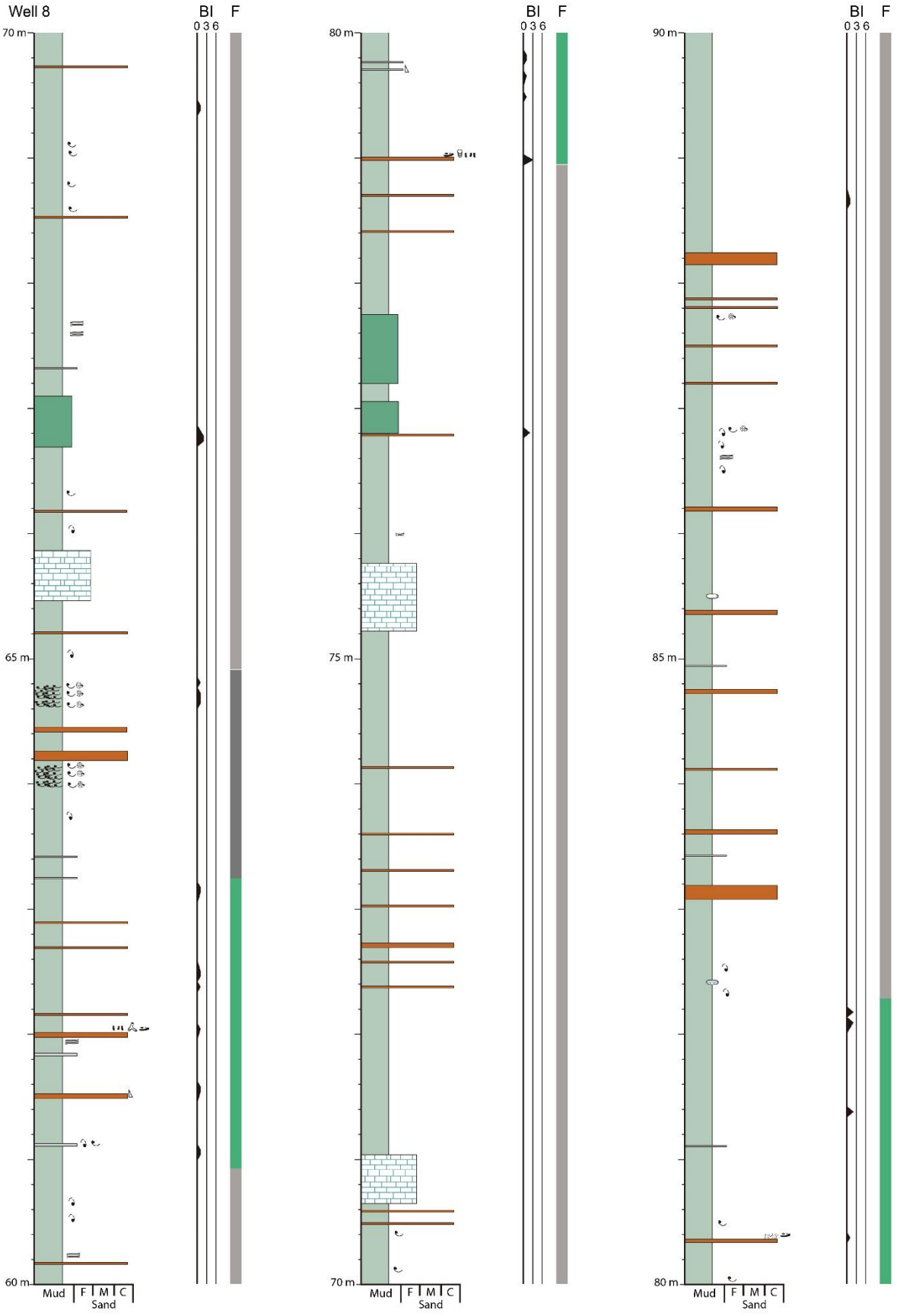
Well 8
BI
0 3 6
F
70 m
65 m
60 m
Mud
F
M
C
Sand
80 m
75 m
70 m
90 m
85 m
80 m

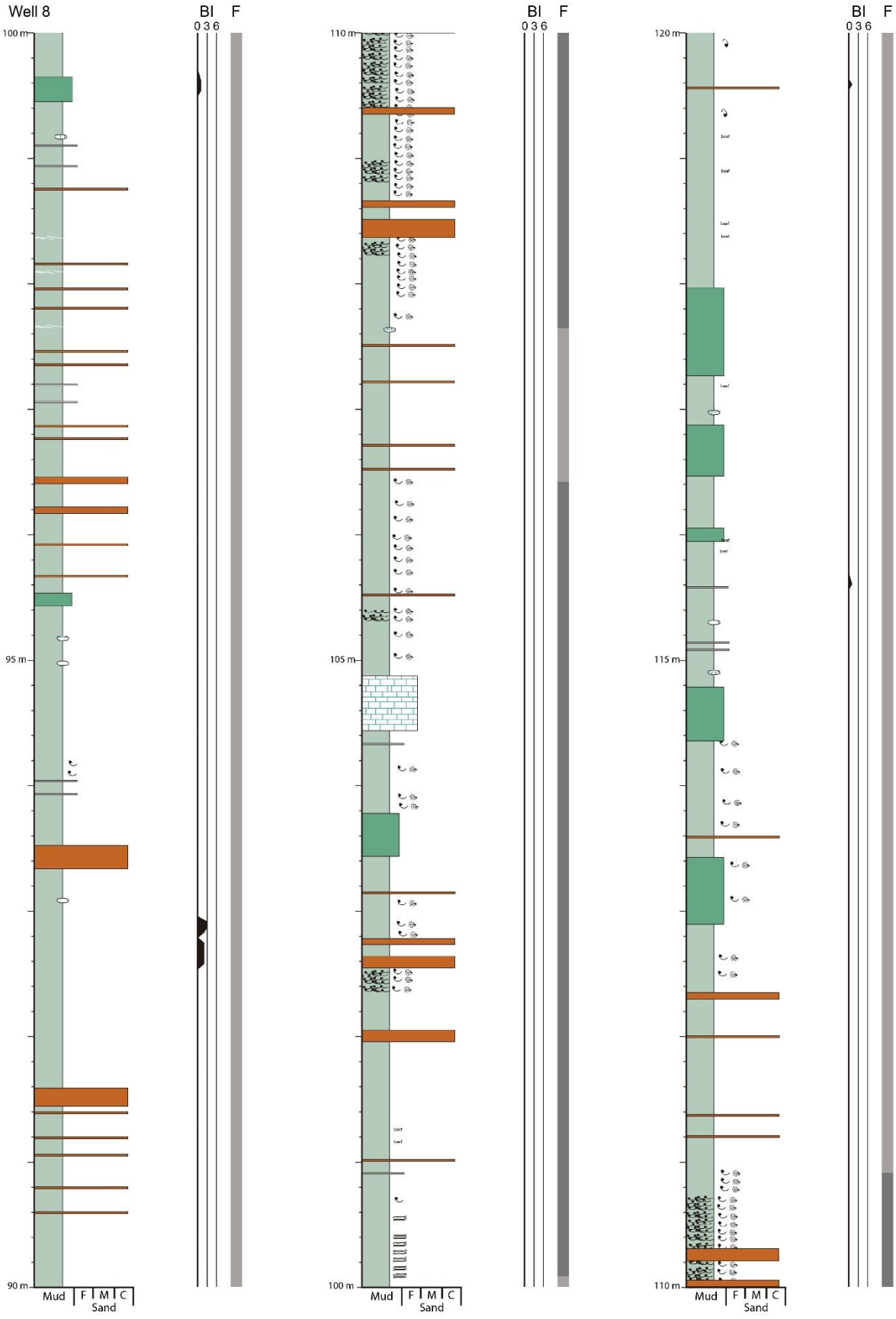
Well 8
BI
0 3 6
F
100 m
95 m
90 m
Mud
F
M
C
Sand
110 m
105 m
100 m
120 m
115 m
110 m

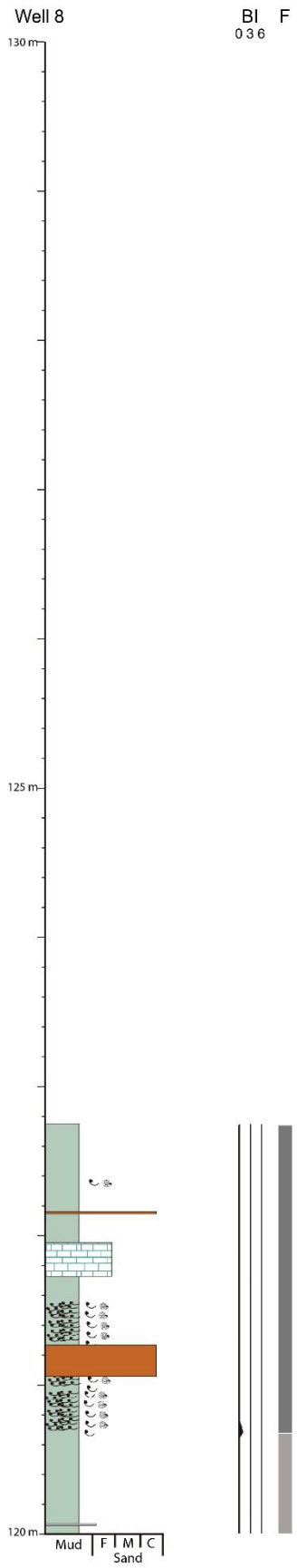
Well 8
BI F
0 3 6
130 m
125 m
120 m
Mud
F
M
C
Sand

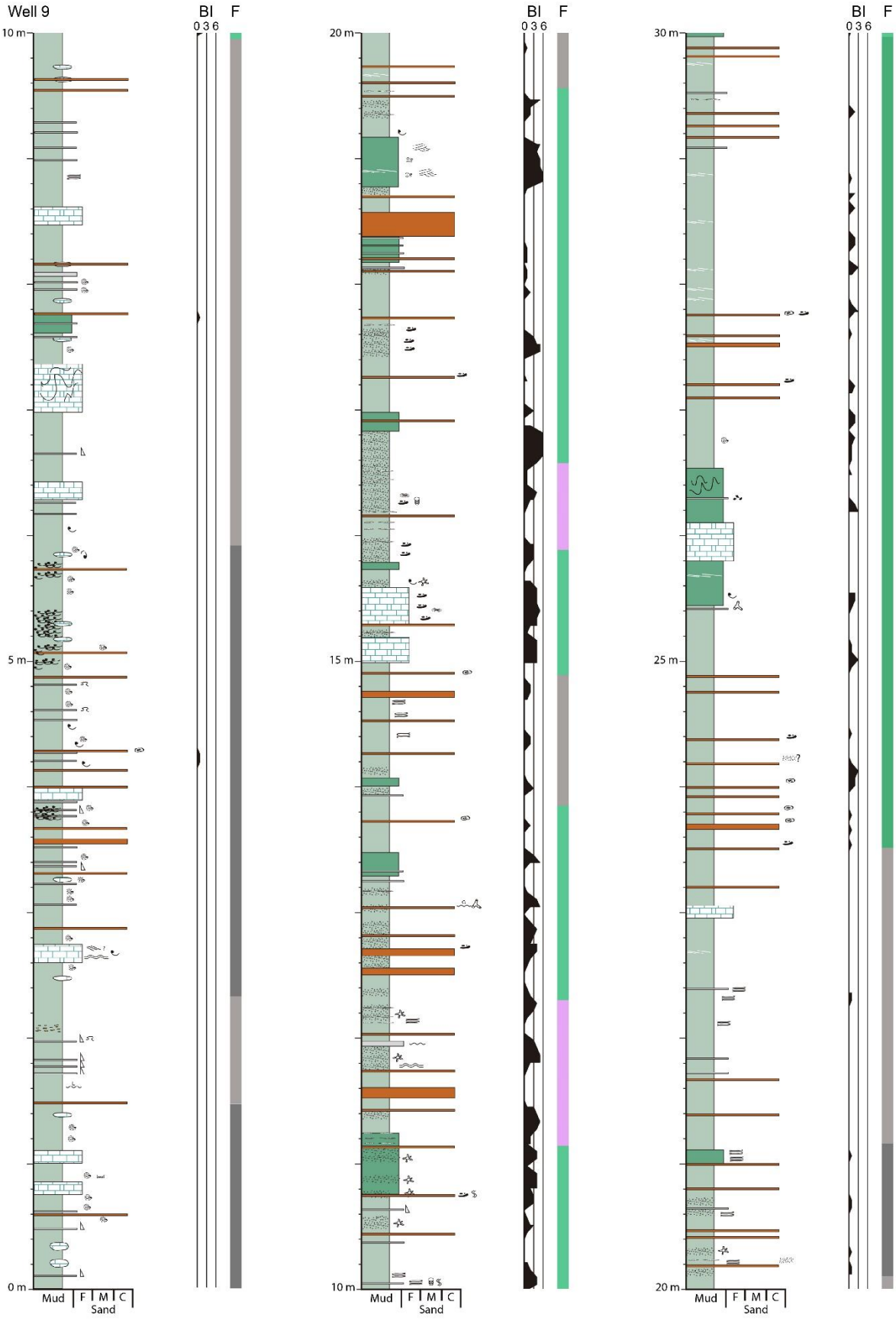
Well 9
BI
0 3 6
F
10 m
5 m
0 m
Mud
F
M
C
Sand
20 m
15 m
10 m
30 m
25 m
20 m

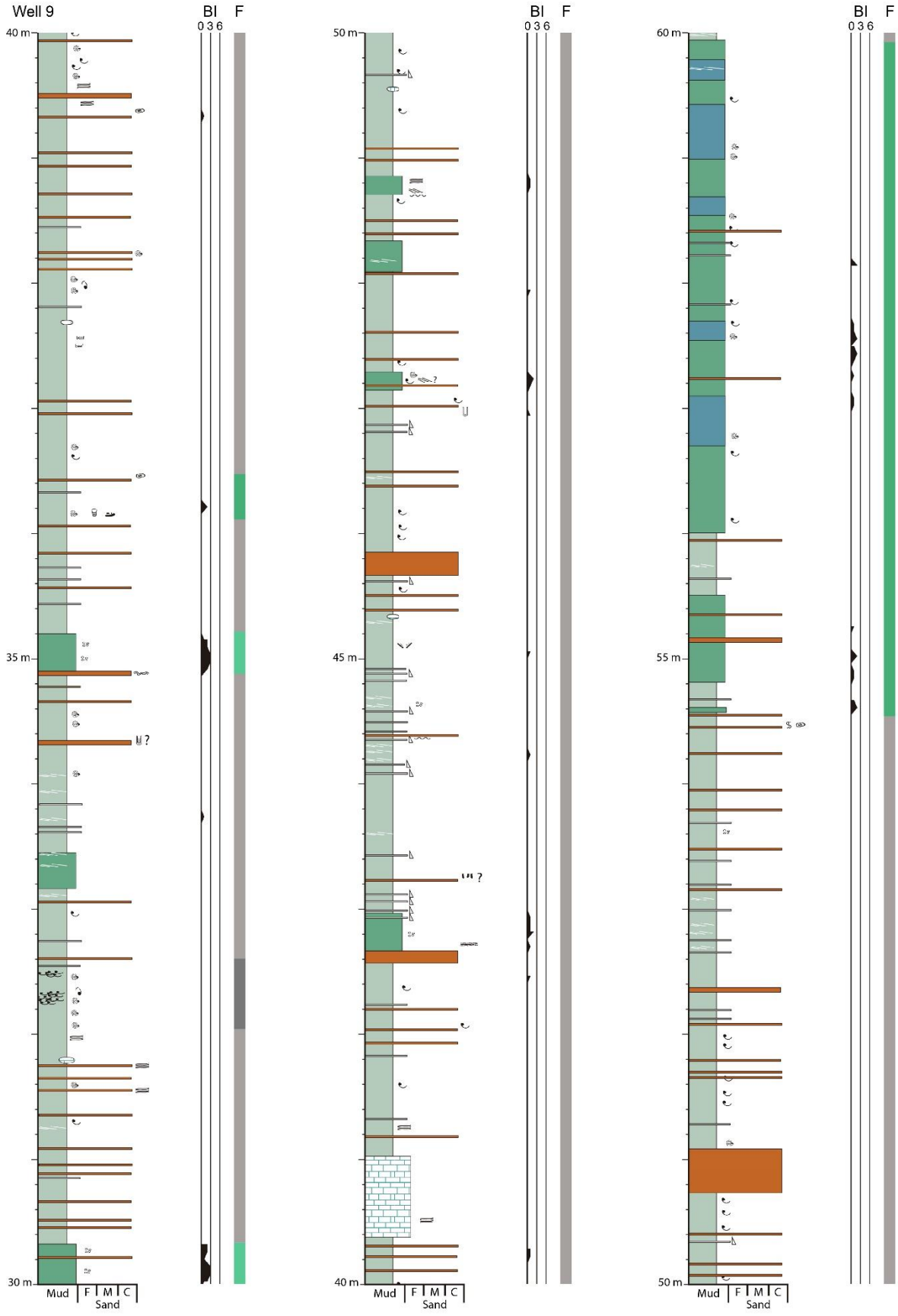
Well 9
BI
0 3 6
F
40 m
35 m
30 m
50 m
45 m
40 m
60 m
55 m
50 m
Mud
F
M
C
Sand

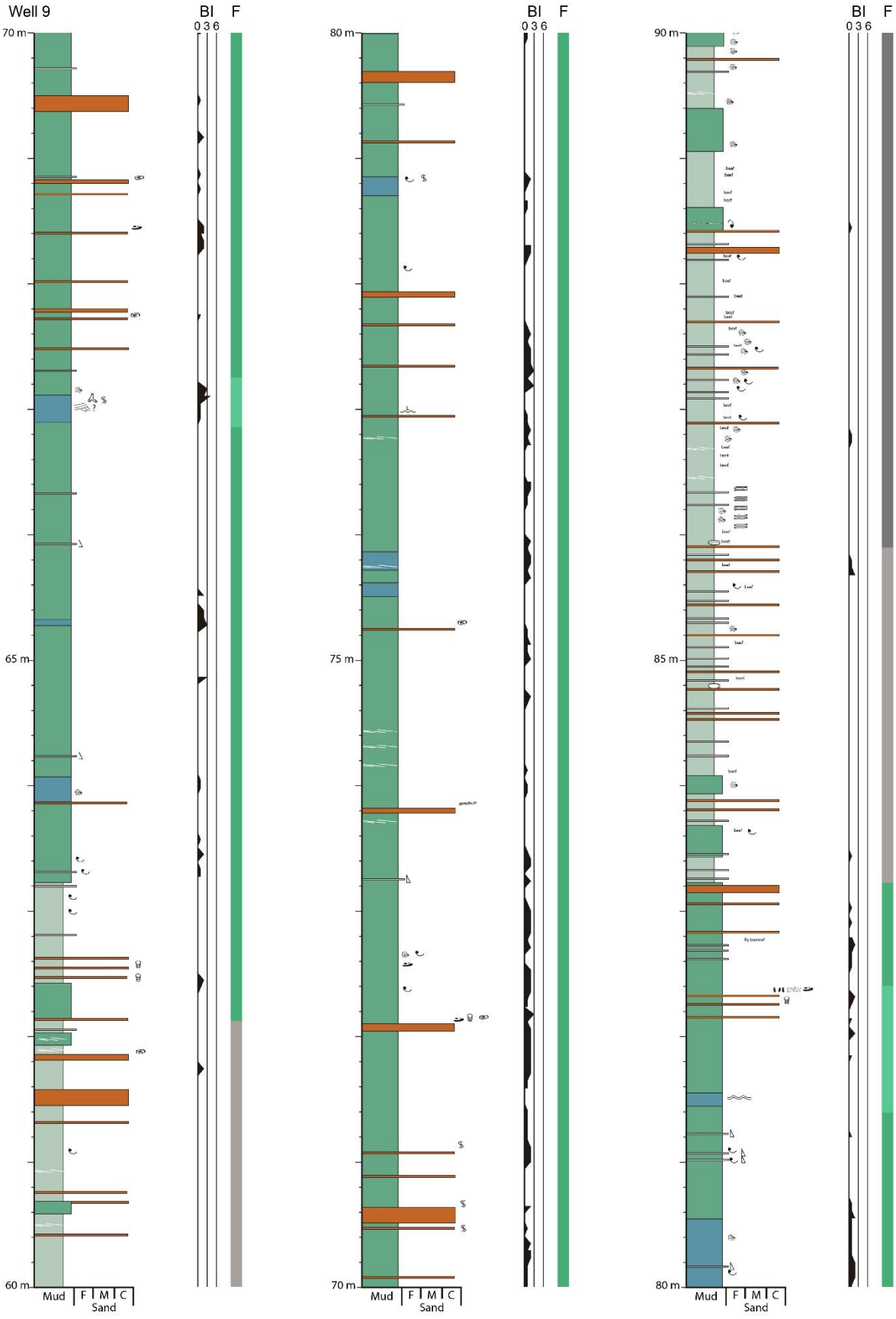
Well 9
BI
0 3 6
F
70 m
65 m
60 m
Mud
F
M
C
Sand
80 m
75 m
70 m
90 m
85 m
80 m

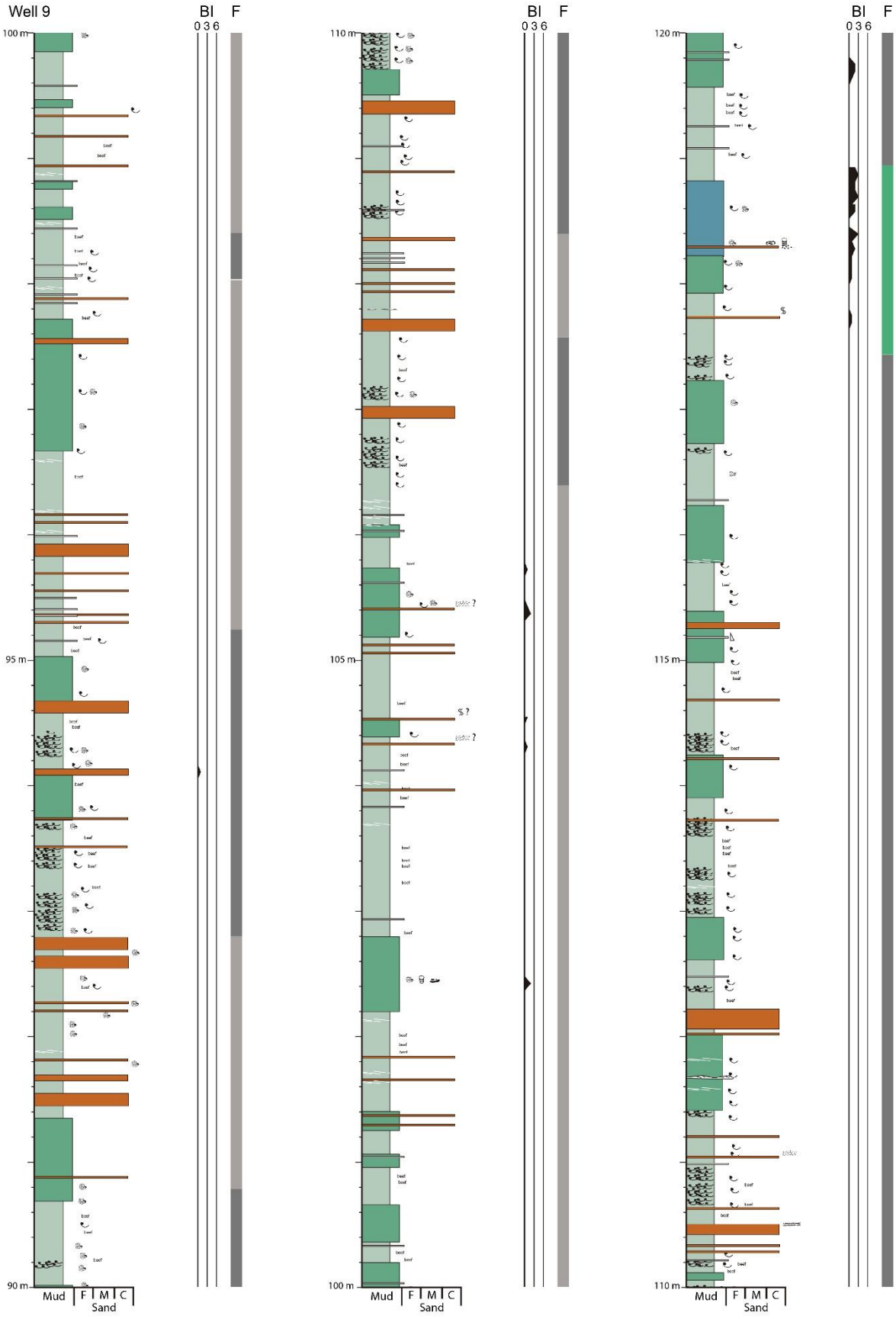
Well 9
BI
F
0 3 6
100 m
95 m
90 m
110 m
105 m
100 m
120 m
115 m
110 m
Mud
F
M
C
Sand

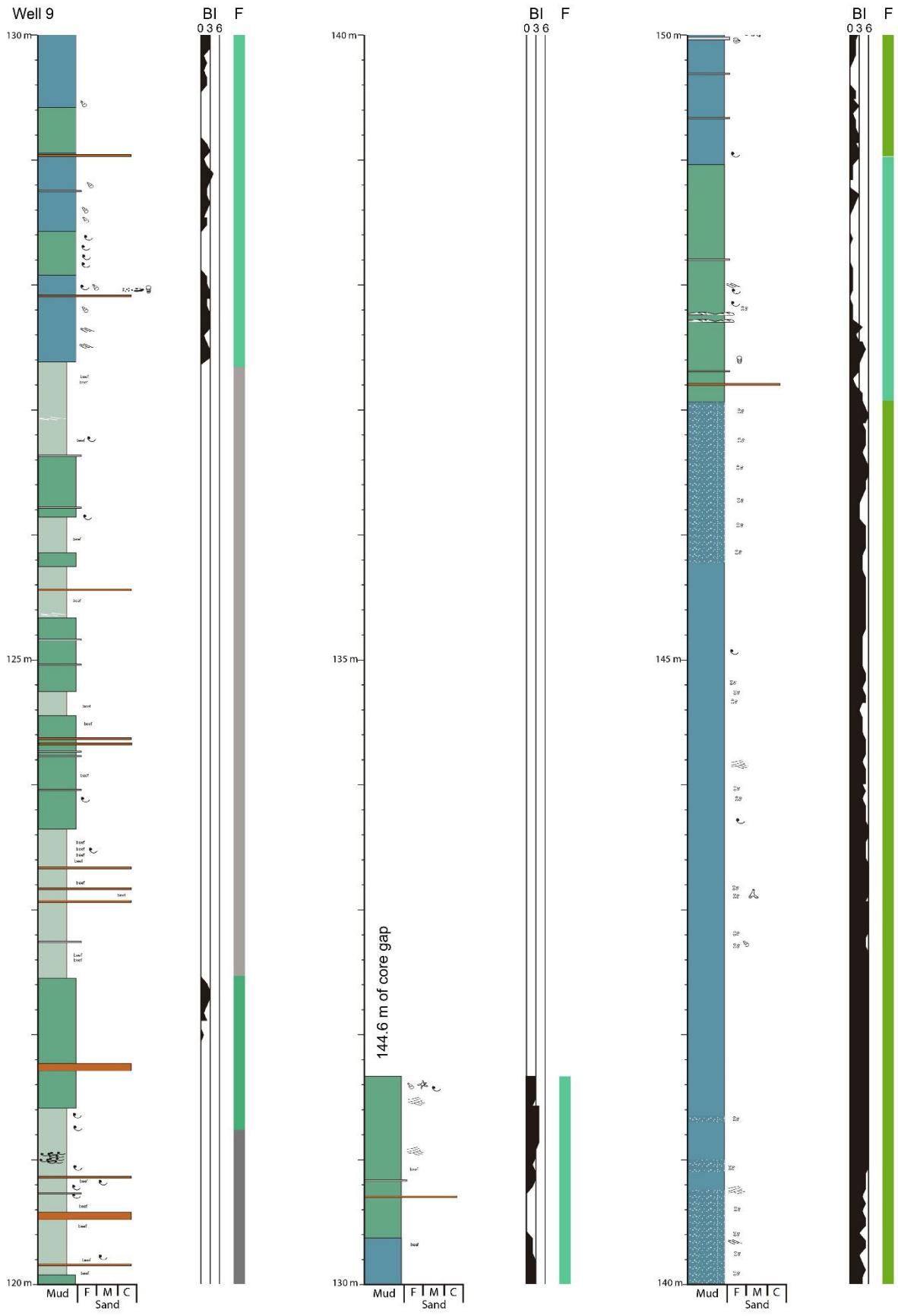
Well 9
BI
0 3 6
F
130 m
125 m
120 m
Mud
F
M
C
Sand
140 m
135 m
130 m
144.6 m of core gap
150 m
145 m
140 m

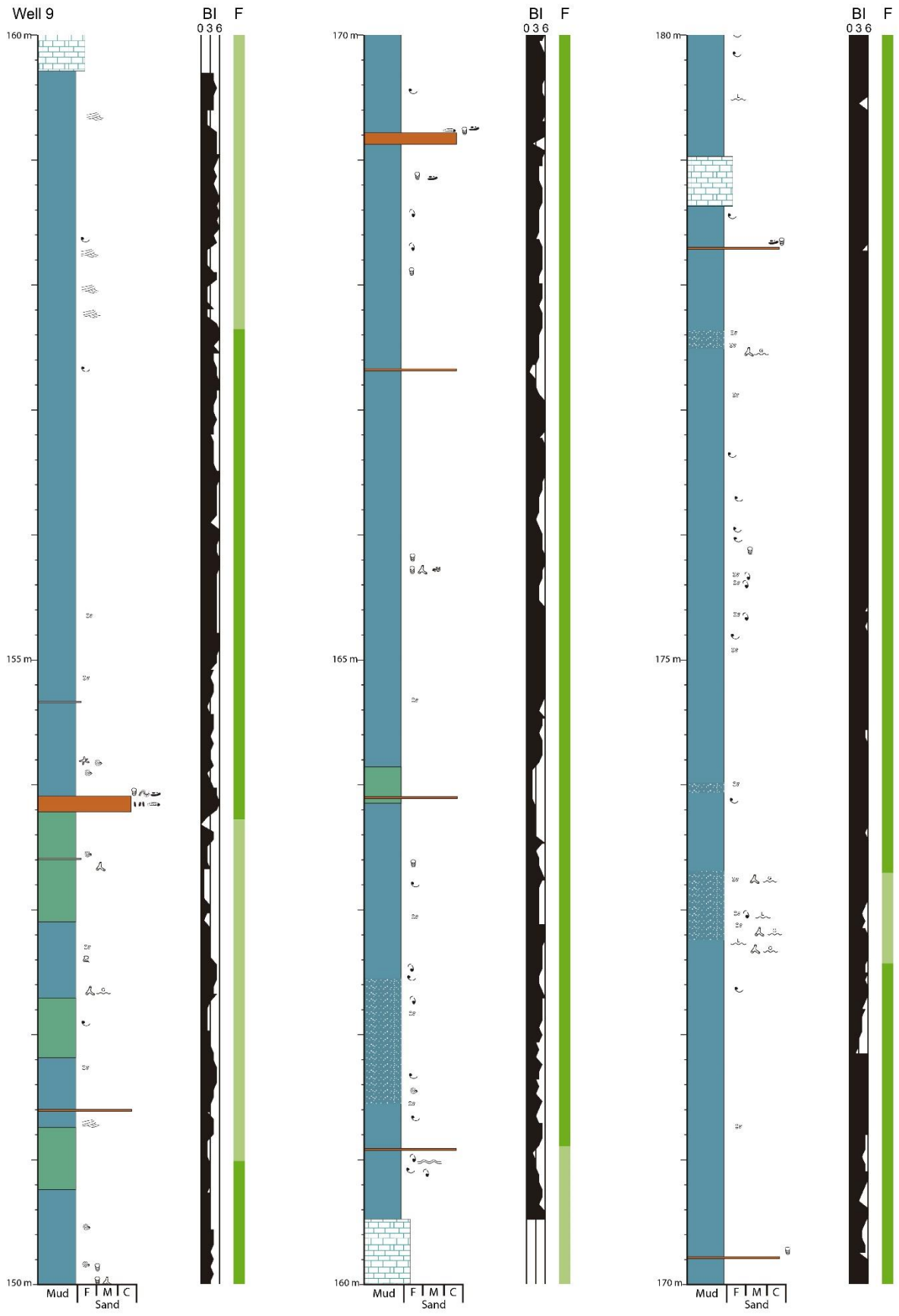
Well 9
BI
0 3 6
F
160 m
155 m
150 m
Mud
F
M
C
Sand
170 m
165 m
160 m
180 m
175 m
170 m

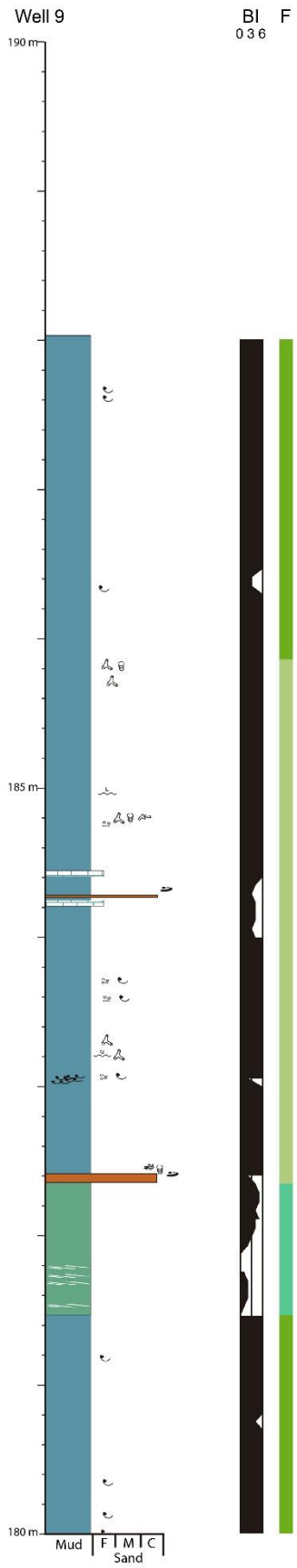
Well 9
BI F
0 3 6
190 m
185 m
180 m
Mud
F
M
C
Sand

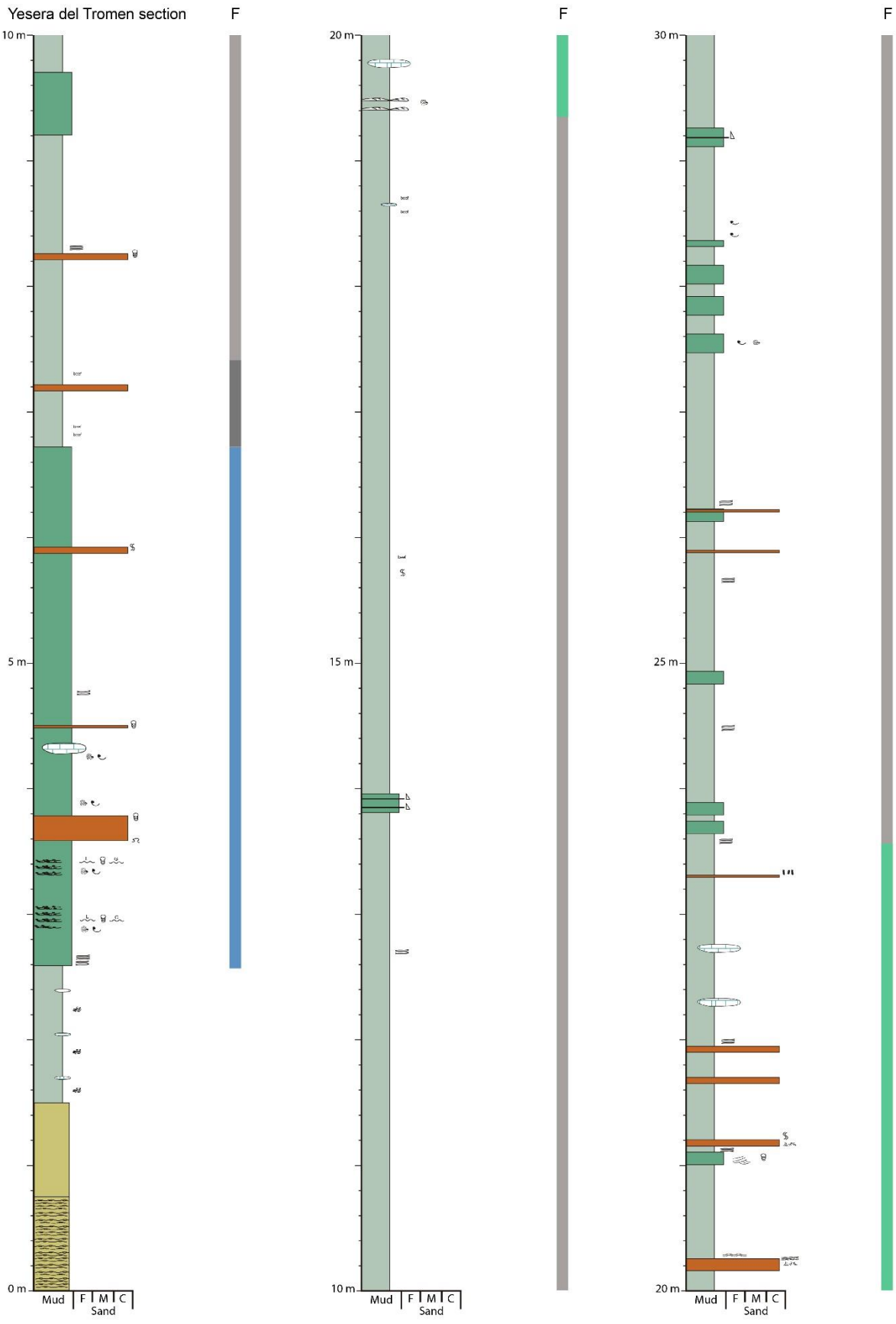
Yesera del Tromen section
F
10 m
5 m
0 m
Mud
F
M
C
Sand
F
20 m
15 m
10 m
Mud
F
M
C
Sand
F
30 m
25 m
20 m
Mud
F
M
C
Sand

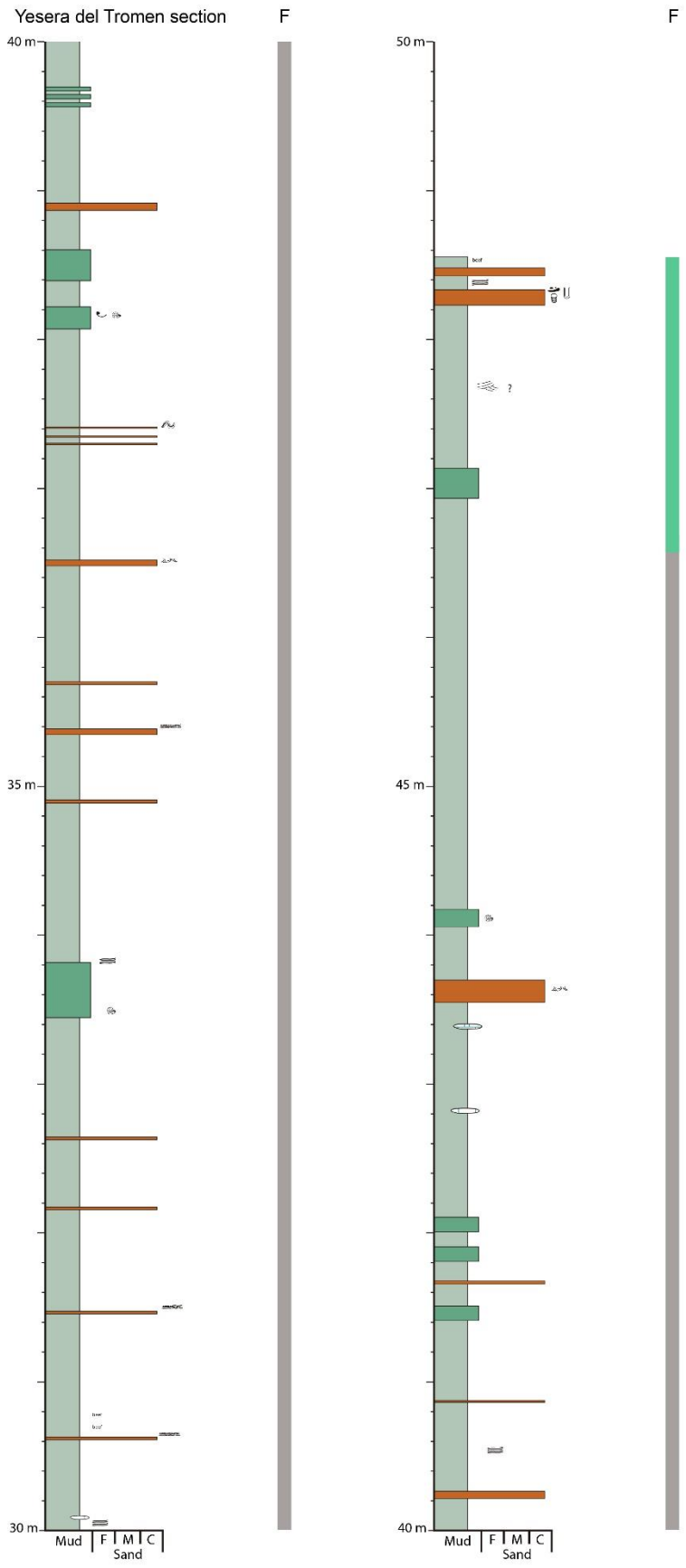
Yesera del Tromen section
F
40 m
35 m
30 m
Mud
F
M
C
Sand
F
50 m
45 m
40 m
Mud
F
M
C
Sand

APPENDIX C

Normalized XRD geochemical data.

Well	Quartz (normalized)	Carbonate (normalized)	Clay (norm)	Facies	BI
2	0.2235	0.5734	0.2031	F4c	5
2	0.2029	0.5895	0.2076	F4c	4
2	0.1793	0.6438	0.1769	F4c	4
2	0.2333	0.5421	0.2246	F4c	4
2	0.2102	0.5802	0.2096	F4c	4
2	0.2176	0.5777	0.2047	F4c	4
2	0.1905	0.6361	0.1734	F4c	3
2	0.1980	0.6028	0.1992	F4b	4
2	0.1832	0.6140	0.2028	F4c	4
2	0.1766	0.6531	0.1704	F4c	3
2	0.1909	0.6215	0.1875	F4c	4
2	0.1773	0.6445	0.1783	F4c	4
2	0.2234	0.5494	0.2272	F4b	3
2	0.1977	0.6002	0.2021	F4b	3
2	0.2127	0.5795	0.2078	F4b	3
2	0.2532	0.4991	0.2477	F4b	3
2	0.2469	0.4978	0.2552	F4b	
2	0.2554	0.5059	0.2386	F4b	2
2	0.2432	0.5309	0.2259	F4b	3
2	0.2593	0.5009	0.2398	F4b	3
2	0.1327	0.6794	0.1879	F4b	
2	0.2303	0.5397	0.2301	F4b	2
2	0.1797	0.6440	0.1763	F4b	4
2	0.2620	0.4776	0.2604	F4b	4
2	0.2616	0.4749	0.2635	F4b	3
2	0.2494	0.5098	0.2407	F4b	2
2	0.2692	0.4743	0.2565	F4b	2
2	0.1493	0.6969	0.1538	F4d	2
2	0.2094	0.6074	0.1832	F4d	2
2	0.2278	0.5702	0.2019	F4d	1
2	0.1779	0.6624	0.1597	F4d	2
2	0.2686	0.5049	0.2265	F4d	1
2	0.2164	0.5720	0.2116	F4d	1
2	0.1838	0.6446	0.1716	F4d	0
2	0.2270	0.5688	0.2042	F4d	1
2	0.2664	0.4949	0.2387	F4d	1

2	0.1839	0.6406	0.1755	F4d	2
2	0.2369	0.5470	0.2161	F4d	0
2	0.3070	0.4167	0.2764	F4d	0
2	0.2228	0.5735	0.2037	F4d	1
2	0.1758	0.6495	0.1747	F4d	2
2	0.2078	0.5958	0.1964	F4d	
2	0.2454	0.5585	0.1960	F4d	
2	0.1963	0.6366	0.1671	F4d	0
2	0.2180	0.5990	0.1830	F4d	0
2	0.2934	0.4430	0.2636	F4d	0
2	0.2735	0.4474	0.2791	F3c	1
2	0.2375	0.5279	0.2346	F3c	0
2	0.3188	0.3566	0.3246	F3c	2
2	0.2371	0.5373	0.2257	F3c	2
2	0.2107	0.6193	0.1700	F3c	2
2	0.2951	0.3660	0.3389	F3c	0
2	0.1315	0.6556	0.2130	F3c	1
2	0.1545	0.6672	0.1783	F3c	2
2	0.2272	0.5885	0.1843	F3c	3
2	0.1330	0.6799	0.1870	F3c	2
2	0.1849	0.6280	0.1871	F3c	2
2	0.4943	0.1606	0.3450	F3c	4
2	0.1623	0.6468	0.1909	F3c	6
2	0.2130	0.6058	0.1812	F3c	4
2	0.1901	0.6545	0.1553	F3c	0
2	0.1365	0.7200	0.1436	F3c	2
2	0.1508	0.7032	0.1459	F3c	2
2	0.1583	0.6840	0.1577	F3c	2
2	0.1606	0.6943	0.1451	F3c	2
2	0.1554	0.6880	0.1566		
2	0.1495	0.7036	0.1469		
2	0.1645	0.6870	0.1485	F4d	1
2	0.1872	0.6289	0.1839	F4d	1
2	0.1999	0.5819	0.2182	F4d	2
2	0.2804	0.4804	0.2392	F4a	0
2	0.2817	0.4755	0.2428	F4a	0
2	0.2796	0.4634	0.2570	F4a	0
2	0.3178	0.3924	0.2898	F4a	0
2	0.2237	0.5491	0.2272	F4a	0
2	0.2003	0.6005	0.1991	F2d	0
2	0.2230	0.5762	0.2008	F2d	0

2	0.2797	0.4505	0.2698	F2d	1
2	0.2906	0.4295	0.2799	F2d	1
2	0.2944	0.4298	0.2758	F2d	1
2	0.2756	0.4620	0.2624	F2d	0
2	0.3478	0.3698	0.2824	F2d	0
2	0.2851	0.4374	0.2775	F2d	2
2	0.3444	0.3469	0.3088	F2d	0
2	0.2583	0.4847	0.2570	F2d	0
2	0.3428	0.3365	0.3208	F2d	0
2	0.2309	0.5602	0.2089	F2d	2
2	0.3566	0.3368	0.3066	F2d	0
2	0.2857	0.4620	0.2523	F2b	2
2	0.2322	0.4977	0.2701	F2b	3
2	0.3532	0.3558	0.2910	F2b	0
2	0.1043	0.7071	0.1886	F2b	0
2	0.3146	0.1924	0.4929	F2b	0
2	0.2987	0.1939	0.5073	F2b	0
2	0.3695	0.3305	0.3000	F2b	0
2	0.3393	0.3696	0.2911	F2b	0
2	0.3006	0.4196	0.2797	F2b	0
2	0.3245	0.3642	0.3113	F2b	0
2	0.3338	0.3681	0.2981	F2b	0
2	0.3269	0.3610	0.3121	F2b	0
2	0.1791	0.5249	0.2961	F2b	0
2	0.1060	0.6915	0.2025	F2b	0
2	0.3384	0.3667	0.2950	F2b	0
2	0.2349	0.4717	0.2934	F2b	0
2	0.3266	0.3866	0.2868	F2b	0
2	0.3261	0.3496	0.3243	F2b	0
2	0.3398	0.3393	0.3209	F2b	0
2	0.3414	0.3575	0.3011	F2b	0
2	0.3249	0.3776	0.2975	F2b	0
2	0.2972	0.4204	0.2824	F2b	1
2	0.3296	0.3481	0.3223	F2b	0
2	0.3231	0.3342	0.3427	F2c	0
2	0.1163	0.6758	0.2079	F2c	0
2	0.3111	0.1472	0.5416	F2c	0
2	0.3189	0.3692	0.3118	F2c	0
2	0.1629	0.6460	0.1911	F2c	2
2	0.1335	0.6541	0.2124	F2c	4
2	0.3284	0.3628	0.3088	F2c	0

2	0.3053	0.3924	0.3023	F2c	2
2	0.3428	0.2804	0.3768	F2c	0
2	0.3039	0.2405	0.4556	F2b	0
2	0.3639	0.2847	0.3514	F2b	0
2	0.3425	0.3363	0.3212	F2b	0
2	0.3001	0.3994	0.3004	F2b	0
2	0.3386	0.3088	0.3526	F2b	0
2	0.3300	0.3463	0.3237	F2b	0
2	0.3707	0.2835	0.3458	F2b	2
2	0.3751	0.3384	0.2865	F2b	0
2	0.3532	0.3279	0.3189	F2b	0
2	0.3004	0.3929	0.3067	F2b	0
2	0.3011	0.4012	0.2977	F2b	0
2	0.3241	0.3455	0.3304	F2b	0
2	0.3617	0.2949	0.3434	F2b	0
2	0.2839	0.4487	0.2673	F2b	0
2	0.3495	0.3282	0.3224	F2b	0
2	0.3068	0.3869	0.3063	F2b	0
2	0.2724	0.4853	0.2423	F2b	2
2	0.3181	0.3569	0.3250	F2b	0
2	0.3086	0.3736	0.3178	F2b	0
2	0.3323	0.3585	0.3091	F2b	0
2	0.1352	0.6460	0.2187	F2b	2
2	0.3197	0.4084	0.2719	F2b	0
2	0.2922	0.4420	0.2658	F2b	0
2	0.3051	0.4075	0.2875	F2b	0
2	0.3478	0.1468	0.5054	F2b	0
2	0.3474	0.3273	0.3253	F2b	0
2	0.3462	0.3241	0.3298	F2b	0
2	0.3234	0.4159	0.2607	F2b	0
2	0.2482	0.5387	0.2132	F2b	3
2	0.3699	0.2638	0.3662	F2b	0
2	0.1093	0.6902	0.2005	F2b	0
2	0.3239	0.1473	0.5288	F2b	0
2	0.3419	0.3545	0.3035	F2b	0
2	0.0967	0.7248	0.1784	F2d	0
2	0.3197	0.3575	0.3228	F2d	2
2	0.2808	0.4845	0.2347	F2d	0
2	0.3208	0.3736	0.3057	F2d	0
2	0.2515	0.4999	0.2486	F2d	0
2	0.3059	0.3811	0.3130	F2d	0

2	0.2397	0.5134	0.2469	F2d	0
2	0.2856	0.4376	0.2768	F2d	0
2	0.1175	0.6907	0.1918	F2d	4
2	0.3554	0.3011	0.3435	F2d	0
2	0.3004	0.4014	0.2982	F2d	0
2	0.2746	0.4902	0.2352	F2d	0
2	0.2873	0.4402	0.2725	F2d	0
2	0.2473	0.5469	0.2058	F2d	4
2	0.2645	0.5390	0.1965	F2d	2
2	0.2766	0.4875	0.2359	F2d	0
2	0.3150	0.4122	0.2728	F2b	0
2	0.3239	0.3378	0.3383	F2b	0
2	0.2725	0.4701	0.2574	F2b	0
2	0.3344	0.3460	0.3196	F2b	1
2	0.3395	0.3439	0.3165	F2b	0
2	0.3185	0.4271	0.2544	F2b	0
2	0.3335	0.3014	0.3650	F2b	0
2	0.3327	0.1204	0.5469	F2b	0
2	0.3456	0.3509	0.3035	F2b	0
2	0.3910	0.3367	0.2723	F2b	0
2	0.3317	0.3704	0.2979	F2b	0
2	0.2677	0.4942	0.2382	F2b	0
2	0.3483	0.3354	0.3163	F2b	0
2	0.3645	0.3200	0.3155	F2b	2
2	0.2255	0.4247	0.3498	F2b	0
2	0.3633	0.3212	0.3155	F2b	0
2	0.3455	0.1222	0.5323	F2b	0
2	0.3995	0.3057	0.2948	F2b	0
2	0.4145	0.2786	0.3069	F2c	0
2	0.1314	0.6388	0.2297	F2c	0
2	0.3239	0.1095	0.5666	F2c	0
2	0.3830	0.3835	0.2335	F2c	0
2	0.1316	0.6544	0.2141	F2c	0
2	0.3505	0.3142	0.3353	F2c	0
2	0.4048	0.2853	0.3099	F2c	0
2	0.3004	0.4298	0.2699	F2c	0
2	0.2038	0.5368	0.2593	F2c	0
2	0.1602	0.6475	0.1923	F3b	2
2	0.3513	0.3612	0.2876	F2b	0
2	0.3729	0.3315	0.2956	F2b	0
2	0.3786	0.2888	0.3326	F2b	0

2	0.3307	0.4103	0.2590	F2b	0
2	0.3642	0.3410	0.2948	F2b	0
2	0.3888	0.3241	0.2871	F2b	0
2	0.2100	0.5554	0.2346	F2b	0
2	0.4275	0.2750	0.2975	F2b	0
2	0.3597	0.1917	0.4485	F3b	4
2	0.3909	0.3013	0.3078	F3b	4
2	0.2952	0.4648	0.2400	F3b	2
2	0.2660	0.5060	0.2279	F3b	2
2	0.1950	0.6232	0.1817	F3b	4
2	0.2350	0.5792	0.1858	F3b	2
2	0.2455	0.5596	0.1950	F3b	2
2	0.2686	0.4983	0.2331	F3b	2
2	0.2357	0.5570	0.2073	F3b	1
2	0.4141	0.2754	0.3105	F3b	0
2	0.4475	0.2437	0.3087	F3b	2
2	0.4513	0.2226	0.3261	F3b	6
2	0.3297	0.1178	0.5525	F2c	0
2	0.1386	0.6402	0.2211	F2c	0
2	0.3273	0.1073	0.5654	F2c	0
2	0.4379	0.2384	0.3237	F2c	0
2	0.4699	0.2190	0.3111	F2c	0
2	0.4474	0.2691	0.2834	F2c	0
2	0.1753	0.6364	0.1882	F2d	4
2	0.1183	0.6803	0.2014	F2d	6
2	0.2633	0.5608	0.1759	F2d	6
2	0.2920	0.5016	0.2064	F2d	6
2	0.3998	0.3107	0.2894	F2c	0
2	0.4192	0.2652	0.3156	F2c	0
2	0.1227	0.6528	0.2244	F2c	0
2	0.1393	0.5941	0.2666	F2c	0
2	0.3184	0.1123	0.5692	F2c	0
2	0.4222	0.2949	0.2829	F2c	0
2	0.3836	0.2862	0.3301	F2c	0
2	0.3322	0.3730	0.2948	F2c	0
2	0.3941	0.2409	0.3651	F2c	0
2	0.2884	0.4514	0.2602	F2c	0
2	0.3892	0.2499	0.3609	F2c	0
2	0.3374	0.3477	0.3149	F2c	0
2	0.3132	0.3631	0.3237	F2c	0
2	0.2671	0.4726	0.2603	F2c	0

2	0.3781	0.2552	0.3667	F2c	0
2	0.4094	0.2716	0.3190	F2c	0
2	0.1177	0.6703	0.2121	F2c	0
2	0.3865	0.2450	0.3685	F2c	0
2	0.3268	0.4220	0.2511	F2c	0
4	0.5254312	0.15351861	0.3210502	F2b	0
4	0.2321908	0.69632924	0.07148	F2a	0
4	0.5360199	0.17214677	0.2918333	F2b	0
4	0.4844718	0.25484894	0.2606793	F2b	0
4	0.3526678	0.08489316	0.562439	F2b	1
4	0.5538987	0.16182487	0.2842764	F2b	0
4	0.4337706	0.30910752	0.2571219		0
4	0.4417044	0.2672234	0.2910722	F2b	0
4	0.1341762	0.75119387	0.1146299	F2b	0
4	0.5370749	0.19649844	0.2664266	F2c	1
4	0.3306647	0.47108578	0.1982495	F2b	0
4	0.2130425	0.70743561	0.0795219	F2b	0
4	0.2563693	0.68384067	0.05979	F2c	0
4	0.4576952	0.28502192	0.2572829	F2c	0
4	0.3424328	0.44561585	0.2119513	F2b	0
4	0.4460328	0.29975117	0.2542161	F2b	0
4	0.4509664	0.29485384	0.2541798	F2c	0
4	0.5081997	0.20101148	0.2907888	F2b	0
4	0.4754716	0.26742659	0.2571018	F2b	0
4	0.583284	0.13106057	0.2856554	F2b	0
4	0.4524843	0.28405737	0.2634583	F2b	0
4	0.582534	0.12756839	0.2898976	F2b	0
4	0.5136943	0.25402888	0.2322768	F2b	0
4	0.1521873	0.81291224	0.0349005	F2b	0
4	0.2583995	0.02562015	0.7159803	F2a	0
4	0.5255954	0.23757571	0.2368289	F2b	0
4	0.5369692	0.32350381	0.139527		
4	0.495321	0.15506292	0.3496161	F2b	0
4	0.5270083	0.16962505	0.3033666	F2b	0
4	0.4722778	0.25241194	0.2753103	F2b	0
4	0.0980103	0.85593911	0.0460506	F2b	0
4	0.5793569	0.0657946	0.3548485	F2c	0
4	0.5438793	0.21776709	0.2383536	F2c	0
4	0.5816193	0.1676287	0.250752	F2c	0
4	0.4747919	0.30791783	0.2172903	F2b	0
4	0.5986803	0.24678709	0.1545326	F2d	0

4	0.3332879	0.58051063	0.0862015	F3a	5
4	0.3908022	0.36306827	0.2461296	F2c	0
4	0.4937031	0.28802417	0.2182727	F3a	0
4	0.3796814	0.45526804	0.1650505	F3a	0
4	0.5475605	0.14871346	0.303726	F2b	0
4	0.4907485	0.2750881	0.2341634	F2b	0
4	0.4530607	0.34509414	0.2018451	F2a	0
4	0.4305839	0.31047265	0.2589434		
4	0.5607858	0.10632856	0.3328856		
4	0.5585635	0.20866064	0.2327759		
4	0.541748	0.18827448	0.2699776		
4	0.5651113	0.11181266	0.323076		
4	0.2936254	0.09425086	0.6121238	F2b	0
4	0.4126926	0.15401656	0.4332908	F2b	0
4	0.4236723	0.38227156	0.1940561	F1b	0
4	0.5575168	0.04984632	0.3926369		
5	0.3941811	0.32478118	0.2810377	0	0
5	0.2705532	0.55998815	0.1694586	F2b	0
5	0.3161287	0.49939917	0.1844721	F2b	0
5	0.4765642	0.17868188	0.3447539	F2b	0
5	0.4816092	0.2433123	0.2750785	F2b	0
5	0.3356668	0.47682169	0.1875116	F2c	2
5	0.3642984	0.42322368	0.212478	F2c	2
5	0.4443829	0.22885867	0.3267585	F2c	0
5	0.5006217	0.12116475	0.3782135	F2c	3
5	0.2627972	0.61184645	0.1253563	F2b	0
5	0.4857075	0.1265391	0.3877534	F2b	0
5	0.5411975	0.16907106	0.2897314	F2b	0
5	0.4808362	0.13438948	0.3847743	F2b	0
5	0.500357	0.1726553	0.3269877	F2b	0
5	0.5676504	0.26385833	0.1684912	F2b	0
5	0.5219602	0.22038841	0.2576514	F2c	2
5	0.6190156	0.14286553	0.2381188	F2c	0
5	0.2644292	0.56499521	0.1705756	F2c	0
5	0.4605232	0.24224446	0.2972323	F2c	0
5	0.4155539	0.31346316	0.2709829	F2b	0
5	0.3694826	0.4031139	0.2274035	F2b	0
5	0.5005183	0.29451289	0.2049688	F2b	0
5	0.4405274	0.33592145	0.2235511	F2b	0
5	0.4219096	0.43988578	0.1382047	F2b	0
5	0.3585113	0.43170896	0.2097797	F2b	0

5	0.3317735	0.55927061	0.1089559	F2b	0
5	0.4280083	0.33933215	0.2326595	F2b	0
5	0.4609758	0.36493763	0.1740866	F2b	0
5	0.4439563	0.30125539	0.2547883	F2b	0
5	0.4742647	0.34084871	0.1848866	F2b	0
5	0.3934897	0.34870142	0.2578089	F2b	0
5	0.461163	0.24679426	0.2920428	F2b	0
5	0.4162315	0.33847124	0.2452972	F2b	0
5	0.5234725	0.23775693	0.2387706	F2b	0
5	0.4333021	0.30463721	0.2620607	F2c	2
5	0.3645831	0.45745876	0.1779581	F2b	0
5	0.5066674	0.29521647	0.1981162	F2d	5
5	0.2423999	0.64824277	0.1093573	F2d	3
5	0.4257384	0.4577802	0.1164814	F3a	3
5	0.4121958	0.34208218	0.245722	F3a	2
5	0.3722136	0.43838416	0.1894022	F2c	0
5	0.3739517	0.29571134	0.330337	F2b	0
5	0.235321	0.7057523	0.0589267	F2b	0
5	0.429343	0.30317885	0.2674781	F2b	0
5	0.0122892	0.96257744	0.0251333	F2b	0
5	0.4668774	0.2470612	0.2860614	F2b	0
5	0.4547427	0.3209905	0.2242668	F2b	0
5	0.1836779	0.75023053	0.0660916	F2b	0
5	0.2907475	0.59302414	0.1162284	F2b	0
5	0.2365551	0.68079376	0.0826511	F1b	5
8	0.5192488	0.09979204	0.3809591	F2a	0
8	0.5709047	0.14365092	0.2854443	F2b	0
8	0.4412079	0.2197409	0.3390512	F2b	0
8	0.369596	0.47599631	0.1544077	F2b	0
8	0.2136339	0.63213939	0.1542267	F2a	0
8	0.3896107	0.36592154	0.2444678	F2b	0
8	0.5105774	0.15952373	0.3298989	F2a	0
8	0.3994908	0.2976908	0.3028184	F2a	0
8	0.3052632	0.42580101	0.2689358	F2b	0
8	0.4630875	0.224755	0.3121575	F2b	0
8	0.4960516	0.14221932	0.361729	F2b	0
8	0.5213747	0.14083026	0.337795	F2b	0
8	0.4830906	0.26065393	0.2562555	F2b	0
8	0.4532459	0.24464173	0.3021123	F2c	0
8	0.285652	0.45927414	0.2550738	F2c	1
8	0.3045687	0.49236883	0.2030625	F2b	0

8	0.3373041	0.49051119	0.1721847	F2b	0
8	0.4795113	0.23371804	0.2867707	F2b	0
8	0.4638936	0.20428503	0.3318214	F2b	0
8	0.5171177	0.20252183	0.2803605	F2a	0
8	0.3684772	0.21615477	0.415368	F2b	0
8	0.5542698	0.17915969	0.2665705	F2b	0
8	0.4429269	0.36385042	0.1932227	F2b	0
8	0.4640049	0.2990455	0.2369496	F2a	0
8	0.4034165	0.39127344	0.2053101	F2b	0
8	0.5066142	0.15540361	0.3379822	F2c	0
8	0.4141634	0.36508138	0.2207553	F2b	0
8	0.5108392	0.22367414	0.2654866	F2b	2
8	0.5592466	0.23489381	0.2058596	F2b	0
8	0.4628275	0.32744999	0.2097225	F2a	0
8	0.3632579	0.49737077	0.1393713	F3a	3
8	0.4129354	0.44179836	0.1452662	F2d	0
8	0.506286	0.33616639	0.1575476	F2b	0
8	0.3531398	0.39931723	0.247543	F2a	0
8	0.3317996	0.50098681	0.1672136	F2b	0
8	0.3498379	0.32461264	0.3255495	F2b	0
8	0.3400253	0.37629598	0.2836787	F2b	0
8	0.5023537	0.17742124	0.3202251	F2b	0
8	0.3534832	0.36200178	0.2845151	F2b	0
8	0.3799884	0.34807925	0.2719323	F2a	0
8	0.3657096	0.5439097	0.0903807	F1b	0
8	0.5336288	0.06940924	0.396962		
8	0.5939505	0.07871951	0.3273299		
8	0.5910788	0.1240809	0.2848403		

Cutting TOC

Well	TOC (%)	Facies	BI
4	2.16		
4	1.71		
4	2.27		
4	1.09	F2b	0
4	4.4		
4	3.63		
4	3.63	F2a	0
4	3.42		
4	2.49		
4	2.82	F2b	0
4	2.82	F2b	0
4	2.82	F2b	0
4	4.92	F2b	1
4	1.96	F2b	0
4	1.77	F3b	0
4	0.86	F3b	1
4	4.12	F3b	1
4	4.12	F2c	2
4	4.2		
4	3.75		

4	4.2		
4	4.2	F2b	0
4	3		
4	3.32		
4	2.53	F2b	0
4	2.83	F2b	0
4	3.49	F2b	0
4	3.49	F2b	0
4	2.86	F2b	0
4	3.37	F2b	0
4	3.37	F2b	0
4	3.37	F2c	0
4	3.54	F2c	2
4	3.06	F2c	2
4	3.96	F2c	2
4	2.05	F2b	0
4	2.56	F2b	0
4	1.57	F2b	0
4	4.5		
4	6.64		
4	7.63		
4	5.32	F2c	0
4	5.32	F2c	0
4	5.8	F2b	0
4	6.08	F2b	0
4	4.98	F2c	1
4	4.16	F2c	1
4	3.23		
4	3.79		
4	7.36		
4	7.36	F2b	0
4	7.36	F2b	0
4	4.2		
4	3.55		
4	4.12	F2b	0
4	3.32	F2b	0
4	1.95	F2b	0
4	4.93	F2b	0
4	4.18	F2b	0
4	1.43	F2b	0
4	6.19	F2b	0

4	4.06	F2b	0
4	5.16	F2b	0
4	3.84	F2b	0
4	4.31	F2b	0
4	5.42		
4	6.74		
4	3.42		
4	2.98		
4	3.06		
4	2.33		
4	3.55	F2c	0
4	4.91	F2c	0
4	3.84	F2c	0
4	3.95	F2d	0
4	1.49	F3a	0
4	4.61	F3a	0
4	3.78	F3a	0
4	2.59	F2c	0
4	2.21	F2c	0
4	2.75	F3a	1
4	5.28	F2b	0
4	5.37	F2b	0
4	5.37	F2b	0
4	5.37	F2b	0
4	8.73	F2b	0
4	6.37	F2a	0
4	5.64	F2a	0
4	7.48	F2b	0
4	5.57		
4	7.63		
4	9.71		
4	7.25	F2b	0
4	3.73	F2b	0
4	2.75	F2b	0
4	0.34	F2b	0
4	2.58		
4	2.58	F2b	0
4	3.09	F2b	0
4	3.28	F1b	0
4	2.62	F1b	0
4	1.57	F1b	0

4	0.98	F1b	0
8	3.81	F2b	0
8	1.06	F2b	0
8	1.53	F2b	0
8	3.54	F2a	0
8	4.8	F2b	0
8	4.58	F2a	0
8	5.14	F2a	0
8	5.31	F2b	0
8	6.6	F2b	0
8	10.28	F2b	0
8	6.3	F2b	0
8	5.26	F2b	0
8	3.43	F2b	0
8	4.93	F2b	0
8	6.63	F2b	0
8	5.57	F2c	0
8	7.46	F2b	0
8	3.52	F2b	0
8	5.08	F2b	0
8	5.03	F2b	0
8	6.86	F2b	0
8	2.62	F2b	0
8	5.14	F2b	0
8	0.92	F2c	0
8	6.44	F2b	0
8	5.62	F2b	0
8	6.08	F2b	0
8	6.89	F2a	0
8	6.3	F2b	0
8	7.24	F2c	3
8	6.85	F2b	0
8	6.55	F2b	0
8	6.18	F2b	0
8	4.27	F2a	0
8	6.58	F3a	6
8	6.21	F2d	2
8	5.77	F2d	6
8	3.18	F2d	0
8	6.05	F2b	0
8	6.27	F2b	0

8	8.64	F2b	0
8	12.16		
8	4.02		
8	7.04		
8	7.64	F2b	0
8	13.12	F2b	0
8	12.59	F2b	0
8	10.99	F2a	0
8	7.69	F1b	5
8	2.28	F1b	0
8	0.88		
8	0.42		
8	0.27		
8	0.1		
8	0.91	F2a	0
8	5.54	F2b	0
8	1.78	F2b	0
8	6.3	F2b	0
8	7.63	F2b	0
8	5.54	F2b	0
8	1.86	F2b	0
5	6.28	F2b	0
5	4.87	F2b	0
5	3.98	F2b	0
5	4.35	F2c	2
5	4.85	F2c	2
5	3.65	F2c	0
5	3.16	F2c	0
5	4.51	F2c	0
5	3.18	F2c	2
5	6.99	F2b	0
5	5.48	F2b	0
5	4.77	F2b	0
5	5.47	F2b	0
5	3.41	F2b	0
5	5.72	F2b	0
5	4.47	F2b	0
5	5.46	F2b	0
5	6.04	F2b	0
5	5.05	F2b	0
5	7.26	F2b	0

5	6.77	F2b	0
5	6.9	F2b	3
5	3.13	F3a	2
5	3	F3a	3
5	6.99	F3a	0
5	3.2	F2b	0
5	4.59	F2b	0
5	8.92	F2b	0

5	6.95	F2a	0
5	8.16	F2a	0
5	9.4	F2b	0
5	3.54	F2a	0
5	8.65	F2b	0
5	6.61	F2b	0
5	2.82	F1b	3

Outcrop TOC

Section	Location (m)	TOC (%)	Facies
YdT outcrop	58.5	1.33	F2c
YdT outcrop	64.8	1.31	F2c
YdT outcrop	81.2	1.49	F2b
YdT outcrop	88.7	2.35	F2b
YdT outcrop	92.9	2.27	F2b
YdT outcrop	98.8	2.33	F2b
YdT outcrop	100.1	1.76	F2b
YdT outcrop	114.9	2.31	F2d
YdT outcrop	151	3.65	F2b
YdT outcrop	176.9	2.01	F2c
YdT outcrop	228.6	1.84	F2c
YdT outcrop	254.25	2.55	F2d
YdT outcrop	254.25	2.03	F2d
YdT outcrop	260.4	1.79	F2d
YdT outcrop	275.5	1.21	F2d
YdT outcrop	285.5	2.19	F2d
YdT outcrop	316.5	1.17	F2b
YdT outcrop	354.35	2.18	F5a